Drilling Fluid Additives for Wellbore Strengthening and Reservoir Protection

by

Karl Ronny Klungtvedt

Thesis submitted in fulfilment of
the requirements for the degree of
PHILOSOPHIAE DOCTOR
(PhD)

Faculty of Science and Technology
Department of Energy and Petroleum Engineering
2023

ISBN: 978-82-8439-194-6
ISSN: 1890-1387
PhD: Thesis UiS No. 726

University of Stavanger
NO-4036 Stavanger
NORWAY
www.uis.no

ISBN: 978-82-8439-194-6
ISSN: 1890-1387
PhD: Thesis UiS No. 726

Acknowledgements

The research and work leading up to this thesis has been conducted during my employment at European Mud Company AS (EMC). A significant part of the work has been conducted together with my colleagues Bjørn Berglind and Jan Kristian Vasshus. In addition, I have had the benefit of valuable discussions with Dr. Swapan Kumar Mandal and Nicola Santarelli. They have contributed with their experiences and insights and provided a positive environment for research and development. I would like to thank them for their advice, support, curiosity, and enthusiasm.

Most of the laboratory work was conducted at EMC's research laboratory in Stavanger, Norway. Great contributions were made from students from the University of Stavanger, conducting research for their BSc and MSc thesis work.

The access to EMC's client network has been very valuable, with numerous technical discussions on real-life challenges in current drilling operations. This has been very insightful and facilitated a link between the in-house research and experience from field applications.

My supervisors at the University of Stavanger, Professor Arild Saasen and Professor Mahmoud Khalifeh, have been instrumental in guiding me on the path of scientific investigations and openly shared their thoughts and views. Their insights are highly valued.

I would also like to thank EMC and the Research Council of Norway for funding the research leading to this thesis.

In summary, the combined access to current industry challenges, the scientific approach and intellect of academia and an enthusiastic and open-minded workplace has provided we with an ideal arena for conducting the work leading up to this thesis.

Summary

The objective of the research was to optimise drilling fluid additives for wellbore strengthening, preventing lost circulation and avoiding drilling fluid induced formation damage. Industry standard testing, such as HTHP fluid loss tests following API 13B, yield limited insight into important areas such as wellbore strengthening and formation damage.

Therefore, new testing methodologies were developed and evaluated. These provided new insight into important areas for designing and evaluating drilling fluids and drilling fluid additives for wellbore strengthening and reservoir protection.

Key conclusions were that exposing particles to mechanical wear significantly impacted the relative performance of materials used for preventative treatments.

Oil-based fluids were found to create a high-degree of internal formation plugging, whereas water-based fluids more predominantly isolated the wellbore pressure from the pore-pressure though an external filter-cake. Inclusion of cellulose based fibres where the D90 value value $\lesssim 3/2$ the median pore size was shown to reduce internal plugging and reduce formation damage, in both water-based fluids and oil-based fluids.

Particle degradation studies showed that $CaCO_3$ degraded rapidly for particles > 23 μm and that the most wear resistant particles were selected cellulose-based materials. Combinations of fine CaCO3 and slightly coarser cellulose mixtures were found to be effective for creating low-permeability filter-cakes and preventing formation damage.

For preventative treatment in drilling conditions with large differences between the matrix pore-size and the aperture of natural or induced fractures, a dual mode particle size distribution was found to be effective

in both laboratory studies and field applications. In such situations, the fine mode of the PSD provided low filter-cake permeabilities when the particles followed an Andreasen distribution with a packing factor of around 0.08-0.10. Natural and induced fractures were most effectively sealed when granular cellulose particles made up the coarse mode of the PSD and these particles were sized similar to or slightly larger than the fracture aperture.

Preface

The research was conducted in an industrial environment with close contact with academic institutions. This facilitated the study of current operational and practical challenges and simultaneously reflecting over these from an academic and scientific perspective. The key interfaces of the research were thus the internal research and development activities within EMC, the academic environment and guidance from the University of Stavanger, the operations of EMC and its clients and interaction with other industry players. A part of the EMC research contains intellectual property rights such as patents and product recipes. Another important part of the work is field applications, where the data is owned by EMC's clients. These elements are not published as part of this work, except where this has been a part of published research and agreed between the parties.

A critical factor in the research was the investigation into and establishment of alternative test equipment and procedures. Rather than focusing entirely on either of filtration control, loss prevention or remedial treatments of lost circulation, the research aimed at looking into each of these areas in parallel. The idea was that discoveries made in one area might provide useful insight into other areas and hence contribute towards a fuller understanding of fluid loss and lost circulation mechanisms. The wide range of test methodologies facilitated obtaining

new knowledge related to reaching the objectives of the research. The understanding gained when applying the new testing methodologies remain the core of the work leading to the thesis. Figure 0.1 presents the context and content of the PhD Thesis.

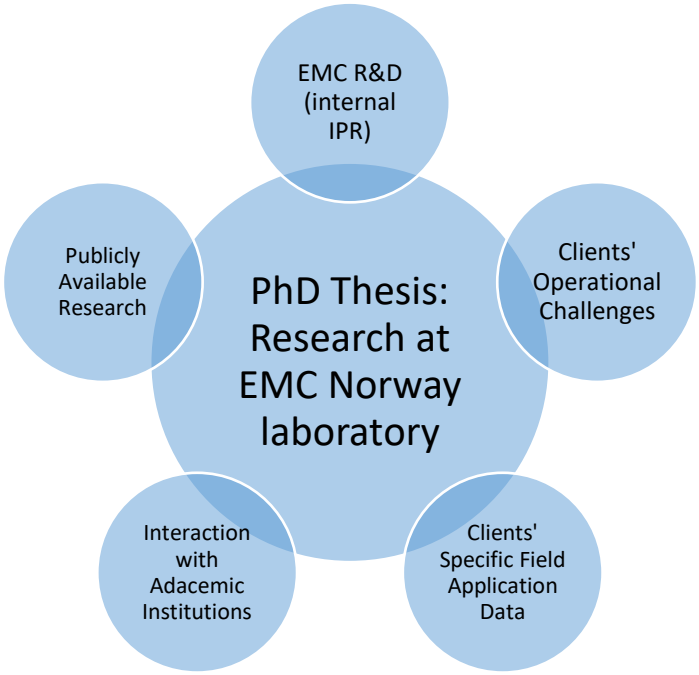

Figure 0-1 Context and content of the PhD Thesis

The objective of the first two chapters is to provide a brief guide to principles within drilling fluid functionality, design and testing. It will cover areas which may provide useful for a student of drilling fluids, a person starting as a drilling fluid engineer or others which have an interest in obtaining a fundamental understanding of drilling fluids. The discussions in these chapters will be on an elementary level to explain basic principles and to identify areas where the reader may seek further depth of study elsewhere. In order to create a natural flow in the document, data from the articles attached in the appendix is included in the thesis text and not referred to in each case.

The majority of the tests presented have been conducted with water-based drilling fluids, due to the wide usage of such fluids as well as an industry drive to move towards more environmentally friendly fluid systems. To retain a low difference in the base fluids for the different tests, a KCl-Polymer fluid is typically used as the base fluid. By retaining relatively similar base-fluids, the impact of weighting agents, filtration agents and lost circulation materials may be more clearly observed. Certain of the tests have been conducted with both water- and oil-based drilling fluids, to better understand the different functions of the fluid systems.

The research has been centred around materials that can be applied preventatively into the active drilling fluid or materials that can be pumped in non-complex pills. This has been done as drilling time often is a critical factor in controlling the cost of a well and also because wellbore stability problems may escalate if time is passing without adequate treatment. Therefore, time- or temperature setting pills, resin plugs or other cementing like treatments are not considered as part of the research scope. Similarly, the focus has been on studying biodegradable and environmentally friendly materials, to reduce the HSE risks of the drilling operations.

In summary, it was a great personal experience to conduct the research leading to the thesis. The overall result is a product of high level of interaction with discussion partners and a large volumes of laboratory testing. Numerous choices were made along the way and most of them bore fruit. Looking back, it is not clear which role lady Fortuna played, however, I have no doubt that daring to make a choice and trying new approaches was critical to making progress in the research. Many have described the choices they made in life, and in retrospect they can often be rationalised and justified. Bearing this in mind, it may also be useful to humbly listen to the elegant words of Robert Frost.

The Road Not Taken

Two roads diverged in a yellow wood,
And sorry I could not travel both
And be one traveler, long I stood
And looked down one as far as I could
To where it bent in the undergrowth;

Then took the other, as just as fair,
And having perhaps the better claim,
Because it was grassy and wanted wear;
Though as for that the passing there
Had worn them really about the same,

And both that morning equally lay
In leaves no step had trodden black.
Oh, I kept the first for another day!
Yet knowing how way leads on to way,
I doubted if I should ever come back.

I shall be telling this with a sigh
Somewhere ages and ages hence:
Two roads diverged in a wood, and I-
I took the one less traveled by,
And that has made all the difference.

Robert Frost, 1916.

List of papers and contributions

The thesis is based on the research enclosed in the appendix. These are referred to by Roman numerals [I] to [IX]. Reference [X and XI] refers to work that the undersigned has co-authored and references [XII] to [XVII] refer to work conducted by bachelor and master students that have been a part over the overall research and where undersigned have been a supervisor or co-supervisor.

I. Klungtvedt, K.R., Saasen, A., Vasshus, J.K., Trodal, V.B., Mandal, S.K., Berglind, B. and Khalifeh, M. "The Fundamental Principles and Standard Evaluation for Fluid Loss and Possible Extensions of Test Methodology to Assess Consequences for Formation Damage." *Energies*, VOL No. 18 (8), Paper 2252 – MDPI, 2021. (open access)

II. Klungtvedt, K.R., Berglind, B., Vasshus, J.K., Khalifeh, M. "Preventing Drilling Fluid Induced Reservoir Formation Damage", SPE-202187-MS, *SPE/IADC Middle East Drilling Technology Conference and Exhibition*, 25-27 May 2021.

III. Klungtvedt, K.R. and Saasen, A. "A Method for Evaluating Drilling Fluid Induced Permeable Formation Damage", *Journal of Petroleum Science and Engineering*. https://doi.org/10.1016/j.petrol.2022.110324. (open access)

IV. Klungtvedt, K.R. and Saasen, A. "Invasion of CaCO3 particles and polymers in porous formations in presence of fibres", *Journal of Petroleum Science and Engineering 2022*. https://doi.org/10.1016/j.petrol.2022.110614 (open access)

V. Klungtvedt, K.R. and Saasen, A. "The Role of Particle Size Distribution for Fluid Loss Materials on Formation of Filter-Cakes and Avoiding Formation Damage". OMAE2022-79501.

Journal of Energy Resources Technology 22-1217, 2023. https://doi.org/10.1115/1.4056187 (open access)

VI. Klungtvedt, K.R. and Saasen, A. "Comparison of Lost Circulation Material Sealing Effectiveness in Water-Based and Oil-Based Drilling Fluids and Under Conditions of Mechanical Shear and High Differential Pressures". OMAE2022-79502 and *Journal of Energy Resources Technology 22-1218, 2022*. https://doi.org/10.1115/1.4054653 (open access)

VII. Klungtvedt, K.R., Pedrosa, C., and Saasen, A. «Measuring Filter-cake Cohesive Strength and Flowability", *Geoenergy Science and Engineering, Volume 221, February 2023, 111298*. https://doi.org/10.1016/j.petrol.2022.111298 (open access)

VIII. Klungtvedt, K.R., Vasshus, J.K., Nesheim, G., Scott, P.D. "Managing High Differential Pressures in Fractured Carbonate Reservoir by use of Wellbore Strengthening Material", OTC-32173-MS, *Offshore Technology Conference* 2023, Houston, Texas, USA. https://dx.doi.org/10.4043/32173-MS

IX. Klungtvedt, K.R., Vasshus, J.K., Saasen, A. "Assessment of induced fracturing and fracture sealing during drilling", *Geoenergy Science and Engineering, Volume 226 (2023) 211816.* https://doi.org/10.1016/j.geoen.2023.211816 (open access)

X. Khalifeh, M., Saasen, A., Vorland, K.A., Djuve, J., Klungtvedt, K.R. «Rheological Characteristics of Oil-Based and Water-Based Drilling Fluids", August 2021, Nordic Rheology Conference 2021.

XI. Khalifeh, M.; Klungtvedt, K.R.; Vasshus, J.K.; Saasen, A. "Drilling Fluids—Lost Circulation Treatment"; SPE-195609-MS; 2019, SPE Seminar in Bergen, Norway.

XII. Trodal, V.B. “Using ceramic discs to evaluate fluid loss and formation damage”, Bachelor Thesis 2021, University of Stavanger.

XIII. Bergsvik, I.S. “Optimizing formulations for reservoir drilling fluids”, Bachelor Thesis 2022, University of Stavanger.

XIV. Trodal, T. “Optimization of LCM formulations for wellbore integrity”, Bachelor Thesis 2022, University of Stavanger.

XV. Grelland, S.S. “Analysis of lost circulation on the Norwegian Continental Shelf”, Master Thesis 2021, University of Stavanger.

XVI. Høgmo, E. “Prevention of loss of drilling fluid when drilling with overbalance”, Bachelor Thesis 2023, University of Stavanger.

XVII. Trodal, V. “Efficiency of lost circulation materials”, Master Thesis 2023, University of Stavanger.

Table of Contents

1 Introduction

1.1 Main purpose and objectives of the research

The research was directed towards obtaining a greater understanding of phenomenon such as lost circulation of drilling fluid, wellbore strengthening or stabilisation, and drilling fluid induced permeable formation damage, and in relation to this develop improved products and methods for dealing with realistic operational challenges. Two primary objectives were established, each with a set of subobjectives, before the research project was initiated.

1) Primary objective: Optimise drilling fluid additives for wellbore strengthening and avoiding lost circulation when drilling oil/gas/geothermal wells. The main objective will be achieved through the subobjectives.

   Subobjectives are addressed as following:

   a) Presenting various sealing mechanisms for avoiding pressure transmission from the wellbore to the surrounding formation, hereunder:
      i) Understanding testing methodologies and their effectiveness in estimating behaviour of drilling fluids additives for wellbores strengthening and avoiding lost circulation
      ii) Identifying optimal testing methodologies or test matrices for understanding effectiveness of drilling fluid additives
      iii) Understanding impact of drilling fluid additives on other important drilling fluid properties such as viscosity and inhibition

   b) Optimising design and application of drilling fluid additives for wellbore strengthening in relation to solids control systems, various fluid systems and fluid densities, hereunder:

   i) Testing various products for resilience towards degradation during circulation and/or ease of passing through solids control systems
   ii) Understanding current operational challenges and integrating product development and testing with such real-life challenges

2) Primary objective: Optimise reservoir protection and extended reach when drilling reservoir formations, by optimising design and application of additives for:
   a) Secondary objective: minimising fluid invasion into the reservoir formation
   b) Secondary objective: easy and efficient removal of filter cake
   c) Secondary objective: maximising wellbore strengthening and minimising rheology impact

Testing was primarily concentrated around commonly used lost circulation materials such as $CaCO_3$, graphite, nutshells and cellulose-based fibres. A selection of biogenic products from EMC, based on proprietary technology (Vasshus et al. 2019, 2020), was used during the testing.

1.2 Functionality of drilling fluids

The objective of the introduction is to provide a guide to fundamental principles within drilling fluid functionality, design and testing. It will cover areas which may provide useful for a student of drilling fluids, a drilling fluid engineer or others which have an interest in obtaining a fundamental understanding of drilling fluids. Also, the information provided in the introduction as considered prerequisites for understanding the research presented in later chapters.

Drilling fluids serve multiple purposes when drilling a well. The primary functions are to transport drilled cuttings out of the wellbore, to stabilise the rock formations by providing a support pressure or prevent formation swelling, to control formation fluids and preventing them from migrating

into the wellbore as well as sealing the wellbore to prevent the drilling fluid from being lost into the formation. Further, the drilling fluids are cooling and lubricating the bit and downhole tools, and in some cases the hydraulic energy of the fluid is used to drive tools such as downhole motors. If the drilling fluid is inadequately designed, the result may be that the wellbore collapses or that hydrocarbons escape the well in an uncontrolled way and cause a blowout.

To serve these purposes, the drilling fluid need to be designed with a series of functions such as adequate viscosity, density, filtration control properties, capacity for inhibition and lubrication, and to retain these functions under realistic conditions of flow, temperatures, pressures and mechanical wear.

When drilling into the reservoir, special attention is paid to the functionality of the fluid with regards to causing permeable formation damage. Drilling fluids used for such operations are generally referred to as drill-in fluids (DIF) or reservoir drilling fluids (RDF).

1.2.1 Water-based drilling fluids and viscosifiers for water-based fluids

Water-based drilling fluids are designed specifically for the formations that are being drilled. For shallow top-hole sections, simple drilling fluids known as spud muds are being used. A spud mud is typically consisting of bentonite and flocculated with lime if it is used onshore and either guar gum or salt gel is used offshore to create sufficient viscosity.

As the drilling progresses deeper into the formation, the technical complexity increases, and thus more advanced fluid compositions are required. Water-based fluids are typically divided into:

- Nondispersed systems. These systems are often gel-and-water compositions used for drilling of shallower sections, although complex polymer-based systems may also be nondispersed.

- Dispersed systems are water-based systems where dispersants are added to deflocculate clay particles to control the fluid viscosity. This approach may be used to allow higher fluid densities by use of weighting agents and to increase the tolerance of drilled solids. Lignosulphonates and lignitic chemicals are commonly used as dispersants. To maintain the system performance, a pH in the range of 10-11 is normally required and achieved through the addition of chemicals such as NaOH (Caustic Soda).
- Brine-based systems may be used to increase the fluid density without the addition of weighting agents, or it may be applied to achieve improved inhibition when drilling clay, shale and salt formations.
- Polymer-based systems are used to further increase the inhibitive functionality of brine-based systems, particularly when drilling formations containing shale. Such systems will therefore often contain either glycols or amines in addition to salts. KCl (Potassium chloride) is an effective inhibitor for shale and is the most widely used salt for polymer-based fluids. These chemicals are incompatible with using bentonite as a viscosifier, and hence separate polymers are added to regulate viscosity and filtration properties.

Bentonite is often used as a viscosifier in non-inhibitive water-based drilling fluids. It is an old clay mineral formed with the ageing of volcanic ash. The name comes from the Fort Benton, Wyoming, whereas also montmorillonite clay from France is a well-known source, and hence this name is also commonly used. Smectite is another name for montmorillonite. Bentonite swells readily in water and increases the fluid viscosity and forms a gel at certain concentrations. The particles also contribute to filtration control by forming a filter-cake. Bentonite may be divided into sodium bentonite and calcium bentonite as the main ingredient. The sodium bentonite has a greater swelling capacity and has very good colloidal properties, making it the ideal choice for drilling

fluids. When suspended in water, bentonite helps to form a shear thinning/pseudoplastic or thixotropic fluid. The gelling properties of bentonite help to suspend weighting agents and drilled solids in the fluid, without or with little particle settling (Luckham and Rossi, 1999). Studies have shown that water-based fluid containing clay or using bentonite is as a viscosifier caused formation damage and that by introducing a polymer-based fluid loss material, the formation damage was reduced (Osode et al., 2016, and Iscan et al., 2007).

Guar gum is a non-ionic polysaccharide that traditionally has been a cost-effective viscosifier in water-based drilling fluids. The application is however limited as it has low thermal stability and degrades quickly in alkaline solutions.

Another more commonly used viscosifier is xanthan gum, otherwise known as XC polymer. This is an anionic polysaccharide that is highly shear-thinning or pseudoplastic, thus making it an effective additive to suspend weighting agents and drilled solids. Due to it being anionic, it also has a positive impact on reducing fluid loss, limits flocculation of clays and works well in brines. Depending on the fluid composition, xanthan gum shows thermal stability to around 120°C (Zou et al., 2019). The thermal stability will vary with the presence of monovalent, divalent or formate salts as these may shield the charged groups of the xanthan gum.

Water-based systems are widely used due to their low cost and generally being environmentally friendly. Therefore water-based fluids are almost always used for drilling of the less complex upper sections of wells. The main disadvantage of water-based fluids is that the polar molecules of water react with many substances which change the properties of the fluid. A key challenge is presented by clays and shales, where hydration commonly leads to wellbore instability issues. For the deeper and sometimes more difficult well sections, oil- or synthetic-based fluids are often preferred due to their inherent stability. To enable drilling of

complex formations or challenging well-sections with water-based fluids, more advanced fluid recipes are prepared, often referred to as high-performance water-based mud, or HPWBM. Such fluids may contain chemicals such as glycols for shale inhibition or to prevent gas hydration, amine-based shale inhibitors and partially hydrolysed polyacrylamide (PHPA). A series of other challenges need to be overcome with water-based fluids to maintain a stable performance. The fluids are therefore often treated with other chemicals such as e.g. NaOH to maintain pH and alkalinity, MgO as an alkalinity agent and pH buffer, Na_2CO_3 to treat Ca^{2+} contamination (hard water).

1.2.2 Oil-based or synthetic-based drilling fluids

Oil-based drilling fluids are primarily invert emulsion systems, where water or brine is sheared into a base oil in the presence of an emulsifier. By applying high shear-rates, the water or the internal phase is broken up into small droplets which are carried by the oil, which is the external phase. Further, organophilic clay is mixed in to provide viscosity. For the clays to work in the oil-based fluid, they have been chemically treated with oil-wetting agents, to ensure the particles are dispersed. The clays that are made organophilic are typically either bentones, which are plate-shaped, and contribute to both viscosity and filtration control or it may be sepolite or attapulgite, which are spike- or rod-like clays, and only regulate the viscosity.

By adjusting the oil to water ratio, the viscosity and density of the fluid may be adjusted. A lower oil to water ratio will normally lead to increased viscosity over the whole shear rate range and also higher yield stress (Ofei et al., 2020).

Synthetic-based fluids are designed to replicate the functional advantages of oil-based fluids, with the objective of obtaining lower toxicity. In such fluids, the external phase or the continuous phase is a

synthetic organic material, whereas the internal phase is typically a brine (Neff et al., 2000).

Oil- or synthetic-based drilling fluids have some inherent benefits relative to water-based drilling fluid systems. In a simple water-based system shale and clay formations will swell and salt formations will start to dissolve. The continuous phase of an oil- or synthetic-based fluid does typically not react with neither the shale nor the salts, so that only the salinity of the internal brine phase needs to be regulated to limit the interaction with the formation being drilled. Also, this helps to prevent drilled solids from breaking up into fine particles, which are difficult for the solids control systems to remove. Oil-based systems naturally have good fluid loss characteristics, temperature stability, good lubricity, and corrosion resistance. All these elements contribute to providing a stable fluid system performance and promote effective drilling and high rate of penetration (ROP).

The main technical disadvantage of an oil-based system is related to health, safety and environmental (HSE) factors. This has led to a drive for both lower toxicity base fluids, but also for more advanced water-based drilling fluids.

1.2.3 Weighting agents

Salts are commonly used in water-based fluids to stabilise the formation, as an inhibitor by preventing it from hydrating, and to increase the density of the fluid. The most used salts are NaCl, KCl and $CaCl_2$. NaCl may increase the density of a brine to 1.197 g/cm^3, KCl may be used to create density up to 1.162 g/cm^3, and $CaCl_2$ up to 1.396 g/cm^3. The K^+ cation, from dissolving KCl in water, is particularly effective in stabilising bentonite or other clays as it is effectively adsorbed on smectite/montmorillonite already at a concentration of 5% by weight, which gives a brine density of 1.03 g/cm^3. For very high densities, brines may be made with e.g. KCOOH (Potassium formate) up to a density of

1.58 g/cm^3, $CaBr_2$ (Calcium bromide) up to a density of 1.80 g/cm^3 or CsCOOH (Cesium formate) up to 2.40 g/cm^3. When applying brines, special care should be taken to consider other effects such as corrosion, as chloride ions are aggressive in inducing corrosion (Lyasara et al., 2015). When brines are mixed into an oil-based fluid, it is also used to regulate the density.

In addition to, or as an alternative to salts, high density minerals are commonly used as weighting agents. Table 1.1 list some weighting agents. The weighing agents available in the market may have different purities, and different mineral combinations, and hence the data may deviate from the values in the table.

Material	**Density (g/cm^3)**	**Solubility**	**Mohs hardness**	**Tenacity**	**Other information**
$BaSO_4$ (Barite)	4.2-5, or 4.48 for pure $BaSO_4$	Low in most acids, moderately in EDTA	3-3.5	Brittle	
$CaCO_3$ (Calcium carbonate)	2.71	Fully soluble in most acids	2-3	Brittle	Degrades very rapidly in size
Fe_2O_3 (Hematite)	5.26	Low	5-6.5	Brittle	Abrasive and very weakly magnetic
$FeTiO_3$ (Ilmenite)	4.70-4.79	Low	5-6	Brittle	Abrasive and weakly magnetic

Table 1-1: Examples of weighting agents

The two most widely used weighting agents are barite and calcium carbonate. Although both are brittle materials, barite is harder than calcium carbonate and the particle size degrades more slowly. Due to the higher density, barite is typically the preferred weighting agent for drilling of well-sections above the reservoir. This enables a higher fluid density with lower volumetric concentration of solids. Calcium

carbonate is often the preferred weighting agent for drilling of reservoir sections due to its acid solubility.

1.2.4 Filtration control materials

Filtration control materials are introduced to prevent or limit fluid filtrate from migrating into the formation and thus reduce the loss of drilling fluid. Water-based drilling fluid may be composed in a series of different ways and hence also use different filtration control materials. The two most common groups of materials are bentonite and polymers. Bentonite is used to both create viscosity and control fluid loss. As bentonite is known to cause permanent permeability damage, it is not used in reservoir drilling fluids (Iscan et al., 2007). The most widely used filtration control materials in water-based drilling fluids are polymers such as starch and poly-anionic cellulose (PAC). These come in different varieties and are often mixed to achieve a certain level of fluid loss and viscosity. PAC is often considered to have better thermal stability and salt resistance than starch, whereas some starches provide effective fluid loss control with lower viscosity impact than PAC. PAC is provided in different grades of viscosity and may be thermally stable to around 150°C. Starches are made from different materials such as potato and corn. Some starches are chemically modified or cross-linked to achieve certain characteristics such as enhanced temperature stability or filtration control. The starches used for drilling fluids typically have a temperature stability up to 90-120°C.

For oil-based fluids, different materials are typically used to improve filtration control. Commonly used alternatives are organophilic clay (bentones) and asphaltic resins, such as gilsonite.

1.2.5 Lost circulation and lost circulation materials

Whereas filtration control materials target sealing of low-permeability formations, lost circulation materials (LCM) are introduced to prevent

or stop loss of fluid to the surrounding formation when the permeabilities are higher or in the presence of natural or induced fractures. It is critical to maintain a control over the wellbore pressure, prevent incidents such as blow outs, collapse of the wellbore, differential sticking, or permeability change of the formation in a producer or injector well.

Losses are typically categorized depending on the loss rate, although, for each situation the loss rate may be highly dependent on the circulation rate of the drilling fluid. A higher circulation rate will normally lead to higher pressures and larger losses. To accurately describe a loss situation, it is therefore beneficial to distinguish between static losses, when the drilling fluid is not circulated, and dynamic losses, where the drilling fluid is circulated at a certain rate. In an An example of categorization of losses is shown in Table 1.2

Category	**Loss rate (m^3/hr)**	**Loss rate (bbl/hr)**
Seepage losses (or minor losses)	0-1.5	0-10
Partial losses	1.5-10	10-60
Severe losses	>10	>60
Complete losses		

Table 1-2: Example of categorization of dynamic losses of drilling fluid in a wellbore

A simplified overview of lost circulation application categories and materials is presented in Figure 1.1

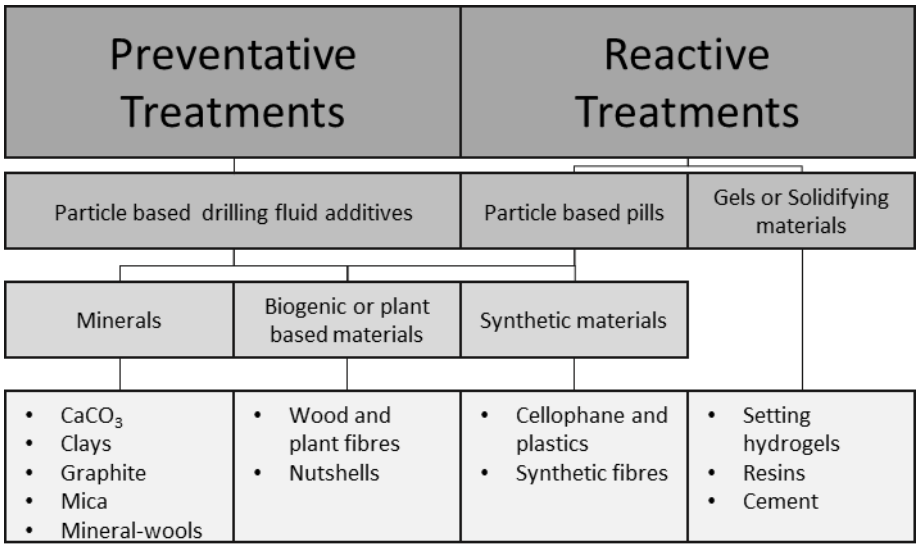

Figure 1-1 Simplified overview over lost-circulation application categories and materials

In very high or total loss situations, it may be required to revert to gels or solidifying materials to obtain a good isolation between the wellbore and the formation fluids. Such applications typically involve either time- or temperature setting mixtures that may be pumped to the loss sone and thereafter cures to form a more rigid structure.

In most wells, loss situations are less severe, and particle-based materials may be applied preventatively or reactively to limit or stop the fluid loss. The general functionality of such lost circulation materials (LCM), otherwise known as bridging particles or loss prevention materials, is that they have a mixture of particles with different sizes to facilitate either a plugging into pores or fractures or to form an external low-permeability filter-cake, to prevent further fluid loss (Whitfill, 2008, and Vickers et al., 2006). Particle based systems are often based on minerals such as calcium carbonate or mica, mineral wools, natural or synthetic graphite, plastics, or by-products of manufacturing of organic materials such as saw-dust, nutshells or other processed cellulose-based products. For preventative treatment, particles are often

selected to minimise screening out at the solids-control stage, and thus typical particle size distributions (PSD) will be up to 100-250 µm. Typical concentrations of preventative LCM materials may be in the range of 14-114 kg/m^3 (5-40 ppb). Unless the formation drilled is pre-fractured, loose sand or vugular, preventative treatments are often sufficient to control fluid loss. A well-designed preventative LCM treatment may avoid or stop seepage losses and certain partial losses.

With partial or severe losses, special mixtures of LCM-pills may be applied to seal high-permeability formations or fractures. Such fractures may be natural or caused by the drilling operation. The general materials used are often the same as for preventative treatments, however the PSD range may be up to 1-4 mm or more, and concentrations may range from 85-430 kg/m^3 (30-150 ppb). In practice, the tolerances of the bottom hole assembly (BHA) may limit the particle size and concentration of LCM that may be applied.

1.3 Geology, permeability, and rock mechanics

A primary function of the drilling fluid is to create a barrier between the circulating fluid in the wellbore and the solids and fluids of the surrounding formation. The barrier takes the form of an internal- and/or external filter-cake against a permeable formation. Therefore, understanding the physical and chemical properties of the formation is key to a good drilling fluid design.

The primary formations drilled during hydrocarbon exploration or production drilling will be sedimentary rocks or sediments of clay, silt, sand or gravel.

Common sedimentary rocks and are sandstone, siltstone, shale, limestone and dolomite, and Karst limestone. Due to the sedimentary nature, these rocks generally have anisotropic characteristics, where the mechanical properties or fluid conductivity may be different if measured

along or perpendicular to the sedimentary layers. The typical porosities also vary greatly, where shale generally will have porosity of 0-10%, limestones and dolomite may be anything from 0-20%, sandstones from 5-30% and siltstones from 20-40%. Karst limestone is a limestone where the exposure to water including e.g. CO_2 or H_2S has led to dissolution of calcite and hence an increase in porosity. Karstified limestone may therefore prove to be particularly difficult to drill as porosities may be up to 50% and the formation may contain large vugs. In conditions where the sediments are yet to form a solid rock, the porosities may be higher and 25-60% could be representative values.

The reservoir porosity, φ, is related to its permeability, K, and the average diameter of the grains, D_g. The specific relationships are modelled in numerous ways and where the Kozeny-Carman or Kozeny equation is a commonly used model. The model appears to be a good predictor of the relationship in conditions where $0.08 \leq \varphi \leq 0.25$ and the Reynolds number is ≤ 1 (Civan, 2020). The Kozeny equation for single phase permeability is presented in equation 1.1, where Φ_s represents the sphericity of the grains.

$$K = \Phi_s^2 \frac{\varphi^3 D_g^2}{180(1-\varphi)^2} \tag{1.1}$$

The most common reservoir rocks are limestones and sandstones. As the typical porosity is lower for the limestones than for sandstones the matrix permeabilities are also typically lower for limestones and higher for sandstones. As an example, the matrix permeabilities of the carbonate reservoirs at Auk and Ekofisk in the North Sea are in the region of 0.025-5 mD. Røgen and Fabricius (2002) analysed core samples from the Tor and Ekofisk Formation chalk reservoirs and found that the permeabilities were successfully predicted by using the Kozeny equation. In contrast to the carbonate reservoirs, the matrix permeabilities of the sandstone reservoirs at Statfjord East and Oseberg are in excess of 1000 mD. The most recently developed giant field in

the North Sea is Johan Sverdrup. The coarse grain size, scarcity of cementation and porosity in the region of 28% provide a reservoir where the permeabilities are in the range of 25 – 27 Darcies in large parts of the reservoir, Olsen et al. (2017).

Wennberg et al. (2013) presented a discussion on characteristics of fractured carbonate reservoirs and found indications that fluid flow tends to be channelled through a fracture network. This is normally a result of large matrix and fracture heterogeneity. Heterogeneous characteristics of formations may be important to consider with regards to drilling fluid design, both with regards to wellbore strengthening, lost circulation and formation damage.

Nelson (2009) conducted a study on pore-throat sizes in siliciclastic rocks and found that they form a continuum from the submillimetre to the nanometer scale. He found that reservoir sandstones generally have pore sizes greater than 20 µm and pore-throat sizes greater than 2 µm. The data reported by Nelson are hence consistent with also using discs with a median pore-throat size of 10-20 µm to represent a sandstone formation. Gao et al. (2021a, 2021b) investigated nanomaterials in relation to Mancos Shale and Eagle Ford Shales, which have pore-sizes in the low nanometre to low µm range.

Kirsch (1898) formulated a series of equations which describe the linear elastic stresses that form around a cylindrical hole in an infinite plate. These equations are referred to as the Kirsch Equations and are commonly used to determine the minimum and maximum horizonal stresses, which are important for modelling wellbore stability. As an example, extended leak-off tests (XLOT) are conducted to measure stresses in wellbores and typically use the Kirsch equations for calculating the different stresses. When conducting an XLOT, a pressure is applied to the fluid to determine the pressures at which e.g. a fracture is opened, when a fracture propagates into the formation and the pressure for re-opening a closed fracture. The analysis aims at

understanding elements such as the local stresses, unconfined compressive strength, internal friction angle and cohesive strength. In general, the pressures in the formation are compressive. If the density of the drilling fluid is sufficiently high, the applied pressure may balance the compressive forces and induce tensile forces in the formation. These tensile forces may ultimately lead to fracturing. If, however, the fluid pressure is too low, the compressive forces on the formation may lead to a collapse of the wellbore.

During drilling, fluid filtrate penetrates the formation and alters the near-wellbore pore pressure. This effect is partially time-dependant as the formation of an effective external filter-cake will to a large degree isolate the wellbore pressure from the pore-pressure. The differences between the fluid pressure in the wellbore, the formation pore-pressure and the stresses in the rock itself impact when a fracture is induced in the wellbore. The Mohr-Coulomb shear failure criterion is a method commonly used for estimating the conditions under which fracturing of brittle materials such as rocks occur. The fundamental version of the model is shown in equation (1.2), where τ_f represents the shear stress at failure, c represents the cohesive strength of the formation, σ is the normal or inter-granular stress and φ the friction angle or the slope of the failure envelope. Alternatively, the friction angle may be used to calculate μ, which represents the internal friction factor as per equation 1.3.

$$\tau_f = c + \sigma \tan(\varphi) \tag{1.2}$$

$$\mu = \tan(\varphi) \tag{1.3}$$

The Terzaghi effective stress, σ', is used to describe stresses in porous media such as soils and is calculated as the difference between the intergranular stress or total stress, σ, and the pore-pressure, P_f, as per equation 1.4. The term η expresses the portion of the pore-pressure that contributes to the effective stress. Originally, Terzaghi set η =1,

however, a wide amount of research has been conducted to obtain expressions for η as a part of analysing stress-strain behaviour in various porous solids, rocks and soils [39, 27]. For the discussions of this text, the original proposal of η =1 has been applied for simplicity.

$$\sigma' = \sigma - \eta P_f \tag{1.4}$$

Mohr-Coulomb shear failure criterion with Terzaghi effective stress concept can thus be represented by equation (1.5) and graphically presented in Figure 1.2.

$$\tau_f = c + \mu\,(\sigma - P_f) \tag{1.5}$$

Following the principles of the combined Mohr-Coulomb failure criterion and the Terzaghi effective stress concept, it is clear that any change in the near-wellbore fluid pore-pressure may impact the strength of the formation and the ability to withstand fracturing. If induced fracturing is perceived to be a risk when a well-trajectory is being planned, it is important to consider the effect that the selection of drilling fluid may have on the pore-pressure transmission.

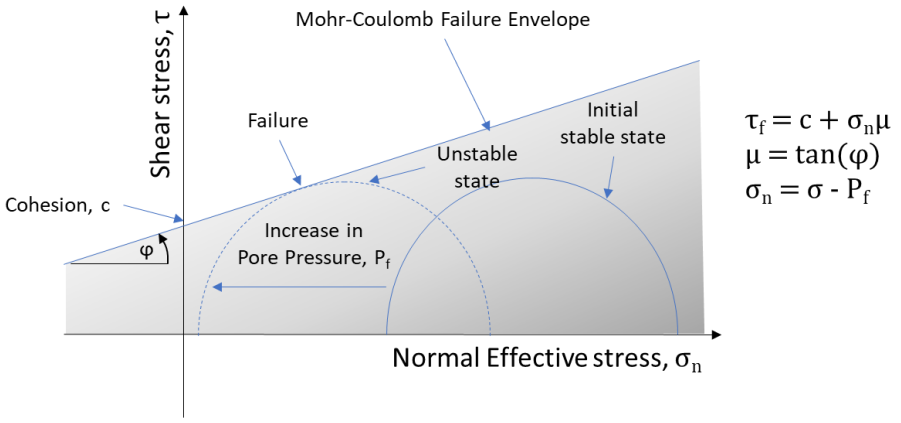

Figure 1-2 Mohr-Coulomb Failure Envelope with Terzaghi effective stress concept for modelling impact of pore-pressure

For specific analysis of failure conditions, the Mohr-Coulomb criterion may be applied along each axis in three dimensions. In a formation, the horizontal stresses are a function of the overburden stress and the Poisson's ratio of the formation. In this application, the Poisson's ratio will determine the portion of vertical stress that is transmitted to horizontal stress. The minimum horizontal stress is often approximated as the fracture closure pressure in a leak-off test.

1.4 Drilling fluid rheology and practical implications

Rheology is defined as the study of flow and deformation of matter, which covers both fluids and solids which show plastic flow. Viscoelastic materials show both elastic and viscous behaviour when being deformed. As an example, a fluid may form a gel, which can suspend higher density particles, when it is at rest and show viscous behaviour when it is being pumped or sheared. Drilling fluid rheology is often limited to the study of viscous flow assumptions and measured using a viscometer. Conventional rotational viscometers typically measure shear stress, τ, at shear rates, $\dot{\gamma}$, ranging from 1.7 to 1021 reciprocal seconds and calculate dynamic viscosity, η, by reformulating Newton's law as presented in equation 1.6.

$$\eta = \frac{\tau}{\dot{\gamma}} \tag{1.6}$$

Drilling fluids are generally viscoelastic, and hence exhibit both viscous and elastic properties. Fluids that establish more stable and stronger internal networks show higher gel strengths than fluids where the internal networks are weak. A gel strength measurement using a viscometer may give some insight into understanding this property, whereas a rheometer may allow for a more detailed study of the viscoelastic behaviour of a fluid.

Flow curves can be plotted using data from viscometers. Plots of shear stress versus shear rate will reveal if the fluid is Newtonian, shear thinning or shear thickening. Figure 1.3 and 1.4 presents flow curves which may be obtained using a conventional viscometer.

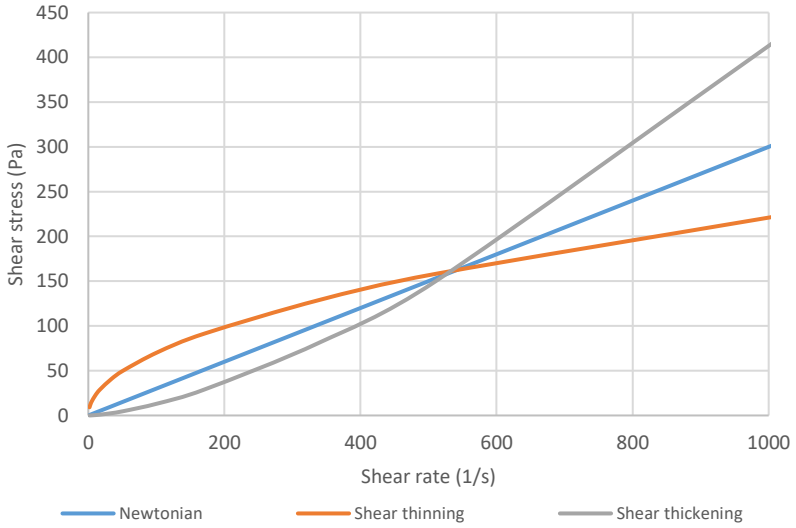

Figure 1-3: Examples of flow curves, Shear stress versus shear rate plot

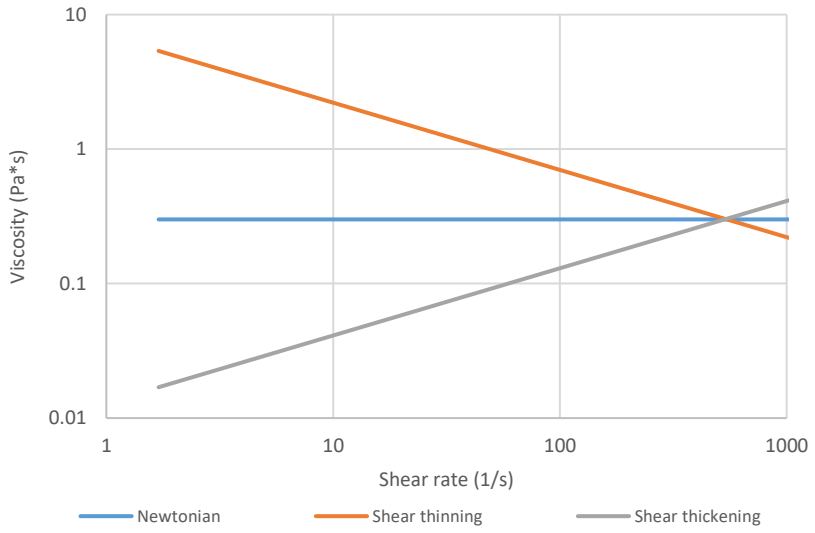

Figure 1-4: Examples of flow curves, Viscosity versus shear rate

To characterise the behaviour of non-Newtonian fluids, various rheological models have been developed. The Bingham plastic model (equation 1.7) follows the linear relationship between shear stress and shear rate, like the Newtonian model, but introduces an initial shear stress, τ_y, that needs to be overcome for the fluid to start flowing. τ_y is also described as the yield stress or yield point. The slope of the curve is defined by the plastic viscosity, μ_p.

$$\tau = \tau_y + \mu_p \dot{\gamma} \tag{1.7}$$

The Power law model uses a dimensionless flow behaviour index, n, and and a consistency index, k, to form the relationship shown in equation 1.8. With values of $n < 1$, the fluid becomes shear thinning, with values of $n > 1$, the fluid is dilatant or shear thickening, and with $n = 1$ and $k = 1$ it described a Newtonian fluid. The models does, however, not have an element that describes yield stress.

$$\tau = k\dot{\gamma}^n \tag{1.8}$$

By combining elements of the Bingham plastic model and the Power law, the Herschel-Bulkley model expressed by equation 1.9 is a more detailed method for describing the characteristics of a fluid.

$$\tau = \tau_y + k\dot{\gamma}^n \tag{1.9}$$

The Herschel-Bulkley may be used to describe the flow curve of most fluids relatively accurately. A weakness of the model is that the consistency index, *k*, and the behaviour index, *n*, are related. Saasen and Ytrehus (2018) provide examples of fluids with nearly identical flow curves, but where the values of *k* and *n* become very different when using least squares fit for slightly different share rate ranges. By using input from Nelson and Ewoldt (2017), Saasen and Ytrehus presented a re-arranged version of the Herschel-Bulkley equation. They first selected a relevant shear rate, $\dot{\gamma}_s$, and determined the surplus shear stress, τ_s, at this shear rate. The modified version is presented by Equation 1.10, where τ_y is the yield stress and $\tau_s = \tau - \tau_y$ at a specified shear rate $\dot{\gamma} = \dot{\gamma}_s$, and the curvature component, *n*.

$$\tau = \tau_y + \tau_s \, (\dot{\gamma} / \dot{\gamma}_s)^n \tag{1.10}$$

The re-arranged version of Herschel-Bulkley thus avoids the interdependence between *k* and *n*, and thereby facilitates a clearer understanding of changes in fluid behaviour by factors such as temperature and solids content. More advanced understanding of rheology may be obtained by studying fluids using a rheometer. A rheometer may be set up with a plate-plate configuration and oscillatory motion may be introduced to separate the elastic and viscous properties of a fluid or a powder. This enables studying time and frequency dependent behaviour and isolating energy storage or elastic properties from viscous or plastic properties (Kulicke et al., 1989, and Lomellini, 1992).

When the drilling fluid is used in the field, it will be exposed to different shear rates as it is pumped down through the drill-pipe and then

circulated back up the annulus. The fluid will normally be sheared at the highest rate when pumped through the nozzles in the bit. The rate of circulation is important to control to remove drilled cuttings from the wellbore. The main factor determining the hole cleaning is the frictional pressure drop caused by the circulation of the drilling fluid. The fluid share rate in the wellbore, $\dot{\gamma}_w$, can be calculated using equation (1.11), from Saasen et al. (2004), where *U* represents the fluid velocity, *D* the wellbore diameter and *d* the outer diameter of the drill-pipe.

$$\dot{\gamma}_w = \frac{12U}{D-d} \tag{1.11}$$

Werner (2018) presented some examples of shear rates for different hole diameters using a 5.5 inch drillpipe. In a 17.5 inch section, a pump-rate of 6 m^3/minute gives a shear rate of 28 s^{-1}, in a 12 ¼ inch hole a pump-rate of 4 m^3/minute yields a shear rate of 77 s^{-1}, and in an 8.5 inch hole a pump-rate of 2 m^3/minute yields a shear rate of 247 s^{-1}. These shear rates may be a good starting point for understanding fluid behaviour in relation to practical challenges such as barite sag, suspension of LCM particles and hole cleaning.

Barite sag is the settling of barite particles as a consequence of gravitational forces overcoming the viscoelastic forces of the drilling fluid. The risk of barite sag increases at low shear rates or at static conditions. It is therefore important to understand the viscoelastic properties of the fluid under such conditions. If the fluid is incapable of holding the barite suspended, the settling of particles will lead to a reduction of fluid density and hence a reduction in the wellbore fluid pressure. The risk of barite settling is increased for inclined sections of the wellbore. A phenomenon called the Boycott effect (Boycott, 1920) describes how the fluid density may be unevenly distributed across the wellbore, where lower density fluid occupies the upper end of the hole and higher density fluid accumulates at the lower end of the wellbore.

Similarly, the viscoelastic properties of the fluid are critical to achieve good hole cleaning and cuttings transportation, Pedrosa et al. (2021). In summary, optimising the fluid rheology profile is an act of balancing multiple considerations such as rate of penetration, hole-cleaning and particle sagging, induced fracturing and lost circulation.

1.5 Categorisation and prevention of permeable formation damage

Reservoir formation damage may take place through different mechanisms (Bennion, 2002 and Civan, 2020). It is a generic term that refers to impairment of the permeability of petroleum-bearing formations by various adverse processes. The impairment may take the form of a mechanical mechanism, such as, e.g., fines migration, solids invasion or phase trapping, or in the form of biological, chemical, or thermal mechanisms.

Some of the impairment factors are briefly introduced below, to give a brief insight into the effects in relation to permeable formation damage.

Permeability is impacted by how the solid formation interacts with the liquid that it is exposed to, Abdallah et al. (2007). The concept of wettability can be described as the ability of a material, an example being the the rock formation, to reduce the surface tension of a liquid so that the liquid naturally spreads over the surface. In contrast, with a non-wetting surface, the liquid will retain a near spherical shape with minimum contact area, as shown in Figure 1.5. The concept of wettability is in the context of formation damage often treated as a scale between oil-wetting and water-wetting. The degree of wettability is determined by the balance between the adhesive forces between the two materials and the cohesive forces within the liquid.

When considering a reservoir drilling operation, understanding the impact of wettability becomes very complex, as the reservoir rocks will typically consist of a combination of different minerals, that each has different wettability. To further complicate the matter, the saturation history of the rock will also impact the surface wetting. Common reservoir minerals such as dolomite, carbonate and quartz are naturally water-wet. However, with extended exposure to hydrocarbons, such surfaces may appear oil-wet or the wetting may be heterogeneous. Therefore, when the formation rock is exposed to the drilling fluid,

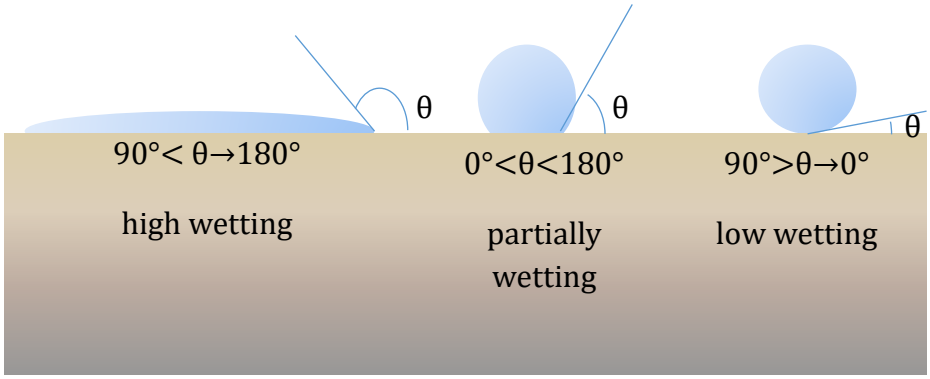

Figure 1-5: Wettability and contact angle

complex interactions may occur. This interaction may lead to a change in the permeability of the formation to the hydrocarbons contained. Similarly, the interaction between an oil-based drilling fluid and a water-wet formation may impact fluid loss differently than if the drilling fluid is water-based. The wettability may therefore both impact fluid loss and formation damage. Wettability will not be discussed in detail in this text, but it is introduced to give an insight into the relevance of understanding the interaction between drilling fluids, formation fluids and the rock mineral composition.

The primary forms of formation damage evaluated as part of the research are the mechanical mechanisms related to the selection of drilling fluid additives. Figure 1.6 present a schematic overview of some of the forms

of mechanical mechanisms of formation damage. Civan (2020) presents a thorough overview of mechanisms of formation damage.

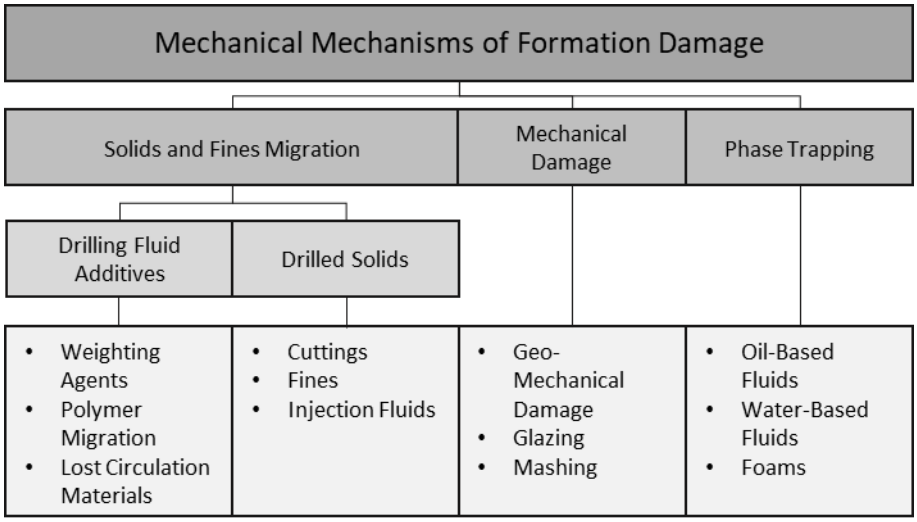

Figure 1-6: Overview of possible categorisation of mechanical mechanisms of formation damage

1.6 Solids control systems

Solids control systems are critical in removing drilled solids (cuttings) and other impurities which may enter the drilling fluid during circulation. The solids control systems may use principles such a filtration screens, particle settling, centrifuges and gas separations to remove unwanted particles, fluids and gases from the drilling fluid. When designing and optimising a drilling fluid, there are some key factors which need to be considered in relation to the solids control systems available on the rigsite.

Firstly, the drilling fluid should be designed on the basis that there will be a level of drilled solids retained in the fluid even after passing the solids control system, and that these levels will increase over time if not properly managed. The inclusion of drilled solids will impact the fluid viscosity as well as the concentration and PSD of solid particles in the

fluid. Therefore, when optimising a drilling fluid, these elements should be considered as part of the drilling fluid design.

A key factor in the solids control system is the selection of shaker screens as these will impact the size distribution of particles that will be retained in the system. Special consideration will therefore need to be made when adding particles to the active drilling fluid to control fluid filtration and prevent fluid loss. If high-permeability or finely fractured formations are being drilled, it may be beneficial to select a coarse screen and add materials adequately sized to seal the pore throats or fracture apertures.

Screens are typically rated following API guidelines. Note that different screen weaves lead to openings of different shapes and hence also different sieving functionality. Table 1.3 is an extract from the USA Standard Testing Sieves, ASTM E – 11 table. Within this Thesis, particle size is generally considered or evaluated using API rated test sieves. This has been done to better correlate particle size with particle retention in a solids control system. Other size measurement systems, such as laser measurements will thus yield different results.

Sieve Designation - Standard	**Sieve Designation - Alternative**	**+/- Variation for Average Opening (µm)**	**+ Maximum Variation for Opening (µm)**
1.0 mm	#18	30	130
600 µm	#30	19	91
300 µm	#50	10.4	58
180 µm	#80	6.8	43
150 µm	#100	6.0	38
125 µm	#120	5.2	34
90 µm	#170	4.2	29
75 µm	#200	3.7	26
45 µm	#325	2.8	20

Table 1-3: Extract from ASTM E11

2 Standard methods for testing of drilling fluids

The standards API 13B-1 (2019), API 13B-2 (2014) and API 13C (2014) cover conventional testing of water-based and oil-based drilling fluids for drilling of wells for the petroleum and natural gas industries. The API 13B and 13C are designed as standards which may be followed for field testing of drilling fluids to ensure that the characteristics of the fluid may be measured in a consistent way. Such measurements cover drilling fluid density, viscosity and gel strength, filtration, content of water, oil and solids, sand content, methylene blue capacity for measuring amount of reactive solids, pH, alkalinity and lime content, chloride content and total hardness as calcium. The standards are designed to provide a drilling fluid engineer with a practical approach to monitor the characteristics of the drilling fluid so that critical levels or trends may be identified. This will allow the engineer to design and execute remedial actions to modify the fluid such that desired parameters may be reached. These standards are used across the industry to compare functionality of drilling fluids. Since the development of the standards, great advances have been made in drilling, and more complex wells are being drilled with requirements for very high drilling fluid performance.

2.1 Filtration control

The standard fluid loss test, commonly referred to as the "API fluid loss test" measured fluid filtrate volume over a period of 30 minutes through a filter-paper with pore-size of 2.5 µm and with an applied pressure of 100 psi at ambient temperature. Thereafter the thickness of the filter-cake is measured, and subjective descriptions of the filter-cake may be added. Notice should be taken of signs of settling of weighting agents, as this signals that the fluid viscosity and gel strength may be too low to prevent settling. This test is applied to a filter-area of 45.8 cm^2 (+/- 0.6 cm^2). The

HTHP fluid loss test is also measured over 30 minutes, but the applied differential pressure is typically 500 psi, and the temperature typically ranging from 80-150°C, although different temperatures and pressured may be used. For the HTHP test, the test medium may be a filter-paper with pore-size of 2.5 µm or permeable discs, with median pore-size ranging from 10 µm to 250 µm. For comparison with the low-pressure/low-temperature test, the fluid loss needs to be corrected for the relevant filter-area. For HTHP tests, it is common practice to also note the 30 second spurt loss volume as well as the total volume after 30 minutes.

The low-pressure/low-temperature test is more convenient than insightful as it may mask significant flaws in the performance of a fluid relative to the formation being drilled. At low temperatures, the fluid viscosity will typically be higher, thus likely reducing the fluid loss, and thermal degradation of chemicals may be overlooked. At HTHP conditions, the sealing capacity of different fluid constituents may start to show greater variability in performance and varying the differential pressures and temperatures may further highlight such differences.

For both tests, the permeability of the 2.5 µm filter-paper is very low, and an effective plugging of this specific pore-size will lead to very low fluid loss. Therefore, if the filer-paper is not reflecting the pore size and permeability of the formation that is to be drilled, the difference in measured fluid loss for different fluids may be artificially low. Also, the hardened filter-papers typically only work up to a pressure of 3.49 MPa (500 psi) and temperatures of less than 150°C. For testing with higher differential pressures, different formation pore-sizes and higher temperatures, permeable ceramic discs are preferred.

2.2 Wellbore strengthening and lost circulation

Annex J in the API RP13B-1 refers to testing of HTHP filtration testing of drilling fluids using a permeability plugging apparatus (PPA). This

involves using ceramic discs at higher pressures and temperatures than conventional HTHP tests. Testing may typically be conducted up to 34.9 MPa (5000 psi) and 260°C (500°F). The recommended reporting follows the same principles as for the standard HTHP filtration tests. The additional insight gained by testing using a PPA relative to the HTHP test is thus generally related to facilitating testing at differential pressures or temperatures that may better reflect operating conditions in certain wells. The testing may thus detect the operating limits of certain drilling fluid compositions.

Some PPAs are designed to use slotted steel discs to simulate sealing of open fractures and the functionality that LCM may have to seal these. The slotted steel discs may have one or multiple slots, which may be straight (90° angle) or tapered. For tapered slots, the fracture aperture is wider than the fracture tip. A fracture occurring in a natural rock will normally have an irregular surface and aperture. It is therefore often considered that the tests on the steel discs are more demanding than the sealing of a rock fracture with similar aperture.

Although there is no specific API recommendation on testing functionality of drilling fluids and drilling fluid additives for lost circulation, the application of slotted steel discs in a PPA may at least represent testing which should be repeatable in a different test facility.

When it comes to testing fluids with regards to wellbore strengthening, the API recommended practices has no specific guidelines. The deficiency is likely caused by multiple factors. The first is that the mechanism and theory of wellbore strengthening is debated and the second is that equipment that facilitates testing of induced fracturing is very limited and complex. The current research aims to provide insight into the sealing functionality of different materials by introducing alternative testing methodologies.

2.3 Formation damage

The step from conventional fluid loss testing to formation damage testing is considerable in terms of technical complexity, equipment requirements, cost and time. Formation damage tests are often conducted on rock cores that are placed into a confining pressure and flooded with fluids to measure initial permeability, fluid loss and subsequent return permeability. This would constitute a core flood test. In general, and in particular for new field developments, actual rock cores may not be available or may be of limited availability. Generic cores may be available for testing, such as e.g. Berea Sandstone cores. A disadvantage of core-flood tests is that the respective formation may be heterogeneous, such that specific samples may yield limited information about the reservoir as a whole. If multiple rock cores from different parts of the reservoir are available, this may help to provide a better representation of the performance on the drilling fluid and the extent of formation damage. However, availability of representative cores and core heterogeneity limits the possibility for conducting comparable studies covering a range of different fluid compositions.

Alternative studies conducted to assess formation damage includes various image, X-ray and microscope analyses amongst others.

As conventional fluid loss testing provides very limited information on formation damage, and core flood tests are scarce and time consuming, methods were developed to facilitate better studies of fluid loss, formation of internal- and external filter-cakes and drilling fluid induced formation damage. These methods are presented in Chapter 3.

3 Extensions of testing methodology

In light of the shortcomings in conventional testing referenced in chapter 2, improved methods are described [I, III, IV, V] for extending the test practices using commercially available permeable discs to study formation of filter-cakes, fluid loss and formation damage. The methods facilitate high-volume testing of fluids for a range of formation permeabilities. Additional methods [VI,VII,VIII] were developed to gain further insight into areas such as wellbore stabilisation or wellbore strengthening. The main objective when designing the methods was to increase the understanding of the functionality of the drilling fluid additives. A secondary objective was to design test methods and equipment that preferably should be low cost and could be used in a portable or rig-site drilling fluid laboratory.

The methods are presented along with relevant test results, as these results are building blocks upon the conclusions of the research are built. KCl-Polymer fluids were selected as the main family of fluids for testing due to the wide range of usage and the ability to enhance the functionality of these fluids through application of specialty additives.

3.1 Simulating mechanical wear and measuring particle degradation

As a part of drilling fluid testing a process of hot-rolling is typically introduced to allow for ageing of the fluid components at a relevant temperature and under low shear-rates. Hot-rolling is conducted by placing a fluid sample in a closed steel cell and placing it in a heated oven with rollers to provide a continuous movement of the fluid. Such a process will facilitate good mixing of the fluid components and also expose the fluid to a desired temperature, before testing the fluids properties.

When components such as lost circulation materials are added to an active drilling fluid in a preventative manner, the LCM particles become a part of the fluid system and hence will be exposed to both the temperature and the mechanical wear of the whole fluid circulation process. Therefore, when testing a material's function with regards to controlling fluid loss or preventing formation damage, it is important to also allow for mechanical wear during the hot-rolling process and before the testing of the fluid. This is particularly important for particles that are brittle and exhibit low mechanical toughness or particles that otherwise are likely to change size, shape or function as a result of circulation in a wellbore. Alternatively, certain combinations of chemicals may react and create agglomeration or accretion on the drill pipe or tools being used in the wellbore.

3.1.1 High shear-rate mixing and impact on particle degradation and fluid loss and fracture sealing ability

A method of applying 30 minutes of high-speed mixing process ahead of the hot-rolling procedure was used to identify mechanical degradation of LCM particles [I]. Two different sets of fluids were prepared, to test LCM materials for sealing of permeable formations and for sealing of fractures under high pressures, as presented below.

3.1.1.1 Degradation tests of LCM for sealing of permeable formations

When drilling formations with high permeability and pore sizes in the range up to 250 µm, seepage losses would normally be encountered unless adequate LCM materials are added to the circulating fluid. For effective loss prevention, LCM materials and shaker screens may be selected to allow the materials to be retained in the active system for multiple circulations. The products selected for the test had a PSD where

at least 85% of the particles would pass through an API 80 rated shaker screen or a 180 µm test sieve.

In total, 11 different samples were tested according to the procedure described in Appendix 1, including 16 h of hot-rolling at 90 °C, six of which were tested on ceramic discs with a specified median pore-throat size of 120 µm (Ofite #170-53-4) and five of which were tested on 250 µm discs (Ofite #170-53-6). All tests were conducted at 6.9 MPa (1000 psi) differential pressure and 90°C. The recipe and mixing procedure of series W-1 are listed in Table 3.1 and further details about particle size of the materials in Table 3.2. An overview of the tests is shown in Table 3.3. Fibre A (FEBRICOAT® C) and Fibre B were selected from two different manufacturers of cellulose-based lost circulation materials, based on relatively similar specified particle size distributions.

Mixing Sequence	**Material/Additive**	**Mass (g) for 350 ml sample**
1	H_2O	328
2	Na_2CO_3	0.02
3	NaOH	0.25
4	Xanthan Gum	1.2
5	Poly-Anionic Cellulose, Low Viscosity	4.0
6	MgO	1.0
7	KCl	17.5
8	Bentonite	5.0
9	$CaCO_3$ (D50 of 50 µm, D90 of 150 µm)	30.0
10	With or without FIBRE A or FIBRE B at given concentration	8.0

Table 3-1: W-1: Recipe and mixing sequence for 350 ml sample of drilling fluid for tests 1-11[I]

Additive	**<90 µm**	**90–180 µm**	**>180 µm**
$CaCO_3$	74.2%	24.8%	1.0%
FIBRE A	56.3%	30.6%	13.1%
FIBRE B	29.5%	56.5% *	13.9%

Table 3-2: Dry sieving of drilling fluid additives for tests 1-11 [I]

Test Number	Description of Test
1	Base fluid (with bentonite and $CaCO_3$), normal mixing, 120 µm disc
2	Base fluid, high-shear mixing, 120 µm disc
3	Base fluid, high-shear mixing, 250 µm disc
4	Base fluid plus FIBRE A, normal mixing, 120 µm disc
5	Base fluid plus FIBRE A, high-shear mixing, 120 µm disc
6	Base fluid plus FIBRE A, normal mixing, 250 µm disc
7	Base fluid plus FIBRE A, high-shear mixing, 250 µm disc
8	Base fluid plus FIBRE B, normal mixing, 120 µm disc
9	Base fluid plus FIBRE B, high-shear mixing, 120 µm disc
10	Base fluid plus FIBRE B, normal mixing, 250 µm disc
11	Base fluid plus FIBRE B, high-shear mixing, 250 µm disc

Table 3-3: Test overview for high-permeability discs [I]

Five of the tests were conducted after a 30-min high-shear mixing procedure to identify any particle degradation. The same degradation test was conducted separately for some of the wet-sieving tests referenced in Figure 3.1. The degradation tests indicated that $CaCO_3$ degraded partially during the high shear-rate mixing procedure. Initially, the wet sieving showed 15.7% and 15.8% of particles being larger than 90 µm, equivalent to a concentration of 13.4–13.5 kg/m^3 in the respective fluid samples. After the high-shear mixing, the concentrations of particles larger than 90 µm was reduced to 9.7% and 9.2%, respectively, implying that circa 40% of the particles above 90 µm had been degraded, and that the resulting concentrations in the fluid samples would be 8.3 kg/m^3 and 7.9 kg/m^3. In contrast, the high shear-rate mixing of FIBRE A did not show signs of degrading, and the concentration was kept stable around 10.6 kg/m^3. One test, which

included bentonite, showed an increase in concentrations of FIBRE A above 90 µm after high-shear mixing. Since the high shear-rate mixing of FIBRE A without bentonite did not show the same effect, it was considered that a potential cause of the apparent increase in the concentration of larger particles may be bentonite particles piggybacking on the coarser FIBRE A particles to increase the measured concentration of such particles.

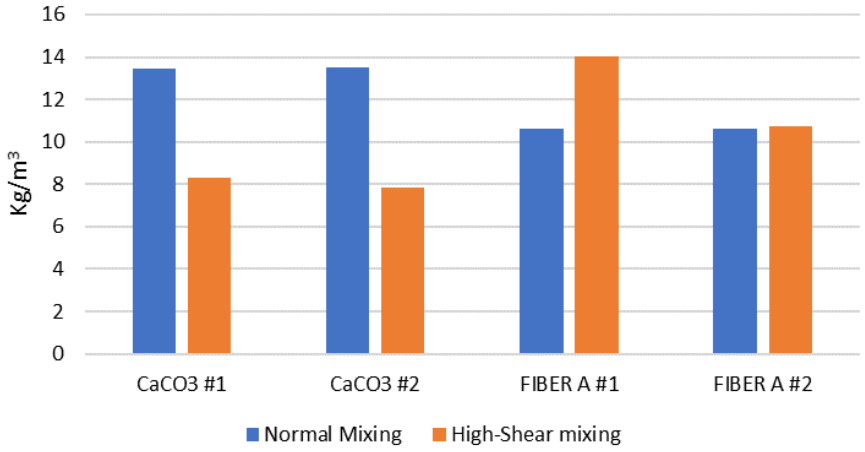

Figure 3-1: Final concentration in kg/m^3 of particles >90 µm after different mixing procedures [I]

Figure 3.2 (a) shows the HTHP tests on the 120 µm discs, with each of the three mixtures of (i) the base fluid being KCl-Polymer drilling fluid with CaCO3, (ii) the base fluid plus FIBRE A, and (iii) the base fluid plus FIBRE B. The tests were conducted with and without high-shear degradation. The fluid loss tests showed that the base fluid produced a fluid loss of 31 ml before degradation and that the fluid loss increased to 42 ml after degradation. The fluid with FIBRE A showed a fluid loss of 31 ml before degradation, but unlike the base fluid, the sealing efficiency increased after the high-shear degradation and gave a fluid loss of 25 ml. The fluid with FIBRE B also showed an improvement

after the degradation test, where the fluid loss was 45 ml without degradation and just over 31 ml after degradation.

The fluid loss profiles were generally consistent throughout the testing on the 120 µm discs. After the initial spurt-loss, the loss-rates were gradually falling during the test and appeared to approach a linear curve with a fluid loss rate of around 0.2 ml/min after 20 min. The development of the fluid loss may indicate that the filter-cake had substantially been formed within the first 15 s, but that further thickness was built over time and that a more stable permeability achieved after 10–20 min.

The testing on 250 µm discs, shown in Figure 3.2 (b), was planned to be identical to the testing on the 120 µm disc, however, the base fluid with $CaCO_3$ recorded a total loss during the first few seconds of the test, so no further tests were conducted with the base fluid alone.

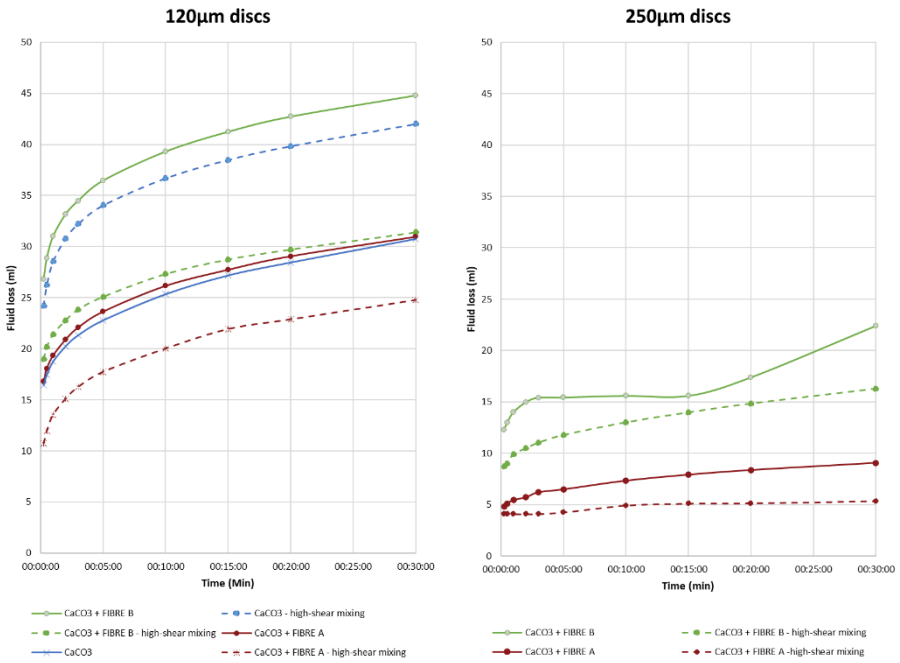

(a) (b)

Figure 3-2: Fluid loss on high-permeability discs, (a) 120 µm discs and (b) 250 µm discs [I]

The testing of the two fibre-based products FIBRE A and FIBRE B showed considerably improved results relative to the testing on the 120 µm ceramic. Contrary to expectations, the fluid losses recorded on the 250 µm discs were significantly smaller than on the 120 µm disc, and the fluid loss rates were showing a different profile. Again, the tests showed lower fluid losses after the high-shear degradation tests. The main difference, however, was the observation of more erratic fluid losses during the 30-min test. It was several times observed that the fluid loss appeared to stop, and then restarted again at more irregular intervals.

By comparing the filter-cakes from the different tests, it was clear that the building of the filter-cakes followed a different mechanism on the coarser discs. The filter-cakes formed on the 120 µm discs were of a

uniform nature and thicker than the more irregular filter-cakes on the 250 µm discs, as seen in Figure 3.3. The impression was that the combined particles of the $CaCO_3$ and the fibres created a layered mat on the surface of the 120 µm disc, whereas the single or collections of particles were plugging larger pores on the 250 µm discs.

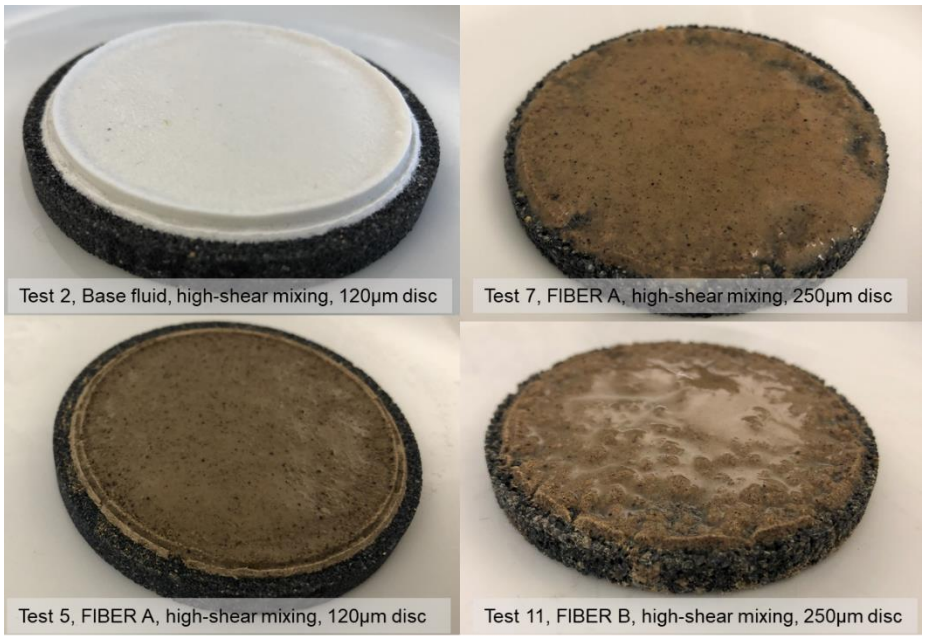

Figure 3-3: Filter-cakes after the 6.9 MPa (1000 psi) HTHP fluid loss test [I]

Dry-sieving tests indicated that both FIBRE A and FIBRE B had a weight concentration of 13–14% with particles larger than 180 µm, indicating that the D90 value of the fibres were around 0.8 times the median pore size. In contrast, only 1% of the $CaCO_3$ was larger than 180 µm. As such a lower sealing ability of the 250 µm discs without the presence of any of the fibre products could be expected.

Summary of findings:

- $CaCO_3$ particles degraded significantly after high shear-rate mixing and lost sealing capacity of high-permeability discs

- Cellulose based fibre particles showed no significant degradation after high shear-rate mixing
- Fluid mixtures where the D90 particle size exceeded the median pore size of the test medium produced a smooth external filter-cake
- Fluid mixtures where the D90 particle size was around 0.8 times the median pore size led to internal plugging and reduced fluid loss
- Although FIBRE A and FIBRE B had comparable particle size distribution, FIBRE A outperformed FIBRE B in all tests, showing that the selection of fibre mixture is important

3.1.1.2 Degradation tests of LCM for sealing of fractured formations

To further test the method of applying mechanical wear to determine particle degradation of particles designed for sealing of fractures in the 500 µm range, three different materials were selected where the D50 value were in the 350-600 µm range. The materials were selected based on having a significant portion of particles in the range between 200 µm and 1000 µm for ease of sieving. The materials were each mixed into a fluid containing xanthan gum (3.3 kg/m^3) and low viscosity poly-anionic cellulose (11 kg/m^3), to reflect the viscosity of a typical drilling fluid. One same of each product was then wet-sieved after 10 minutes of mixing at normal speed. The other sample was sheared at full speed on a Hamilton Beach mixer for 30 minutes and then wet-sieved. Table 3.4 shows a summary of the degradation data.

Additive	>420 µm before degradation	>420 µm after degradation	Reduction in particles >420 µm	Manufacturer specifications
$CaCO_3$	65.6%	0.9%	99%	D50 of 600 µm, D90 of 1125 µm
Resilient Graphite	50.2%	35.4%	30%	D50 of 400 µm, D90 of 744 µm
Granular Cellulose	64.1%	61.0%	5%	D99 of 600 µm

Table 3-4: Exposure of LCM particles to high shear-rate mixing to assess particle toughness and particle size degradation [VI]

Figures 3.4, 3.5 and 3.6 show the PSD of the respective materials with the normal mixing process to represent the material before degradation and after the high-speed mixing to represent the materials after degradation. The measurements were conducted using wet-sieving on a sieve shaker with API rated sieves.

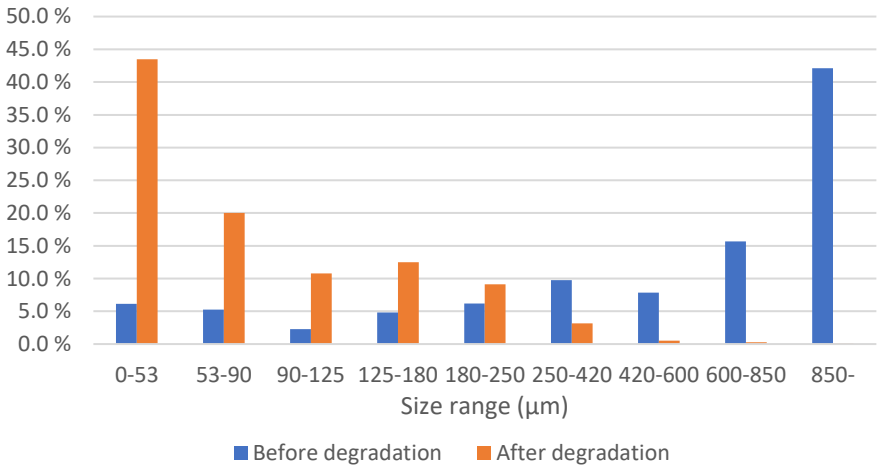

Figure 3-4: PSD of CaCO3 before and after degradation [VI]

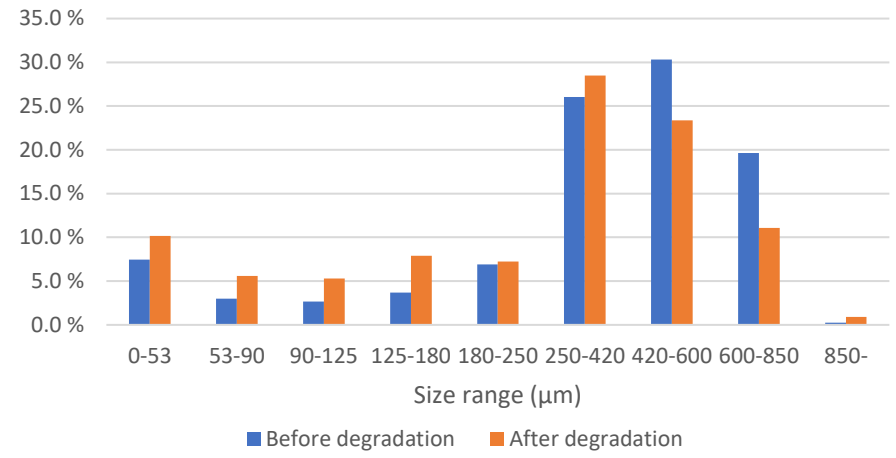

Figure 3-5: PSD of Resilient Graphite before and after degradation [VI]

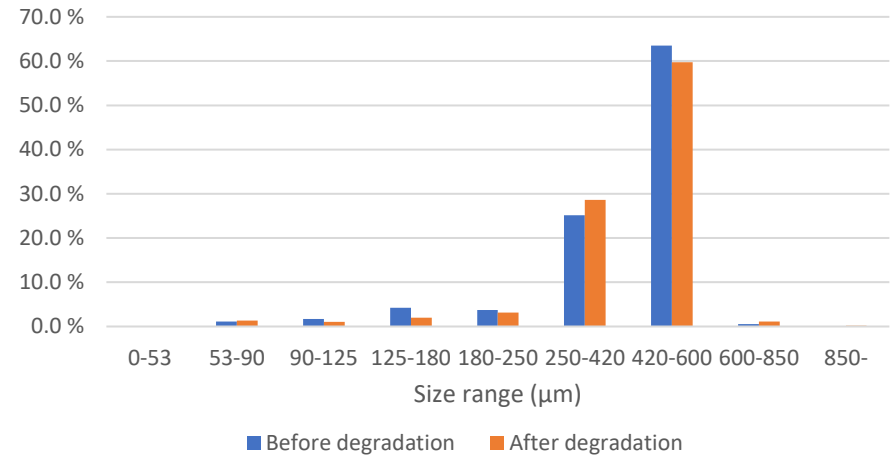

Figure 3-6: PSD of Granular Cellulose before and after degradation [VI]

The degradation process showed considerable change in the particle size distribution of the $CaCO_3$ particles, some reduction in the PSD of the Resilient Graphite and very little change in the PSD of the Granular Cellulose. For the $CaCO_3$, 99% of the particles initially above 420 µm

were finer than 420 µm after the high-speed shearing. For the Resilient Graphite, the reduction in particles above 420 µm was 30% and for the Granular Cellulose it was only 5%.

Summary of findings:

- $CaCO_3$ particles degraded heavily after high shear-rate mixing
- Resilient graphite showed significant degradation after high-shear mixing
- Granular cellulose showed very little signs of degradation after high shear-rate mixing

3.1.2 Hot rolling with threaded steel rod and impact on particle degradation and fluid loss

The process of introducing exposure to mechanical wear through high shear-rate mixing was shown in section 3.1.1 to differentiate the degradability of certain materials. Since it involved the additional time-consuming step of conducting the 30-minute mixing process, an alternative method for studying mechanical wear was introduced.

Figure 3.7 show the stainless-steel rods of 13.5 cm length and of M16 grade that were added into the hot-rolling cells [VI]. By using threaded rods, the force from the rolling rod would be exerted on both smaller and larger particles within the fluid. In contrast, a straight rod would generally be rolling over the larger particles, and would hence exert more wear on larger particles, and potentially less wear on very small particles. Also, the larger surface area of a threaded rod may provide a better indication of any accretion to the steel rod caused by the drilling fluid.

Studies were conducted with various particles added to a water-based drilling fluid, and wet-sieving of the particles were done before and after the hot-rolling process to detect differences in particle size distribution and HTHP fluid loss sealing capacity. The results obtained through this

process were comparable to the degradation measured after exposure to the high shear-rate degradation method in section 3.1.1.

(a) (b)

Figure 3-7: 13.5 cm long M16 threaded rod and hot rolling cell (a) and examples of different level of accretion (b)

Different LCM combinations were mixed into a weighted oil-based field fluid, series O-1, as per Table 3.5. The measured density of the fluid prior to mixing of LCM was 1.49 kg/m^3. The fluid contained barite as weighting agent and drilled solids from a North Sea drilling operation.

LCM Additive for 1 litre of fluid	**Fluid 1: Granular LCM**	**Fluid 2: Granular and Cellulose LCM**
Oil-based drilling fluid (g)	1432	1417
$CaCO_3$ with D50 of 150 µm (g)	24.5	24.5
$CaCO_3$ with D50 of 600 µm (g)	24.5	24.5
Resilient Graphite with D50 of 100 µm (g)	24.5	
Resilient Graphite with D50 of 400 µm (g)	12.5	
Ultra-fine cellulose with D90 of 75 µm (g)		8.6
Granular Cellulose with D99 of 600 µm (g)		28.5

Table 3-5: O-1: LCM mixture in oil-based drilling fluid for 1 litre sample for degradation and fracture sealing test [VI]

Two samples of each fluid were hot rolled for 16 hours at 90°C temperature. For each fluid, one sample included a threaded steel rod to

test the functionality with regards to sealing of a 500 µm slotted disc with and without exposure to mechanical degradation.

The metric proposed to determine the sealing strength of the lost circulation materials was calculated as a moving average over time periods of 10 or 60 seconds and the highest average value over 10 and 60 second periods selected as the Peak Hold Pressure and Sustainable Hold Pressure, respectively. Equations 3.1, 3.2 and 3.3 present the methods of calculation.

$$P(MA_n) = \sum_{t=0}^{t=n} P_t \, / n \tag{3.1}$$

$$\textit{Peak Hold Pressure} = \text{Max P}(MA_{10}) \tag{3.2}$$

$$\textit{Sustainable Hold Pressure} = \text{Max P}(MA_{60}) \tag{3.3}$$

The tests were conducted with the objective of obtaining the highest sealing pressure for each combination of material and slotted disc. Limitations were set for fluid loss of 275 ml out of an applied volume of 400 ml, to ensure that sufficient fluid was left in the test cylinder, pressures exceeding and holding above 34.9 MPa (5000psi) or a period of 20 minutes.

The pressure plots are presented in Figure 3.8. For the tests with normal hot rolling, both fluids performed well, and enabled high sealing pressures over a 60 second period. For Fluid 1, without cellulose-based LCM, the highest Sustainable Hold Pressure was 4182 psi before the fluid loss reached 275 ml, whereas the test for Fluid 2 (with cellulose-based LCM) was stopped with a SHP of 5374 psi, due to the pressure

approaching the set limit at 5500 psi. At the time, the measured fluid loss was only 13 ml.

Thereafter, the tests were repeated with the fluid samples that has been exposed to mechanical wear by the inclusion of a threaded steel rod in the hot-rolling cell. For Fluid 1, the highest recorded SHP was 302 psi when a fluid loss of 275 ml was reached. For Fluid 2, also a noticeable change was recorded relative to the first sample. A larger fluid loss was recorded; however, the pressure reached a SHP level of 4689 psi. Following the degradation tests in section 2.2 it may be assumed that only the Granular Cellulose particles of Fluid 2 were intact and equivalent to the slot size after the hot-rolling process with the steel rod. Therefore, in these tests, the concentration of LCM that was similar to or larger than the slot aperture size was around 28.5 kg/m^3 or slightly in excess of 2% by volume.

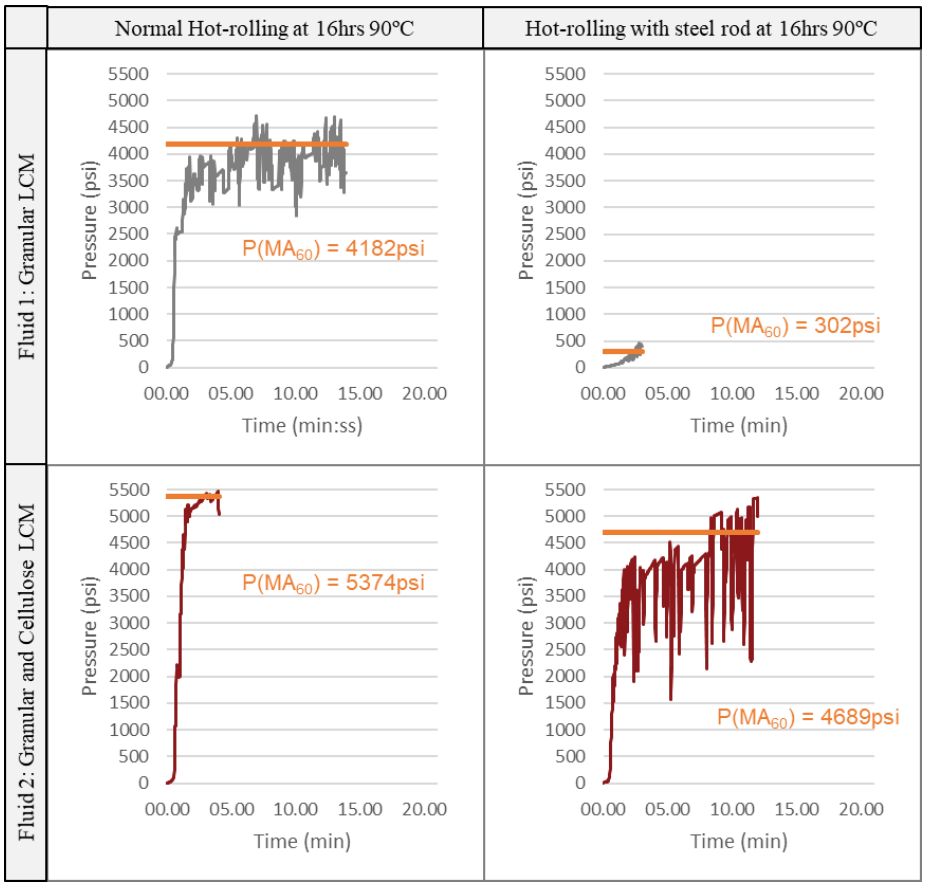

Figure 3-8: Pressure build-up charts for preventative LCM in oil-based drilling fluid [VI]

The preventative LCM mixtures used in section 3.2 were mixed into a water-based drilling fluid, series W-2, as presented in Table 3.6 and hot-rolled with and without a threaded steel rod. The recipes included bentonite to represent fine drill solids.

LCM Additive for 1 litre of fluid	Fluid 3: Granular LCM (g)	Fluid 4: Granular and Cellulose LCM (g)
H_2O	817	817
Na_2CO_3	0.055	0.055
NaOH	0.69	0.69
Xanthan Gum	3.32	3.32
Poly-anionic Cellulose	11.05	11.05
MgO	2.77	2.77
KCl	48.3	48.3
Bentonite	13.8	13.8
Barite	464	464
$CaCO_3$ with D50 of 150 µm	24.5	24.5
$CaCO_3$ with D50 of 600 µm	24.5	24.5
Resilient Graphite with D50 of 100 µm	24.5	
Resilient Graphite with D50 of 400 µm	12.5	
Ultra-fine cellulose with D90 of 75 µm		8.6
Granular Cellulose with D99 of 600 µm		28.5

Table 3-6: W-2: LCM mixture in water-based drilling fluid for 1 litre sample for degradation and fracture sealing test [VI]

The pressure tests were conducted on a slotted disc with 0.50 mm apertures, as for the tests with the oil-based drilling fluid. The pressure plots are presented in Figure 3.9. Also in these tests, a significant difference was recorded for the samples where the fluid had been exposed to mechanical wear during the hot-rolling process. Without the mechanical wear, the results for Fluid 3, with the granular LCM, were very similar to the results obtained for Fluid 1 as a SHP pressure in the region of 4200 psi was achieved. For the sample with the mechanical shear, Fluid 3 registered a SHP in excess of 1000 psi, or more than 3 times the SHP for the Fluid 1, with Granular LCM in an oil-based drilling fluid. In contrast, the SHP of 3981 psi obtained for Fluid 4 after mechanical wear was a little lower than for Fluid 2 after the same mechanical exposure. However, in all tests, the fluid samples with the combined granular and cellulose-based LCM showed significant improvements in sealing strength and fluid loss over the formulations with granular LCM only. Also, it appears that the addition of cellulose-based LCM provided significantly higher sealing strength after exposure to mechanical wear.

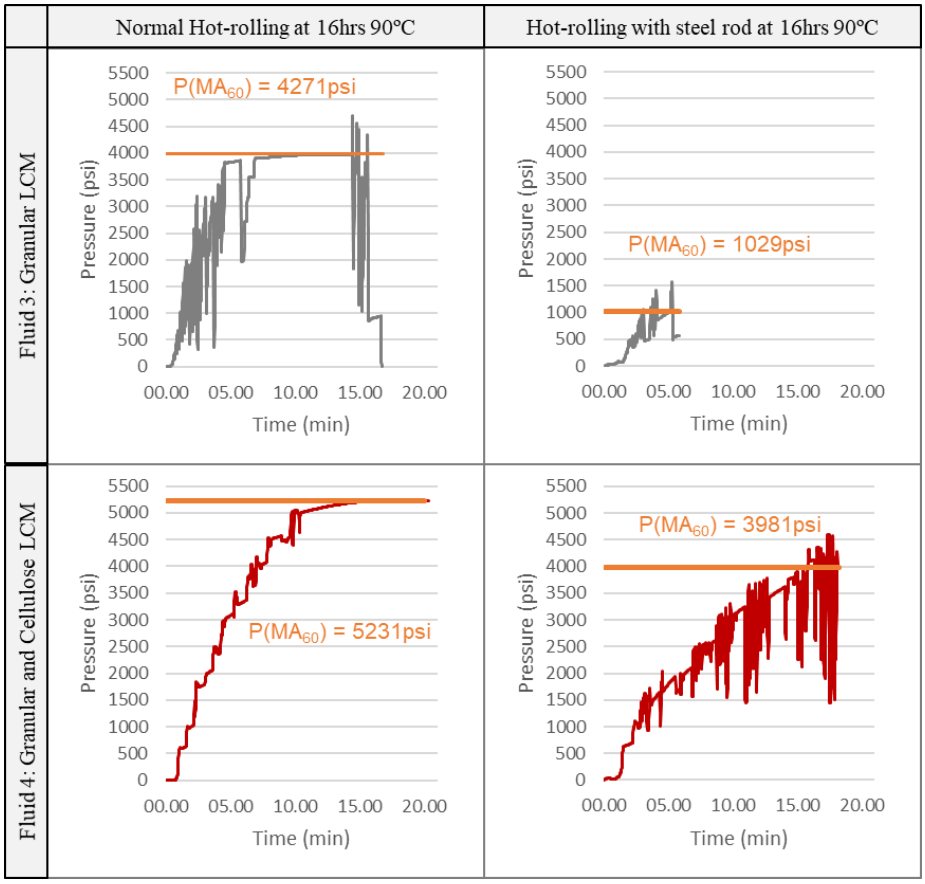

Figure 3-9: Pressure build-up charts for preventative LCM in water-based drilling fluid [VI]

Summary of findings:

- The method of including a threaded steel rod was less time consuming than conducting high-shear mixing to simulate mechanical wear, but produced comparable degradation results.
- The Fluids using a combination of $CaCO_3$, and resilient graphite lost nearly all sealing effect after exposure to mechanical wear, indicating that both types of particles were significantly

degraded. Sealing effectiveness was lower in OBM than in WBM for the fluids with $CaCO_3$ and resilient graphite.

- The Fluids using a combination of $CaCO_3$, and granular cellulose experienced little deterioration in sealing performance after exposure to mechanical wear. The results are consistent with the high-shear degradation tests which showed that the selected granular cellulose showed high resistance towards mechanical wear. The sealing results in OBM and WBM were comparable for this combination of LCM materials.

3.2 Measuring particle invasion in porous formations

A fundamental factor in both fluid loss control, formation damage and wellbore stabilisation is the presence of particles in the drilling fluid and the build-up of internal or external filter-cakes. Since representative core samples may be unavailable or limited, a method was developed on the basis of using industry standard permeable discs [I]. The methodology was built around the API 13 standards for HTHP fluid loss, but extended the studies conducted on the permeable discs used. The primary extension was using a moisture analyser to precisely measure the disc mass prior to the HTHP tests and after the completion of the test and the subsequent removal of the external filter-cake.

An experimental setup was therefore used with the following main objectives and functionalities:

- Enabling reverse flow of a fluid through the discs, after the HTHP tests, to understand filter-cake removal and lift-off pressures.
- Enabling measurement of disc mass before and after the HTHP test and filter-cake removal to obtain indications of polymer or solids invasion into the discs.
- Studying filter-cake formation.

- Understanding how application of fluid degradation methods may impact the fluid loss and reservoir formation damage.

A moisture analyser was set up with a program where the disc was heated to 105°C and the mass of the disc measured continuously. It provided a resolution of 1 mg, and the test condition used was to continue weighing until the change in mass was less than 1 mg over a 60 second period. The discs were wet in water prior to the HTHP test and reverse flowed with water after the tests to remove salts and any loose particles within the disc. By comparing the mass of the disc before and after the test, changes in disc mass were accurately measured. The diagram of the equipment for reverse flow of fluid is shown in Figure 3.10.

The measurement of changes in disc mass facilitated the measurement of particle invasion into the permeable formation. Any fluid may easily be tested against a range of formation permeabilities and pore-sizes. For studies of reservoir drilling fluids, the method would enable measuring the invasion of particles as a sign of potential reduction in formation permeability. Hence, the drilling fluid additives' effectiveness in preventing migration of particles into the formation may be studied. Similarly, the same functionality may provide valuable insight into additives for wellbore stabilisation or wellbore strengthening purposes. During the drilling of a high permeability section in a non-reservoir well section, migration of solids into the near wellbore formation may be beneficial. Such particle migration may create a robust internal filter-cake and thereby reduce the dependence on the presence of a low-permeability external filter-cake.

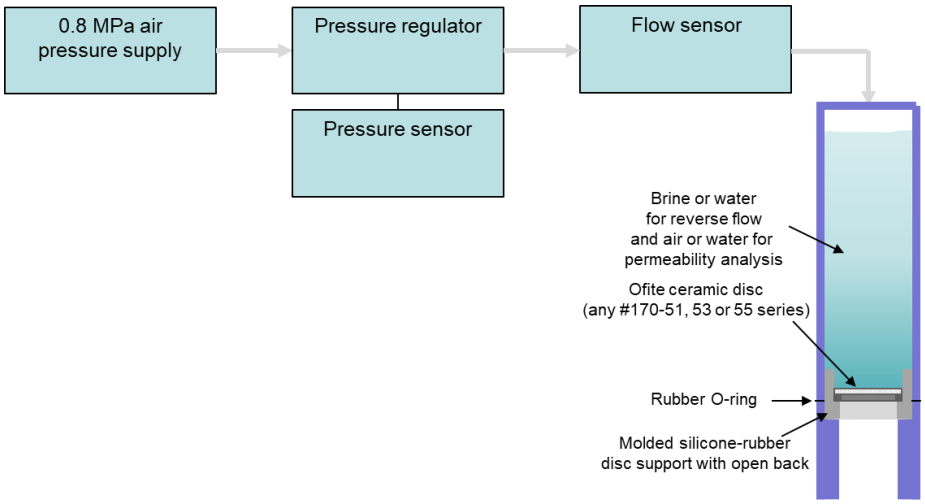

Figure 3-10: Infographic of the system developed for permeability measurement of reverse flow of fluids through permeable discs [I]

3.2.1 Results and observations

The discs with filter-cakes from the tests presented in section 3.1.1 were used to measure particle invasion. This was done by measuring changes to the disc mass, excluding the external filter-cake, using the system for reverse flow and the procedure presented in Appendix A [I].

When conducting the low-pressure reverse flow of brine through the discs (<7 psi or <0.05 MPa), the filter-cakes were easily removed from the 120 µm discs as the filter-cakes came off either whole or in large pieces. Little visual trace of the filter-cakes was left on the disc other than along the circumference, which was held back by the silicone mold, which held the disc inside the acrylic cell, see Figure 3.11 as an example.

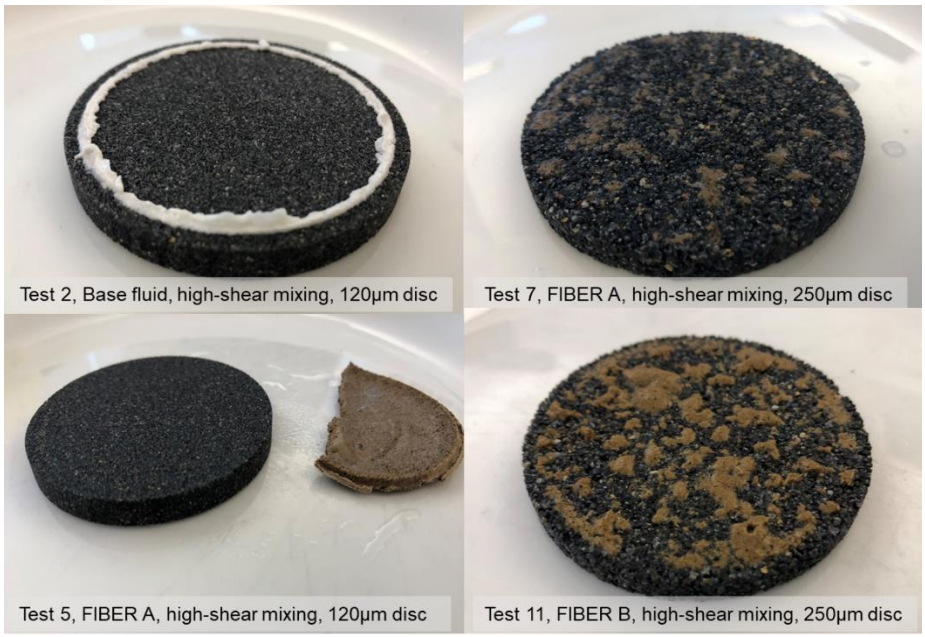

Figure 3-11: Discs after reverse flow with brine at 0.05 MPa pressure [I]

On the 250 µm discs, the filter-cakes were noticeably more separated as they were washed off the discs. This may be due to the filter-cake being thinner than for the 120 µm discs and/or pin-holing effects caused by the larger pore-openings. Visual inspection showed minor particles protruding from the surface of the discs, giving further substance to the impression of particles partly penetrating and plugging the pore-throats of the discs, rather than forming an external filter-cake.

Following the reverse flow, the discs were placed in a liquid oxidizing breaker and kept at a temperature of 90–100 °C for four hours [I,II]. The discs were thereafter flowed with water to remove any loose residue and dried in the moisture analyzer. The discs were visually inspected for traces of residue and the final disc masses compared with the original disc masses to identify any invasion of polymer, solids or fibre. Figure 3.12 shows the discs from testing of FIBRE A after removal of filter-cakes. By visual inspection no particle or filter-cake residue could be

identified. In contrast, some residue could be seen into the pore-throats of the 250 µm discs in Figure 3.13, after testing of FIBRE B, thereby the indicating particle-plugging inside the disc.

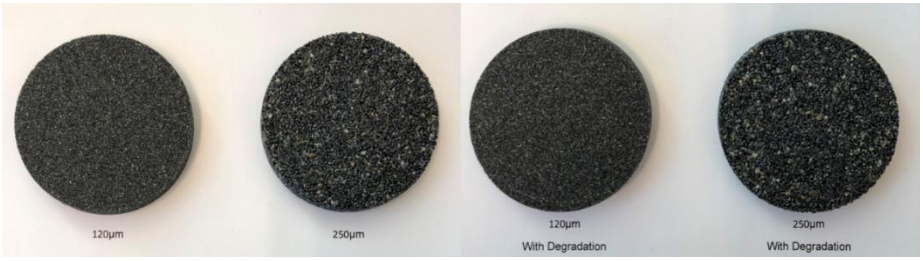

Figure 3-12: Discs for testing of FIBRE A after breaker application [I]

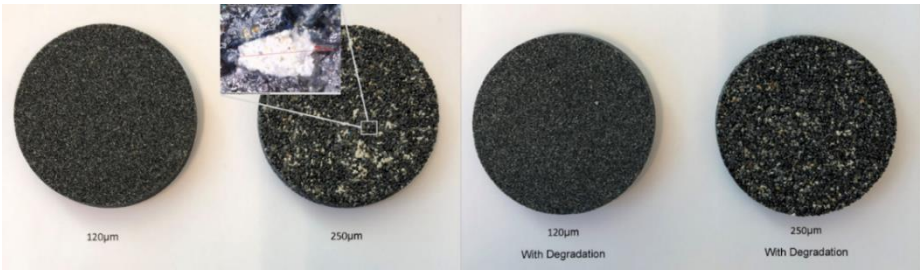

Figure 3-13: Discs for testing of FIBRE B after breaker application [I]

By placing both the fluid loss measurements and disc mass gain data into one chart, some interesting observations can be made, see Figure 3.14.

Tests 1 and 2 with the base fluid including $CaCO_3$ show that nearly all of the filter-cake and potential invasion of polymers and solids into the 120 µm discs have been removed by the reverse flow and breaker application, as the mass increases were only 8 mg and 9 mg, respectively. In contrast, test number 3 recorded a total loss of fluid and a subsequent mass increase of 80 mg on the 250 µm disc. The higher mass increase may be due to residue of polymers and solids and represents formation damage occurring when the fluid particles are of insufficient size to create an external filter-cake.

The four tests conducted with FIBRE A show an inverse relationship between increase in disc mass and fluid loss. After visual inspection of the filter-cakes, it looked like the filter-cakes on the 250 µm showed more of a particle-plugging nature, whereas the filter-cakes on the 120 µm discs to a greater extent were created uniformly and externally to the disc. The mass increases of the 120 µm discs were 6 mg for test 4 and 18 mg for test 5, thus indicating a low degree of internal plugging and formation damage. This is consistent with the uniform external filter-cakes that were observed. For tests 6 and 7, the mass increases on the 250 µm discs were 47 mg and 190 mg, respectively. The higher disc mass corresponds with observed internal plugging and lower fluid loss than for the 120 µm discs. The sieve results of FIBRE A showed a D87 value of 180µm. The overall observation is a consistent pattern where presence of particles above the median pore-size promotes the formation of an external filter-cake, whereas internal plugging and increase in disc mass is more predominant when the particles are smaller than the median pore-size. The ratio of the D87 FIBRE A particle size to the pore-size was 3/2 for the 120 µm discs and 0.72 for the 250 µm discs. This may indicate that formation damage is limited if D87 value of the selected FIBRE A are $\gtrsim$ 3/2 the pore size.

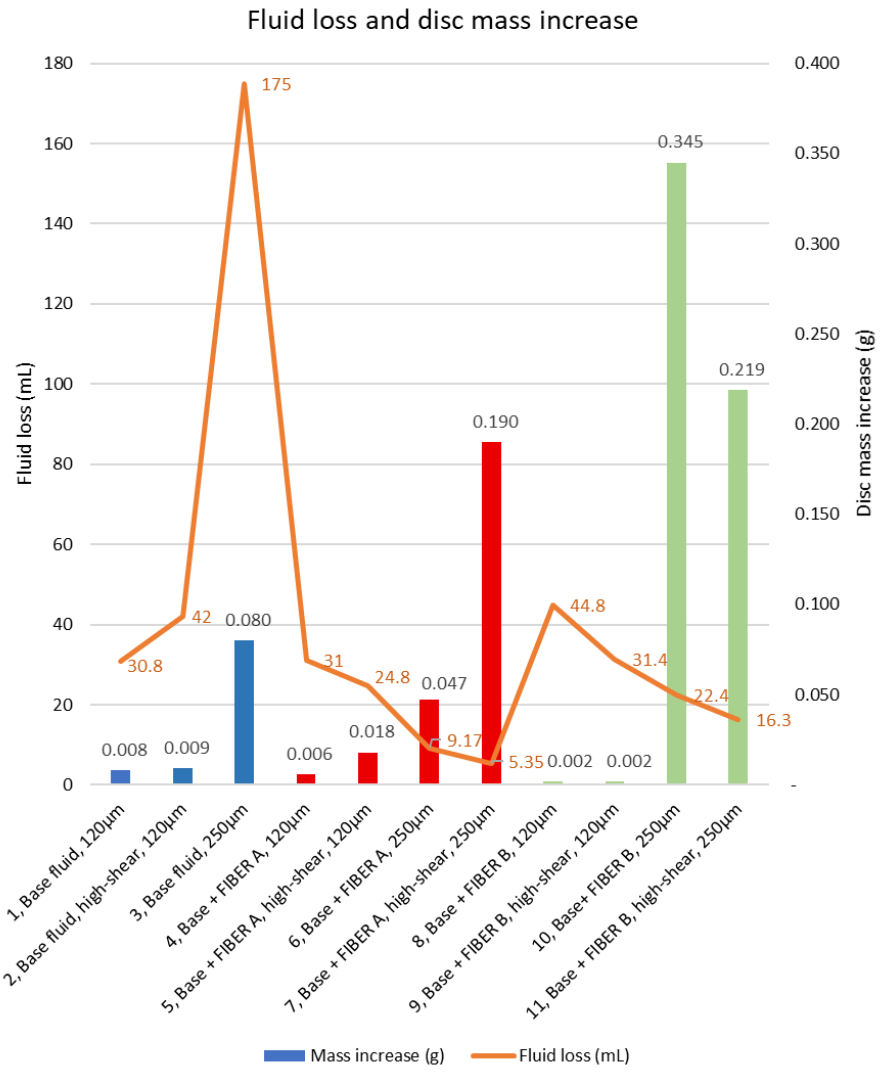

Figure 3-14: Fluid loss and disc mass increase [I]

3.2.2 Discussion

The tests with FIBRE B were consistent with the observations from the testing of FIBRE A. Disc mass increases were negligible on the finer discs, whereas the mass increases of the coarser discs were the largest in the test.

An interesting result of the study was that whilst the fluid with only $CaCO_3$ performed worse with higher pore-sizes and with mixing at high shear-rates, the opposite was the results for the fluids with a combination of either of the two fibre products and $CaCO_3$. The fluid with only $CaCO_3$ failed the test on the 250 µm discs. In Figure 3.2 (a) the fluid loss curves show the typical behaviour where the fluid loss rate falls over time. This is typical when the external filter-cake is the primary barrier that separates the high-pressure side from the low-pressure side. As the filter-cake grows thicker, the resistance to flow increases and the fluid loss rate falls. The graphs in Figure 3.2 (b) present a different story. Here the initial spurt-loss constitutes a more significant part of the total fluid loss, and the fluid loss thereafter are more inconsistent. The total fluid loss is, however, considerably less for the tests with both fibre products on the 250 µm discs than on the 120 µm discs. The cause of this is particle migration into the discs and the formation of an internal filter-cake.

By combining the 30-minute fluid loss values with the measured disc mass increases, it is clear that the low fluid-loss for the fluids with fibre on the 250 µm discs is due to particle invasion and the formation of a rigid internal filter-cake.

Summary of findings:

- By extending the testing procedure with a moisture analyser and reverse flow equipment it was possible to measure the increases in disc mass accurately.
- Reverse flow of fluid through the disc with filter-cake enables studying the removal of filter-cake by back pressure.

- As the discs median pore-throat size was varied relative to the particle size of the fibres and $CaCO_3$, for tests 1–11, it appeared that different mechanisms for sealing the disc and creating a filter-cake was obtained. For the 250 µm disc tests, with the largest solids and fibres being 10-20% smaller than the pore-throat openings, fluid loss was reduced, and the sealing appeared to partial plugging of the pore-throats. In contrast, the tests on the 120 µm discs showed that with sufficient portion of the particles was larger than the mean pore-throat size, a uniform external filter-cake was building on the disc.
- In the tests where the D90 value of the fibre-based particles were around 0.8 times the median pore size, the fluid loss was lower than when the fibres had a D90 value which exceeded the median pore size
- In the tests where the LCM particles plugged into the pores, the fluid loss was reduced, and the disc mass significantly increased relative to when the sealing appeared to be primarily by the establishment of an external filter-cake.
- The LCM D90 value relative to the median pore size appears to be the determining factor of the sealing mechanism being primarily an internal- or external filter cake. The data indicates that D90 values > than the median pore size may facilitate the creation of an external filter-cake or a surface sealing, whereas a D90 value < median pore size tends to plug into the pores of the formation and create and internal filter-cake.
- Application of an oxidizing breaker did in certain cases allow the test discs to return to almost its original state, with mass changes so low that they may be considered to be within the tolerances of the tests.

3.3 Measuring permeability change in porous formations

The methodology is centered around conventional HTHP test for fluid loss using permeable discs as these are commonly used in the industry. The main addition to the process is to document the permeability and mass of the discs prior to the HTHP tests and thereafter measure changes in these parameters after conducting the fluid loss test and reverse flow for filter-cake removal. This enables studying the changes a fluid may have on the permanent permeability of the formation, without needing to conduct a more comprehensive dynamic core flooding test. The change in disc mass was described in chapter 3.2 [I], however, further studies were conducted to verify if the method of detecting formation damage by measuring changes in permeability could provide reliable results.

The key elements of the process are to first measure the mass and permeability of ceramic discs before conducting an HTHP test using the procedure from ANSI/API 13B-1, or potentially under a higher applied differential pressure. The permeability of the discs was first measured by flowing air through the discs and measuring applied pressure, flowrate, and air temperature. By restricting the flow area of the disc to an area slightly smaller than that of the HTHP test, the change in permeability after exposure to the drilling fluid may be measured quite accurately. The equipment was first calibrated by measuring the pressure drop in the system when flowing air at different flowrates without the disc present. Using tables of viscosity of air, the dimensions of the flow area, disc thickness, applied pressure and air flowrate, it was possible to calculate the average permeability. Thereafter, a similar process was applied for flowing water through the disc. Prior to the flow test, the fluid and the disc were placed in a vacuum for 5 minutes to remove air bubbles.

The HTHP tests were conducted at 6.9 MPa (1000psi) using a nitrogen pressure source. Thereafter the discs are placed in a customized acrylic cell, where brine is flushed through the discs in the reverse direction of

the HTHP test to study the ease of lifting the filter-cakes, as earlier shown in Figure 3.11. Thereafter the discs are submerged into a breaker fluid before permeability and disc mass is measured and compared with the original values. At this stage of the process, the permeability to water was measured first, then the disc was dried in the Moisture Analyser and weighed before the permeability to air was measured. The methodology used for the testing is presented in detail in Appendix 1, and the equipment in Appendix 2.

3.3.1 Drilling fluid composition

Four fluid compositions were used to make up series W-3, shown in Table 3.7, were selected, and tested with a one-month interval and tested by different personnel to evaluate reproducibility. Fluid 1 was selected to be a KCl polymer fluid without any solids or fibres, using conventional xanthan gum and low viscosity poly-anionic cellulose. Such a fluid was expected to result in high fluid loss and formation damage following the findings of Khan et al. (2003, 2007), where polymer damage to the formation was detected. The other three fluids contained solids to reflect the findings of Pitoni et al. (1999), who found that the solids composition impacted fluid loss and return permeability. Fluid 2 used the same base mixture as Fluid 1. However, bentonite was added to represent fine drill solids or clay. Fluid 3 and 4 were also KCl polymer fluids. These had the same concentration of $CaCO_3$ and a cellulose-based fibre with a D90 value of 75 µm. (AURACOAT® UF, provided by EMC AS). The difference between Fluids 3 and 4 were the polymers used for viscosity and fluid loss. Fluid 4 used conventional xanthan gum and low viscosity poly-anionic cellulose, whereas Fluid 3 used a designed mixture of starch-based polymers (PureBore and PureBore ULV, provided by Clear Solutions International Limited). The concentration of KCl was selected as an average between what might be applied when drilling oil and gas wells and geothermal wells.

Component and Mixing sequence for 1 litre sample	**Fluid 1 (g)**	**Fluid 2 (g)**	**Fluid 3 (g)**	**Fluid 4 (g)**
Water	971	961	928	926
Soda Ash	0.06	0.06	0.06	0.05
Caustic Soda	0.71	0.71	0.66	0.66
Xanthan Gum	3.43	3.39		3.17
Low viscosity poly-anionic cellulose	14.3	14.2		13.23
Polymer blend for viscosity and fluid loss (PureBore)			6.6	
Polymer blend for fluid loss (PureBore ULV)			8.0	
MgO	2.86	2.83	2.65	2.65
KCl	50.0	49.5	46.3	46.3
Bentonite		28.3		
Ground marble ($CaCO_3$) < 53µm			52.9	52.9
Cellulose fibre for fluid loss control (AURACOAT UF)			13.2	13.2

Table 3-7: W-3: Drilling fluid recipes 1-4 for 1 litre sample [III]

3.3.2 Ceramic discs and permeability measurements

Prior to the HTHP tests, the ceramic discs were weighted and permeabilities to air and water were measured. The respective data for each disc used for the tests are presented in Figure 3.15. The discs are specified as having a mean pore-throat size of 20 µm and permeability to air of 2 D. Given that the outer dimensions are identical and uniform materials are used for manufacturing the discs, a low disc mass may indicate high porosity and permeability, and visa-versa for a high mass disc. Figure 3.16 shows the plot of permeability to air against disc mass for the discs used. The relationship between disc mass and air

permeability is negative, and the calculated correlation is -0.961. This confirms the relationship between disc mass and permeability, where a higher disc mass is correlated to a reduction in permeability (thus the negative correlation coefficient). Table 3.8 lists the correlation between the three measurements for each disc, showing positive correlation between permeability to air and water. Correlation between disc mass and permeability to water was also negative. The difference in permeabilities might also be a factor that should be considered when comparing results of experiments where the specific discs have been used, rather than assuming that any two discs with a specified mean pore-throat size of 20 µm have the same porosity, permeabilities and pore-throat sizes. As an example, From Figure 3.15 it can be seen that the discs used for Fluid 2 had slightly higher permeability and lower mass than then discs used for Fluid 4. The least permeable discs were used when testing Fluid 3.

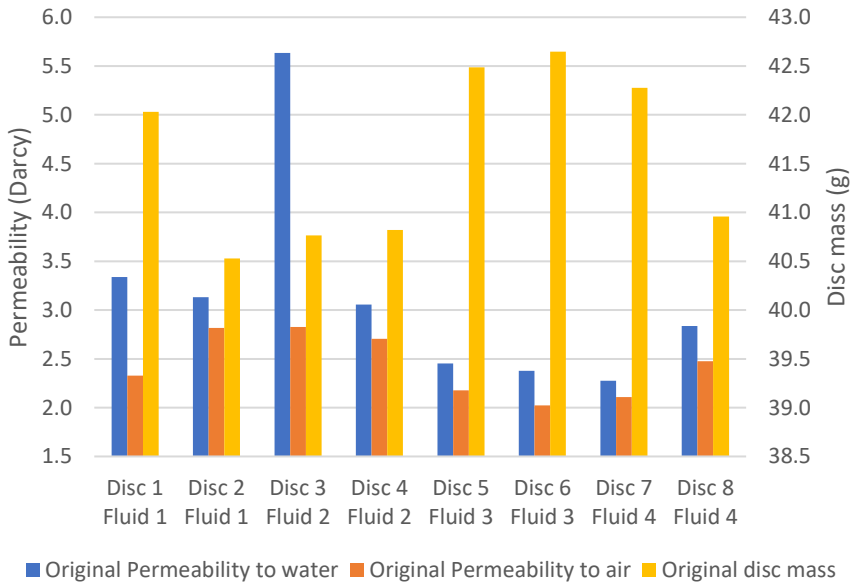

Figure 3-15: Measurements of 20 µm ceramic discs before HTHP testing [III]

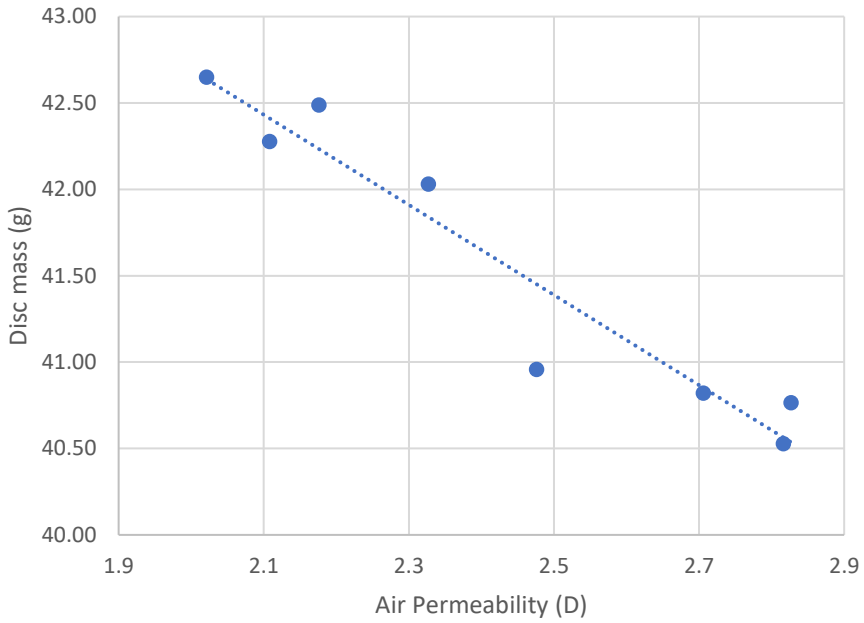

Figure 3-16: Plot of disc mass vs air permeability of 20 µm discs [III]

Correlation	Permeability to air	Disc mass
Permeability to water	0.693	-0.561
Permeability to air		-0.961

Table 3-8: Correlations between measured permeabilities and mass for each disc [III]

3.3.3 Fluid loss measurements

The fluid loss curves are represented in Figure 3.17, for testing at a differential pressure of 6.9 MPa (1000psi) and temperature of 90°C. All tests were conducted using ceramic discs with specified median pore size of 20 µm. The two test-series yielded consistent results, with less than 8% difference in fluid loss between any of the two corresponding tests. For both tests of Fluid 1, containing XC and PAC, a total loss was

recorded, and the tests stopped within the first few seconds. Fluid 2 replicated the recipe of Fluid 1, however, with the addition of 28.3 kg/m^3 (10 lb/bbl) of bentonite, which was sufficient to limit the fluid loss to 32-35 ml. Fluids 3 and 4 contained the same concentration of $CaCO_3$ particles and the short fibres, whereas Fluid 3 contained the starch-based polymer blends instead of xanthan gum and ultra-low viscosity poly-anionic cellulose used in Fluid 4. The two tests with Fluid 3 and Fluid 4 recorded fluid losses of around 17 ml and around 21 ml, respectively.

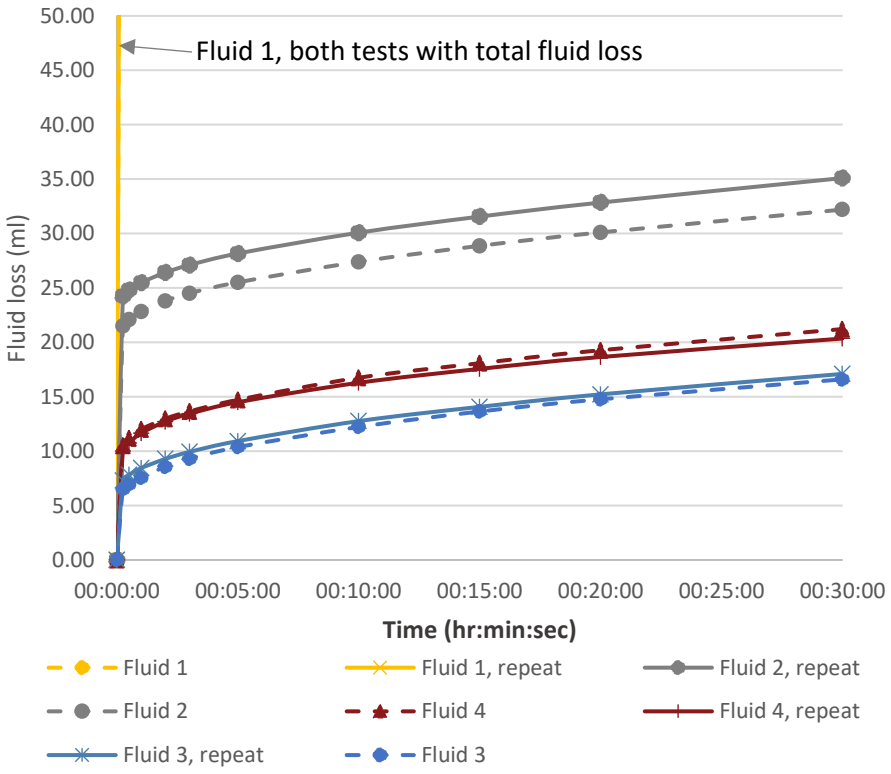

Figure 3-17: Fluid loss of Fluid 1-4 at 6.9 MPa differential pressure at 90°C [III]

The fluid loss data as a loss rate of ml/min are presented in Figure 3.18. It excludes the test with Fluid 1 on the 20 µm ceramic disc as this yielded a total loss. The figure gives an insight into the gradual development of the fluid loss rates over time implicitly also the development of the

permeability of the filter-cakes. The two tests with Fluid 2 saw the loss rates fall to 0.21 ml/min and 0.23 ml/min. Fluid 3 and 4 both showed lower loss rates than Fluid 2, where the loss rates fell to 0.18 ml/min and 0.19 ml/min for Fluid 3 and 0.17 ml/min and 0.19 ml/min for Fluid 4. The low differences in fluid loss rates over time also highlight that the main difference in fluid loss between Fluids 2, 3 and 4 occur during the initial spurt-loss recorded during the first 15 seconds of the test, and hence during the initial build-up of the filter-cakes. The lower spurt-losses of Fluids 3 and 4, relative to Fluid 2 may be attributed to the higher concentration of solids in Fluid 3 and 4. However, the relative difference between Fluid 3 and 4 may be related to the different polymers used, given that the concentration of $CaCO_3$ and fibres were similar. The indications or arguments can, however, not be considered as conclusive evidence given that the discs had different original permeabilities and disc mass.

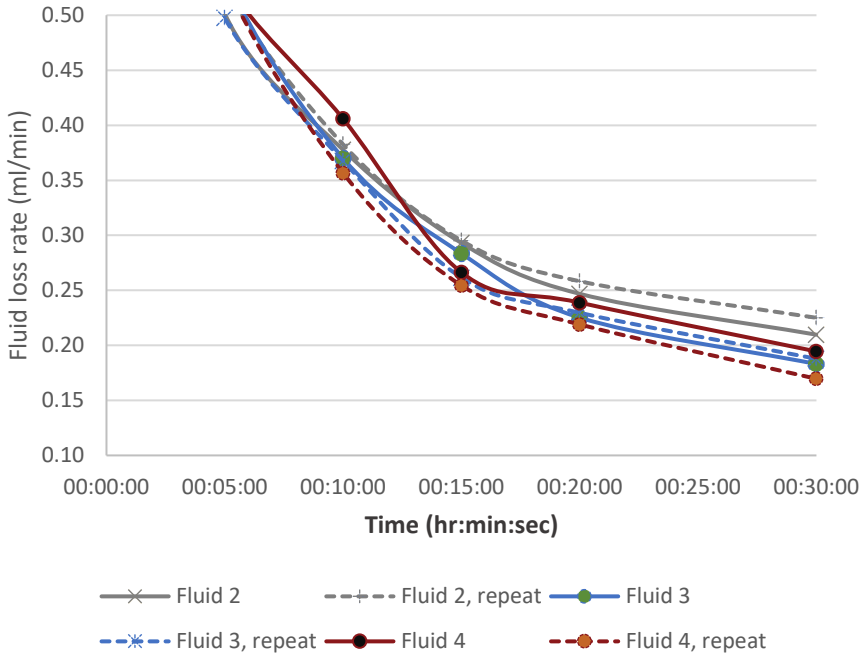

Figure 3-18: Fluid loss rate development for Fluid 2-4 [III]

A comparison of the original disc permeability and the measured fluid loss is shown in Figure 3.19 for Fluids 2-4. For each of the respective fluids there was a negative correlation between the original disc permeability and the fluid loss, i.e., each of the tests with the higher permeability disc recorded a smaller fluid loss given the same fluid has been used.

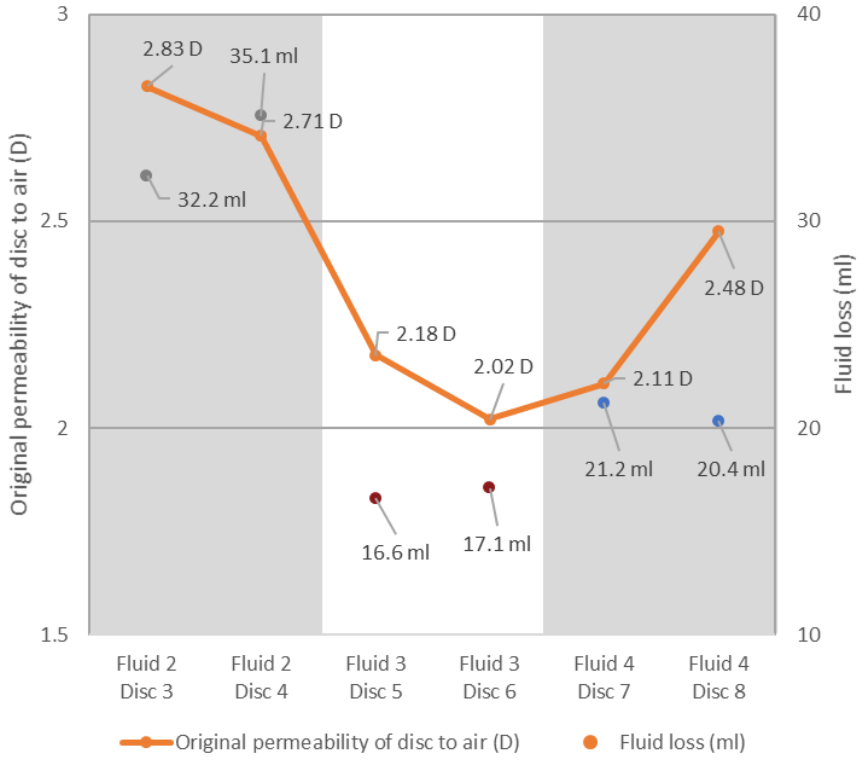

Figure 3-19: Fluid loss (right axis) and original disc permeability (left axis) comparison [III]

With the original disc permeability and the fluid loss rate development data, it is possible to provide some simple estimates for the combined permeability of the internal and the external filter-cakes. In reality, the fluid filtrate composition will vary a little for each test, and hence also

the viscosities of the fluid filtrates and the thickness of the filter-cakes. As a reference, the original disc permeabilities were in the range of 2.3-5.6 Darcy. The filtercakes were circa 1mm thick, and for simplicity, assuming that the fluid filtrate showed Newtonian behaviour with a viscosity of 1 Pa*s, the permeabilities of the filter-cakes may be calculated. In the period from 20 to 30 minutes, the fluid loss rates were ranging from 0.17 ml/min to 0.225 ml/min. This yields that the filter-cakes obtained a permeability as of 0.16-0.21 mD.

3.3.4 Filter-cakes

The polymer residue from Fluid 1 on the ceramic disc is shown in Figure 3.20, together with the filter-cakes from testing of Fluid 2 and 4. The disc from testing of Fluid 1, had no distinct filter-cake, but more of a semi-sticky polymer coating. Also, the rear of the disc showed signs of polymers after the total loss during the HTHP test. The filter-cakes made by Fluid 2 and Fluid 4 were even and shiny.

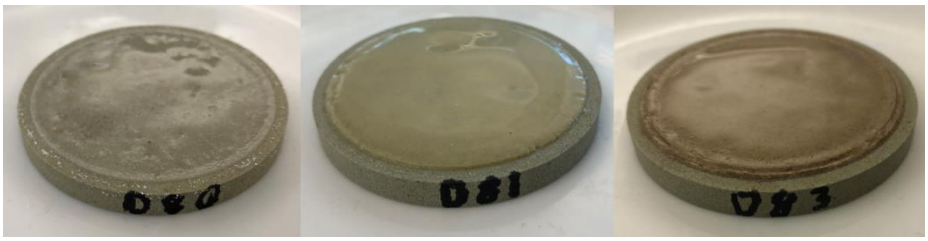

Figure 3-20: From left: Residue from Fluid 1 (Disc 2) after total loss, and filter-cakes from Fluid 2 (Disc 4) and Fluid 4 (Disc 8) [III]

The filter-cake formed by Fluid 3 (Disc 7), was a little distinct as it appeared to be a continuous piece or mat. The filter-cake and the disc and after filter-cake removal, with reverse flow of brine, is shown in Figure 3.21. Even before the application of the breaker fluid, the traces of the filter-cake had almost disappeared.

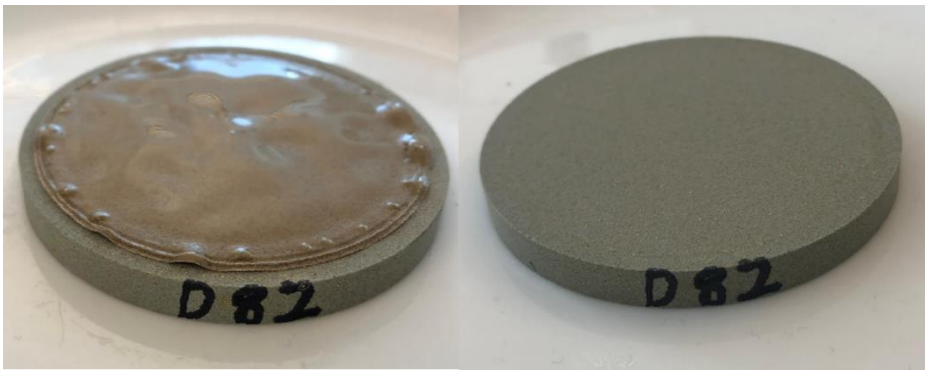

Figure 3-21: Disc 7, from testing of Fluid 3 with filter-cake (left) and after filter-cake had been lifted by reverse flow (right) [III]

3.3.5 Estimation of formation damage

Following the HTHP tests with the water-based fluids, the discs with the filter-cakes were back-flowed with brine and the discs placed in a bath with an oxidizing breaker fluid at 90°C for four hours. Thereafter permeability changes and disc mass increases were measured. The results of these tests are presented in Figure 3.22. The data indicate that both the permeability to air and water were considerably reduced after the HTHP tests with Fluid 1, with measured permeability reductions ranging from 65-78%. This was considerably higher than for any of the other fluids, and the permeability data were also supported by the tests for Fluid 1 also having the largest mass increases. Considering that Fluid 1 contained polymers, but no solids nor fibres, the mass increase and reduction in permeability is highly related to the polymers being used. Also, it showed that the breaker that had been applied did not fully dissolve the polymers nor remove the polymers from the ceramic disc. Further, it should be considered that since the test yielded a total loss, drilling fluid or drilling fluid filtrate would penetrate the formation considerably deeper than the near wellbore region that the ceramic disc represents. Therefore, when comparing the results from testing of Fluid

1 with the other fluids in the tests, it needs to be understood that the consequential formation damage of deeper penetration into the reservoir is likely to be much higher for Fluid 1 than for the other fluids. Disc mass increases were 248-275 mg.

For Fluid 2, the inclusion of bentonite reduced the fluid loss and improved the results with regards to avoiding formation damage relative to Fluid 1, with permeability reductions ranging from 5-44% and lower disc mass increases of 29-62 mg.

Fluid 3, with $CaCO_3$ and the short fibres, yielded much lower permeability reductions of 9-28% and disc mass increases of only 21-23 mg. The best results were obtained with Fluid 4 with reductions in permeability of 2-16% and disc mass increases of 7-13 mg. Given that Fluid 4 yielded a higher fluid loss then Fluid 3, there is, however, a possibility that more formation damage might occur further into the reservoir formation than for Fluid 3, where the fluid losses were lower in both tests.

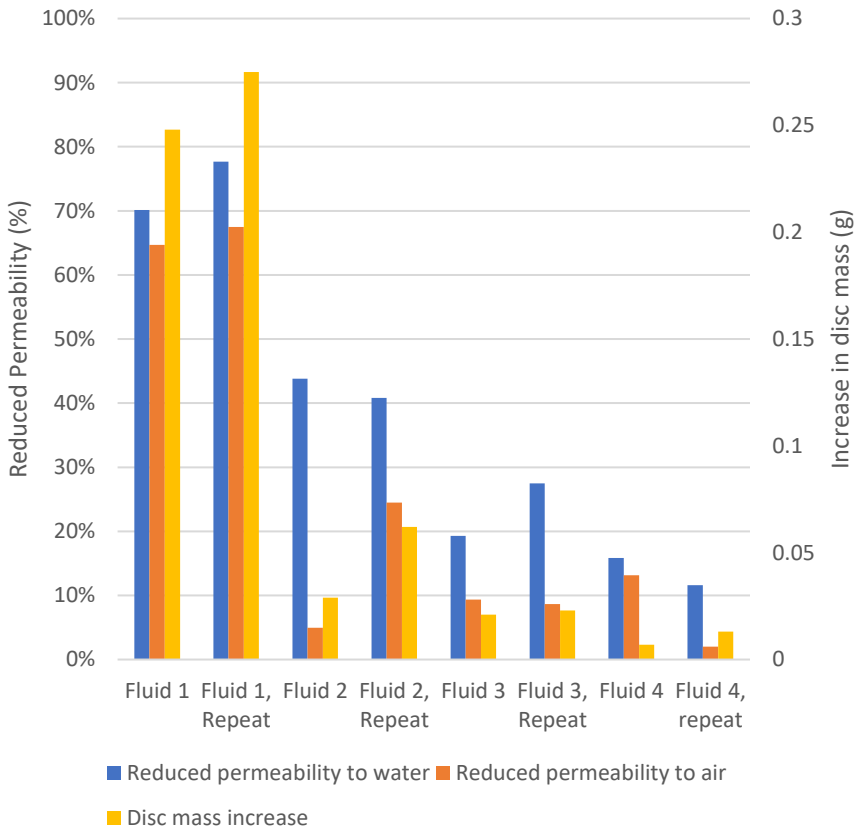

Figure 3-22: Indicators of formation damage for tests with Fluid 1-4, with original test and repetition test for each fluid [III]

The data presented in Figure 3.22 indicate high consistency in the data obtained for changes in permeability to air and water as well as increases in disc mass. Some inconsistency appears in the measurements related to Fluid 2, where reduction in permeability to air and disc mass increase was higher for the repeat test than for the first test. It should be noted that the initial measurements for disc 3, used for the first test of Fluid 2, deviated from the other discs by having a higher permeability to water, see Figure 3.15. The slight inconsistency in results for Fluid 2 may therefore be due to disc heterogeneity. The calculated correlations between the three indicators of formation damage are shown in Table

3.9. With all correlations being positive and above 0.9, it can be concluded that the overall data obtained have a high consistency. The highest correlation was obtained between changes in permeability to air and increase in disc mass, with a correlation as high as 0.984. Relative to the data in Table 2, the correlations are calculated to a reduction in permeability, and hence the coefficients of correlation with changes in disc mass are positive.

Correlations	**Reduced Permeability to air**	**Disc mass increase**
Reduced Permeability to water	0.906	0.932
Reduced Permeability to air		0.984

Table 3-9: Correlations between indicators of formation damage [III]

Further, the correlations between the first and the second test of each individual fluid with regards to the three indicators of formation damage are listed in Table 3.10. Although the data set is small, it is reassuring to see that the correlation data are positive and in the range of 0.686 to 0.997.

Correlation	**Fluid 1**	**Fluid 2**	**Fluid 3**	**Fluid 4**
Correlation: 1st and 2 tests (reduced permeability to water and air and increase in disc mass)	0.997	0.872	0.982	0.686

Table 3-10: Correlation of results between first and second tests for each fluid [III]

3.3.6 Discussion

The tests were conducted with the objective of assessing if the methodology could be applied consistently and if the indicators of formation damage would yield consistent results. All the evidence

collected strongly support that the methodology yields consistent results and that the three indicators of formation damage yield consistent results.

From a practical point of view, it was most difficult to measure the permeability to water, as inclusion of air bubbles in the fluid significantly impacted the fluid flow at a given pressure, and hence also the calculation of permeability. This was solved by placing the disc and the fluid in vacuum before the permeability tests.

It may, however, be argued that neither of the indicators of formation damage as tested here fully replicate the damage that might occur when drilling a reservoir formation and therefore a core-flood test would be a more correct representation of such. From a purely scientific perspective each of the methods have limitations in replicating wellbore and reservoir conditions. When testing using ceramic discs, the size and shape of pore-throat openings will differ from those appearing in actual rock formations. However, when testing is carried out using actual reservoir cores, there will be an uncertainty with regards to the heterogeneity of the reservoir section, where the production zone may extend hundreds or thousands of meters. One might therefore consider that the applied testing methodology in the present study assesses the performance of the drilling fluids against a generic formation, whereas a core-flooding test assesses the performance of the drilling fluid in a specific rock formation. From a practical perspective, a core-flooding test is generally considered to be a time-consuming and costly exercise, leading to a low number of tests being conducted for each relevant reservoir. Also, for a new field, representative cores may be non-existent before the selection process of the drilling fluid is concluded. When testing using ceramic discs, it is a relatively fast and low-cost process. This enables higher volumes of testing and testing using different permeabilities, which may represent different parts of a reservoir formation. The higher volumes may be used to reduce the statistical uncertainty of the results, it may allow for testing of different fluid compositions with different breaker applications, and also assess the

performance of the fluid is parts of the reservoir formation exhibit other properties than any specific core. Also, from a field perspective, it may be possible to monitor the performance of the drilling fluid as the drilling progresses and obtain relevant data to adjust the fluid properties during drilling.

Further testing should be conducted to compare the results of the test method used with equivalent core flooding tests. This may give valuable insight into the benefits of each testing methodology.

The application of the methodology did, however, replicate other results obtained by applying core flood tests. The test with Fluid 1 showed strong signs of formation damage using a polymer fluid without bridging materials. This is consistent with the findings of both Khan et al. (2003, 2007) and Audibert et al. (1999). Khan et al. concluded that xanthan gum solutions could cause significant reduction in permeability and that this may be caused by adsoption and retention of the polymer molecules on the rock surface. Audibert et al. used computer tomography imaging to detect formation damage by polymers in cores.

Green et al. (2017) conducted a series of core flooding tests and subsequent Micro-CT scanning to detect particle migration and formation change. They concluded that the key "zone" for permeability alteration in the samples was the first pores in the wellbore, regardless of the volume of filtrate loss or thickness of remnant drilling fluid filter-cake. This supports the idea of studying formation damage in the near wellbore region and that ceramic discs with a thickness of 6.3 mm will have considerably more depth than what might be necessary to study formation damage as the thickness represents around 25 times the pore size of a 250 µm disc and more than 300 times the pore size of a 20 µm disc. Further, the study revealed that with the specific breaker fluid applied, the higher fluid loss of Fluid 4 relative to Fluid 3 did not correspond with a higher formation damage. In contrast, Fluid 1 and Fluid 2 both led to higher fluid loss and formation damage than Fluid 3

and Fluid 4. These results are also consistent with the mentioned findings of Green et al. (2017), where there the lowest permeability alterations did not correlate with the lowest drilling fluid filtrate loss volume.

Civan (2020), provide a deep insight into a number of causes of formation damage. He presented challenges such as drilling fluid to formation fluid incompatibilities, drilling fluid to rock incompatibilities, phase trapping, chemical adsorption or wettability alteration and biologic activity. These types of formation damage are not covered in the present study.

Given that the methodology focusses on the formation damage occurring in the depth of the disc only, no quantitative measure of deeper formation damage caused by the fluid filtrate is provided.

Summary of findings:

- The methodologies of measuring disc mass change and measuring change in permeability to air and water provided highly correlated and consistent results.

3.4 Describing formation of internal and external filter-cakes and filter-cake permeability

For a fluid loss test, the emphasis is often placed on the 30-minute reading, and less importance is places on the various readings during the period of the test. By logging the fluid loss using a digital scale, it is possible to get very accurate measurements of the mass of the fluid loss and the fluid loss-rate at any point in time during the fluid loss test. The information gathered on the development of the fluid may be used together with the disc mass measurement to gain valuable insight into the formation of an internal filter-cake, as a deposit of particles into the permeable disc, and the formation of an external filter-cake.

Two approaches were used to model the formation of an internal- and external filter-cake. One approach was to model the fluid loss as a linear function of the square root of time using a fluid loss coefficient and a spurt loss constant. The other approach was to analyse the fluid loss as a flow through a series of flow resistances, equivalent to an electric circuit where the resistances would be separated into the flow resistance of the formation, the flow resistance of the internal filter-cake and the flow resistance of the external filter-cake.

Three fluid compositions were used for the tests. The basis for the study was a water-based reservoir drilling fluid composed with xanthan gum, starch, and sized ground marble ($CaCO_3$) as a bridging agent. The particle sizes were chosen to replicate a drilling fluid recipe used in a field operation. Two cellulose-based fluid loss materials were partly replacing ground marble for two of the fluid samples. One cellulose-based product is referred to as Non-Invasive Fluid Additive Ultra-Fine (NIF UF) with a D90 value of 75 µm and another referred to as Non-Invasive Fluid Additive Fine (NIF F) with a D90 value of 125 µm, both having a density of 1.35 g/cm^3. The fluid compositions for series W-4 were as presented in Table 3.11.

Recipe for 350 ml fluid	**Fluid 1 Base Fluid (g)**	**Fluid 2 NIF UF (g)**	**Fluid 3 NIF F (g)**
Water	318.5	318.5	318.5
Soda Ash	0.02	0.02	0.02
Caustic Soda	0.25	0.25	0.25
Xanthan Gum	1.3	1.3	1.3
Starch	7.0	7.0	7.0
MgO	1.0	1.0	1.0
NaCl	20.0	20.0	20.0
$CaCO_3$ <23µm	10.0	10.0	10.0
$CaCO_3$ <53µm	10.0	10.0	10.0
$CaCO_3$ D50 of 50 µm and D90 of 125 µm	20.0	10.0	10.0
NIF UF, D90 of 75 µm (AURACOAT UF)		5.0	
NIF F, D90 of 125 µm (AURACOAT F)			5.0
Polymer volume concentration	2.25%	2.25%	2.25%
Solids and fibre volume concentration	4.23%	4.23%	4.23%

Table 3-11: W-4: Drilling fluid recipes 1-3 for 350 ml fluid samples

The three fluids were hot-rolled for a period of 16 hours at a temperature of 112°C in a hot-rolling cell where a threaded steel rod was included to simulate mechanical wear. A wet-sieving study was conducted of the base fluid showing that > 99% of the ground marble particles were finer than 53 µm after hot-rolling. The hot-rolling temperature was selected to replicate a certain reservoir temperature. Fluid loss tests were thereafter conducted on 2.5 µm filterpaper at 500psi differential pressure and on ceramic discs with specified median pore-sizes of 10, 20, 50 and 120 µm, respectively.

The HTHP fluid loss tests were conducted in accordance with ANSI/API 13B-1 (2019) at 500 psi differential pressure, although the tests on ceramic discs were conducted with 1000 psi differential pressure, in order to identify if higher applied pressure could impact the sealing abilities and formation damage. The fluid loss tests were conducted at 90°C, unless stated otherwise. By selecting a temperature below the

boiling point, it was more practical to measure fluid loss accurately during the test.

3.4.1 Fluid loss tests and regression model

The fluid loss for the test on the 120 µm ceramic disc is plotted in Figure 3.23. For the Base Fluid, the test was stopped after a short period of time as the fluid loss was high and uncontrolled. For the two other fluids, the fluid loss fell to a very low level shortly after an initial spurt loss. When plotting the fluid loss against the square root of time, the graph appears to be linear after the spurt loss is experienced, whereas models commonly describe it as a function of the square root of time, without considering the spurt loss separately, as used by for example Skjeggestad (1989).

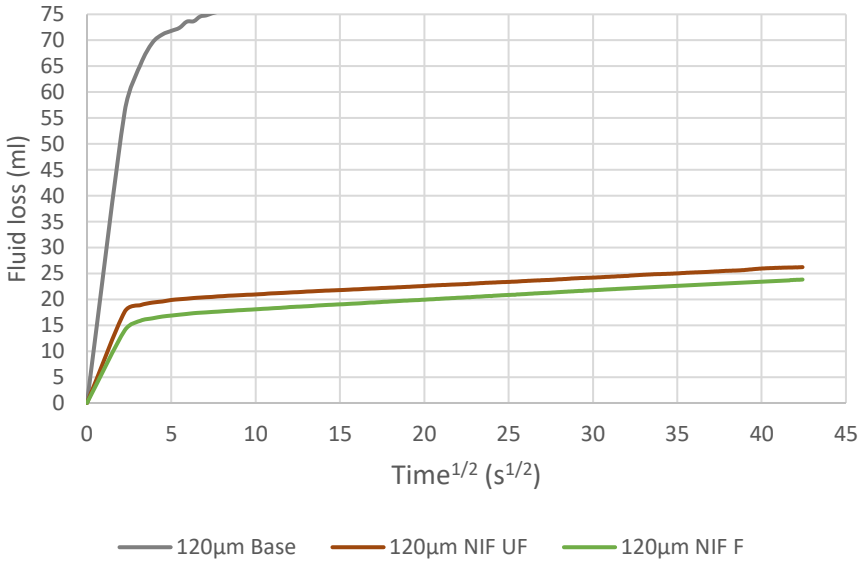

Figure 3-23: Fluid loss test on 120 µm disc [V]

A method for modelling the spurt loss and the fluid loss over time was attempted by plotting fluid loss (ml) versus the square root of the time ($s^{0.5}$). To separate the spurt loss from the linear loss phase, the first data point in the regression was the fluid loss value recorded after 15 seconds. Thereafter, a trendline was calculated using a linear regression model as presented in Equation 3.4. The fluid loss model calculated the fluid loss (ml), FL_T, as a fluid loss coefficient C_{FL} multiplied by the square root of time, $T^{0.5}$, plus a spurt loss constant, SL (ml). The fluid loss graphs for fluids NIF UF and NIF F on the 120 µm discs are presented together with the linear regression models in Figure 3.24. For both tests, the goodness of fit value, R^2, was in excess of 0.998, thereby indicating that the linear regression describes the underlying data in a very good way.

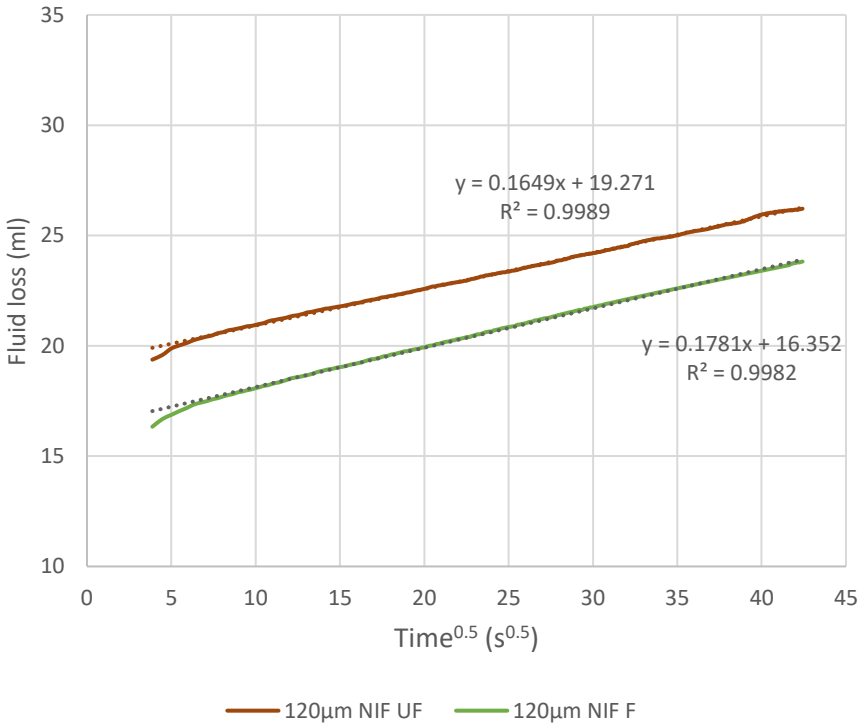

Figure 3-24: Regression of fluid loss test on 120 µm disc [V]

$$FL_T = C_{FL} * T^{0.5} + SL \tag{3.4}$$

Further, similar regressions were made of the other fluid loss tests. The regressions of all three fluids on the 50 µm ceramic disc is shown in Figure 3.25, and similarly the regressions of the fluid loss on the 2.5 µm filterpaper in Figure 3.26. In contrast to a ceramic disc, the filter-paper is not pre-wet in vacuum. The negative *SL* values obtained in some of the tests on filterpaper may therefore reflect that it takes some time for the fluid to penetrate and pass through the paper. Thus, with a more viscous base fluid, it will take more time for the fluid to pass through the paper, and a lower value of *SL* may be recorded. Looking at the C_{FL} values for the samples with NIF UF, these are lower than for the base fluid and the fluid with NIF F, thereby indicating that the filtercake is less permeable and will produce lower fluid loss over time.

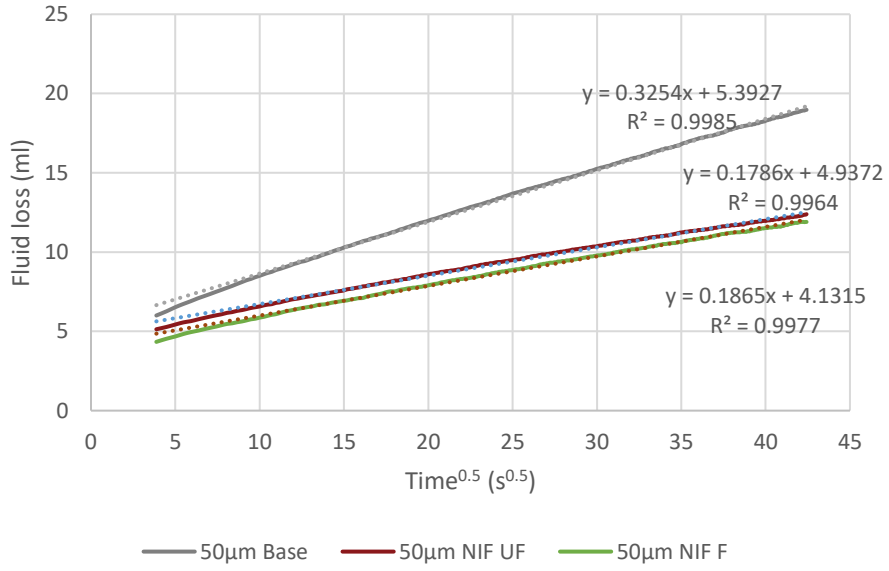

Figure 3-25: Regression of fluid loss test on 50 µm disc [V]

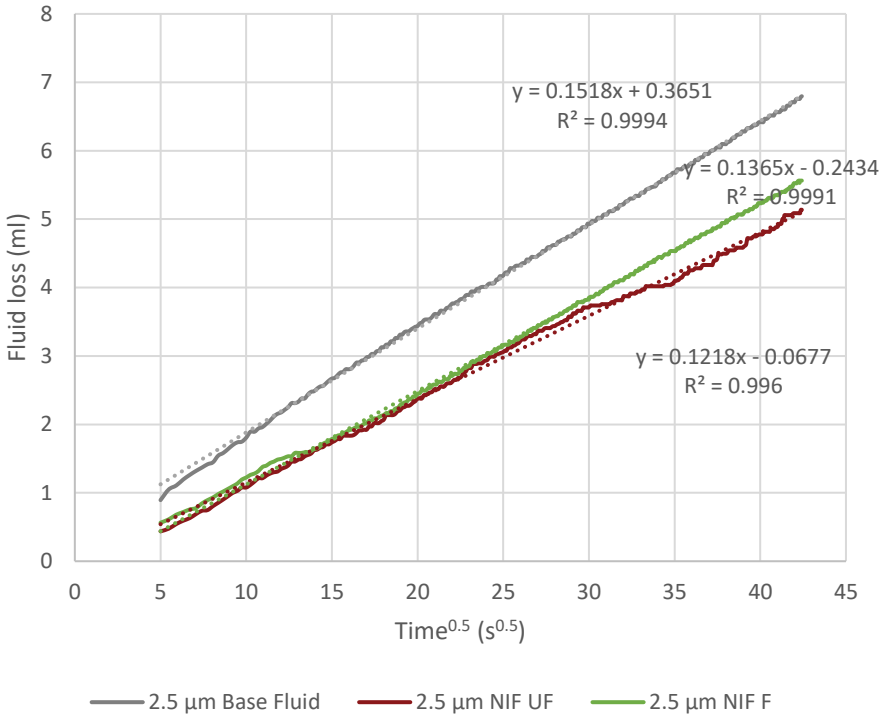

Figure 3-26: Regression of fluid loss test on 2.5µm filterpaper [V]

The Fluid Loss Coefficient data for the whole test-series in presented in Figure 3.27. For the Base Fluid, the coefficient more than doubles its value from the test on the filterpaper to the tests on the ceramic discs. In contrast, the coefficient only increases marginally for the fluid with NIF UF and NIF F. For the latter two, the coefficient gradually increases with higher disc pore size and reaches a maximum with the 50 µm discs, before it falls marginally when using the 120 µm discs.

The large change for the Base Fluid may be related to the increase in sealing pressure, from 500 psi on the filterpaper to 1000 psi on the ceramic discs. This may be natural as the ground marble particles are not believed to elastically compress, and hence the fluid-loss may increase in a near linear fashion with pressure in the pressure range that has been

investigated. In contrast, the increased pressure does not lead to a similar increase in fluid loss for NIF UF and NIF F, likely due to the compressibility of the cellulose fibres reducing the filter-cake permeability with higher pressure. For the test with similar pressures, it may be assumed that the permeability of the external filter-cake is consistent irrespective of the formation permeability and the internal filter-cakes, as long as the disc is sufficiently sealed during the spurt-loss phase to facilitate the formation of an external filter-cake. For the Base Fluid, the C_{FL} is consistently higher than the other fluids in all the tests, indicating that the filter-cake of the Base Fluid is higher than the filter-cakes of NIF UF and NIF F at 1000 psi.

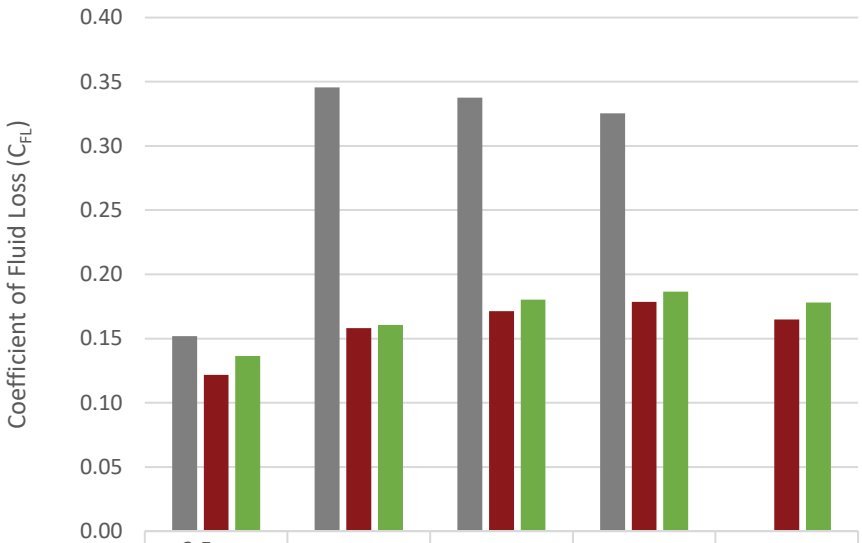

	2.5 µm paper (500 psi)	10 µm disc (1000 psi)	20 µm disc (1000 psi)	50 µm disc (1000 psi)	120 µm disc (1000 psi)
Base Fluid	0.15	0.35	0.34	0.33	
NIF UF	0.12	0.16	0.17	0.18	0.16
NIF F	0.14	0.16	0.18	0.19	0.18

Figure 3-27: Coefficient of fluid loss [V]

For the regressions the corresponding Spurt Loss Constant data are presented in Figure 3.28. The *SL* value for the Base Fluid on the 120 µm disc was set to 70, which was the reading after 15 seconds. No regression could be made as the test was aborted due to high and uncontrolled fluid loss. The calculated *SL* values are as expected very low for the tests on filter-paper and highest on the tests with 120 µm ceramic disc. The latter signifies that a larger volume of fluid was required to establish an effective internal filter-cake, against which an external filter-cake could be built. For the tests with 10, 20 and 50 µm discs, the three *SL* values were in a relatively narrow range, for each fluid. The highest values in the tests were for the Base Fluid and the lowest for the NIF F fluid.

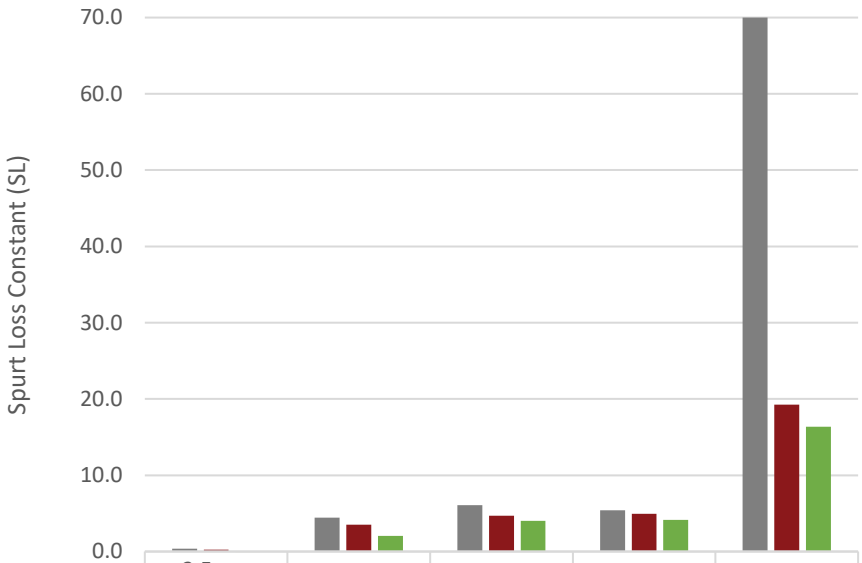

	2.5 µm paper (500 psi)	10 µm disc (1000 psi)	20 µm disc (1000 psi)	50 µm disc (1000 psi)	120 µm disc (1000 psi)
Base Fluid	0.4	4.4	6.1	5.4	70.0
NIF UF	0.2	3.5	4.7	4.9	19.3
NIF F	-0.1	2.0	4.0	4.1	16.4

Figure 3-28: Spurt loss constant from regressions, please note that the value of 70 for the Base Fluid was set manually as test was terminated [V]

When designing a fluid for wellbore strengthening purposes or for reservoir drilling purposes it is necessary to know to which degree particles migrate into the formation and form an internal filter-cake and to which degree the sealing is substantially enabled by the external filter-cake. To model this behaviour, a simplification was made, where the formation of the internal and external filter-cakes was separated in time. It was assumed that the internal filter-cake was formed it its entirety during the spurt loss phase, whilst the external filter-cake was formed after the spurt loss phase. As such, the volume of filtrate in each loss-phase and the concentration of polymers and solids in the fluid can be used to re-construct the process of building the internal and external filter-cakes. Using the linear regression model, the Spurt Loss Constant, *SL*, describes the relative amount of fluid required to form an internal filter-cake or the internal plugging in the disc. The fluid loss after the initial spurt loss is described by the Coefficient of Fluid Loss, which then describes the phase where the external filter-cake is built. In the case of a test on filter-paper, the pore-openings are so small that it may be assumed that particle invasion and internal plugging is negligible. This would result in a Spurt Loss Constant equal to 0, and the only factor required to calculate the fluid filtrate at any point in time would be the Coefficient of Fluid Loss. A test on filter-paper may hence be seen as a test of the flow resistance of the filter-cake, or inversely it may be used to describe the filter-cake permeability. In contrast, it may also be possible to imagine a fluid loss test where the particle invasion during the spurt loss led to a complete sealing of the disc, with no subsequent fluid loss. In this test the Coefficient of Fluid Loss would be 0 and the Spurt Loss Constant would be fully describing the fluid loss at any point in time after the initial spurt loss. Therefore, by calculating a simple metric of the ratio of the two factors, it may be possible to get a good description of the relative control each factor has in terms of controlling the fluid loss. The ratio may be defined as per Equation 3.5 and named the Relative Plugging Factor, *RPF*, which has the unit of $s^{0.5}$. As the volumetric concentration of solids impact the spurt loss and potentially

also the subsequent fluid loss, the *RPF* is likely most useful for comparing fluids of similar solids concentrations or when testing one fluid on different permeability discs.

$$RPF = \frac{SL}{C_{FL}} \tag{3.5}$$

A high *RPF* would indicate that the fluid loss may be highly impacted by the spurt loss and thereby formation plugging, this hence reduces the time dependence of the fluid loss, which conventionally grows following the square root of time. A high value may therefore be ideal for wellbore-stabilisation purposes, as a disturbance of the external filter-cake during drilling may have lower consequences. It is assumed that the formation of an internal filter-cake, as measured by the mass increase of discs or the estimated permeability of the internal filter-cake, will make the formation less exposed to disturbances in the wellbore. Circulation of drilling fluid or swabbing effects are less likely to lead to increased losses or differential sticking if the internal filter-cake limits the pressure communication between the wellbore and the formation. In contrast, a lower degree of formation plugging may be desired for reservoir drilling purposes, where formation plugging may lead to permanent permeability reduction and hence formation damage. Given that the ratio does not say anything about the absolute level of fluid loss, fluids should not be evaluated using the metric alone.

The *RPF* values for the tests are presented in Figure 3.29. Given that the C_{FL} remained reasonably consistent for each fluid at a given pressure, the difference in *SL* also translates into the *RPF* readings. As expected, the *RPF* values for the tests on filterpaper are very low, indicating that the external filter-cake is the primary barrier towards fluid loss. This is in clear contrast with the values calculated for the 120 µm ceramic disc tests. The high ratio's indicate high particle migration and significant plugging of these discs during the HTHP tests. Another observation is

that the *RPF* values for NIF F are considerably lower than for NIF UF in all tests. For practical purposes, these fluids are identical except for the different PSD of the cellulose fibres. This may indicate that the finer fibres of NIF UF need a slightly higher initial fluid loss to form an internal filter-cake, whereas the larger NIF F particles build an initial bridging faster.

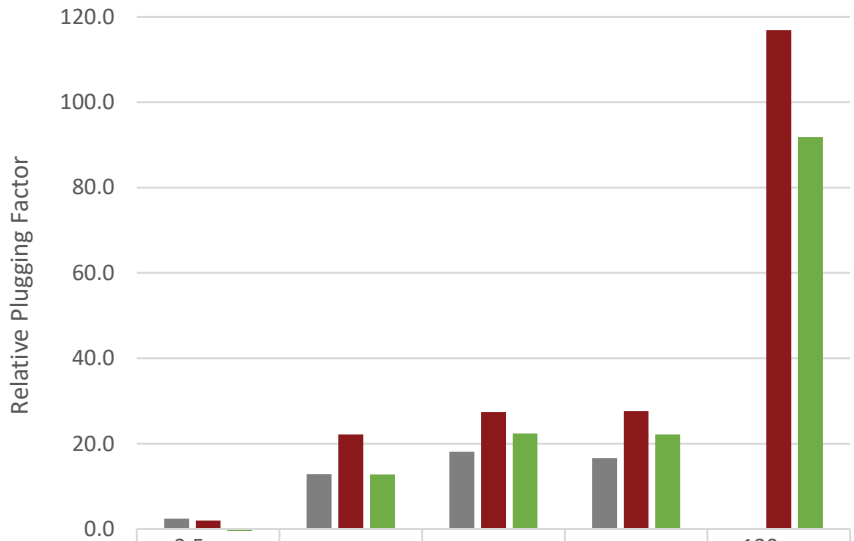

	2.5 µm paper (500 psi)	10 µm disc (1000 psi)	20 µm disc (1000 psi)	50 µm disc (1000 psi)	120 µm disc (1000 psi)
Base Fluid	2.4	12.8	18.1	16.6	
NIF UF	2.0	22.2	27.4	27.6	116.9
NIF F	-0.5	12.8	22.4	22.2	91.8

Figure 3-29: Relative plugging factor [V]

3.4.2 Permeability and disc mass measurements

For the tests conducted on 10, 20 and 50 µm ceramic discs, permeability tests were conducted using air both before the HTHP tests and after reverse flow through the discs to remove the external filter-cake and

potentially parts of the internal filter-cake. The data on retained permeability to air are presented in Figure 3.30. For all the ceramic discs, the changes in mass were measured using a moisture analyzer after reverse flow with water to lift off the external filter-cake and remove loose deposits within the disc. Figure 3.31 presents the data on disc mass change.

Overall, the best retained permeability results were recorded on the 20 µm ceramic discs. Considering the high concentration of $CaCO_3$ in all three fluids, this may indicate that the size of the $CaCO_3$ after degradation works most effectively in this range of pore sizes. Considering both disc mass increases and permeability measurements, NIF F appears to provide the best formation protection for any formation above 20 µm, whereas the NIF UF may be more effective in the 10-20 µm range. It should be noted how the permeability is clearly reduced with the Base Fluid on the 10 µm disc. The result of 54% from the 30-minute test was replicated with multiple tests with small variance.

In summary, the average retained permeability for the tests with the base fluid was 73%, with a standard deviation of 21%, whereas the tests with the cellulose-based fibres yielded an average retained permeability of 88%, with a standard deviation of 10%.

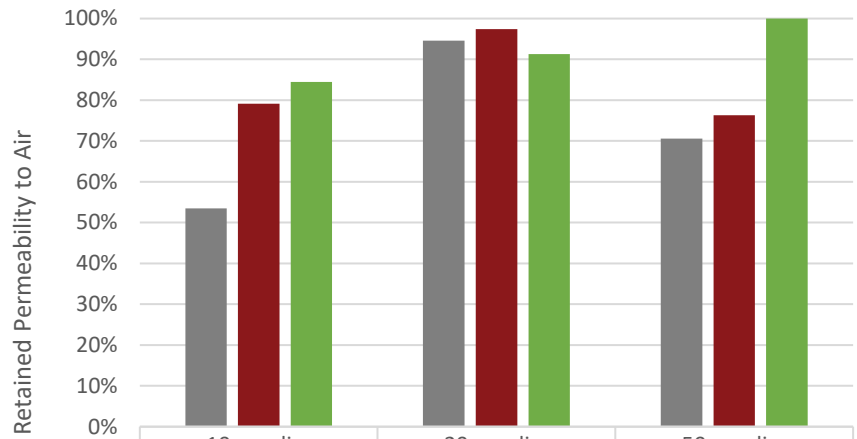

	10 µm disc (1000 psi)	20 µm disc (1000 psi)	50 µm disc (1000 psi)
Base Fluid	54%	95%	71%
NIF UF	79%	97%	76%
NIF F	85%	91%	100%

Figure 3-30: Retained permeability to air [V]

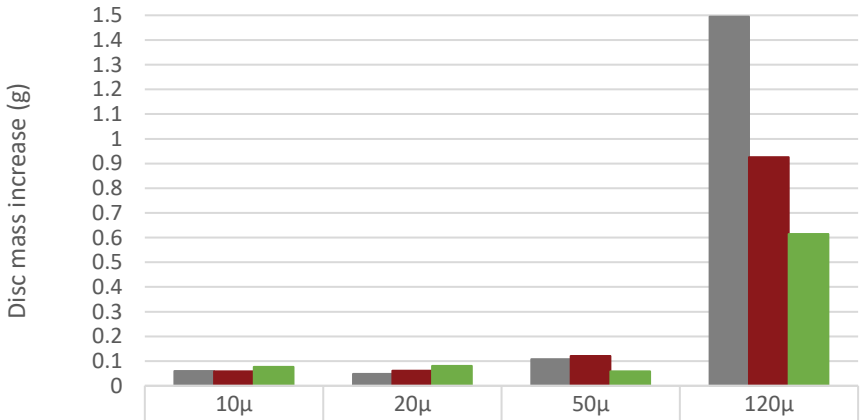

	10µ	20µ	50µ	120µ
Base Fluid	0.06	0.048	0.108	1.495
NIF UF	0.058	0.061	0.121	0.925
NIF F	0.077	0.081	0.058	0.615

Figure 3-31: Disc mass increase [V]

For the two test-series for fluids NIF UF and NIF F it was possible to calculate both the *RPF* and measure the disc mass increase for all four disc grades. The correlations between the two variables were 0.998 for NIF UF and 0.99 for NIF F. When plotting the *RPF* against the ratio of the NIF particle D90 value to the median disc pore size, it is clear that the disc mass retains a relative stable level until the particle D90 to pore-size ratio approaches the range of around 1.5 – 2.2. With lower ratios, the disc mass increase rises sharply, as presented in Figures 3.32 and 3.33. This is a strong indicator that, with the applied concentration of the specific cellulose-based fibres and by selecting a D90 value ≳ 3/2 times the pore opening, a low-permeability external filter-cake is created and the invasion of solid particles into the formation is limited.

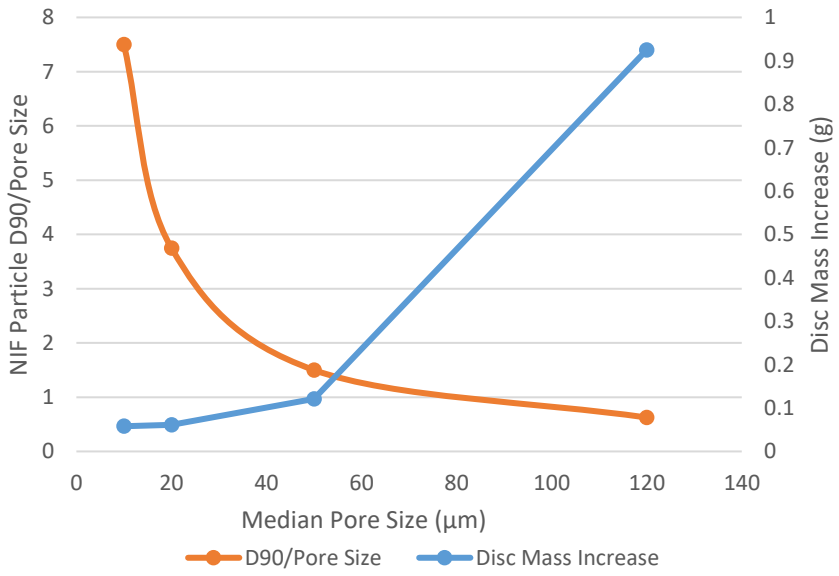

Figure 3-32: Particle to pore size ratio vs disc mass increase for fluid NIF UF [V]

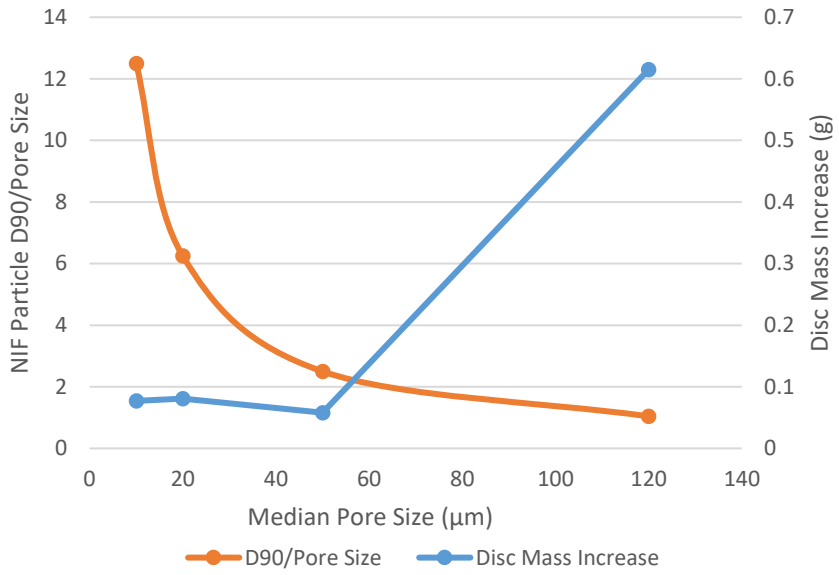

Figure 3-33: Particle to pore size ratio vs disc mass increase for fluid NIF F [V]

When plotting the particle D90 to pore size ratio versus the *RPF*, a very similar pattern emerges, as presented in Figures 3.34 and 3.35. When the particle D90 to pore size ratio falls below the 1.5-2.2 range, the *RPF* increases sharply, indicating that the particles of the fluid enter the formation, rather forming an external filter-cake. The *RPF* maintains a level in the range of 20-30 as long as the size ratio does not fall below the 1.5-2.2 range. This may indicate that $30 \gtrsim RPF$ represents a limit where solids invasion is limited.

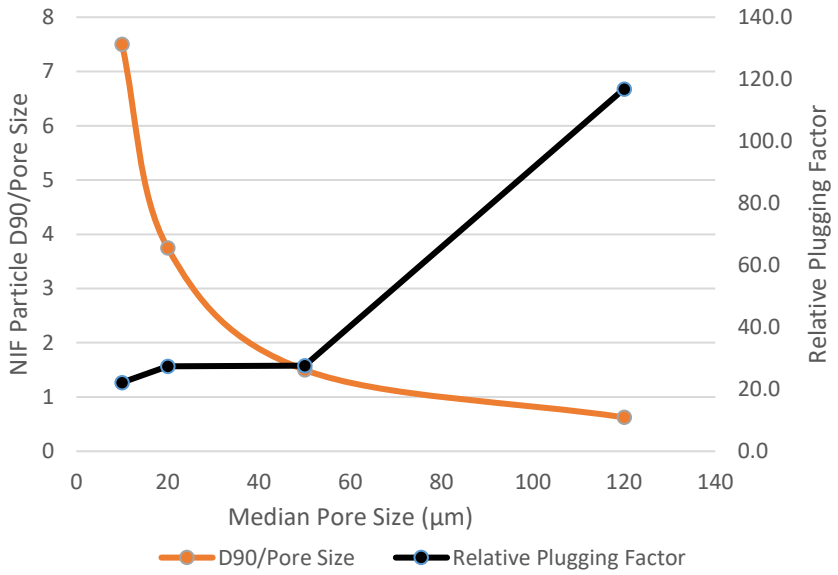

Figure 3-34: Particle to pore size ratio vs Relative Plugging Factor for fluid NIF UF [V]

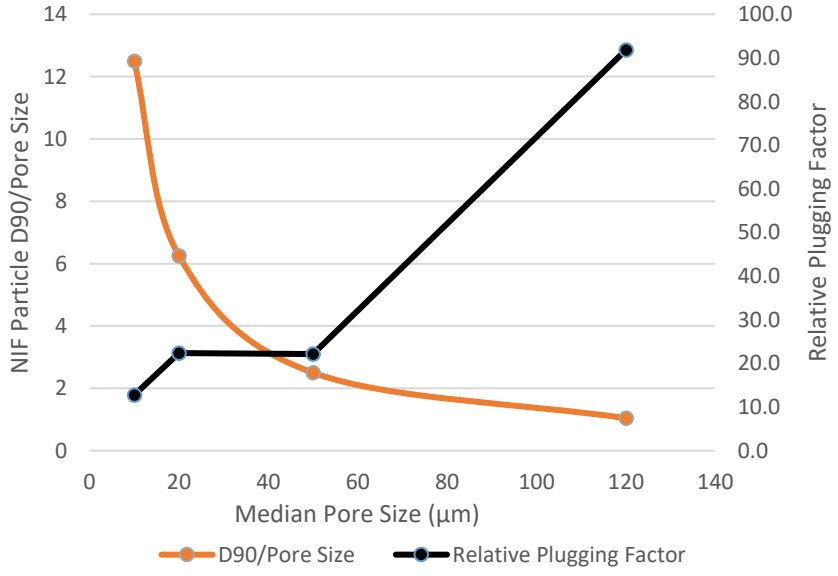

Figure 3-35: Particle to pore size ratio vs Relative Plugging Factor for fluid NIF F [V]

The three fluid samples all have a volume concentration of polymers of 2.25%, with a specific gravity of 0.95, whereas the volume concentration of solids (ground marble and fibres) was 4.23% for the Base fluid, with a specific gravity of 2.7, and 4.63% for the fluids with NIF UF and NIF F, with an average specific gravity of 2.16. By combining these values with the calculated spurt loss constants, it is possible to analyze the creation of an internal filter-cake.

A numerical model was developed analogous to the principles of Ohm's law, where U = voltage, I = current and R = resistance, as represented in Equation 3.6. Converting this to a flow of fluid through a formation, the applied differential pressure, ΔP, would be equivalent to the voltage, U, and a volume flow of a specific Newtonian fluid, Q, equivalent to the current, I. Further, the resistance to flow may be divided up into the flow resistance of the formation R_F, the flow resistance of the internal filter-cake, R_{IF} and the flow resistance of the external filter-cake R_{EF}, as per Equation 3.7 modelling the elements as serial resistance to flow, and thereafter re-arranged into Equation 3.8.

$$\mathrm{U} = \mathrm{I} * \mathrm{R} \tag{3.6}$$

$$R_T = R_F + R_{IF} + R_{EF} \tag{3.7}$$

$$\Delta P/Q = R_F + R_{IF} + R_{EF} \tag{3.8}$$

Darcy's law of flow through a porous medium is presented in re-arranged integral forms in Equations 3.9 and 3.10, where K is the permeability, Q the flowrate, η the assumed constant viscosity of the fluid and A the area of flow. For simplicity, the area A and the fluid viscosity η can be set equal for the formation and the internal- and external filter-cakes. By substitution, Equations 3.8 and 3.10 may be combined to form Equation 3.11. Here, the length and permeabilities of formation, internal filter-cake and external filter-cake are separated and named with subscript *F*, *IF* and *EF*.

$$_{\mathrm{K}} = \eta * \frac{Q*\Delta L}{A*\Delta P} \tag{3.9}$$

$$\Delta P/Q = \eta * \frac{\Delta L}{A*K} \tag{3.10}$$

$$\Delta P/Q = \frac{\eta}{A} * \left(\frac{\Delta L_F}{K_F} + \frac{\Delta L_{IF}}{K_{IF}} + \frac{\Delta L_{EF}}{K_{EF}} \right) \tag{3.11}$$

When applying this to a study using ceramic discs, the area *A* is defined by the actual flow area through the discs, and ΔL_F as the thickness of the disc. The permeability of each disc, K_F, can be assumed to be unchanged during the test. Following the logic of the linear regression model, Equation 3.4, the flow resistance of the internal filter-cake is modelled as a function of the spurt loss and is assumed to be constant thereafter. With such an approach, the flow resistance of the external filter-cake is the only flow resistance factor changing after the initial spurt loss. The build-up of the flow resistance of the formation, R_F, the internal filter-cake, R_{IF}, and the external filter-cake, R_{EF}, may hance be schematically presented as per Figure 3.36. Due to the significant differences in value, the Flow Resistance is illustrated using a logarithmic scale.

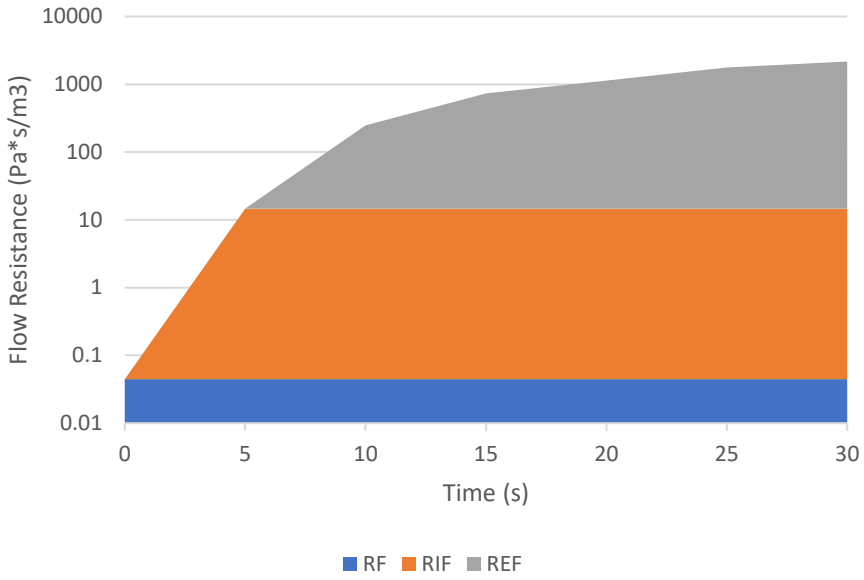

Figure 3-36: Schematic description of evolvement of flow resistance during fluid loss test using the resistance to flow of the formation, R_F, the resistance to flow by the internal filtercake, R_{IF} and the resistance to flow of the external filter-cake R_{EF} [V]

During a fluid loss test, the content and behavior of the fluid filtrate normally changes character over time. The higher the spurt loss, the more the initial filtrate will resemble the drilling fluid in look, content and viscosity. After an internal and external filter-cake has been established, the fluid filtrate gradually changes to become similar to the base fluid. For a water-based fluid, this implies that the filtrate will gradually move towards showing Newtonian behavior.

A simplified model was used as an estimate of the viscosity of the fluid filtrate where the initial flow rate, during the spurt loss phase, was high and the viscosity near that of the drilling fluid, and as the fluid loss reduced, the viscosity moved asymptotically towards the viscosity of the base fluid.

Further, 4 filter-cakes were weighed in a wet condition and thereafter dried to measure the water content of the filter-cake. For the four

measured filter-cakes, the moisture level varied in the range of 48-50%. For modelling purposes, the value of 50% was used. The moisture content did not vary significantly between the fluids used. If another value is to be applied, Equation 3.13 would need to be amended to reflect the applicable moisture level. The build-up of the filter-cake may be calculated by separating the content of the drilling fluid into the filtrate portion and the solids portion. For simplicity it is assumed that all the polymers and solids are retained in the external filter-cake after the initial spurt loss. It can be assumed that the fluid consumed, F_T (ml) at time, T, is separated into a portion of solids, polymers, and some of the fluid base to form the filter-cake, denoted FC_T (ml) and a clear fluid portion which escapes the filter-cake and becomes the measured fluid loss, CL_T (ml) after the initial spurt loss SL. Equation 3.12 presents this relationship.

$$F_T = FC_T + CL_T \tag{3.12}$$

We already know that 50% of the filter-cake mass was calculated to be water for these specific tests. Therefore, in addition to the direct volumetric concentration of the polymers and the solids, a volumetric concentration of water needs to be added which corresponds to the mass of the polymers and the solids. This means that the relationship presented in Equation 3.12 may be extended. Defining the volumetric concentration of polymers v_P (%) the volumetric concentration of solids v_S (%) and the average specific gravity of the polymers, ρ_P, and the specific gravity of the solids, ρ_S, we get Equation 3.13.

$$FC_T = F_T * (v_P + v_S + v_P * \rho_P + v_S * \rho_S) \tag{3.13}$$

During the filtration phase, the consumed drilling fluid volume is separated into a fluid filtrate and the filter-cake, which will consist of both solids and base fluid. Equation 3.13 may be simplified for each fluid

where the portion of the consumed drilling fluid that is used to build the filter-cake is k_F, thus forming Equation 3.14.

$$FC_T = F_T * k_F \tag{3.14}$$

Or, alternatively the volumes may be expressed as Equation 3.15.

$$CL_T = \frac{FC_T}{k_F} - FC_T \tag{3.15}$$

For the Base Fluid, this computes to a factor where k_F = 0.2 and substituting into Equation 3.12, FC_T = 0.25 * CL_T. For the NIF UF and NIF F fluids, the factors are similar with k_F = 0.20 and substituting into Equation 3.12, FC_T = 0.25 * CL_T. Thus, for all three fluids, the volume of the filter-cake after time = *T*, FC_T (ml), is 0.25 times the volume of the measured clear fluid filtrate CL_T (ml) at time = *T*.

Since we already have Equation 3.4 which calculates the fluid filtrate volume over time, where the spurt loss volume is defined as *SL*, the element CL_T can be represented as per Equation 3.16. The thickness of the filter-cake, ΔL_{EF} (cm), is calculated as per Equation 3.17 and the permeability, *K* (D or mD, where 1 D = 0.9869233 μm^2), as per Equation 3.18. Care should be taken when applying equations 3.17 and 3.18 to use consistent units of measurement.

$$CL_T = C_{FL} * T^{0.5} \tag{3.16}$$

$$\Delta L_{EF} = \frac{1}{A}\frac{C_{FL} * T^{0.5}}{1+\frac{1}{k_F}} \tag{3.17}$$

$$K = \frac{\eta}{2PA^2} \frac{C_{FL}^2}{1+\frac{1}{k_F}} \tag{3.18}$$

A numerical analysis was set up based on the assumptions described and Equations 3.4, 3.11, 3.17 and 3.18 together with the logging data from a fluid loss test to simulate the development of the internal and external filter-cakes and their permeabilities. Figure 3.37 presents such a data plot. For the test, a ceramic disc with median pore size of 50 µm was used. The permeability to water was measured to be 22.4 D. In contrast, the internal filter-cake permeability was calculated to be 69 mD and he external filter-cake < 0.1 mD. In the modelling, the ΔL_{IF} was set to 4.5 times the median pore size of the disc. This was done after fracturing discs to make a visual inspection of particle invasion. By applying the regression data into equation 3.18, the permeability was calculated to be a 0.054 mD, which was marginally lower than that of the numerical analysis. Equations 3.17 and 3.18 will be less useful if there is a substantial plugging into the disc during the spurt loss phase, as the internal filter-cake may then be the critical factor reducing the fluid loss. In situations with high degree of plugging, the actual permeable area of the disc will be smaller than the initial area, *A*. For the 120 µm discs, the invasion was considerably larger, and for the test with the Base Fluid, deposits of $CaCO_3$ were seen almost through the thickness of the disc even though the HTHP test was aborted within 2 minutes.

Analysing equation 3.18 further, it is clear that C_{FL} gives an insight into the permeability of the filter-cake as K is a function of $C_{FL}^{\ 2}$. It is, however, important to also consider the k_F factor, as high solids content in the fluid will lead to a larger portion of the fluid being deposited as part of the filter-cake. Therefore, C_{FL} values of fluids may be more relevant to compare directly if the solids concentrations or particle concentrations of the fluids are relatively similar.

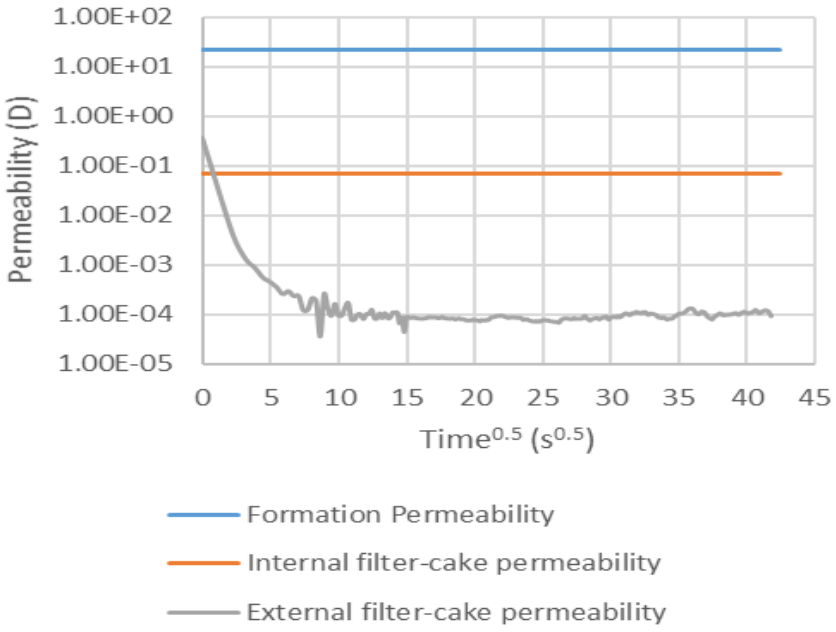

Figure 3-37: Calculated permeability development based on fluid loss logging data [V]

3.4.3 Discussion

The fluid loss tests were conducted under static conditions. The linear regression model applied is consistent with common theory, where fluid loss is calculated as a constant multiplied by the square root of time, Skjeggestad (1989) is one example. In the current study, the model is slightly amended to separate the spurt loss phase from the steadier loss rate. During a static filtration test, the filter-cake is allowed to build steadily as there is no mechanical disturbance of the filter-cake surface. In contrast, a dynamic fluid loss test would experience a continuous disturbance to the wellbore side of the filter-cake due to circulation of fluid. In such a condition, an equilibrium condition is likely to be met where the rate of erosion of the filter-cake equals the rate of build-up due to fluid loss. Hence, in a dynamic condition, the fluid loss will remain higher, and the filter-cake will reach a maximum thickness depending on the rate of erosion. With the assumption that the filter-cake is tight

enough to prevent particle migration, the difference between a static and a dynamic fluid loss test will not impact the formation of the internal filter-cake to any significant degree.

The hot-rolling procedure included a threaded steel-rod to simulate mechanical degradation. Studies have shown that $CaCO_3$ particles degrade during circulation and exposure to mechanical shear [VI]. In the same study, a cellulose-based LCM was found to show very low levels of particle size degradation. Applying these findings to the three fluids used in these studies, it may be assumed that the $CaCO_3$ particles, with an initial D 90 value in the region of 125 µm and D50 value of 50 µm may have been ground down in size, and that the largest particles in fluids NIF UF and NIF F may be the cellulose-based fibres. The test with the Base Fluid did not effectively seal the 120 µm disc. The Abrams Rule (Abrams 1977) recommends particles with a D50 value equal to or larger than 1/3 of the pore size for effective sealing. The result thus indicates that the D50 value of the CaCO3 particles in the Base Fluid likely had a D50 value of less than 40 µm after hot-rolling. Similarly, the Base Fluid sealed the 50 µm disc, suggesting that the D50 may be equal to or larger than 50/3 µm or the D90 value is $\gtrsim$ 45 µm after the hot-rolling process, applying the findings of Alsaba et al. (2017). The tests thus showed that if a circulating fluid is exposed to mechanical wear like that of the applied hot-rolling process, the PSD of $CaCO_3$ before circulation cannot be applied using known particle size selection methods. For the 50 µm discs, the tests with NIF F provided the lowest fluid loss, disc mass increase and permeability reduction. For this test, the NIF UF fluid would likely contain particles around 3/2 times the pore opening, whereas NIF F would likely contain particles $\gtrsim$ 3/2 times the pore opening, indicating that the latter would be preferrable to limit formation damage.

The tests presented in section 3.1 showed that with particles present in the fluid that were equal to or larger than the pore size of the discs, the mass increase of each disc was moderately low at 48 mg and 121 mg.

For the 120 µm discs, where the particle size was equal to or smaller than the pore size, the mass increase was much higher and in the region of 615 mg to 1495 mg. Also, comparing the tests with the fluids NIF UF and NIF F it is clear that the larger particles in NIF F better protects against solids invasion and fluid loss with pore openings in the range from 50 – 120 µm, whereas the differences between NIF UF and NIF F are small in the range from 20 µm and smaller pore openings. Applying the findings of Nelson, that sandstone reservoirs could effectively be simulated by using discs or cores with 10-20 µm pore openings [47], NIF UF and NIF F would thus effectively seal most sandstone reservoirs with lower fluid loss and reduced formation damage relative to common polymer and $CaCO_3$ based reservoir drilling fluids.

The experimental method applied to identify and measure polymer concentration in fluid filtrate showed consistent differences between the fluids with fibres and the Base Fluid. It is an interesting observation which may be explained by polar interaction and thereby increased adhesive and frictional forces between the cellulose-based fibres and the polymers used for fluid loss and viscosity. Such interaction may also be consistent with increased tensile strength or cohesive strength of the filter-cake. Further analysis should be conducted to better verify the experimental method and its applicability. Further studies should also be conducted to understand potential interaction between cellulose-based fibres and polymers and its impact on filter-cake strength and also the impact on dynamic fluid loss tests. With higher filter-cake cohesion, less erosion should be expected in a dynamic condition, and hence the fluid loss could be further reduced.

The extension of the model for analysis of filter-cake formation increases the complexity of the modelling. It was possible to calculate estimates of the permeability of internal and external filter-cakes, but with very significant increases in computation relative to the regression model. The extension of the model indicates that, once established, the external filter-cake was the dominant factor in controlling the fluid loss for the

tests conducted in this experiment. This observation was also expected given that the fluid compositions used were designed for reservoir drilling purposes. If similar modelling had been conducted with a fluid designed for wellbore strengthening purposes, the results of the modelling might be different. As such, with such a numerical model being established it may provide useful information for further understanding of how the internal and external filter-cakes are being built.

The linear regression model obtained very high goodness of fit values which may be useful to predict fluid loss under static conditions. Applying this together with Equation 3.17 one can also predict how the thickness of the external filter-cake will evolve over time. As an example, under the test conditions for the test on 10 µm discs, a 72-hour test could be forecasted to yield 180 ml of fluid loss for the Base Fluid and 84 ml of fluid loss for each of NIF UF and NIF F. The corresponding filter-cake thicknesses would be 11.1 mm for the Base Fluid and 4.9 mm for NIF UF and NIF F.

The Relative Plugging Factor appeared to give meaningful information regarding when a fluid changed from primarily producing an external filter-cake, to when the discs were plugged through solids migration. This inflection point was observed when the *RPF* was around 30. The tested fluids had relatively similar concentrations of solids. It could be expected that a higher solids concentration would lead to a lower spurt loss. A higher concentration of the same solids may, however, not necessarily cause a change in the filter-cake permeability, and hence in the Coefficient of Fluid Loss, as the same distribution of particles would be present to build the filter-cake. Therefore, it would be natural that a fluid with higher volumetric concentration of solids would produce an inflection point for the *RPF* at values less than 30.

The permeability of the filter-cake is consistently calculated for tests where the flow resistance is predominantly caused by the external filter-

cake, i.e. when the internal plugging is low and the *RPF* is below the inflection point. In such situations, the area used to calculate the permeability is the area of the external filter-cake. For tests where the internal plugging is high, the external filter-cake is not formed uniformly over the whole exposed area of the disc and the calculation of the external filter-cake permeability becomes difficult. Figure 3.3. shows examples of such tests.

Summary of findings:

- The regression model yield insight into formation of internal and external filter-cakes and facilitates the calculation of filter-cake permeabilities and filter-cake thickness.
- For the water-based reservoir drilling fluids, the average retained permeability for the tests with the base fluid was 73%, with a standard deviation of 21%, whereas the tests with the cellulose-based fibres yielded an average retained permeability of 88%, with a standard deviation of 10%.
- It was found that cellulose particles with size $\gtrsim 3/2$ the pore size limited polymer and solids invasion into the formation, whereas invasion of particles were higher when the largest particles were equal to or smaller than the pore openings.

3.5 Measuring filter-cake cohesion and shear strength

During testing of drilling fluids, the fluid's ability to seal the formation is tested using API fluid loss tests or HTHP filtration tests. The properties of the filter-cake are typically described in terms of thickness and surface texture, whereas measurements of the filter-cakes' strength and flowability are not normally studied. During an over-balance drilling operation, the filter-cake is the primary barrier that isolate the higher wellbore fluid pressure from the formation pore-pressure, and thereby prevents fluid loss and pressure communication. Ideally, the filter-cake

should have very low permeability and high cohesive strength. This would enable low fluid loss, a thin filter-cake and prevent differential sticking.

Differential sticking may appear when the drill-pipe comes in contact with the filter-cake. At the time of first contact, there is no suction pressure on the pipe. If the pipe is allowed to sink into the filter-cake, the fluid pressure on the filter-cake side of the pipe will start to fall and gradually move towards the formation pore pressure. Therefore, in a long-term static condition, the suction pressure on the pipe will move asymptotically towards being equal to the difference between the fluid pressure in the wellbore and the pore pressure in the formation. By multiplying the suction pressure with the contact area and the coefficient of friction between the drill-pipe and the filter-cake, the frictional force on the pipe is calculated.

The rate at which the suction pressure builds up is governed by the permeability of the filter-cake and the ease of disturbing or eroding the filter-cake in a dynamic setting, or alternatively seen as the cohesive strength and flowability of the filter-cake. Studies were conducted by Sheerwood and Meetin (1997) with water-based fluids containing bentonite on the ratio of volume of liquid to volume of solids within the filter-cake. They found that lower void ratio was correlated with lower filter-cake permeability. In earlier studies, Sherwood et al. (1991) used a squeeze-film rheometry approach to study filter-cake yield stress, σ_0. They concluded that with a solids volume fraction, ϕ, between 0.09 and 0.6, the yield stress could be expressed as function of ϕ for the fluid studied. Also, they showed that the bentonite filter-cakes compacted over time, and that ϕ reached an equilibrium value for a given applied pressure. Falahati et al. (2020) conducted a study on filter-cake strength using a hole punch tester and found that broadening the particle size distribution tended to make the filter-cakes stronger.

An intact and low-permeability filter-cake will substantially prevent the build-up of suction pressure on the drill-pipe leading to differential sticking. In contrast, a high-permeability filter-cake will lead to higher fluid loss and a faster growth of the filter-cake thickness. As the filter-

cake thickness grows, the potential area of contact with the drill-pipe increases. Further, if the cohesion of the filter-cake is low it becomes easier for the pipe to become «tucked-in» so that the contact area increases further, and the pressure barrier is damaged. Therefore, to prevent differential sticking, a filter-cake with very low permeability and high cohesive strength is ideal.

Studies of static fluid loss tests shown that after the initial spurt loss, the fluid loss follows a linear function when plotted against the square root of time [V]. In a dynamic condition, the filter-cake will reach a state where the rate of erosion equals the rate of filter-cake build-up, such that the fluid loss follows a linear function against time. By measuring the cohesive strength and flowability of the filter-cake, the differences between static and dynamic fluid loss may be better understood.

The study of powder rheology can be done by measuring the dynamic flow and the shear properties of the powders, where the powder itself may be a combination of liquids, solids and gases. Pedrosa et al. (2021) applied the methodology of measuring wet-granular rheology to calculate the internal friction coefficient of cuttings bed, which provides an insight into the particle cohesion properties. The test methodology used in the study by Pedrosa was also selected for the present study. The primary function is to use a powder shear cell to measure the resistance to flow at low shear rates.

The findings that Pedrosa made when studying cuttings beds may also have some relevance to drilling fluid filter-cakes. He concluded that water-based fluids made with KCl and polymers packed cuttings in a dense manner, where the particles moved in clusters. In contrast, the particles were packed in a loose configuration when submerged in an oil-based fluid, and hence single particles could be moved more freely. These data may indicate that an external filter-cake formed by oil-based drilling fluids may erode more readily than that of a water-based drilling fluid.

Two water-based reservoir drilling fluids were used to produce filter-cakes under high differential pressures. The filter-cakes were thereafter

analysed using a rheometer with a specially designed cell for accurate powder shear rheology. This enabled measurement of the cohesive strength and flowability of the filter-cakes.

The flow behaviour of powders is mostly non-Newtonian, where the resistance to flow falls with higher shear rates. Typically filter-cakes have moisture levels in the range of 15-50% by weight, primarily depending on the solids content of the fluids. Therefore, in order to study the rheology of the filter-cakes, it is important that they are kept in original condition, without being dried. The filter-cakes were made in HTHP tests using ceramic discs.

The tests were conducted using a 4.5 ml Anton Paar powder shear cell on an Anton Paar MCR-301 Rheometer. The shear cell was designed for analysis of powders and uses standard test loops with high precision measurements. The methodology uses the Mohs-Coulomb failure envelop theory, which is conventionally used to describe brittle materials or materials where the compressive strength significantly exceeds the tensile strength, by comparing the measured shear stress with the applied normal stress. Labuz and Zang (2012) provides a good insight into the mechanisms and governing equations. The Mohr-Coulomb failure is expressed by equation 1.2 and the internal friction factor calculate using equation 1.3.

Figure 3.38 shows the shear cell and the stem with the blades. The test material is placed into the cell without initial compaction. Excess materials is scraped off to provide an even surface.

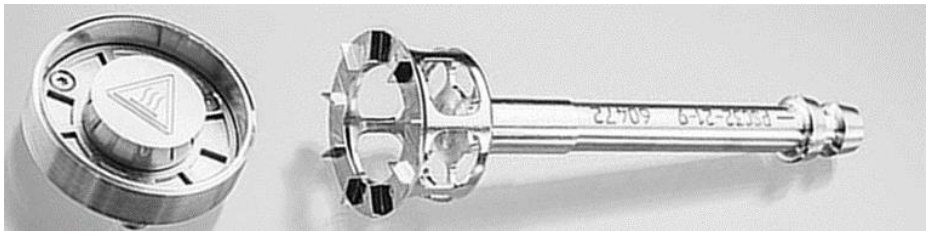

Figure 3-38: Anton Paar Powder Shear Cell and stem [VII]

After the filter-cakes were placed in the test cell, a pre-set maximum normal stress was applied, before the sample was sheared at constant rotation until reaching the cake's failure and the shear stress was measure. This procedure was repeated at 30%, 50% and 70% of the maximum initial normal stress. The test cell has been designed with a small open area around the top of the test cell, so that it can identify if powders simply overflow when a given normal pressure is applied. For certain free flowing powders, there will hence we a limit to the applied normal pressure. With the three shear-to-failure points is possible to obtain the yield locus of the Mohr-Coulomb failure envelop, and from there calculate the unconfined yield strength and the major principal stress as shown in Figure 3.39.

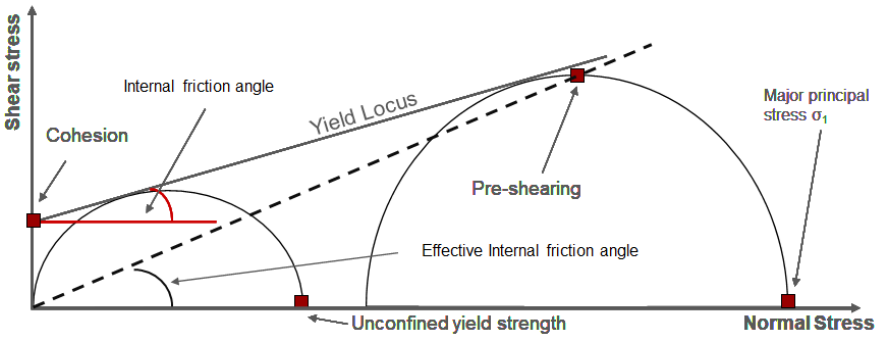

Figure 3-39: Mohr-Coulomb failure envelope obtained by rheometry [VII]

The unconfined yield stress (σ_c) which represents the major principal stress that will cause the cake to shear in an unconfined state, together with the major principal stress (σ_1) under normal stress, will provide the flowability of the cake in terms of its Flow Function Coefficient (ffc), as described in equation 3.19. This flowability is divided into five regions, according to the ffc as follows: not flowing (ffc <1), very cohesive (1< ffc <2), cohesive (2< ffc <4), easy flowing (4< ffc <10) and free flowing (ffc>10).

$$ffc = \frac{\sigma_1}{\sigma_c} \tag{3.19}$$

3.5.1 Drilling fluid composition and fluid loss tests

Four fluid compositions for test series W-5, shown in Table 3.12, were selected to represent typical water-based reservoir drilling fluids. Xanthan Gum was used to provide viscosity, starch for fluid loss control and $CaCO_3$ (ground marble) and cellulose based fibres to provide bridging. To ensure sufficient filter-cake thickness for conducting the tests in the powder shear cell, the concentration of starch was kept a little lower than what might be ideal from a fluid loss perspective. The filter-cakes were made by testing the fluids under high differential pressures on 50 µm ceramic discs. Fluid 1 and 2 were tested with average pressures of 1500 psi for 30 minutes, whereas Fluid 3 and 4 were tested with average pressures of 2400 psi for 40 minutes.

Component and mixing sequence for 1 litre of fluid	**Fluid 1 (g)**	**Fluid 2 (g)**	**Fluid 3 (g)**	**Fluid 4 (g)**
Water	950.6	936	947.6	933
Na_2CO_3	0.057	0.057	0.057	0.057
NaOH	0.71	0.71	0.71	0.71
Xanthan Gum	4.29	4.29	4.29	4.29
Starch	11.4	11.4	14.25	14.25
MgO	1.43	1.43	1.43	1.43
NaCl	28.57	28.57	28.57	28.57
$CaCO_3$ (<53µm)	57.14	57.14	57.14	57.14
Cellulose based material with D90 of 75 µm (AURACOAT UF)		14.29		14.29

Table 3-12: W-5 Drilling fluid recipes 1-4 for 1 litre sample [VII]

3.5.2 Filter-cake shear rheology measurements

Fluid 1 was tested with a maximum applied normal pressure of 3 kPa, as the sample disintegrated and overflowed above this pressure. The

disintegration of the filter-cake is evidence of low cohesion and high flowability. The Mohr-Coulomb failure envelope is presented in Figure 3.40. The obtained cohesion was 495 Pa and the internal friction angle 14°.

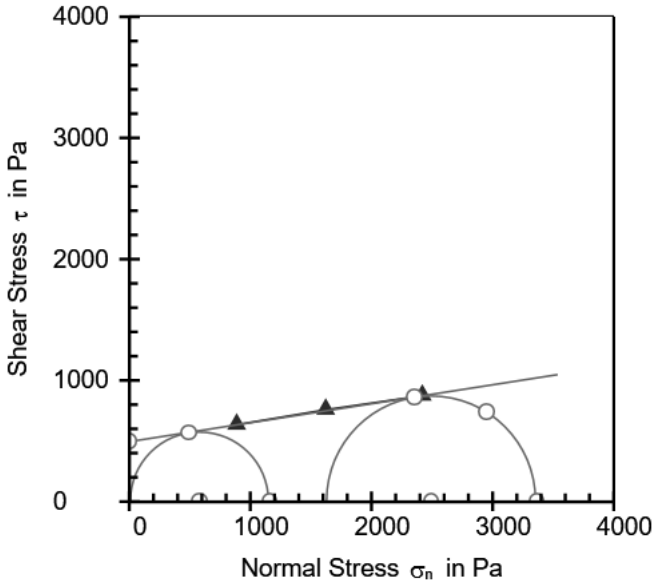

Figure 3-40: Mohr-Coulomb failure envelope for W-5 Fluid 1 at 3 kPa [VII]

For Fluid 2, testing was conducted at 3, 6 and 9 kPa applied normal pressures as presented in Figure 3.41. The cohesion ranged from 2271 Pa to 3167 Pa, which is around 5 to 6 times that of Fluid 1, and the internal friction angles were from 31° to 44°, indicating lower flowability.

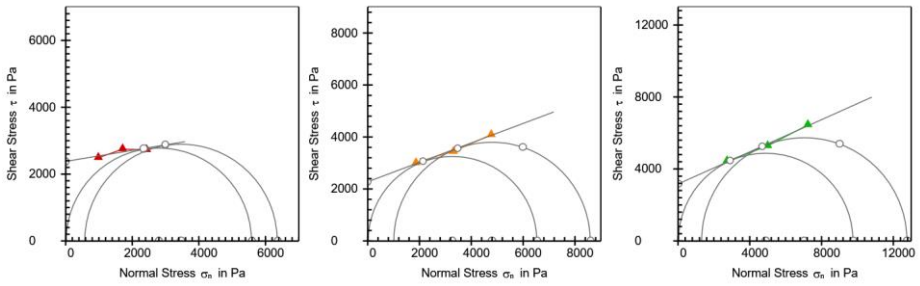

Figure 3-41: Mohr-Coulomb failure envelope for W-5 Fluid 2 at 3, 6 and 9 kPa [VII]

Fluid 4 showed similar characteristics as Fluid 1, and were tested at 1, 2 and 3 kPa normal pressures. Figure 3.42 presents these plots, and as for Fluid 1, it can be seen that the Mohr's circles did not overlap for most test conditions. The Cohesion was measured to range from 261 Pa to 361 Pa and the friction angles in the range from 14° to 19°.

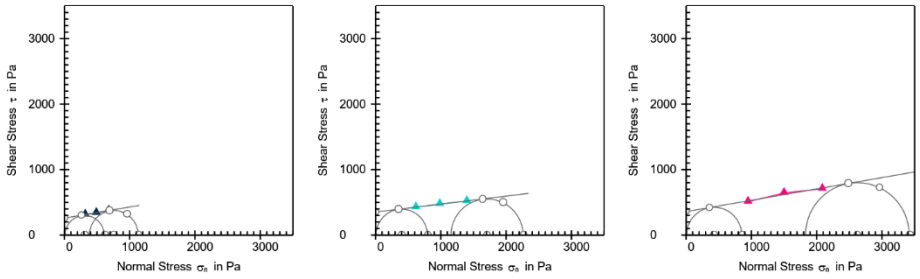

Figure 3-42: Mohr-coulomb failure envelope for W-5 Fluid 3 at 1, 2 and 3 kPa [VII]

Fluid 4 was tested at normal pressures of 1, 2 and 3 kPa, to facilitate a comparison with Fluid 3. The Mohr-Coulomb failure envelopes are presented in Figure 3.43. The Cohesion was measured to range from 1032 Pa for the 1 kPa normal pressure test to 1731 Pa for the 3 kPa normal pressure test, and the internal friction angles ranged from 53° to 34°. Relative to Fluid 3, the Cohesion was 4-5 times higher under the same normal pressure conditions, and the friction angle more than double.

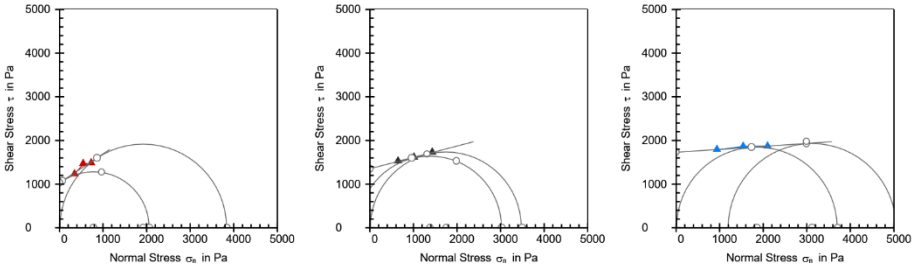

Figure 3-43: Mohr-coulomb failure envelope for W-5 Fluid 4 at 1, 2 and 3 kPa [VII]

The overall unconfined yield strengths were plotted against the major principal stresses for each of the tests. These data are presented in Figure 3.44. Using the separation into different flow regimes, it is clear that Fluid 2 and 4 show significantly higher levels of cohesion than Fluid 1 and 3, which appear to be in the range from cohesive to easy flowing. For Fluids 3 and 4, the unconfined yield strength appears to potentially be independent of the major principal stress, within the tested principal stress range. Given that Fluids 2 and 4 are very similar, but tested at different major principal stresses, viewing the two plots together may be relevant. Using this approach, it may be interpreted that the unconfined yield strength is constant below a certain major principal stress level, and that when this stress level is exceeded, the unconfined yield strength follows a linear relationship with the major principal stress.

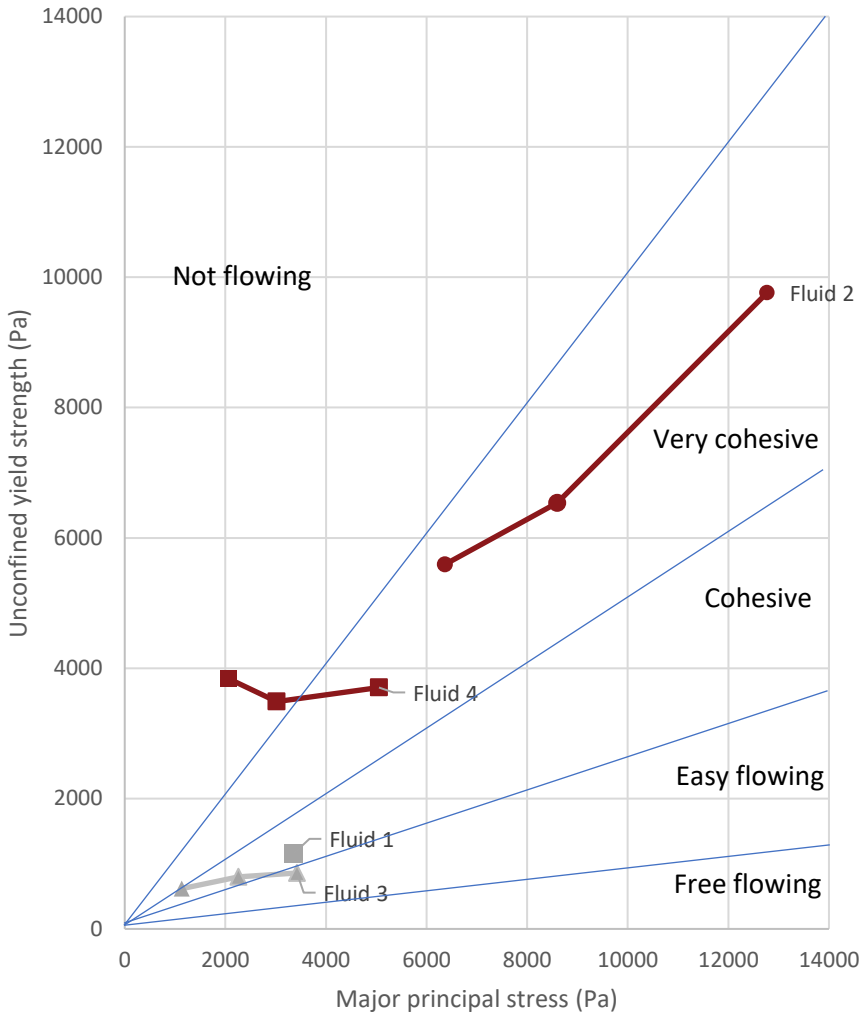

Figure 3-44: Flowability of W5 Fluid 1-4 [VII]

The datapoints for each of the tests are listed in Table 2. Herein, the calculated internal friction angles were lower for higher values of applied normal pressure for all the tests where multiple normal pressures were applied. This also corresponds to higher flowability factors coefficients, for higher applied normal pressures.

	Applied normal pressure (Pa)	Cohesion, c (Pa)	Unconfined yield strength, σ_c (Pa)	Major principal stress, σ_1 (Pa)	Flowability factor coefficient, ffc	Internal fricion angle, ϕ	Coefficient of internal friction, $\mu=\tan(\phi)$
Fluid 1	3000	495	1156	3360	2.91	14.14	0.252
Fluid 2	3000	2375	5593	6365	1.14	44	0.966
Fluid 2	6000	2271	6538	8598	1.32	31.07	0.603
Fluid 2	9000	3167	9762	12770	1.31	30.99	0.601
Fluid 3	1000	261	618	1136	1.84	18.79	0.340
Fluid 3	2000	354	799	2263	2.83	14.39	0.257
Fluid 3	3000	361	858	3425	3.99	13.83	0.246
Fluid 4	1000	1032	3841	2060	0.54	52.92	1.323
Fluid 4	2000	1349	3488	3022	0.87	37.74	0.774
Fluid 4	3000	1731	3704	5054	1.36	33.53	0.663

Table 3-13: Flowability data [VII]

3.5.3 Discussion

The method of testing filter-cakes using advanced rheometry introduces sources or error and conditions which are unlike those seen in a wellbore. As an example, the filter-cakes were produced under high differential pressures, whereas the rheology studies were conducted without a confining fluid pressure.

The testing using the Anton Paar powder shear cell functioned in a satisfactory manner. The cell required a filter-cake volume of at least 4 ml, and hence the drilling fluid composition and filtration tests need to be conducted in a way that would produce a filter-cake with sufficient thickness. The fluid compositions applied included concentrations of starch ranging from 11.4-14.25 kg/m3 to ensure a slightly higher fluid-

loss and filter-cake build up. This is somewhat lower than what is conventionally used in wellbore application. Given that the testing was successful, it is natural to conduct future tests with fluid compositions that more closely resemble a field fluid with optimised values of polymers and presence of drilled solids.

The results showed very clear differences between the fluids with and without the cellulose-based fibres. It was clear that the fluid containing $CaCO_3$ as the only solid, created a filter-cake with low cohesive strength and high flowability.

Extending the results to field applications, it may be expected that the fluid without cellulose-based non-invasive fluid additives would be exposed to rapid filter-cake erosion, higher fluid-loss and greater risk of differential sticking, whereas the addition of the tested cellulose-based additives may present a significant reduction of these risk factors.

A cause of the improved filter-cake cohesion for Fluid 2 and 4 may be polar interaction of the cellulose-based fibres and the dispersed polymers in the fluid. Such interaction may take the form of higher adhesive and frictional forces between the particles, and thereby increased shear strength.

Studying the data in further detail, the internal friction angle, or alternatively the coefficient of internal friction, was not constant for either Fluid 2, 3 and 4 as the applied normal stresses varied. For the filter-cakes of each of the three fluids, a higher applied normal pressure led to a lower coefficient of internal friction. For the mentioned filter-cakes, also the highest applied normal pressure led to the largest recorded cohesion. The classical Mohr-Coulomb shear strength criterion describes the shear strength as a linear function of the normal stress and the coefficient of internal friction plus the cohesion constant. The observed behaviour indicates that a nonlinear relationship exists when different normal stresses are applied. Shen et al. (2018) presented a nonlinear modified Mohr-Coulomb shear strength criterion for analysing intact rocks. Their model also showed a transition from brittle to ductile behaviour upon reaching a critical level of normal stress, following

Barton (1976). At this critical state, the failure envelope becomes horizontal, and the maximum shear strength is half of the normal compressive strength. The tests conducted using the filter-cakes of Fluid 1-4 showed some of the same behaviour as observed by Shen et al. and Barton, however, the testing conducted did not replicate a wide enough range of normal stresses to fully describe the behaviour of the filter-cakes.

Summary of findings:

- The application of the powder shear cell for measuring the flowability and cohesion of drilling fluid filter-cakes worked well. The test results showed that fluids with relatively similar compositions also yielded similar results.
- A total of four test were conducted successfully and where the primary differences were the addition of an ultra-fine cellulose based non-invasive fluid additive in fluids 2 and 4. The addition of the cellulose-based additive created a significantly higher cohesive strength and lower flowability of the filter-cakes.
- The results from the testing indicate that a Fluid 2 and 4, containing the cellulose-based additive, would provide improved resistance towards erosion of the filter-cake due to fluid circulation and potentially reduced risk of differential sticking.

3.6 Studying fluid filtrate content and viscosity

When conducting a fluid-loss test, the drilling fluid is separated into a portion which makes up the internal- and external filter-cake and a filtrate portion which penetrates deeper into the formation. By analyzing the content and viscosity of the fluid filtrate, information may be obtained about potential deeper formation damage or alteration of the fluid pressure in the near wellbore region of the formation. Two separate studies were conducted where one study focused on identifying polymer

content in water-based fluid filtrate using light and portable devices that may be used in a field application. The other study was conducted to understand the viscosity of the fluid filtrate.

3.6.1 Studying fluid filtrate content in water-based drilling fluids

An experimental analysis was conducted to measure the contents of the fluid filtrate relative to the drilling fluid before application. By using a series of test including turbidity, salinity, conductivity, and refractive index (BRIX or °Bx), as being used in the food industry (Hu et al., 2023), each of the components of the fluids were mapped and the values of the fluids and the fluid filtrates measured. Each component thus made a unique "fingerprint" in terms of relative readings on the different parameters measured. Using this method, it was possible to estimate the relative polymer concentrations in the fluid filtrates. This was calculated by measuring the BRIX value and subtracting the BRIX value resulting from other constituents in the filtrate such as salts. Further, by combining the volume of the filtrate and the polymer concentration in the filtrate, it was possible to plot the polymer content in the filtrate for certain fluid loss tests. The filtrate tests were conducted after fluid loss tests with fluids listed in Table 3.11, series W-4 Fluid 1-3.

Figure 3.45 presents the estimated polymer content in the filtrate from the 3.49 MPa (500 psi) tests on filterpaper for the three respective fluids. Here the concentration of polymers in the test with the Base Fluid was around twice that of the NIF UF and the NIF F fluids. The area of each indicator reflects the product of the BRIX value (polymer concentration) and the Fluid Loss value, to reflect the absolute volume of polymers. The equipment used is listed in the appendix. For the first test series it was decided to use portable equipment that easily could be used in a small field laboratory.

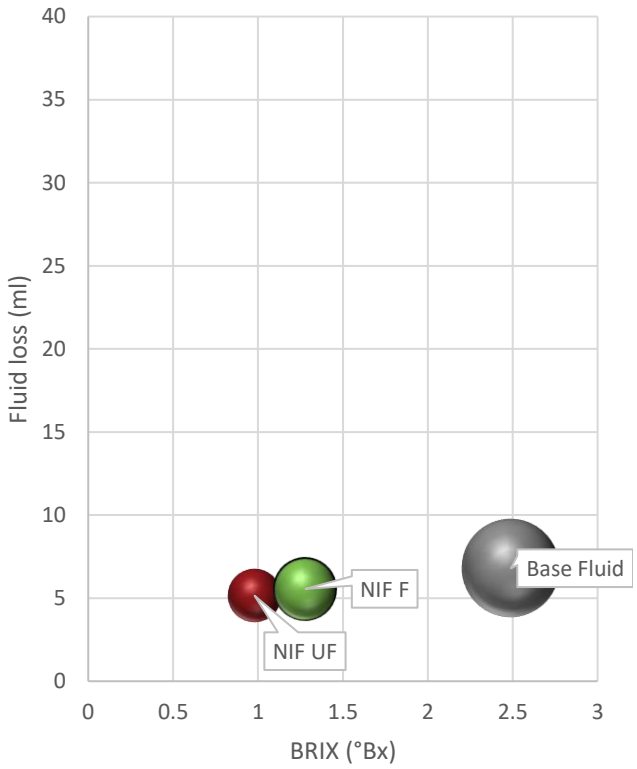

Figure 3-45: Estimated polymer content in fluid filtrate (BRIX residual) for HTHP test on 2.5µm filterpaper. The area of each circle refers to the product of the concentration of polymers and the volume of the filtrate. [V]

The fluid loss test with 20 µm ceramic discs had been conducted at a higher pressure than the test on filterpaper. The plot of the fluid loss and BRIX is presented in Figure 3.46. For the tests with fluids NIF UF and NIF F, the estimated absolute volume of polymers was slightly lower than that found in the test with filterpaper. This may be due to some deposit of the polymers within the disc itself. In contrast, the volume of polymers calculated for the test with the Base Fluid nearly doubled relative to the test on filterpaper, likely indicating that more polymers escape the Base fluid filter-cake as the pressure is doubled.

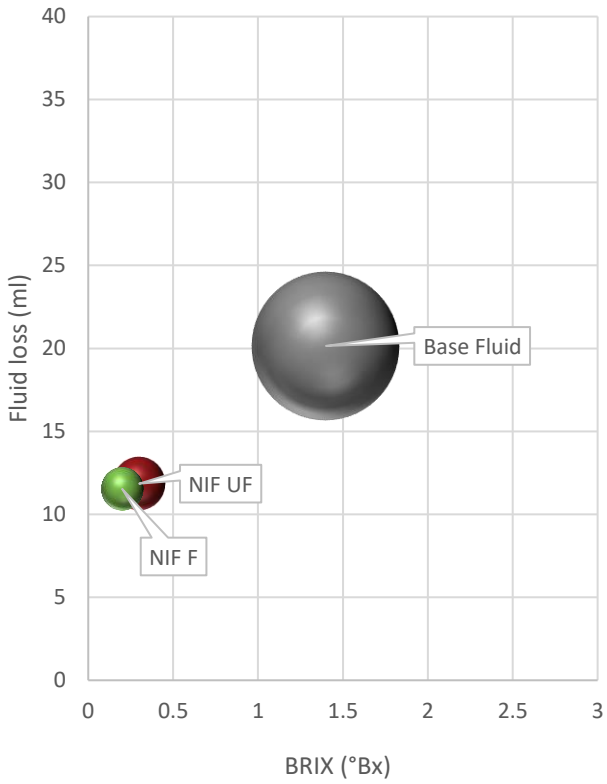

Figure 3-46: Estimated polymer content in fluid filtrate (BRIX residual) for 6.9 MPa (1000 psi) test on 20 µm disc. The area of each circle refers to the product of the concentration of polymers and the volume of the filtrate. [V]

The analysis results of a third test conducted on 10 mm ceramic discs over a period of 24 hours and with 3.49 MPa (500 psi) applied pressure is presented in Figure 3.47. In this test, the measured polymer content in the filtrate from the Base Fluid was noticeably smaller than presented in Figure 3.45 and 3.46. It should be noted that some dilution of the fluid filtrate will naturally occur for the tests conducted on ceramic discs, pre-wetted in water.

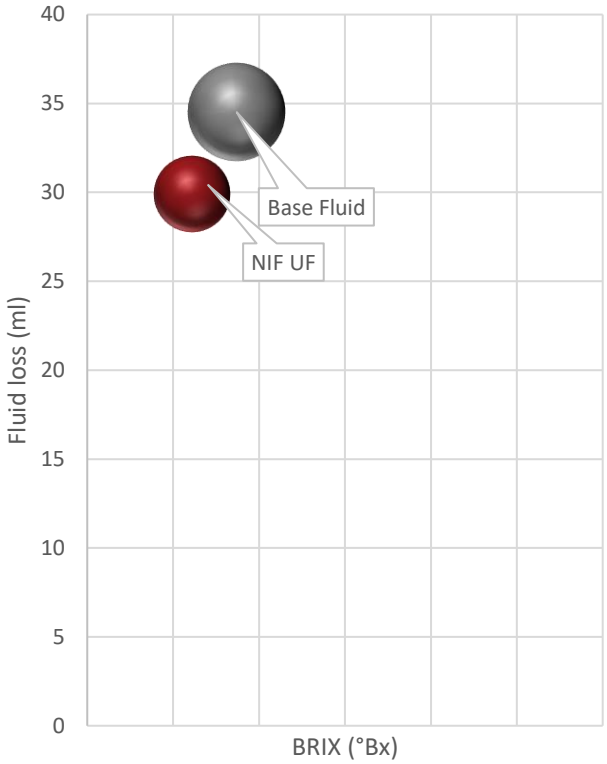

Figure 3-47: Estimated polymer content in fluid filtrate (BRIX residual) for 24 hour and 3.49 MPa (500 psi) test on 10 µm disc. The area of each circle refers to the product of the concentration of polymers and the volume of the filtrate. [V]

The results from the test on Filterpaper may indicate that the fluids containing cellulose fibre bind the polymers better in the filter-cake and hence release less polymers into the formation. Given that the cellulose particles and the polymers both exhibit polar properties, it may be that the polar interaction causes increased inter-particle adhesive and frictional forces. This hypothesis is also supported with the results from the test on 20 µm ceramic discs, where the higher applied pressure nearly doubles the calculated polymer volume in the filtrate for the Base Fluid, whereas it remains relatively unchanged for the two fluids containing fibres.

The 24-hour test on 10 µm ceramic discs yielded lower calculated values of polymers in the filtrate for the Base Fluid. The cause of this may be that due to the finer pore-openings of the disc, more polymers are deposited within the disc, and hence less are transferred as part of the fluid filtrate. The permeability measurements of the 24-hour tests on 10 µm discs were in line with those for the 10 µm discs in the 30-minute test presented in Figure 3.31. A possible conclusion is therefore that the relative reduction in permeability for the Base Fluid on the 10 µm discs are polymer invasion and partial plugging of the discs. In contrast, the two fluids with fibres hold the polymers firmer within the filter-cake and hence lead to a smaller formation damage. This explanation is also consistent with the finding that the inclusion of the cellulose-based fibres (AURACOAT® UF) in test series W-5 lead to significant increases in filter-cake cohesiveness and share strength, as described in Figure 3.44.

Summary of findings:

- The method of mapping fluid filtrate components provides good indications of which of the fluid components that migrate through the test medium and become a part of the fluid filtrate.
- Testing of fluids on filterpaper and discs of different grades yield insight into whether polymers become trapped in the filter-cake, case permeable formation damage within ceramic discs, or become a part of the fluid filtrate.
- Test data become partially distorted as ceramic discs are pre-soaked prior to filtration tests. This does not happen when testing on filter-paper.

3.6.2 Measuring fluid filtrate viscosity

When observing a fluid loss test with a water-based drilling fluid, the initial spurt loss is typically a cloudy and viscous liquid. As the test progresses, the fluid filtrate tends to become clearer and less viscous. Due to the small volumes of fluid filtrate, it is impractical to measure the

viscosity using oilfield viscometers. A method was therefore developed, where the fluid filtrate was flowed through a 0.9 mm diameter and 40 mm long cylindrical needle. By measuring the applied pressure and the flow-rate, the viscosity could be calculated at different shear rates. Figure 3.48 shows an overview of the set-up. The system was calibrated with water as a base fluid, and the standard deviation of the measurements was calculated to be 3.1% with fluid temperatures ranging from 17-20°C.

The method was thereafter applied to a series of fluid loss tests, and the filtrate was divided into a primary and a secondary filtrate. The primary filtrate was collected during the first 30 seconds of the test or until circa 2 ml had been collected. The secondary filtrate was the remaining filtrate collected during the test. The minimum filtrate of 2 ml was set to facilitate effective measurement of the viscosity.

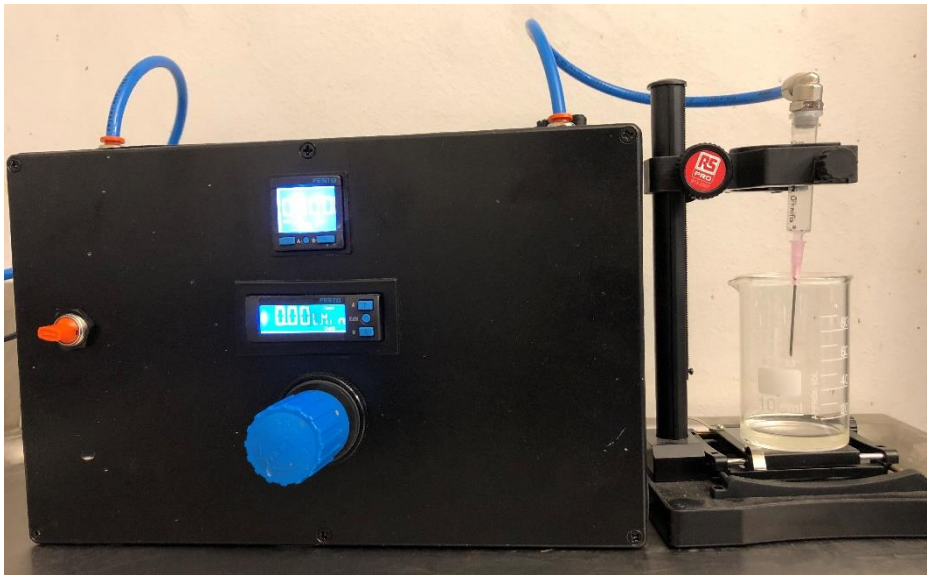

Figure 3-48: Equipment for measuring fluid filtrate viscosity

A series of tests was conducted with fluids W-4 Fluid 1 and 2, as listed in Table 3.11. and the fluid filtrate viscosity was thereafter measured. The fluid loss tests were conducted on filterpaper with thickness of

around 150 µm. Test temperature was 90°C and the applied pressure 3.45 MPa (500 psi). The pore sizes were specified to be 2.5 µm and 22 µm for the two grades of paper being used. Through visual inspection it was evident that the primary filtrates had varying viscosities, whereas the secondary filtrates were much more similar and considerably less viscous. The fluid loss data are presented in Figure 3.49.

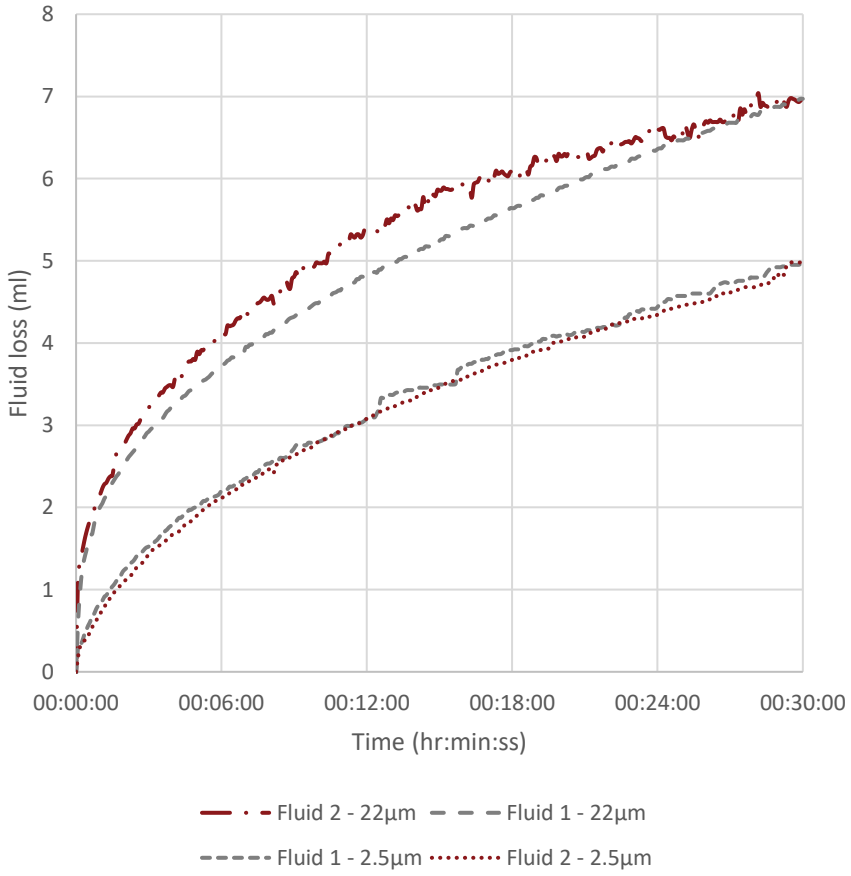

Figure 3-49: Fluid loss measurements

As a reference, the primary filtrates from the 22 µm tests appeared very viscous and more gel-like than rapeseed oil under low-shear conditions. The rapeseed oil is a Newtonian fluid with viscosity of around 60-70

mP*s at 20°C. The dynamic viscosity of water is temperature dependent and circa 1.080 mP*s at 17°C, 1.053 at 18°C and 1.002 at 20°C. At 90°C, the viscosity of water is as low as 0.315 mP*s. The observed properties of the filtrate indicate that viscosifying polymers and other fine particles migrated through the filterpaper during the spurt loss phase. Table 3.14 present the data from the viscosity measurements, conducted at circa 18°C. For the tests conducted, the viscosity of the secondary filtrate was measured to be 1-7% higher than water, with 3 of 4 test being within 2.5% of the viscosity of water. These numbers were calculated as an average of several measurements. No evidence was found regarding the secondary fluid filtrate having a shear rate dependent viscosity. In contrast, the calculated viscosities of the primary filtrates varied with the grading of the filter-paper and with the shear rate. The fluid loss tests showed a distinct spurt loss when the 22 µm filterpaper was used, whereas the spurt loss was minimal with the 2.5 µm filterpaper tests.

Fluid	**Filter-paper**	**Primary**	**filtrate**	**Secondary**	**filtrate**
		Viscosity (mP*s)	Shear rate (1/s)	Viscosity (mP*s)	Shear rate (1/s)
Fluid 1, ($CaCO_3$)	2.5 µm	1.58	4891	1.13	6288
Fluid 1, ($CaCO_3$)	22 µm	9.39 4.91	932 5123	1.06	6113
Fluid 2, ($CaCO_3$ and Ultra-fine fibre)	2.5 µm	1.09	6870	1.06	6171
Fluid 2, ($CaCO_3$ and Ultra-fine fibre)	22 µm	7.65 7.54 7.09 6.72 5.58 5.57 5.12	2329 2795 3027 3726 4891 5589 6754	1.08	6676

Table 3-14: Example of fluid filtrate viscosity measurements

The calculated viscosities of the primary filtrates show clear shear-thinning behaviour for the tests with 22 µm filterpaper, however, the

testing methodology prevents analysis of the filtrate at low shear rates. For these tests, visible traces of $CaCO_3$ particles could be seen in the filtrate, particularly for Fluid 1. Xanthan Gum was used as the viscosifier in both Fluid 1 and 2 and is considered to form a non-gelling hydrocolloid in pure form. However, when mixed with other substances gelling may occur (BeMiller, 2008). Therefore, based on the data collected it is not clear if the primary fluid filtrate is exhibiting Herschel-Bulkley or Power Law behaviour. A simple Power Law regression of the Primary filtrate of Fluid 2 tested on 22 µm filter-paper yields a consistency index, *k*, value of 0.188 $Pa*s^n$ and a flow behaviour index, *n*, of 0.59.

The analysis shows that the secondary filtrate exhibits viscous properties close to that of water at shear rates > 6000 1/s. Neither measured results nor observed behaviour at low shear rates showed signs of the secondary fluid filtrate being distinctively non-Newtonian nor that the viscosity is significantly different from water. In absence of better and more specific data, this indicates that modelling of flow of the secondary filtrate for the tested fluids may be approximated using the dynamic viscosity of water.

A second series of tests were conducted using an oil-based drilling fluid under similar test conditions. The fluid recipe, O-3 Fluid 1, is presented in table 3.15.

Component	**Mass (g) for 350 ml sample**
Base oil, SipDril 4.0	189.6
$CaCl_2$ brine, 30%	98.3
Primary emulsifier	5
Secondary emulsifier	7
Lime – Ca (OH)2, for emulsion stability	7
Organophilic clay, for yield stress and viscosity enhancement	6.5
Gilsonite, for fluid loss control	4
Organophilic lignite, for fluid loss control	2
$CaCO_3$, for density and fluid loss control	40

Table 3-15: Recipe for O-3 Fluid 1 for 350 ml sample

After hot-rolling for 19 hours at 90°C, the electrical stability was measured to be 560 V. The sample was thereafter tested on 2.5 µm and 22 µm filterpaper at 90°C and 3.49 MPa (500 psi). For the tests on 2.5 µm filterpaper, the fluid filtrate was 1.17 ml after 30 minutes and 2.42 ml after 90 minutes. The fluid filtrate had a slight tanned colour, but was transparent, and a measured density of 0.839 g/cm^3 at 20.4°C. The measured viscosity of the filtrate was 5.5 mP*s, calculated as an average of 7 measurements at a temperature of 20.5°C and the fluid appeared to be Newtonian. For reference, the base oil had a measured density of 0.825 g/cm^3 at 19.1°C and a viscosity of 4.93 mP*s at 19.8°C. With the density of the $CaCl_2$ brine being 1.28 g/cm^3 and the viscosity 3.33 mP*s at 20°C, the measured density and viscosity of the fluid filtrate indicates that it contained almost exclusively base oil, likely with some trace of emulsifier. The brine droplets are hence retained as part of the filter-cake.

The test with 22 µm filterpaper yielded a distinct spurt-loss where the fluid was opaque and dark. The fluid loss was 1.70 ml after 30 minutes and 2.37 ml after 1 hour. The measured viscosity and density of the primary filtrate (first 1.2 ml) was 10.26 mP*s and 0.94 g/cm^3 at 20.4°C and no clear deviation from Newtonian behaviour could be observed. The secondary filtrate was transparent and had a viscosity of 5.6 mP*s at 21°C with Newtonian characteristics and a measured density of 0.83 g/cm^3. Due to the higher density and viscosity of the primary filtrate it appears that some of the brine droplets may have passed through the 22 µm filter-paper during the spurt loss phase, whereas the secondary filtrate mainly consists of base oil.

Table 3.16 presents the fluid loss data together with the mass of the filter-cakes and the measured filtrate viscosities. The significantly lower fluid loss values for the oil-based Fluid 3 is also associated with much higher filter-cake mass and higher secondary filtrate viscosities. The fluid filtrate volume was around 4.3 times higher with the water-based fluids than the oil-based fluid on the 2.5 µm filter-paper and 4.1 times higher on the 22 µm filter-paper. In contrast, the secondary viscosities were

around 5 times higher with the oil-based fluid. Also, the filter-cakes with the oil-based fluid had around twice the mass of the filter-cakes of the water-based fluids. Following Darcy's law and estimating fluid viscosities at 90°C it appears that the lower fluid loss for Fluid 3, relative to Fluids 1 and 2, is caused by the higher viscosity of the base oil relative to water, and not due to a lower permeability filter-cake.

Fluid	**Filter-Paper**	**30 min fluid loss (ml)**	**Mass of wet filter-cake (g)**	**Mass of dry filter-cake (g)**	**Primary filtrate viscosity (mP*s)**	**Secondary filtrate viscosity (mP*s)**	**Estimated filter-cake permeabilities (mD)**
Fluid 1 (WBM)	2.5 µm	4.98	2.871	1.228	1.58	1.13	≈ 0.007
Fluid 1 (WBM)	22 µm	6.97	3.126	1.562	≥4.91	1.06	≈ 0.010
Fluid 2 (WBM)	2.5 µm	4.99	2.246	1.033	1.09	1.06	≈ 0.007
Fluid 2 (WBM)	22 µm	6.99	3.125	1.239	≥5.12	1.08	≈ 0.009
Fluid 3 (OBM)	2.5 µm	1.17	5.325	2.164	5.5	5.5	≈ 0.008
Fluid 3 (OBM)	22 µm	1.70	6.111	2.775	10.26	5.6	≈ 0.010

Table 3-16: Summary of filtration and filter-cake data

Summary of findings:

- The method of measuring fluid filtrate viscosity yielded a precise mean value and a standard deviation of 3.1% when measuring the viscosity of a known fluid.
- The measurements indicate that the viscosity of secondary filtrate is around 5-15% higher than the viscosity of the base fluid.
- The viscosity of the primary filtrate varies considerably and reflects that different components of the drilling fluid migrate through the test medium during the spurt-loss phase until an effective filter-cake is formed.

3.6.3 Discussion

The method of mapping fluid components and fluid filtrate using analysis such as turbidity, salinity, conductivity and refractory index (BRIX) functioned to identify concentration of polymers in the fluid filtrate, although the test could not differentiate between the different filtrates. By applying tests on different grades of filterpaper and discs, it was possible to identify polymer migration in water-based fluids.

The testing of fluid filtrate viscosity proved to be quick method for assessing if fluid additives migrate through the test medium or form a part of an internal or external filter-cake. The filtrate viscosity measurements gave consistent results with both water-based fluids and oil-based fluids.

3.7 Determining sealing strength and lift-off pressures for seals in fractured formations

When drilling fractured or vugular formations, partial, severe or even complete losses of drilling fluid may occur. In such situations, the first remedial treatment is typically a pill application with high concentration of LCM materials. The testing of LCM pills is typically conducted using a permeability plugging apparatus and either straight or tapered slotted discs. Table 3.17 list some information on particle size distribution of selected LCM materials used in subsequent tests in this chapter.

Material	D50 (µm)	D90 (µm)	D99 (µm)	Specific gravity	Description
$CaCO_3$ 50	50	150		2.7-2.78	Ground marble
$CaCO_3$ 150	150	325		2.7-2.78	Ground marble
$CaCO_3$ 600	600	1125		2.7-2.78	Ground marble
$CaCO_3$ 1200	1200	1489		2.7-2.78	Ground marble
Graphite 100	100	182		1.82	Resilient graphite
Graphite 400	400	744		1.71	Resilient graphite
Ultra-Fine Cellulose A (AUARFIX UF)		75	90	0.97-1.0	Cellulose Fibre
Ultra-Fine Cellulose B (AURACOAT UF)		75	90	0.97-1.0	Cellulose Fibre
Medium Cellulose (FEBRICOAT C)		197		0.97-1.0	Cellulose Fibre
Granular Cellulose (AURACOAT C)			600	1.3	Cellulose Fibre
Cellulose LCM blend C (BOREMAT C)	425	<3200		1.02-1.04	Cellulose Fibre
Cellulose LCM blend A (AURABRIDGE C)		3800		1.25-1.28	Cellulose Fibre

Table 3-17: Particle size distribution of selected Lost Circulation materials

3.7.1 Testing on slotted discs

A series of tests were conducted following LCM pill application recipes frequently used in the North Sea according to Grelland [XV]. The LCM mixtures were blended into a 1.4 kg/m^3 barite-weighted water-based fluid and a 1.49 kg/m^3 barite-weighted oil-based field fluid as per Table 3.18 and conducted on slotted discs of different slot widths as presented in Figure 3.50 [VI]. The LCM pills were not hot-rolled prior to testing to illustrate the application of a freshly mixed lost circulation pill.

Recipe for 1 litre	**Pill 4: 350 kg/m3 granular LCM (g)**	**Pill 5: 450 kg/m3 granular LCM (g)**	**Pill 6: 155 kg/m3 Cellulose LCM blend (g)**
Base fluid (ml)	850	808	850
$CaCO_3$ 150	100	100	
$CaCO_3$ 600	100	100	
$CaCO_3$ 1200		75	
Graphite 100	100	100	
Graphite 400	50	75	
Cellulose LCM blend C (BOREMAT C)			155

Table 3-18: LCM blends for slotted disc tests for 1 litre sample [VI]

Figure 3-50: Examples of slotted discs [VI]

The primary findings of the tests were that the LCM pills with $CaCO_3$ and resilient graphite showed limited sealing capacity above 1.5 mm slot widths and that the performance was significantly better in the water-based fluid than in oil-based fluid. In these recipes, the D90 value of the coarsest component, applied at 100 kg/m^3, was specified to be 1489 µm. The results with $CaCO_3$ and graphite thus do not refute the conclusions of Alsaba et al. [5], which suggest that the D90 value of the particles should be ≥ 6/5 of the fracture width. In contrast, the cellulose LCM blend C sealed fractures up to 5 mm in both fluids, with a D90 value of 3200 µm, and no significant differences were observed in sealing capacity when the base fluid was changed from water-based to oil-based. The pressure charts for the tests are presented in Figure 3.51 and 3.52. The results for the cellulose LCM blend C indicate that certain LCM types may seal openings significantly wider than the recommendation of Alsaba et al. based on the size of the particles. A reason for this may be high cohesive or frictional forces between the particles of LCM blend C when these are forces together due to differential pressures.

A limitation with such tests is that they do not present any information on the stability of the LCM seal with regards to disturbances in the wellbore, such as e.g. swabbing, where the annular pressure is reduced and potentially leads to a temporary underbalance. Another disadvantage is that the straight slotted discs do not replicate the tapering that may typically be found in induced fractures nor the friction which is experienced when LCM is pumped into a natural facture.

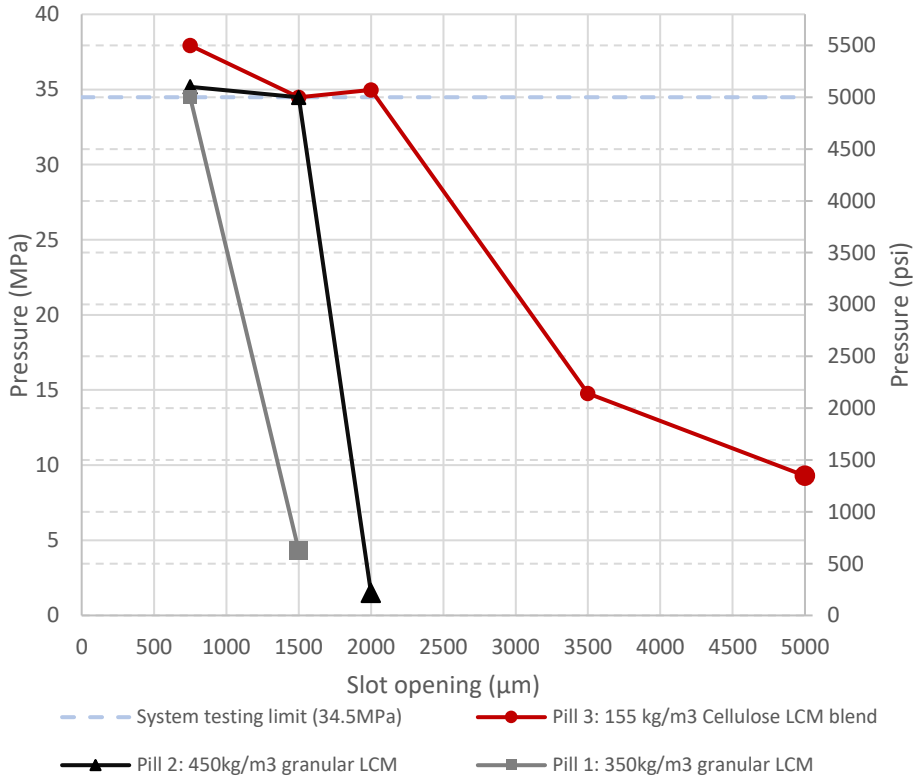

Figure 3-51: Pressure build-up charts for LCM pills in water-based fluids [VI]

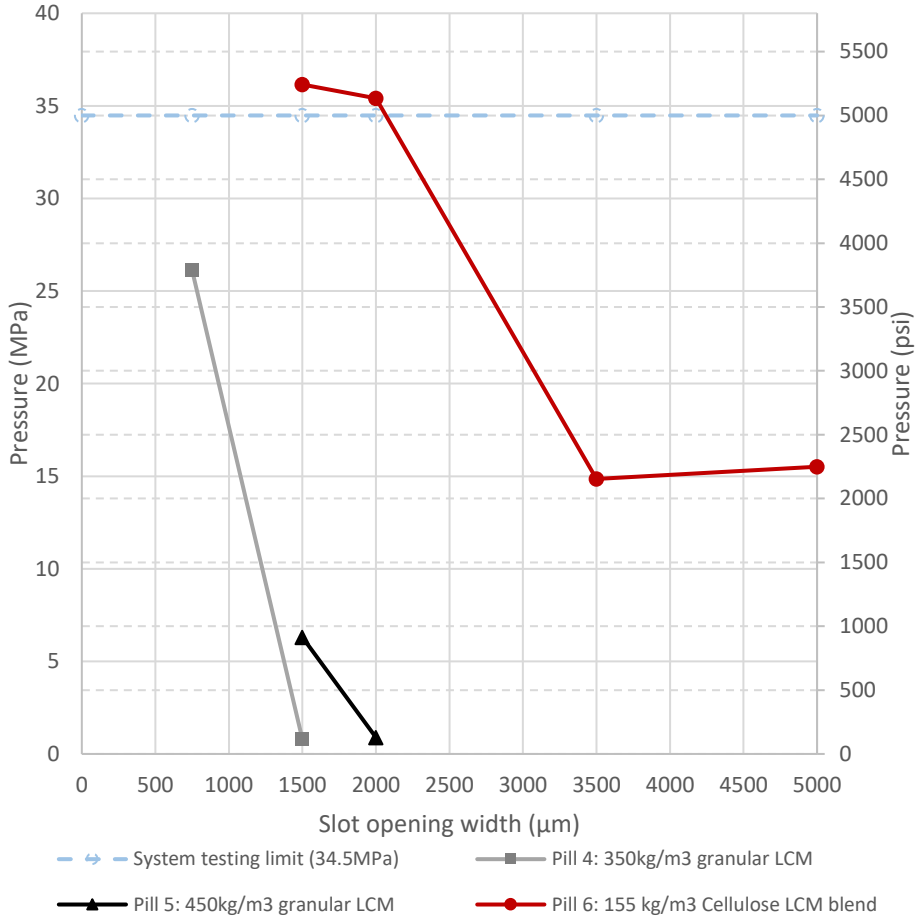

Figure 3-52: Pressure build-up charts for LCM pills in oil-based fluids [VI]

3.7.2 Testing on tapered discs

A set-up was designed where tapered discs could be made up of two halves placed into a steel holder. The assembly could then be placed into the test cell in both axial directions. This enabled first measuring the sealing pressure of the LCM, and thereafter reverse the assembly into the test cell and measure the brine pressure required to remove the LCM plug from the tapered slot. The surfaces of the tapered slots were a bit rough

to simulate friction between the LCM and a formation fracture. Figure 3.53 shows an example with various disc halves and how they were placed into the holder.

(a) (b)

Figure 3-53: Example with tapered discs placed into the holder (a) and the disc halves (b)

Tests with different fluid and LCM mixtures were conducted with three different plug arrangements, where the smallest slot opening was a taper from 1.6 mm to 0.9 mm, the medium tapered from 3.4 mm to 2.5 mm and the widest from 5.0 mm to 3.4 mm. The plugs each had a depth of 22 mm where LCM particles could be deposited.

The first tests were conducted with a 350 kg/m^3 $CaCO_3$ pill in a WBM, where the largest particles (100 kg/m^3) had a D50 value of 1200 µm and a D90 value of 1489 µm. The pill effectively sealed the 1.6 mm to 0.9 mm slot but failed to seal the others. Figure 3.54 present the sealing pressure, which exceeded 32 MPa, without failing, and the reverse pressure plot. When reversing the fluid pressure, only a pressure of 0.07 MPa was required to dislocate the entire LCM plug from the slot. This indicates that an LCM plug made from $CaCO_3$ alone, may have a low

cohesive strength or for other reasons could be easily disturbed by circulation of the wellbore fluid or changes in wellbore pressure.

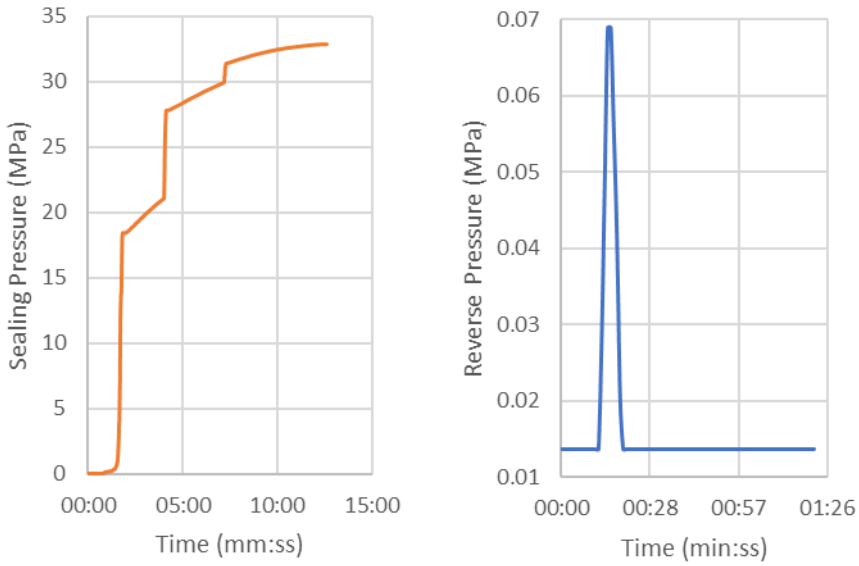

(a) (b)

Figure 3-54: Sealing Pressure build-up chart (a) and Reverse Pressure chart (b) for test of CaCO3 on 1.6 to 0.9 mm tapered slot

As a contrast to the test with $CaCO_3$, the cellulose LCM blend C was tested both as a self-sealing pill and a squeeze pill with the slot which tapered from 5.0 mm to 3.4 mm. The squeeze pill application was mixed with 200 kg/m^3 of the LCM blend into saltwater viscosified by addition of 1.15 kg/m^3 xanthan gum. The pill was placed into the test cell and dehydrated for 5 minutes by application of a low pressure (0.1 MPa). Thereafter, a water-based drilling fluid containing 85.5 kg/m3 of $CaCO_3$ (< 53 µm) and 14.25 kg/m^3 of Ultra-fine Cellulose (AURACOAT® UF, D90 of 75 µm) was applied to provide the fine sealing before higher pressures were applied. For the self-sealing pill, the LCM blend C was

applied at a concentration of 155 kg/m^3 into a barite-weighted water-based drilling fluid with specific gravity of 1.4. The sealing pressure plots are presented in Figure 3.55.

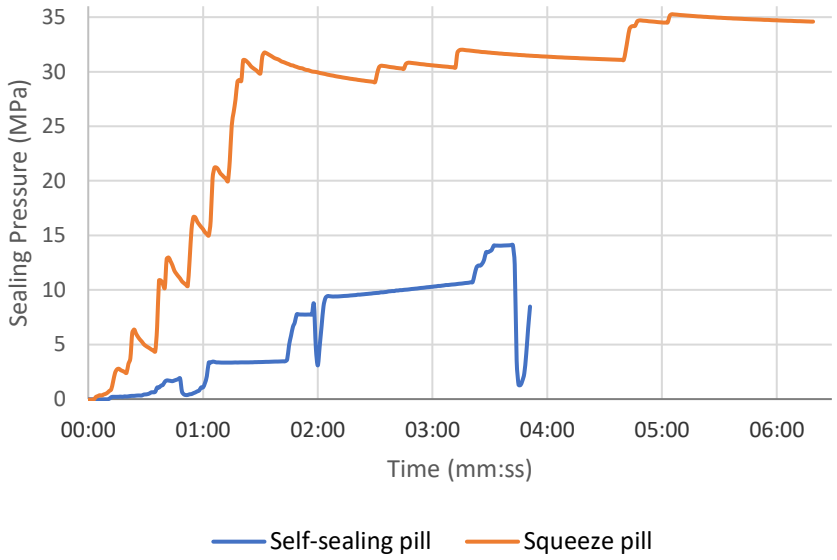

Figure 3-55: Sealing pressure build-up of self-sealing and squeeze pills on 5.0 to 3.4 mm tapered slot

For the tests with cellulose LCM blend C, the squeeze pill obtained a higher integrity seal of the largest tapered slot. Once the squeeze pill had been de-fluidized, and the drilling fluid with ultra-fine cellulose had been applied, a sealing pressure exceeding 35 MPa was achieved without intermediate seal failure. To remove the LCM plug from the slot, a reverse pressure of nearly 1.4 MPa was required, as shown in Figure 3.56. The self sealing pill obtained a much lower sealing pressure of 14 MPa, and since the seal was ruptured, no reverse pressure could be tested.

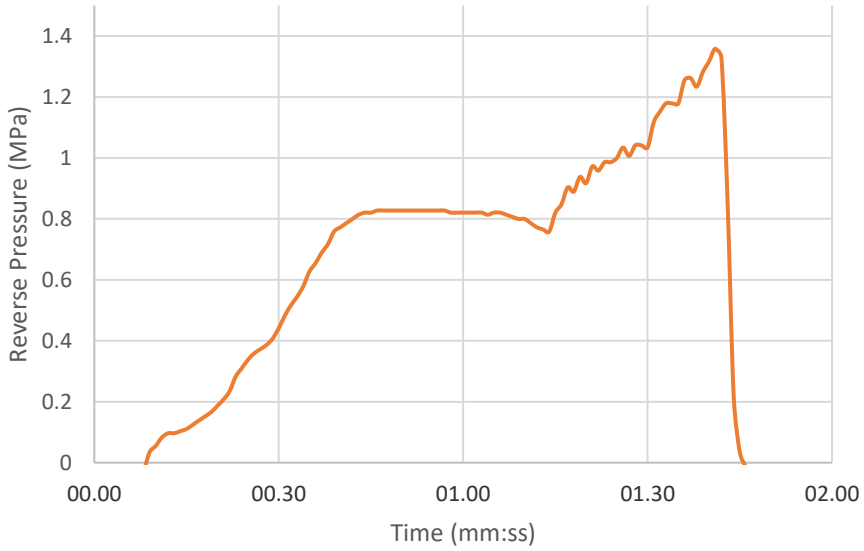

Figure 3-56: Reverse pressure build-up of squeeze pill

A summary of sealing and reverse pressures is presented in Table 3.19. The maximum sealing pressures held over a 60 second period were in line with the results from tests on straight slotted discs for the CaCO3 and Graphite mixtures. For the cellulose blends, the sealing strength increased considerably for the widest slots when the squeeze pill application was applied. Additional information was also obtained from applying a reverse pressure with brine to dislocate the LCM plugs from the tapered slots. A consistent observation was that the inclusion of $CaCO_3$ in an LCM blend reduced the reverse pressure resistance. The highest reverse pressures were measured with squeeze pills with cellulose LCM blends, with the single highest value being 1.36 (MPa), or around 200 psi, on the 5.0-3.4 mm tapered slot.

LCM pill	Largest particle D90 (µm)	Slot (mm)	Max. Sealing Pressure (MPa)	Max. Reverse Pressure (MPa)
350 kg/m^3 $CaCO_3$ pill	1489	1.6-0.9	>32	0.07
350 kg/m^3 $CaCO_3$ pill	1489	3.4-2.5	Failed to seal	-
450 kg/m^3 $CaCO_3$ /Graphite pill	1489	1.6-0.9	>45	0.27
450 kg/m^3 $CaCO_3$ /Graphite pill	1489	3.4-2.5	Failed to seal	-
85.5 kg/m^3 Granular cellulose and 28.5 kg/m^3 Medium cellulose squeeze pill	D99 of 600µm	1.6-0.9	>35	0.20
85.5 kg/m^3 Granular cellulose and 28.5 kg/m^3 Medium cellulose squeeze pill, $CaCO_3$ weighted	D99 og 600µm	1.6-0.9	>35	0.14
155 kg/m^3 LCM blend C self-sealing pill, 1.25 sg $CaCO_3$ weighted fluids	3200	1.6-0.9	>35	0.48
155 kg/m^3 LCM blend C 1.25 sg self-sealing pill, $CaCO_3$ weighted fluids	3200	3.4-2.5	>35	0.43
155 kg/m^3 LCM blend C self-sealing pill	3200	5.0-3.4	14	Broken disc
200 kg/m^3 LCM blend C squeeze pill	3200	1.6-0.9	>35	0.78
200 kg/m^3 LCM blend C squeeze pill	3200	3.4-2.5	>35	0.43
200 kg/m^3 LCM blend C squeeze pill	3200	5.0-3.4	>35	1.36
172 kg/m^3 LCM blend A squeeze pill	3800	1.6-0.9	>35	0.97
172 kg/m^3 LCM blend A squeeze pill	3800	3.4-2.5	>31	0.42
172 kg/m^3 LCM blend A squeeze pill	3800	5.0-3.4	>35	0.82
172 kg/m^3 LCM blend A squeeze pill, weighted with 261 kg/m^3 $CaCO_3$	3800	3.4-2.5	>31	0.11
172 kg/m^3 LCM blend A squeeze pill, weighted with 261 kg/m^3 $CaCO_3$	3800	5.0-3.4	>35	0.05

Table 3-19: Summary of maximum Sealing and Reverse Pressures

Summary of findings:

- Testing on tapered discs were consistent with results obtained with slotted discs although identical slot openings were not tested.
- Granular LCM such as $CaCO_3$ and resilient graphite consistently sealed slot openings up to 1 mm at pressures exceeding 30 MPa (4350 psi). With slot openings of 1-2 mm, sealing pressures were variable, and with slots larger than 2 mm, no seals were achieved.
- The tested cellulose-based LCM showed sealing abilities up to 5 mm slots at high applied pressures.
- For cellulose-based LCMs, the squeeze pill method showed higher sealing strength then the self-sealing pills.
- Higher reversal pressures were obtained with cellulose-based materials than granular materials for the tapered disc tests.
- Addition of $CaCO_3$ to the cellulose-based LCM mixtures consistently reduced the reverse pressures required to dislocate the LCM plug from the tapered slots.

3.8 Assessing induced fracturing and fracture sealing during drilling

When designing a fluid for sealing permeable formations, particles are normally selected based on one of several recognised particle size selection methods. A selection of these is described in section 4.1. Two such methods are the Ideal Packing Theory (IPT), proposed by Kaeuffer (1973) and Abrams rule (Abrams, 1977). The IPT aims at selecting particles to form a low porosity and low permeability filter-cake. Particle sizing is claimed to be ideal when a linear relationship between the cumulative volume percentage of particles and the square root of the particle diameter is obtained. The Abrams rule aims at sealing a formation effectively without causing excessive solids-invasion and

permeable formation damage. Other methods, such as the one proposed by Alsaba et al. (2017) is aimed at sealing fractures.

Fracture initiation and fracture growth are conditions required for lost circulation to occur through an induced fracture. During drilling, leak-off tests (LOT) may be conducted to identify the fracture initiation pressure (FIP) and the fracture propagation pressure (FPP). These pressures are a function of the in-situ stresses, the mechanical properties of the formation, the drilling fluid and the complex interaction of these factors. Feng et al. [23] presented a review on fracture initiation and fracture propagation and highlighted some important findings. They concluded that the recorded leakoff pressure may be higher than the actual FIP as the drilling fluid may contain particles that seal the initial fracture. Therefore, an observed leakoff pressure may be a filter-cake breakdown pressure. Further, they conclude that wellbore strengthening may be achieved through fracture plugging and that this is particularly effective in conditions where the pore pressure is significantly smaller than the minimum horizontal stress, such as for depleted reservoirs.

Ma et al. (2019) tested various fluids as part of a core fracturing experiment. They used 100 mm diameter and 140-150 mm length cores with a circular hole of 10 mm. The cores were made of Portland cement and quartz sand. Their studies showed that water-based fluids achieved fracture pressures ranging from 19 MPa to 26.6 MPa, whereas the fracture pressures for OBM, with the same LCM additives, ranged from 12.3 MPa to 22.5 MPa. On average, the fracture pressures were 52% higher with WBM and at the same time the API fluid loss values being on average 26% higher with WBM. They concluded that adding barite as a weighting agent increased the fracture pressure, whereas the inclusion of nanomaterials was found to have little effect.

The challenge of induced fracturing is relevant for drilling of wells for oil and gas production, geothermal wells and wells for CO_2 injection. When it comes to laboratory testing, the testing of static fluid loss using

ceramic discs is normally separated from testing with a Permeability Plugging Apparatus and slotted steel discs.

A method was therefore developed to assess the functionality of drilling fluids in situations where a fracture is induced in a permeable medium. The method involves using a conventional permeability plugging apparatus designed for application of industry standard ceramic discs. By making the surface of the end cap slightly uneven, the inflexible ceramic discs fracture at certain applied fluid pressures. Samples of laboratory made WBM and OBM field fluid were treated with different LPMs and hot-rolled for 16 hours at either 112° or 120°C to reflect different reservoir temperatures. Included in each hot-rolling cell was a 135 mm long threaded M16 stainless steel bar, to simulate mechanical wear that LPM particles would be exposed to during circulation in a field operation. The testing was conducted at an initial temperature of 70°C and rising towards 75-78°C during each test. An overview of the equipment is presented in Figure 3.57.

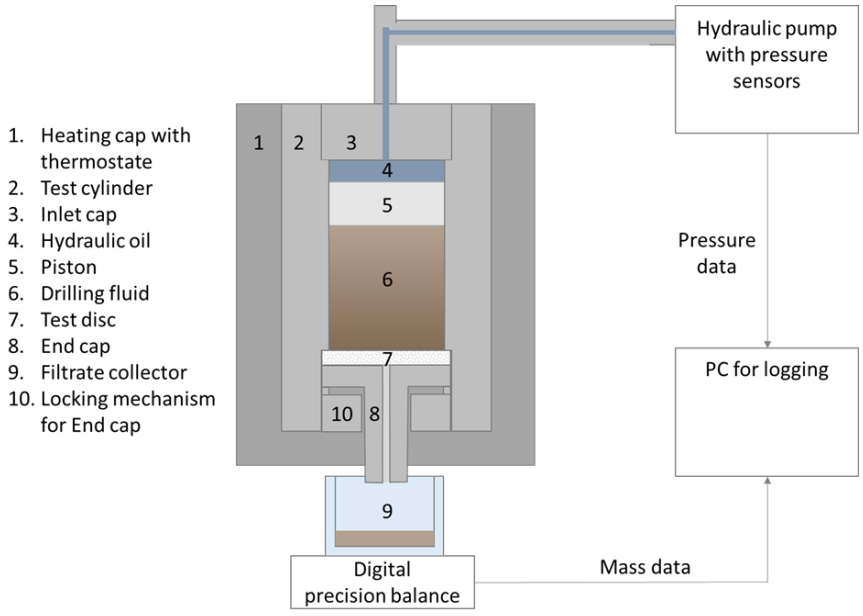

Figure 3-57: Schematic of Permeability Plugging Apparatus and data capture setup [IX]

3.8.1 Results and observations

Three base fluids were used for the study. Each of these were tested with different combinations of loss prevention materials. The LPMs were added prior to hot-rolling with the threaded steel rod. For Fluid 1, hot rolling was conducted at 112°C for 16 hours. For Fluids 2 and 3, the temperature was 120°C. Fluids 1 and 2 were laboratory fluids that had been optimised for reservoir drilling, however without the presence of drilled solids. To simulate the accumulation of fine drilled solids in a carbonate reservoir, $CaCO_3$ particles with a D50 value of 50 µm was added to some of the tests to identify any differences in sealing performance. The tests were also conducted with and without various cellulose based LPMs as presented in Table 3.20.

Description	**Fluid 1**	**Fluid 2**	**Fluid 3**
Base Fluid	Fluid 1: 1.09 sg KCl-polymer fluid, 85.5 kg/m^3 $CaCO_3$, 1-150µm	Fluid 2: 1.10 sg KCl-polymer glycol fluid, 57 kg/m^3 $CaCO_3$, 1-15µm	Fluid 3: 1.62 sg oil-based field fluid with drilled solids, sieved through API140, 106 µm sieve
A) Cellulose fibre A (D90=75µm)	14.25 kg/m^3	8.55 kg/m^3	
B) Cellulose fibre B (D90=75µm)		8.55 kg/m^3	
C) $CaCO_3$ (D50 = 50µm, D100 = 150 µm)	28.5 kg/m^3	57 kg/m^3	
G) Granular cellulose (D99=600µm)		28.5 kg/m^3	28.5 kg/m^3

Table 3-20: Fluid descriptions and additives, series W-6 Fluid 1 and 2 and series O-4 Fluid 3 [IX]

Earlier studies have shown that non-degraded $CaCO_3$ with a D50 value of 50 µm can effectively seal 120 µm pore-size ceramic discs when applied in a concentration of 85.5 kg/m^3 [I]. This is in line with the Abrams rule, which recommends using particles with a D50 value ≥ 1/3 of the formation average pore size. However, after exposing the fluid to mechanical wear during the hot-rolling process it has been shown that the $CaCO_3$ degrades sufficiently to fail a 120 µm ceramic disc test even

when applied in 114 kg/m^3 concentration [V]. Applying the logic of the Abrams rule, this indicates that the D50 value of the $CaCO_3$ particles degraded to significantly less than 40 µm during the hot-rolling process using the threaded steel rod. This is also consistent with the findings of Scott et al. [60], where $CaCO_3$ (ground marble) particles larger than 44 µm were shown to degrade during exposure to shearing.

Fluids 1 and 2 were both water-based. The main differences were the finer size of $CaCO_3$ particles in Fluid 2 and the inclusion of polyethylene glycol (PEG) and slightly higher concentration of Xanthan Gum. Jiang et al. (2011) showed that PEG has good effect on shale and gas-hydrate inhibition and can prevent pollution related to presence of calcium and magnesium ions. The specified D50 value of the $CaCO_3$ in Fluid 2 was 5 µm, thus indicating that it would be effective for sealing of formations with pore-size up to 15 µm, following the Abrams rule. The viscosity (at 49°C) of Fluid 2 was noticeably higher than that of Fluid 1 after hot-rolling, as presented in Figure 3.58. The difference in viscosity could be expected to impact the fluid-loss and fracture sealing ability of the fluid.

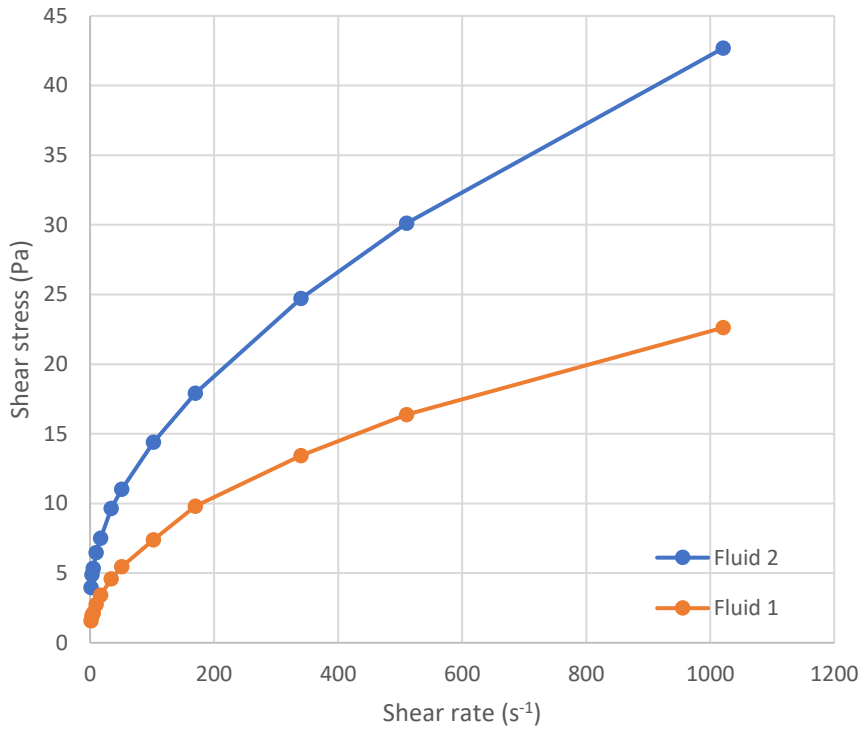

Figure 3-58: Flow curves of Fluids 1 and 2 after hot-rolling [IX]

The fractured disc tests were conducted on ceramic discs with a mean pore-size of 10µm. The discs were selected on the basis of representing a low- to moderate permeability formation such as chalk or limestone, thus creating a contrast to the size of the induced fractures. This enabled a clear separation of when fracturing occurred and a steady state situation before fracturing or after a fracture had been successfully sealed. Figure 3.59 shows the pressure and fluid loss plots for Fluid 1 with an additional concentration of $CaCO_3$, referenced as Fluid 1+C, and with the addition of cellulose fibre A, referenced as Fluid 1+A. During the early stages of the test with Fluid1+C, a slight cracking noise could be heard when the pressure reached 7-8 MPa, and a fluid loss of circa 10 ml was observed. Thereafter, the fluid loss remained at a steady state until the pressure reached 16 MPa, after which, a more severe fracturing of the disc

occurred. After this point, no stable pressure could be achieved above ca 1 MPa.

The test with Fluid 1+A started in a similar manner, with light fracturing occurring around 7-9 MPa and a corresponding fluid loss of around 2 ml. Thereafter, with higher applied pressure the disc fractured multiple times and was repeatedly re-sealed as pressure was increased to 21 MPa.

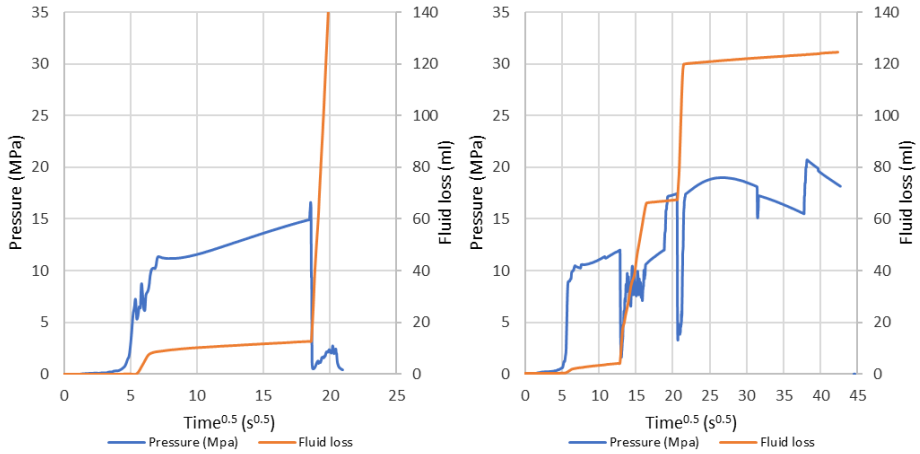

(a) (b)

Figure 3-59: Pressure build-up and fluid loss for Fluid 1+C (a), and Fluid 1+A (b) [IX]

Figure 3.60 shows the disc and the induced fracture when testing with Fluid 1+C. A clear thin cut can be seen in the filter-cake. This crack led to the high fluid loss. The fracture was measured to be in the range of 74-126 µm on the disc surface. The applied $CaCO_3$ was not able to re-seal this fracture because of the too small a particle size distribution or low filter-cake cohesion.

(a) (b) (c)

Figure 3-60: Disc after test with Fluid 1+C, with filter-cake (a), after removing filter-cake (b) and measurement of fracture opening (c) [IX]

The disc with filter-cake for the tests with Fluid 1+A is presented in Figure 3.61. After fracturing, the filter-cake re-formed and thus an intact filter-cake can be observed, despite the induced fracture being in the range of 224-365 µm on the surface. Comparing the results with the test with Fluid 1+C, it is clear that the addition of the ultra-fine cellulose fibres improved the capacity to re-seal the disc and hold a much higher pressure after re-sealing. Given that the fracture width greatly exceeded the size of the Cellulose fibre A particles, the re-sealing was likely not due to particle plugging at the surface, but potentially due to the properties of the filter-cake. It may be that higher cohesion and shear strength in the filter-cake facilitates the re-establishment of a filter-cake after the fracture is induced. Following Klungtvedt et al. [VII], such a cohesion is expected. However, the strength of the present cohesion is unknown.

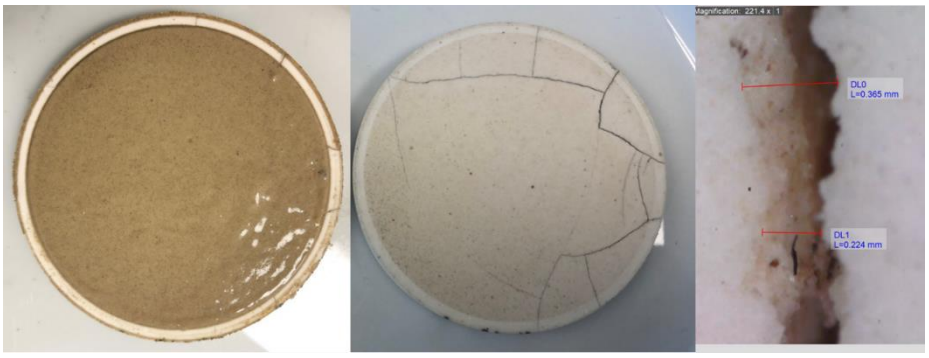

(a) (b) (c)

Figure 3-61: Disc after test with Fluid 1/ 14.25 kg/m3 Cellulose fibre A, with filter-cake (a), after removing filter-cake (b) and measurement of fracture opening (c) [IX]

The experiments with the other fluids followed the same procedure and the results are presented as two tests side-by side for ease of comparison. To assess the consistency of the testing, two tests were conducted with Fluid 2 without additives and Fluid 2 with extra $CaCO_3$, to reflect the accumulation of fine drilled solids. These two fluid compositions are thus relatively similar to the test with Fluid 1+C. The recorded pressure and fluid loss data are presented in Figure 3.62 and show a behaviour consistent with Fluid 1+C. Both tests show low fluid loss as the pressure builds towards the first significant fracturing. The test with Fluid 2 without additional LCM was terminated after being fractured at a pressure of 16 MPa, after which it was difficult to obtain a good sealing of the induced fracture. The test with Fluid 2+C fractured at around 9 MPa and could not be re-sealed to achieve higher pressures thereafter. The addition of coarser size $CaCO_3$ could not be seen to improve the ability of Fluid 2 to re-seal the disc after fracturing. This may be due to inadequate size of the added particles, or it may be related to low filter-cake cohesion, or more likely a combination of the two factors, given that Fluid 1+A effectively re-sealed the fractured disc.

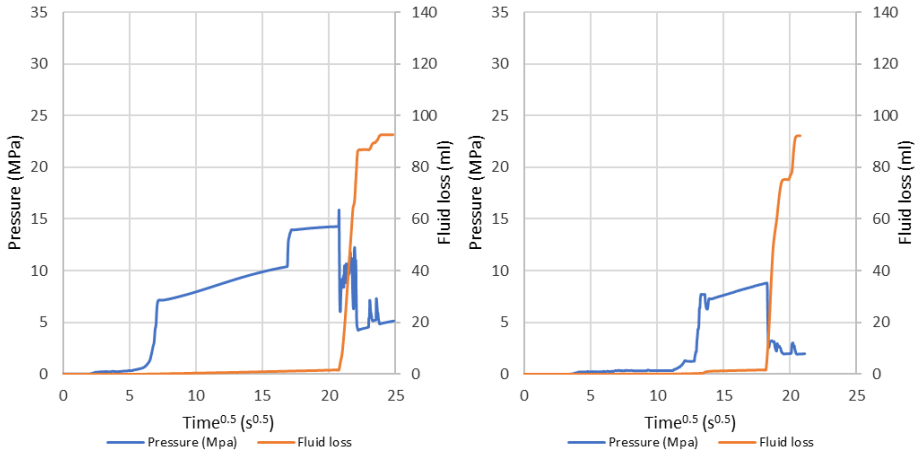

(a) (b)

Figure 3-62: Pressure build-up and fluid loss for Fluid 2 (a), and Fluid 2+C (b) [IX]

The testes with Fluid 2 were then repeated with the addition of 28.5 kg/m3 of the Granular cellulose, with and without additional $CaCO_3$. The pressure and fluid loss plots, shown in Figure 3.63, reveal a very significant improvement in performance. As the discs fractured, a seal was re-established with steps in the fluid loss of only 0.2-0.5 ml, hence showing an excellent ability to seal fractures as they were occurring. The total fluid loss for each of the tests were around 4 ml and peak pressures of 27-28 MPa were held without the seals failing. From the pressure and fluid loss plots it is not evident that the additional $CaCO_3$ alters the performance of the fluid.

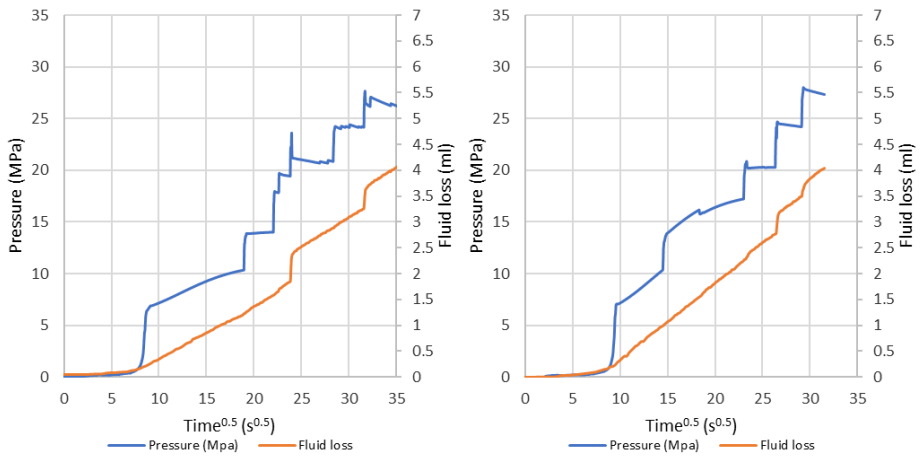

(a) (b)

Figure 3-63: Pressure build-up and fluid loss for Fluid 2+G (a), and Fluid 2+G+C (b) [IX]

As a next step, the tests with Fluid 2+G and Fluid 2+G+C were repeated with the addition of 8.55 kg/m^3 of Cellulose fibre B in two tests and Cellulose fibre A in another test. The pressure and fluid loss data of the tests with Cellulose fibre B are shown in Figure 3.64. Overall, the data show similar results as those from the first two tests with the Granular cellulose, with fluid loss ranging from 3.7 – 5 ml under pressures ranging up to 28 MPa. The test with Cellulose fibre A yielded a consistent result as with Cellulose fibre B, since the 2% lower recorded fluid loss is likely within the normal variations of testing.

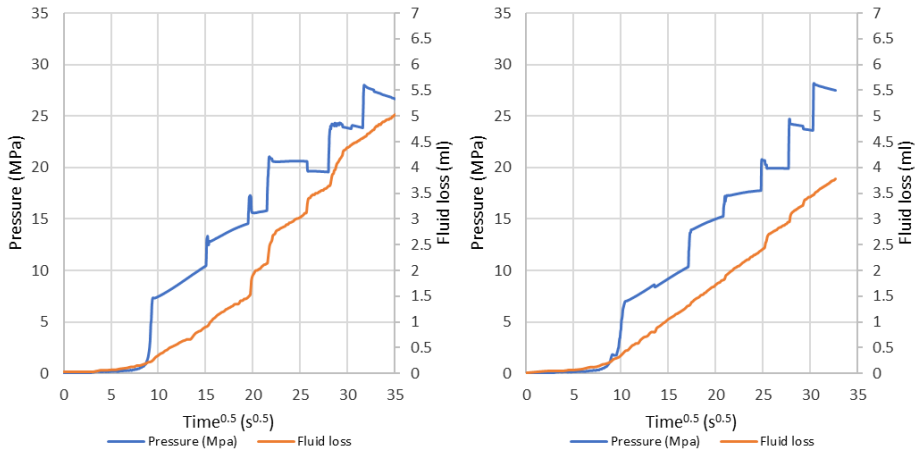

(a) (b)

Figure 3-64: Pressure build-up and fluid loss for Fluid 2+G+B, and Fluid 2+G+B+C (b) [IX]

In summary, the results with water-based fluids provided a consistent set of data, thus indicating that the testing methodology provided data that were repeatable and reliable, despite the natural variations in disc fracturing.

To test the methodology with oil-based fluids, two tests were set up with a 1.62 sg oil-based field fluid, with and without the addition of 28.5 kg/m^3 of the Granular cellulose. The pressure and fluid loss plots of Fluid 3 and Fluid 3+G are presented in Figure 3.65. For Fluid 3 the results are almost identical to the test results with the water-based Fluids 1 and 2 without Granular cellulose. Once the disc fractured at around 9 MPa, a satisfactory re-sealing could not be achieved, despite the high solids content of the drilling fluid. As for the water-based fluids, the addition of 28.5 kg/m^3 of the Granular cellulose enabled a re-sealing of the disc after fracturing and the pressure was elevated as high as 32 MPa. The oil-based fluid loss was, however, considerably higher than that of the tests with water-based once the fractures were induced. The fluid loss was around 30 ml with Fluid 3+G vs around 4 ml with Fluid 2+G.

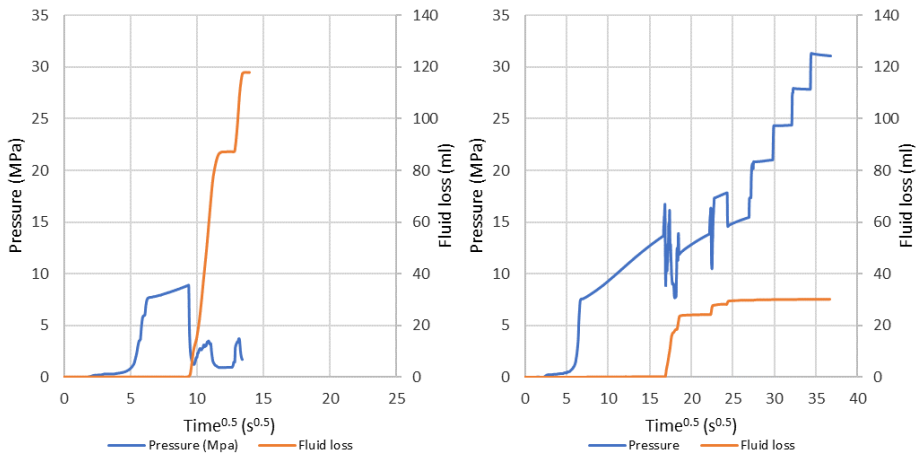

(a) (b)

Figure 3-65: Pressure build-up and fluid loss for Fluid 3 (a), and Fluid 3+G (b) [IX]

For time periods without any noticeable disc fracturing, the permeability of the filter-cakes for Fluid 2 were estimated using Equations 3.4 and 3.18 [V]

For simplicity, the viscosity of the fluid filtrate was set to 2 mPa*s, which is equivalent to twice the dynamic viscosity of water at 20°C. The value of k_F was based on a measurement of the moisture content of the filter-cakes, which averaged 50%, and the calculated solids, fibre and polymer contents of the fluids, taken from the fluid recipes. As such, the calculated permeabilities are primarily to be used for comparison within a series of tests for one base fluid, rather than being scientifically precise. A measurement of the fluid filtrate viscosity at the relevant temperature would yield more precise results and may facilitate comparison between fluids.

Figure 3.66 shows the estimated filter-cake permeabilities for Fluid 2. For Fluid 2, without any other additives, the permeability was calculated to be 0.017 and 0.019 mD for two different average pressures. Fluid 2+C contained only a very fine $CaCO_3$ particles, with a D50 value of 5 µm

before hot-rolling and degradation, which may explain the low permeability values. With only two data-points, no trend or correlation between permeability and differential pressure can be established with an acceptable level of precision. Once coarser $CaCO_3$ particles were added, the calculated permeability more than doubled to 0.047 mD for Fluid 2+C. As expected, this indicates that the larger particles, which may be adequate for sealing a coarser formation, increases the permeability of the external filter-cake. For all the three tests with additional $CaCO_3$, the permeabilities increased relative to the tests with only the 5 µm $CaCO_3$. It was noted that all the tests containing cellulose, showed lower permeabilities at higher pressures. The effect is likely caused by the compression of the fibres and hence an improved sealing of the gaps between the particles in the filter-cake. For the test with Granular cellulose, but without Cellulose fibre B, the permeability was significantly higher when the slightly coarser $CaCO_3$ particles were added to the fluid. This effect was eliminated when Cellulose fibre B or A were present. Considering that the Cellulose fibre B and A particles were of relatively similar size as the $CaCO_3$ particles added to reflect drilled solids, the results indicate that the fibres adapt better than the $CaCO_3$ to reduce filter-cake permeability.

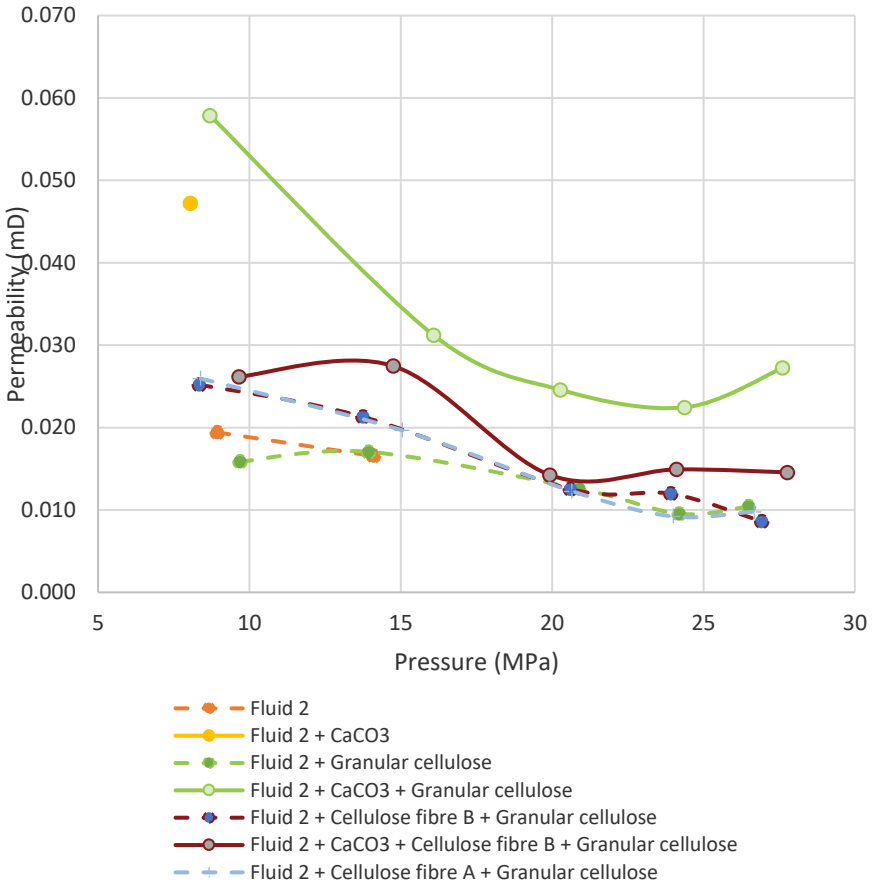

Figure 3-66: Calculated permeability of the filter-cakes of Fluid 2 with different additives and at different pressures [IX]

Further, when analysing the test discs and the filter-cakes, the patterns observed in the pressure and fluid loss charts were further established. Firstly, Figure 3.67 shows the discs for base Fluid 2 and Fluid 2+C with $CaCO_3$. Only small fractures in the discs could be observed, and thin hair-like cuts could be seen in the filter-cakes. Considering that both the tests yielded very high fluid loss once the discs had fractured, this indicates that the cohesive strength of the filter-cake or the sealing ability of the particles were ineffective to control the flow at the applied pressure.

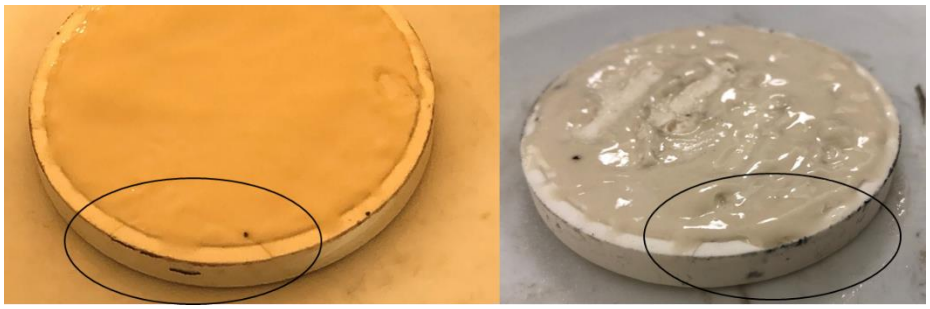

(a) (b)

Figure 3-67: Discs from tests of Fluid 2 (a) and Fluid 2+C (b) [IX]

For the tests with Granular Cellulose, higher pressures had been applied, and more severe disc fracturing had occurred despite the fluid loss being limited to 4 ml for both tests. As presented in Figure 3.68, the dark Granular Cellulose particles can be seen at the fracture opening. A similar sealing mechanism is presented in Figure 3.69, for Fluid 2+G+C, although the disc fracturing was even more severe. Specifically, it can be seen in Figure 3.69 (b) that the Granular cellulose particles gathered to form a seam in the filter-cake above the induced fractures in the disc.

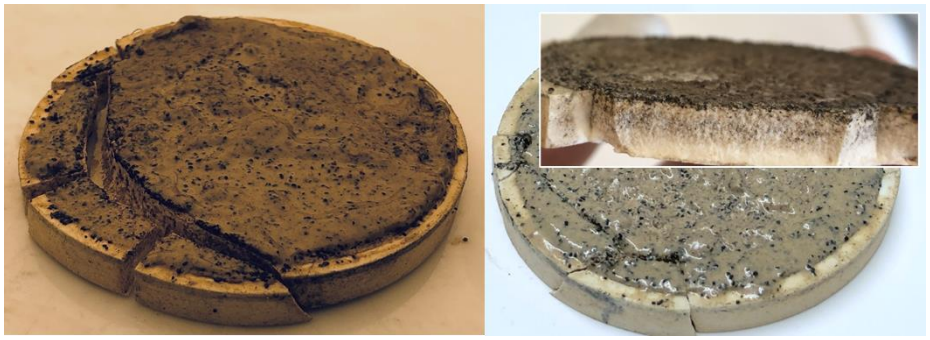

(a) (b)

Figure 3-68: Discs from tests of Fluid 2+G (a) and Fluid 2+G+C (b) [IX]

(a) (b)

Figure 3-69: Disc from tests of Fluid 2+G+B (a) and reverse side of filter-cake with Granular cellulose seams (b) [IX]

Two tests were conducted with a barite weighted oil-based field fluid, Fluid 3. The test without any Granular cellulose yielded a pressure and fluid loss plot which was consistent with tests with Fluids 1 and 2 without Granular cellulose. Figure 3.70 presents images of the disc for the test of Fluid 3. The filter-cake can be seen to have hair-like cuts in multiple places.

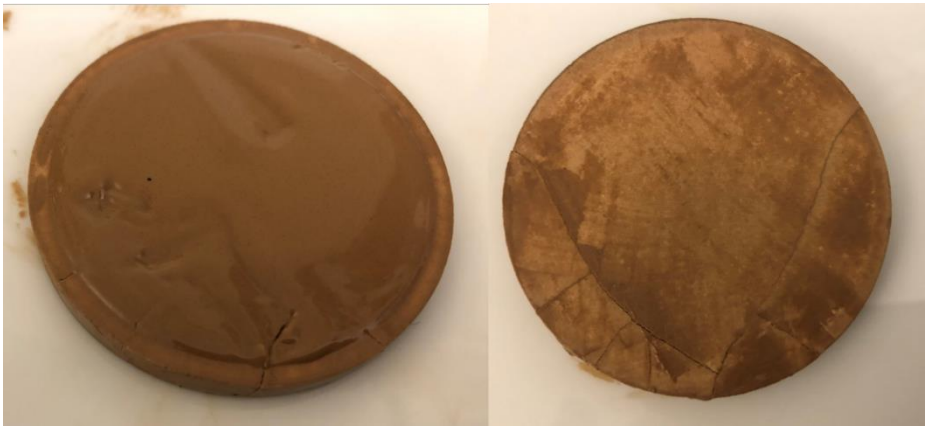

(a) (b)

Figure 3-70: Disc from test with Fluid 3, with filter-cake (a) and with filter-cake removed (b) [IX]

Fluid 3 was also tested with the addition of Granular cellulose. Figure 3.71 shows the disc with the filter-cake intact in the test cell and also how the disc was fractured. The picture taken with the disc inside the cell clearly shows how the LPM has built ridges over the fractures, which is consistent with the building of LPM seams shown in Figure 3.69 (b).

(a) (b)

Figure 3-71: Disc from test with Fluid 3+G, with filter-cake and LPM ridges (a) and broken disc when taken out of cell (b) [IX]

3.8.2 Discussion

The methodology was applied to attempt studying the transition from a steady-state fluid loss test to the repeated sealing of induced fractures. The results obtained were remarkably similar for fluids with small variations in composition, such as Fluids 1 and 2. Also, the results were considerably different for different LPM combinations, where addition of $CaCO_3$ had no significant impact on sealing induced fractures, Cellulose fibre A and B improved filter-cake permeability, whereas the Granular Cellulose particles were very effective in sealing the induced fractures. Figure 3.72 shows six of the disc's tested, and the similarities

in the fracture patterns are evident. The fractures were consistently towards the edge of the discs and often on both sides, thus limiting the fracture width to half of the gap between the disc and the test cylinder, or around 0.3-0.4 mm. This indicates that the test methodology could compare the applied fluids' capability of sealing induced fractures from around 0.1-0.4 mm. With higher applied pressures, more significant disc fracturing was induced, thus potentially enabling distinguishing the performance of more similar LPM materials than those tested.

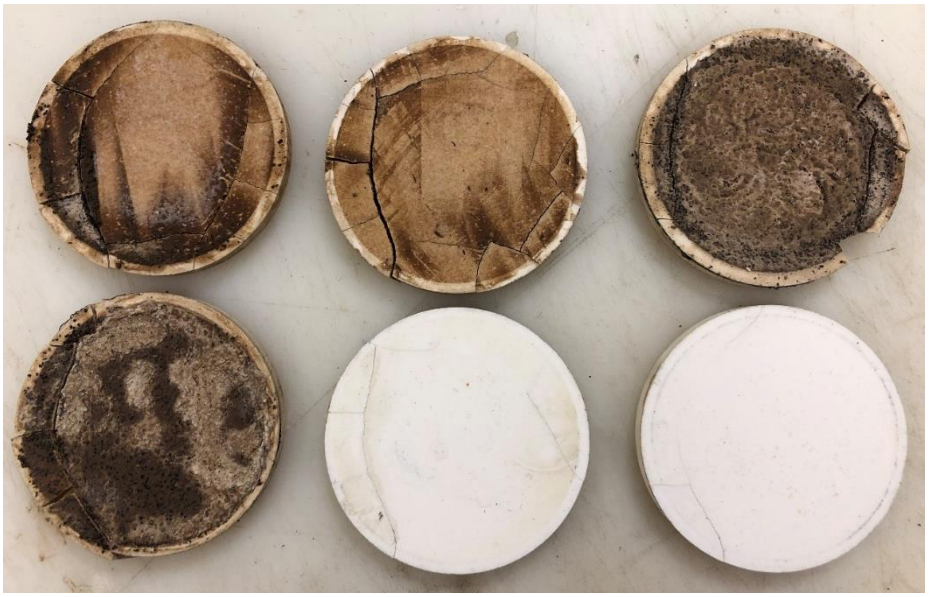

Figure 3-72: Fracture patterns in discs [IX]

A weakness of the method is comparing test results conducted with different equipment. This may be solved by establishing a standardized method for inducing the disc fractures, such as e.g. placing thin needles, or cones at fixed locations between the disc and the end cap. An alternative may be to weaken the discs in certain points to control the fracturing patterns, or discs may even be pre-fractured to simulate a situation where natural fractures are present when new formation is being drilled. For the current study, a microscope was used to measure fracture

openings. More advanced imaging and scanning analysis may provide additional data to assess fluid and particle invasion into the fractures.

The permeabilities calculated for many of the data-points also include the area of the sealed fractures. As the permeabilities trended downwards with higher pressures where the Granular cellulose had been applied, and more fractures had been induced, it is clear that if the fractures were effectively healed, the permeability of the filter-cake must have been fully restored also over the fracture openings.

The similarity between the water-based Fluids 1 and 2 with the oil-based Fluid 3, when $CaCO_3$ was the only applied LPM is apparent. For Fluids 1 and 2 the similarities were also remarkable when the Granular cellulose was applied, as the five tests were successful to above 27 MPa and with very small variations in fluid loss. The contrast was however clear with the oil-based Fluid 3 with Granular Cellulose as the fluid loss during fracturing was around 7.5 times that of the water-based fluids.

The fluid loss recorded for the tests with water-based fluid and Granular Cellulose was very low at around 4 ml. This is evidence that the fluid composition performed well with regards to sealing of the permeable disc with median pore-size of 10 µm as well as sealing the induced fractures which could be up to 0.3-0.4 mm. When considering the particle size distribution of Fluid 2 with the Granular Cellulose and the Cellulose Fibre B, the results deviate considerably from the recommendations of the Ideal Packing Theory, Abrams rule and the Alsaba method. The closest model is the recommendation that Fuh (1993) proposed, although the volumetric concentration of Cellulose Fibre B is considerably lower than Fuh's proposal. The polymer and the $CaCO_3$ particles provide a volumetric concentration of particles <10µm of around 5.6%, the Cellulose fibre B are sized between 5 and 80 µm at a concentration of 0.63% and the Granular cellulose are sized between 250 and 600 µm at a concentration of 2.1%. In combination this provides a multimodal particle size distribution. The combined functionality is

that the fine particles, effectively seal the surface of the formation with a low-permeability filter-cake and the Granular cellulose effectively seal the fracture openings as they are induced. Figure 3.73 show the cumulative particle size distribution of Fluid 2 with the Cellulose fibre B and the Granular cellulose compared with the Ideal Packing Theory.

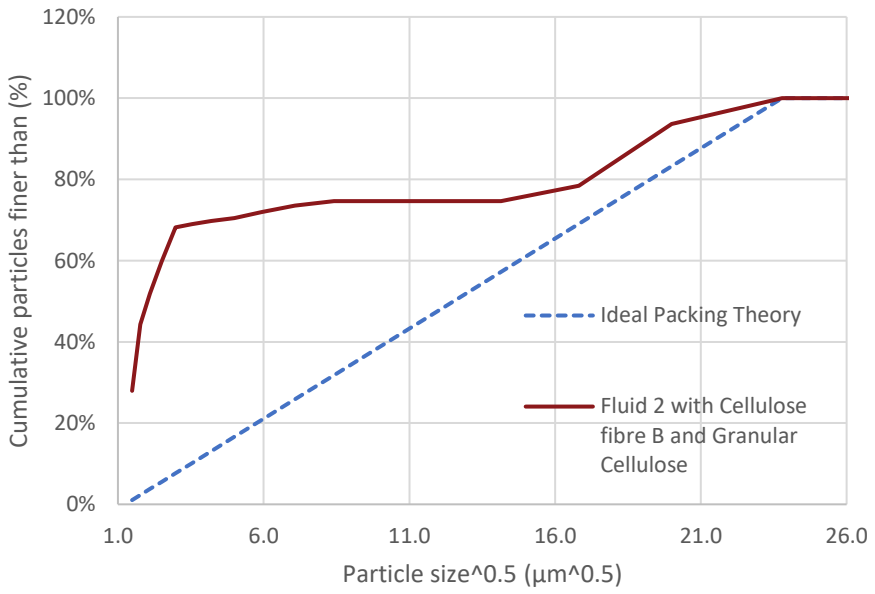

Figure 3-73: Particle size distribution of all particles in Fluid 2+G+B [IX]

Andreasen (1930) presented a model for designing concrete slurries to optimize the strength of concrete. The model is described by Equation 3.20, where D is the particle size, D_L is the size of the largest particle and q is the Andreasen packing factor. Through experiments it was shown that smaller values of q led to less voids and higher concrete density.

$$\text{Cumulative Particles Finer Than (\%)} = 100 * \left(\frac{D}{D_L}\right)^q \tag{3.20}$$

By studying the finer particles in Fluid 2, which are the polymers, $CaCO_3$ and the Cellulose fibre B particles, these may be compared in isolation to the Ideal Packing Theory and the Andreasen packing model. Figure

3.73 shows that the particles of Fluid 2 with Cellulose fibre B more closely resemble an Andreasen model with a q of 0.08 than the Ideal Packing Theory.

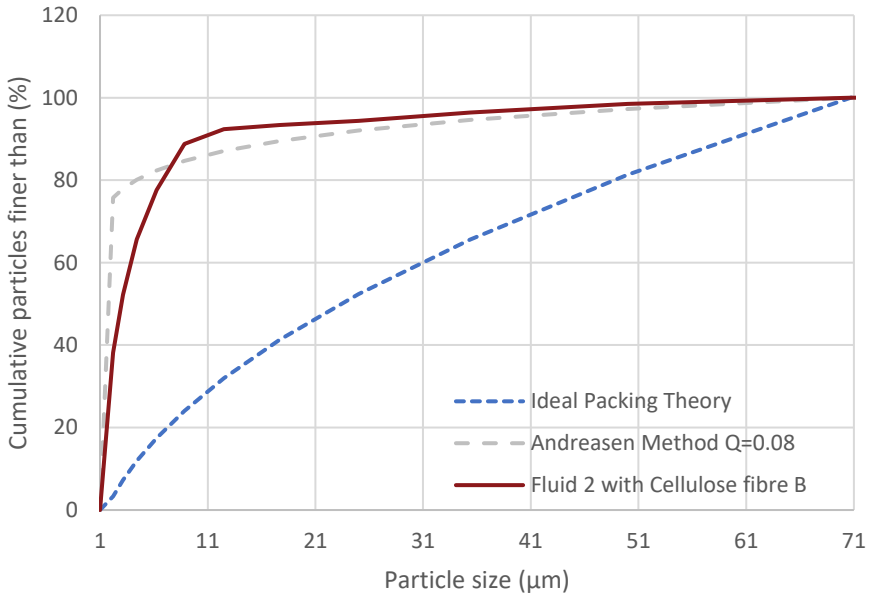

Figure 3-74: Particle size distribution of finer particles in Fluid 2+G+B [IX]

The Granular cellulose materials was sized consistently with the practical approach introduced by Fuh (1993a, 1993b and 2007), although at considerably lower concentrations. The fractures that were induced during the experiments were of a size equivalent to the particle size of the Granular cellulose, and thus also reasonably consistent with the Alsaba method for sealing of fractures as well as the Fuh approach.

Considering the very low fluid loss achieved during the induced fracture tests with Fluid 2+G+B, it may be concluded that multimodal particle size distributions may be useful when a fluid is to be designed for sealing of both a permeable formation and induced fractures simultaneously. Also, the analysis of the finer particles indicate that the Andreasen

method may be relevant for optimising fluids to provide a low-permeability filter-cake.

The hydraulic pump used for the tests provided an accurate measurement of the applied pressure, however, if could not be automatically controlled to provide a constant flowrate or constant applied pressure. For future testing, an automated pump may provide additional insight, particularly if specific differential pressures are to be simulated. Similarly logging of temperature may be relevant as this may facilitate studying any changes in sealing performance as a function of temperature, which may impact particle integrity and fluid viscosity.

Summary of findings:

The experimental method for testing of fracture induction and fracture sealing using ceramic discs yielded consistent results in terms of fluid loss and fracture patterns, with the fluids tested.

- The methodology facilitated gradual fracturing of the discs as higher pressures were applied
- The fracture patterns were relatively similar for discs tested up to the same pressures
- The addition of the Granular cellulose LPM enabled effective sealing of the induced fractures with very low fluid loss
- The lowest filter-cake permeabilities were obtained when applying a combination of very fine $CaCO_3$, with D50 of 5 µm, with cellulose based LPM
- The addition of cellulose based LPM eliminated the negative impact that certain sizes of $CaCO_3$ particles had on the filter-cake permeability
- The losses occurring with oil-based fluid was higher than for water-based fluid when fractures were induced
- A multi-modal particle size distribution proved to be effective for simultaneous sealing of a permeable formation and induced fractures

Further development of the methodology might be attempted to achieve a more standardized methodology which may be transferrable to other permeability plugging apparatuses designed for using ceramic discs

4 Sealing Mechanisms and Impact on Wellbore Stabilisation and Formation Damage in Permeable Formations

4.1 Theories for optimizing particle size distribution to seal permeable formations

Losses into permeable formations are normally limited to seepage or partial losses, where the loss rates are 10 m^3/hour or less. Such losses may be costly on their own, or they may also lead to more problematic situations. Differential sticking is an example of a problem caused when a thin and low-permeability filter-cake is not effectively formed. Also, if partial losses are permitted to persist, the formation may we washed out and the losses may escalate.

Numerous studies have been conducted to optimize particle size distribution of solids to reduce fluid loss and prevent formation damage in both static and dynamic conditions. Some of the studies are described as attempting to seal a fracture tip, some studies refer to pore-throat sizes in a permeable formation, while other studies focus on selecting a PSD of solids that minimizes filter-cake porosity and permeability. In practical applications these different approaches are often simplified as a rule of thumb approach and applied in the same manner for permeable and finely fractured formations.

Kaeuffer (1973) created what was called the Ideal Pacing Theory also described as the $D^{1/2}$ rule, based on earlier theories by such as Fuller and Thompson (1907), and Bolomey (1927) which were developed for mixing of concrete. The $D^{½}$ rule claims that ideal packing of solid particles occurs when a linear relationship is found between the cumulative volume percentage of particles and the square root of the particle diameter ($D^{1/2}$). The packing theory is focused on forming a

filter-cake where the particles are densely packed, and permeability thereby minimised.

Abrams (1977) conducted a study on particle size distribution and impact on formation damage in permeable formations. He concluded that drilling fluids typically contained sufficient concentrations of particles to limit formation damage in lower permeability rocks, whereas formation damage if more likely in higher permeability rocks, due to insufficiently sized particles in the fluid. Further, he found that once solids had invaded into the formation, backflushing could not remove the impairment of the formation. Abrams proposed a rule where the mean particle size of the solids, as he descried as bridging particles, should be $\lesssim 1/3$ times the median pore size of the formation. He further proposed that the concentration of bridging particles should be 5% by volume or more for an effective bridging to start.

Alsaba et al. (2017) presented a new criterion for optimizing the PSD based on the objective of effectively sealing a fracture. The criterion was developed based on testing lost circulation materials' effectiveness of sealing tapered slotted discs, where the fracture width varied between 1000 µm and 3000 µm. A statistical analysis was conducted, and resulted in the new criterion, where the LCM D50 particle size should be $\geq 3/10$ of the fracture width and the D90 particle size $\geq 6/5$ of the fracture width. This method thus proposes a larger D90 particle size for sealing of fractures than what previously had been recommended for sealing of permeable formations.

A selection of PSD optimization methods is listed chronologically in Table 4.1.

Reference and year	Proposed LCM PSD selection for various applications
Kaeuffer (1973)	Packing of filter-cake is optimal when cumulative volume (%) forms a linear relationship with the square root of the particle diameter
Abrams (1977)	Median particle size ≥ 1/3 times the median pore size to limit formation damage, with minimum 5% volumetric concentration
Vickers et al. (2006)	D10 particle size > smallest pore throat D25 = 1/7 of mean pore throat D50 ≈ 1/3 of mean pore throat D75 < 2/3 of largest pore throat D90 = largest pore throat
Whitfill (2008)	D50 particle size = 1/3 of the pore throat and D90 particle size = pore throat
Alsaba et al. (2017)	D50 particle size ≥ 3/10 of the fracture width and D90 particle size ≥ 6/5 of the fracture width

Table 4-1: Examples of PSD optimization methodologies

Of the listed PSD selection methods, only the Alsaba method specifically addresses fracture sealing as the objective. The other methods refer to pore sizes and permeable formations.

However, due to the practical limitations related to conducting testing and verification of particle size selection methods, some weaknesses of the proposed methods naturally exist.

The general weaknesses of conventional PSD optimization may be summarized as follows:

- Actual formation pore size distribution is not considered, as the PSD selection is typically related to the median pore size or to the smallest, median or largest pore throats, without a consideration of the relative distribution of pore sizes within a formation.
- Particle degradation during circulation is often neglected, leading to situations in the wellbore where the actual PSD is significantly different to the simulated laboratory conditions. Deviations may be considerable, in particular for wellbore

strengthening applications for induced- or finely fractured formations. [I, IV, V]

- Density of added LCM particles and potential impact on evenness of distribution of particles in the fluid or settling of particles during circulation may have been considered. [9]
- Presence of drilled solids and variations in PSD of drilled solids during the progression of the drilling of the well may impact effectiveness in terms of creating an internal filter-cake or the permeability of an external filter-cake [IX].
- Differences in sealing abilities and sealing mechanism of oil- or synthetic based drilling fluids versus water-based drilling fluids are generally not considered as part of the PSD selection methodology [VI, VIII, IX].
- Compressibility and particle shape of added LCM particles are generally not considered [V, VI, IX].
- Particle-to-particle interaction in the form of friction or particle adhesion is not considered [V, VI, VII, IX].

4.2 Theories of wellbore strengthening

A large study was conducted by the Drilling Engineering Association in the 1980's (DEA, Whitfill and Nance, 2008) on investigation of formation fracturing and lost circulation. In their studies, they found no significant differences between oil-based and water-based fluids with regards to the pressure required to initiate fracturing (FIP) or to re-open a fracture (FRP). They concluded that the FIP was a function of the in-situ stresses, and that the FIP needed to be sufficiently large to induce a tensile stress in the near-wellbore formation. In contrast, they found that the wellbore pressures required for the formation to break down (FBP) or for fractures to propagate (FPP) depended on the type of fluid and composition. Water-based fluids showed an ability to elevate the FPP more than oil-based fluids, and further, DEA found that water-based fluids with higher concentrations of weighting materials were superior in

deferring fracture propagation. In general terms, wellbore strengthening may be defined as methods for treating drilling fluids, or other methods, where either of the FBP or FPP are increased relative to an untreated condition. The consequence is that the formation may be drilled with a higher wellbore pressure and/or with reduced loss of drilling fluid, each factors which may impact the design and reach of the wellbore.

Following the DEA study, a series of studies have been conducted using mathematical modelling and experimental methods for describing wellbore strengthening effects. A summary of such research was published by Feng and Gray (2017), They conclude that the studies are limited with regards to investigating fracture propagation and fracture healing. Further, they point out that the experimental studies are limited to vertical wells.

The method for wellbore strengthening described by Scott et al. (2020) takes into consideration that a typical field fluid will contain particles up to and above 100 µm. Following a tetrahedral packing of spherical solids, a 100 µm diameter particle will fit perfectly between spheres with a diameter of 645 µm, or a ratio of 0.155 to 1. Therefore, to achieve an effective fracture sealing, there is no need for a continuous particle size distribution such as proposed by Kaeuffer (1973), for optimal packing of filter-cakes. Scott et al. therefore recommends selecting particles equal to or slightly larger than the loss zone opening, given that other solids in the fluid have a diameter of at least 0.155 times the diameter of the larger particles. The method is based on earlier US patents (Fuh, 1993a and 1993b) and with further developments by Fuh et al. (2007). According to one of the claims of Fuh et al. (1993b) the volumetric concentration of the LPM needs to be 3.5% or greater.

Fekete et al. (2013) studied wellbore stability management, focusing on depleted and low-pressure reservoirs. They also concluded that wellbore strengthening should be targeted through preventative treatment, as the

stress caging concept does not work after a loss has occurred (Alberty and McLean, 2004).

Alshubbar et al. (2018) studied the performance of LCM when circulating in a wellbore. By changing the flowrates, they discovered that higher flowrates defer the establishment of a seal. Further, it was established that LCM with lower specific gravity was less dependent on flowrates, thereby making such materials more effective for preventative treatment of losses.

Some of the mechanisms descried for wellbore strengthening are presented in Figures 4.1-4.4.

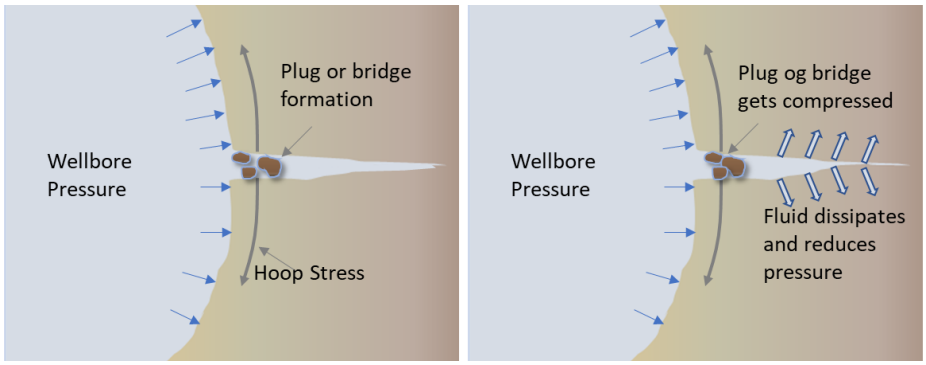

Figure 4-1: Schematic of stress caging process, after Alberty and McLean (2004)

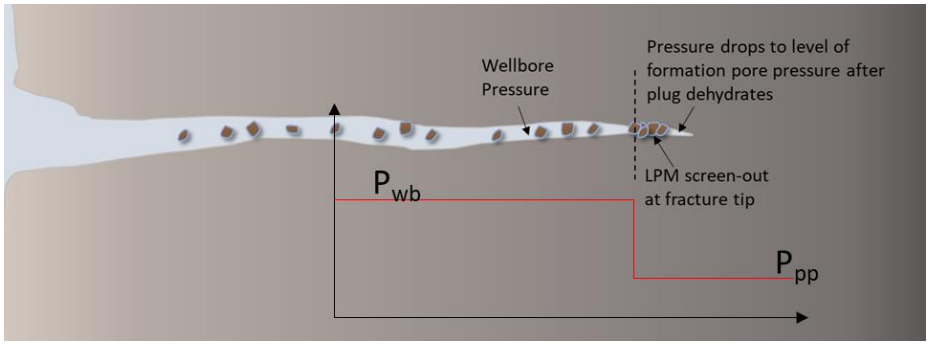

Figure 4-2: Schematic of LPM screen-out at fracture tip, after Fuh et al. (2007)

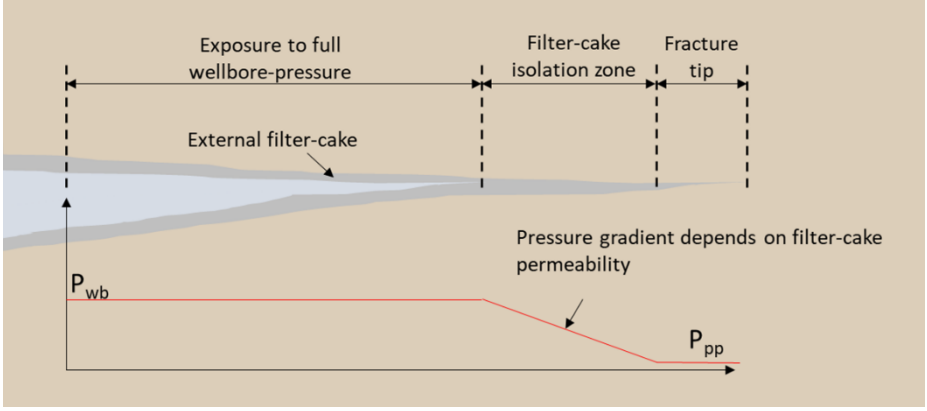

Figure 4-3: Schematic of external filter-cake in water-based fluid in fracture, after concept of van Oort et al. (2009)

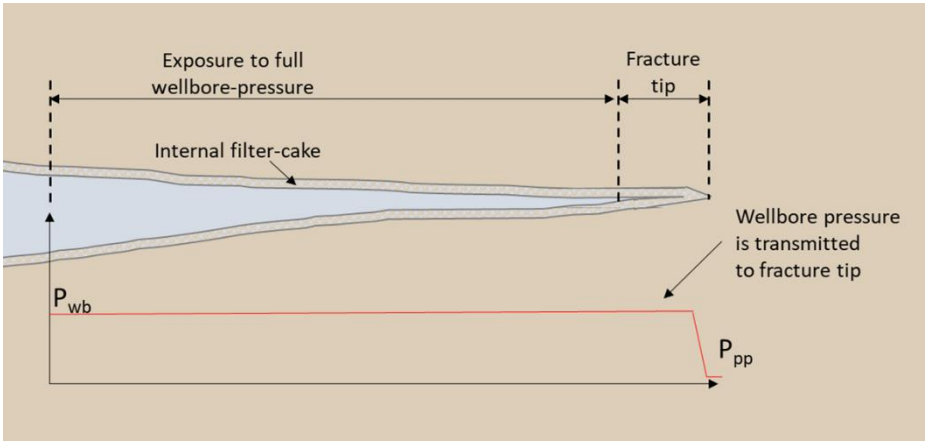

Figure 4-4: Schematic of internal filter-cake in oil-based fluid in fracture, after concept of van Oort et al. (2009)

4.3 Filter-cake formation in water-based drilling fluids

The liquid base of a water-based fluid is typically a combination of water and various salts such as NaCl, KCl, $CaCl_2$. The densities of these fluids without weighting agents will be in the range of 1.0-1.4 g/cm^3, or higher with more specialised brines. The fluid bases will exhibit Newtonian viscosity behaviour, with apparent viscosities in the order of 1-1.5 mP*s. at 20°C. The required viscosity of the drilling fluid is therefore achieved

by adding particles in the form of polymers such as xanthan gum or swellable clays like bentonite. To enhance the fluid-loss characteristics, starch or poly-anionic cellulose (PAC) is commonly used. The recipes used in references I to X have volumetric concentrations of xanthan gum of 0.2-0.6% and combined concentrations of PAC and starch of 1.1-2.4%, or in total averaging circa 2.5%. Before the presence of drilled solids, weighting agents or lost circulation materials, the volumetric concentration of particles, other than water and ions of salts are therefore low.

4.3.1 Fluid loss test using fluids with low concentration of solids

15 tests were conducted with five different low-solid fluids to assess the sealing capacities at HTHP conditions on 2.5 µm filter-paper and ceramic discs with median pore size ranging from 10 µm to 120 µm. The recipes of the fluids in series W-7 are presented in table 4.2. The tests on filter-paper were conducted at 3.45 MPa (500 psi), whereas the tests on ceramic discs were conducted at 6.9 MPa (1000 psi).

Component	**Fluid 1 (Polymer) (g)**	**Fluid 2 (Polymer/ Fibre UF) (g)**	**Fluid 3 (Polymer/ Fibre F) (g)**	**Fluid 4 (Polymer/ Solids) (g)**	**Fluid 5 (Polymer/ Solids/ Fibre UF) (g)**
H_2O	337	333	333	333	328
KCl	17.5	17.5	17.5	17.5	17.5
Xanthan Gum	1.2	1.2	1.2	1.2	1.2
PAC	5.0	5.0	5.0	5.0	5.0
AURACOAT UF (D90 of 75 µm)		4.0			5.0
AURACOAT F (D90 of 120 µm)			4.0		
Bentonite				10.0	10.0
Volumetric Concentrations:					
Polymer	1.77%	1.77%	1.77%	1.77%	1.77%
Cellulose Fibre		0.85%	0.85%		1.06%
Solids				1.10%	1.10%
Total particle concentration	1.77%	2.62%	2.62%	2.87%	3.93%

Table 4-2: W-7 Low-solid water-based drilling fluid recipes for 350 ml samples

The fluid loss data were analysed using the regression methodology introduced in reference [V] and presented in chapter 3.4. Table 4.3 presents the data, including the calculated a spurt loss constant, *SL*, the Coefficient of Fluid Loss, C_{FL}, and the filter-cake permeability. The permeabilities were calculated on the average basis of a 50% water content in the filter-cakes, and with the simplification that the fluid filtrate had a dynamic viscosity of 1 mPa*s, which is equal to water at 20°C.

It was discovered that the KCl/Polymer fluid (Fluid 1), lost its sealing ability with pore-sizes larger than 10 µm with the given particle concentration of 1.77%. All fluids were tested on the 20 µm ceramic discs and Fluid 3 was tested on the whole range of mediums from 2.5 µm filterpaper to 120 µm ceramic discs. From the table a general trend of

higher fluid loss with more permeable discs can be observed. Figure 4.5 shows the fluid loss regressions of Fluid 1 and Fluid 3 on different discs and filter-paper, whereas Figure 4.6 shows Fluids 2-5 tested on the 20 µm disc. The test of Fluid 1 on 20 µm disc resulted in a total loss and is hence not included in the Figures.

	Pressure (MPa)	**Pore size (µm)**	**30 second fluid filtrate (ml)**	**30 minute fluid filtrate (ml)**	**Coefficient of Fluid Loss ($ml/s^{1/2}$)**	**Spurt Loss Constant (ml)**	**Filter-cake permeability (mD)**
Fluid 1 (Polymer)	3.45	2.5	2.79	16	0.358	0.8	0.091
Fluid 1 (Polymer)	6.9	10	31.45	48.2	0.453	29.0	0.073
Fluid 1 (Polymer)	6.9	20	150+				
Fluid 2 (Polymer/ Fibre UF)	3.45	2.5	3.27	12.8	0.258	1.9	0.076
Fluid 2 (Polymer/ Fibre UF)	6.9	10	11.80	23.5	0.317	10.1	0.057
Fluid 2 (Polymer/ Fibre UF)	6.9	20	19.40	32.1	0.344	17.5	0.068
Fluid 2 (Polymer/ Fibre UF)	6.9	50	38.60	63.98	0.687	34.8	0.270
Fluid 3 (Polymer/ Fibre F)	3.45	2.5	3.40	13.1	0.263	2.0	0.079
Fluid 3 (Polymer/ Fibre F)	6.9	10	15.50	26.2	0.290	13.9	0.048
Fluid 3 (Polymer/ Fibre F)	6.9	20	21.25	31.55	0.279	19.7	0.044
Fluid 3 (Polymer/ Fibre F)	6.9	50	41.00	52.75	0.318	39.3	0.058
Fluid 3 (Polymer/ Fibre F)	6.9	120	52.75	66.65	0.376	50.7	0.081
Fluid 4 (Polymer/ Solids)	6.9	20	24.79	35.1	0.279	23.3	0.044
Fluid 5 (Polymer/ Solids/ Fibre UF)	6.9	20	11.75	19.75	0.217	10.6	0.039

Table 4-3: Fluid loss data for low-solid water-based drilling fluids

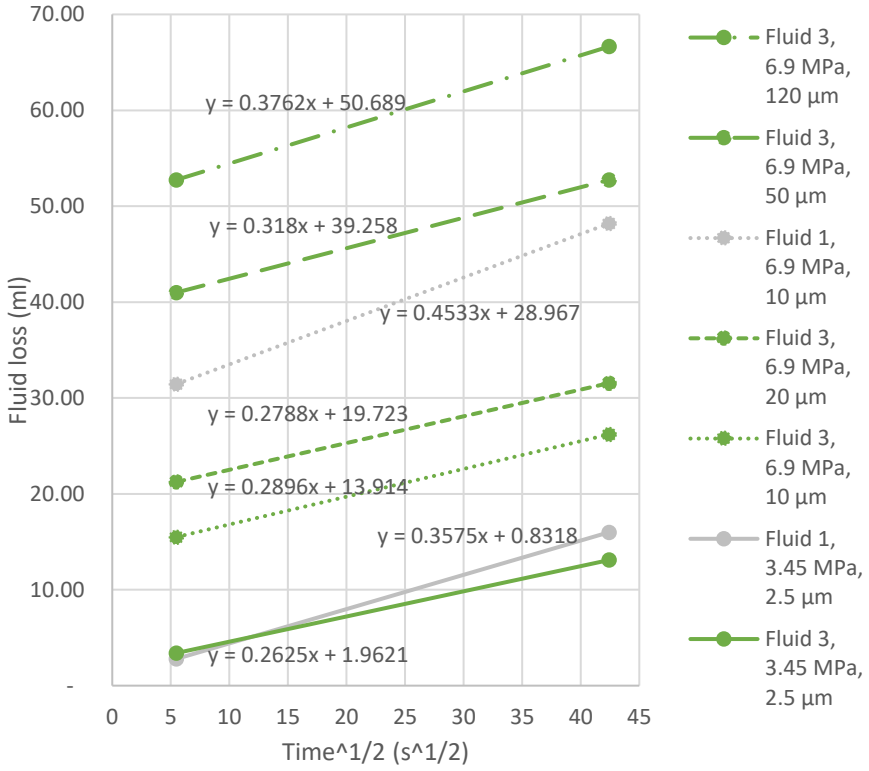

Figure 4-5: Fluid loss regressions for Fluid 1 and 3

The regressions help to distinguish between the formation of an internal filter-cake and the subsequent build-up of the external filter-cake. For Fluid 3, with a volumetric concentration of particles of 2.62%, the Coefficient of Fluid Loss, which represents the steepness of the curve, varies considerably less than the Spurt Loss Constant. The C_{FL} has an average value of 0.305 ml/s$^{1/2}$ and a standard deviation of 0.044, or 15%. The Spurt Loss Constant has an average value of 25.1 ml and a standard deviation of 19.7, or 78%. This implies that for this Fluid a higher formation pore-size and permeability will require a higher spurt-loss to form an internal filter-cake. The lower variations of the C_{FL} indicates that the permeability of the external filter-cake is less dependent on the formation permeability, once a seal or an internal filter-cake is

established. The tendency is the same for Fluid 2 with a volumetric concentration of particles of 1.77%, however, the significantly higher C_{FL} values indicate that the external filter-cake is more permeable. Comparing the tests on 2.5 µm filter-paper at 3.45 MPa pressure, the permeability of the filter-cake is reduced by 13% by adding 0.85% of fibres, whereas the permeability falls by 35% for the 10 µm and 6.9 MPa tests when the fibres are included.

The tests conducted on the 20 µm discs add some more information to the understanding of the filter-cake formation. Having excluded Fluid 1, which yielded a total loss, the overall results are relatively similar for Fluids 2-4. This may be seen as reasonable as the volumetric concentrations of particles are relatively similar, with 2.62% for Fluids 2 and 3 and 2.87% for Fluid 4. By multiplying the particle concentration with the spurt loss volume, an estimate of the volume of particles required to form an internal filter-cake can be made. The volumes were calculated to be 0.46 ml for Fluid 2, 0.52 ml for Fluid 3 and 0.59 ml for Fluid 4. The permeabilities are identical for Fluid 3 and 4 at 0.044 mD, whereas the permeability of the filter-cake of Fluid 2 was 0.068 mD. Differences in PSD may explain the small variations between the three Fluids. A slight deviation in the data can be seen in the regression data of Fluid 5. With a higher particle concentration of 3.93%, the Spurt Loss Constant is around half that of Fluids 2-4, indicating that here the internal filter-cake is formed with a lower overall presence of particles, 3,93%*10.564 ml = 0.42 ml. Further, the C_{FL} is also reduced, and the calculated permeability is as low as 0.039 mD. This may indicate that the combination of drilled clays or bentonite particles and the fibres are more effectively sealing, than either of the particles on its own. This may be due to complementary particle size distributions, cohesive forces between the clay/bentonite particles and the fibres or a combination of both factors.

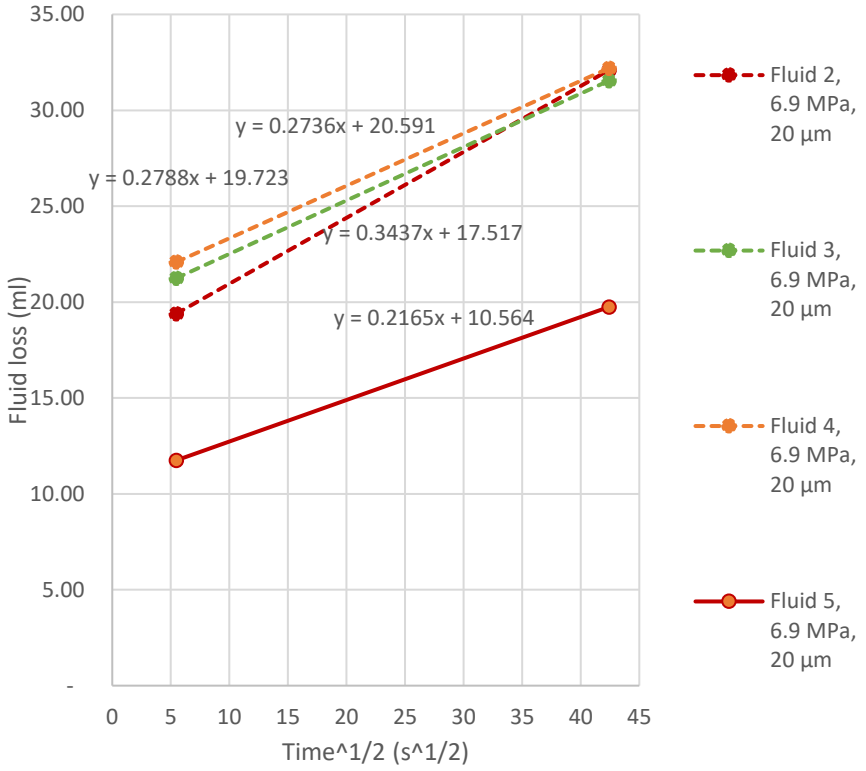

Figure 4-6: Fluid loss regressions of Fluid 2-5 on 20 µm disc

The Mohr-Coulomb model modified with the Terzaghi effective stress concept determines the shear failure mode for a brittle and porous material under different conditions of normal stresses and internal pore pressure, (Terzaghi, 1923). Applying these principles to understand the functionality of a filter-cake, both the cohesion of the filter-cake and the transfer of fluid pressure into the filter-cake fluid phase (the internal pore-pressure) will impact its shear strength. During dynamic circulation, the filter-cake's cohesion will be important to prevent erosion. Filter-cakes made from particles where there is significant cohesion, increases the strength of the filter-cake before shear failure occurs in a situation where tensile and normal forces are equal, relative to a filter-cake made from particles with less cohesion [VII]. This implies

that the stability of a filter-cake will increase in proportion to its cohesive forces when it is exposed to circulation of fluid in the wellbore. Similarly, when a filter-cake exhibits lower permeability, less pressure will be transported from the wellbore into the fluid part of the filter-cake, and hence also increase the effective shear strength of the filter-cake. Considering a water-based drilling fluid with solid particles with low compressibility, a reduction in permeability is obtained when the porosity is reduced and the PSD of the solids packs in the most effective manner. References may here be made to the Ideal Packing Theory (Kauffer, 1973) or alternatively to the Andreasen method for packing of solids to minimise porosity in concrete (Ribeiro, 2014). In contrast, if a significant portion of the particles are softer, compressible, deformable or in another way adapts to obtain a tighter seal, the importance of an exact PSD is reduced, as the adaptable particles will adjust to the open pores between the less compressible solids, without being permanently deformed or broken [V, IX]. An intermediate solution to reduce the permeability is the application of different types of solids, where the compressive strength and/or mechanical toughness are significantly different. In such a condition, the more brittle materials may break up into smaller pieces to pack the filter-cake tighter. This mechanism may describe the benefits observed when using fine $CaCO_3$ particles, due to its brittle nature, to reduce fluid loss in a fluid in combination with harder particles. In contrast, harder materials such as barite, may require the support of more adaptable particles, like cellulose-based fibres, or more brittle particles like $CaCO_3$ to form a satisfactory low permeability seal.

4.3.2 Fluid loss test with barite weighted fluids

To illustrate the importance of using materials with different mechanical properties, two fluids were composed with a high concentration of solids. In one of the fluids, a small concentration of cellulose-based fibres was added. The added fibre had a D90 value of < 75 µm, which does not deviate considerably from the specifications of the API barite. The

recipes for series W-8 are presented in Table 4.4. Due to the small concentration of fibres, and the relatively similar PSD of API barite, the overall PSD distribution would hence not change significantly, whereas the impact of a tighter packing with flexible materials may be observed.

Component	**Fluid 1 (Barite weighted KCl/Polymer)**	**Fluid 2 (As Fluid 1 with Fibres)**
H_2O	300.5 g	295.5 g
KCl	17.5 g	17.5 g
Xanthan Gum	1.2 g	1.2 g
PAC	4.0 g	4.0 g
API Barite	178.0 g	178.0 g
AURAFIX UF (D90 of <75 µm, cellulose fibre)		5.0 g
Bentonite	10.0 g	10.0 g
Volumetric Concentrations:		
Polymers	1.49%	1.49%
Solids	12.66%	12.66%
Cellulose Fibre		1.06%
Total particles (incl. Polymers)	14.14%	15.21%
Total particle (excl. Polymers)	12.66%	13.72%

Table 4-4: W-8 Recipes for Fluid 1-2 for 350 ml samples

In contrast to the low-solids fluids, where the water-content in the filter-cakes was estimated to be around 50% by volume, the average number was estimated to be 25% for the fluids with high levels of solids. As shown in Figure 4.7, the tests conducted on 2.5 µm filter-paper does not significantly differentiate the performance of the fluids. The calculated filter-cake permeabilities were 0.090 mD for Fluid 1 and 0.079 mD for Fluid 2, or a reduction of 12% with the inclusion of the fibres. For the 50 µm discs, the filter-cake permeabilities were calculated to be 0.218 mD for Fluid 1 and 0.125 mD for Fluid 2, or a reduction of 43%.

The large difference in permeabilities for the 50 µm discs indicates that the 1.06% volumetric addition of the selected fibres has a strong

contribution towards either reducing the permeability of the internal filter-cake or the external filter-cake or both.

After the HTHP test, the discs were reverse flowed with 2 litres of water at a pressure of 0.07 MPa (or 10 psi) and any filter-cake residue on the surface of the disc was removed. The discs were thereafter dried to measure the mass increases. The disc for Fluid 1 showed a mass increase of 0.083 g and the disc for Fluid 2 showed a mass increase of 0.038 g. This indicates that the fibres in Fluid 2 reduced the invasion of solids into the disc, relative to the Fluid 1, where no fibres were added. The difference in the *SL* for the disc tests, was only around 3.2% (2.59 ml for Fluid 1 vs 2.68 ml for Fluid 2). The slightly higher *SL* for Fluid 2 is consistent with the hypothesis that the fibres limit initial solids invasion. With rapid invasion of solids to plug the pores, the spurt-loss will be lower before an external filter-cake may effectively be built. If the fibres reduce the plugging effect, the initial control of the fluid loss is more dependent on the building of an external filter-cake, which may require a larger initial spurt loss. The evidence of lower increase in disc mass for Fluid 2 supports this hypothesis.

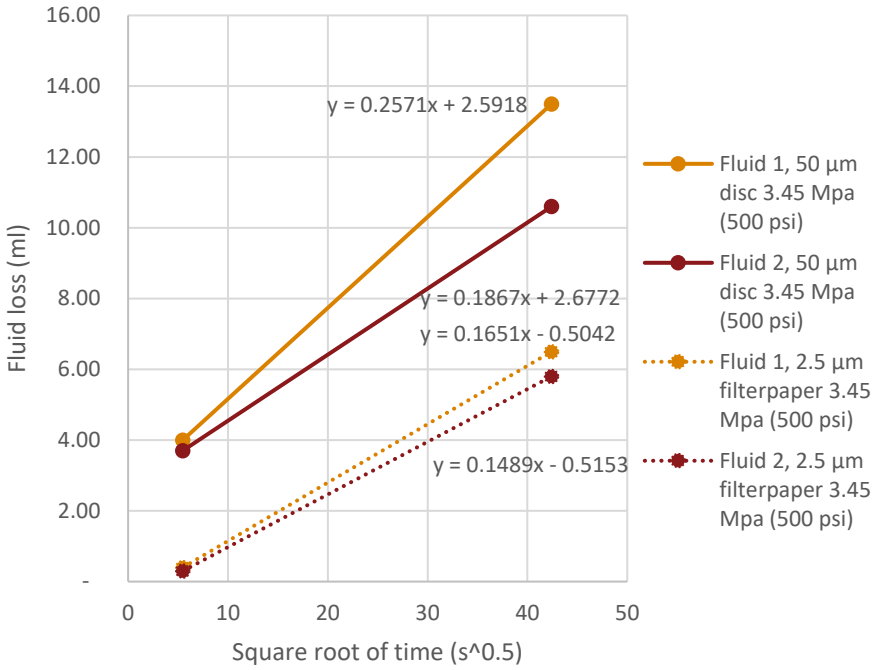

Figure 4-7: Fluid loss regressions of Fluid 1-2

A hypothesis is that the fibres increase the particle-to-particle adhesion and friction as the solids and the cellulose fibres are squeezed together during the spurt-loss phase. As the cellulose fibre particles are elastically deformable, the contract area between the particles may be allowed to increase as higher pressure is applied. With a higher particle-to-particle friction and adhesion, it may be easier to create a barrier over a pore-opening, than if low inter-particle friction is dominant, thus creating lower particle invasion.

4.4 Filter-cake formation in oil-based drilling fluids and comparison with water-based fluids

An oil-based drilling fluid is conventionally built by mixing a base oil with brine, emulsifier and organophilic clay. Through mixing at high

shear-rates, a water-in-oil emulsion is established, and the water portion can be seen as very small droplets within the oil base. The observed size of these droplets are typically less than 10 µm, and potentially with a D50 value of around 5 µm (Agarwal et al., 2013 and Sadian et al., 2015). The viscosity of the fluid may be tuned by the relative concentration of these components. By adding more organophilic clay, brine or based oil, the viscosity may be changed. At the same time the concentration of emulsifier needs to be maintained to achieve a good emulsion. Although not studied in detail as part of this research, it was found that volumetric concentrations of emulsifier of 2.0-2.4% yielded stable emulsions. The concentration of emulsifier will impact the viscosity of the fluid at different temperatures, and hence it may be important to conduct fluid loss tests at relevant field temperatures to get realistic data. The oil-to-water ratios are normally within the range of 60/40 to 95/5.

Fluid loss tests with a low-solids oil-based fluid was presented in section 3.6.2, as part of the method for analysing fluid filtrate viscosity. The tests were conducted on 2.5 µm and 22 µm filterpaper, and clearly showed how the brine droplets formed a part of the filter-cake rather than being a part of the fluid filtrate. This thus makes a clear difference in how filter-cakes are formed in oil-based drilling fluids relative to water-based drilling fluids. With a low oil-to-water ratio, a large portion of the fluid is used to form the filter-cake, even before considering the solids content in the fluid.

4.4.1 Fluid loss test with barite weighted fluids

An oil-based fluid was used for circulating on a MudCube filter-belt machine and thereafter for fluid loss tests. The MudCube uses a filter-belt which circulates over a vacuum suction area. The rotating filter-belt is thus not tensioned in the same way as a vibrating shaker screen and may therefore screen particles in a different way. Filter-belts with different apertures were used for circulation. Table 4.5 shows the laboratory composition of series O-2, for different fluids with and

without the addition of fibres. The actual fluid tested was mixed as an 8 m^3 sample and may hence deviate from the laboratory specification. The barite used was specified as an API-grade barite with maximum 3.0% particles above 75µm (ASTM sieve 200) and minimum 5.0% particles above 45µm (ASTM sieve 325). Due to circulation in the system and through the filter-belt, the PSD of the barite was likely finer than the specification, although specific PSD analysis was not conducted.

Component	**Density (g/cm^3)**	**Fluid 1 (352 ml)**	**Fluid 2 (356 ml)**	**Fluid 3 (357 ml)**
Base oil	0.822	167.5 g	167.5 g	167.5 g
Emulsifier	0.95	9.7 g	9.7 g	9.7 g
$CaCl_2$ brine (36% wt)	1.349	116 g	116 g	116 g
Ca (OH)2	2.21	8.5 g	8.5 g	8.5 g
Organophilic clay	1.57	5.5 g	5.5 g	5.5 g
API Barite	4.2	178.0 g	178.0 g	178.0 g
Organophilic lignite	1.8	4.0g	4.0g	4.0g
AURAFIX UF, cellulose fibre (D90 <75 µm)	0.98		5.0 g	2.0 g
FEBRICOAT C, cellulose fibre (D90 <197 µm)	0.97			5.0 g
Measured Density of large sample		1.37 g/cm^3	1.37 g/cm^3	1.37 g/cm^3
Particle concentration (Clay, barite and fibre)		13.8%	14.8%	15.25%
Particle concentration including brine droplets		38.2%	39.2%	40.45%

Table 4-5: O-2 Recipe for mixing laboratory sample of Fluids 1-3 for 352-357 ml samples.

A hypothesis for the discussion is that from a fluid loss perspective, the brine-droplets act as particles, given that the emulsion is not broken, and evidenced by the tests of oil-based fluid presented in Tables 3.15 and 3.16. For testing of the hypothesis, let us assume a D50 brine particle size of 5 µm. Following the established particle size selection methods presented in Table 4.1, this suggests that the brine droplets will very effectively aid the sealing of formations up to around 3 times the D50 value, or here around 15 µm. Further, with the presence of larger particles in the fluid, the droplets will aid the sealing between such

particles, given that the apertures between the particles are 15 µm or smaller. Thus, the brine particles may also aid in creating a low-permeability external filter-cake. Due to the high concentration of brine droplets in Fluid 1-3 of around 25%, the anticipated fluid loss should be lower than for a water-based fluid, given that the concentrations of other particles such as barite, $CaCO_3$ or LCM are similar in all fluids and that the viscosity of the base oil is higher than that of water.

Figure 4.8 presents the fluid loss collected over 30 minutes of Fluids 1-3, with the application of a pressure of 6.9 MPa (1000 psi). The fluids tested do not contain drilled solids, and thus represent relatively clean fluids. Here it can be seen that the Fluid 1, which is the barite-weighted oil-based fluid, shows excellent sealing of a 50 µm ceramic disc, but that a total loss occurred with the 120 µm ceramic disc. For Fluid 2, the 120 µm disc was effectively sealed, although with a higher fluid loss than for the 50 µm disc. This shows that the addition of 14.2 kg/m^3 (5 ppb) of selected cellulose fibres significantly changed the sealing ability of the fluid, despite the D90 value being only 0.625 times the median pore size. Further, the PSD of the added cellulose particles was specified as being reasonably similar to the API barite specification. This may be an indicator supporting the hypothesis that the cellulose particles create more adhesive and frictional forces, thus improving the ability to create an external seal, or it may indicate that the actual PSD of the barite had been changed during circulation. Fluid 3 contained a slightly higher concentration of cellulose fibres, where one of the blends applied had a D90 value of 197 µm. This corresponds to around 0.8 times the pore size of the 250 µm disc. This fluid reduced the fluid loss with the 120 µm disc with around 57% relative to Fluid 2. Further, Fluid 3 enabled a sealing of the 250 µm disc, although with a high fluid loss of around 40 ml.

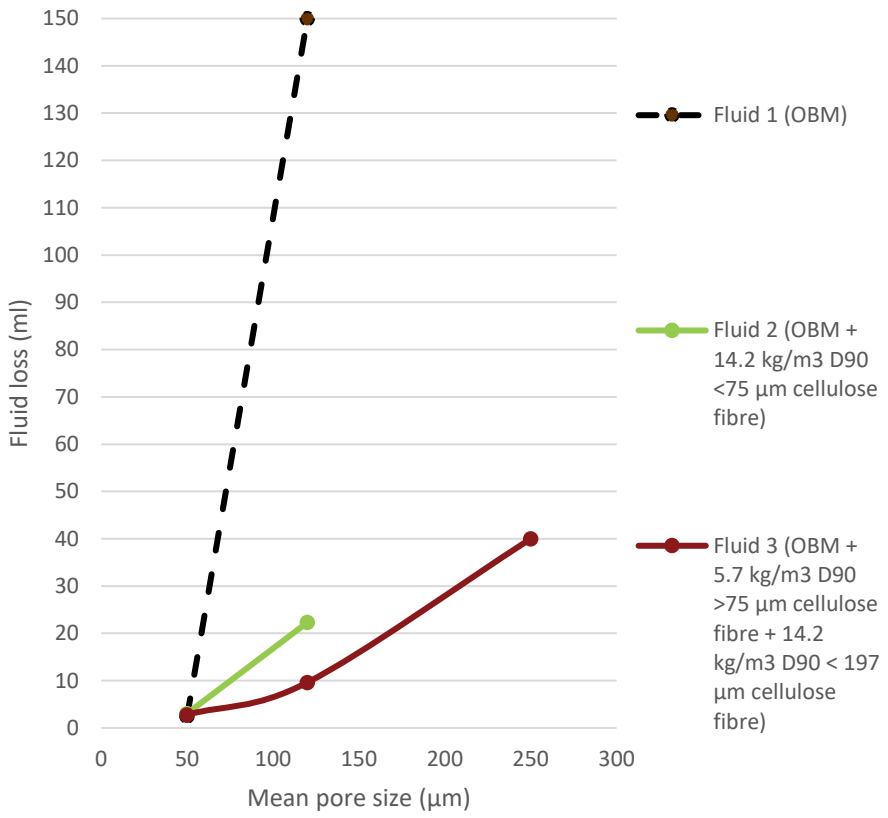

Figure 4-8: 30-minute fluid loss vs pore size at 6.9 MPa (1000 psi)

Figure 4.9 presents the same fluid loss tests as a plot against the square root of time. This facilitates the application of a linear regression model which achieved a high goodness of fit for all the tests. The chart shows that the three fluids yield relatively similar plots for the tests on 50 µm discs, with *SL* in the region of 1.4 to 1.8 ml and C_{FL} ranging from 0.02-0.04 ml/s$^{1/2}$. However, looking at the data for the tests on 120 µm discs, the C_{FL} values for Fluid 2 and Fluid 3 are quite similar at 0.038 ml/s$^{1/2}$ and 0.034 ml/s$^{1/2}$, and hence comparable to those with the 50 µm discs. The main deviations are the *SL* values, where higher spurt-losses are required for a seal to start to form. This tendency is extended to the test on 250 µm disc with Fluid 3, where the *SL* was even higher, and here the

curve also shows some more inconsistency after the initial spurt loss. This fluid loss test showed the highest C_{FL}, at 0.07 ml/s$^{1/2}$, as well as the lowest goodness of fit. Following the recommendations of the particle-size selection methods listed in table 4.1, only the largest cellulose- fibres with a D90 value of around 0.8 times the pore size and a D50 value of 0.28 times the pore size could be large enough to create a seal. For this product, the volume concentration was 1.04%. Given that the fluid loss was high, and slightly erratic, it may be concluded that the size and concentration of cellulose particles were near the limit for a seal to be formed.

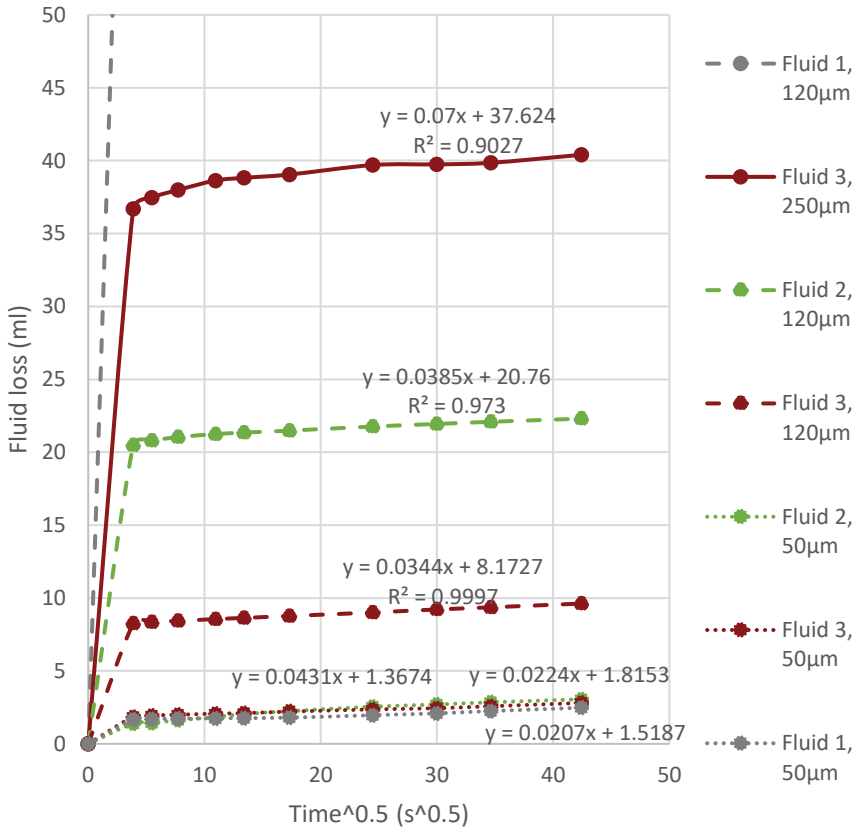

Figure 4-9: Fluid loss vs time1/2 at 6.9 MPa (1000 psi)

4.4.2 Comparing fluid loss and filter-cake formation of oil-based fluids with water-based fluids

When conducting fluid loss tests with filter-paper, there is no need to pre-wet the filter-paper due to the thickness being around 0.137 mm, and hence the volume required to wet the paper is minimal. In contrast, the ceramic discs have a thickness of around 6.35 mm, a diameter of 63.5 mm (2.5 in) and a porosity of 30-40%. Therefore, when submerging a ceramic disc in a fluid and placing it in a vacuum, around 6-8 ml of fluid may be absorbed into the disc. During a fluid loss test, this fluid may be partially or fully displaced by the drilling fluid filtrate and solids. The normal practice is to pre-wet the discs using the base fluid of the drilling fluid. By following this practice, effects related to saturating the disc with fluid are largely eliminated and the filtration performance observed are primarily those of the particles in the fluid. However, when the measured fluid loss is equal to or lower than the base fluid absorbed by the disc, the viscosity of the fluid used to soak the disc will also impact the fluid loss rate and hence also the implied filter-cake permeability, if this factor is not accounted for. As an example, the viscosity of water is 1 mPa*s at 20°C and 0.315 mPa*s at 90°C. For oil or synthetic based fluids, the viscosity is likely to be significantly different to that of water and with different dependence on temperature. Examples of base oils tested showed viscosities in the range of 3-6 mPa*s at 20°C.

If information about the formation fluid is available, more exact fluid loss data may be obtained if the discs are pre-wet with a fluid representing the formation fluid. Important data may be obtained from such testing, as e.g. an oil-based drilling fluid may seal a formation differently if it is pre-wet with brine than with a hydrocarbon oil. Similarly, a water-based drilling fluid may exhibit different fluid loss and formation damage characteristics depending on the formation fluid.

The element of wetting and capillary pressures may also impact pore-pressure transmission and rock fracturing. When conducting fluid loss

tests, the fluid filtrate may be studied and factors such as filtrate density and filtrate viscosity may yield information regarding how the wellbore pressure is isolated from the formation pore-pressure and how the higher pressure of the fluid filtrate may dissipate into the formation. A low viscosity fluid filtrate is likely to dissipate more effectively than a higher viscosity fluid filtrate, and thus cause a lower increase in pore-pressure near the wellbore.

A barite-weighted water-based fluid, series W-9, Fluid 1, with recipe shown in Table 4.6, was mixed to compare with the results of the barite weighted oil-based fluid, series O-2, Fluid 3 presented in Table 4.5. The concentration and size of fibres were identical, and the concentration of other solids including barite were also very similar. As such, it could be expected that any differences in fluid loss would be related to the functionality of the base fluid, base fluid viscosity, or how the base fluid interacted with the other solids.

Component	**Fluid 1 (Barite weighted fluid with Fibres)**
H_2O	293 g
KCl	17.5 g
Xanthan Gum	1.2 g
Starch	6.0 g
API Barite	157.0 g
CaCO3 (D50 of 50 µm)	15.0 g
AURAFIX UF (D90 of <75 µm, cellulose fibre)	2.0 g
FEBRICOAT C (D90 of <197µm, cellulose fibre)	5.0 g
Volumetric Concentrations:	
Polymers	2.05%
Solids	12.27%
Cellulose Fibre	1.48%
Total particles (incl. Polymers)	15.8%
Total particle (excl. Polymers)	13.75%

Table 4-6: Fluid recipe for W-9 Fluid 1 for 350 ml samples

Figure 4.10 shows the fluid loss versus time$^{0.5}$ for W-9 Fluid 1. As for O-2 Fluid 3, both the 120 µm and 250 µm discs were sealed effectively,

however, the regression data indicated larger differences in how the seals were obtained.

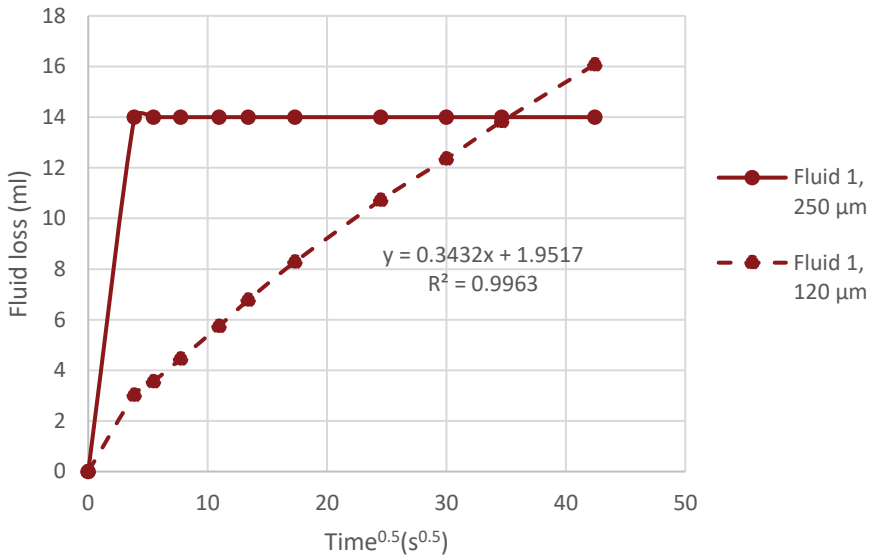

Figure 4-10: Fluid loss vs time$^{0.5}$ at 6.9 MPa (1000 psi)

Table 4.7 list the regression data alongside the 30 minute 6.9 MPa (1000 psi) fluid loss measurement. Considering that the concentrations of solids and fibres are very similar for the two fluids, the regression data indicates some clear differences in the functionality of the base fluid or how the base fluid interacts with the solids and fibres. For the 120 µm discs, the differences in *SL* and C_{FL} are significant. With the oil-based fluid, the *SL* is around 4 times that of the water-based fluid. In contrast, the C_{FL} of the oil-based fluid is only 1/10th of that of the water-based fluid. Part of this difference can be explained by the base oil being around 3-5 times more viscous than water. Further difference in C_{FL} may be caused by the brine droplets in the oil-based fluid acting as fine particles from a fluid loss perspective, thereby supporting the hypothesis presented in section 4.4.1. Analysing the C_{FL} data first, the high concentration of fine brine droplets in Fluid 3, may explain why the C_{FL} is lower than for the water-based fluid, once an initial seal is established.

The high concentration of small (< 10 µm) and potentially elastically deformable brine particles could be functioning as a fine sealant between the coarser barite and fibre particles, thus leading to the lower fluid loss rate. So why is the observed spurt loss so much higher with the oil-based fluid than the water-based fluid? One potential explanation is that the brine droplets act as "roller bearing" particles during the spurt-loss phase or that is causes a "crowding out" effect and effectively separate the larger barite and fibre particles, so that it takes more time or a higher flow of fluid for a sufficient volume of larger particles to make contact to form an internal filter-cake or surface seal [VI, IX]. An alternative explanation may be that the higher viscosity of the base fluid delays de-fluidisation which would otherwise enable solid particles to come together and form an internal filter-cake. Rough estimates of the filter-cake permeabilities were made by first estimating the portion of the fluids used to form the filter-cake, k_f, together with an estimated filtrate viscosity. The viscosity of the filtrate from Fluid 1 was set to that of water at atmospheric pressure at 90°C, and the viscosity of the base oil was assumed to be 3x times that of water. The calculated *RPF* was 240 or higher for 3 of the 4 tests. For the water-based fluids tested in section 3.4.1 and 3.4.2, it was found that $30 \lesssim RPF$ represented an inflection point below which solids invasion was limited. The test with Fluid 1 on 120 µm disc yielded a low *RPF* value and indicated that the filter-cake was mostly external, whereas for the other three tests the high *RPF* indicates substantial plugging of the discs. For the three tests with *RPF* of 240 and above, the estimated filter-cake permeabilities, marked with *, will be incorrect as the actual filtration area is substantially reduced through the internal plugging of the discs.

		Fluid loss (ml)	**SL (ml)**	**C_{FL} (ml/s$^{0.5}$)**	***Estimated k_F***	***Assumed filtrate viscosity, η (mP*s) at 90°C***	***Estimated filter-cake Permeability, K (mD)***	***Relative Plugging Factor, RPF***
Fluid (OBM), 120 µm	3	9.6	8.17	0.034	≈ 0.54	≈ 0.90	≈ 0.004*	240
Fluid (WBM), 120 µm	1	16.1	1.95	0.34	≈ 0.21	≈ 0.30	≈ 0.084	5.7
Fluid (OBM), 250 µm	3	40.4	37.6	0.07	≈ 0.54	≈ 0.90	≈ 0.016*	537
Fluid (WBM), 250 µm	1	14	14	0	≈ 0.21	≈ 0.30	≈ 0*	Infinite as C_{FL} = 0

Table 4-7: Fluid loss regression and filter-cake permeability data, * signifies likely misleading value, see text.

Looking at the data for the tests on 250 µm discs, again it is clear that the *SL* is considerably higher with the oil-based fluid, which supports the "roller bearing" or "crowding out" behaviour hypothesis or the alternative explanation that a higher base fluid viscosity reduces de-fluidisation and hence plug formation. It should be noted that once the spurt-loss phase had passed, no further fluid loss was recorded with the water-based fluid and hence the C_{FL} became 0. This behaviour is sometimes observed when the particles in the fluid entirely plug the pores of the disc during the spurt-loss phase.

Additional insight may be gained by analysing the two fluids from a particle size distribution perspective. Figure 4.11 present the PSD of the fluids and compare it to the Ideal Packing Theory and the Andreasen Method with a Q = 0.10. The water-based Fluid 1 and the oil-based Fluid 3 both have particle size distributions that more closely resemble the Andreasen Method curve than the Ideal Packing Theory curve. If the

brine droplets are excluded from the PSD plot of Fluid 3, the PSD plot is nearly identical to that of Fluid 1, even though the fluid loss performance of the two fluids were very different. With considerable differences in fluid loss, it is evident that comparing the PSD of fluids without considering the influence on brine particles yield limited insight into filtration and fluid loss performance. Given that the brine droplets form a part of the filter-cake of an oil-based fluid, the most correct way to analyse the fluid PSD may be with taking the size distribution of the droplets into consideration. The PSD of the brine droplets were assumed to have a D50 value of 5 µm [3, 59]. The PSD plot of Fluid 3 including the brine droplets much more closely resemble the curve of the Andreasen Method with a Q = 0.10. Further, the PSD plot is relatively similar to the water-based fluid W-6 Fluid 2, from Table 3.20, which provided very low fluid loss results and low filter-cake permeabilities on 10 µm ceramic discs.

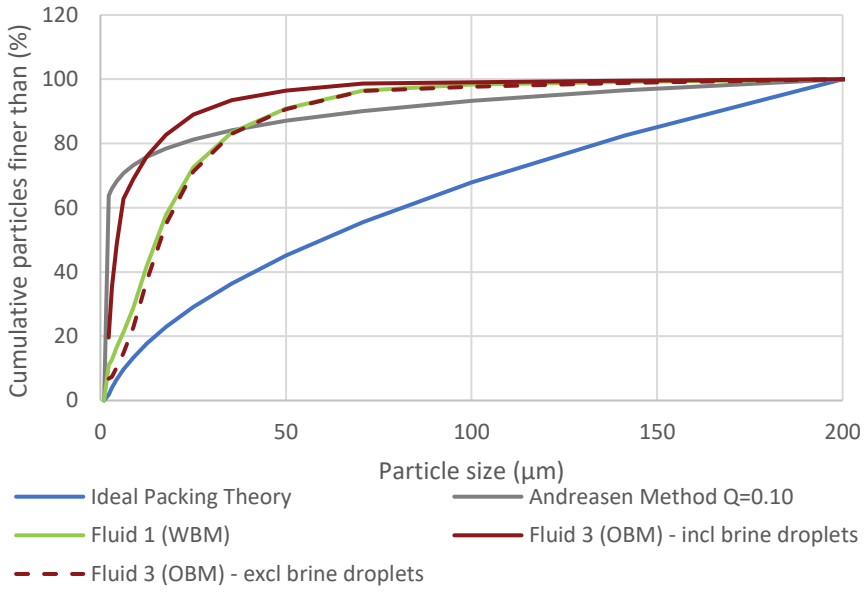

Figure 4-11: Particle Size Distribution of Fluids

In summary, oil-based and water-based fluids create internal and external filter-cakes in a very different ways and therefore produce different fluid-loss results. For an oil-based fluid, the brine droplets constitute a large volumetric portion of the fluid and become a key component in the filter-cake. Figure 4.12 present an example of an unweighted oil-based drilling fluid without bridging particles. With the small size of the droplets, they may be viewed as particles from a filtration and fluid loss perspective and included in any PSD considerations. The volumetric portion of the oil-based fluids that makes up the filter-cake, k_f, was found to typically be in the range of 0.3-0.6 for oil-based drilling fluids. Due to the small size of the brine droplets, they are likely to penetrate the pores of a permeable formation and contribute towards building a low-permeability internal filter-cake.

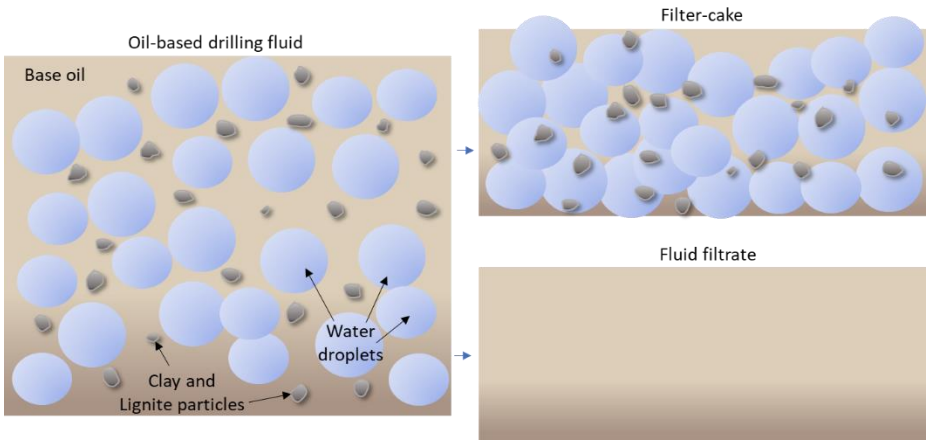

Figure 4-12: Schematic of separation of OBM into filter-cake and fluid filtrate

In contrast, the portion of the drilling fluid that makes up the filter-cake is considerably lower for a water-based fluid. Figure 4.13 is a schematic presentation of an unweighted water-based fluid without bridging particles. The value of k_f was found to typically be in the range of 0.05-0.35 for water-based drilling fluids.

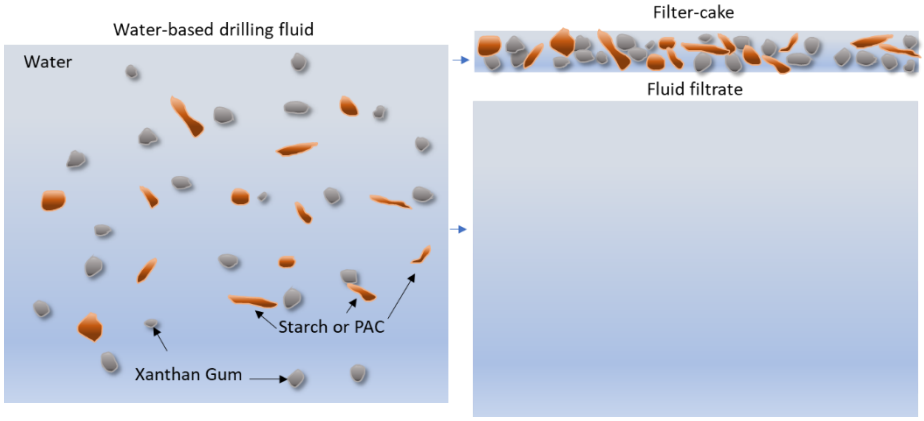

Figure 4-13: Schematic of separation of WBM into filter-cake and fluid filtrate

Another factor which may impact the filter-cake formation and the fluid loss rate is the drilling fluid viscosity at different shear rates. Khalifeh et al. (2021) concluded that a yield stress is likely to develop in an oil-based drilling fluid mixture, but not in a water-based drilling fluid mixture. In certain conditions, the yield strength of the fluid may be sufficient to temporarily prevent or reduce shearing and fluid flow through the filter-cake.

4.5 Discussion and summary

Comparing the unweighted and weighted fluids, there is a large reduction in spurt loss, *SL*, with higher solids concentrations, whereas the change in the coefficient of fluids loss, C_{FL}, is more complex to describe. The lowest C_{FL} values and filter-cake permeabilities were obtained with the presence of fibres and falling with higher differential pressures.

It was found that the brine droplets in oil-based drilling fluids act as a fine particle in the formation of a filter-cake. Due to small the size of the brine droplets, they will penetrate the pore-throats of ceramic discs which are ≥ 10 µm and create an internal plugging effect. The creates a substantial permeability reduction through the formation of an internal filter-cake. The effect is also noticed through a high relative plugging

factor, *RPF*. The *RPF* is lowered by adding cellulose based fibres where the particle size is larger than the median pore size, thus reducing the degree of solids invasion and plugging.

For water-based fluids, the fluid base itself does not contribute towards fluid loss reduction, and thus the fluid loss is exclusively controlled by other additives into the drilling fluid. To a larger degree than for oil-based fluids, the filter-cake formation is predominantly external, and less internal plugging is naturally occurring. This is also evidenced by lower *RPF* values on average. During drilling, the concentration of fine solids increases over time, as drilled solids, weighting agents or LPM particles grind down. This leads to more solids-invasion during the spurt-loss phase and hence increases permeable formation damage. It is therefore important to select LPM particles that are resistant to degradation during circulation.

The internal plugging effect of oil-based fluids reduces fluid loss efficiently; however, it was observed to have negative effects with regards to permeable formation damage and likely in certain cases wellbore strengthening. In situations where the wellbore pressure is approaching the fracture pressure, the transmission of pressure from the wellbore into the formation pores will reduce the formation strength, following the Terzaghi effective stress concept. With water-based fluids, the formation of an external filter-cakes more effectively isolates the wellbore pressure from the formation pore-pressure, and thus reduces the risk of induced fracturing.

When testing for mechanical formation damage, it appears that nearly all the formation damage occurs during the spurt-loss phase. Tests conducted over different lengths of time, show similar levels of formation damage, given that the fluid recipe and test conditions are similar. A lower spurt-loss does, however, not guarantee reduced formation damage as the most effective mechanism for reducing the spurt-loss is to size solids or cellulose fibres so that they invade the pore-

throats and create an internal filter-cake. By selecting cellulose-based particles larger than the pore-throats, less solids migrate into the formation and the filter-cake formation becomes predominantly external. The benefit of using larger cellulose-based particles relative to materials such as $CaCO_3$ or resilient graphite as LPM, is that they degrade less with circulation and also compress to form a low permeability filter-cake. If solid particles are sized larger than the pore-throats, there is a tendency for a thick and high-permeability external filter-cake to be formed. For fluids with evenly sizes solids, e.g. with a D100 value of 100 µm, it was discovered that the fluid loss could be greatly reduced by introducing 1-2% volumetric concentrations of cellulose based fibres even when they were of relatively similar PSD.

5 Lost Circulation and Wellbore Stabilisation in Fractured Formations

5.1 Losses to induced or natural fractures

One of the costliest and highest risk occurrences during drilling is severe or complete losses of drilling fluid. In such conditions, the wellbore pressure may be lost, and the worst-case outcomes may be collapse of the wellbore or a blow-out of formation fluids. In certain situations, the wellbore may be open to different formation pore-pressures, resulting in high overbalance drilling. This may lead to induced fracturing and severe cases of lost circulation. The most effective treatment of induced fracturing is to treat the active fluid system with loss prevention materials, which act immediately when a fracture is starting to propagate. If the fluid loss into the fracture is high, the fracture may continue to propagate, and the loss may escalate further and become uncontrollable. If induced fractures are not effectively sealed using preventative treatments, they may also be treated with LCM pills. For pill applications into induced fractures, it is important to minimise fluid loss, so that the LCM pill does not contribute to fracture propagation.

For naturally occurring fractures, preventative treatment may also be effective if the size of the loss prevention materials are adequate to seal the fracture. Low fluid loss, or self-sealing, LCM pills may also be used to seal off natural fractures. Unlike for induced fractures, natural fractures may also be effectively treated with squeeze pills. Squeeze pills are often mixed using low density LCM materials such as cellulose fibres, as these are more easily suspended in a low viscosity fluid. As the squeeze pill is pumped into the loss-sone, the pill is de-fluidized so that the solids particles form a plug into the fracture. If the fluid viscosity is high, the pill will not effectively de-fluidize, and hence the LCM is more likely to be transported further into the fracture system together with the fluid.

5.2 Functionality of different lost circulation materials

Alsaba et al. 2014 [6] concluded that fibrous materials showed the best performance among conventional LCM in terms of sealing fractures in tapered discs and in maintaining the integrity of the formed seal within the fractures. Further, they concluded that the superior performance of the fibrous materials was considered to be due to the wide range of particle sizes and the irregularity in particle shapes and degree of deformability. In contrast, they concluded that granular materials such as $CaCO_3$ and graphite formed seals with relatively low integrity. In 2019, Khalifeh et al. [XII] conducted high-pressure slot testing of fibre-based LCM demonstrating sealing performance where the seal did not fail even with pressures of more than 34.5 MPa (5000 psi) being applied. Further, it was shown that seals were dynamically built to withstand higher differential pressure.

Studies show that LCM with lower specific gravity is less prone to variations in the circulating conditions making them better preventative approach candidates (Alshubbar et al., 2018).

The observation of particle size degradation of $CaCO_3$ and graphite, primarily due to the influence of shear, was also observed by Hoxha et al. (2016). In their studies the D50 values of medium grade $CaCO_3$ decreased by 25–40% after 30 min of shearing. Further, it was found that various methods for measuring the PSD yielded different results. As an example, the change in D50 value of regular grade graphite was recorded to be reduced between 20% to circa 70%. These results are hence consistent with the material degradation results found in the current research, where $CaCO_3$ was consistently found to degrade faster than synthetic or resilient graphite, whereas cellulose based materials showed the highest resistance towards size degradation due to mechanical weal under temperatures ranging from ambient temperature of circa 22°C to extended hot-rolling at 112°C [I, V, VI].

To further understand the degradation of $CaCO_3$, a water-based fluid was mixed with a wide PSD of $CaCO_3$ particles. The base fluid was equivalent to W-4 Fluid 1 used in section 3.4, but with the total concentration of CaCO3 increased to 55 g/350 ml or 157 kg/m^3. The fluid thus had a volumetric concentration of polymers and solids of 2.25% and 5.81%, respectively. The fluid was wet sieved before and after hot-rolling with a threaded steel rod. Table 5.1 presents the particle size distribution before and after the exposure to the hot-rolling process with mechanical wear. The change in PSD shows that the $CaCO_3$ particles degraded rapidly and that more than 85% of the particles were finer than 23 µm.

Particle size	Concentration before hot-rolling	Concentration after hot-rolling with rod	Change
>420 µm	0.09 %	0.00 %	-100 %
250-420 µm	2.64 %	0.00 %	-100 %
180-250 µm	0.40 %	0.00 %	-100 %
150-180 µm	6.44 %	0.00 %	-100 %
125-150 µm	2.93 %	0.00 %	-100 %
90-125 µm	5.78 %	0.13 %	-98 %
75-90 µm	4.76 %	0.15 %	-97 %
53-75 µm	9.49 %	0.76 %	-92 %
23-53 µm	21.84 %	13.75 %	-37 %
<23 µm	45.64 %	85.22 %	87 %

Table 5-1: Degradation and change in PSD of $CaCO_3$ after hot-rolling with mechanical wear

Fluid loss tests were conducted with the fluid using samples that were hot-rolled with and without a threaded steel rod. The fluid that had not been exposed to mechanical wear sealed a 250 ceramic disc with a fluid loss of circa 5 ml after 30 minutes, when tested at 90°C and 6.9 MPa (1000 psi). For the fluid that had been exposed to mechanical wear, a total loss was recorded on the 250 µm disc.

Table 5.2 shows an overview of selected materials used for lost circulation treatment.

Material	Density (g/cm^3)	Typical sealing range	Mechanical stability	Solubility	Other considerations	Environmental
Asphaltenes	1.0-1.4	0-20 µm	Variable with composition and temperature	Insoluble in most acids and bases	Normally low viscosity impact, cause formation damage	Harmful to the environment
$CaCO_3$ in various forms, e.g. ground marble	2.7	0-1500 µm	Degrades very rapidly, Mohs hardness of 3 for pure mineral.	Acid soluble	Low viscosity impact	Environmentally friendly in pure form.
Cellulose, flexible/ fibrous, such as ground wood	1.0-1.5	0-1500 µm	Degrades very slowly du to high mechanical toughness relative to other typical LCM materials	Typically 30-70% soluble in acid and/or oxidizing breaker	Some increase in viscosity with concentration > 14-28 kg/m^3, may enhance low end viscosity in polymer-based fluids	Organic and biodegradable
Cellulose, hard/ granular, such as e.g. walnut shells	1.0-1.5	0-2000 µm	Degrades very slowly due to high mechanical toughness. Mohs hardness may be in the range of 2-4.	Typically 30-70% soluble in acid and/or oxidizing breaker	Low viscosity impact	Organic and biodegradable
Cellulose, mixtures	1.0-1.5	0-10 mm or more	Degrades very slowly du to high mechanical toughness relative to other typical LCM materials	Typically 30-70% soluble in acid and/or oxidizing breaker	Viscosity impact depends on specific blend and concentration	Organic and biodegradable
Graphite	2.27 for pure graphite, product range from 1.7-2.4	0-1500 µm	Resilient graphite degrades at moderate rate, but particle disintegration is part of sealing mechanism. Typical Mohs hardness of 1-2.	Insoluble in most acids and bases	Low viscosity impact	Environmentally friendly in pure form.

Table 5-2: Overview of selected LCM material properties

5.3 Wellbore stabilisation and prevention of fracture propagation

Natural fractures may occur in both carbonate formations, sandstones, and shales. The cause of the fractures may be due to tectonic stress or thermal stress. Due to the high acid solubility of carbonate formations, these are also particularly exposed to fracture due to chemical or biological activity. When drilling naturally fractured formations, the width of the fractures will typically deviate considerably from the pore-size in the rock matrix. This presents a special challenge when designing the drilling fluid and selecting loss prevention materials to form an effective bridging strategy to cover both the matrix permeability and the fractures.

Section 3.8 presented a laboratory method for testing for the dual function of sealing a low-permeability formation and induced fractures [IX]. A successful fluid design involved a dual mode particle size distribution, where the coarser particles sealed the fracture apertures, whereas the finer particles sealed the matrix and the gaps between the larger particles.

Ma et al. (2019) conducted a study on core fracturing to assess the impact of different drilling fluid compositions on fracture pressures and implications for wellbore strengthening. They found that water-based fluids consistently enabled higher formation fracturing pressures than oil-based fluids, when the same weighting agents or plugging materials were used. This was despite the oil-based fluids showing lower API fluid loss values. They concluded that the combination of deformable and particulate materials can increase the fracture pressure of the core. Also, they concluded that nanomaterials had little impact on the fracture pressure of the core. In their discussions, they reflect upon the high fluid phase content of the filter-cakes of the oil-based fluids and observe that adding solids such as polyester and barite to the fluid increases the respective fracture pressures. They argue that the difference in the filter-

cakes result in a large difference in the core fracture pressure of the two drilling fluid systems. The data from the study also reveals an interesting contrast. When water was pumped through the core, the fracture pressure was very low at 5.73 MPa, whereas the fracture pressure increased to 18.99 MPa, when using a water-based drilling fluid without lost circulation materials. Here they make the comment that under the protection of the filter-cake formed by the drilling fluid, the migration of fluid filtrate had little effect on the fracturing of the core. Their conclusion is thus consistent with the findings presented in chapter 4.

Nagaso et al. (2015) investigated the impact of fluid viscosity on propagation of hydraulic fractures. They found that high viscous fluid was better than low viscous fluid for effective fracturing as the high viscous fluid promoted fracture propagation. Therefore, if the objective is to design a drilling fluid where induced fracturing is prevented, it may be beneficial to use a fluid system with a base fluid with low viscosity.

When conducting fluid loss tests with water-based fluids on permeable discs, it is generally observed that the spurt loss may contain a certain concentration of particles and that the filtrate retains some of the viscosity of the drilling fluid. After the initial spurt-loss, the fluid filtrate becomes clearer and less viscous and to a high degree resembles the liquid base of the drilling fluid. The analysis of fluid filtrate viscosity in section 3.6.2 confirms the observation that the primary fluid filtrate is viscous and shear thinning, whereas the secondary filtrate can be approximated by the Newtonian properties of the base fluid. For the fluids tested, the viscosity of the base oil used had a viscosity at room temperature which was 5 times higher than that of water. Bringing this observation into the studies of Ma et al. (2019), the main difference between the fracture pressure obtained with water and the water-based drilling fluid is the pressure drop in the fluid particles across the external filter-cake and hence lower pore-pressure inside the core for the fluid filtrate of the water-based fluid relative to when water is pumped. When water is pumped, the full wellbore pressure is transmitted into the first

pores of the core, and the pore-pressure gradient within the core is determined by the permeability of the core to water and the applied pressure or pump rate. When applying a water-based drilling fluid and once the external filter-cake is established, the fluid filtrate viscosity approaches that of water. As the fluid filtrate has a low viscosity any pressure initially transmitted into the core is readily dissipated through the core and local pore-pressure elevation near the wellbore is minimised.

In contrast, a higher viscosity base fluid, will lead to a higher viscosity fluid filtrate. Following the findings of Nagaso et al., a higher viscosity fluid will be more effective in inducing fracture propagation, likely due to higher localised pressure build-up and slower pressure dissipation.

Transferring these observations into the Mohr-Coulomb shear failure criterion and including the Terzaghi effective stress concept (Terzaghi, 1923), as introduced in chapter 1.2, the filter-cake's ability to isolate the pore-pressure within the formation from the higher fluid pressure in the wellbore will greatly impact the formation shear strength.

Field applications were conducted with the granular cellulose loss prevention material, AURACOAT® C [VIII]. The granular cellulose material had been selected due to its high mechanical and thermal wear resistance and high sealing strength. The LPM was introduced into barite weighted oil-based drilling fluids with specific gravities in the range from 1.5 to 1.75. Figure 5.1 presents a PSD of the solids in one such fluid before the addition of the granular cellulose material. The solids in the fluid were predominantly below 100 µm, and the D50 value was in the region of 10 µm, without considering the particle size of the brine droplets. The LPM material was sized between 200 µm and 600 µm, and when added to the fluid it would thus create a dual mode particle size distribution for the total fluid system. The LPM material was successfully recovered and recycled using a triple-deck shaker system. The triple-deck shaker system allows for stage-wise removal of particles,

where coarser particles are first removed at the top screen, of e.g. API grade 20-25, then a finer middle screen of e.g. API grade 60 may be used to recover the LPM particles before fine drilled solids are removed at the finer bottom screen of e.g. API 270 grade.

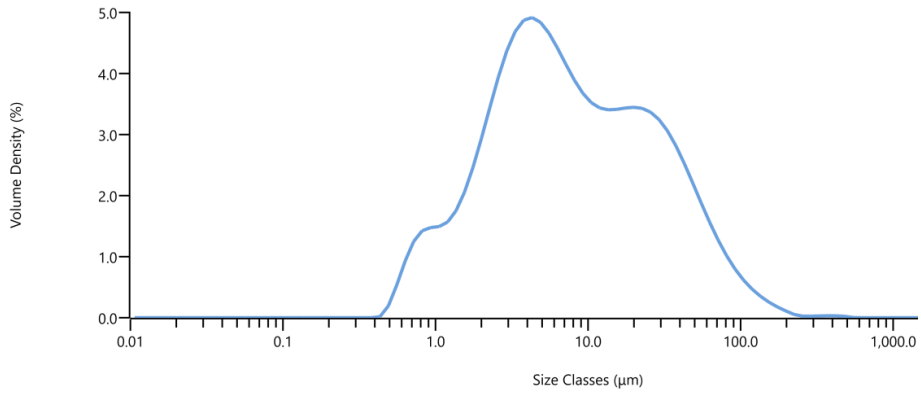

Figure 5-1: Particle size distribution of an oil-based field fluid without LPM [VIII]

The granular cellulose based LPM was shown to be effective in sealing natural fractures and stopped fracture propagation in chalk formations. The highest recorded overbalance was 3300 psi without losses, with a concentration of 28.5 kg/m^3 (10 lb / bbl) of LPM in the system. Earlier studies had shown fractures in the formation up to circa 500 µm. The field applications were thus consistent with the results in the laboratory studies of the granular cellulose material on fractured ceramic discs and slotted discs [VI, VIII and IX].

5.4 Treatment of high-loss situations

High-loss situations present a great technical and commercial challenge during drilling operations. Lost Circulation Materials of various kinds are typically applied as a first attempt to cure severe or total losses of drilling fluids. If such attempts are not successful, alternative remedies such as cementing, and resin plugs are used as alternatives. High cost

and time of application is a disadvantage of both cementing and resin plugs. Cementing may also be unsuccessful as it may be difficult to retain the cement in the fracture near the wellbore. With resins, the technical application is often challenging as the materials set at certain temperatures and time intervals. Therefore, if LCM can be effectively applied to seal off the loss zone, the savings may be very significant.

Alternatives to cementing and resin plugs are various versions of hydrogels. These typically need to be customized to specific conditions to obtain a balance between factors such as acceptable rheology for pumping, setting time and sufficient sealing strength. Pereira et al. (2022) shows an example of such an optimisation. In their study, a solid-free gel system was optimised for the Brazilian pre-salt formations where rheological properties at 70°C and high concentration of NaCl were critical. Their conclusions show that it is a complex system and that there is a critical balancing between pH, concentration of acrylic acid, initiator, helper polymer and crosslinker required to obtain the desired properties.

Various biogenic, synthetic or mineral-based materials are used alone or in combinations to create lost circulation material pills. $CaCO_3$, graphite, nutshells, mica, and cellulose fibres are examples of such materials. Khoshmardan et al. (2022) optimised and tested bagasse fibre-reinforced polypropylene (BFRP) material for sealing slotted discs up to 5 mm (0.2 inches) and found a 40% fibre and 60% polypropylene mixture to be partially effective in sealing before failing at 4.8 MPa (700 psi). In contrast, slots of 2, 3 and 4 mm (0.08, 0.12 and 0.16 inches) were successfully sealed at 6.9 MPa (1000 psi) pressure. In these tests, the BFRP mixture outperformed conventional LCM such as Mica, Oyster shells and Nutshells.

A series of tests were set up using conventional combinations of $CaCO_3$ and resilient graphite and compared with custom blends of cellulose particles in section 3.7 [VI, XI]. It was shown that the custom cellulose blends effectively sealed slotted discs up to 5mm, when mixed into either

oil-based or water-based fluids. The conventional blends of $CaCO_3$ and resilient graphite functioned better in water-based fluids than in oil-based fluids with the sealing effectiveness being good up to 1.5 mm slots in water-based fluids and up to circa 1.0 mm in oil-based fluids. A general challenge with high-density LCM materials such as $CaCO_3$ and other minerals is that particles with diameter of 1-2 mm and more require a very high viscosity or high-density fluid to remain suspended. In fully hydrated condition, the effective density of cellulose-based materials is typically in the range of 1-1.5 g/cm^3, and thus much easier to suspend in a typical drilling fluid. Since the cellulose-based materials are easier to suspend, they may also be used in high fluid loss squeeze pills for sealing of large fractures. With high fluid loss squeeze pills containing the cellulose-based material FEBRIBRIDGE® (D90 of 4500 µm), 10 mm slots were effectively sealed, thus extending the sealing range considerably relative to materials such as $CaCO_3$ and resilient graphite. Field applications of the same material was used to seal total losses of drilling fluid occurring in fractured carbonate formations and transition zones under differential pressures exceeding 21 MPa (3000 psi).

5.5 Discussion and summary

The survey conducted by Grelland [XV] shows that lost circulation in North Sea operations is predominantly treated by use of $CaCO_3$ and various types of graphite. Laboratory studies show that these materials have sealing limits somewhere between 1 and 1.5 mm, nut-shells have a limit around 2 mm, whereas various combinations of cellulose based materials can extend the sealing range and sealing pressures considerably [VI, XI], (Alsaba et al., 2014 and 2017). The size of particles that may be pumped are limited by the bottom hole arrangement used during drilling and the density of the materials used. High-density materials such as $CaCO_3$ are very difficult to keep suspended with particle sizes above 1-2 mm diameter, whereas cellulose-based materials have a density that more often is close to the density of the drilling fluid being

used. Another limiting factor is the nozzle size in the bit or the tolerances of the tools in the bottom hole assembly. Alternatives for pumping LCM pills with high concentrations of larger particles are the inclusion of a ported or circulation sub (PBL sub) or pumping through an open-ended pipe.

When materials are applied as LPM in the active system, the material toughness is critical to retain the particle size during circulation. This is necessary to retain the sealing effectiveness and avoiding a build-up of fine solids in the drilling fluid. Studies show that $CaCO_3$ particles degrade rapidly and have very limited size stability with particles larger than 40-53 µm (Scott et al., 2012 and Jueghale et al., 2023), [V, VI]. The specific degradation study presented in Table 5.1 shows that $CaCO_3$ particles quickly degrade to become smaller than 23 µm. Although $CaCO_3$ may be fully dissolved by use of acid, applying $CaCO_3$ as the only bridging particles in a reservoir drilling fluid causes a great risk of lost circulation and deep formation damage if particles >23 µm are required. Studies simulating mechanical degradation showed that $CaCO_3$ used as the sole bridging particles causes very high fluid loss, particle migration and formation damage in ceramic discs with pore-size of 120 µm after exposure of the LCM to mechanical wear [IV, V]. Although graphite shows better size stability, it is also shown to degrade significantly under conditions of mechanical wear (Scott et al., 2012), [VI]. Nut shells have been shown to degrade less than graphite Scott et al. (2012), although the best results were found with a special hardened granular cellulose [VI, VIII].

6 Summary and Conclusions

The objective of the research was to optimise drilling fluid additives for wellbore strengthening, preventing lost circulation and avoiding drilling fluid induced formation damage. Such optimisation involves the trade-off between different technical parameters, operational considerations, HSE implications and cost. Important technical variables are viscosity, density, effectiveness in fluid loss prevention and formation damage. Further, the selections need to be related to operational restrictions or limitations such as solids control systems.

Industry standard testing, such as e.g. HTHP test on 2.5 µm filter-paper, was found to be inadequate for ranking drilling fluids, and did not provide insight into the fluid's ability to enhance wellbore strengthening nor to prevent permeable formation damage. For this reason, other testing methodologies were evaluated. The application of the new test methodologies enabled new insight into important areas for designing and evaluating drilling fluids and drilling fluid additives for wellbore strengthening and reservoir protection.

Key methodologies applied were the exposure of drilling fluid to mechanical wear, use of ceramic disc to assess formation damage, analysis of fluid filtrate and study of filter-cake formation, filter-cake permeability, and strength. Further, testing with field mud was found to be important to ensure that realistic particle size distributions are present in the fluid during performance testing.

The fluid loss regression analysis yielded insight into formation of internal and external filter-cakes and the permeabilities of these. Further, the methodology may also yield insight into the relative permeability plugging of the internal and the external filter-cake by calculating the Relative Plugging Factor.

The majority of past research on loss prevention and lost circulation treatment is centred around particle size distribution theory. A shortcoming of the research is a lack of consideration for the mechanical properties of the particles included in the applied fluids. Mechanical properties that were found to be important were mechanical toughness, compressibility, elasticity, surface friction and adhesiveness/ cohesiveness.

The introduction of mechanical wear during the hot-rolling process clearly differentiated the drilling fluid additives with regards to retaining the original PSD. The most wear resistant particles were the granular cellulose and cellulose fibre particles. Resilient graphite showed moderate levels of degradation, whereas $CaCO_3$ degraded fastest. Test results indicate that $CaCO_3$ particles $\lesssim$ 23 µm degrade rapidly and hence need continuous replenishment if used as part of a drilling fluid design. The degradation of $CaCO_3$ will increase the build-up of fine particles in the drilling fluid, which may lead to increased formation damage and increased viscosity. Due to having the lowest size degradation rate, cellulose-based fibres or granular cellulose particles should be selected to represent the largest particles in a bridging PSD, up to the limit presented by the solids-control equipment.

It was shown that a commonly used water-based reservoir drilling fluid made with starch and $CaCO_3$ can create formation damage through polymer and solids migration. The formation damage was reduced by introducing cellulose-based fibres with D90 value $\lesssim$ 3/2 the median pore size. For a series of the water-based reservoir drilling fluids tested on a range from 10 µm to 50 µm pore sizes, the average retained permeability for the tests with the polymer/$CaCO_3$ base fluid was 73%, whereas the tests with the selected cellulose-based fibres yielded an average retained permeability of 88%. When tested on 120 µm ceramic discs, polymer/$CaCO_3$ fluids that had been exposed to mechanical wear generally showed high fluid loss and/or high solids invasion.

Although both synthetic/resilient graphite and $CaCO_3$ contributed effectively towards reducing fluid loss, the effectiveness with regards to creating a low-permeability filter-cake was primarily dependent on obtaining an even particle size distribution with significant presence of fine particles to cause internal plugging.

The combination of cellulose-based fibres and starch or PAC reduced the polymer content in the fluid filtrate, increased filter-cake strength and reduced filter-cake permeability. The inclusion of cellulose-based fibres yielded a filter-cake permeability that reduced with higher differential pressures. Filter-cakes made without cellulose-based fibres did not show signs of lower permeability at higher differential pressures.

For preventative treatment in drilling conditions with large differences between the matrix pore-size and the aperture of natural or induced fractures, a dual mode particle size distribution was found to be effective in both laboratory studies and field applications. In such situations, the fine mode of the PSD provided low filter-cake permeabilities when the particles followed an Andreasen distribution with a packing factor of around 0.08-0.10. Natural and induced fractures were most effectively sealed when granular cellulose particles made up the coarse mode of the PSD and these particles were sized similar to or slightly larger than the fracture aperture.

It was shown that typically 30-60% of an oil-based drilling fluid becomes part of the internal or external filter-cake, as the brine droplets form a part of the filter-cake. For water-based fluids the portion of the fluid that forms the filter-cake is typically between 5 and 35%. For oil-based fluids, the formation of an internal filter-cake is more predominant than for water-based fluids. In contrast, the pressure drop across the external filter-cake is more predominant for a water-based fluid. Further, the filtrate of an oil-based fluid typically has 3-6 times the viscosity of the fluid filtrate from water-based drilling fluids. The internal plugging effect caused by the brine particles and the higher base fluid viscosity are

key factors behind the often-observed superior fluid loss performance of oil-based fluids. The combination of brine particle invasion into the formation and a higher filtrate viscosity appears to be important factors behind why oil-based fluids are more prone to transfer the wellbore pressure into the first pores of the formation and thus more likely to cause induced fracturing. Therefore, to enhance wellbore strengthening and reduce induced fracturing when using an oil-based fluid, it is critical to include particles that act to form an external seal on a pore-throat or a fracture opening. For water-based fluids it appears that the sealing performance is gradually reduced as higher permeability test mediums are used. For oil-based fluids the drop in performance appears to be much sharper once the limit has been reached. Two potential causes of this behaviour may be that i) the higher base fluid viscosity of oil-based fluids increase the drag on particles to prevent them from forming a bridge or plug in a large pore opening and/or ii) that a high concentration of brine particles effectively separate bridging particles through a "crowding out" or "roller bearing" principle.

The formation damage was shown to occur during the spurt loss phase, as the length of the filtration test did not have any significant impact on the estimated formation damage. Focusing on the formation damage caused by invasion of solids, polymers or fibres, the formation damage was reduced when particle invasion during the spurt loss phase was limited and less related to the volume of the fluid loss filtrate. In certain tests when selected cellulose-based fibres were introduced, the spurt loss increased marginally, whereas the formation damage was reduced correspondingly. The effect appears to be that the cellulose-based fibres prevented solids and polymer migration when the D90 value was $\gtrsim 3/2$ times the median pore size, and thus limited the formation of an internal filter-cake. In contrast, when the cellulose-based fibres have a D90 value < 0.8 times the median pore size, this enhances the internal plugging effect.

For lost circulation materials for pill application, it was observed that the sealing strength and seal integrity was significantly higher with cellulose-based materials than with granular materials like $CaCO_3$ and resilient graphite. The is believed to be caused by more inter-particle friction and larger adhesive and cohesive forces between the cellulose-based particles. By introducing fine $CaCO_3$ particles into a cellulose-based LCM blend, the seal integrity was reduced, and the reverse pressure required to remove the LCM plug was reduced.

A key observation in the present research was that compressible and adaptable particles, such as cellulose-based materials, could in small concentrations alleviate sealing deficiencies caused by centred unimodal particle size distributions. The effect is likely caused by the cellulose particles elastically adapting to seal openings in pore-throats or between granular inert particles in a filter-cake. An elastic adaption enables an effective sealing even when the sealing particle is larger than what would be mathematically ideal from a particle packing perspective. An elastic adaption also increases the surface contact area between the particles, and hence also the internal friction in a filter-cake or an LCM plug.

7 Bibliography

Abdallah, W., Buckley, J.S., Carnegie, A., Herold, B, Edwards, J., Fordham, E., Graue, A., Habashy, T., Seleznev, N., Signer, C., Hussain, H., Montaron, B., and Ziauddin, M., 2007. Fundamentals of Wettability, *Oilfield Review,* **Summer 2007**, 44-61.

Abrams, A., 1977. Mud Design to Minimize Rock Impairment Due to Particle Invasion. *Journal of Petroleum Technology*, May 1977, **29**(5), 586-592.

Agarwal, S., Phuoc, T.X., Soong, Y., Martello, D. and Gupta, R.K, 2013. Nanoparticle-Stabilised Invert Emulsion Drilling Fluids for Deep-Hole Drilling of Oil and Gas, *The Canadian Journal of Chemical Engineering*, Volume **91**, October 2013.

Alberty, M.W. and McLean, M.R., 2004. A physical model for stress cages. Paper SPE-90493-MS. SPE Annual Technical Conference and Exhibition, Houston, Texas, September 2004. DOI: http://dx.doi.org/10.2118/90493-MS.

Alsaba, M., Al Dushaishi, M. F., Nygaard, R., Nes, O.-M. and Saasen, A., 2017. Updated Criterion to Select Particle Size Distribution of Lost Circulation Materials for An Effective Fracture Sealing. *Journal of Petroleum Science and Engineering*, **149**, 641-648.

Alsaba, M., Nygaard, R. and Hareland, G., 2015. In Review of Lost Circulation Materials and Treatments with an Updated Classification. Paper AADE-14-FTCE-25, AADE, Houston, Texas, USA.

Alsaba, M., Nygaard, R., Saasen, A. and Nes, O.M., 2014. Lost Circulation Materials Capability of Sealing Wide Fractures. Paper SPE-170285-MS; SPE Deepwater Drilling and Completions Conference, September 10-11 2014, Galveston, Texas, USA.

Alsaba, M., Nygaard, R., Saasen, A. and Nes, O.-M., 2016. Experimental investigation of fracture width limitations of granular lost circulation materials. *Journal of Petroleum Exploration and Production Technology*. **6**, 593–603 (2016). https://doi.org/10.1007/s13202-015-0225-3

Alshubbar, G., Nygaard, R. and Jeennakorn, M., 2018. The effect of wellbore circulation on building an LCM bridge at the fracture aperture. *Journal of Petroleum Science and Engineering*. **165**, 550–556, doi:10.1016/j.petrol.2018.02.034.

Andreasen, A.H.M., 1930. Ueber die Beziehung zwischen Kornabstufung und Zwischenraum in Produkten aus losen Körnern (mit einigen Experimenten). *Kolloid-Zeitschrift* **50**, 217–228 (1930). https://doi.org/10.1007/BF01422986 (In German)

ANSI/API RP 13B-1, 2019. Recommended Practice for Field Testing Water-based Drilling Fluids, 5th ed.; 2019, API Publishing Services, Washington, DC, USA.

ANSI/API RP 13B-2, 2014. Recommended Practice for Field Testing Oil-Based Drilling Fluids, 5th ed.; 2014, API Publishing Services, Washington, DC, USA.

ANSI/API RP 13C, 2014. Recommended Practice on Drilling Fluids Processing Systems Evaluation, 5th edition, 2014. API Publishing Services, Washington, DC, USA.

Audibert, A., Argiller, J.F., Ladva, H.K.J., Way, P.W. and Hove, A.O., 1999. Role of Polymers on Formation Damage, Paper SPE-54767-MS, SPE European Formation Damage Conference, The Hague, Netherlands, May 1999. https://doi.org/10.2118/54767-MS

Barton, N., 1976. The shear strength of rock and rock joints. *International Journal of Rock Mechanics and Mining Sciences and Geomechanics Abstracts* 1976; **13(9)**: 255-79

BeMiller, J.N., 2008. Hydrocolloids. *Gluten-Free Cereal Products and Beverages*, pp 203-215, Academic Press 2008. https://doi.org/10.1016/B978-012373739-7.50011-3

Bennion, D.B., 2002. An overview of formation damage mechanisms causing a reduction in the productivity and injectivity of oil and gas producing formations. *J Can Pet Technol* **41**, 29–36. https://doi.org/10.2118/02-11-DAS

Bolomey, J. 1927. Determination of the compressive strength of mortars and concretes. *Bulletin, ASCE, **16**: 22-24.*

Boycott, A., 1920. Sedimentation of Blood Corpuscles. *Nature* **104**, 532 (1920). https://doi.org/10.1038/104532b0

Civan, F., 2020. *Reservoir Formation Damage,* Gulf Professional Publishing: Waltham, MA,, USA. ISBN 978-0-12-801898-9.

DEA, Whitfill,D.L., and Nance,W. 2008. DEA 13-Investigation of Lost Circulation with Oil-based Muds(1985-1988). Technical/Project Report, Drilling Engineering Association (DEA). Houston, TX, USA.

Falahati, N., Routh, A.F. and Chellappah, K. 2020. The effect of particle properties and solids concentration on the yield stress behaviour of drilling fluid filter cakes.

Chemical Engineering Science, X, **7**, 2020: 100062. https://doi.org/10.1016/j.cesx.2020.100062

Fekete, P.O., Dosunmu, A., Anthony, K., Ekeinde, E.B., Anyanwu, C. and Odagme, B.S., 2013. Wellbore stability management in depleted and low pressure reservoirs. Paper SPE-167543, SPE Nigeria Annual International Conference and Exhibition, Lagos, August 5-7, 2013. https://doi.org/10.2118/167543-MS

Feng. Y. and Gray, K.E., 2017. Review of fundamental studies on lost circulation and wellbore strengthening. *Journal of Petroleum Science and Engineering*. **152** (3), February 2017. DOI: 10.1016/j.petrol.2017.01.052

Fuh, G-F., 1993. *Method for inhibiting the initiation and propagation of formation fractures while drilling and casing a well*, U.S. Patent 5,180,020 filed Oct. 31, 1991 and issued Jan. 19, 1993.

Fuh, G-F., 1993. *Method for inhibiting the initiation and propagation of formation fractures while drilling and casing a well*, U.S. Patent 5,207,282 filed Oct. 5, 1992 and issued May 4, 1993.

Fuh, G-F., Beardmore, D. and Morita, N., 2007. Further Development, Field Testing, and Application of the Wellbore Strengthening Technique for Drilling Operations. Paper SPE-105809-MS. SPE/IADC Drilling Conference, Amsterdam, The Netherlands, February 20-22, 2007.

Fuller, W.B. and Thompson, S.E., 1907. The Laws of Proportioning Concrete. *Transactions of the American Society of Civil Engineers*. Vol. **59**, issue 2, December 1907.

Gao, C., Miska, S., Yu, M., Dokhani, V., Ozbayoglu, E. and Takach, N., 2021. Experimental and numerical analysis of effective enhancement of wellbore stability in Shales with nanoparticles. *Journal of Natural Gas Science and Engineering*. **95**. 104197. 10.1016/j.jngse.2021.104197.

Gao, C., Miska, S., Yu, M., Dokhani, V., Ozbayoglu, E. and Takach, N., 2021. Geomechanical characterization of shale samples after pore plugging with nanomaterials. *Journal of Petroleum Science and Engineering* 208(1):109703, October 2021. DOI: 10.1016/j.petrol.2021.109703

Guerriero, V. and Mazzoli, S., 2021. Theory of Effective Stress in Soil and Rock and Implications for Fracturing Processes: A Review. *Geosciences* 2021, **11**, 119. https://doi.org/10.3390/ geosciences11030119

Green, J., Patey, I., Wright, L., Carazza, L. and Saasen, A., 2017. The Nature of Drilling Fluid Invasion, Clean-Up, and Retention during Reservoir Formation

Drilling and Completion. Paper SPE-185889-MS, SPE Bergen One Day Seminar, Bergen, Norway, April 2017.

Hu, S., Meng, Y. and Zhang, Y., 2023. Prediction Method for Sugarcane Syrup Brix Based on Improved Support Vector Regression. *Electronics* 2023, **12**, 1535. https://doi.org/10.3390/electronics12071535

Hoxha, B.B., Yang, L., Hale, A., and van Oort, E., 2016. Automated Particle Size Analysis using Advanced Analyzers. AADE-16-FTCE-78, AADE Fluids Technical Conference and Exhibition, Houston, TX, USA. http://dx.doi.org/10.2118/178877-MS

Iscan, A.G., Civan, F. and Kok, M.V., 2007. Alteration of permeability by drilling fluid invasion and flow reverseal. *Journal of Petroleum Science and Engineering*, **58** (1-2): 227-244. http://dx.doi.org/10.1016/j.petrol.2007.01.002

Jiang, G., Liu, T., Ning, F., Tu, Y., Zhang, L., Yu, Y. and Kuang, L., 2011. Polyethylene Glycol Drilling Fluid for Drilling in Marine Gas Hydrates-Bearing Sediments: An Experimental Study. *Energies*, **4**(1):140-150, 2011. https://doi.org/10.3390/en4010140

Jeughale, R., Khan, R. N., Andrews, K. H., Mendez, F. A., Nakano, S., Toki, T., Alzaabi, M. A., Klungtvedt, K. R., Sarap, G., Meki, Z., Gupta, K., Vallejo, A. V., Ramnarine, N., Nofal, S. F., and A. Y. Alzaabi. First Application of Biogenic Fibres in a Reservoir Drilling Fluid to Enable Safe Drilling and Data Acquisition Across a Depleted, Highly Laminated, Carbonate Reservoir With Heterogenous Characteristics. Paper presented at the ADIPEC, Abu Dhabi, UAE, October 2023. doi: https://doi.org/10.2118/216525-MS

Kaeuffer, M., 1973. Determination de L'Optimum deRemplissage Granulometrique et Quelques proprieties S'y Rattachant. Presented at Congres International de I'A.F.T.P.v., Rouen, Oct. 1973

Khan, R., Kuru, E., Tremblay, B. and Saasen, A., 2003. An investigation of Formation Damage Characteristics of Xanthan Gum Solutions Used For Drilling, Drill-in, Spacer Fluids and Coiled Tubing Applications, Paper 2003-067, Petroleum Society's Canadian International Petroleum Conference, Calgary, Alberta, Canada, June 10-12, 2003. http://dx.doi.org/10.2118/2003-067

Khan, R., Kuru, E., Tremblay, B., and Saasen, A., 2007. Extensional Viscosity of Polymer Based Fluids as a Possible Cause of Internal Cake Formation, *Energy Sources* A, vol**. 29**, pp. 1521-1528. http://dx.doi.org/10.1080/00908310600626630

Khoshmardan, M.A., Behbahani, T.J., Ghotbi, C. and Nasri, A., 2022. Experimental investigation of mechanical behaviour and microstructural analysis of bagasse

fibre-reinforces polypropylene (BFRP) composites to control lost circulation in water-based drilling mud. *Journal of Natural Gas Science and Engineering*. **100** (8): 104490. DOI: 10.1016/j.jngse.2022.104490

Kirsch, E.G., 1898. Die Theorie der Elastizität und die Bedürfnisse der Festigkeitslehre. *Zeitschrift des Vereines deutscher Ingenieure*, **42**, 797-807.

Kulicke, W.-M., Aggour, Y.A., Nottelmann, H. and Elsabee, M.Z., 1989. Swelling and Rheological Studies of Some Starch Hydrogels. *Starch - Stärke* **41**(4), 140–146. https://doi.org/10.1002/star.19890410405

Lade, P.V. and De Boer, R., 1997. The concept of effective stress for soil, *Geotechnique*, **47**(1), March 1997. DOI: 10.1680/geot.1997.47.1.61

Labuz, J.F. and Zang, A., 2012. Mohr-Coulomb Failure Criterion, *Rock Mech Rock Eng* **45**, 975–979. https://doi.org/10.1007/s00603-012-0281-7

Lomellini, P., 1992. Effect of chain length on the network modulus and entanglement. *Polymer* **33**, 1255–1260. https://doi.org/10.1016/0032-3861(92)90771-N

Luckham, P.F. and Rossi, S., 1999. The colloidal and rheological properties of bentonite suspensions. *Advances in Colloid and Interface Science*, **82** (1–3): 43–92. doi:10.1016/S0001-8686(99)00005-6.

Lyasara, A.C. and Ovri, J.E.O., 2015. Corrosion Behaviour and Effects on Drilling Mud. *International Journal of Scientific & Technology Research*. **4**(9) 917-923.

Ma, B., Pu, X., Zhao, Z., Wang, H. and Dong, W., 2019. Laboratory Study on Core Fracturing Simulations for Wellbore Strengthening. **Geofluids**, Volume **2019**, 1-18. Article ID 7942064. https://doi.org/10.1155/2019/7942064

Nagaso, M., Mikada, H. and Takekawa, J., 2015. The effects of fluid viscosity on the propagation of hydraulic fractures at the intersection of pre-existing fractures. The 19th International Symposium on Recent Advances in Exploration Geophysics (RAEG 2015), Chiba, Japan, May 2015. DOI: 10.3997/2352-8265.20140188

Neff, J.M., McKelvie, S. and Ayers, R.C. Jr., 2000. Environmental impacts of synthetic based drilling fluids. Report prepared for MMS by Robert Ayers & Associates, Inc. August 2000. U.S. Department of the Interior, Minerals Management Service, Gulf of Mexico OCS Region, New Orleans, LA. OCS Study MMS 2000-064. 118 pp

Nelson, P.H., 2009. Pore-throat sizes in sandstones, tight sandstones, and shales. *AAPG Bulletin*, **93**(3), 329–340, doi:10.1306/10240808059.

Nelson, A.Z. and Ewoldt, R.H., 2017. Design of yield stress fluids: A rheology-to-structure inverse problem, *Soft Matter* **13**(41) 7578 – 7594. http://dx.doi.org/10.1039/C7SM00758B

Ofei, T.N., Cheng, I., Lund, B., Saasen, A. and Sangesland, S., 2020. On The Stability of Oil-Based Drilling Fluid: Effect of Oil-Water Ratio. OMAE2020-19071, August 3-7 2020, Virtual Conference Online. DOI: 10.1115/OMAE2020-19071

Olsen, H., Briedis, N.A. and Renshaw, D., 2017. Sedimentologial analysis and reservoir characterisation of a multi-darcy, billion barrel oil field – the Upper Jurassic shallow marine sandstones of the Johan Sverdrup field, North Sea, Norway. *Marine and Petroleum Geology*, **84** (2017) 102-134. https://doi.org/10.1016/j.marpetgeo.2017.03.029

Osode, P.I., Hussain, H.A., Bataweel, M.A. and Babbington, J.F., 2016. Drill-in Fluids Design and Selection for a Low-Permeability, SubHydrostatic Carbonate Reservoir Development. Paper SPE-182878-MS, Abu Dhabi International Petroleum Exhibition and Conference, Abu Dhabi, UAE, 7–10 November 2016.

Pedrosa, C., Saasen, A., Lund, B. and Ytrehus, J.D., 2021. Wet Drilled Cuttings Bed Rheology. *Energies* 2021, **14**, 1644. https://doi.org/10.3390/en14061644

Pereira, F.C., Clinckspoor, K.J. and Moreno, R.B.Z.L., 2022. Optimization of an in-situ polymerized and crosslinked hydrogel formulation for lost circulation control. *Journal of Petroleum Science and Engineering*, **208** (D) 109687. https://doi.org/10.1016/j.petrol.2021.109687

Pitoni, E., Ballard, D.A., and Kelly, R.M., 1999. Changes in Solids Composition of Reservoir Drill in Fluids during Drilling and the Impact on Filter Cake Properties. Paper SPE-54753-MS, SPE European Formation Damage Conferences, The Hauge, The Netherlands, May 1999. https://doi.org/10.2118/54753-MS

Ribeiro Borges, P.H., Panzera, T.H., Nunes, V.A. and Martuscelli, C.C., 2014. Andreasen particle packing method on the development of geopolymer concrete for civil engineering. *Journal of Materials in Civil Engineering*, **26**, 692-697, April 2014. DOI: 10.1061/(ASCE)MT.1943-5533.0000838

Røgen, B. and Fabricius, I.L., 2022. Influence of clay and silica on permeability and capillary entry pressure of chalk reservoirs in the North Sea. *Petroleum Geoscience* **8**(3):287-293, September 2002. http://dx.doi.org/10.1144/petgeo.8.3.287

Saasen, A., Svanes, K., Omland, T.H., Mathiassen, E., Vikane, O., 2004. Well Cleaning Performance, Paper SPE-87204-MS, IADC/SPE Drilling Conference, Dallas, TX, USa, March 2004. http://dx.doi.org/10.2118/87204-MS

Saasen, A. and Ytrehus, J.D., 2018. Rheological properties of drilling fluids: Use of dimensionless shear rates in Herschel-Bulkley and Power-Law models. *Applied Rheology*, Vol. **28**, no. 5, 2018, pp 201854515. DOI:10.3933/APPLRHEOL-28-54515

Sadian, M., Prasad, M. and Koh, C.A., 2015. Measurement of the Water Droplet Size in Water-in-Oil Emulsions Using Low Field Nuclear Magnetic resonance for Gas Hydrate Slurry Application, *Canadian Journal of Chemistry*, **93**:1-7, April 2015. DOI: 10.1139/cjc-2014-0608

Scott, P., Beardmore, D.H., Wade, Z.D., Evans, E. and Franks, K.D., 2012. Size Degradation of Granular Lost Circulation Materials. Paper SPE-151227-MS, IADC/SPE Drilling Conference and Exhibition held in San Diego, California, 6-8 March 2012. http://dx.doi.org/10.2118/151227-MS

Scott, P., Redburn, M. and Nesheim, G., 2020. A Pragmatic approach to Lost Circulation Treatments: What every Drilling Engineer Should Know. AADE-20-FTCE-062.

Sharma, M.M., Chenevert, M., Guo, Q., Ji, L., Friedheim, J. and Zhang, R., 2012. A New Family of Nanoparticle Based Drilling Fluids. Paper SPE-160045-MS, SPE Annual Technical Conference and Exhibition, San Antonio, Texas, USA. 5. 10.2118/160045-MS.

Shen, B., Shi, J. and Barton, N., 2018. An approximate nonlinear modified Mohr-Coulomb shear strength criterion with critical state for intact rocks. *Journal of Rock Mechanics and Geotechnical Engineering*. **10** (2018) 645-652. http://dx.doi.org/10.1016/j.jrmge.2018.04.002

Sheerwood, J.D. and Meeten, G.H., 1997. The filtration properties of compressible mud filtercakes. *Journal of Petroleum Science and Engineering*, **18** (1) 73-81. http://dx.doi.org/10.1016/S0920-4105(97)00005-3

Sherwood, J.D. and Meeten, G.H., Farrow, C.A., Alderman, N.J., 1991. Squeeze-film rheometry of non-uniform mudcakes. *Journal of Non-Newtonian Fluid Mechanics*, Volume **39**, Issue 3, 1991, pp 311-334. http://dx.doi.org/10.1016/0377-0257(91)80020-K

Skjeggestad, O., 1989. *Boreslamteknologi, teori og praksis*, ISBN 82-4190010-4, Alma Mater Forlag AS, Bergen, Norway 1989. (in Norwegian)

Terzaghi, K., 1923. Die Berechnung der Durchlassigkeitsziffer des Tones aus Dem Verlauf der Hidrodynamichen Span-Nungserscheinungen Akademie der Wissenschaften in Wien. *Mathematish-Naturwissen-Schaftiliche Klasse*: **132**, 125-138.

van Oort, E., Friedheim, J., Pierce, T. and Lee, J., 2009. Avoiding losses in depleted and weak zones by constantly strengthening wellbore. Paper SPE-125093-MS, *SPE Drilling & Completion*, **26** (4), December 2011.

Vasshus, J.K., Klungtvedt, K.R. and Mandal, S.K., 2019. *Composition for making a solids-free drilling fluid a non-invasive drilling fluid*. Norwegian patent 345560, filed 10.12.2019, granted 19.04.2021.

Vasshus, J.K., Klungtvedt, K.R. and Mandal, S.K., 2020. *Composition for making a solids-free drilling fluid a non-invasive drilling fluid*. UK patent GB2595161. Norwegian patent 345560, filed 13.03.2020, granted 26.10.2022.

Vickers, S., Cowie, M., Jones, T., and Twynam, A. J., 2006. A New Methodology That Surpasses Current Bridging Theories to Efficiently Seal A Varied Pore Throat Distribution as Found in Natural Reservoir Formations, AADE Drilling Fluids Technical Conference, Houston, Texas, April 11-12, (2006).

Whitfill, D., 2008. In Proceedings of the Lost Circulation Material Selection, Particle Size Distribution and Fracture Modelling with Fracture Simulation Software. Paper SPE-115039-MS, IADC/SPE Asia Pacific Drilling Technology Conference and Exhibition, Jakarta, India, 25–27 August 2008. https://doi.org/10.2118/115039-MS

Wennberg, O.P, Casini, G., Jonoud, S. and Peacock, D.C.P., 2016. The Characteristics of Open Fractures in Carbonate Reservoirs and their Impact on Fluid Flow: A Discussion. *Petroleum Geoscience*, **22**(1):91-94, January 2016. DOI: 10.1144/petgeo2015-003

Werner, B., 2018. The Influence of Drilling-Fluid Rheology on Cuttings-Bed Behaviour, PhD thesis, Norwegian Technical University. DOI: 10.13140/RG.2.2.19105.30566

Zou, Z., Zhao, Q., Wang, Q. and Zhou, F., 2019. Thermal stability of xanthan gum polymers and its application in salt-tolerant bentonite water-based mud. *Journal of Polymer Engineering*, vol. **39**, no. 6, 2019, pp. 501-507. https://doi.org/10.1515/polyeng-2018-0386

8 Table of figures

9 List of tables

Appendices

Appendix 1 – Procedure for HTHP testing of fluid loss on permeable discs including measurement of changes in disc mass and permeability

1. Mix drilling fluid according to the recipe allowing sufficient time for mixing of the various additives,
2. Measure pH and rheology,
3. Hot-roll for 16 hours at 90°C, or as otherwise descried, and if applicable degrade by high-shear stirring or other degradation method,
4. Measure pH and rheology after hot-rolling and any degradation,
5. Mark and weigh disc in dry condition using the moisture analyser (M_b). Moisture analyzer shall be set to dry disc at 105 °C until change in mass is less than 1 mg/60 s,
6. Optional step: place disc in acrylic cell and measure air temperature and flowrate at different pressures to calculate average permeability to air (K_{ab}),
7. Optional step: place disc in acrylic cell and place arrangement with water in vacuum (circa −0.96 bar for 5 min) to remove any air from disc or water. Flow thereafter water through disc and measure water temperature and flowrate at different pressures to calculate average permeability to water (K_{wb}),
8. Soak disc in brine (40 g NaCl per 1000 g freshwater) in vacuum,
9. Conduct HTHP test at desired pressure, typically 3.45 MPa (500 psi) or 6.9 MPa (1000 psi), and measure both volume (V_f) and mass (M_f) of fluid filtrate at point in time of 15 s, 30 s, 1 min, 2 min, 3 min, 5 min, 10 min, 15 min, 20 min and 30 min (V_f) or, if available, measure mass of fluid filtrate using digital scale at intervals of 1-10 seconds during the testing period. Calculate fluid filtrate density,
10. Weigh disc with filter-cake and observe filter-cake, note any anomalies
11. Place disc in acrylic cell and reverse flow with 1 L (40 g NaCl per 1000 g water) heated to 60 °C, or other specified temperature, and then with 1 litre water heated to 60°C to remove traces of salt before drying. Note pressure required to enable reverse flow through disc,
12. Optional step: place disc in breaker fluid for required time and at required temperature. (Note that certain acids may partially dissolve

the test discs, so acid application needs to be tested to ensure that the measurements of mass change and permeability are not impacted by part solubilising of the test disc.) Place disc in acrylic cell and flow disc with 1 litre water at ambient temperature to remove any dissolved filter-cake residue,

13. Optional step: place disc in acrylic cell and place arrangement with water in vacuum to remove any air from disc or water. Flow thereafter water through disc and measure water temperature and flowrate at different pressures to calculate average permeability to water (K_{wa}),
14. Weigh disc in dry condition using moisture analyser (M_a) using the same settings as in step 5,
15. Optional step: place disc in acrylic cell and measure air temperature and flowrate at different pressures to calculate average permeability to air (K_{aa}).

Depending on the number of optional steps included in the procedure, it enables collection of a large amount of data in addition to observing the filter-cake and the fluid filtrate volume $V_{f.}$

The moisture analyser used for weighing the discs was set to heating the discs to 105 °C and continue drying until the mass change due to moisture evaporation was less than 1 mg per 60 s. The drying process then stopped automatically, and the mass of the disc displayed. The precision of the instrument is 1 mg. The change in disc mass was then simply calculated as:

$$(M_a) - (M_b) = M_{change}$$

By placing a digital weight under the graduated cylinder used to measure fluid filtrate, it was possible to simultaneously record the mass of the fluid filtrate and read the volume of the filtrate. This enabled a precise estimation of the fluid loss profile and calculating the fluid filtrate density (D_f), calculated as:

$$(M_f)/(V_f) = (D_f)$$

The permeability was calculated as an average of multiple readings within certain flow-rate ranges. Darcy's law was used in a rearranged form as follows:

$$K = \eta \frac{Q * \Delta L}{A * \Delta P}$$

Where K is the calculated permeability coefficient (m^2), η is the viscosity of the fluid (Pa * s), Q the fluid flowrate (m^3/s), ΔL the disc thickness

(m), A the areal of flow into the disc and ΔP the pressure differential over the disc (Pa).

Appendix 2 – List of Equipment

- AEP Transducers JET Pressure Gauge with Data Logger, for measuring and logging applied pressure
- Anton Paar DMA 35n density and specific gravity meter
- Anton Paar MCR-301 Rheometer with powder shear cell
- Apera pH90, pH meter
- Custom built permeability plugging apparatus with hydraulic pump for testing slotted discs, tapered slotted discs or ceramic discs up to 35 MPa (5076 psi)
- Custom built reverse flow and permeability measurement apparatus with Festo pressure regulators, pressure sensors and flow sensors
- DVP EC.20-1, Vacuum chamber
- Hamilton Beach Mixer, for mixing of drilling fluids
- Hanna HI96801 Refractometer
- Haver & Boecker EML Digital Plus sieve-shakers and sieves for dry and wet sieveing
- Heidolph RR-2021 mixer
- Ofite dual capped HTHP cell with nitrogen manifold, #170-01-02
- Ofite single capped HTHP cell for CO_2 cartridge, #170-01
- Ofite ceramic discs, #170-53 and #170-55 series; 10 µm, 20 µm, 50 µm, 120 µm, 160 µm, 180 µm and 250 µm
- Ofite emulsion stability meter, #131-50

- Ofite retort kit 50 ml, #165-14-1
- Ofite roller-oven, #172-00-1-C, for aging the drilling fluid samples
- Ofite viscometer model 900, for measuring fluid rheological parameters
- Ohaus MB120 moisture analyser
- Ohaus Pioneer Precision PX3202, for weighing the drilling fluid ingredients
- Thermo Scientific, Eutech Expert CTS, for measuring fluid filtrate
- Whatman hardened ashless filterpaper, 2.5 µm, 8 µm, 11 µm and 22 µm

Appendix 3 – Nomenclature

ANSI, American National Standards Institute

API, American Petroleum Institute

ASTM, American Society for Testing Materials

BRIX, degrees Brix (°Bx) is a refractive index

ECD, Equivalent circulating density

FBP, Fracture breakdown pressure [Pa]

FIP, Fractur initiation pressure [Pa]

FPP, Fracture propagation pressure [Pa]

FRP, Fracture re-opening pressure [Pa]

HTHP, High temperature and high pressure

IPT, Ideal packing theory

LCM, Lost circulation material

LPM, Loss prevention material

NIF, Non-invasive fluid additive

OBM, Oil-based mud or drilling fluid

PAC, Poly-anionic cellulose
PPA, Permeability plugging apparatus

PSD, Particle size distribution

WBM, Water-based mud or drilling fluid

XC, Xanthan gum or XC polymer

c, Cohesion (Pa)

C_{FL}, Coefficient of fluid loss (ml/s0.5)

FL_T, Fluid loss at time T (ml)

ffc, Flow function coefficient

K, Permeability (D)

k, Power law consistency index

k_f, Portion of a drilling fluid that forms a part of the filter-cake

ΔL, Thickness of filter-cake (m, cm or mm in practical applications)

n, Power law flow behaviour index

P or p, Pressure (Pa)

ΔP, Differential pressure (Pa)

Q, Flowrate (m3/s)

R, Flow resistance (Pa*$s^{0.5}$/m3)

RPF, Relative plugging factor ($s^{0.5}$)

SL, Spurt loss constant (ml)

$\dot{\gamma}$, Shear rate (1/s)
η or μ, Viscosity (Pa*s)
θ, contact angle
ϕ, internal friction angle
μ, Coefficient of friction
v, Volumetric concentration of particles in the fluid (%)
ρ, Density (kg/m3 or g/cm3)
σ, Stress (Pa)
τ, Shear stress (Pa)

Φ, Sphericity of grains
φ, Porosity

Appendix 4 – Published articles, I-IX

I. Klungtvedt, K.R., Saasen, A., Vasshus, J.K., Trodal, V.B., Mandal, S.K., Berglind, B. and Khalifeh, M. “The Fundamental Principles and Standard Evaluation for Fluid Loss and Possible Extensions of Test Methodology to Assess Consequences for Formation Damage.” Energies, VOL No. 18 (8), Paper 2252 – MDPI, 2021. (open access)

energies

MDPI

Article

The Fundamental Principles and Standard Evaluation for Fluid Loss and Possible Extensions of Test Methodology to Assess Consequences for Formation Damage

Karl Ronny Klungtvedt [1,2,*], Arild Saasen [2], Jan Kristian Vasshus [1], Vegard Bror Trodal [2], Swapan Kumar Mandal [1], Bjørn Berglind [1] and Mahmoud Khalifeh [2]

[1] European Mud Company AS, 4033 Stavanger, Norway; jkv@emcas.no (J.K.V.); sm@emcas.no (S.K.M.); bb@emcas.no (B.B.)
[2] Department of Energy and Petroleum Engineering, University of Stavanger, 4021 Stavanger, Norway; arild.saasen@uis.no (A.S.); vegardtrodal@gmail.com (V.B.T.); mahmoud.khalifeh@uis.no (M.K.)
* Correspondence: krk@emcas.no

Abstract: Industry testing procedures such as ANSI/API 13B-1 describe a method for measuring fluid loss and studying filter-cake formation against a medium of either a filter paper or a porous disc, without giving information about potential formation damage. Considering the thickness of the discs, it may also be possible to extend the method to gain an insight into aspects of formation damage. A new experimental set-up and methodology was created to evaluate changes to the porous discs after HTHP testing to generate insight into signs of formation damage, such as changes in disc mass and permeability. Such measurements were enabled by placing the disc in a cell, which allowed for reverse flow of fluid to lift off the filter-cake. Experiments were conducted with different drilling fluid compositions to evaluate the use of the new methodology. The first test series showed consistent changes in disc mass as a function of the additives applied into the fluid. The data yield insights into how the discs are sealed and to which degree solids, fibers or polymers are entering the discs. A second series of tests were set up to extend the procedure to also measure changes in the disc's permeability to air and water. The results showed that there was a positive correlation between changes in disc mass and changes in permeability. The conclusions are that the methodology may enable identifying signs of formation damage and that further studies should be conducted to optimize the method.

Keywords: fluid loss; formation damage; lost circulation; drilling fluids; filter-cake removal

Citation: Klungtvedt, K.R.; Saasen, A.; Vasshus, J.K.; Trodal, V.B.; Mandal, S.K.; Berglind, B.; Khalifeh, M. The Fundamental Principles and Standard Evaluation for Fluid Loss and Possible Extensions of Test Methodology to Assess Consequences for Formation Damage. *Energies* **2021**, *14*, 2252. https://doi.org/10.3390/en14082252

Academic Editor: Ergun Kuru

Received: 17 February 2021
Accepted: 15 April 2021
Published: 16 April 2021

1. Introduction

Different types of lost circulation materials (LCMs) are available for preventative or reactive treatment of fluid loss using procedures such as ANSI/API 13B-1 [1]. Categorization of such materials has been conducted; however, due to different application methods and different design criteria, no consistent evaluation method has been established [2]. For sealing of larger fractures, testing using slotted discs are often used and maximum sealing pressures measured. Jeennakorn et al., 2017 and 2018 [3,4] showed that varying testing conditions might give different results when testing lost circulation materials. Variations in drilling fluid compositions such as using different base fluids, density, and weighting materials impact LCM performance. Additionally, it was shown that different time-dependent degradation could occur under severe downhole conditions.

In 2018, Alshubbar et al. [5] studied the performance of LCM under conditions of an annular flow of fluid. By varying the circulation rates, they found that higher circulation rates led to higher fluid losses before a seal could be established. In addition, they identified that LCM with lower specific gravity was less prone to variations in the circulating conditions making them better preventative approach candidates.

Alsaba et al., 2014 [6] concluded that fibrous materials showed the best performance among conventional LCM in terms of sealing fractures in tapered discs and in maintaining the integrity of the formed seal within the fractures. They obtained sealing pressures up to 20.2 MPa (2925 psi) before failure when sealing a disc with a 1.0 mm fracture tip. Further, they concluded that the superior performance of the fibrous materials was considered to be due to the wide range of particle sizes and the irregularity in particle shapes and degree of deformability. In contrast, they concluded that granular materials such as $CaCO_3$ and graphite formed seals with relatively low integrity. In 2019, Khalifeh et al. [7] conducted high-pressure slot testing of fiber-based LCM demonstrating sealing performance where the seal did not fail even with pressures of more than 34.5 MPa (5000 psi) being applied. Further, it was shown that seals were dynamically built to withstand higher differential pressure.

Saasen et al., 2018 [8] tested lost circulation materials using a coarse gravel bed in addition to testing on slotted discs with the objective of testing materials for healing severe losses of drilling fluid to the formation. They found that addition of short fibers reduced filtration in porous formations and that use of long fibers may heal severe losses in fractured formations. Lee et al., 2020 [9] conducted parametric studies in numerical simulations to better understand thermal effects of sealing mechanisms of lost circulation materials. By studying properties such as fluid viscosity, particle size, friction coefficient, and Young's modulus they found that thermally degraded properties lead to inefficient fracture sealing.

In 1975, Enstad [10] described how dry powders might block hoppers with openings several times larger than the size of the dry powders. However, when transferring particles in a liquid or drilling fluid, different mechanisms will interact and change the particle plugging behavior. Whitfill 2008 [11] proposed a method for selecting a particle size distribution (PSD) based on the expected fracture width, where the D50 value should be equal to the fracture width to ensure the formation of an effective seal or plug. In 2015, Alsaba et al. [12] studied lost circulation materials of different shapes and their ability to seal fractures up to 2000 µm. They concluded that PSD had a significant effect on the seal integrities, and in particular the D90 value. It was found that a D90 value, which was equal or slightly larger than the fracture width, was required to initiate a strong seal. When combined with finer particles, the permeability of the seal would be lower, and the fluid loss reduced. A study of sealing pressure prediction [13] also found that in after the fracture width and fluid density, the D90 value was the most significant influence of sealing pressure.

The observation of particle size degradation of $CaCO_3$ and graphite, primarily due to the influence of shear, was also observed by Hoxha et al., 2016 [14]. In their studies the D50 values of medium grade $CaCO_3$ decreased by 25–40% after 30 min of shearing. Further, it was found that various methods for measuring the PSD yielded different results. As an example, the change in D50 value of regular grade graphite was recorded to be reduced between 20% to circa 70%.

In 1999, Pitoni et al. [15] studied how changes in solids composition of reservoir drilling fluids impacted forming of filter-cakes and return permeabilities. They found that filter-cake became softer and thickness increased with increasing solids content in the fluid. However, they observed that the higher the clay content, the thinner and harder the filter-cake. Additionally, the fluids with higher clay contents gave a lower return permeability. They also concluded that the size of the bridging particles effectively could be increased for high permeability or poorly consolidated formations, by adding coarse bridging particles and running the system in a "sacrificial" manner.

When conducting core flood studies to assist in designing of drilling and completion fluids in 2017, Green et al. [16] found that the lowest permeability alterations did not correlate with the lowest drilling fluid filtrate loss volumes. They concluded that the major formation damage is more likely to be caused by the drilling fluid filter cake's ability to stick to the formation and whether it can be removed during production.

Czuprat et al., 2019 [17] conducted experiments with long-term (14 days) static aging of drilling fluids and testing of fluid properties including filtration behavior and formation damage tests on sandstone samples and reservoir rock. They concluded that lower solids content in the drilling fluid would result in a slower build-up of the filter-cake, thus allowing for a higher amount of fluid filtrate invasion to occur. Additionally, they concluded that the long test period might be impractical for a service company to conduct tests before selecting a drilling fluid.

When drilling a reservoir formation with a water-based drilling fluid, polymers are used to provide viscosity and to control filtration losses. Khan et al. [18] showed that polymers such as xanthan gum, long-chain poly anionic cellulose (PAC) and starch may help in reducing fluid losses to the formation. If the pore-throats are exceeding, e.g., 20 µm and differential pressures exceeding 3.45 MPa (500 psi), such polymer additives may have little effect in preventing solids from entering the formation. PAC with shorter chains and lower viscosity (PAC LV) impact are used to reduce fluid losses through their bonding to solids in the drilling fluid and to pore-throats in the formation.

Cobianco et al., 2001 [19] developed a drill-in fluid for low permeability reservoirs using a fluid consisting of biopolymers, highly crosslinked starch and microfibrous cellulose. The used Portland limestone cores with permeability of ca. 20–100 mD for static filtration tests at differential pressures ranging from 1 to 3 MPa (145–435 psi) at 80 °C and backflowed with a 3% KCl brine to measure permeability to brine. They found that when the drilling fluid including cuttings, the return permeability was slightly lower than the formulation without the cuttings. SEM micrographs indicated that cuttings invasion was limited to the first 100 µm.

Nelson 2009 [20] conducted a study on pore-throat sizes in siliciclastic rocks and found that they form a continuum from the submillimeter to the nanometer scale. He found that reservoir sandstones generally have pore sizes greater than 20 µm and pore-throat sizes greater than 2 µm. The data reported by Nelson are hence consistent with also using discs with a median pore-throat size of 20 µm to represent a sandstone formation.

Reservoir formation damage may take place through different mechanisms [21]. It is a generic term that refers to impairment of the permeability of petroleum-bearing formations by various adverse processes. The impairment may take the form of a mechanical mechanism, such as, e.g., fines migration, solids invasion or phase trapping, or in the form of biological mechanisms or chemical mechanisms.

The literature shows that test procedures (e.g., types of fluids, applied pressure and temperature, type of flooded medium, type and geometry of LCM, etc.) create inconsistency in results obtained by different researchers. Some research study changes in formation damage by measuring changes in permeability to a fluid using rock cores. These cores are of a different nature than the discs used for the day-to-day testing of fluid loss, as per ANSI/API13B-1, thereby making such testing less accessible for a researcher or a fluid engineer.

Therefore, in this article, experiments were set up to understand the data set that is typically collected when conducting HTHP test according to ANSI/API13B-1. Thereafter, new testing methods are investigated to identify if new information about fluid loss and formation damage could be collected by extending the test procedures and using the same permeable discs. The overall objective is to use such methods for further product development and evaluation or optimization of drilling fluids. If cost-effective test methods can be established, it will facilitate more effective research and more consistent comparison of various drilling fluid compositions. The objective of the research was to identify a cost-effective method for testing drilling fluids and drilling fluid additives and to verify if this method could be used to provide reliable information about formation damage or indication of formation damage. The introduction of a moisture analyzer to precisely measure the mass change of the discs may be such a cost-effective method for identifying formation damage.

2. Analytical Approach

An experimental setup was therefore built with the following main objectives and functionalities:

- Enabling reverse flow of a fluid through the discs, after the HTHP tests, to understand filter-cake lift-off pressures.
- Enabling measurement of disc mass before and after the HTHP test and filter-cake removal to obtain indications of polymer or solids invasion into the discs.
- Enabling disc permeability estimation before and after the HTHP test and filter-cake removal to obtain indications of changes in disc permeability.
- Studying fluid loss profiles and filter-cake building.
- Establishing a practical routine for application of breaker fluid or acid to remove filter-cake.
- Understanding how various fluid degradation methods may impact the fluid loss and reservoir formation damage.

In order to investigate these potential changes in methodology, the two different base fluids shown in Appendix A, Tables A1 and A5 with KCl, xanthan gum and PAC were used. The effect of incorporation of different solids particles in the form of bentonite, $CaCO_3$, micronized barite and three types of cellulose-based fibers was investigated. The objective of using different base fluids and different fibers was to verify if the methodology could be valid for different types of fluid compositions. As the verification on the methodology was the primary objective of the research, the actual product names are not used in the descriptions. Experiments were set up with discs of mean pore-throats of 20 µm, 120 µm and 250 µm to reflect different permeability formations.

2.1. Key Factors in Fluid Loss Measurement Using Water-Based Drilling Fluids

Field engineers evaluate the properties of drilling fluid during operations to understand the requirement for potential treatment of the fluid to obtain certain desired parameters. One of these tests will normally be an HTHP test to understand filter-cake properties and the drilling fluid's ability to create a temporary seal against permeable formation.

2.1.1. Equipment for Testing According to ANSI/API 13B-1

In addition to conventional laboratory equipment for mixing (e.g., hot-rolling drilling fluids, pH and rheology measurements), the primary equipment required is an HTHP cell, which allows for testing on filter paper and permeable discs. In the experiments that were conducted, the following equipment was used:

- Hamilton Beach Mixer, Virginia, USA;
- Ohaus Pioneer Precision PX3202, New Jersey, USA;
- Ofite Filter Press HTHP 175 mL, Double Capped, Texas, USA;
- Ofite Viscometer model 900, Texas, USA;
- Ofite roller-oven #172-00-1-C, Texas, USA;
- Apera pH90, pH meter, Wuppertal, Germany.

2.1.2. Test Procedure and Data Collection in Accordance with ANSI/API 13B-1

For the full procedure, please refer to the ANSI/API 13B-1 for water-based drilling fluids or ANSI/API 13B-2 for oil-based drilling fluids [22]. The information contained herein contains only the main elements. The filtration tests are conducted at high temperature and high pressure under static conditions using a pressurized gas source to create a differential pressure across the test medium. The test medium used is either a filter paper, typically with a median pore-throat of 2.5 µm or permeable ceramic discs with means pore throats ranging from 10 to 250 µm. After the differential pressure has been applied and the temperature in the cell has reached the desired level, the cylinder outlet valve is opened to enable the differential pressure to drive the fluid towards the medium. The fluid filtrate

is thereafter collected and measured over a 30-min period. For comparison with other tests, one needs to account for differences in filter area. The data collected according to the procedure is:

- Measure the filter-cake thickness, at its center, to the nearest millimeter (or 1/32 in).
- Observe indications of settling of solids on the filter-cake, such as an abnormally thick cake or coarse texture, and record comments.
- The filtrate volume V_f should be measured and normalized with regards to filter area.

2.2. Extending the HTHP Filtration Tests to Study Signs of Formation Damage

The objective is to collect information related to formation damage and other operational parameters and to identify if the methodology can yield meaningful information about potential formation damage.

2.2.1. Equipment Overview

The experimental set-up was centered around a cell with regulated supply of pressured air to drive a fluid or air through the ceramic discs. The experiments were not planned for filter paper, as the filter paper is not designed for higher pressures than 3.45 MPa (500 psi). By reversing the discs into the cell, fluid can be pumped through the disc at low pressures to study the lift-off pressure of filter-cakes, as shown in Figure 1. Further, by measuring both the supply pressure and flowrate, estimates of disc permeability could be conducted. Extending the procedure further, a moisture analyzer was used to measure the mass of the disc in a standardized dry condition before the HTHP test and after the test including reverse flow and any breaker application. The following equipment was used for the experimental set-up in addition to the standard equipment used for the HTHP test according to ANSI/API 13B-1:

- Ohaus MB120 Moisture Analyzer;
- Custom built transparent acrylic cell with stand for enabling of reverse flow of fluid through the ceramic discs;
- Festo pressure regulator LRP-1/4-2.5 and LRP-1/4-0.25;
- Festo Pressure Sensor SPAN-P025R and SPAN-P10R;
- Festo Flowmeter SFAH-10U;
- Nitrogen source and manifold for pressure up to 9.3 MPa (1350 psi), Ofite #171-24;
- Vacuum machine, DVP EC.20-1.

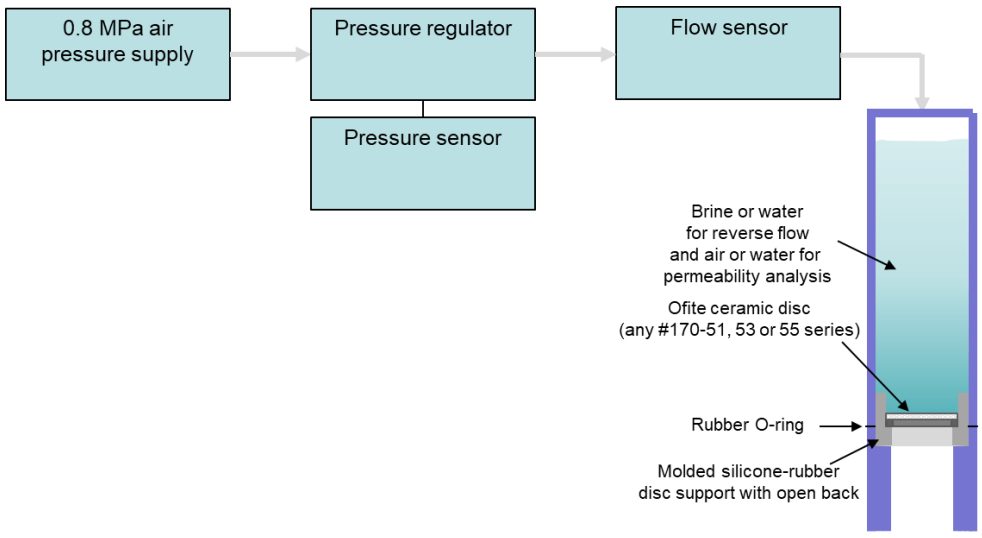

Figure 1. Infographic of the system developed for this study.

2.2.2. Procedures Applied for Testing Using Experimental Set-Up

The main elements of the new procedure are the measurement of disc mass and permeability to water and air before and after the HTHP test. For the full procedure and calculations, please refer to Appendix B. Testing of permeability was restricted to discs with mean pore-throat size of 20 µm as it was difficult to establish precise readings of pressure and flow rate with flow of air or water through the higher permeability discs. A permeability analysis of other disc grades may be practical with a higher viscosity fluid. Otherwise, the procedure was the same for all ceramic disc grades.

3. Experimental Data

3.1. Identifying Signs of Polymer, Solids or Fiber Invasion into Permeable Formations Using a Moisture Analyzer to Measure Changes in Disc Mass

In total, 11 different samples were tested according to the procedure described in Appendix B, including 16 h of hot-rolling at 90 °C, six of which were tested on ceramic discs with a specified median pore-throat size of 120 µm (Ofite #170-53-4) and five of which were tested on 250 µm discs (Ofite #170-53-6). All tests were conducted at 6.9 MPa (1000 psi) differential pressure and 90 °C. An overview of the tests is shown in Table 1. Fiber A and Fiber B were selected from two different manufacturers of cellulose-based lost circulation materials, based on relatively similar specified particle size distributions.

Table 1. Test overview for high-permeability discs.

Test Number	Description of Test
1	Base fluid (with bentonite and $CaCO_3$), normal mixing, 120 µm disc
2	Base fluid, high-shear mixing, 120 µm disc
3	Base fluid, high-shear mixing, 250 µm disc
4	Base fluid plus FIBER A, normal mixing, 120 µm disc
5	Base fluid plus FIBER A, high-shear mixing, 120 µm disc
6	Base fluid plus FIBER A, normal mixing, 250 µm disc
7	Base fluid plus FIBER A, high-shear mixing, 250 µm disc
8	Base fluid plus FIBER B, normal mixing, 120 µm disc
9	Base fluid plus FIBER B, high-shear mixing, 120 µm disc
10	Base fluid plus FIBER B, normal mixing, 250 µm disc
11	Base fluid plus FIBER B, high-shear mixing, 250 µm disc

Five of the tests were conducted after a 30-min high-shear mixing procedure to identify any particle degradation. The same degradation test was conducted separately for some of the wet-sieving tests referenced in Figure 2. The degradation tests indicated that $CaCO_3$ degraded partially during the high-shear mixing procedure. Initially, the wet sieving showed 15.7% and 15.8% of particles being larger than 90 µm, equivalent to a concentration of 13.4–13.5 kg/m^3 in the respective fluid samples. After the high-shear mixing, the concentrations of particles larger than 90 µm was reduced to 9.7% and 9.2%, respectively, implying that circa 40% of the particles above 90 µm had been degraded, and that the resulting concentrations in the fluid samples would be 8.3 kg/m^3 and 7.9 kg/m^3. In contrast, the high-shear mixing of FIBER A did not show signs of degrading, and the concentration was kept stable around 10.6 kg/m^3. One test, which included bentonite, showed an increase in concentrations of FIBER A above 90 µm after high-shear mixing. Since the high-shear mixing of FIBER A without bentonite did not show the same effect, it was considered that a potential cause of the apparent increase in the concentration of larger particles may be bentonite particles piggybacking on the coarser FIBER A particles

to increase the measured concentration of such particles. Tables A2 and A3 in Appendix A gives more detailed information about dry sieving and wet sieving results.

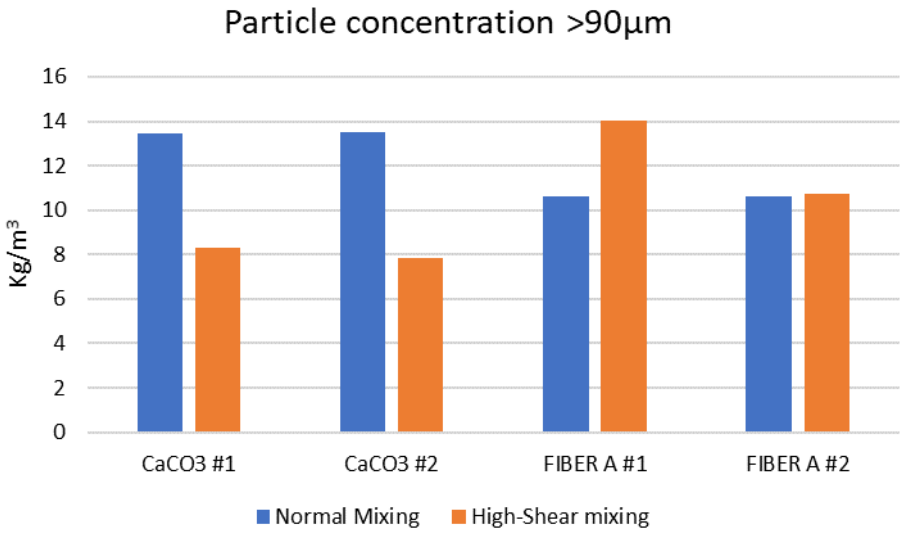

Figure 2. Changes in particle concentration in fluid due to high-shear degradation.

Figure 3 shows the HTHP tests on the 120 µm discs on the left, with each of the three mixtures of (i) the base fluid being KCl-Polymer drilling fluid with CaCO3, (ii) the base fluid plus FIBER A, and (iii) the base fluid plus FIBER B. The tests were conducted with and without high-shear degradation. The fluid loss tests showed that the base fluid produced a fluid loss of 31 mL before degradation and that the fluid loss increased to 42 mL after degradation. The fluid with FIBER A showed a fluid loss of 31 mL before degradation, but unlike the base fluid, the sealing efficiency increased after the high-shear degradation and gave a fluid loss of 25 mL. The fluid with FIBER B also showed an improvement after the degradation test, where the fluid loss was 45 mL without degradation and just over 31 mL after degradation.

The fluid loss profiles were generally consistent throughout the testing on the 120 µm discs. After the initial spurt-loss, the loss-rates were gradually falling during the test and appeared to approach a linear curve with a fluid loss rate of around 0.2 mL/min after 20 min. The development of the fluid loss may indicate that the filter-cake had substantially been formed within the first 15 s, but that further thickness was built over time and that a more stable permeability achieved after 10–20 min.

The testing on 250 µm discs, shown in the right half of Figure 3, was planned to be identical to the testing on the 120 µm disc, however, the base fluid with $CaCO_3$ recorded a total loss during the first few seconds of the test, so no further tests were conducted with the base fluid alone. The testing of the two fiber-based products FIBER A and FIBER B showed considerably improved results relative to the testing on the 120 µm ceramic. Contrary to expectations, the fluid losses recorded on the 250 µm discs were significantly smaller than on the 120 µm disc, and the fluid loss rates were showing a different profile. Again, the tests showed lower fluid losses after the high-shear degradation tests. The main difference, however, was the observation of more erratic fluid losses during the 30-min test. It was several times observed that the fluid loss appeared to stop, and then restarted again at more irregular intervals.

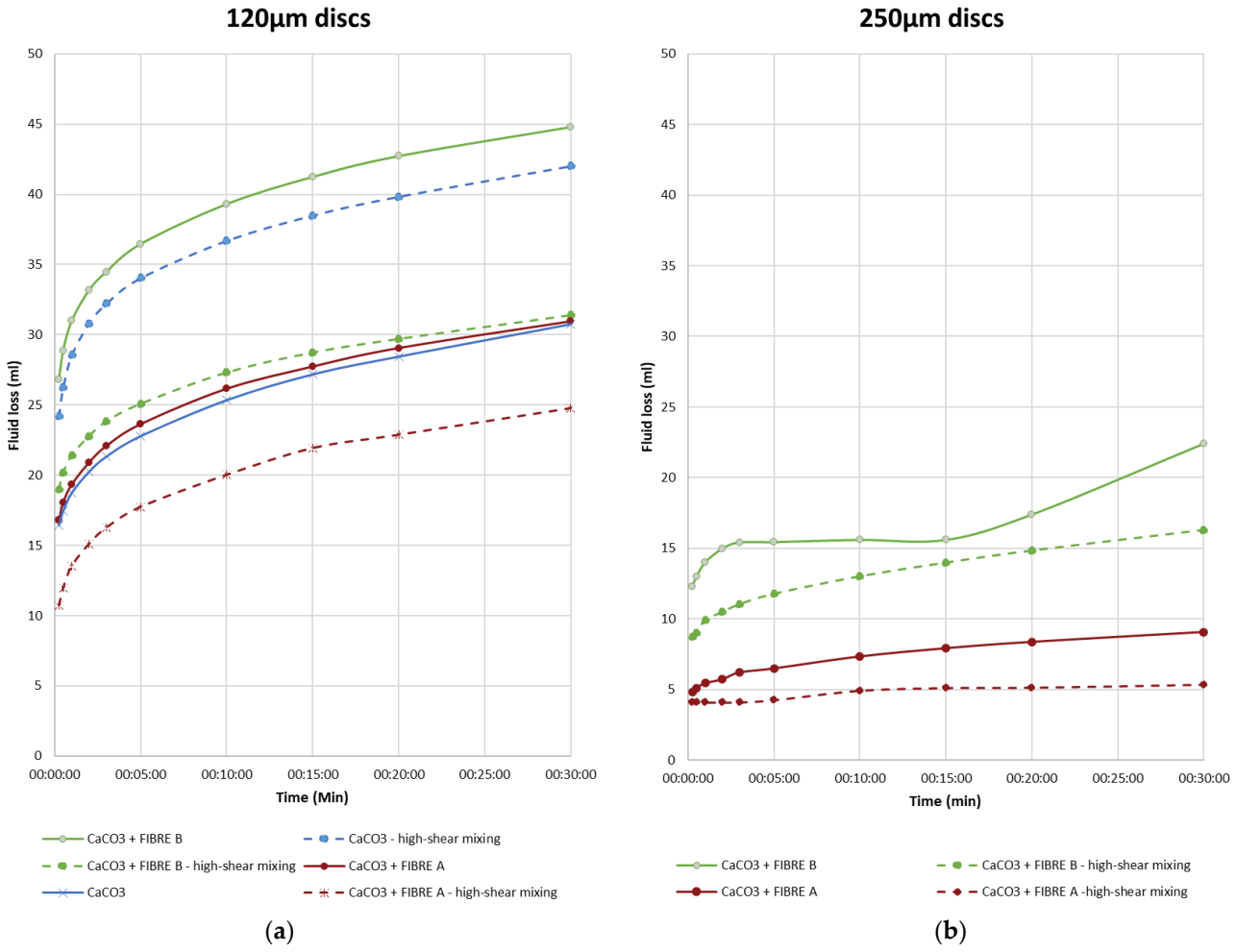

(**a**) (**b**)

Figure 3. Fluid loss on high-permeability discs, (**a**) 120 µm discs and (**b**) 250 µm discs.

By comparing the filter-cakes from the different tests, it was clear that the building of the filter-cakes followed a different mechanism on the coarser discs. The filter-cakes formed on the 120 µm discs were of a uniform nature and thicker than the more irregular filter-cakes on the 250 µm discs, as seen in Figure 4. The impression was that the combined particles of the $CaCO_3$ and the fibers created a layered mat on the surface of the 120 µm disc, whereas the single or collections of particles were plugging larger pores on the 250 µm discs.

When conducting the low-pressure reverse flow of brine through the discs (<7 psi or <0.05 MPa), the filter-cakes were easily removed from the 120 µm discs as the filter-cakes came off either whole or in large pieces. Little visual trace of the filter-cakes was left on the disc other than along the circumference, which was held back by the silicone mold, which held the disc inside the acrylic cell, see Figure 5 as an example.

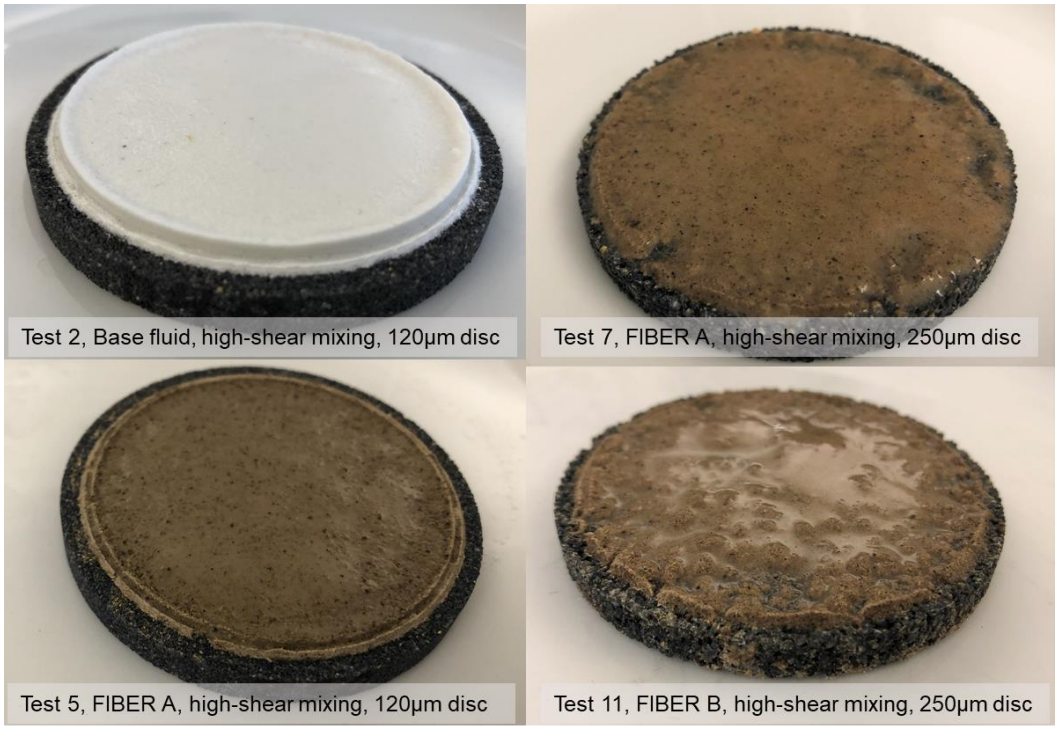

Figure 4. Filter-cakes after the 6.9 MPa (1000 psi) HTHP fluid loss test.

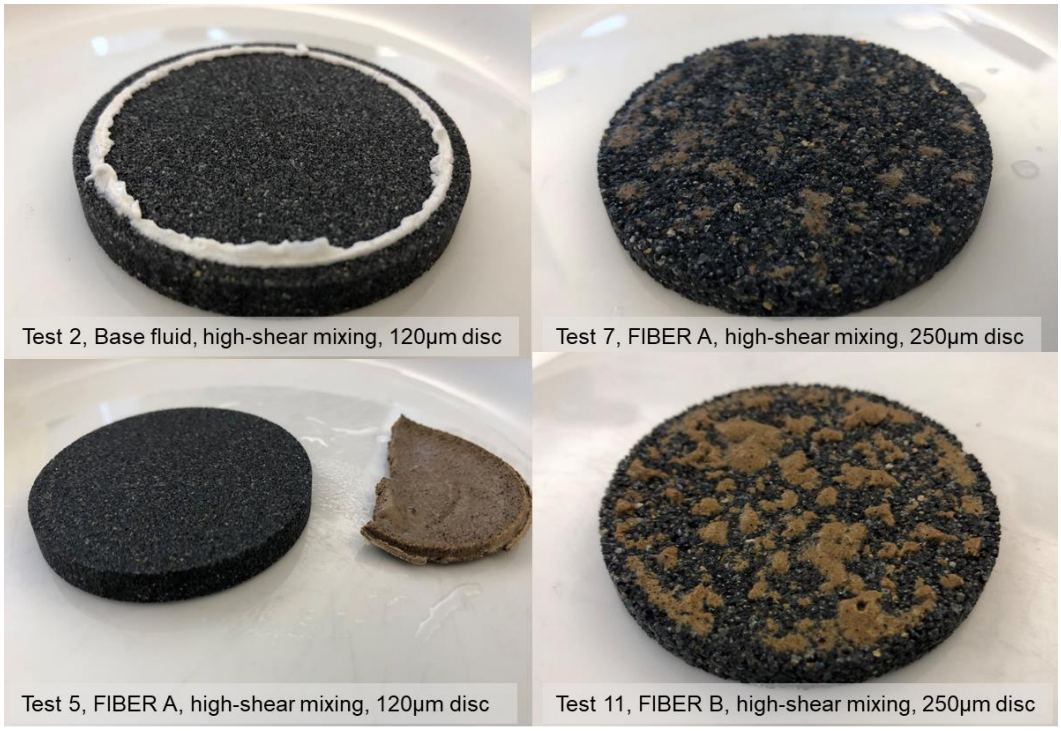

Figure 5. Discs after reverse flow with brine at 0.05 MPa pressure.

On the 250 µm discs, the filter-cakes were noticeably more separated as they were washed off the discs. This may be due to the filter-cake being thinner than for the 120 µm discs. Visual inspection showed minor particles protruding from the surface of the discs, giving further substance to the impression of particles partly penetrating and plugging the pore-throats of the discs.

Following the reverse flow, the discs were placed in a liquid oxidizing breaker and kept at a temperature of 90–100 °C for four hours. The discs were thereafter flowed with water to remove any loose residue and dried in the moisture analyzer. The discs were visually inspected for traces of residue and the final disc masses compared with the original disc masses to identify any invasion of polymer, solids or fiber. Figure 6 shows the discs from testing of FIBER A after removal of filter-cakes. By visual inspection no particle or filter-cake residue could be identified. In contrast, some residue could be seen into the pore-throats of the 250 µm discs in Figure 7, after testing of FIBER B, thereby the indicating particle-plugging inside the disc.

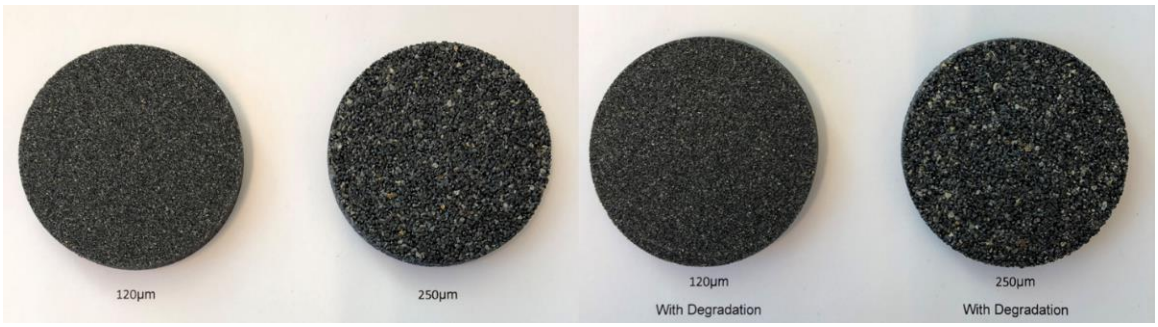

Figure 6. Discs for testing of FIBER A after breaker application.

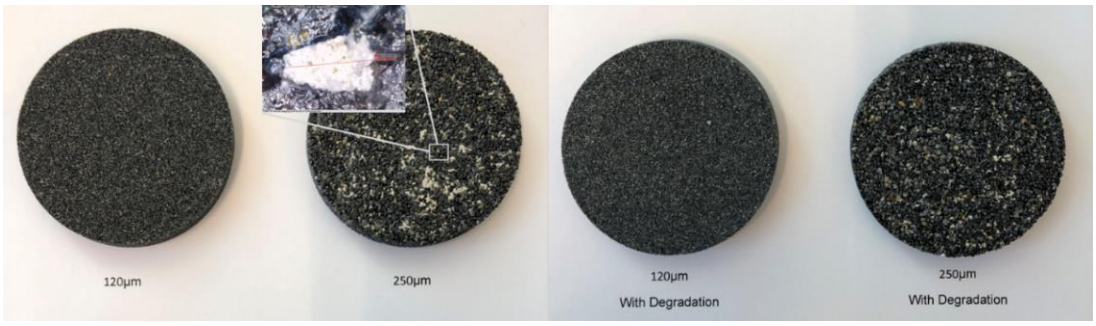

Figure 7. Discs for testing of FIBER B after breaker application.

By placing both the fluid loss measurements and disc mass gain data into one chart, some interesting observations can be made, see Figure 8.

Tests 1 and 2 with the base fluid including $CaCO_3$ show that nearly all of the filter-cake and potential invasion of polymers and solids into the discs have been removed by the reverse flow and breaker application. In contrast, test number 3 recorded a total loss of fluid and no pressure control. This corresponded with a more significant increase in disc mass, which may be due to residue of polymers and solids. This clearly indicates that formation damage may occur when the particles are of insufficient size to create a low-permeability filter-cake.

The four tests conducted with FIBER A show an inverse relationship between increase in disc mass and fluid loss. After visual inspection of the filter-cakes, it looked like the filter-cakes on the 250 µm showed more of a particle-plugging nature, whereas the filter-cakes on the 120 µm discs to a greater extent were created uniformly and externally to the disc. The measurements of increase in disc mass were consistent with this theory, as low increases in disc mass were recorded on the 120 µm discs, and more significant increases in disc mass was recorded on the 250 µm discs, where particle plugging, or deep sealing was suspected.

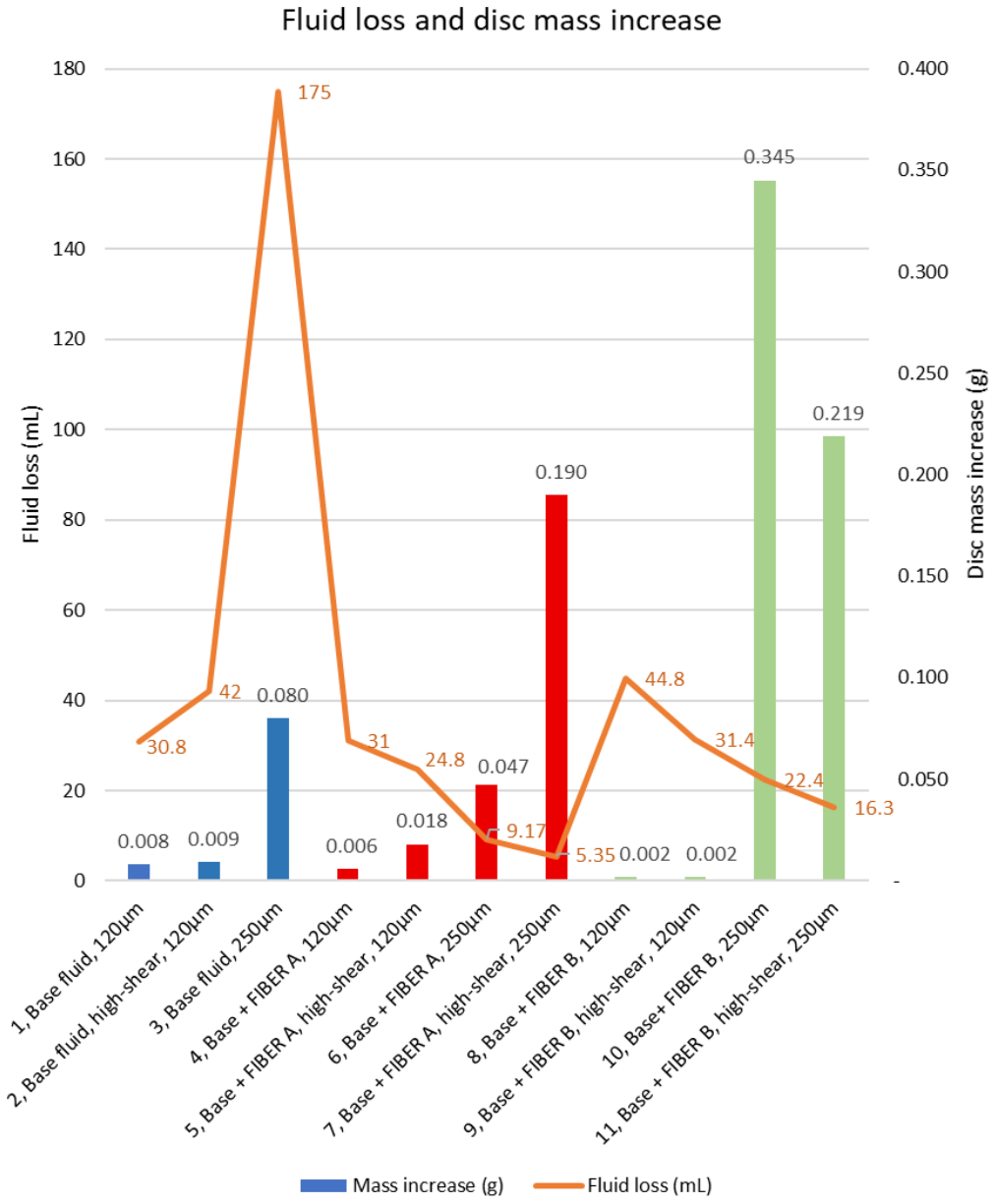

Figure 8. Fluid loss and disc mass increase.

The tests with FIBER B were consistent with the observations from the testing of FIBER A. Disc mass increases were negligible on the finer discs, whereas the mass increases of the coarser discs were the largest in the test. The full data for disc mass measurements can be found in Table A4 in Appendix A.

Dry-sieving tests indicated that both FIBER A and FIBER B had a weight concentration of 13–14% with particles larger than 180 µm, whereas only 1% of the $CaCO_3$ was larger than 180 µm. As such a lower sealing ability of the 250 µm discs without the presence of any of the fiber products could be expected. The sealing of the 120 µm discs was shown to be falling as the percentage of $CaCO_3$ particles was reduced after degradation in test number 2, relative to test number 1, as also shown in Figure 2. A 90 µm particle size represents 75% of the specified median pore-throat size of the 120 µm discs. This may be an indication that particles above 75% of the median pore-throat size of the disc may be required to form an effective filter-cake.

3.2. Extending the Testing Regime to Include Estimation of Disc Permeability Changes

A new set of tests was conducted to study potential changes in the permeability of ceramic discs with specified mean pore-throat size of 20 µm (Ofite #170–53-3). The tests were conducted using the full test-procedure specified in Appendix B. Four tests were conducted with a KCl-Polymer fluid with combinations of Bentonite and FIBER UF as sealing-materials, refer to Appendix A, Table A5 for the full recipe. Due to finer discs being used than in the tests referred to in Section 3.1, a finer grade fiber was selected. FIBER UF was provided by the vendor with a specified D90 of 75 µm and a D100 of 90 µm. The rheology of the various fluid compositions was measured before and after hot-rolling. The measurements showed slight increases in shear stress for a given shear rate as more particles were added to the fluid, as shown in Figure A1, Appendix A.

The disc grade was chosen such that it would be practical to test water-permeability and air-permeability, in addition to the changes in disc mass as described in Section 3.1. Discs with median pore-throat size larger than 20 µm were found to be more difficult to test, as the flowrates of fluid would be very high relative to the low pressures applied. Table 2 show the main data from tests 12–15. As an initial experiment, it was chosen to use water to test permeability even though this would not represent a reservoir fluid. The objective was only to ascertain if the method had practical value, rather than to be an exact replication of a reservoir drilling situation in presence of hydrocarbons.

Table 2. Fluid loss and formation damage data for tests 12–15.

Test	Fluid Loss	Disc Mass Change	Water Permeability Retention	Air Permeability Retention
12, Base fluid 2	Total loss	From 42.031 to 42.279 g = +0.248 g	From 3.338 to 0.997 D = 30%	From 2.327 to 0.822 D = 35%
13, Base fluid 2 + 14.3 kg/m^3 (5 ppb) FIBER UF	24.2 mL	From 41.394 to 41.419 g = +0.025 g	From 4.056 to 2.253 D = 56%	From 2.824 to 2.378 D = 89%
14 Base fluid 2 + 28.5 kg/m^3 (10 ppb) Bentonite	32.2 mL	From 40.776 to 40.795 g = +0.029 g	From 5.633 to 3.166 D = 56%	From 2.823 to 2.686 = 95%
15, Base fluid 2 + 28.5 kg/m^3 (10 ppb) Bentonite and 14.3 kg/m^3 (5 ppb) FIBER UF	19.8 mL	From 40.990 to 40.986 g = −0.004 g	From 5.329 to 3.459 D = 65%	From 3.479 to 3.037 D = 87%

The fluid loss data showed that the Base Fluid 2 (test 12) could not withstand the 6.9 MPa (1000 psi) pressure and build a filter-cake. The HTHP fluid loss test was therefore aborted after around 2–3 s. The reverse-flow of brine through the disc at 0.075 MPa (11 psi) showed very little fluid flow. The disc mass measurement showed that the test with the Base Fluid 2 created a significant increase in the disc mass of 248 mg. Due to the fluid not containing either solids or fiber, the disc mass increase was likely reflecting polymer damage to the formation. The measurements of permeability to water indicated that only 30% of initial permeability had been retained during the test. A thin layer of residue was visible on the surface of the disc where the filter-cake should have been formed.

Test 13 showed that the addition 14.3 kg/m^3 (5 ppb) of FIBER UF could seal the disc without the presence of solids and produced a fluid loss of 24.2 mL. The reverse-flow of brine through the disc at 0.075 MPa (11 psi) showed very moderate fluid flow, but the filter-cake did not lift off directly. After application of breaker, the filter-cake was dissolved and the measurement of permeability to water showed that 56% of original permeability had been retained. The disc mass measurement showed a low increase of mass of 25 mg. Only a slight change in color on the surface showed that there had been a filter-cake on the disc prior to the application of the breaker fluid.

By adding 28.5 kg/m^3 (10 ppb) of bentonite instead of the fiber, test 14 was completed with a fluid loss of 32.2 mL. Reverser flow of brine lifted off the filter-cake and fluid flow appeared relatively similar to test 13. After application of the breaker, the filter-cake was dissolved and the measurement of permeability to water showed that 56% of the original permeability had been retained. The disc mass measurement showed a low increase of

mass of 29 mg. Some light gray residue was visible on the surface of the disc after reverse flow and breaker fluid application.

The lowest fluid loss was recorded when both 14.3 kg/m^3 (5 ppb) of FIBER UF and 28.5 kg/m^3 (10 ppb) of bentonite was added to the base fluid. For this test, the fluid loss was reduced to 19.8 mL. There was no visible residue on the disc surface and the mass measurement indicated a very minor fall in disc mass of 4 mg. The measurement of permeability to water showed retention of 65%.

The information on changes in disc mass, permeability to water and air were gathered in attempt to find practical method for studying indicators of any formation damage caused by the drilling fluid in a real-life application. A differential pressure of 6.9 MPa (1000 psi) was considered to be adequately reflecting what might be experienced in certain drilling situations. Similarly, it was of interest to see if a relatively low reverse pressure of 0.075 MPa (11 psi) could start the process of filter-cake removal before any chemical cleaning of the reservoir was applied.

It was shown that the addition of either FIBER UF or bentonite reduced the invasion of drilling fluid into the formation and also that less damage appeared to have been made to the formation permeability. Further, the combination of FIBER UF and bentonite showed even lower fluid loss and the visual inspection and the mass measurement indicated that no or little damage to the formation had been caused. In contrast, the estimation of permeability to water showed that some change in permeability might have occurred. In this context one should consider the polarity of water and its potential interaction with bentonite and the cellulose based FIBER UF.

When studying the results of the tests it should be considered that only the first 6.35 mm (1/4″) or of the formation has been studied. The content of the fluid filtrate has not been studied, and hence it may be difficult to provide clear evidence for which further damage could have been caused to formation further away from the wellbore. During tests 13–15, the applied pressure of 6.9 MPa (1000 psi) was successfully held, and a moderate amount of fluid filtrate was collected. This may be an indication that such fluid compositions would be quite effective in preventing fluid loss to the formation. Test 12 showed that polymers alone could not seal the disc under the applied differential pressure nor prevented polymers from migrating into the disc. Figure 9 shows the discs after breaker application and drying.

Figure 9. Discs from tests 12–15 after breaker application and drying.

4. Observations and Lessons Learned from the Experimental Procedure

Measurement of disc mass using the moisture analyzer, weighing the fluid filtrate continuously during the HTHP process and calculation of fluid filtrate were practical exercises that yielded consistent results without complications.

The process of reverse flow using brine and water for lifting of filter-cake functioned very well within certain limitations. For tests where the applied differential pressure during the HTHP test was 6.9 MPa (1000 psi), certain fluid combinations showed little or no reverse flow with applied reverse pressure of 0.069 MPa (10 psi) and a brine temperature

of 60 °C. It was experimented with applying higher reverse pressures and higher brine temperatures whilst developing the method that was applied. Higher temperatures were avoided to avoid deforming of the acrylic cylinder, and higher pressures were avoided as some discs fractured if the reverse pressure exceeded 0.1 MPa (15 psi).

Calculating the average permeability to dry air functioned very well and yielded quite consistent and repeatable results on dry discs prior to any HTHP testing. The primary ambition was to identify changes to the calculated permeability of each individual disc. One observation was that the permeability of discs coming from different batches varied considerably, whereas discs coming from the same batch appeared to be more similar. The method has a weakness when used after an HTHP test as it is based on the disc being predried before flowing of air. Using this method, the effects of drying may impact discs with the presence of, e.g., polymers, solids, and fibers and their ability to obstruct flow of air differently. These data may therefore be imprecise relative to flow of fluids in a reservoir formation.

Adapting the permeability estimation to a fluid such as water appeared to be more complex. The primary observation was that the calculated permeability of an individual disc could vary, even when correcting for changes in viscosity due to temperature changes. The process that enabled a stabilization of the readings included to place the disc in fluid in vacuum to remove any air-bubbles from the disc and fluid before the test. This yielded considerably more consistent results, particularly on low-permeability discs. A cause of the uncertainty of measurement was thought to be capillary forces at the air–water interface, and the improvement obtained by placing the disc and fluid in vacuum strengthened this idea.

Additionally, it should be considered that the thickness of the discs (ΔL) is low relatively to the depth of a typical core sample for a return permeability test. The testing of the discs can therefore be considered to reflect the skin damage of a formation.

5. Conclusions

The inclusion of additional procedures to those described in ANSI/API 13B-1 yielded information relevant to obtaining a better understanding of fluid loss and giving an insight into how various drilling fluid compositions seal permeable formations and how they may impact future reservoir permeability. The main conclusions are as follows:

- By extending the testing procedure with (i) a moisture analyzer and (ii) reverse flow equipment and a procedure for reverse flow and breaker fluid application it was possible to measure the increases in disc mass accurately.
- Reverse flow of fluid through the disc with filter-cake enables studying the removal of filter-cake by back pressure.
- Application of an oxidizing breaker did in certain cases allow the test discs to return to almost its original state, with mass changes so low that they may be considered to be within the tolerances of the tests.
- As the discs median pore-throat size was varied relative to the particle size of the fibers and $CaCO_3$, for tests 1–11, it appeared that different mechanisms for sealing the disc and creating a filter-cake was obtained. Hereunder, when the solids or fibers were equal or marginally smaller than the pore-throat openings, fluid loss was reduced, and the sealing appeared to partial plugging of the pore-throats. In contrast, when a significant portion of the particles was larger than the mean pore-throat size, a thicker and more uniform filter-cake was building on the disc. Without the presence of fibers or when the solids were smaller than the pore-throats, no low-permeability filter-cake was formed, and disc mass increases were significant.
- In the tests on the 120–250 μm discs where either of the fiber products was present, there was an inverse relationship between fluid loss and disc mass increases. In the tests on the 20 μm discs, the fibers appeared to be larger than the pore-throats, and there was a positive relationship between lower fluid loss and lower disc mass increase.

- Testing of disc mass change and change of permeability to water and air suggested that ranking 20 µm discs in terms of lowest increase in mass and lowest calculated change to water-permeability would yield consistent results in terms of indicating formation damage. Since the other disc grades are built up in the same way as the 20 µm discs, it may be possible to obtain equivalent results with discs of other grades.
- The findings on using the new testing methodologies are indicating that valuable information concerning reservoir formation damage may be observed and estimated using a relatively simple set-up and test procedure. To further investigate this potential, it is recommended to conduct further experiments. One of the natural extensions of the methodology is to investigate using a non-polar hydrocarbon-based fluid for testing of permeability and for presoaking discs before the fluid loss test.

Author Contributions: Conceptualization, K.R.K.; methodology, K.R.K. and J.K.V.; formal analysis, K.R.K., B.B. and V.B.T.; writing—original draft preparation, K.R.K.; writing—review and editing, K.R.K., A.S., M.K. and S.K.M.; supervision, S.K.M. All authors have read and agreed to the published version of the manuscript.

Funding: This research was funded by The Research Council of Norway, grant number 320646, Innovation Norway, grant number 2020/527515 together with European Mud Company AS.

Institutional Review Board Statement: Not applicable.

Informed Consent Statement: Not applicable.

Data Availability Statement: Data availability on request due to intellectual property rights of EMC.

Conflicts of Interest: The authors confirm that this article content has no conflict of interest.

Appendix A

Appendix A contains recipes and data from the tests.

Table A1. Recipe and mixing sequence of drilling fluid for tests 1–11.

Mixing Sequence	Material/Additive	Mass (g)
1	H_2O	328
2	Na_2CO_3	0.02
3	NaOH	0.25
4	Xanthan Gum	1.2
5	Poly-Anionic Cellulose, Low Viscosity	4.0
6	MgO	1.0
7	KCl	17.5
8	Bentonite	5.0
9	$CaCO_3$ (D50 of 50 µm)	30.0
10	With or without FIBER A or FIBER B at given concentration	8.0

Table A2. Dry sieving of drilling fluid additives for tests 1–11.

Additive	<90 μm	90–180 μm	>180 μm
$CaCO_3$	74.2%	24.8%	1.0%
FIBER A	56.3%	30.6%	13.1%
FIBER B	29.5%	56.5% *	13.9%

* When sieving of FIBER B it was noted that the particles had some magnetic properties. Visual inspection indicated that this might have increased amount of product collected in 90 μm sieve.

Table A3. Wet sieving of drilling fluid sample with additives before and after high-shear degradation for tests 1–11.

Wet Sieving before and after High-Shear Degradation	<90 μm	>90 μm
$CaCO_3$ Sample #1, normal mixing	84.3%	15.7%
$CaCO_3$ Sample #2, normal mixing	84.2%	15.8%
$CaCO_3$ Sample #1, 30 min high-shear mixing	90.3%	9.7%
$CaCO_3$ Sample #2, 30 min high-shear mixing	90.8%	9.2%
FIBER A Sample #3, normal mixing	53.4%	46.6%
FIBER A Sample #4, normal mixing	53.5%	46.5%
FIBER A Sample #5, 30 min high-shear mixing together with bentonite	38.6%	61.4%
FIBER A Sample #4, 30 min high-shear mixing	52.9%	47.1%

Table A4. Disc mass measurements in dry condition before and after whole test sequence for tests 1–11.

Test with Changes in Disc Mass	Original Disc Mass (g)	Final Disc Mass (g)	Mass Increase (g)
1, Base fluid (with bentonite and $CaCO_3$), normal mixing, 120 μm disc	50.098	50.106	0.008
2, Base fluid, high-shear mixing, 120 μm disc	50.069	50.078	0.009
3, Base fluid, normal mixing, 250 μm disc (TOTAL LOSS)	50.249	50.329	0.080
4, Base fluid plus FIBER A, normal mixing, 120 μm disc	50.419	50.425	0.006
5, Base fluid plus FIBER A, high-shear mixing, 120 μm disc	49.970	49.988	0.018
6, Base fluid plus FIBER A, normal mixing, 250 μm disc	50.624	50.671	0.047
7, Base fluid plus FIBER A, high-shear mixing, 250 μm disc	50.457	50.647	0.190
8, Base fluid plus FIBER B, normal mixing, 120 μm disc	49.789	49.791	0.002
9, Base fluid plus FIBER B, high-shear mixing, 120 μm disc	49.927	49.929	0.002
10, Base fluid plus FIBER B, normal mixing, 250 μm disc	50.139	50.484	0.345
11, Base fluid plus FIBER B, high-shear mixing, 250 μm disc	50.204	50.423	0.219

Table A5. Recipe and mixing sequence of base fluid 2 for tests 12–15.

Mixing Sequence	Material/Additive	Mass (g)
1	H_2O	328
2	Na_2CO_3	0.02
3	NaOH	0.25
4	Xanthan Gum	1.2
5	Poly-Anionic Cellulose, Low Viscosity	4.0
6	MgO	1.0
7	KCl	17.5
8	With or without Bentonite at given concentration	10.0
9	With or without FIBER UF at given concentration	5.0

Energies **2021**, *14*, 2252 17 of 19

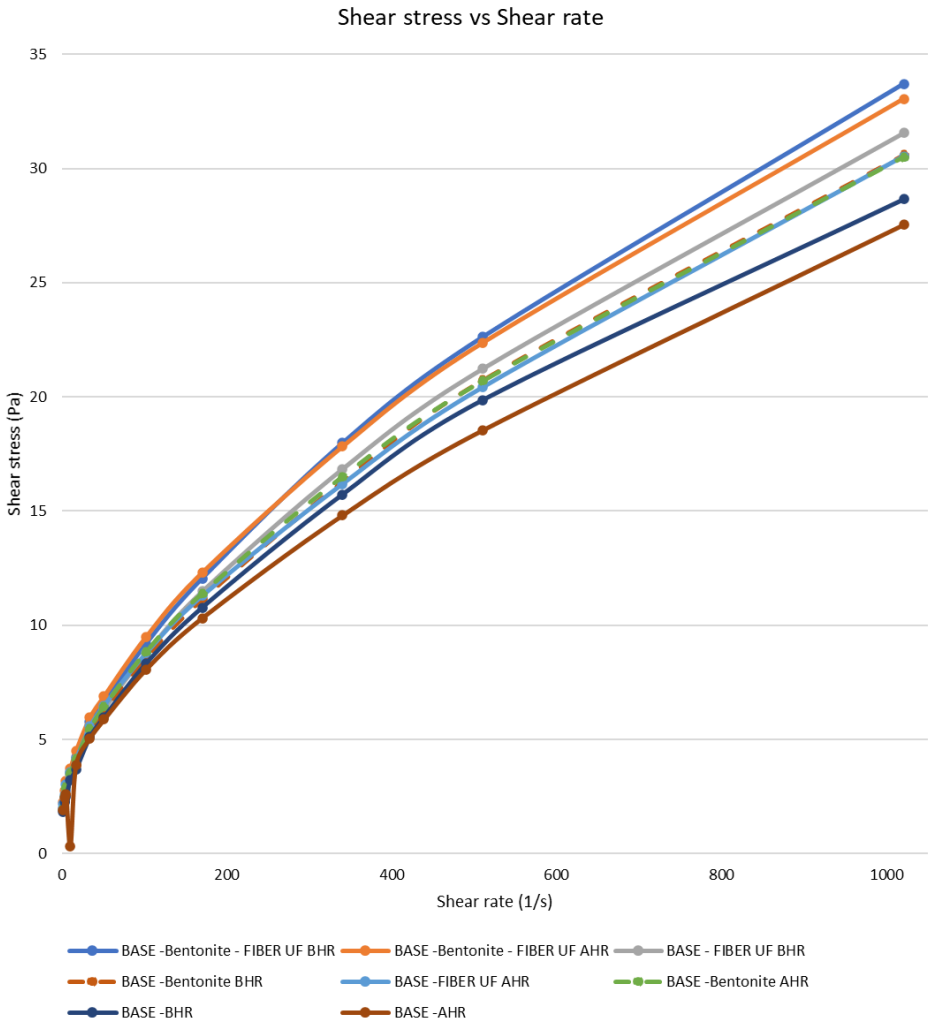

Figure A1. Rheology before hot-rolling (BHR) and after hot-rolling (AHR) of fluids for tests 12–15.

Figure A1. Rheology before hot-rolling (BHR) and after hot-rolling (AHR) of fluids for tests 12–15.

Appendix B

Procedure for measuring change in disc mass and change in permeability and relevant calculations.

1. Mix drilling fluid according to the recipe;
2. Measure pH and rheology;
3. Hot-roll and if applicable degrade by high-shear stirring or other degradation method;
4. Measure pH and rheology after hot-rolling and any degradation;
5. Mark and weigh disc in dry condition using the moisture analyzer (M_b). Moisture

Appendix B

Procedure for measuring change in disc mass and change in permeability and relevant calculations.

1. Mix drilling fluid according to the recipe;
2. Measure pH and rheology;

3. Hot-roll and if applicable degrade by high-shear stirring or other degradation method;
4. Measure pH and rheology after hot-rolling and any degradation;
5. Mark and weigh disc in dry condition using the moisture analyzer (M_b). Moisture analyzer shall be set to dry disc at 105 °C until change in mass is less than 1 mg/60 s;
6. Optional step: place disc in acrylic cell and measure air temperature and flowrate at different pressures to calculate average permeability to air (K_{ab});
7. Optional step: place disc in acrylic cell and place arrangement with water in vacuum (circa −0.96 bar for 5 min) to remove any air from disc or water. Flow thereafter water through disc and measure water temperature and flowrate at different pressures to calculate average permeability to water (K_{wb});
8. Soak disc in brine (40 g NaCl per 1000 g freshwater) in vacuum;
9. Conduct HTHP test at desired pressure, typically 3.45 MPa (500 psi) or 6.9 MPa (1000 psi), and measure both volume (V_f) and mass (M_f) of fluid filtrate at point in time of 15 s, 30 s, 1 min, 2 min, 3 min, 5 min, 10 min, 15 min, 20 min and 30 min (V_f). Calculate fluid filtrate density;
10. Weigh disc with filter-cake and observe filter-cake;
11. Place disc in acrylic cell and reverse flow with 1 L (40 g NaCl per 1000 g water) heated to 60 °C and then with 1 L water heated to 60 °C. Note pressure required to enable reverse flow through disc;
12. Optional step: place disc in breaker fluid for required time and at required temperature. Place disc in acrylic cell and flow disc with 1 L water at ambient temperature to remove any dissolved filter-cake residue;
13. Optional step: place disc in acrylic cell and place arrangement with water in vacuum to remove any air from disc or water. Flow thereafter water through disc and measure water temperature and flowrate at different pressures to calculate average permeability to water (K_{wa});
14. Weigh disc in dry condition using moisture analyzer (M_a) using the same settings as in step 5;
15. Optional step: place disc in acrylic cell and measure air temperature and flowrate at different pressures to calculate average permeability to air (K_{aa}).

Depending on the number of optional steps included in the procedure, it enables collection of a large amount of data in addition to observing the filter-cake and the fluid filtrate volume $V_{f.}$

The moisture analyzer used for weighing the discs was set to heating the discs to 105 °C and continue drying until the mass change due to moisture evaporation was less than 1 mg per 60 s. The drying process then stopped automatically, and the mass of the disc displayed. The precision of the instrument is 1 mg. The change in disc mass was then simply calculated as:

$$(M_a) - (M_b) = M_{change}$$

By placing a digital weight under the graduated cylinder used to measure fluid filtrate, it was possible to simultaneously record the mass of the fluid filtrate and read the volume of the filtrate. This enabled a precise estimation of the fluid loss profile and calculating the fluid filtrate density (D_f), calculated as:

$$(M_f)/(V_f) = (D_f)$$

The permeability was calculated as an average of multiple readings within certain flow-rate ranges. Darcy's law was used in a rearranged form as follows:

$$K = \eta \frac{Q * \Delta L}{A * \Delta P}$$

where K is the calculated permeability coefficient (m^2), η is the viscosity of the fluid (Pa * s), Q the fluid flowrate (m^3/s), ΔL the disc thickness (m), A the areal of flow into the disc and ΔP the pressure differential over the disc (Pa).

References

1. ANSI/API 13B-1. In *Recommended Practice for Field Testing Water-based Drilling Fluids*, 5th ed.; API Publishing Sevices: Washington, DC, USA, 2019.
2. Alsaba, M.; Nygaard, R.; Hareland, G. AADE-14-FTCE-25. In *Review of Lost Circulation Materials and Treatments with an Updated Classification*; AADE: Houston, TX, USA, 2014.
3. Jeennakorn, M.; Alsaba, M.; Nygaard, R.; Saasen, A.; Nes, O.-M. The effect of testing conditions on the performance of lost circulation materials: Understandable sealing mechanism. *J. Pet. Explor. Prod. Technol.* **2018**, *9*, 823–836. [CrossRef]
4. Jeennakorn, M.; Nygaard, R.; Nes, O.-M.; Saasen, A. Testing conditions make a difference when testing LCM. *J. Nat. Gas Sci. Eng.* **2017**, *46*, 375–386. [CrossRef]
5. Alshubbar, G.; Nygaard, R.; Jeennakorn, M. The effect of wellbore circulation on building an LCM bridge at the fracture aperture. *J. Pet. Sci. Eng.* **2018**, *165*, 550–556. [CrossRef]
6. Alsaba, M.; Nygaard, R.; Saasen, A.; Nes, O.M. *Lost Circulation Materials Capability of Sealing Wide Fractures*; SPE-170285-MS; SPE International: Houston, TX, USA, 2014.
7. Khalifeh, M.; Klungtvedt, K.R.; Vasshus, J.K.; Saasen, A. *Drilling Fluids—Lost Circulation Treatment*; SPE-195609-MS; SPE Norway: Bergen, Norway, 2019.
8. Saasen, A.; Hodne, H.; Ronæs, E.; Aarskog, S.A.; Hetland, B.; Løvereide, M.B.; Mohammadi, R. *Wood Fibre Based Lost Circulation Materials*; OMAE2018-77662; ASME: Madrid, Spain, 2018.
9. Lee, L.; Taleghani, A.D. Simulating Fracture Sealing by Granular LCM Particles in Geothermal Drilling. *Energies* **2020**, *13*, 4878. [CrossRef]
10. Enstad, G. On the theory of arching in mass flow hoppers. *Chem. Eng. Sci.* **1975**, *30*, 1273–1283. [CrossRef]
11. Whitfill, D. In Proceedings of the Lost Circulation Material Selection, Particle Size Distribution and Fracture Modelling with Fracture Simulation Software, SPE-115039-MS, IADC/SPE, Jakarta, India, 25–27 August 2008.
12. Alsaba, M.; Nygaard, R.; Saasen, A.; Nes, O.M. Experimental investigation of fracture width limitations of granular los circulation materials, 2015. *J. Petrol. Explor. Prod. Technol.* **2016**, *6*, 593–603. [CrossRef]
13. Alsaba, M.; Aldushaishi, M.; Jeennakorn, M.; Nygaard, R.; Saasen, A.; Nes, O.M. *Sealing Pressure Prediction Model for Lost Circulation Treatments Based on Experimental Investigations*; AADE-17-NTCE-21; American Association of Drilling Engineers: Houston, TX, USA, 2017.
14. Hoxha, B.B.; Yang, L.; Hale, A.; van Oort, E. *Automated Particle Size Analysis using Advanced Analyzers*; AADE-16-FTCE-78; AADE: Houston, TX, USA, 2016.
15. Pitoni, E.; Ballard, D.A.; Kelly, R.M. *Changes in Solids Composition of Reservoir Drill in Fluids during Drilling and the Impact on Filter Cake Properties*; SPE 54753; SPE International: The Hauge, The Netherlands, 1999.
16. Green, J.; Patey, I.; Wright, L.; Carazza, L.; Saasen, A. *The Nature of Drilling Fluid Invasion, Clean-Up, and Retention during Reservoir Formation Drilling and Completion*; SPE-185889-MS; SPE Bergen: Bergen, Norway, 2017.
17. Czuprat, O.; Dahle, B.O.; Dehmel, U.; Ritschel, R.; Storhaug, J.; Adrian, T.; Patley, I. *Systematic Selection of Drill-in and Completion Fluids for Development of the Dvalin HT Gas Field*; SPE-195601-MS; SPE Norway: Bergen, Norway, 2019.
18. Khan, R.; Kuru, E.; Tremblay, B.; Saasen, A. Extensional Viscosity of Polymer Based Fluids as a Possible Cause of Internal Cake Formation. *Energy Sources A* **2007**, *29*, 1521–1528. [CrossRef]
19. Cobianco, S.; Bartosek, M.; Lezzi, A.; Previde, E. *New Solids-Free Drill.in Fluid for Low Permeability Reservoirs*; SPE-64979; SPE: Houston, TX, USA, 2001.
20. Nelson, P.H. Pore-throat sizes in sandstones, tight sandstones, and shales. *AAPG Bull.* **2009**, *93*, 329–340. [CrossRef]
21. Civan, F. *Reservoir Formation Damage 2020*; Gulf Professional Publishing: Waltham, MA, USA, 2020; pp. 1–6, ISBN 978-0-12-801898-9.
22. ANSI/API 13B-2. In *Recommended Practice for Field Testing Oil-Based Drilling Fluids*, 5th ed.; API Publishing Services: Washington, DC, USA, 2014.

II. Klungtvedt, K.R., Berglind, B., Vasshus, J.K., Khalifeh, M. "Preventing Drilling Fluid Induced Reservoir Formation Damage", SPE-202187-MS, SPE/IADC Middle East Drilling Technology Conference and Exhibition, 25-27 May 2021.

Please note: This paper is not included in the repository due to copyright restrictions.

III. Klungtvedt, K.R. and Saasen, A. “A Method for Evaluating Drilling Fluid Induced Permeable Formation Damage”, Journal of Petroleum Science and Engineering. https://doi.org/10.1016/j.petrol.2022.110324. (open access)

Journal of Petroleum Science and Engineering 213 (2022) 110324

Contents lists available at ScienceDirect

Journal of Petroleum Science and Engineering

journal homepage: www.elsevier.com/locate/petrol

A method for assessing drilling fluid induced formation damage in permeable formations using ceramic discs

Karl Ronny Klungtvedt [a], Arild Saasen [b,*]

[a] EMC AS, NO-4033 Stavanger, Norway
[b] University of Stavanger, NO-4036, Stavanger, Norway

ARTICLE INFO

Keywords:
Measuring permeable formation damage
Methodology for screening drilling fluids

ABSTRACT

When drilling an oil and gas or geothermal well, the formation's ability to produce or flow may be reduced because of exposure to the drilling fluid during the drilling operation. To evaluate such formation damage, core flooding tests are typically conducted using representative samples of rock to measure the change in the formation permeability in the zone near the wellbore. Disadvantages of core flooding tests include time and cost of a test and potential limited access to representative cores. Therefore, core flooding tests are generally not practical to use for screening and adjustment of drilling fluid compositions when a high number of tests are planned.

A method has been suggested to allow for time and cost-effective testing of mass change of ceramic discs, such that a high number of tests may be completed within a limited timeframe and budget. However, so far only limited testing had been conducted to understand the potential for measuring permeability change. In the present study, the method was applied to test for change in permeability of ceramic discs following HTHP tests. A reverse flow of fluid was applied to lift off the filter-cakes and then a breaker fluid was applied. Thereafter the permeabilities to air and water and the dry disc mass was measured and compared with the original value to detect any changes.

The repeated tests showed very high correlations between changes in permeability to air, permeability to water and changes in disc mass, ranging from 0.906 to 0.984. The tests were repeated by different researchers and the results of the two test-series showed high correlations between the original and repeated test series. The overall results provide a high degree of consistency and confirmed findings in past research conducted on core flooding tests.

Present study inferred that the simplified method for assessing formation damage produces consistent results and may be used as a cost-effective method for comparing different drilling fluids and methods for removing the filter cakes, ahead of potential core flooding tests.

1. Introduction

The standard, ANSI/API 13B-1 (2019), describes a procedure for measuring fluid loss under high temperature and high-pressure conditions (HTHP), related to drilling of wells for oil or gas production. These conditions are typically a temperature requirement of 90 °C, a differential pressure of 3.45 MPa (500psi) and a test period of 30 min. These procedures are designed to be practical for a drilling fluid engineer to conduct at a rig site to monitor the performance of the fluid. The procedure neither cater for measuring the fluid's ability to seal fractured formations nor any impact on drilling fluid induced formation damage. Materials used for preventing or treating lost circulation (LCM) of drilling fluid are tested using different methods. For functionality beyond the limitations of the procedure described by ANSI/API 13B-1, however, no consistent method seems to have been established.

Lost circulation materials have been categorised by Alsaba et al. (2014a) and classified into seven categories based on physical and chemical characteristics, appearance, and application: granular, flaky, fibrous, LCM's mixture, acid/water soluble, high fluid loss squeeze, swellable/hydratable combinations, and nanoparticles.

Jeennakorn et al. (2017, 2019)identified that different test conditions could yield different results when testing lost circulation materials. Their testing was focused on identifying maximum sealing pressures using slotted discs to simulate fractures. Further, the performance of

* Corresponding author.
E-mail address: arild.saasen@uis.no (A. Saasen).

https://doi.org/10.1016/j.petrol.2022.110324
Received 7 October 2021; Received in revised form 10 December 2021; Accepted 20 February 2022
Available online 4 March 2022

LCM will be impacted by the characteristics of the base fluid they are blended into, and the wear the fluid is exposed to over time in downhole conditions and at the solids-control stage. A study was conducted by Alshubbar et al. (2018) on LCM performance under conditions of annular flow. It was found that higher circulation rates led to higher fluid losses, potentially as the particles forming the seal were more disturbed by a higher flow compared to a lower flow. Also, they identified that LCM particles with lower specific gravity were less impacted by the annular flow conditions, and hence might be more suitable for preventative treatment of lost circulation.

In a study comparing LCM from different categories of materials, Alsaba et al. (2014a,b), showed that LCM made of fibers should give the best sealing ability and seal integrity on tapered slotted discs. In their study they obtained sealing pressures up to 20.2 MPa (2925 psi) for slotted discs with a 1.0 mm fracture tip. They compared fibrous materials with granular materials such as $CaCO_3$ and graphite and found that the seal integrity was lower with granular materials. The performance of fibre-based LCM was further studied by Khalifeh et al. (2019), where LCM materials sealed slotted discs from 400 μm and up to 2500 μm at pressures exceeding 34.5 MPa (5000 psi) without failing. In this study it was shown that the seals were dynamically built to withstand higher pressures, which may indicate that LCM pill applications should be pressurised to the equivalent circulating density (ECD) to ensure good integrity during the drilling operation.

Saasen et al. (2018) used an alternative approach, where LCM were tested using a coarse gravel bed as well as on slotted discs. The objective was to study curing of large losses of drilling fluids. They found that the addition of short fibers could reduce fluid loss in porous and permeable formations, whereas longer fibers were more effective in curing large losses in fractured formations.

Particle size distribution (PSD) has been widely used with regards to understand mechanisms for treating lost circulation. An early study of the ability of dry powders to block hopper openings was conducted by Enstad (1975), where he showed that granules could block openings of several times their own dimensions. When studying similar effects in a drilling fluid, the mechanical properties of the fluid will also interact and change the mechanism of sealing. Whitfill (2008) proposed a method where the D50 value of the particles should be equal to the fracture width to ensure the formation of an effective seal. Alsaba et al. (2016) built further on these studies and investigated how the shapes and PSD of LCM materials impacted sealing of fractures up to 2000 μm. They found that a D90 value which was equal to or slightly larger than then fracture width, was required for a strong seal to form. However, to reduce the fluid loss, finer particles were needed to reduce the permeability of the seal.

Alsaba et al. (2017) conducted a study of sealing prediction and found that after the fracture width and fluid density, the D90 value was the most significant factor influencing the sealing pressure. Hoxha et al. (2016) also studied the degradation of $CaCO_3$ and graphite due to exposure to fluid shear. They found a 25–40% reduction in the D50 values of medium grade $CaCO_3$ after 30 min of shearing. Using different methods for measuring PSD, they noted that the D50 value of graphite was recorded to be reduced between 20% and 70%. The methods for particle size selection do not provide evidence regarding how the seals or plugs impact the permanent permeability of the formation, after the drilling operation has been completed. Klungtvedt et al. (2021a) showed that a specially designed cellulose-based drilling fluid additive could enable effective HTHP sealing of permeable discs, even without the presence of solids that are conventionally applied as bridging particles.

Lee and Taleghani (2020) studied properties lost circulation in relation to geothermal drilling and found that parameters such as fluid viscosity, particle size and friction coefficient and Youngs' modulus were important. By applying a parametric study, they discovered that thermal degradation reduced the capacity to seal fractures.

A study of filter-cakes and return permeability was conducted by Pitoni et al. (1999). They found that the solids composition of the fluids impacted the filter-cakes and return permeability. With higher solids content, they discovered that the filter-cakes became softer and thicker. In contrast, higher clay content gave thinner and harder filter-cakes, suggesting that the clay particles pack together tightly. Also, the increasing concentration of clay reduced the measured return permeability. They also proposed a method of using coarser bridging particles in a sacrificial manner, as increasing the PSD yielded better return permeability values.

Complementing the results from Pitoni et al. a study by Green et al. (2017) found that the lowest fluid filtrate loss did not necessarily correspond to the lowers permeability damage. They concluded that the filter-cakes ability to stick to the formation and if it could be removed during operation were the determining factors of formation damage. Czuprat et al. (2019) conducted long term (14 days) static aging tests and formation damage tests on sandstone samples. They concluded that slower build-up of the filter-cake would be a result of lower solids content in the drilling fluid. After conducting the experiments, they also concluded that the extended test period may make it impractical for service companies to conduct tests using the methodology before selecting a drilling fluid.

Numerous studies have been conducted on water-based drilling fluids and impact on return permeability. Khan et al. (2003) studied the formation damage characteristics of xanthan gum using core flow experiments, also investigating the extensional viscosity of the fluid in addition to shear viscosity, filtration loss and pressure drop. The xanthan gum solutions tested had low yield stresses but showed increasing extensional viscosity with increasing concentration of xanthan gum and that higher extensional viscosity led to lower fluid filtrate volumes. Also, they found that flow of xanthan gum through a porous media may significantly reduce the original permeability. Khan et al. (2007) showed that polymers such as xanthan gum, poly-anionic cellulose and starch had little impact of reducing fluid loss on its own in conditions where pore-throats were exceeding 20 μm, differential pressures exceeding 3.45 MPa (500 psi).

For low permeability reservoirs, Cobianco et al. (2001) developed a fluid using biopolymers, highly crosslinked starch and micro fibrous cellulose. They found that when the fluid contained cuttings, the return permeability was slightly lower than for the fluid without cuttings. SEM micrographs indicated that the cuttings invasion was limited to the first 100 μm of the 20–100 mD Portland limestone cores. Nelson (2009) found that reservoir sandstones generally had pore-sizes greater than 20 μm, however, with pore-throat openings greater than 2 μm, and that testing sandstone reservoirs on 20 μm ceramic discs may be representative of many reservoir formations.

Further challenges in optimal fluid design appear when reservoir formations exhibit significant heterogeneity in terms of pore sizes and permeability. Yang et al. (2020) conducted a study on selective plugging of such reservoir formations using microfoam selective water plugging agent, where the core permeabilities ranged from 7.87×10^{-3} μm^2 – 736×10^{-3} μm^2. Considering the presence of such high formation heterogeneity, a reservoir drilling fluid may need to be tested on a large range of permeable formations to provide a robust picture of the performance through the various parts of the reservoir.

Siddig et al. (2020) conducted a review of different approached for chemically removing the filter-cake when using water-based drilling fluids. Their findings were that different approaches were recommended for different weighting materials and different reservoir rock conditions. Also, with high concentrations of weighting agents, the filter-cakes would become heterogeneous, where one layer would consist mainly of the weighting agent and one layer of polymers, thereby also potentially introducing the need for a dual- or multistage chemical treatment.

Viewing reservoir formation damage in multiple contexts, Civan (2020) shows different forms of formation damage, such as e.g., fines and solids migration, phase trapping, biological and chemical mechanisms. The research literature shows that results using different test methodology to a certain degree are inconsistent. A considerable part of

the research is conducted using rock cores, which are tested using a different procedure than the practical testing using ANSI/API 13B-1. Therefore, such testing is normally not available to a drilling fluid engineer in a practical situation.

The conclusions of Czuprat et al. (2019) and Green et al. (2017) support the need for a cost-effective screening method for selecting a drilling fluid before a verification test on a representative core or when no core is available for testing. Klungtvedt et al. (2021b) developed a methodology for assessing signs of formation damage by measuring changes to permeable discs, as a sign of invasion of e.g., solids, polymers or fibers. Data showed that it was possible to measure changes in disc mass accurately, however, the experiments did not sufficiently study changes in permeability to verify its applicability. Therefore, the methodology developed by Klungtvedt et al. was applied in the present study to investigate the changes in disc permeability after HTHP tests and compare these results with changes in disc mass. Further, the tests were repeated by a different researcher, and the data compared.

The objective of present study was to identify if multiple indicators of formation damage would yield consistent and reliable results, thereby enabling a cost-effective method for assessing formation damage. A series of experiments were set up to test application of the method proposed by Klungtvedt and verify if the extension to measure changes in permeability would provide consistent results.

The present objectives are:

- To verify if the methodology proposed by Klungtvedt et al. (2021b) would yield consistent results when applied to measure changes in permeability in ceramic discs by using different fluid compositions and repeated tests with different researchers.
- To verify if the three indicators of formation damage, namely disc mass change, change in permeability to air and change in permeability to water, yield consistent results.
- To apply the methodology to very that a KCl Polymer fluid may produce formation damage and further to verify that such formation damage may be reduced by addition of $CaCO_3$ and cellulose fibres.
- To apply the methodology to investigate if xanthan gum and low viscosity poly-anionic cellulose may be replaced by modified starch additives and provide satisfactory results with regards to formation damage as well as rheology and fluid loss.

The tests were designed to assess the consistency of the results obtained when calculating the disc' change in permeability to water and air following the HTHP tests and a subsequent process of applying a reverse flow for filter-cake lift-off and an oxidizing breaker for further removal of filter-cake residue. Four different fluid compositions were tested for rheology, fluid loss and signs of formation damage, particularly related to change in permeability. The four tests were repeated by a different researcher using the same procedure, recipe, and equipment, but separated by a period of four weeks. The fluid composition was designed to replicate a typical fluid that might be used for drilling either a producer or injector well for oil and gas or a geothermal well. Also, by using inert ceramic discs, the study focuses on the functionality of the drilling fluid and the breaker application alone, without considering any chemical or mechanical interaction between the fluid and the rock formation.

2. Methods

The methodology is centered around conventional HTHP test for fluid loss using permeable discs as these are commonly used in the industry. The main addition to the process is to document the permeability and mass of the discs prior to the HTHP tests and thereafter measure changes in these parameters after conducting the fluid loss test and reverse flow for filter-cake removal. This enables studying the changes a fluid may have on the permanent permeability of the formation, without needing to conduct a more comprehensive dynamic core flooding test. The change in disc mass was documented by Klungtvedt et al. (2021b), however, the present study was conducted to verify if the method of detecting formation damage by measuring changes in permeability could provide reliable results.

The key elements of the process are to first measure the mass and permeability of ceramic discs before conducting an HTHP test using the procedure from ANSI/API 13B-1, or potentially under a higher applied differential pressure. The permeability of the discs was first measured by flowing air through the discs and measuring applied pressure, flowrate, and air temperature. By restricting the flow area of the disc to an area slightly smaller than that of the HTHP test, the change in permeability after exposure to the drilling fluid may be measured quite accurately. The equipment was first calibrated by measuring the pressure drop in the system when flowing air at different flowrates without the disc present. Using tables of viscosity of air, the dimensions of the flow area, disc thickness, applied pressure and air flowrate, it was possible to calculate the average permeability. Thereafter, a similar process was applied for flowing water through the disc. Prior to the flow test, the fluid and the disc were placed in a vacuum for 5 min to remove air bubbles.

The HTHP tests were conducted at 6.9 MPa (1000psi) using a nitrogen pressure source. Thereafter the discs are placed in a customized acrylic cell, where brine is flushed through the discs in the reverse direction of the HTHP test to study the ease of lifting the filter-cakes, as shown in Fig. 1. Thereafter the discs are submerged into a breaker fluid before permeability and disc mass is measured and compared with the original values. At this stage of the process, the permeability to water was measured first, then the disc was dried in the Moisture Analyser and weighed before the permeability to air was measured. The methodology used for the testing is presented in detail in the Appendix.

Conventional equipment used for HTHP Fluid loss testing according to ANSI/API13-B.

- Hamilton Beach Mixer, for mixing of drilling fluids
- Ohaus Pioneer Precision PX3202, for weighing the drilling fluid ingredients
- Ofite Filter Press HTHP 175 ml, Double Capped cell for HTHP fluid loss test
- Ofite Viscometer model 900, for measuring fluid rheological parameters
- Ofite roller-oven #172-00-1-C, for aging the drilling fluid samples
- Apera pH90, pH meter, for pH measurements

Special experimental set-up.

- Ohaus MB120 Moisture Analyser, for weighing the discs in dry conditions at 105 °C
- Custom built transparent acrylic cell with stand for enabling of reverse flow of fluid through the ceramic discs and viewing of filter-cake removal
- Festo pressure regulator LRP-1/4–2.5 and LRP-1/4–0.25, for regulating air pressure that is driving the reverse flow of fluid through the disc or for permeability measurements
- Festo Pressure Sensor SPAN-P025R and SPAN-P10R for measuring the applied pressure for filter-cake lift-off or for permeability measurement
- Festo Flowmeter SFAH-10U, for measuring the flow of fluid through the disc
- Nitrogen source and manifold for pressure up to 1350psi, Ofite #171-24
- Vacuum machine, DVP EC.20–1, for removal of air from fluid and discs when conducting HTHP tests and permeability measurements

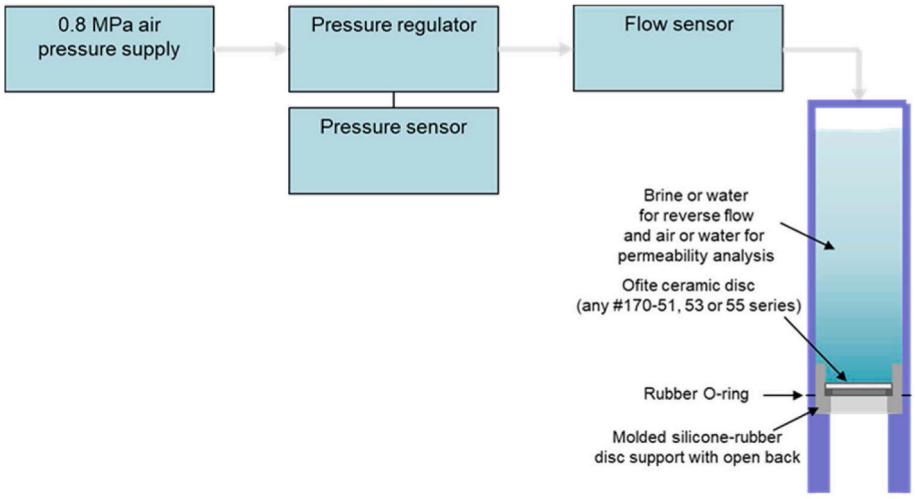

Fig. 1. Schematic of equipment for reverse flow and permeability measurement.

3. Results

3.1. Drilling fluid composition and rheology

Four fluid compositions, shown in Table 1, were selected, and tested with a one-month interval and tested by different personnel to evaluate reproducibility. Fluid 1 was selected to be a KCl polymer fluid without any solids or fibres, using conventional xanthan gum and low viscosity poly-anionic cellulose. Such a fluid was expected to result in high fluid loss and formation damage following the findings of Khan et al. (2003, 2007), where polymer damage to the formation was detected. The other three fluids contained solids to reflect the findings of Pitoni et al. (1999), who found that the solids composition impacted fluid loss and return permeability. Fluid 2 used the same base mixture as Fluid 1. However, bentonite was added to represent fine drill solids or clay. Fluid 3 and 4 were also KCl polymer fluids. These had the same concentration of $CaCO_3$ and a cellulose based fibre with a D90 value of 75 μm. (AURACOAT UF, provided by EMC AS). The difference between Fluids 3 and 4 were the polymers used for viscosity and fluid loss. Fluid 4 used conventional xanthan gum and low viscosity poly-anionic cellulose, whereas Fluid 3 used a designed mixture of starch-based polymers (PureBore and PureBore ULV, provided by Clear Solutions International Limited). The concentration of KCl was selected as an average between what might be applied when drilling oil and gas wells and geothermal wells.

Figs. 2 and 3 show the shear stress vs shear rate diagrams for the fluids after hot-rolling and at a temperature of 49 °C, focussing on the dynamic conditions on the drilling operation. All the fluids showed shear-thinning or thixotropic behaviour. At shear rates more than 200 (1/s), Fluid 3 showed the lowest viscosity and Fluid 4 showed the highest viscosity. The only difference between the two fluids were the polymers selected for viscosity and fluid loss. In the range up to a shear rate of 34 (1/s), Fluid 3 showed the highest viscosity and Fluid 1 showed the lowest viscosity. In total, Fluid 3 showed the most shear thinning or thixotropic behaviour. If the fluids were applied in a 17 ½" or 12 ¼" sections, the shear rates would typically be in the range below 200 reciprocal seconds, and the rheological properties would be relatively similar. For a permeable well section of 8 ½" or smaller diameter, the shear rates may be more variable depending on the selection of drill-pipe outer diameter etc.

Table 1
Drilling fluid recipes 1-4.

Component and Mixing sequence	Fluid 1	Fluid 2	Fluid 3	Fluid 4
Water	971g	961g	928g	926g
Soda Ash	0.06g	0.06g	0.06g	0.05g
Caustic Soda	0.71g	0.71g	0.66g	0.66g
Xanthan Gum	3.43g	3.39g		3.17g
Low viscosity poly-anionic cellulose	14.3g	14.2g		13.23g
Polymer blend for viscosity and fluid loss (PureBore)			6.6g	
Polymer blend for fluid loss (PureBore ULV)			8.0g	
MgO	2.86g	2.83g	2.65g	2.65g
KCl	50.0g	49.5g	46.3g	46.3g
Bentonite		28.3g		
Ground marble ($CaCO_3$) < 53 μm			52.9g	52.9g
Cellulose fibre for fluid loss control (AURACOAT UF)			13.2g	13.2g

3.2. Ceramic discs and permeability measurements

Prior to the HTHP tests, the ceramic discs were weighted and permeabilities to air and water were measured. The respective data for each disc used for the tests are presented in Fig. 4. The discs are specified as having a mean pore-throat size of 20 μm and permeability to air of 2 D. Given that the outer dimensions are identical and uniform materials are used for manufacturing the discs, a low disc mass may indicate high porosity and permeability, and visa-versa for a high mass disc. Fig. 5 shows the plot of permeability to air against disc mass for the discs used. The relationship between disc mass and air permeability is negative, and the calculated correlation is −0.961. This confirms the relationship between disc mass and permeability, where a higher disc mass is correlated to a reduction in permeability (thus the negative correlation coefficient). Table 2 lists the correlation between the three measurements for each disc, showing positive correlation between permeability to air and water. Correlation between disc mass and permeability to water was also negative. The difference in permeabilities might also be a factor that should be considered when comparing results of experiments where the specific discs have been used, rather than assuming that any two discs with a specified mean pore-throat size of 20 μm have the same porosity, permeabilities and pore-throat sizes. As an example, From Fig. 4 it can be seen that the discs used for Fluid 2 had slightly higher permeability and lower mass than then discs used for Fluid 4. The least permeable discs were used when testing Fluid 3.

3.3. Fluid loss measurements

The fluid loss curves are represented in Fig. 6, for testing at a differential pressure of 6.9 MPa (1000psi) and temperature of 90 °C. All

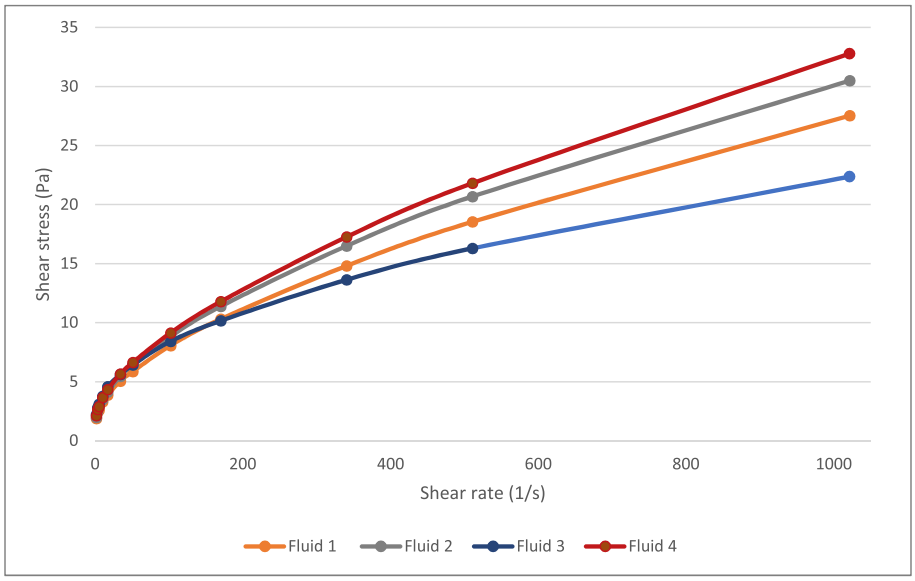

Fig. 2. Rheological flow curves of Fluid 1–4 at full share rate range.

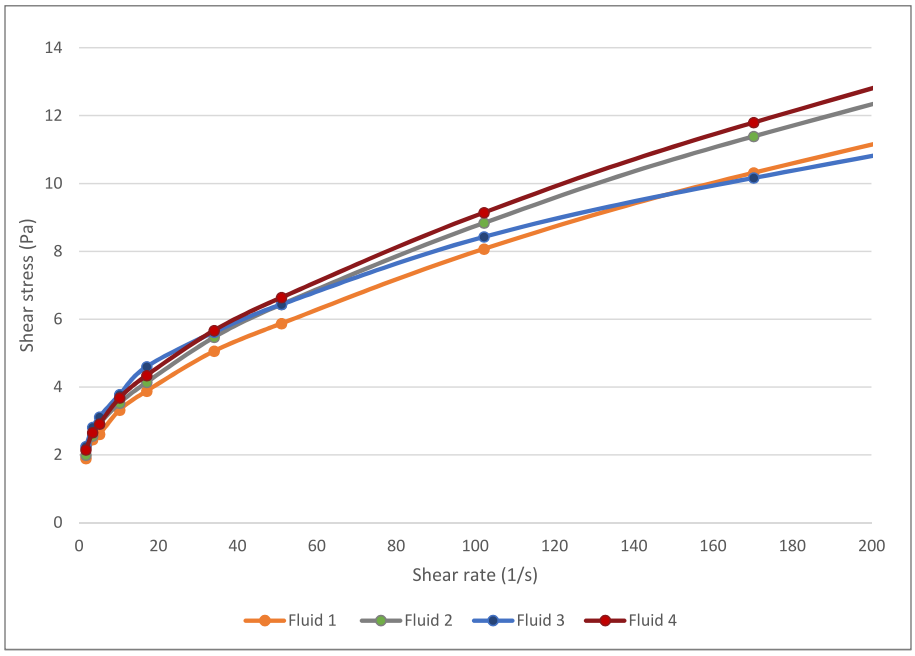

Fig. 3. Rheological flow curves of Fluid 1–4 at low-to moderate shear rates.

tests were conducted using ceramic discs with specified median pore size of 20 μm. The two test-series yielded consistent results, with less than 8% difference in fluid loss between any of the two corresponding tests. For both tests of Fluid 1, containing XC and PAC, a total loss was recorded, and the tests stopped within the first few seconds. Fluid 2 replicated the recipe of Fluid 1, however, with the addition of 28.3 kg/m^3 (10 lb/bbl) of bentonite, which was sufficient to limit the fluid loss to 32–35 ml. Fluids 3 and 4 contained the same concentration of $CaCO_3$ particles and the short fibers, whereas Fluid 3 contained the starch-based polymer blends instead of xanthan gum and ultra-low viscosity poly-anionic cellulose used in Fluid 4. The two tests with Fluid 3 and Fluid 4 recorded fluid losses of around 17 ml and around 21 ml, respectively.

The fluid loss data as a loss rate of ml/min are presented in Fig. 7. It excludes the test with Fluid 1 on the 20 μm ceramic disc as this yielded a total loss. The figure gives an insight into the gradual development of the fluid loss rates over time implicitly also the development of the permeability of the filter-cakes. The two tests with Fluid 2 saw the loss rates fall to 0.21 ml/min and 0.23 ml/min. Fluid 3 and 4 both showed lower loss rates than Fluid 2, where the loss rates fell to 0.18 ml/min and 0.19 ml/min for Fluid 3 and 0.17 ml/min and 0.19 ml/min for Fluid 4. The low differences in fluid loss rates over time also highlight that the main difference in fluid loss between Fluids 2, 3 and 4 occur during the initial spurt-loss recorded during the first 15 s of the test, and hence during the initial build-up of the filter-cakes. The lower spurt-losses of Fluids 3 and 4, relative to Fluid 2 may be attributed to the higher concentration of solids in Fluid 3 and 4. However, the relative difference between Fluid 3 and 4 may be related to the different polymers used, given that the concentration of $CaCO_3$ and fibers were similar. The indications or arguments can, however, not be considered as conclusive

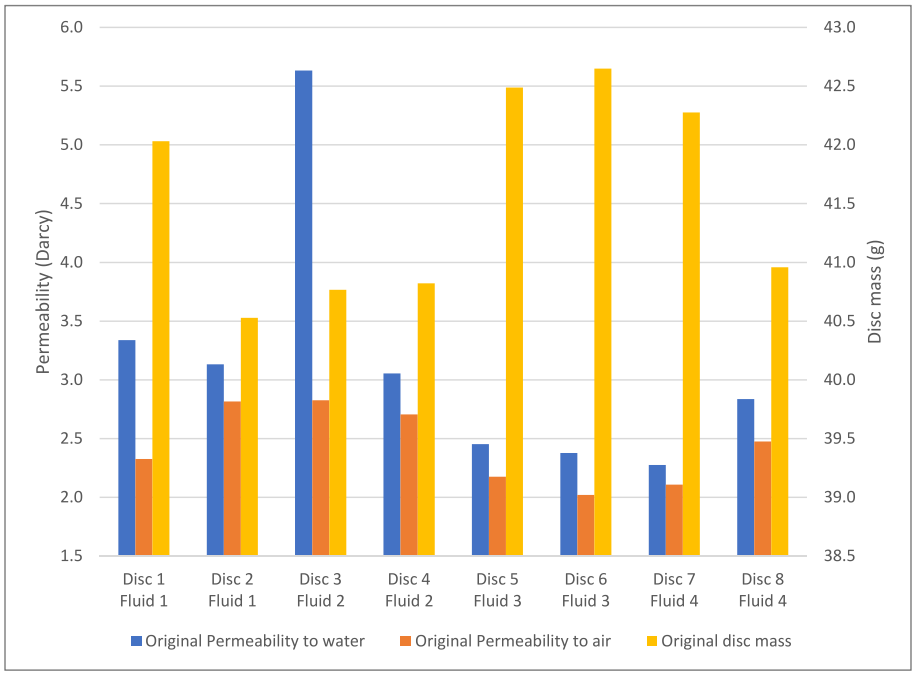

Fig. 4. Measurements of 20 μm ceramic discs before HTHP testing.

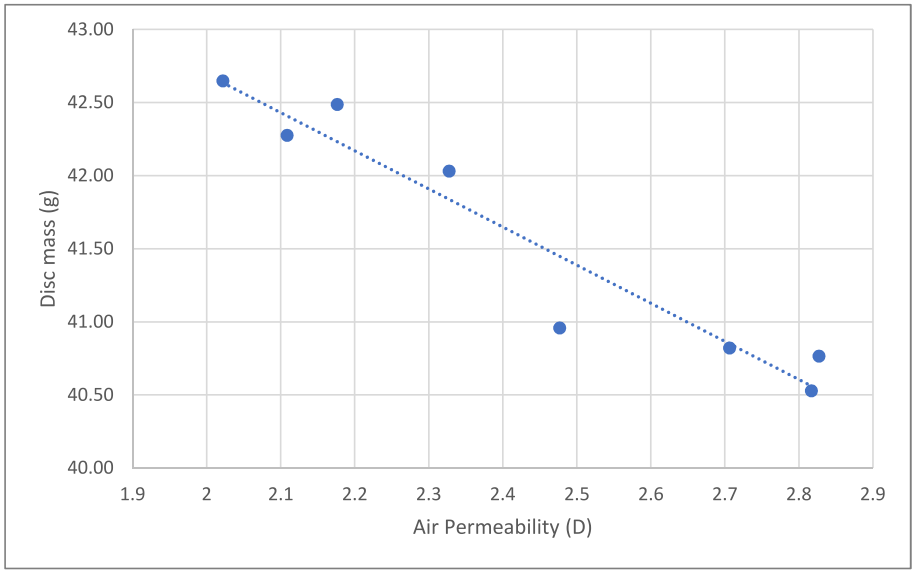

Fig. 5. Plot of disc mass vs air permeability of 20 μm discs.

Table 2
Correlations between measured permeabilities and mass for each disc.

Correlation	Permeability to air	Disc mass
Permeability to water	0.693	−0.561
Permeability to air		−0.961

evidence given that the discs had different original permeabilities and disc mass.

A comparison of the original disc permeability and the measured fluid loss is shown in Fig. 8 for Fluids 2–4. For each of the respective fluids there was a negative correlation between the original disc permeability and the fluid loss, i.e., each of the tests with the higher permeability disc recorded a smaller fluid loss given the same fluid has been used.

With the original disc permeability and the fluid loss rate development data, it is possible to provide some simple estimates for the combined permeability of the internal and the external filter-cakes. In reality, the fluid filtrate composition will vary a little for each test, and hence also the viscosities of the fluid filtrates and the thickness of the filter-cakes. As a reference, the original disc permeabilities were in the range of 2.3–5.6 Darcy. The filtercakes were circa 1 mm thick, and for simplicity, assuming that the fluid filtrate showed Newtonian behaviour with a viscosity of 1 Pa*s, the permeabilities of the filter-cakes may be calculated. In the period from 20 to 30 min, the fluid loss rates were ranging from 0.17 ml/min to 0.225 ml/min. This yields that the filter-cakes obtained a permeability as low as $1.6–2.1*10^{-7}$ Darcy.

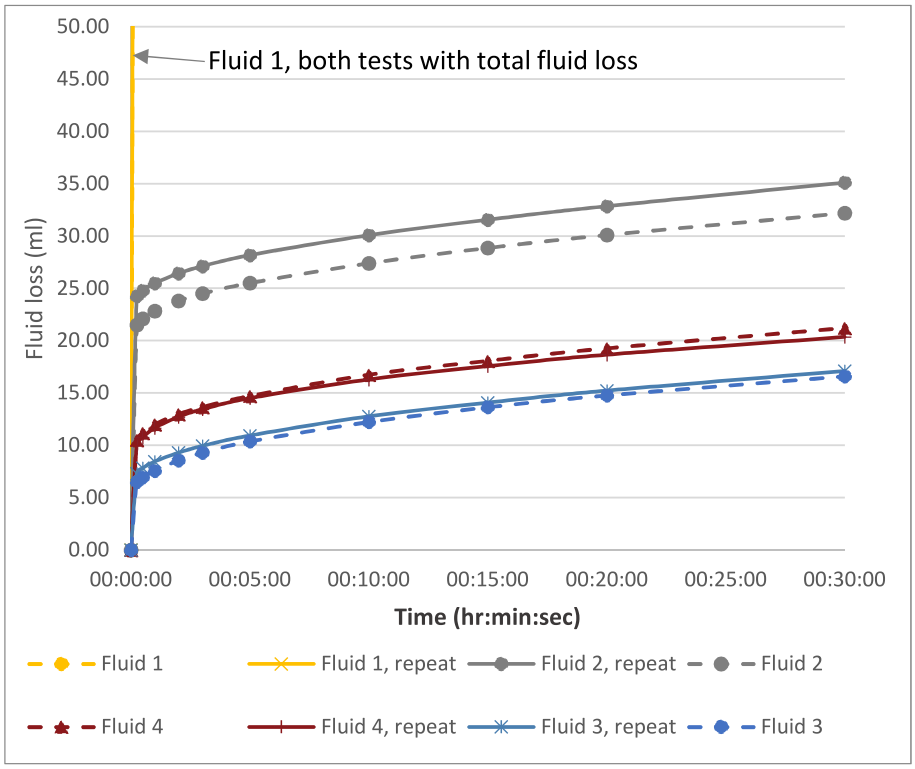

Fig. 6. Fluid loss of Fluid 1–4 at 6.9 MPa differential pressure at 90 °C.

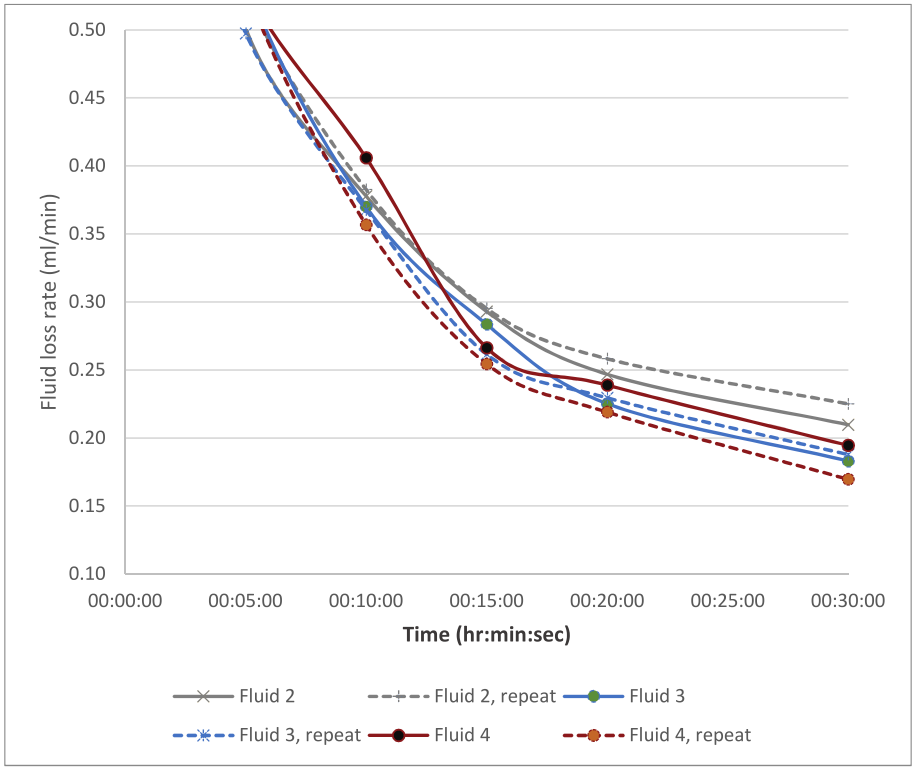

Fig. 7. Fluid loss rate development for Fluid 2-4.

3.4. Filter-cakes

The polymer residue from Fluid 1 on the ceramic disc is shown in Fig. 9, together with the filter-cakes from testing of Fluid 2 and 4. The disc from testing of Fluid 1, had no distinct filter-cake, but more of a semi-sticky polymer coating. Also, the rear of the disc showed signs of polymers after the total loss during the HTHP test. The filter-cakes made by Fluid 2 and Fluid 4 were even and shiny.

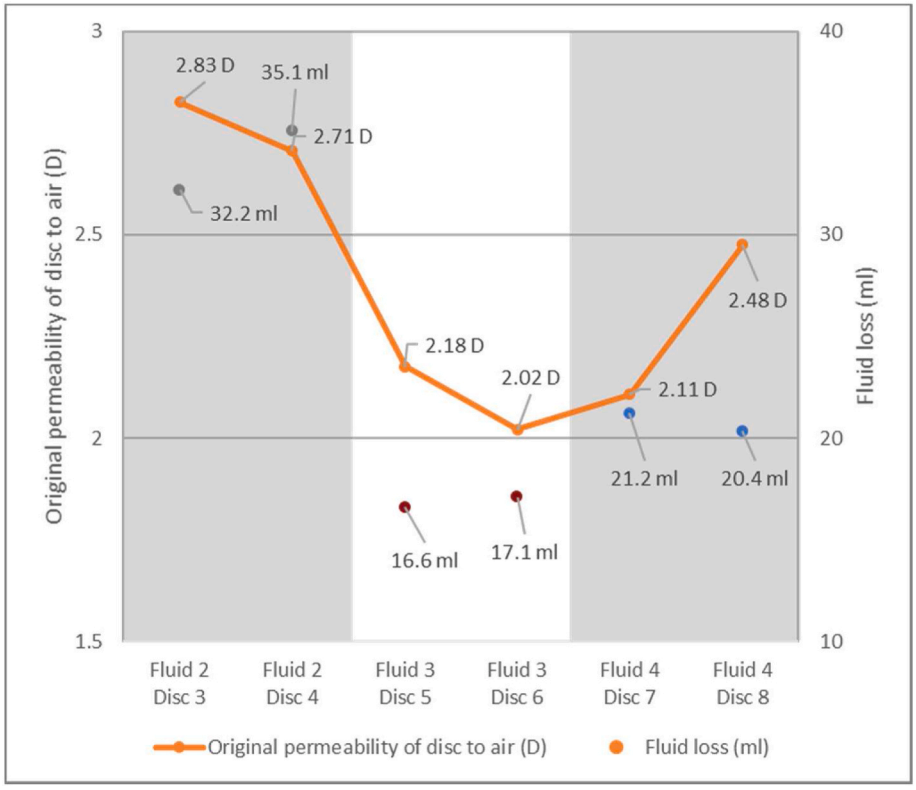

Fig. 8. Fluid loss (right axis) and original disc permeability (left axis) comparison.

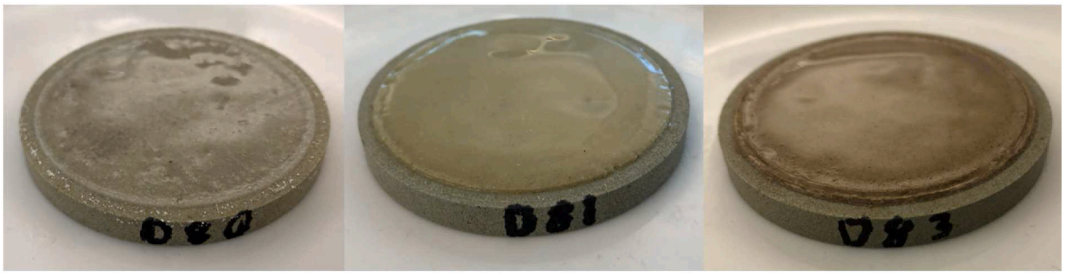

Fig. 9. From left: Residue from Fluid 1 (Disc 2) after total loss, and filter-cakes from Fluid 2 (Disc 4) and Fluid 4 (Disc 8).

The filter-cake formed by Fluid 3 (Disc 7), was a little distinct as it appeared to be a continuous piece or mat. The filter-cake and the disc and after filter-cake removal, with reverse flow of brine, is shown in Fig. 10. Even before the application of the breaker fluid, the traces of the filter-cake had almost disappeared.

3.5. Estimation of formation damage

Following the HTHP tests, the discs with the filter-cakes were back-flowed with brine and the discs placed in a bath with an oxidizing breaker fluid at 90 °C for 4 h. Thereafter permeability changes and disc

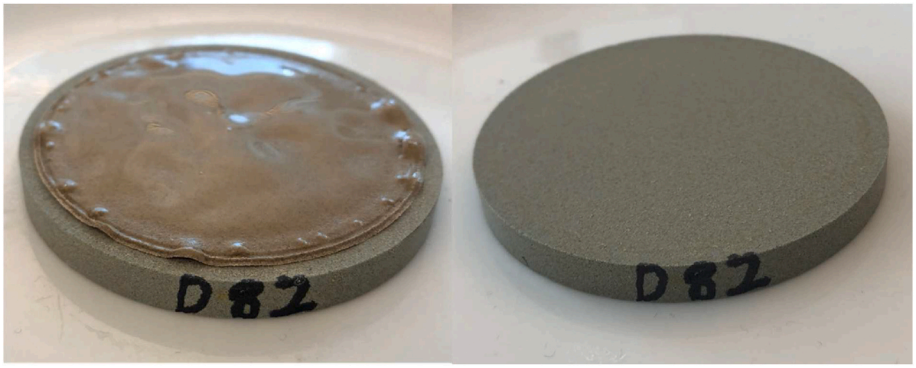

Fig. 10. Disc 7, from testing of Fluid 3 with filter-cake (left) and after filter-cake had been lifted by reverse flow (right).

mass increases were measured. The results of these tests are presented in Fig. 11. The data indicate that both the permeability to air and water were considerably reduced after the HTHP tests with Fluid 1, with measured permeability reductions ranging from 65 to 78%. This was considerably higher than for any of the other fluids, and the permeability data were also supported by the tests for Fluid 1 also having the largest mass increases. Considering that Fluid 1 contained polymers, but no solids nor fibers, the mass increase and reduction in permeability is highly related to the polymers being used. Also, it showed that the breaker that had been applied did not fully dissolve the polymers nor remove the polymers from the ceramic disc. Further, it should be considered that since the test yielded a total loss, drilling fluid or drilling fluid filtrate would penetrate the formation considerably deeper than the near wellbore region that the ceramic disc represents. Therefore, when comparing the results from testing of Fluid 1 with the other fluids in the tests, it needs to be understood that the consequential formation damage of deeper penetration into the reservoir is likely to be much higher for Fluid 1 than for the other fluids. Disc mass increases were 248–275 mg.

For Fluid 2, the inclusion of bentonite reduced the fluid loss and improved the results with regards to avoiding formation damage relative to Fluid 1, with permeability reductions ranging from 5 to 44% and lower disc mass increases of 29–62 mg.

Fluid 3, with $CaCO_3$ and the short fibers, yielded much lower permeability reductions of 9–28% and disc mass increases of 21–23 mg. The best results were obtained with Fluid 4 with reductions in permeability of 2–16% and disc mass increases of 7–13 mg. Given that Fluid 4 yielded a higher fluid loss then Fluid 3, there is, however, a potential that more formation damage might occur further into the reservoir formation than for Fluid 3, where the fluid losses were lower in both tests.

The data presented in Fig. 11 indicate high consistency in the data obtained for changes in permeability to air and water as well as increases in disc mass. The calculated correlations between the three indicators of formation damage are shown in Table 3. With all correlations being positive and above 0.9, it can be concluded that the data obtained have a high consistency. The highest correlation was obtained between changes in permeability to air and increase in disc mass, with a correlation as high as 0.984. Relative to the data in Table 2, the correlations are calculated to a reduction in permeability, and hence the coefficients of correlation with changes in disc mass are positive.

Table 3
Correlations between indicators of formation damage.

Correlations	Reduced Permeability to air	Disc mass increase
Reduced Permeability to water	0.906	0.932
Reduced Permeability to air		0.984

Further, the correlations between the first and the second test of each individual fluid with regards to the three indicators of formation damage are listed in Table 4. Although the data set is small, it is reassuring to see that the correlation data are positive and in the range of 0.686–0.997.

4. Discussion

The tests were conducted with the objective of assessing if the methodology could be applied consistently and if the indicators of formation damage would yield consistent results. All the evidence collected strongly support that the methodology yields consistent results and that the three indicators of formation damage yield consistent results.

From a practical point of view, it was most difficult to measure the permeability to water, as inclusion of air bubbles in the fluid significantly impacted the fluid flow at a given pressure, and hence also the calculation of permeability. This was solved by placing the disc and the fluid in vacuum before the permeability tests.

It may, however, be argued that neither of the indicators of formation damage as tested here fully replicate the damage that might occur when drilling a reservoir formation and therefore a core-flood test would be a more correct representation of such. From a purely scientific

Table 4
Correlation of results between first and second tests for each fluid.

Correlation	Fluid 1	Fluid 2	Fluid 3	Fluid 4
Correlation: 1st and 2 tests (reduced permeability to water and air and increase in disc mass)	0.997	0.872	0.982	0.686

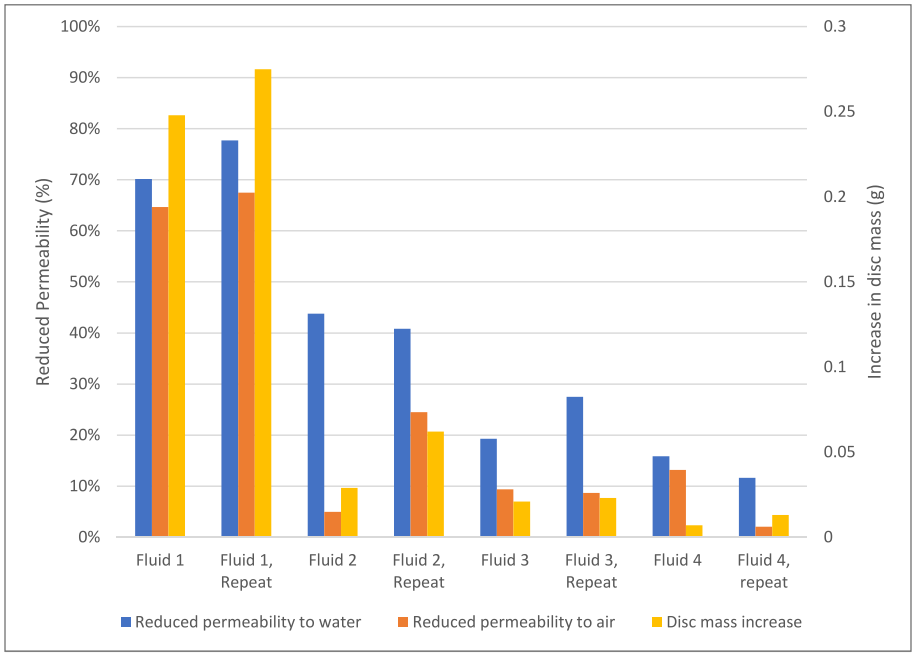

Fig. 11. Indicators of formation damage for tests with Fluid 1–4, with original test and repetition test for each fluid.

perspective each of the methods have limitations in replicating wellbore and reservoir conditions. When testing using ceramic discs, the size and shape of pore-throat openings will differ from those appearing in actual rock formations. However, when testing is carried out using actual reservoir cores, there will be an uncertainty with regards to the heterogeneity of the reservoir section, where the production zone may extend hundreds or thousands of meters. One might therefore consider that the applied testing methodology in the present study assesses the performance of the drilling fluids against a generic formation, whereas a core-flooding test assesses the performance of the drilling fluid in a specific rock formation. From a practical perspective, a core-flooding test is generally considered to be a time-consuming and costly exercise, leading to a low number of tests being conducted for each relevant reservoir. Also, for a new field, representative cores may be non-existent before the selection process of the drilling fluid is concluded. When testing using ceramic discs, it is a relatively fast and low-cost process. This enables higher volumes of testing and testing using different permeabilities, which may represent different parts of a reservoir formation. The higher volumes may be used to reduce the statistical uncertainty of the results, it may allow for testing of different fluid compositions with different breaker applications, and also assess the performance of the fluid is parts of the reservoir formation exhibit other properties than any specific core. Also, from a field perspective, it may be possible to monitor the performance of the drilling fluid as the drilling progresses and obtain relevant data to adjust the fluid properties during drilling.

Further testing should be conducted to compare the results of the test method used with equivalent core flooding tests. This may give valuable insight into the benefits of each testing methodology.

The application of the methodology did, however, replicate other results obtained by applying core flood tests. The test with Fluid 1 showed strong signs of formation damage using a polymer fluid without bridging materials. This is consistent with the findings of both Khan et al. (2003, 2007) and Audibert et al. (1999).

Green et al. (2017) conducted a series of core flooding tests and subsequent Micro-CT scanning to detect particle migration and formation change. They concluded that the key "zone" for permeability alteration in the samples was the first pores in the wellbore, regardless of the volume of filtrate loss or thickness of remnant drilling fluid filter-cake. This supports the idea of studying formation damage in the near wellbore region and that ceramic discs with a thickness of 6.3 mm will have considerably more depth than what might be necessary to study formation damage as the thickness represents around 25 times the pore size of a 250 μm disc and more than 300 times the pore size of a 20 μm disc.

Further, the study revealed that with the specific breaker fluid applied, the higher fluid loss of Fluid 4 relative to Fluid 3 did not correspond with a higher formation damage. In contrast, Fluid 1 and Fluid 2 both led to higher fluid loss and formation damage than Fluid 3 and Fluid 4. These results are also consistent with the findings of Green et al. (2017), where there the lowest permeability alterations did not correlate with the lowest drilling fluid filtrate loss volume.

Civan (2020), provide a deep insight into a number of causes of formation damage. It gives an insight into challenges such as drilling fluid to formation fluid incompatabilities, drilling fluid to rock incompatabilities, phase trapping, chemical adsorption or wettability alteration and biologic activity. These causes of formation damage are not covered in the present study. Further studies may be conducted where e.g. the original and final permeabilies are measured using a fluid replicating the reservoir fluid, which may yield an insight into aspects of fluid to fluid incompatabilities.

Given that the methodology focusses on the formation damage occurring in the depth of the disc only, no quantitative measure of deeper formation damage caused by the fluid filtrate is provided. Further testing could be conducted to measure the constituents and the characteristics of the fluid filtrate, as this might yield further information about likely formation damage beyond the near wellbore region of the part of the formation represented by the ceramic disc.

5. Conclusions

The primary conclusion of the study is that high correlations were found between the measured changes in disc mass and changes in permeability to air and water. This was verified by the two independently run test series which yielded highly correlated results.

The conclusions regarding the main objectives of the study are as follows:

- The method proposed by Klungtvedt yielded consistent results also when applied to measure changes in permeability in ceramic discs by using different fluid compositions and repeated tests with different researchers.
- The three indicators of formation damage, namely disc mass change, change in permeability to air and change in permeability to water, yield consistent results with high correlations.
- The method provided evidence that a KCl Polymer without bridging particles may produce formation damage, which is in line with past research conducted on core samples.
- Polymer formation damage may be significantly reduced by addition of a combination of $CaCO_3$ and cellulose fibres.
- The methodology provided evidence that xanthan gum and low viscosity poly-anionic cellulose may potentially be replaced by modified starch additives and provide satisfactory results with regards to formation damage, rheology, and fluid loss. Further analysis using breaker fluids designed for starch should be investigated.
- The overall results support the practical application of the methodology for assessing near wellbore formation damage. This may be particularly beneficial when it is important to test a series of different fluids and potentially with different formation permeabilities.
- The methodology, including permeability analysis, may be beneficial as part of a screening process ahead of a core flood test or in situations when a core flood test is not practical.
- The application should be relevant for both drilling of oil- and gas wells and geothermal wells, where the permanent permeability of the formation may be important.
- The tests were conducted using an oxidizing breaker fluid. Further test should be conducted without a breaker fluid or using different breaker fluids to identify how different clean-up methods may impact the removal of the filter-cakes and the consequences for estimated formation damage

Credit author statement

Karl Ronny Klungtvedt: Conceptualization, Methodology, Validation, Investigation, Writing – original draft, Writing – review & editing, Funding acquisition, Arild Saasen: Writing – original draft, Writing – review & editing, Supervision

Declaration of competing interest

The authors declare that they have no known competing financial interests or personal relationships that could have appeared to influence the work reported in this paper.

Acknowledgements

The authors would like to thank The Research Council of Norway for financially supporting the project through RCN# 320646.

Appendix

Procedure for measuring change in disc mass and change in permeability and relevant calculations following Klungtvedt et al. [24],

1. Mix drilling fluid according to the recipe allowing sufficient time for mixing of the various additives.
2. Measure pH and rheology.
3. Hot-roll for 16 h at 90 °C and if applicable degrade by high-shear stirring or other degradation method.
4. Measure pH and rheology after hot-rolling and any degradation.
5. Mark and weigh disc in dry condition using the moisture analyser (M_b). Moisture analyzer shall be set to dry disc at 105 °C until change in mass is less than 1 mg/60 s.
6. Optional step: place disc in acrylic cell and measure air temperature and flowrate at different pressures to calculate average permeability to air (K_{ab}).
7. Optional step: place disc in acrylic cell and place arrangement with water in vacuum (circa −0.96 bar for 5 min) to remove any air from disc or water. Flow thereafter water through disc and measure water temperature and flowrate at different pressures to calculate average permeability to water (K_{wb}).
8. Soak disc in brine (40 g NaCl per 1000 g freshwater) in vacuum.
9. Conduct HTHP test at desired pressure, typically 3.45 MPa (500 psi) or 6.9 MPa (1000 psi), and measure both volume (V_f) and mass (M_f) of fluid filtrate at point in time of 15 s, 30 s, 1 min, 2 min, 3 min, 5 min, 10 min, 15 min, 20 min and 30 min (V_f). Calculate fluid filtrate density.
10. Weigh disc with filter-cake and observe filter-cake.
11. Place disc in acrylic cell and reverse flow with 1 L (40 g NaCl per 1000 g water) heated to 60 °C and then with 1 L water heated to 60 °C to remove traces of salt before drying. Note pressure required to enable reverse flow through disc.
12. Optional step: place disc in breaker fluid for required time and at required temperature. Place disc in acrylic cell and flow disc with 1 L water at ambient temperature to remove any dissolved filter-cake residue.
13. Optional step: place disc in acrylic cell and place arrangement with water in vacuum to remove any air from disc or water. Flow thereafter water through disc and measure water temperature and flowrate at different pressures to calculate average permeability to water (K_{wa}).
14. Weigh disc in dry condition using moisture analyser (M_a) using the same settings as in step 5.
15. Optional step: place disc in acrylic cell and measure air temperature and flowrate at different pressures to calculate average permeability to air (K_{aa}).

Depending on the number of optional steps included in the procedure, it enables collection of a large amount of data in addition to observing the filter-cake and the fluid filtrate volume V_f.

The moisture analyser used for weighing the discs was set to heating the discs to 105 °C and continue drying until the mass change due to moisture evaporation was less than 1 mg per 60 s. The drying process then stopped automatically, and the mass of the disc displayed. The precision of the instrument is 1 mg. The change in disc mass was then simply calculated as:

$$(M_a) - (M_b) = M_{change}$$

By placing a digital weight under the graduated cylinder used to measure fluid filtrate, it was possible to simultaneously record the mass of the fluid filtrate and read the volume of the filtrate. This enabled a precise estimation of the fluid loss profile and calculating the fluid filtrate density (D_f), calculated as:

$$(M_f)/(V_f) = (D_f)$$

The permeability was calculated as an average of multiple readings within certain flow-rate ranges. Darcy's law was used in a rearranged form as follows:

$$K = \eta \frac{Q * \Delta L}{A * \Delta P}$$

where K is the calculated permeability coefficient (m^2), η is the viscosity of the fluid (Pa * s), Q the fluid flowrate (m^3/s), ΔL the disc thickness (m), A the areal of flow into the disc and ΔP the pressure differential over the disc (Pa).

References

Alsaba, M., Aldushaishi, M., Jeennakorn, M., Nygaard, R., Saasen, A., Nes, O.M., 2017. Sealing Pressure Prediction Model for Lost Circulation Treatments Based on Experimental Investigations. American Association of Drilling Engineers. AADE-17-NTCE-21.

Alsaba, M., Nygaard, R., Hareland, G., 2014a. Review of Lost Circulation Materials and Treatments with an Updated Classification. AADE-14-FTCE-25.

Alsaba, M., Nygaard, R., Saasen, A., Nes, O.M., 2014b. Lost Circulation Materials Capability of Sealing Wide Fractures. SPE-170285-MS.

Alsaba, M., Nygaard, R., Saasen, A., Nes, O.M., 2016. Experimental investigation of fracture width limitations of granular los circulation materials. J Petrol Explor Prod Technol 6 (2016), 593–603.

Alshubbar, G., Nygaard, R., Jeennakorn, M., 2018. The effect of wellbore circulation on building and LCM bridge at the fracture aperture. J. Petrol. Sci. Eng. 165, 550–556, 2018.

ANSI/API 13B-1 5th edition, 2019. Recommended Practice for Field Testing Water-Based Drilling Fluids.

Audibert, A., Argiller, J.F., Ladva, H.K.J., Way, P.W., Hove, A.O., 1999. Role of Polymers on Formation Damage. SPE 54767.

Civan, F. Reservoir Formation Damage 2020. Gulf Professional Publishing, ISBN 978-0-12-801898-9, PP. 1-6.

Cobianco, S., Bartosek, M., Lezzi, A., Previde, E., 2001. New solids-free drill. In: Fluid for Low Permeability Reservoirs. SPE-64979.

Czuprat, O., Dahle, B.O., Dehmel, U., Ritschel, R., Storhaug, J., Adrian, T., Patley, I., 2019. Systematic Selection of Drill-In and Completion Fluids for Development of the Dvalin HT Gas Field. SPE-195601-MS.

Enstad, G., 1975. On the theory of arching in mass hoppers. Chem. Eng. Sci. 30, 2173-1283.

Green, J., Patey, I., Wright, L., Carazza, L., Saasen, A., 2017. The Nature of Drilling Fluid Invasion, Clean-Up, and Retention during Reservoir Formation Drilling and Completion. SPE-185889-MS.

Hoxha, B.B., Yang, L., Hale, A., van Oort, E., 2016. Automated Particle Size Analysis Using Advanced Analyzers, AADE-16-FTCE-78.

Jeennakorn, M., Alsaba, M., Nygaard, R., Nes, O.M., Saasen, A., 2017. Testing conditions make a difference when testing LCM. J. Nat. Gas Sci. Eng. 46, 375–386. https://doi.org/10.1016/j.jngse.2017.08.003, 2017.

Jeennakorn, M., Alsaba, M., Nygaard, R., Saasen, A., Nes, O.M., 2019. The effect of testing conditions on the performance of lost circulation materials: understandable sealing mechanism. Journal of Petroleum Exploration and Production Technology 9, 823–836.

Khalifeh, M., Klungtvedt, K.R., Vasshus, J.K., Saasen, A., 2019. Drilling Fluids - Lost Circulation Treatment. SPE-195609-MS.

Khan, R., Kuru, E., Tremblay, B., Saasen, A., 2007. Extensional viscosity of polymer based fluids as a possible cause of internal cake formation. Energy Sources 29, 1521–1528.

Khan, R., Kuru, E., Tremblay, B., Saasen, A., 2003. An Investigation of Formation Damage Characteristics of Xanthan Gum Solutions Used for Drilling, Drill-In, Spacer Fluids and Coiled Tubing Applications, PAPER 2003-067, Petroleum Society's Canadian International Petroleum Conference. Calgary, Alberta, Canada, June 10-12, 2003.

Klungtvedt, K.R., Khalifeh, M., Saasen, A., Berglind, B., Vasshus, J.K., 2021a. Drilling Fluids – Preventing Drilling Fluid Induced Reservoir Formation Damage, SPE-202187-MS.

Klungtvedt, K.R., Saasen, A., Vasshus, J.K., Trodal, V.B., Mandal, S.K., Berglind, B., Khalifeh, M., 2021b. The fundamental principles and standard evaluation for fluid loss and possible extensions of test methodology to assess consequences for formation damage. Energies – MDPI.

Lee, L., Taleghani, A.D., 2020. Simulating fracture sealing by granular LCM particles in geothermal drilling. Energies 13, 04878.

Nelson, P.H., 2009. Pore-throat sizes in sandstones, tight sandstones and shales. Am. Assoc. Petrol. Geol. Bull. 93, 329–340. NO. 3 (March 2009).

Pitoni, E., Ballard, D.A., Kelly, R.M., 1999. Changes in Solids Composition of Reservoir Drill in Fluids during Drilling and the Impact on Filter Cake Properties. SPE 54753.

Siddig, O., Mahmoud, A.A., Elkatantny, S., 2020. A review of different approaches for water-based drilling fluid filter cake removal. J. Petrol. Sci. Eng. Online publication April 29, 2020. Https//doi.org/10.1016/j.petrol.2020.107346.

Saasen, A., Hodne, H., Ronæs, E., Aarskog, S.A., Hetland, B., Løvereide, M.B., Mohammadi, R., 2018. Wood Fibre Based Lost Circulation Materials, pp. OMAE2018–77662.

Whitfill, D., 2008. Lost Circulation Material Selection, Particle Size Distribution and Fracture Modelling with Fracture Simulation Software. IADC/SPE, 25-27 August, Jakarta. SPE-115039-MS.

Yang, E., Fang, Y., Liu, Y., Li, Z., Wu, J., 2020. Research and application of microfoam selective water plugging agent in shallow low-temperature reservoirs. J. Petrol. Sci. Eng. 193, 107354, 2020.

IV. Klungtvedt, K.R. and Saasen, A. “Invasion of CaCO3 particles and polymers in porous formations in presence of fibres”, Journal of Petroleum Science and Engineering 2022. https://doi.org/10.1016/j.petrol.2022.110614 (open access)

Journal of Petroleum Science and Engineering 215 (2022) 110614

Contents lists available at ScienceDirect

Journal of Petroleum Science and Engineering

journal homepage: www.elsevier.com/locate/petrol

Invasion of $CaCO_3$ particles and polymers into porous formations in presence of fibres

Karl Ronny Klungtvedt [a,b,*], Arild Saasen [b]

[a] EMC AS, NO-4033, Stavanger, Norway
[b] University of Stavanger, NO-4036, Stavanger, Norway

ARTICLE INFO

Keywords:
Formation damage
Drilling fluid LCM

ABSTRACT

Formation damage can occur through migration of drilling fluid particles and polymers into porous formations. A methodology for assessing formation damage was applied to measure invasion of $CaCO_3$ and polymers into porous formations, where the $CaCO_3$ particles size had been selected using established particle size selection methods. Tests were conducted with and without the presence of a cellulose-based additive, to study if the fibres could reduce the fluid loss and limit the formation damage.

Input factors such as applied differential pressures, ranging from 6.9 to 34.9 MPa (1000-5000psi), and median pore-throat openings of discs were also varied to investigate which parameters affected the significance of the formation damage.

The results showed invasion of $CaCO_3$/ground marble into the formation and that particle size selection methods used to reduce fluid loss also led to formation damage. Further it was discovered that the presence of fibres limited the invasion of both $CaCO_3$ and polymers into the porous formations when the D90 of the fibres were $\geq$3/2 times the pore-throat size, and that higher applied pressures led to larger formation damage. The fluid loss tests also showed both lower total fluid losses and lower fluid loss rates over time with the fibres added to the fluids, indicating that the filter-cake permeability was reduced with the addition of the fibre particles.

1. Introduction

A simplified method for assessing formation damage experimentally was introduced by Klungtvedt et al. (2021, 2022) for the study of formation damage when drilling either oil-, gas- or geothermal wells. In this method, formation damage was studied by measuring changes in the mass of a porous formation as well as changes in the formation's permeability to a fluid. They concluded that it was possible to measure the increases in disc mass accurately and that for certain tests there were inverse relationships between fluid losses and disc mass increases. Further, in the second study, it was concluded that the high correlations obtained between the changes in disc mass and changes in permeabilities indicate that the different indicators of formation damage yield consistent results.

$CaCO_3$ is used worldwide as a fluid loss additive and weighting agent in reservoir drilling fluids due to factors such as low cost, a density of around 2.7 sg and acid solubility. Numerous studies have been conducted on selection of sealing materials (Alsaba et al., 2014; Jennakorn et al., 2019) and particle size distribution (PSD) for sealing of pore-throats and fine fractures (Whitfill, 2008; Alsaba et al., 2015; 2017) leading to particle size selection methods typically selecting a D50 or D90 value relative to a given median pore-throat size. As an example, both the D90 Rule (Smith et al., 1996) and the Vickers Method (Vickers et al., 2006) suggest selecting a D90 value which is equal to the pore throat size, whilst Abrams Rule suggest selecting particles with a D50 $\geq$ 1/3 of the formation average pore size (Abrams, 1977). The selection methods do, however, not consider compressible or elastically deformable particles like fibres as part of their models to limit fluid loss and prevent formation damage. However, it has also been shown that $CaCO_3$ and graphite particles degrade readily when exposed to fluid shear (Hoxha et al., 2016). It can therefore be questioned how accurate the particle size selection methods are from a field perspective, as the particle size distribution of the particles in the drilling fluid will change during circulation.

Alternative materials such as cellulose-based additives have been proven to seal permeable discs without the presence of solids in the form of weighting agents or drill solids (Klungtvedt et al., 2021b). Other studies have shown that the solids composition of fluids play a role in

* Corresponding author. EMC AS, NO-4033, Stavanger, Norway.
E-mail addresses: krk@emcas.no (K.R. Klungtvedt), arild.saasen@uis.no (A. Saasen).

https://doi.org/10.1016/j.petrol.2022.110614
Received 2 February 2022; Received in revised form 25 March 2022; Accepted 6 May 2022
Available online 13 May 2022

reducing the formation permeability, and that increasing the PSD may yield higher return permeability (Pitoni et al., 1999).

When studying the roles of specific materials, it has been shown that polymers such as xanthan gum may significantly reduce formation permeability (Khan et al., 2003, 2007), whilst the presence of cuttings may yield a lower return permeability than a fluid without cuttings (Cobianco et al., 2001).

The scope of the present tests is to apply the method of selecting $CaCO_3$ particles with D90 values equal to the pore-throat size to evaluate the impact on formation damage. Considering that $CaCO_3$ particles added to the fluid will be grinded down in size during circulation, it may be argued that the particles will eventually be reduced to a size smaller than the pore-throat size of the formation. To prevent them from migrating into the formation, $CaCO_3$ particles need to be combined with more shear resistant particles where the D90 value is more stable. A second objective was to see if the fibres also could enable an effective fluid loss control and prevent polymers from damaging the formation permeability, with no $CaCO_3$ present in the fluid. For convenience, the specified median pore-throat size of the ceramic discs will be treated as the relevant pore-throat size. Therefore, two test series were set up to apply the methodology to separately assess the impact of $CaCO_3$ invasion and polymer invasion on permeability and disc mass. These tests were conducted with and without fibres present in the fluid.

The primary objectives of the present tests can be summarised as follows:

- Verify if the recognised particle selection methods are optimal for reducing formation damage
- To identify the formation damage caused by a solids-free polymer fluid or a polymer fluid containing $CaCO_3$ particles.
- To identify if higher applied differential pressures are likely to increase the formation damage
- To identify if application of cellulose fibres may reduce any formation damage caused by either polymers or $CaCO_3$ particles.

2. Methods, results and discussions

The experiments were set up to measure changes in the mass and permeability of porous ceramic discs to provide potential evidence of formation damage caused by $CaCO_3$ and polymers. The methodology used for the testing is presented in detail in the Appendix and in Klungtvedt and Saasen (2022). The key elements of the process are to measure changes in the discs before and after HTHP filtration tests with regards to disc mass and permeability, either after reverse flow with water to remove the filter-cake or after an application of a chemical breaker fluid. The first test series uses a drilling fluid with presence of both polymers and $CaCO_3$, whereas the second test series uses a KCl polymer fluid with no solids present.

Studies have been conducted in the past on application of various breaker fluids for removing polymers such as starch from core samples (AlKhalid et al., 2011). Since the objective of this study partially is to investigate the potential formation damage of polymers, a combination of xanthan gum and low viscosity poly-anionic cellulose was selected for viscosity and fluid loss and a benign oxidizing breaker fluid was selected for light cleaning of the ceramic discs only. It was therefore expected that the application of the breaker would mainly function to disperse the external filter-cake, without removing internal polymer residue or alternatively deposited carbonate or fiber particles.

2.1. $CaCO_3$ invasion into porous discs under high-pressure conditions

Tests were set up to measure the effect of $CaCO_3$ invasion into ceramic discs of mean pore-throat size of 50 μm under different differential pressures and with/without the presence of an Ultra-Fine cellulose-based fibre product which has a specified D90 value of 75 μm (AURACOAT UF, provided by European Mud Company AS). The $CaCO_3$ used was a ground marble and had been sieved to ensure a maximum particle size of 53 μm and an even distribution of particles above and below 23 μm to reflect the guidance of particle selection methods like the D90 Rule, Vickers Method, and the Abrams Rule. In this article, the terms $CaCO_3$, carbonate and ground marble are used interchangeably. The recipe and mixing sequence of the two fluids used is shown in Table 1. The fluids were KCl polymer-based drilling fluids with a concentration of around 56–57 kg/m^3 of $CaCO_3$, with the differences between the fluids being the inclusion of a fibre at a concentration of 13.9 kg/m^3 in Fluid 2, whereas Fluids 1 contained no fibres. The concentration of KCl was kept low, to reflect a drilling composition which may be relevant both for hydrocarbon and geothermal wells. KCl was selected due to its inhibitive effect on reactive clays. The concentration of xanthan gum was around 3.4 g/100 ml to provide sufficient viscosity for barite suspension and suspension of drill solids in wells with low angles of deviation. The fluids were designed with low solids contents and low salinity to be representative of fluids using for drilling of geothermal wells in addition to drilling of a permeable section of an oil- or gas well.

Table 1
Recipe of test Fluids 1-2.

Component and Mixing sequence	Fluid 1	Fluid 2
Water	961g	948g
Soda ash	0.06g	0.06g
Caustic soda	0.71g	0.70g
Xanthan gum	3.39g	3.35g
Low viscosity poly-anionic cellulose	14.1g	13.9g
MgO	2.83g	2.80g
KCl	49.5g	48.8g
$CaCO_3$ (<53 μm)	56.6g	55.8g
Cellulose fibre with D90 of 75 μm		13.9g

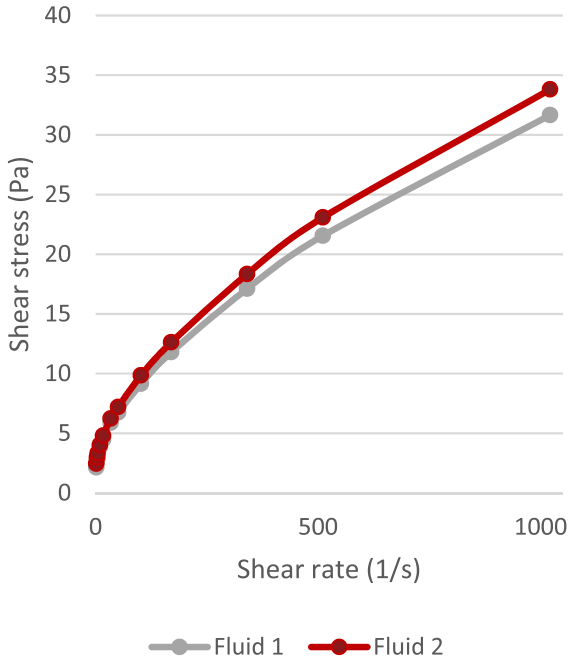

Fig. 1. Flow curves of Fluids 1-2.

The rheological flow curves of Fluids 1 and 2 at 49 °C are presented in Fig. 1. The inclusion of cellulose fibre increases the concentration of particles in the fluid and increases the measure shear stress slightly at higher shear rates. Shear rates in the annulus will typically be less than 200 reciprocal seconds, and in this region the differences between the

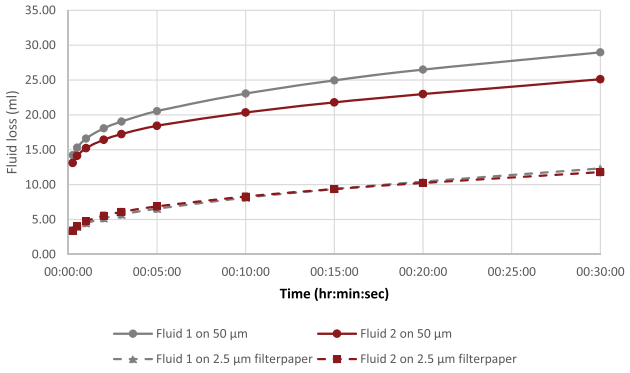

Fig. 2. Fluid loss for Fluids 1 and 2 on filter paper and 50 µm ceramic disc.

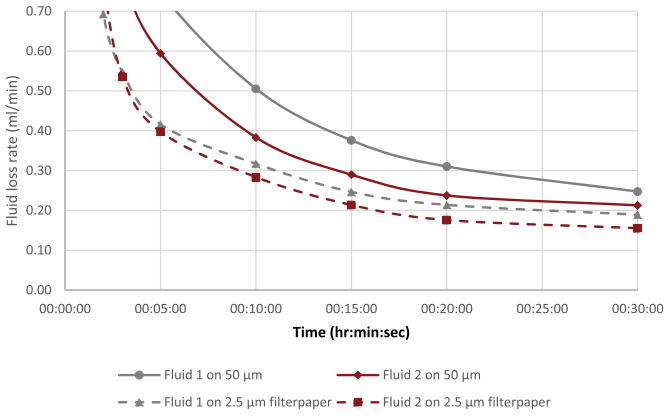

Fig. 3. Fluid loss rate development for Fluid 1 and 2.

measured shear stresses between the two fluids are small.

Fluid loss test were conducted using a conventional HTHP cell at 90 °C with applied differential pressures of 3.49 MPa (500 psi) for the tests on 2.5 µm filterpaper and 6.9 MPa (1000 psi) for the tests on 50 µm ceramic discs, as presented in Fig. 2. Higher pressures were applied for the tests on ceramic discs to reflect that drilling of depleted reservoirs often occur at higher differential pressures than the 500 psi recommended for API HTHP testing. The measured total fluid loss for the tests on filterpaper were relatively similar for Fluid 1 and 2, with 4% lower fluid loss for Fluid 2, indicating that the filter-cakes exhibit similar permeability at 3.49 MPa or that the permeability of the filterpaper is very low and hence does not adequately differentiate the filter-cake permeabilities. In contrast, the test on 50 µm ceramic discs showed a 13% reduction in fluid loss after the addition of Ultra-Fine cellulose fibre to the fluid. The differences in spurt-loss were not large and hence the difference in fluid loss over time may indicate that the filter-cakes exhibit different permeabilities with higher differential pressures applied. A reason for this may be compression of the fibres under higher applied differential pressure, and consequently a tighter packing of the filter-cake. The slight increases in shear stress and reduction in fluid loss for Fluid 2 relative to Fluid 1 may indicate some affinity between the cellulose fibres and the polymers of the base fluid.

To understand the development of the filter-cake permeability and the fluid loss over time, the fluid loss data were converted to a fluid loss rate for any given period of the HTHP test. This is presented in Fig. 3. Here it can be seen that the tests with Fluid 2, with fibre products and ground marble, have a lower fluid loss rate than Fluid 1, with ground marble, at any given point in time, given the same test medium. After 30 min, the recorded loss-rates were 0.25 ml/min and 0.21 ml/min respectively. This is evidence that the inclusion of the cellulose fibres reduced the permeability of the filter-cakes.

Subsequently, Fluids 1 and 2 were tested in a permeability plugging apparatus up to a maximum pressure of circa 34.9 MPa (5000psi) using 50 µm ceramic discs. After the target peak pressure had been achieved, no further fluid was pumped into the cell, and hence the pressure was allowed to fall gradually in line with fluid filtrate passing through the

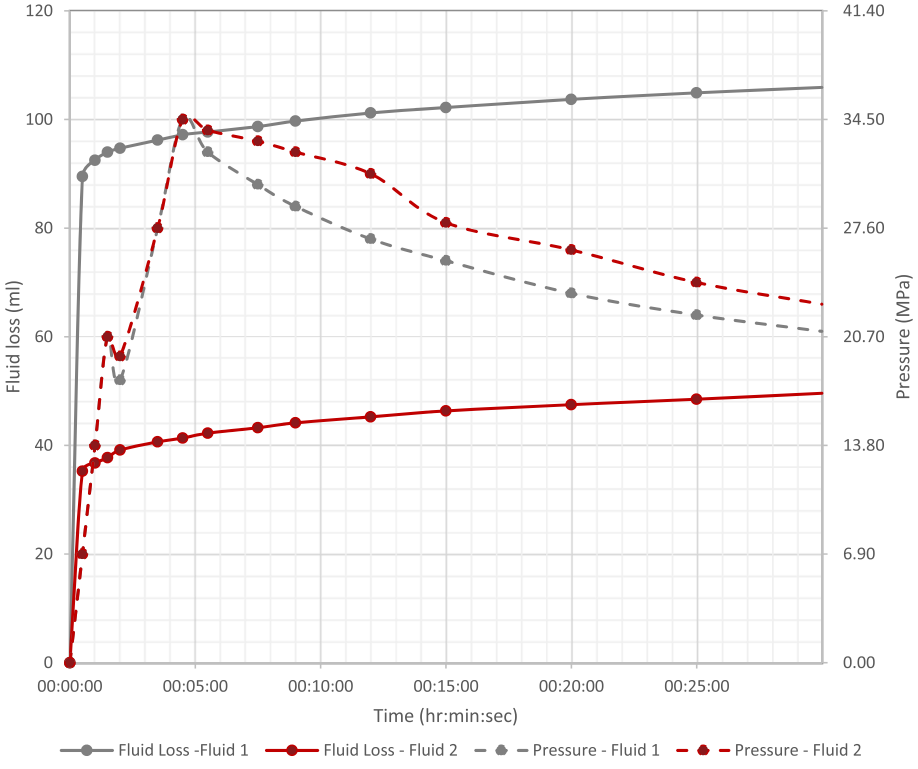

Fig. 4. Fluid loss and pressure development using tests on 50 µm ceramic discs for Fluid 1 with $CaCO_3$/ground marble and Fluid 2 with fibres.

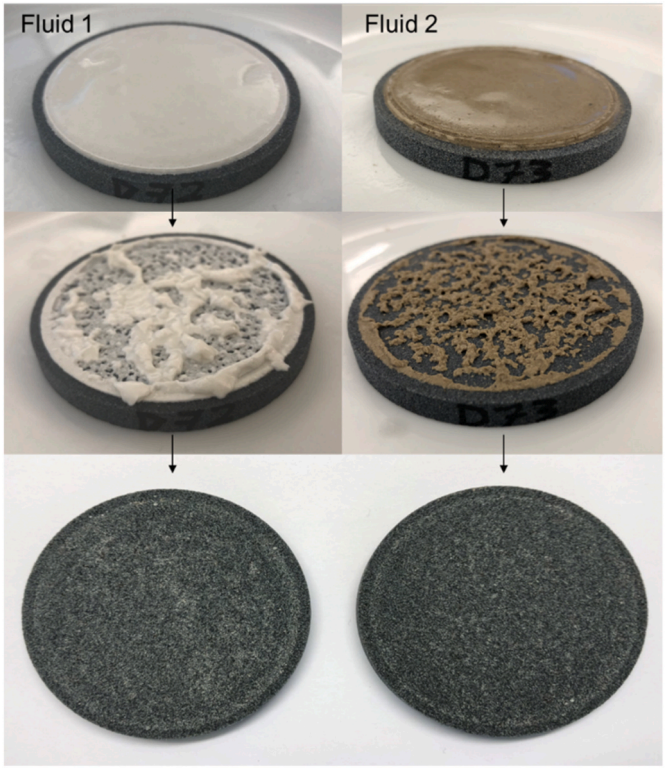

Figs. 5. 50 μm discs used for testing of Fluid 1 and 2.

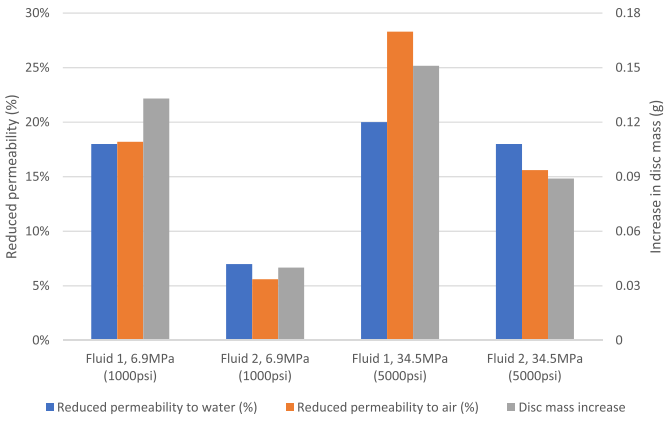

Fig. 6. Indicators of formation damage for Fluid 1 and 2 at different pressures.

ceramic disc and the corresponding de-compression of the fluid in the test cell. The pressure and fluid loss curves are presented in Fig. 4. Relative to the test conducted at 6.9 MPa, the differences in fluid loss between Fluid 1 and 2 increased considerably, with a 53% lower fluid loss with Fluid 1 containing $CaCO_3$ than with Fluid 2 containing fibres and $CaCO_3$.

After the HTHP fluid loss tests, the respective discs were analysed for changes in permeability and disc mass. The tested discs are presented in Fig. 5 at different stages through the process. First, with the discs of Fluid 1 and Fluid 2 after the 6.9 MPa (1000 psi) HTHP test, and in the middle with the filter-cakes partially removed by reverse flow, and then finally after applying an oxidizing breaker for 4 h at 90 °C and drying. During the reverse flow with brine, the filter cakes started disintegrating before a pressure of 0.05 MPa (7 psi) had been reached, but due to the high disc permeability, flow of brine rapidly builds at certain points of the disc and the filter-cakes were washed off in fragments. More of the filter-cake appeared to be lifted off the disc with Fluid 2, relative to the disc with Fluid 1, potentially due to the filter-cake being more cohesive with bonding between the cellulose fibres and the polymers. After the breaker application and drying, there was a visible difference, with less filter-cake residue remaining on the surface of the disc where Fluid 2 has been applied.

Changes in permeability and mass were measured. The results of these measurements are shown in Fig. 6. The three indicators of formation damage yield consistent results between the respective tests. For the 6.9 MPa tests, exposure to Fluid 1 reduced both the permeability to air and water by 18% and the increase in disc mass was 133 mg. After the test with Fluid 2, the permeability to water and air was reduced by 7% and 6%, respectively, whereas the increase in disc mass was only 4 mg, clearly indicating that the presence of cellulose fibre reduced the formation damage to a very low level. The significantly lower mass increase of the disc indicate that the fibres prevented $CaCO_3$ or polymers from migrating into the disc. Also, the tests confirmed the expectation that the oxidizing breaker did not dissolve or otherwise remove all polymers or deposited particles from the ceramic discs, whereas the external filter-cakes were successfully dissolved.

When the applied pressure increased to 34.9 MPa, the fluid loss increased relative to the 6.9 MPa test fluid loss values. This also corresponded with greater signs of formations damage. For Fluid 1 with carbonate particles, the reduction in permeability to water and air increased from 18% to 20% and 28%, respectively, whereas the disc mass increased from 133 mg to 151 mg. For Fluid 2 with cellulosic fibres, the reduction in permeability to water increased from 7% to 18% and the reduction in permeability to air increased from 6% to 16%. The increase in disc mass was more considerable as it increased from 4 mg to 89 mg.

It should, however, be noted that the data on formation damage was better for Fluid 2 at 34.9 MPa, than for Fluid 1 at 6.9 MPa, despite a higher fluid loss. This may indicate that the higher applied pressure for the test with Fluid 2 caused a higher filtrate volume, but that the presence of the fibres still reduced the invasion of solids or polymers into the disc. This observation is also consistent with Green et al. (2017), who concluded that lower fluid loss did not always correspond with lower formation damage.

The overall results of tests indicate that presence of $CaCO_3$, in a concentration of 5.6% by mass, facilitates a sealing of permeable formations up to median pore-throat sizes of 50 μm when the $CaCO_3$ particles were sieved to a size less than 53 μm, supporting the D90 Rule and the Vickers Method. However, the indicators of formation damage show that with presence of polymers and $CaCO_3$, the formation's permeability is significantly reduced. Further, with the addition of cellulose fibre in a concentration of 1.4% by mass, both fluid loss and indicators of formation damage are considerably improved. This indicates that presence of fibre particles with D90 $\geq$ 3/2 times the median pore-throat size may reduce invasion of solids and polymers and thereby reduce formation damage. For both the tests with Fluid 1 on ceramic discs, the disc mass increase was significantly larger than that for the tests with Fluid 2. This indicates that Fluid 1 led to more solids-invasion and hence more particles were forming an internal filter-cake with Fluid 1 than with Fluid 2. Comparing the fluid loss after the first 15 s of the tests conducted at 1000 psi, the fluid loss with Fluid 2 was 20% lower than that of Fluid 1. This is also consistent with the lower fluid loss rate of Fluid 2 than Fluid 1 after 30 min, Shown in Fig. 3. The fact that Fluid 1 likely had formed more of an internal filter-cake and that the fluid loss rate was lower for Fluid 2 after the initial spurt loss, indicates that the filter-cake also has a lower permeability.

2.2. *Limitation of polymer invasion in a solids-free fluid by introducing cellulose-based fibre particles*

To study the potential formation damage of polymers alone and the combination of polymers and fibres, a second series of tests were setup. An Ultra-Fine fibre product proved to limit formation damage in the first

Table 2
recipe of fluids 3-5.

Component and Mixing sequence	Fluid 3	Fluid 4	Fluid 5
Water	971g	961g	961g
Soda Ash	0.06g	0.06g	0.06g
Caustic Soda	0.71g	0.71g	0.71g
Xanthan gum	3.43g	3.39g	3.39g
Low viscosity poly-anionic cellulose	14.3g	14.1g	14.1g
MgO	2.86g	2.82g	2.82g
KCl	50.0g	49.5g	49.5g
Cellulose fibre Fine, D90 of 125 μm		11.3g	
Cellulose fibre Ultra-Fine, D90 of 75 μm			11.3g

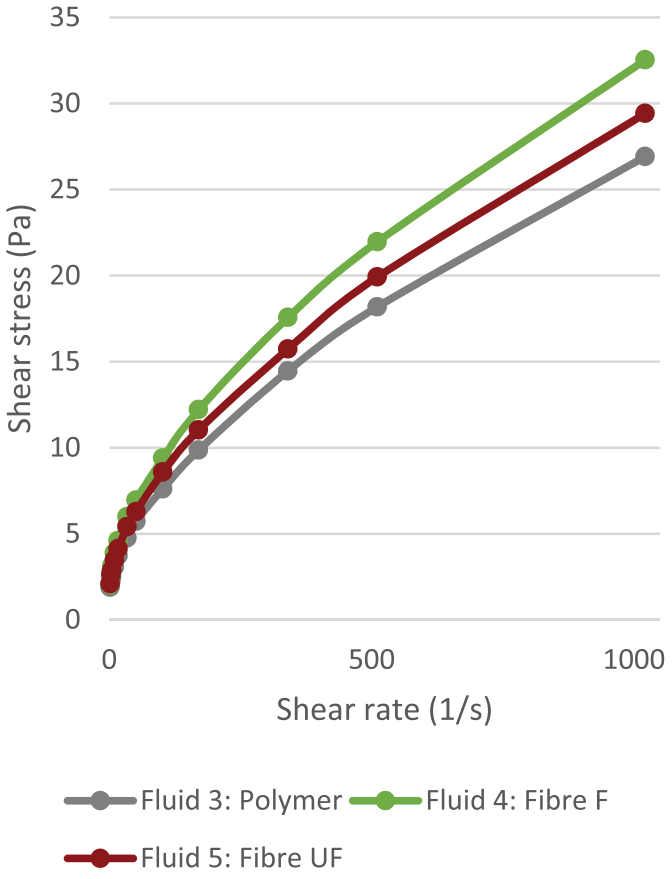

Fig. 7. Flow curves of Fluid 3–5, full viscometer share rate range.

test series when added to a fluid containing both polymers and $CaCO_3$. In addition to the Ultra-Fine fibre used in section 2.1, another Fine cellulose-based fibre product with D90 of 125 μm was selected for testing (AURACOAT F, provided by European Mud Company AS) in a drilling fluid free of solids in the form of drilled solids and weighting agents. The underlying objective was to assess if the fibre products could limit fluid loss and prevent formation damage when drilling with a solids-free drilling fluid. Tests were conducted on discs with a specified mean pore-throat size of 10 μm and 20 μm, with and without the presence of fibres. The recipe and mixing sequence of the three fluids used are presented in Table 2. Fluid 3 is the base fluid, composed as a KCl polymer drilling fluid where the polymers used are xanthan gum and low viscosity poly-anionic cellulose. The Fine fibre product was added in concentration of 11.3 kg/m^3 in Fluid 4 and the Ultra-Fine fibre product was added in a concentration of 11.3 kg/m^3 in Fluid 5.

The rheological flow curves of Fluids 3–5 at 49 °C are presented in Fig. 7. The inclusion of the fibres introduces particles in the fluid and increased the measured shear stress for a given shear rate. The increase

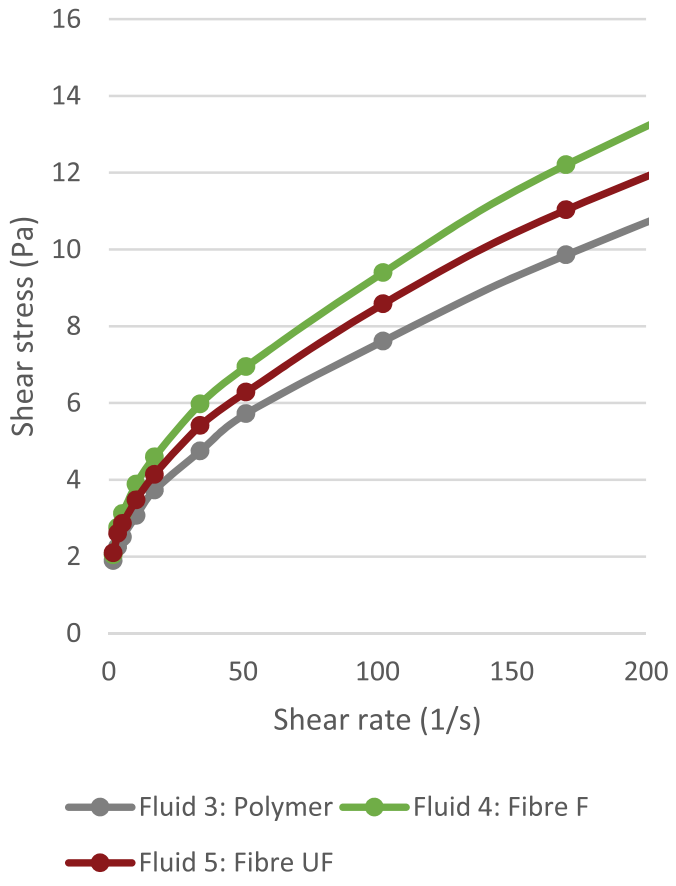

Fig. 8. Flow curves of Fluid 3–5, annulus flow share rate range.

in shear stress is slightly larger for the Fine fibre than for the Ultra-Fine fibre, likely due to the larger particle size, particularly when seen relative to the shear gap of the Ofite 900 viscometer that was used. With a viscometer shear gap of 1.17 mm and D90 particle size of 125 μm for the Fine fibre, the largest particles will be more than 1/10th of the shear gap, which may lead to incorrect readings on the viscometer. In Fig. 8, the lower share rate readings are presented. Here it can be seen that the differences in measured shear-stress between the three fluids reduce with lower shear-rates.

The plots for the fluid loss of Fluids 3–5 are represented in Fig. 9. For Fluid 3, a total loss was recorded on the 20 μm ceramic disc, whereas it managed to seal the 10 μm ceramic disc with a total fluid loss of 48 ml. In the solids-free fluid, the inclusion of the Fine fibre in Fluid 4 enabled effective sealing of the 10 μm disc with a fluid loss of 26 ml and the 20 μm ceramic disc with a fluid loss of 29 ml. With Fluid 5, the inclusion of the Ultra-Fine fibre effectively sealed the 10 μm ceramic disc with a total fluid loss of 19 ml and the 20 μm disc with a fluid loss of 32 ml. Fluids 4 and 5 have the same total concentration of fibre particles. However, due to the smaller particle size of the fibres in Fluid 5, naturally the concentration of particles below 75 μm will be higher than that of Fluid 4. This difference in particle size distribution may explain why the fluid loss is lower for Fluid 5 on the 10 μm ceramic disc. Another factor may be polar forces between the fibres and the polymers. With smaller fibre particles, the surface area will be larger for the same concentration of the Ultra-Fine fibres than for Fine fibres, and hence any polar interaction may be increased. In total, these factors may explain why the fluid loss was particularly low for Fluid 5 when tested on the 10 μm disc.

The fluid loss rate development is presented in Fig. 10. It excludes the test with Fluid 3 on the 20 μm ceramic disc as this yielded a total loss. The fluid loss rates appear very similar for the two fluids with fibres (Fluid 4 and Fluid 5), already after 2 min into the test. During the testing period, the fluid loss rates gradually fall towards a loss rate of 0.2–0.24

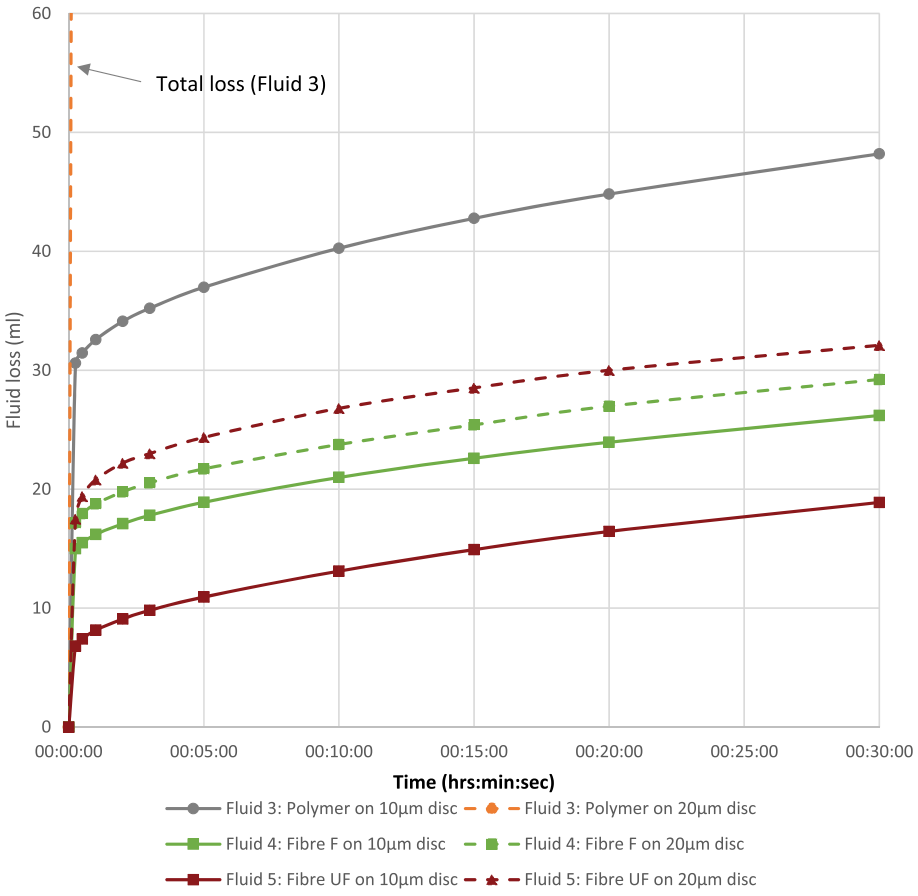

Fig. 9. Fluid loss at 6.9 MPa (1000 psi) for Fluid 3-5.

ml/min, when calculating as the average over the final 10 min of the tests. The main differences between the tests for Fluid 4 and 5 were during the first 15 s, when the internal and initial external filter-cakes were established. It appears that as time progressed, the fluid loss rate was more dependent on the permeability of the filter-cake being developed and less on the original disc permeability. In contrast, the fluid loss rate for Fluid 3 was consistently higher and fell to a rate of 0.34 ml/min during the final period of the test.

The measurements of air permeability and disc mass after reverse flow, and treatment with an oxidizing breaker, are presented in Fig. 11. The two discs that had been tested with Fluid 3 showed signs on considerable formation damage, with 53% and 66% reduction in permeability to air and 146 mg and 262 mg increases in the disc mass. Given that no solids nor fibres were present in Fluid 3, it may be concluded that the damage is due to polymer invasion.

In contrast, the results from the discs tested with Fluid 4 and 5 showed very low signs of formation damage. The recorded reduction in air permeability was 0.9% (10 µm disc) and 32% (20 µm disc) and disc mass increases of 27 mg (10 µm disc) and 21 mg (20 µm disc), where Fluid 4 had been applied. The corresponding numbers were 4.3% (10 µm disc) and 1.0% (20 µm disc) for reduction in air permeability and 0 mg (10 µm disc) and 32 mg (20 µm disc) increases in disc mass where Fluid 5 has been applied. The overall results indicate that the fibres were able to limit the fluid loss and reduce formation damage considerably when a breaker fluid was used to remove the external filter-cake residues. For the tests with Fluids 4 and 5, the D90 values of the fibre particle size distribution were larger than the specified pore sizes. Also, the D90 values of the fibres were higher than the ratio of 3/2 times the median pore-throat size. For Fluid 4, the D90 value was 12.5 times the rated pore size and 6.25 times the pore size, for the 10 µm and 20 µm discs. For Fluid 5, the D90 value was 7.5 and 3.75 times the median pore size. Comparing the formation damage indicators with the tests with Fluid 2, from the first test series, it is not clear if a further increase in the ratio of D90 value of the fibres to the median pore-throat size increases beyond the ration of 3/2 would yield any further reduction of formation damage.

It was observed a significant reduction in permeability to air for Fluid 4 after the test on the 20 µm disc. This is in slight contrast to the measurement of changes in disc mass, which was very low. The observation is also in contrast with the other tests with fluids containing fibres. No clear evidence was found of this deviating data, but a cause may be large differences in initial disc permeabilities and hence pore-sizes The 20 µm disc used for testing Fluid 5 has a low initial permeability to air of 646 mD and a disc mass of 41.768g. In contrast, the initial permeability of the 20 µm disc used for testing Fluid 4 was 8.36 D and the disc mass was 41.461g. Given that the differences in mass was relatively low at only 0.74% it is likely that the large difference in permeability is related to larger pore-sizes on the disc used for Fluid 4. Any surface plugging of some large pore openings may lead to significant reduction in permeability, but with little measured disc mass increase. The specified permeability to air is 2 D, so it is clear that the supplied discs varied greatly from the specification. Other potential causes may be the functioning of the breaker fluid or that the polymers and/or fibres may have combined in a certain way during the drying process.

The overall test results of test series 2 clearly indicates that the cellulose fibres enable HTHP sealing of permeable formations without the presence of solids in the form of drill solids or weighting agents, even in concentrations as low as 11.3 kg/m^3. Also, a fluid with polymers, but without fibres or solids present a great risk of formation damage if used in a reservoir section. Further, the inclusion of cellulose fibres show that formation damage may be substantially limited even with a 6.9 MPa (1000 psi) differential pressure applied and given that the particles have

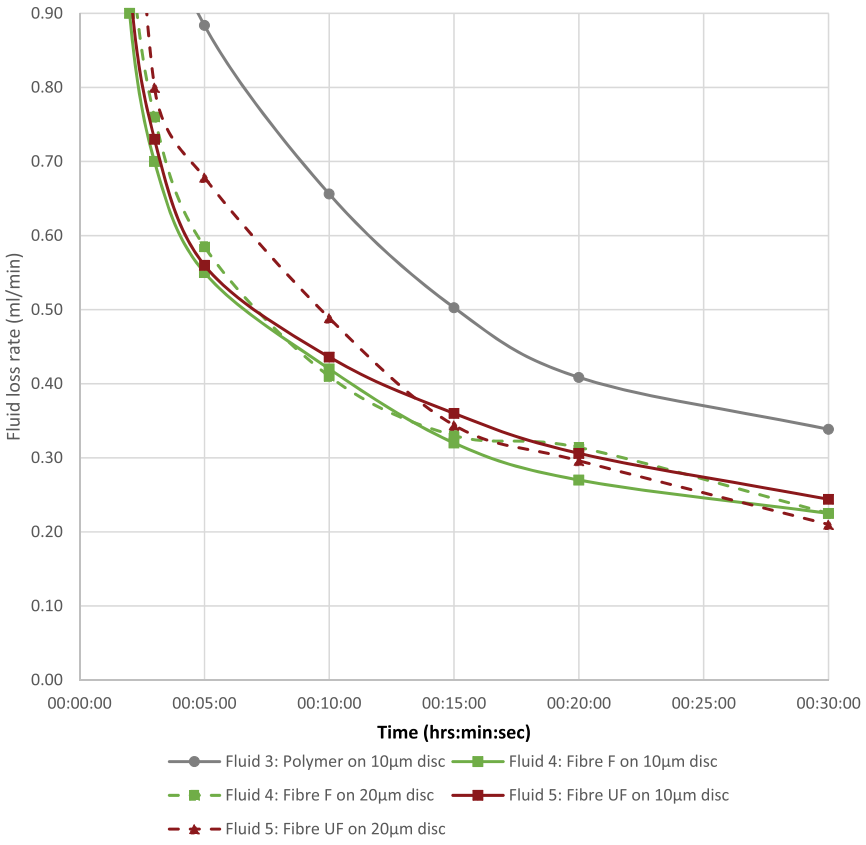

Fig. 10. Fluid loss rate development of Fluid 3-5.

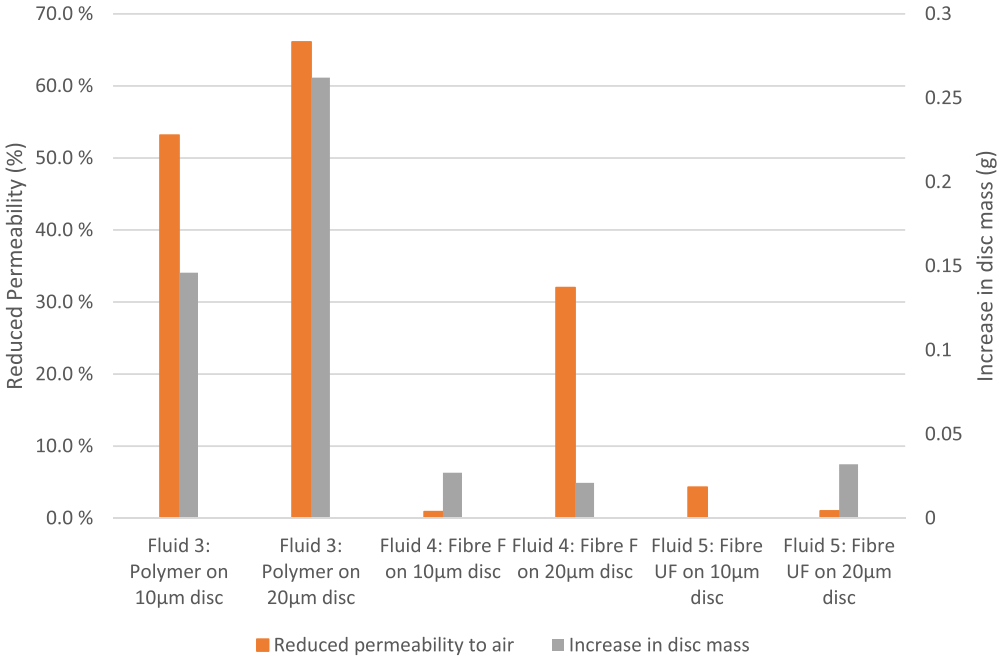

Fig. 11. Indicators of formation damage after testing with Fluid 3-5.

a D90 value that is equal to or greater than 3/2 times the pore-throat size. Klungtvedt et al. (2021a,b) tested fibres containing cellulose with D90 values of around 0.8 times the pore-size and found that this led to very low fluid loss, but with significant increases in disc mass. Such application may be ideal for wellbore stabilisation purposes but may induce formation damage in a reservoir drilling application.

By viewing the fluid loss rate development together with the measurement of changes in disc mass, it may be possible to assess if the development of the fluid loss rate was dictated by the building of an internal or external filter-cake. For the tests with Fluids 4 and 5, the fluid loss rate fell much faster than for Fluid 3. At the same time, the disc mass increases were considerably lower. This indicates that for Fluids 4 and 5, relative to Fluid 3, the improvement in fluid loss over time was a result of lower external filter-cake permeability rather than more particles migrating to form a low-permeability internal filter-cake.

2.3. Overall discussion of test results

The tests show that fluid loss is reduced when $CaCO_3$ and fibres are added to a KCl polymer drilling fluid, and that an effective sealing may be achieved all the way up to differential pressures of 34.5 MPa (5000psi) in certain cases. Further, it shows that the formation damage is considerably reduced when fibres with a D90 $\geq$ 3/2 the pore size is added to the fluid. This suggests that the fibres can form a more impermeable external filter-cake which prevents solids from entering the formation, given that the size exceeds 3/2 times the median pore-throat size.

Considering that $CaCO_3$ particles are known to degrade rapidly after exposure to shear, there results of this study indicates that application of sized $CaCO_3$ particles to prevent fluid loss and formation damage will only have temporary effect. For optimum results, $CaCO_3$ particles need to be combined with materials where the PSD deteriorates much less during a typical drilling operation.

The analysis has been based on comparing the D90 value of the fibers with the median pore size of the permeable discs. In a permeable rock formation, there will likely be heterogeneity in the pore-sizes, where the largest pore-networks may yield higher permeability than the average of the formation. If such heterogeneity is significant, the high permeability parts of the formation is likely to provide an above average fluid flow when the well is brought into operation. To optimise the retention of the formation permeability, it may therefore also be important to ensure that particles are of a sufficiently large size to protect the largest pore openings from solids invasion and polymer damage. It may also be the case that the ceramic discs are heterogenous and hence that fibres with a larger D90 value than then median pore size are particularly important in protecting the high-permeability parts of the discs.

3. Conclusions

The tests provided good evidence with regards to understanding how fluid loss and formation damage may be reduced. It was shown that polymer fluids alone and in combination with $CaCO_3$ can lead to substantial formation damage. The main variable factor in the tests were the inclusion of fibres with a known D90 value $\geq$ 3/2 the pore size, to both reduce the fluid loss and the formation damage.

- It was identified that a solids-free polymer fluid without cellulose fibres led to large formation damage on permeable discs with 10 μm and 20 μm pore sizes.
- It was identified that $CaCO_3$ particles can lead to formation damage when the D90 value is around the pore size. The tests showed a permeability reduction of 17–18%.
- When cellulose fibres with D90 value $\geq$ 3/2 the pore size were introduced, the formation permeability reduction was limited to 6–7%. This indicates that the recognised particle size selections methods may be further optimised when applying fibrous materials, and that larger fibre particles prevent migration of solids and polymers into the formation.
- When higher differential pressure was applied, the measured formation damage increased.
- The recognised particle selection methods focussing on either D50 or D90 values proved to provide good fluid loss values. However, such particle selection method led to formation damage, measured as reduction in permeability and increased disc mass.
- The tests conducted at 6.9 MPa (1000 psi) indicated that the permeability of the external filter-cake was reduced when fibre particles were added to the fluid.

Credit author statement

Karl Ronny Klungtvedt: Conceptualization, Methodology, Validation, Investigation, Writing – original draft, Writing – review & editing, Funding acquisition. **Arild Saasen**: Writing – original draft, Writing – review & editing, Supervision.

Declaration of competing interest

The authors declare that they have no known competing financial interests or personal relationships that could have appeared to influence the work reported in this paper.

Acknowledgements

The authors would like to thank the Research Council of Norway for financially supporting the project through RCN# 320646.

Appendix

The special experimental set-up was as follows:

- Ohaus MB120 Moisture Analyser
- Custom built transparent acrylic cell with stand for enabling of reverse flow of fluid through the ceramic discs
- Festo pressure regulator LRP-1/4–2.5 and LRP-1/4–0.25
- Festo Pressure Sensor SPAN-P025R and SPAN-P10R
- Festo Flowmeter SFAH-10U
- Nitrogen source and manifold for pressure up to 1350 psi, Ofite #171-24
- Vacuum machine, DVP EC.20-1
- Custom build Permeability Plugging Apparatus with hydraulic pump for testing on slotted discs or ceramic discs up to 35 MPa (5076 psi)
- AEP Transducers JET Pressure Gauge with Data Logger

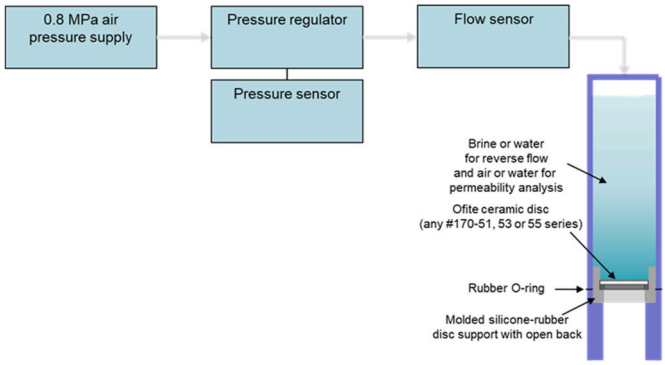

Fig. 12. Schematic of equipment for reverse flow and permeability measurement.

In additional, the following equipment was used for the conventional preparation of the fluid and HTHP fluid loss testing according to ANSI/API 13B:

- Hamilton Beach Mixer, for mixing of drilling fluids
- Ohaus Pioneer Precision PX3202, for weighing the drilling fluid ingredients
- Ofite Filter Press HTHP 175 ml, Double Capped cell for HTHP fluid loss test
- Ofite Viscometer model 900, for measuring fluid rheological parameters
- Ofite roller-oven #172-00-1-C, for aging the drilling fluid samples
- Apera pH90, pH meter, for pH measurements

References

Abrams, A., 1977. Mud design to minimize rock impairment due to particle invasion. J. Petrol. Technol. 586–592. May 1977.

AlKhalid, M.H., Ghosh, B., Ghosh, D., 2011. A novel enzyme breaker for mudcake removal in high temperature horizontal and multi-lateral wells. In: SPE Asia Pacific Oil and Gas Conference and Exhibition Held in Jakarta, Indonesia, pp. 20–22. September 2011, SPE-147863.

Alsaba, M., Aldushaishi, M., Jeennakorn, M., Nygaard, R., Saasen, A., Nes, O.M., 2017. Sealing Pressure Prediction Model for Lost Circulation Treatments Based on Experimental Investigations. American Association of Drilling Engineers. AADE-17-NTCE-21.

Alsaba, M., Nygaard, R., Saasen, A., Nes, O.M., 2014. Lost circulation materials capability of sealing wide fractures. In: SPE-170285-MS.

Alsaba, M., Nygaard, R., Saasen, A., Nes, O.M., 2015. Experimental investigation of fracture width limitations of granular lost circulation materials. J. Pet. Explor. Prod. Technol. 2016 (6), 593–603.

Cobianco, S., Bartosek, M., Lezzi, A., Previde, E., 2001. New Solids-free Drill-In Fluid for Low Permeability Reservoirs. SPE-64979.

Green, J., Patey, I., Wright, L., Carazza, L., Saasen, A., 2017. The Nature of Drilling Fluid Invasion, Clean-Up, and Retention during Reservoir Formation Drilling and Completion. SPE-185889-MS.

Hoxha, B.B., Yang, L., Hale, A., van Oort, E., 2016. Automated Particle Size Analysis Using Advanced Analyzers, AADE-16-FTCE-78.

Khan, R., Kuru, E., Tremblay, B., Saasen, A., 2003. An investigation of formation damage characteristics of xanthan gum solutions used for drilling, drill-in, spacer fluids and coiled tubing applications. In: PAPER 2003-067, Petroleum Society's Canadian International Petroleum Conference. Calgary, Alberta, Canada, June 10-12, 2003.

Khan, R., Kuru, E., Tremblay, B., Saasen, A., 2007. Extensional viscosity of polymer based fluids as a possible cause of internal cake formation. Energy Sources 29, 1521–1528.

Klungtvedt, K.R., Khalifeh, M., Saasen, A., Berglind, B., Vasshus, J.K., 2021a. Drilling Fluids – Preventing Drilling Fluid Induced Reservoir Formation Damage, SPE/IADC Middle East Drilling Technology Conference and Exhibition, Abu Dhabi, UAE 25-27 May 2021, SPE-202187-MS.

Klungtvedt, K.R., Saasen, A., 2022. A method for evaluating drilling fluid induced reservoir formation damage. J. Petrol. Sci. Eng. 213, 110324, 2022.

Klungtvedt, K.R., Saasen, A., Vasshus, J.K., Trodal, V.B., Mandal, S.K., Berglind, B., Khalifeh, M., 2021b. The fundamental principles and standard evaluation for fluid loss and possible extensions of test methodology to assess consequences for formation damage. Energies 14 (8), 2252. https://doi.org/10.3390/en14082252.

Pitoni, E., Ballard, D.A., Kelly, R.M., 1999. Changes in Solids Composition of Reservoir Drill in Fluids during Drilling and the Impact on Filter Cake Properties. SPE 54753.

Smith, P.S., Browne, S.V., Heinz, T.J., Wise, W.V., 1996. Drilling Fluid Design to Prevent Formation Damage in High Permeability Quartz Arenite Sandstones, SPE-36430-MS.

Vickers, S., Cowie, M., Jones, T., Twynam, A.J., 2006. A New Methodology that Surpasses Current Bridging Theories to Efficiently Seal a Varied Pore Throat Distribution as Found in Natural Reservoir Formations, AADE-06-DF-HO-16.

Whitfill, D., 2008. Lost Circulation Material Selection, Particle Size Distribution and Fracture Modelling with Fracture Simulation Software. IADC/SPE, 25-27 August 2008, Jakarta. SPE-115039-MS.

V. Klungtvedt, K.R. and Saasen, A. “The Role of Particle Size Distribution for Fluid Loss Materials on Formation of Filter-Cakes and Avoiding Formation Damage”. OMAE2022-79501. Journal of Energy Resources Technology 22-1217, 2023. https://doi.org/10.1115/1.4056187 (open access)

The Role of Particle Size Distribution for Fluid Loss Materials on Formation of Filter-Cakes and Avoiding Formation Damage

Karl Ronny Klungtvedt
EMC,
Stavanger 4033, Norway;
Department of Energy and Petroleum Engineering,
University of Stavanger,
Stavanger 4036, Norway
e-mail: krk@emcas.no

Arild Saasen[1]
Department of Energy and Petroleum Engineering,
University of Stavanger,
Stavanger 4036, Norway
e-mail: arild.saasen@uis.no

Numerous studies have shown that careful particle size selection is the main parameter for reducing fluid loss when drilling permeable or fractured formations. The methods are generally built around either the D50 or D90 values of the particles in the fluid as a relative size to the pore openings of the formation to minimize fluid loss. A series of studies were conducted with the aim of assessing if analysis of fluid loss could be used to separate the formation of internal and external filter-cakes, thereby enabling a more accurate estimate of the permeabilities of the internal and external filter-cakes. It was concluded that conventional particle size methods were found to be adequate for designing a fluid for wellbore stabilization purposes. This led to higher solids invasion and a more impermeable internal filter-cake. However, for optimization of reservoir drilling fluids, a different particle size selection method was found to be more useful to prevent reservoir formation damage. This method involves selecting particles that are resistant towards shear-degradation and with a D90 particle size $\gtrsim 3/2$ the pore size of the formation. By analyzing fluid loss regression data and correlating these with indicators of formation damage, such as disc mass and permeability change, it was found that a ratio defined as the relative plugging factor could provide insight into the extent of solids invasion into the formation and potential formation damage. [DOI: 10.1115/1.4056187]

Keywords: drilling fluid, lost circulation, sealing mechanism, lost circulation materials, formation damage, return permeability, solids invasion, geothermal energy, petroleum engineering

1 Introduction

Static fluid loss tests are conducted daily during drilling operations to assess the drilling fluid's ability to seal off permeable formations. When conducting tests on ceramic discs, it is possible to measure the mass change of the discs and hence also obtain an indication of particle invasion into the near-wellbore part of the formation [1]. An extension of this is to also measure permeability changes of ceramic discs to obtain further information about potential formation damage, as demonstrated by Klungtvedt and Saasen [2].

It is known that polymers may control fluid loss in formations with pore sizes up to 10 μm but fail to seal formations with 20 μm pore sizes and pressures exceeding 500 psi, as shown by Khan et al. [3]. A typical water-based reservoir drilling fluid using starch and sized marble to control fluid loss and bridging was therefore designed as a basis for testing formations with pore openings up to 120 μm. To also test the functionality and general validity of the fluid loss and formation damage models, two differently sized cellulose-based fiber products were included in the tests.

Experiments by Alvi et al. [4] have shown that it is possible to reduce filtration loss measured on filterpaper by addition of 0.5 wt % iron oxide nanoparticles to an oil-based drilling fluid. In a series of experiments, such filtration loss was nearly halved. Contreras et al. [5] found an optimum effect by addition of 0.5 wt% graphite together with 0.5 wt% nanoparticles based on iron or calcium. These additions seem to provide a formation strengthening effect. Razzaq et al. [6] demonstrated for water-based drilling fluids that silicon manganese fume can have a potential to reduce fluid losses in porous formations either alone or together with calcium carbonate. This fume seems to have a relatively large fraction of sub-micron particles. Hence, these results fall along the same results as the previous mentioned nano-particle effects. Nano-particle addition can be used in many respects to control drilling fluid performance. In the following, such effects will not be discussed. Several nano-particle additions can be evaluated based on the findings in the present article. A study by Jiang et al. [7] showed the results of expanding existing methods by including internal and external factors for improving the borehole during drilling to enhance, e.g., the cementation and cohesive forces between the rock particles and to transform capillary suction forces into resistance.

For a fluid loss test, the emphasis is often placed on the 30-min reading, and less importance is placed on the various readings during the period of the test. By logging the fluid loss using a digital scale, it is possible to get very accurate measurements of the mass of the fluid loss and the fluid loss rate at any point in time during the fluid loss test. The information gathered on the development of the fluid may be used together with the disc mass measurement to gain valuable insight into the formation of an internal filter-cake, as a deposit of particles into the permeable disc, and the formation of an external filter-cake.

Two approaches were used to model the formation of internal and external filter-cakes. One approach was to model the fluid loss as a linear function of the square root of time using a fluid loss coefficient and a spurt loss constant. The other approach was to analyze the fluid loss as a flow through a series of flow resistances, equivalent to an electric circuit where the resistances would be

[1]Corresponding author.

Contributed by the Advanced Energy Systems Division of ASME for publication in the Journal of Energy Resources Technology. Manuscript received March 25, 2022; final manuscript received October 30, 2022; published online November 22, 2022. Assoc. Editor: Tatiana Morosuk.

separated into the flow resistance of the formation, the flow resistance of the internal filter-cake and the flow resistance of the external filter-cake. A series of experiments was therefore conducted where the objectives were to:

- Determine if the formation of internal and external filter-cakes may be adequately modeled using numerical models.
- Assess if factors used in the numerical modeling also can be correlated with other tests conducted to assess formation damage.
- Assess the lost circulation material (LCM) particle size impact on formation damage.
- Employ an experimental method for measuring the content of the fluid filtrate to assess if it is possible to trace polymers in the fluid filtrate.

2 Materials and Methods

Three fluid compositions were used for the tests. The basis for the study was a water-based reservoir drilling fluid composed with xanthan gum, starch, and sized ground marble ($CaCO_3$) as a bridging agent. The particle sizes were chosen to replicate a drilling fluid recipe used in a field operation. Two cellulose-based fluid loss materials were partly replacing ground marble for two of the fluid samples. One cellulose-based product is referred to as non-invasive fluid additive ultra-fine (NIF UF) with a D90 value of 75 μm and another referred to as non-invasive fluid additive fine (NIF F) with a D90 value of 125 μm, both having a density of 0.98 g/cm^3. The fluid compositions were as presented in Table 1.

The three fluids were hot-rolled for a period of 16 h at a temperature of 112 °C in a hot-rolling cell where a threaded steel rod was included to simulate mechanical wear. A wet-sieving study was conducted of the base fluid showing that >99% of the ground marble particles were finer than 53 μm after hot-rolling. The hot-rolling temperature was selected to replicate a certain reservoir temperature. Fluid loss tests were thereafter conducted on 2.5 μm filterpaper at 500 psi differential pressure and on ceramic discs with specified median pore sizes of 10, 20, 50, and 120 μm, respectively.

The high temperature and high pressure (HTHP) fluid loss tests were conducted in accordance with ANSI/API 13B-1 [8] at 500 psi differential pressure, although the tests on ceramic discs were conducted with 1000 psi differential pressure, in order to identify if higher applied pressure could impact the sealing abilities and formation damage. The fluid loss tests were conducted at 90 °C, unless stated otherwise. By selecting a temperature below the boiling point, it was more practical to measure fluid loss accurately during the test.

Permeability measurements and disc mass measurements were made according to Refs. [1,2].

Table 1 Fluid recipes

Recipe for 350 ml fluid	Base fluid	NIF UF	NIF F
Water (g)	318.5	317.1	317.1
Soda ash (g)	0.02	0.02	0.02
Caustic soda (g)	0.25	0.25	0.25
Xantham gum (g)	1.3	1.3	1.3
Starch (g)	7.0	7.0	7.0
MgO (g)	1.0	1.0	1.0
NaCl (g)	20.0	20.0	20.0
$CaCO_3$ (g) < 23 μm	10.0	10.0	10.0
$CaCO_3$ (g) < 53 μm	10.0	10.0	10.0
$CaCO_3$ (g) D50 of 50 μm and D90 of 125 μm	20.0	10.0	10.0
NIF UF (g), D90 of 75 μm		5.0	
NIF F (g), D90 of 125 μm			5.0
Polymer volume concentration	2.25%	2.25%	2.25%
Solids volume concentration	4.23%	4.63%	4.63%

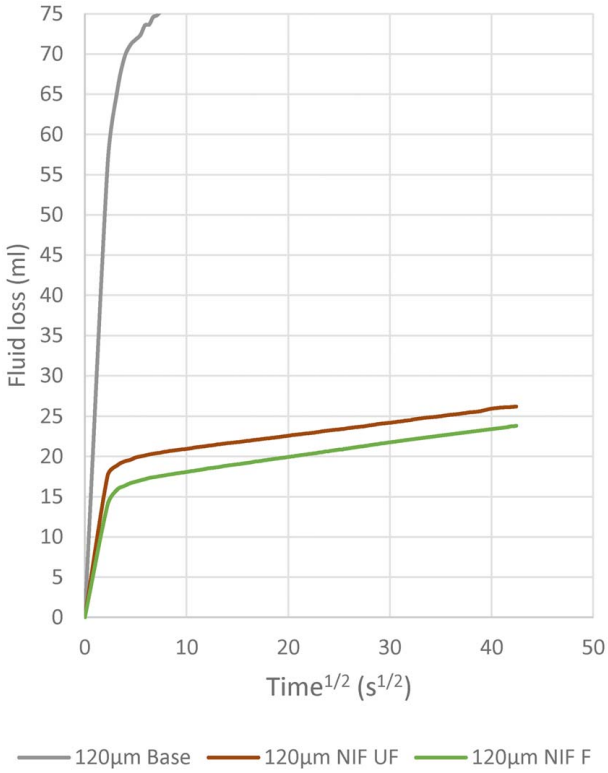

Fig. 1 Fluid loss test on 120 μM discs

3 Results and Discussion

3.1 Fluid Loss Tests and Regression Model. The fluid loss for the test on the 120 μm ceramic disc is plotted in Fig. 1. For the base fluid, the test was stopped after a short period of time as the fluid loss was high and uncontrolled. For the two other fluids, the fluid loss fell to a very low level shortly after an initial spurt loss. When plotting the fluid loss against the square root of time, the graph appears to be linear after the spurt loss is experienced, whereas models typically only describe it as a function of the square root of time, without considering the spurt loss separately [9].

A method for modeling the spurt loss and the fluid loss over time was attempted by plotting fluid loss (ml) versus the square root of the time (s$^{0.5}$). To separate the spurt loss from the linear loss phase, the first data point in the regression was the fluid loss value recorded after 15 s. Thereafter, a trendline was calculated using a linear regression model as presented in Eq. (1). The fluid loss model calculated the fluid loss (ml), FL_T, as a fluid loss coefficient C_{FL} multiplied by the square root of time, $T^{0.5}$, plus a spurt loss constant, SL (ml). The fluid loss graphs for fluids NIF UF and NIF F on the 120 μm discs are presented together with the linear regression models in Fig. 2. For both tests, the goodness of fit value, R^2, was in excess of 0.998, thereby indicating that the linear regression describes the underlying data in a very good way.

$$FL_T = C_{FL} * T^{0.5} + SL \quad (1)$$

Furthermore, similar regressions were made of the other fluid loss tests. The regressions of all three fluids on the 50 μm ceramic disc are shown in Fig. 3, and similarly the regressions of the fluid loss on the 2.5 μm filterpaper in Fig. 4. In contrast to a ceramic disc, it may be argued that a test on 2.5 μm filterpaper presents less of formation plugging and thereby a clearer study of the external filter-cake itself.

The fluid loss coefficient data for the whole test-series are presented in Fig. 5. For the base fluid, the coefficient is more than double its value from the test on the filterpaper to the tests on the

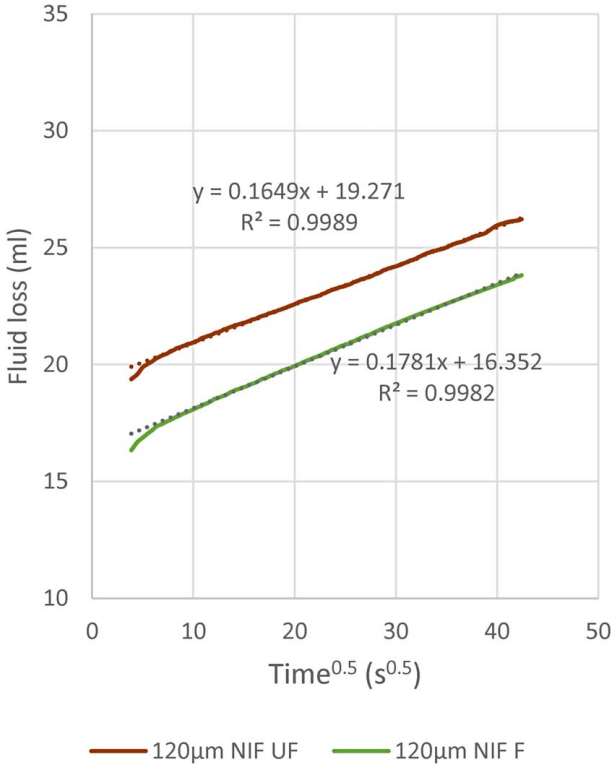

Fig. 2 Regression of fluid loss test on 120 μM disc

ceramic discs. In contrast, the coefficient only increases marginally for the fluid with NIF UF and NIF F. For the latter two, the coefficient gradually increases with higher disc pore size and reaches a maximum with the 50 μm discs, before it falls marginally when using the 120 μm discs.

The large change for the base fluid may be related to the increase in sealing pressure, from 500 psi on the filterpaper to 1000 psi on the ceramic discs. This may be natural as the ground marble particles are not believed to elastically compress, and hence the fluid loss may increase in a near linear fashion with pressure in the pressure range that has been investigated. In contrast, the increased pressure does not lead to a similar increase in fluid loss for NIF UF and NIF F, likely due to the compressibility of the cellulose fibers making them crate a compact filter-cake. For the test with similar pressures, it may be assumed that the permeability of the external filter-cake is consistent irrespective of the formation permeability and the internal filter-cakes, as long as the disc is sufficiently sealed during the spurt loss phase to facilitate the formation of an external filter-cake. For the base fluid, the C_{FL} is consistently higher than the other fluids in all the tests, indicating that the filter-cake of the base fluid is roughly twice as permeable as the filter-cakes of NIF UF and NIF F at 1000 psi.

For the regressions, the corresponding spurt loss constant data are presented in Fig. 6. The value for the base fluid on the 120 μm disc of >70 ml was taken from the fluid loss measurement as no regression could be made as the test was aborted. The calculated SL values are as expected very low for the tests on filterpaper and highest on the tests with 120 μm ceramic disc. The latter signifies that a larger volume of fluid was required to establish an effective internal filter-cake, against which an external filter-cake could be built. For the tests with 10, 20, and 50 μm discs, the three SL values were in a relatively narrow range, for each fluid. The highest values in the tests were for the base fluid and the lowest for the NIF F fluid.

When designing a fluid for wellbore strengthening purposes or for reservoir drilling purposes, it is necessary to know to which degree particles migrate into the formation and form an internal filter-cake and to which degree the sealing is substantially enabled by the external filter-cake. To model this behavior, a simplification was made, where the formation of the internal and external filter-cakes was separated in time. It was assumed that the internal filter-cake was formed in its entirety during the spurt loss phase, whilst the external filter-cake was formed after the spurt

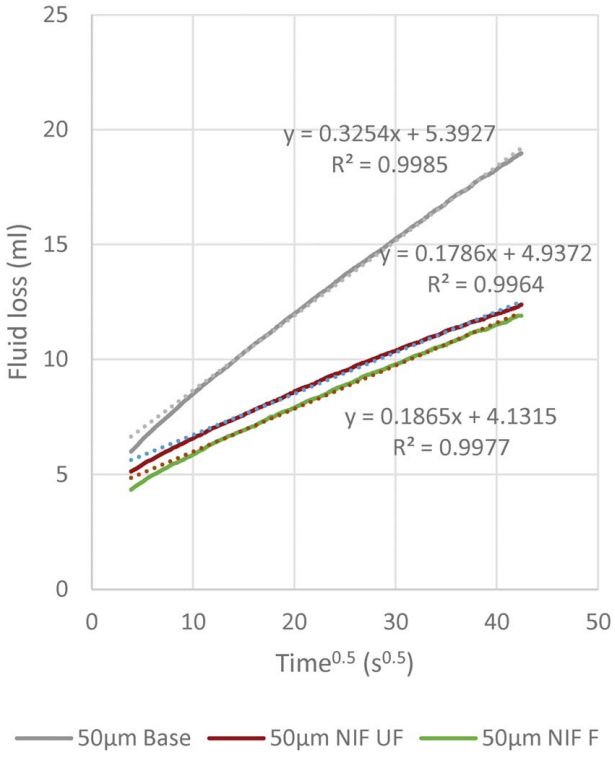

Fig. 3 Regression of fluid loss test on 50 μM disc

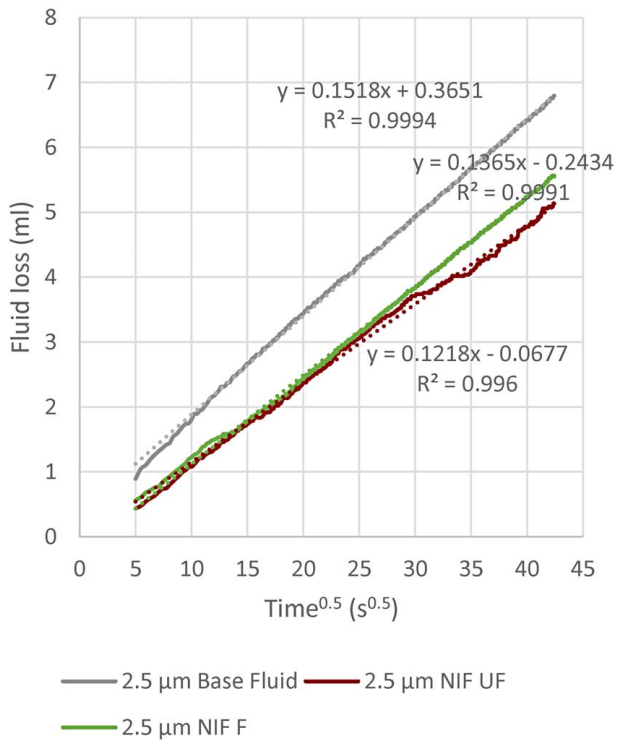

Fig. 4 Regression of fluid loss test on filterpaper

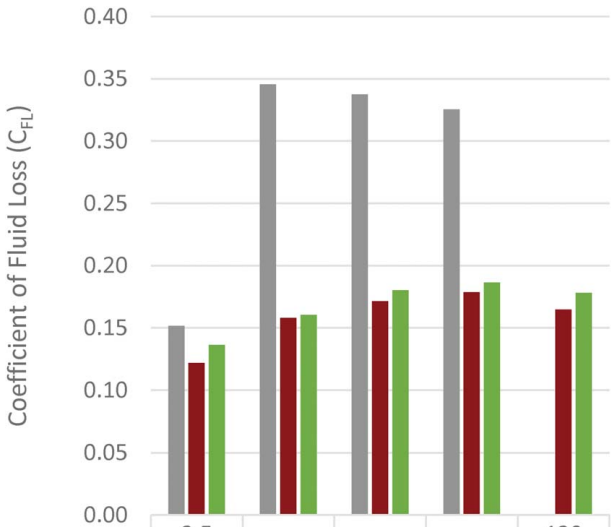

	2.5 µm paper (500 psi)	10 µm disc (1000 psi)	20 µm disc (1000 psi)	50 µm disc (1000 psi)	120 µm disc (1000 psi)
Base Fluid	0.15	0.35	0.34	0.33	
NIF UF	0.12	0.16	0.17	0.18	0.16
NIF F	0.14	0.16	0.18	0.19	0.18

Fig. 5 Coefficient of fluid loss

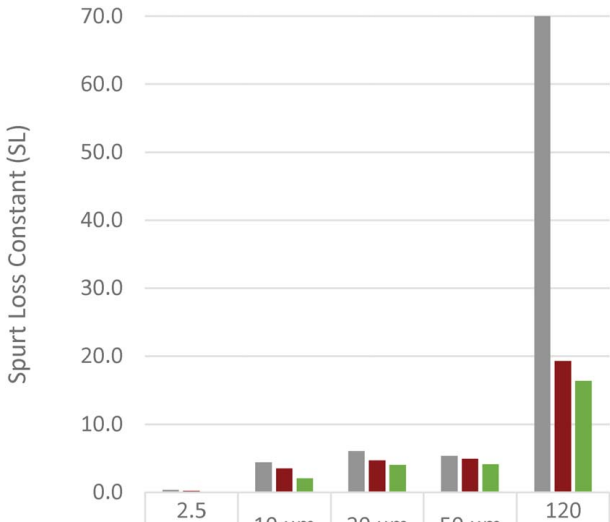

	2.5 µm paper (500 psi)	10 µm disc (1000 psi)	20 µm disc (1000 psi)	50 µm disc (1000 psi)	120 µm disc (1000 psi)
Base Fluid	0.4	4.4	6.1	5.4	70.0
NIF UF	0.2	3.5	4.7	4.9	19.3
NIF F	-0.1	2.0	4.0	4.1	16.4

Fig. 6 Spurt loss constant

loss phase. As such, the volume of filtrate in each loss phase and the concentration of polymers and solids in the fluid can be used to re-construct the process of building the internal and external filter-cakes. Using the linear regression model, the spurt loss constant, SL, describes the relative amount of fluid required to form an internal filter-cake or the internal plugging in the disc. The fluid loss after the initial spurt loss is described by the coefficient of fluid loss, which then describes the phase where the external filter-cake is built. In the case of a test on filterpaper, the pore openings are so small that it may be assumed that particle invasion and internal plugging are negligible. This would result in a spurt loss constant equal to 0, and the only factor required to calculate the fluid filtrate at any point in time would be the coefficient of fluid loss. A test on filterpaper may hence be seen as a test of the flow resistance of the filter-cake, or inversely it may be used to describe the filter-cake permeability. In contrast, it may also be possible to imagine a fluid loss test where the particle invasion during the spurt loss led to a complete sealing of the disc, with no subsequent fluid loss. In this test, the coefficient of fluid loss would be 0 and the spurt loss constant would be fully describing the fluid loss at any point in time after the initial spurt loss. Therefore, by calculating a simple metric of the ratio of the two factors, it may be possible to get a good description of the relative control each factor has in terms of controlling the fluid loss. The ratio may be defined as per Eq. (2) and named the relative plugging factor (RPF). As the volumetric concentration of solids impact the spurt loss and potentially also the subsequent fluid loss, the RPF is likely most useful for comparing fluids of similar solids concentrations or when testing one fluid on different permeability discs.

$$\mathrm{RPF} = \frac{\mathrm{SL}}{C_{\mathrm{FL}}} \tag{2}$$

A high RPF would indicate that the fluid loss may be highly impacted by the spurt loss and thereby formation plugging. A high value may therefore be ideal for wellbore stabilization purposes, as a disturbance of the external filter-cake during drilling may have lower consequences. It is assumed that the formation of an internal filter-cake, as measured by the mass increase of discs or the estimated permeability of the internal filter-cake, will make

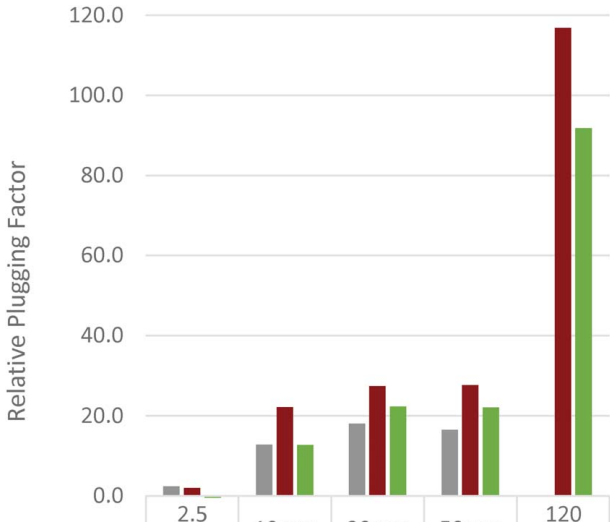

	2.5 µm paper (500 psi)	10 µm disc (1000 psi)	20 µm disc (1000 psi)	50 µm disc (1000 psi)	120 µm disc (1000 psi)
Base Fluid	2.4	12.8	18.1	16.6	
NIF UF	2.0	22.2	27.4	27.6	116.9
NIF F	-0.5	12.8	22.4	22.2	91.8

Fig. 7 Relative plugging factor (Eq. (2))

the formation less exposed to disturbances in the wellbore. Circulation of drilling fluid or swabbing effects are less likely to lead to increased losses or differential sticking if the internal filter-cake limits the pressure communication between the wellbore and the formation. In contrast, a lower degree of formation plugging may be desired for reservoir drilling purposes, where formation plugging may lead to permanent permeability reduction and hence formation damage. Given that the ratio does not say anything about the absolute level of fluid loss, fluids should not be evaluated using the metric alone.

The RPF values for the tests are presented in Fig. 7. Given that the C_{FL} remained reasonably consistent for each fluid at a given pressure, the difference in SL also translates into the RPF readings. As expected, the RPF values for the tests on filterpaper are very low, indicating that the external filter-cake is the primary barrier towards fluid loss. This is in clear contrast with the values calculated for the 120 μm ceramic disc tests. The high ratios indicate high particle migration and significant plugging of these discs during the HTHP tests. Another observation is that the RPF values for NIF F are considerably lower than for NIF UF in all tests. For practical purposes, these fluids are identical except for the different particle size distribution (PSD) of the cellulose fibers. This may indicate that the finer fibers of NIF UF need a slightly higher initial fluid loss to form an internal filter-cake, whereas the larger NIF F particles build an initial bridging faster.

3.2 Permeability and Disc Mass Measurements. For the tests conducted on 10, 20, and 50 μm ceramic discs, permeability tests were conducted using air both before the HTHP tests and after reverse flow through the discs to remove the external filter-cake and potentially parts of the internal filter-cake (see Figs. 8 and 9). For all the ceramic discs, the changes in mass were measured using a moisture analyzer after reverse flow with water to lift off the external filter-cake and remove loose deposits within the disc. Overall, the best permeability results were recorded on the 20 μm ceramic discs. Considering the high concentration of $CaCO_3$ in all three fluids, this may indicate that the size of the $CaCO_3$ after degradation works most effectively in this range of pore sizes. Considering both disc mass increases and permeability measurements,

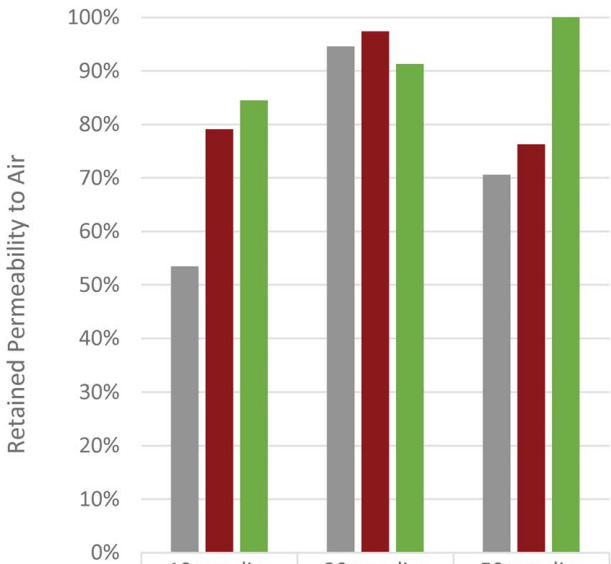

	10 µm disc (1000 psi)	20 µm disc (1000 psi)	50 µm disc (1000 psi)
Base Fluid	54%	95%	71%
NIF UF	79%	97%	76%
NIF F	85%	91%	100%

Fig. 8 Retained permeability to air

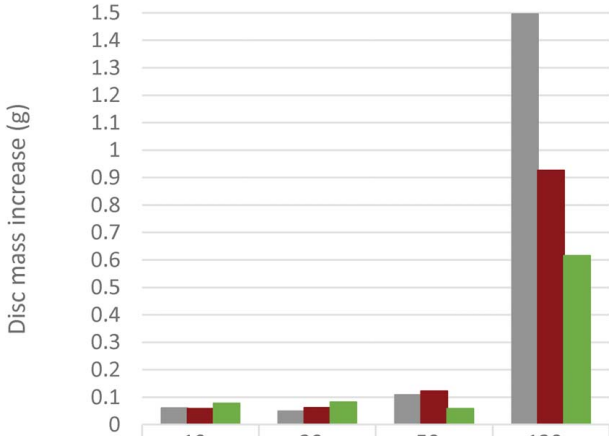

	10µ	20µ	50µ	120µ
Base Fluid	0.06	0.048	0.108	1.495
NIF UF	0.058	0.061	0.121	0.925
NIF F	0.077	0.081	0.058	0.615

Fig. 9 Disc mass increase

NIF F appears to provide the best formation protection for any formation above 20 μm, whereas the NIF UF may be more effective in the 10–20 μm range. It should be noted how the permeability is clearly reduced with the base fluid on the 10 μm disc. The result of 54% from the 30-min test was replicated with multiple tests with small variance.

In summary, the average retained permeability for the tests with the base fluid was 73%, with a standard deviation of 21%, whereas the tests with the cellulose-based fibers yielded an average retained permeability of 88%, with a standard deviation of 10%.

For the two test-series for fluids NIF UF and NIF F, it was possible to calculate both the RPF and measure the disc mass increase for all four disc grades. The correlations between the two variables were 0.998 for NIF UF and 0.99 for NIF F. When plotting the RPF against the ratio of the NIF particle D90 value to the median disc pore size, it is clear that the disc mass retains a relative stable level until the particle D90 to pore size ratio approaches the range of around 1.5–2.2. With lower ratios, the disc mass increase rises sharply, as presented in Figs. 10 and 11. This is a strong indicator that, with the applied concentration of the specific cellulose-based

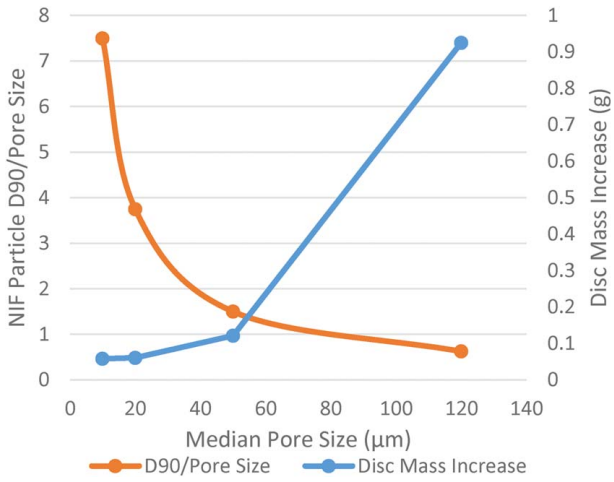

Fig. 10 Particle to pore size ratio versus disc mass increase for NIF UF

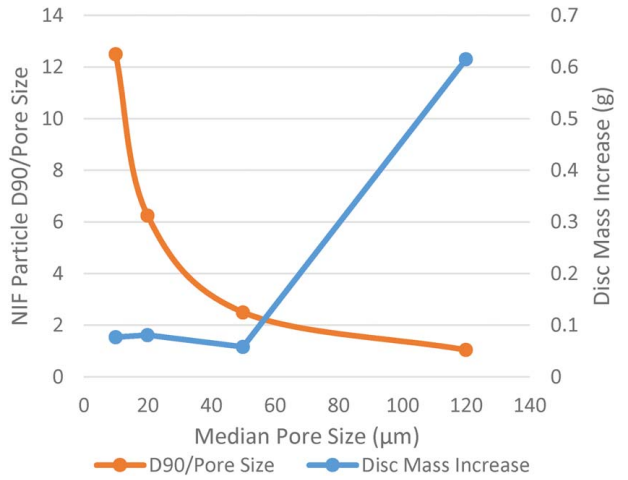

Fig. 11 Particle to pore size ratio versus disc mass increase for NIF F

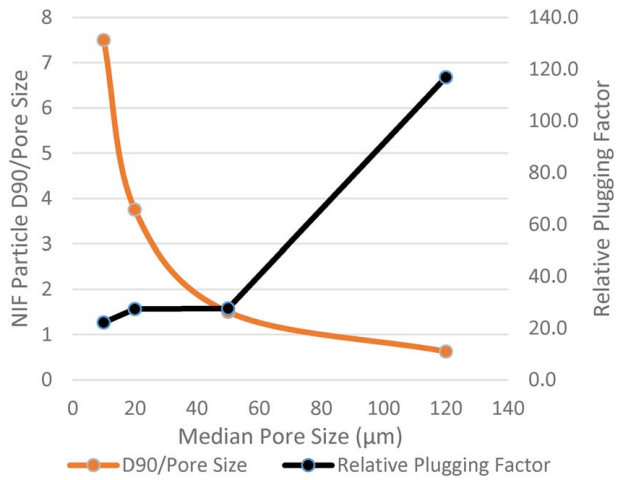

Fig. 12 Particle to pore size ratio versus relative plugging factor for NIF UF

fibers and by selecting a D90 value ≳ 3/2 times the pore opening, a low-permeability external filter-cake is created and the invasion of solid particles into the formation is limited.

When plotting the particle D90 to pore size ratio versus the RPF, a very similar pattern emerges, as presented in Figs. 12 and 13. When the particle D90 to pore size ratio falls below the 1.5–2.2 range, the RPF increases sharply, indicating that the particles of the fluid enter the formation, rather forming an external filter-cake. The RPF maintains a level in the range of 20–30 as long as the size ratio does not fall below the 1.5–2.2 range. This may indicate that 30 ≳ RPF represents a limit where solids invasion is limited.

3.3 Polymer Content in the Fluid Filtrate. An experimental analysis was conducted to measure the contents of the fluid filtrate relative to the drilling fluid before application. By using a series of test including turbidity, salinity, conductivity, and refractive index (BRIX), each of the components of the fluids were mapped and the values of the fluids and the fluid filtrates measured. Each component thus made a unique "fingerprint" in terms of relative readings on the different parameters measured. Using this method, it was possible to estimate the relative polymer concentrations in the fluid filtrates. This was calculated by measuring the BRIX value and subtracting the BRIX value resulting from other constituents in the filtrate such as salts. Furthermore, by combining the

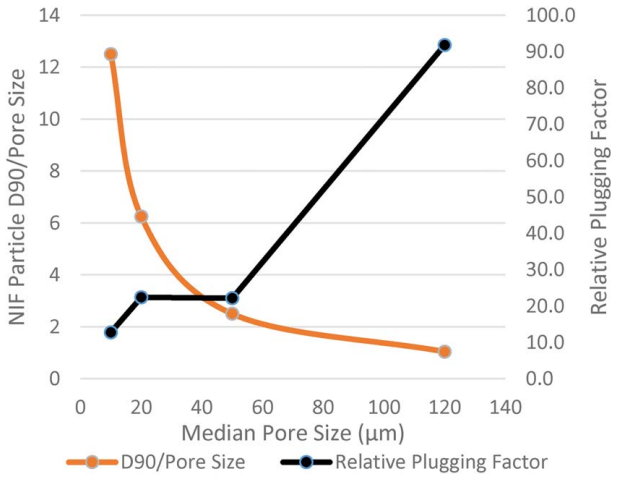

Fig. 13 Particle to pore size ratio versus relative plugging factor for NIF F

volume of the filtrate and the polymer concentration in the filtrate, it was possible to plot the polymer content in the filtrate for certain fluid loss tests.

Figure 14 presents the estimated polymer content in the filtrate from the 500 psi tests on filterpaper for the three respective fluids. Here the concentration of polymers in the test with the base fluid was around twice that of the NIF UF and the NIF F fluids. The area of each indicator reflects the multiple of the BRIX value and the fluid loss value to reflect the absolute volume of polymers. The equipment used is listed in the Appendix. For the first test-series, it was decided to use portable equipment that easily could be used in a small field laboratory.

The fluid loss test with 20 μm ceramic discs had been conducted at a higher pressure than the test on filterpaper. The plot of the fluid

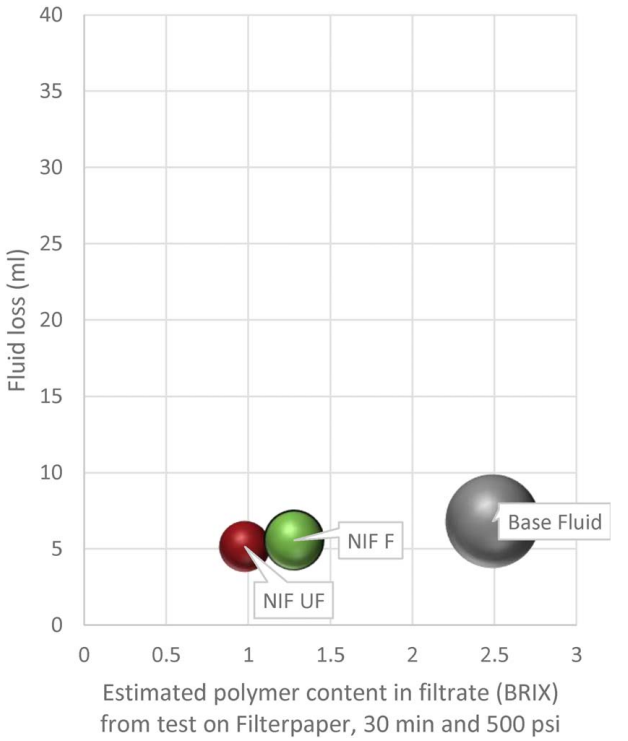

Fig. 14 Estimated polymer content in fluid filtrate for test on filterpaper

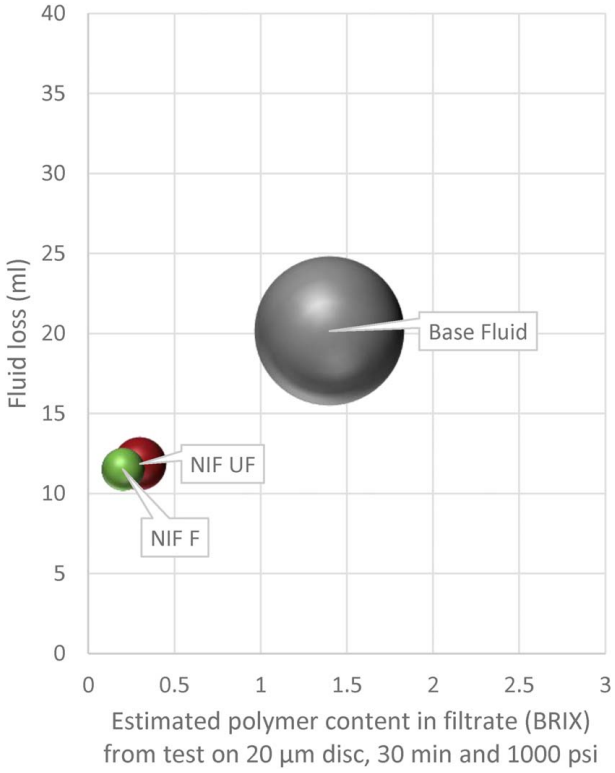

Fig. 15 Estimated polymer content in fluid filtrate for test on 20 μm disc

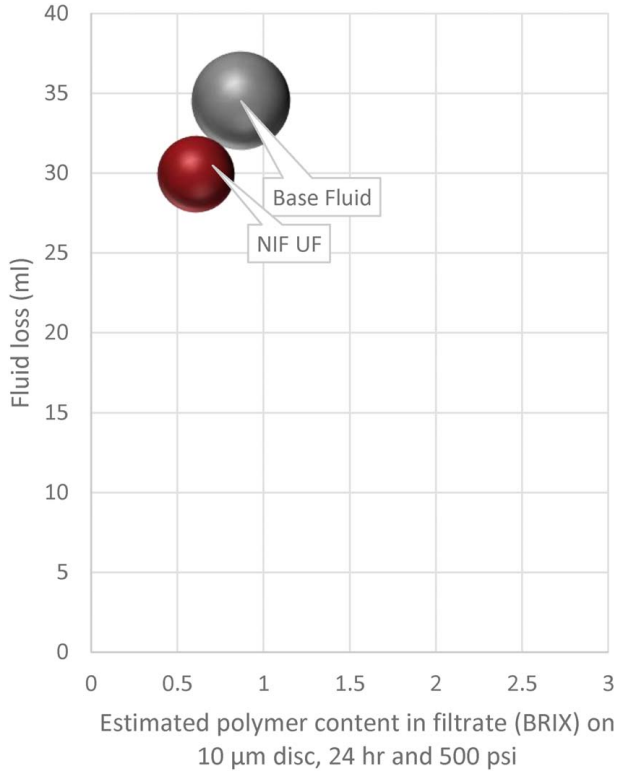

Fig. 16 Estimated polymer content in fluid filtrate for test on 10 μm disc

loss and BRIX is presented in Fig. 15. For the tests with fluids NIF UF and NIF F, the estimated absolute volume of polymers was slightly lower than that found in the test with filterpaper. This may be due to some deposit of the polymers within the disc itself. In contrast, the volume of polymers calculated for the test with the base fluid nearly doubled relative to the test on filterpaper, likely indicating that more polymers escape the base fluid filter-cake as the pressure is doubled.

The analysis results of a third test conducted on 10 mm ceramic discs over a period of 24 h and with 500 psi applied pressure is presented in Fig. 16. In this test, the measured polymer content in the filtrate from the base fluid was noticeably smaller than presented in Figs. 14 and 15.

The results from the test on filterpaper may indicate that the fluids containing cellulose fiber bind the polymers better in the filter-cake and hence release less polymers into the formation. Given that the cellulose particles and the polymers both exhibit polar properties, it may be that the polar interaction causes increased inter-particle adhesive and frictional forces. This hypothesis is also supported with the results from the test on 20 μm ceramic discs, where the higher applied pressure nearly doubles the calculated polymer volume in the filtrate for the base fluid, whereas it remains relatively unchanged for the two fluids containing fibers.

The 24-h test on 10 μm ceramic discs yielded lower calculated values of polymers in the filtrate for the base fluid. The cause of this may be that due to the finer pore openings of the disc, more polymers are deposited within the disc, and hence less are transferred as part of the fluid filtrate. The permeability measurements of the 24-h tests on 10 μm discs were in line with those for the 10 μm discs in the 30-min test presented in Fig. 8. A possible conclusion is therefore that the relative reduction in permeability for the base fluid on the 10 μm discs is polymer invasion and partial plugging of the discs. In contrast, the two fluids with fibers hold the polymers firmer within the filter-cake and hence lead to a smaller formation damage.

3.4 Extension of Model for Filter-Cake Formation. The three fluid samples all have a volume concentration of polymers of 2.25%, with a specific gravity of 0.95, whereas the volume concentration of solids (ground marble and fibers) was 4.23% for the base fluid, with a specific gravity of 2.7, and 4.63% for the fluids with NIF UF and NIF F, with an average specific gravity of 2.16. By combining these values with the calculated spurt loss constants, it is possible to analyze the creation of an internal filter-cake.

A numerical model was developed analogous to the principles of Ohm's law, where U = voltage, I = current, and R = resistance, as represented in Eq. (3). Converting this to a flow of fluid through a formation, the applied differential pressure, ΔP, would be equivalent to the voltage, U, and a volume flow of a specific Newtonian fluid, Q, equivalent to the current, I. Furthermore, the resistance to flow may be divided up into the flow resistance of the formation R_F, the flow resistance of the internal filter-cake, R_{IF}, and the flow resistance of the external filter-cake R_{EF}, as per Eq. (4) modeling the elements as serial resistance to flow, and thereafter re-arranged into Eq. (5).

$$U = I * R \tag{3}$$

$$R_T = R_F + R_{IF} + R_{EF} \tag{4}$$

$$\Delta P/Q = R_F + R_{IF} + R_{EF} \tag{5}$$

Darcy's law of flow through a porous medium is presented in re-arranged integral forms in Eqs. (6) and (7), where K is the permeability, Q is the flowrate, η is the assumed constant viscosity of the fluid, and A is the area of flow. For simplicity, the area A and the fluid viscosity η can be set equal for the formation and the internal and external filter-cakes. By substitution, Eqs. (5) and (7) may be combined to form Eq. (8). Here, the length and permeabilities of formation, internal filter-cake, and external filter-cake are separated

and named with subscript F, IF, and EF.

$$K = \eta * \frac{Q * \Delta L}{A * \Delta P} \tag{6}$$

$$\Delta P/Q = \eta * \frac{\Delta L}{A * K} \tag{7}$$

$$\Delta P/Q = \frac{\eta}{A} * \left(\frac{\Delta L_F}{K_F} + \frac{\Delta L_{\mathrm{IF}}}{K_{\mathrm{IF}}} + \frac{\Delta L_{\mathrm{EF}}}{K_{\mathrm{EF}}} \right) \tag{8}$$

When applying this to a study using ceramic discs, the area A is defined by the actual flow area through the discs, and ΔL_F as the thickness of the disc. The permeability of each disc, K_F, can be assumed to be unchanged during the test. Following the logic of the linear regression model, Eq. (1), the flow resistance of the internal filter-cake is modeled as a function of the spurt loss and is assumed to be constant thereafter. With such an approach, the flow resistance of the external filter-cake is the only flow resistance factor changing after the initial spurt loss. The buildup of the flow resistance of the formation, R_F, the internal filter-cake, R_{IF}, and the external filter-cake, R_{EF}, may hence be schematically presented as per Fig. 17. Due to the significant differences in value, the flow resistance is illustrated using a logarithmic scale.

During a fluid loss test, the content and behavior of the fluid filtrate normally change character over time. The higher the spurt loss, the more the initial filtrate will resemble the drilling fluid in look, content, and viscosity. After internal and external filter-cakes have been established, the fluid filtrate gradually changes to become similar to the base fluid. For a water-based fluid, this implies that the filtrate will gradually move towards showing Newtonian behavior.

A simplified model was used as an estimate of the viscosity of the fluid filtrate where the initial flowrate, during the spurt loss phase, was high and the viscosity near that of the drilling fluid, and as the fluid loss reduced, the viscosity moved asymptotically towards the viscosity of the base fluid.

Furthermore, four filter-cakes were weighed in a wet condition and thereafter dried to measure the water content of the filter-cake. For the four measured filter-cakes, the moisture level varied in the range of 48–50%. For modeling purposes, the value of 50% was used. The moisture content did not vary significantly between the fluids used. If another value is to be applied, Eq. (10) would need to be amended to reflect the applicable moisture level. The buildup of the filter-cake may be calculated by separating the content of the drilling fluid into the filtrate portion and the solids portion. For simplicity, it is assumed that all the polymers and solids are retained in the external filter-cake after the initial spurt loss. It can be assumed that the fluid consumed, F_T, at time, T, is separated into a portion of solids, polymers, and some of the fluid base to form the filter-cake, denoted FC_T and a clear fluid portion which escapes the filter-cake and becomes the measured fluid loss, CL_T after the initial spurt loss SL.

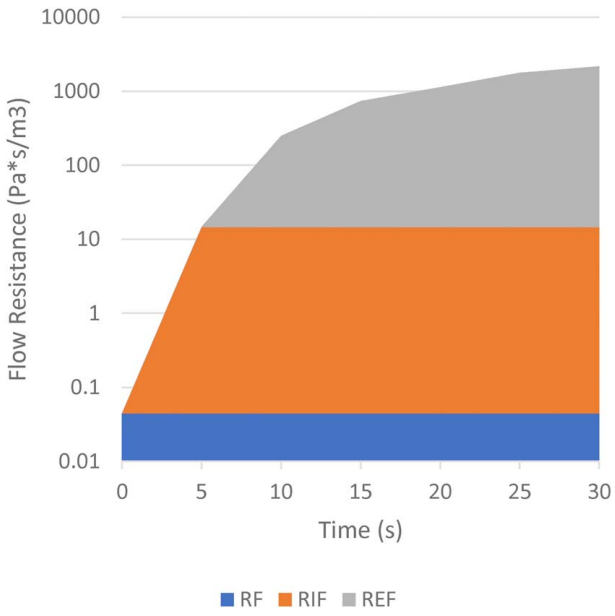

Fig. 17 Schematic description of evolvement of flow resistance during fluid loss test

$$F_T = \mathrm{FC}_T + \mathrm{CL}_T \tag{9}$$

We already know that 50% of the filter-cake mass was calculated to be water for these specific tests. Therefore, in addition to the direct volumetric concentration of the polymers and the solids, a volumetric concentration of water needs to be added which corresponds to the mass of the polymers and the solids. This means that the relationship presented in Eq. (9) may be extended. Defining the volumetric concentration of polymers v_P (%), the volumetric concentration of solids v_S (%), and the average specific gravities of the polymers and solids ρ_P and ρ_S, we get Eq. (10).

$$FC_T = F_T * (v_P + v_S + v_P * \rho_P + v_S * \rho_S) \tag{10}$$

Equation (10) may be simplified for each fluid where the portion of the fluid used to build the filter-cake is k_F.

$$FC_T = F_T * k_F \tag{11}$$

Or, alternatively expressed as Eq. (12).

$$\mathrm{CL}_T = \frac{\mathrm{FC}_T}{k_F} - \mathrm{FC}_T \tag{12}$$

For the base fluid, this computes to a factor where $k_F = 20\%$ and substituting into Eq. (9), $\mathrm{FC}_T = 0.25 * \mathrm{CL}_T$. For the NIF UF and NIF F fluids, the factors are almost similar as $k_F = 19\%$ and substituting into Eq. (9), $\mathrm{FC}_T = 0.234 * \mathrm{CL}_T$.

Since we already have Eq. (1) which calculates the fluid filtrate over time, where the spurt loss is defined as SL, the element CL_T can be represented as per Eq. (13). The thickness of the filter-cake is calculated as per Eq. (14) and the permeability, K, as per Eq. (15).

$$\mathrm{CL}_T = C_{\mathrm{FL}} * T^{0.5} \tag{13}$$

$$\Delta L_{\mathrm{EF}} = \frac{1}{A} \frac{C_{\mathrm{FL}} * T^{0.5}}{1 + (1/k_F)} \tag{14}$$

$$K = \frac{\eta}{2PA^2} \frac{C_{\mathrm{FL}}^2}{1 + (1/k_F)} \tag{15}$$

A numerical analysis was setup based on the assumptions described and Eqs. (1), (8), (14), and (15) together with the logging data from a fluid loss test to simulate the development of the internal and external filter-cakes and their permeabilities. Figure 18 presents such a data plot. For the test, a ceramic disc with median pore size of 50 μm was used. The permeability to water was measured to be 22.4D. In contrast, the internal filter-cake permeability was calculated to be 69 mD and he external filter-cake <0.1 mD. In the modeling, the ΔL_{IF} was set to 4.5 times the median pore size of the disc. This was done after fracturing discs to make a visual inspection of particle invasion. By applying the regression data into Eq. (15), the permeability was calculated to be 0.054 mD, which was marginally lower than that of the numerical analysis. Equations (14) and (15) will be less useful if there is a substantial plugging into the disc during the spurt loss phase, as the internal filter-cake may then be the critical factor reducing the fluid loss. For the 120 μm discs, the invasion was considerably larger, and for the test with the base fluid, deposits of $CaCO_3$ were seen

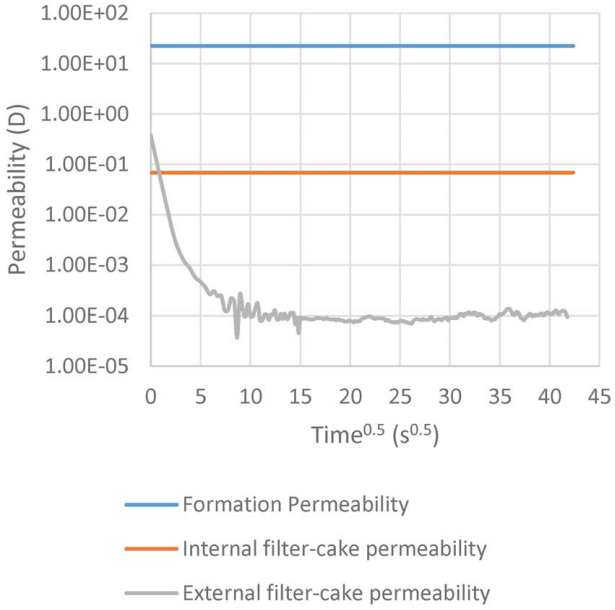

Fig. 18 Calculated permeability development

almost through the thickness of the disc even though the HTHP test was aborted within 2 min.

3.5 Discussion. The fluid loss tests were conducted under static conditions. The linear regression model applied is consistent with common theory, where fluid loss is calculated as a constant multiplied by the square root of time [2]. In the current study, the model is slightly amended to separate the spurt loss phase from the steadier loss rate. During a static filtration test, the filter-cake is allowed to build steadily as there is no mechanical disturbance of the filter-cake surface. In contrast, a dynamic fluid loss test would experience a continuous disturbance to the wellbore side of the filter-cake due to circulation of fluid. In such a condition, an equilibrium condition is likely to be met where the rate of erosion of the filter-cake equals the rate of buildup due to fluid loss. Hence, in a dynamic condition, the fluid loss will remain higher, and the filter-cake will reach a maximum thickness depending on the rate of erosion. With the assumption that the filter-cake is tight enough to prevent particle migration, the difference between a static and a dynamic fluid loss test will not impact the formation of the internal filter-cake to any significant degree.

The hot-rolling procedure included a threaded steel rod to simulate mechanical degradation. Studies have shown that $CaCO_3$ particles degrade during circulation and exposure to mechanical shear [10]. In the same study, a cellulose-based LCM was found to show very low levels of particle size degradation. Applying these findings to the three fluids used in these studies, it may be assumed that the $CaCO_3$ particles, with an initial D90 value in the region of 125 μm and D50 value of 50 μm, may have been ground down in size and that the largest particles in fluids NIF UF and NIF F may be the cellulose-based fibers. The test with the base fluid did not effectively seal the 120 μm disc, thus suggesting that the new D50 value of the $CaCO_3$ is less than 120/3 or 40 μm, following the Abrams rule [11]. Similarly, the base fluid sealed the 50 μm disc, suggesting that the D50 is likely larger than 50/3 μm or the D90 value is $\lesssim$45 μm after the hot-rolling process, applying the findings of Alsaba et al. [12]. The tests thus showed that if a circulating fluid is exposed to mechanical wear like that of the applied hot-rolling process, the PSD of $CaCO_3$ before circulation cannot be applied using known particle size selection methods. For the 50 μm discs, the tests with NIF F provided the lowest fluid loss, disc mass increase, and permeability reduction. For this test, the NIF UF fluid would likely contain particles around 3/2 times the pore opening, whereas NIF F would likely contain particles $\lesssim$3/2 times the pore opening, indicating that the latter would be preferrable to limit formation damage.

The tests presented in Sec. 3.1 showed that with particles present in the fluid that were equal to or larger than the pore size of the discs, the mass increase of each disc was between 48 and 121 mg. For the 120 μm discs, where the particle size was equal to or smaller than the pore size, the mass increase was in the region of 615–1495 mg. Also, comparing the tests with the fluids NIF UF and NIF F, it is clear that the larger particles in NIF F better protects against solids invasion and fluid loss with pore openings in the range from 50 to 120 μm, whereas the differences between NIF UF and NIF F are small in the range from 20 μm and smaller pore openings.

The experimental method applied to identify and measure polymer concentration in fluid filtrate showed consistent differences between the fluids with fibers and the base fluid. It is an interesting observation which may be explained by polar interaction and thereby increased adhesive and frictional forces between the cellulose-based fibers and the polymers used for fluid loss and viscosity. Such interaction may also be consistent with increased tensile strength or cohesive strength of the filter-cake. Further analysis should be conducted to better verify the experimental method and its applicability. Further studies should also be conducted to understand potential interaction between cellulose-based fibers and polymers and its impact on filter-cake strength and also the impact on dynamic fluid loss tests. With higher filter-cake cohesion, less erosion should be expected in a dynamic condition, and hence the fluid loss could be further reduced.

The extension of the model for analysis of filter-cake formation increases the complexity of the modeling. It was possible to calculate estimates of the permeability of internal and external filter-cakes, but with very significant increases in computation relative to the regression model. The extension of the model indicates that, once established, the external filter-cake was the dominant factor in controlling the fluid loss for the tests conducted in this experiment. This observation was also expected given that the fluid compositions used were designed for reservoir drilling purposes. If similar modeling had been conducted with a fluid designed for wellbore strengthening purposes, the results of the modeling might be different. As such, with such a numerical model being established it may provide useful information for further understanding of how the internal and external filter-cakes are being built.

The linear regression model obtained very high goodness of fit values which may be useful to predict fluid loss under static conditions. Applying this together with Eq. (14), one can also predict how the thickness of the external filter-cake will evolve over time. As an example, under the test conditions for the test on 10 μm discs, a 72-h test could be forecasted to yield 180 ml of fluid loss for the base fluid and 84 ml of fluid loss for each of NIF UF and NIF F. The corresponding filter-cake thicknesses would be 11.1 mm for the base fluid and 4.9 mm for NIF UF and NIF F.

The relative plugging factor appeared to give meaningful information regarding when a fluid changed from primarily producing an external filter-cake to when the discs were plugged through solids migration. This inflection point was observed when the RPF was around 30. The tested fluids had relatively similar concentrations of solids. It could be expected that a higher solids concentration would lead to a lower spurt loss. A higher concentration of the same solids may, however, not necessarily cause a change in the filter-cake permeability, and hence in the coefficient of fluid loss, as the same distribution of particles would be present to build the filter-cake. Therefore, it would be natural that a fluid with higher volumetric concentration of solids would produce an inflection point for the RPF at values less than 30.

The two approaches used for modeling of the filter-cake permeabilities clearly show that already within the first seconds of the tests, the original formation permeability becomes insignificant in controlling the fluid loss, relative to the much lower permeabilities

of the internal and external filter-cakes. As such, the microflow of polymers through the permeable discs were not studied in detail. Other studies such as Ref. [13] have been conducted to understand the viscoelastic flow of polymer fluids in permeable formations, and in particular the microflow mechanisms of polymer displacements. Such findings may bring further insight if applied to the study of fluid filtrate when using water-based drilling fluids with polymers.

4 Conclusion

Numerical modeling of the formation of internal and external filter-cakes provided to be a useful approach. New information was discovered, and further studies should be conducted to assess if additional insight into filter-cake formation might be gained.

- It was verified that a modified linear regression model could describe a static fluid loss test with very high goodness of fit by separating the factors into a spurt loss constant and a coefficient of fluid loss and plotting against the square root of time.
- The modified regression model enables a separation of the calculation of the internal and external filter-cake permeabilities.
- The calculated relative plugging factor provided consistent results with the measurements of disc mass increases. This indicates that 30 $\lesssim$ relative plugging factor represents situations where fluid loss, for the tested fluids, is primarily controlled by an external filter-cake and that formation damage is limited.
- Average retained permeability for the tests with the base fluid was 73%, whereas the tests with cellulose-based additives showed an average retained permeability of 88%.
- It was found that cellulose particles with size $\lesssim$3/2 the pore size limited polymer and solids invasion into the formation, whereas invasion of particles were higher when the largest particles were equal to or smaller than the pore openings. Using the experimental analysis of fluid filtrate, it was found that the presence of cellulose particles in the filter-cake led to reduced polymer invasion into the formation relative to a fluid with only $CaCO_3$ used as bridging material.

The experimental analysis of fluid filtrate should be further applied and analyzed to determine its consistency and accuracy.

Acknowledgment

The authors would like to thank Jan Kristian Vasshus, Bjørn Berglind, Swapan Mandal, and Nicola Santarelli for advice and the Research Council of Norway for financially supporting the project through RCN# 320646.

Conflict of Interest

There are no conflicts of interest.

Data Availability Statement

The authors attest that all data for this study are included in the paper.

Nomenclature

A = cross-sectional flow area (m^2)
I = current (A)
K = permeability (m^2), where 1 Darcy = 1 μm^2
Q = flowrate (m^3/s)
R = electrical resistance (ohm)
R = flow resistance (Pa s/m^3)
U = voltage (V)
C_{FL} = coefficient of fluid loss (ml/$s^{0.5}$)
R_X = flow resistance (Pa s/m^3), where the subscript refers to the medium
R^2 = goodness of fit for the regression model
BRIX = degrees of refraction (°Bx)
RPF = relative plugging factor ($s^{0.5}$)
SL = spurt loss constant (ml)
FL_T = fluid loss at time T (ml)
ΔL = length (m)
ΔP = applied differential pressure (Pa)
η = viscosity (Pa s)

Appendix

The equipment setup was as follows:
Equipment used for testing:

- Hamilton Beach Mixer
- Ohaus Pioneer Precision PX3202
- Ofite Filter Press HTHP 175 ml, double capped
- Ofite Viscometer model 900
- Ofite roller-oven #172-00-1-C
- Apera pH90, pH meter
- Ohaus MB120 Moisture Analyser
- Custom built transparent acrylic cell for enabling of reverse flow of fluid through the ceramic discs
- Festo Pressure Regulator LRP-1/4-2.5 and LRP-1/4-0.25
- Festo Pressure Sensor SPAN-P025R and SPAN-P10R
- Festo Flowmeter SFAH-10U
- Nitrogen source and manifold for pressure up to 1350 psi, Ofite #171-24
- Vacuum machine, DVP EC.20-1
- Thermo Scientific, Eutech Expert CTS
- Hanna, HI96801 Refractometer

References

[1] Klungtvedt, K. R., Saasen, A., Vasshus, J. K., Trodal, V. B., Mandal, S. K., Berglind, B., and Khalifeh, M., 2021, "The Fundamental Principles and Standard Evaluation for Fluid Loss and Possible Extensions of Test Methodology to Assess Consequences for Formation Damage," Energies, **18**(8), p. 2252.
[2] Klungtvedt, K. R., and Saasen, A., 2022, "A Method for Evaluating Drilling Fluid Induced Permeable Formation Damage," J. Pet. Sci. Eng., **213**, p. 110324.
[3] Khan, R., Kuru, E., Tremblay, B., and Saasen, A., 2007, "Extensional Viscosity of Polymer Based Fluids as a Possible Cause of Internal Cake Formation," Energy Sources Part A, **29**(16), pp. 1521–1528.
[4] Alvi, M. A. A., Belayneh, M., Fjelde, K. K., Saasen, A., and Bandyopadhyay, S., 2020, "Effect of Hydrophobic Iron Oxide Nanoparticles on the Properties of Oil-Based Drilling Fluid," ASME J. Energy Resour. Technol., **143**(4), p. 043001.
[5] Contreras, O., Alsaba, M., Hareland, G., Hussein, M., and Nygaard, R., 2016, "Effect on Fracture Pressure by Adding Iron-Based and Calcium-Based Nanoparticles to a Nonaqueous Drilling Fluid for Permeable Formations," ASME J. Energy Resour. Technol., **138**(3), p. 032906.
[6] Razzaq, W., Elkatatny, S., Gamal, H., and Samsuri, A., 2022, "The Utilization of Steelmaking Industrial Waste of Silicomanganese Fume as Filtration Loss Control in Drilling Fluid Application," ASME J. Energy Resour. Technol., **144**(2), p. 023004.
[7] Jiang, G., Sun, J., He, Y., Cui, K., Dong, T., Yang, L., Yang, X., and Wang, X., 2021, "Novel Water-Based Drilling and Completion Fluid Technology to Improve Wellbore Quality During Drilling and Protect Unconventional Reservoirs," Engineering.
[8] ANSI/API 13B-1 5th edition, "Recommended Practice for Field Testing Water-Based Drilling Fluids," ANSI/API 2019.
[9] Skjeggestad, O., 1989, *Boreslamteknologi, Teori og Praksis*, Alma Mater Forlag AS, Bergen (in Norwegian).
[10] Klungtvedt, K. R., and Saasen, A., 2022, "Comparison of Lost Circulation Material Sealing Effectiveness in Water-Based and Oil-Based Drilling Fluids and Under Conditions of Mechanical Shear and High Differential Pressures," ASME J. Energy Resour. Technol., **144**(12), p. 123011.
[11] Abrams, A., 1977, "Mud Design to Minimize Rock Impairment Due to Particle Invasion," J. Pet. Technol., **29**(5), pp. 586–592.
[12] Alsaba, M. T., Al Dushaishi, M., Jeennakorn, M., Nygaard, R., Saasen, A., and Nes, O. M., 2017, "Sealing Pressure Prediction Model for Lost Circulation Treatments Based on Experimental Investigations," American Association of Drilling Engineers, AADE-17-NTCE-21.
[13] Zhong, H., He, Y., Yang, E., Bi, Y., and Yang, T., 2022, "Modelling of Microflow During Viscoelastic Polymer Flooding in Heterogeneous Reservoirs of Daqing Oilfield," J. Pet. Sci. Eng., **210**, p. 110091.

VI. Klungtvedt, K.R. and Saasen, A. “Comparison of Lost Circulation Material Sealing Effectiveness in Water-Based and Oil-Based Drilling Fluids and Under Conditions of Mechanical Shear and High Differential Pressures”. OMAE2022-79502 and Journal of Energy Resources Technology 22-1218, 2022. https://doi.org/10.1115/1.4054653 (open access)

Comparison of Lost Circulation Material Sealing Effectiveness in Water-Based and Oil-Based Drilling Fluids and Under Conditions of Mechanical Shear and High Differential Pressures

Karl Ronny Klungtvedt
EMC AS and Department of Energy and Petroleum Engineering,
University of Stavanger,
Stavanger 4033, Norway
e-mail: krk@emcas.no

Arild Saasen
Department of Energy and Petroleum Engineering,
University of Stavanger,
Stavanger 4036, Norway
e-mail: arild.saasen@uis.no

A study was conducted to assess the performance of granular and fibrous lost circulation materials as preventative treatments and in remedial treatment of lost circulation in water-based and oil-based drilling fluids. For the preventative treatments, a factor that introduced increased mechanical wear on the particles was added to the hot-rolling process, to identify signs of deterioration of performance of certain materials. The study of remedial treatments of lost circulation was conducted on slotted discs with apertures of 750 μm and up to 5 mm and with a differential pressure of up to 34.5 MPa (5000 psi). To compare the sealing pressures of the different tests, a simple statistical analysis was introduced to differentiate between the peak holding pressures and the sustainable holding pressures of the various material and fluids combinations. The material degradation studies showed that $CaCO_3$-based lost circulation materials rapidly experienced significant particle degradation after exposure to fluid shear and mechanical degradation and that this considerably reduced the sealing performance of the materials. Also, synthetic graphite-based products showed clear signs in particle size degradation and a significant reduction in sealing performance. Cellulose-based products showed superior resistance toward mechanical wear and only small changes in sealing performance. When comparing water-based and oil-based fluids, it was clear that granular lost circulation materials showed considerably lower sealing efficiency in oil-based drilling fluids compared to water-based drilling fluids. In contrast, cellulose-based materials showed similar sealing performance in oil-based fluids and water-based fluids. [DOI: 10.1115/1.4054653]

Keywords: lost circulation, lost circulation material sealing effectiveness, particle size degradation, sealing pressure, geothermal energy, petroleum engineering, petroleum wells-drilling/production/construction

1 Introduction

Lost circulation is a critical factor that may reduce drilling efficiency, increase cost, and increase the risk of well collapse. Oil-based drilling fluids are often considered as superior to water-based drilling fluids with regards to obtaining a low fluid loss and achieving high rates of penetration. Water-based drilling fluids are in contrast often preferred due to a lower cost if the risk of large or total losses of drilling fluid is expected.

A considerable number of studies have been conducted on the classification of lost circulation materials (LCMs) and the sealing abilities of different materials. Alsaba et al. [1] classified lost circulation materials into categories based on physical and chemical characteristics. Alshubbar et al. [2] found that higher circulation rates led to higher fluid loss and observed that lost circulation materials with lower density were less impacted by annular flow, and that such materials therefore may be more effective for preventative treatment. Alsaba et al. [3] compared lost circulation materials from different material categories and found that fibers gave the best seals on tapered slotted discs. Furthermore, they found that granular materials such as $CaCO_3$ and graphite created seals with lower integrity. Khalifeh et al. [4] also tested fiber-based lost circulation materials and found that these seals were dynamically built to withstand gradually higher pressures without failing.

The use of nanoparticles in drilling fluids has received significant attention recently. For example, Alvi et al. [5] have shown that it is possible to reduce filtration loss measured on filter paper by the addition of 0.5 wt% iron oxide nanoparticles to an oil-based drilling fluid. In a series of experiments, such filtration loss was nearly halved. Most attention with the nanoparticle studies has been directed toward conventional fluid loss tests against filter paper or porous formation like Contreras et al. [6]. They found also an optimum effect by the addition of 0.5 wt% graphite together with 0.5 wt% nanoparticles based on iron or calcium. The role of particle size distribution (PSD) for fluid loss materials without nanoparticles on the formation of filter cakes and avoiding formation damage can be found consulting Klungtvedt and Saasen [7].

The main cost related to lost circulation treatment is normally the nonproductive time incurred to treat the loss or to remedy other consequences of the lost circulation, such as differential sticking. Grelland [8] studied how lost circulation is treated by most companies in the North Sea area and found that only 1–2% of the costs of treating lost circulation was related to the lost circulation material cost. He also found that the main materials used for treating losses on the Norwegian continental shelf were $CaCO_3$ and

Contributed by the Petroleum Division of ASME for publication in the Journal of Energy Resources Technology. Manuscript received March 25, 2022; final manuscript received May 18, 2022; published online June 10, 2022. Assoc. Editor: Saeed Salehi.

graphite. These materials were used alone or in combination and most of these treatments were insufficient to cure lost circulation. Furthermore, he concluded that the LCM treatments did not differ between formations drilled even though there were different pore and fracture sizes in different formations. Application of LCM with higher density than the typical fluid density was used consistently. As such, his findings related to actual field application procedures appear to be in contrast with the conclusions of Alshubbar et al. [2] and Alsaba et al. [3], where Alshubbar et al. concluded that in a circulating well LCM with lower specific gravity were better preventative candidates and Alsaba et al. showed that LCMs that have irregularity in particles shapes and a degree of deformability are effective in improving sealing strength and reducing fluid loss.

The research on lost circulation materials and sealing effectiveness does not provide a standard for determining which sealing pressure should be recorded for a given test as it may be a pressure held over time of the maximum pressure obtained before the seal broke. The present study proposes a simple metric for measuring a peak hold pressure (PHP) and a sustainable hold pressure (SHP) to provide as a minimum method for classifying a sealing pressure using slot testing of lost circulation materials.

To test the proposed metric for measuring sealing pressures, a typical lost circulation treatment recipe for both preventative treatments and remedial treatments of lost circulation following the findings of Grelland [8] was used. These recipes were applied to both an oil-based drilling fluid and a water-based drilling fluid and compared with a recipe like that tested by Khalifeh et al. [4]. This would allow for comparing the different treatments of lost circulation and to compare performances in oil-based and water-based drilling fluids.

Scott et al. [9] presented a pragmatic approach to lost circulation treatment and concluded that bridging is achieved when the particles are equal to or slightly larger than the loss zone opening and present in the fluid at a concentration of 10–20 lb/bbl (28.5–57 kg/m^3). Furthermore, due to solids content in field mud, for the LCM to be effectively enhancing the performance of a field mud, LCM should have a D_{50} value of 400 μm or larger.

Hoxha et al. [10] used a flow loop and shearing facilities to test the degradation of the particle size distribution of lost circulation materials under the influence of shear. They found that both $CaCO_3$ and graphite suffer from shear degradation. To build on these findings and the conclusions of Alsaba et al. [3], a method was proposed and tested in the present study to introduce mechanical wear into an ordinary hot-rolling process for drilling fluids. The method was applied to lost circulation materials that are designed to be a part of the circulating system, and this will experience mechanical wear and potential degradation.

To summarize, a series of experiments were conducted where the objectives were to:

- apply a simple statistical method for measuring the sealing strength of lost circulation materials against a specific fracture size;
- identify if lost circulation treatment is equally effective in KCl/polymer water-based drilling fluids and oil-based drilling fluids;
- investigate sealing mechanisms and sealing strength of granular and fibrous lost circulation materials; and
- identify how a method for applying mechanical shear in the hot-rolling process impacts particle size distribution and sealing ability of lost circulation materials for preventative treatment.

2 Materials and Methods

The tests were conducted using a permeability plugging apparatus where drilling fluid can be tested on either ceramic discs or slotted steel discs with a 63 mm diameter. Pressure can be applied by either a pressured gas source or by a hydraulic pump which allows for logging the applied pressure digitally at 1 s intervals during the test. The tests were conducted at a temperature of 60 °C.

Fig. 1 Slotted steel discs for testing of LCM pills

The slotted steel discs each have multiple slots without any tapering. With limited side wall friction, the sealing would primarily need to take place at the fracture tip, thus likely making the test more difficult than to seal a subterranean fracture where the friction within the fracture may help to form a deep seal. As such, the tests will not fully replicate the deep sealing of a fracture, but they may be a practical approach to understand the potential for sealing the fracture opening. For the testing of high-concentration LCM pills, discs with slot widths of 0.75, 1.5, 2.0, and 3.5 mm were used. In addition, a disc with a combination of single slots of sizes 0.5, 1.0, 2.0, 3.0, and 5.0 mm was selected. The discs used for testing LCM pills are shown in Fig. 1.

The metric proposed to determine the sealing strength of the lost circulation materials was calculated as a moving average over time periods of 10 or 60 s and the highest average value during 10 and 60 s averaging periods was selected as the peak hold pressure and sustainable hold pressure, respectively

$$P(MA_n) = \sum_{t=0}^{t=n} P_t/n \tag{1}$$

$$\text{Peak hold pressure} = \max P(MA_{10}) \tag{2}$$

$$\text{Sustainable hold pressure} = \max P(MA_{60}) \tag{3}$$

The tests were conducted with the objective of obtaining the highest sealing pressure for each combination of the material and slotted disc. Limitations were set for the fluid loss of 275 mL out of an applied volume of 400 mL, to ensure that sufficient fluid was left in the test cylinder, pressures exceeding and holding above 34.9 MPa (5000 psi) or a period of 20 min.

An overview of the equipment used is presented in the Appendix.

2.1 Particle Size Distribution of Materials. The materials were selected to replicate the materials references by Grelland [8] and Khalifeh et al. [4], with some additions. A description of each material is shown in Table 1. The granular products are ground marble, hereinafter referred to as $CaCO_3$, and resilient graphite, whereas the cellulose-based products have three different natures. One is an ultra-fine cellulose powder, another is a hard and granular cellulose, and the third is a mixture of various cellulose fibers and granular particles.

2.2 Mechanical Wear and Particle Degradation. For materials used as part of the active system, the particles will experience wear as part of the circulation in the well. To simulate this, a

Table 1 LCM materials

Material	D_{50} (μm)	D_{90} (μm)	D_{99} (μm)	Specific gravity	Description
$CaCO_3$ 150	150	325		2.7–2.78	Ground marble
$CaCO_3$ 600	600	1125		2.7–2.78	Ground marble
$CaCO_3$ 1200	1200	1489		2.7–2.78	Ground marble
Graphite 100	100	182		1.82	Resilient graphite
Graphite 400	400	744		1.71	Resilient graphite
Ultra-fine cellulose	–	75	90	0.97–1.0	Cellulose fiber
Granular cellulose	–	–	600	1.3	Cellulose fiber
Cellulose LCM blend	425	<3200		1.02–1.04	Cellulose fiber

threaded steel rod was placed into the hot-rolling cell for some of the samples, and the pressure testing was compared with samples where ordinary hot rolling had been conducted. For the tests with high-concentration LCM pills, no hot rolling was used as the pill would normally be prepared just before application in the well.

One representative was selected for testing particle degradation from each of the material categories using a simple high-speed shearing process, as an alternative method to the hot-rolling process for testing material degradation. The materials were selected based on having a significant portion of particles in the range between 200 μm and 1000 μm for ease of sieving. The materials were each mixed into a fluid containing xanthan gum (3.3 kg/m^3) and low viscosity poly-anionic cellulose (11 kg/m^3), to reflect the viscosity of a typical drilling fluid. One same of each product was then wet-sieved after 10 min of mixing at normal speed. The other sample was sheared at full speed on a Hamilton Beach mixer for 30 min and then wet-sieved.

Figures 2–4 show the PSD of the respective materials with the normal mixing process to represent the material before degradation and after the high-speed mixing to represent the materials after degradation. The measurements were conducted using wet sieving on a sieve shaker with American Petroleum Institute (API) rated sieves. It should be noted that the samples that were hot rolled were not exposed to the high-speed mixing process.

The degradation process showed considerable change in the particle size distribution of the $CaCO_3$ particles, some reduction in the PSD of the resilient graphite, and very little change in the PSD of the granular cellulose. For the $CaCO_3$, 99% of the particles initially above 420 μm were finer than 420 μm after the high-speed shearing. For the resilient graphite, the reduction in particles above 420 μm was 30% and for the granular cellulose, it was only 5%.

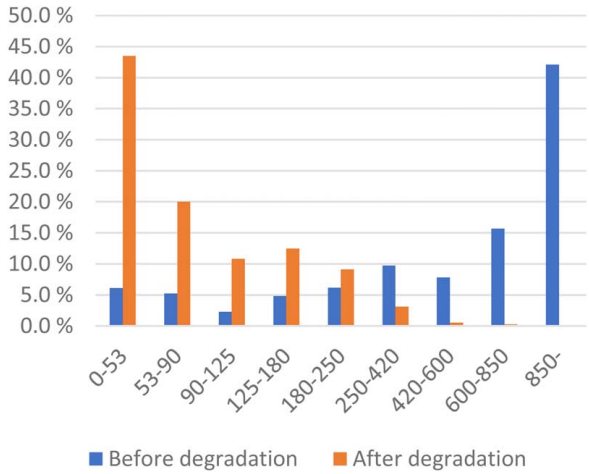

Fig. 2 PSD of $CaCO_3$ with D_{50} approximately at 600 µm before and after degradation

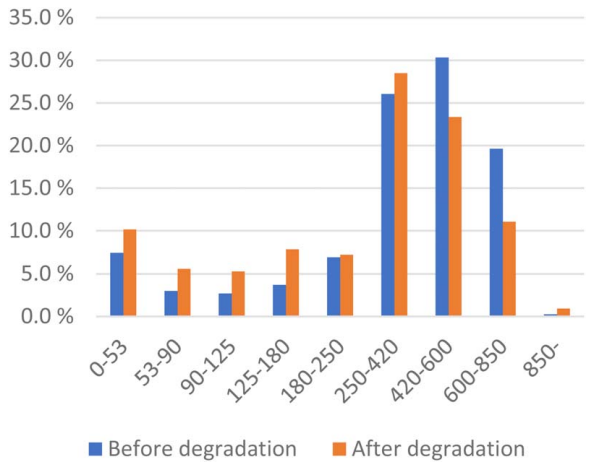

Fig. 3 PSD of graphite with D_{50} approximately at 400 µm before and after degradation

3 Measurements and Results

The tests are separated into four different test series. Tests were conducted in oil-based and water-based drilling fluids with high-concentration LCM pills and with lower concentration preventative treatment recipes.

3.1 Pressure Measurement. The tests were by recording the applied pressure relative to ambient pressure every second. The pressure source was a hydraulic hand pump where the pressure was applied through regular pumping. The applied hydraulic pressure moves a piston within the test cell, which then transfers the pressure to the drilling fluid.

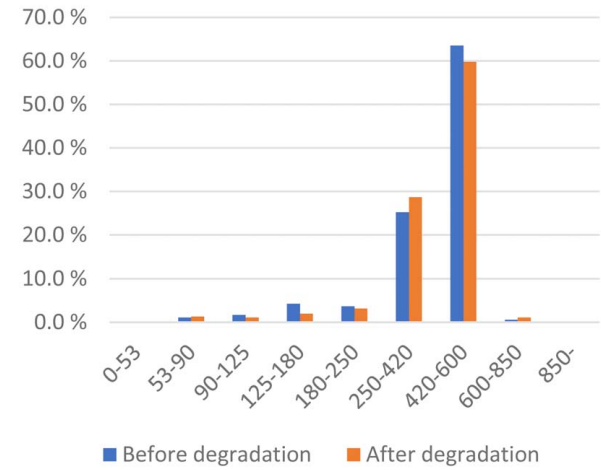

Fig. 4 PSD of granular cellulose before and after degradation

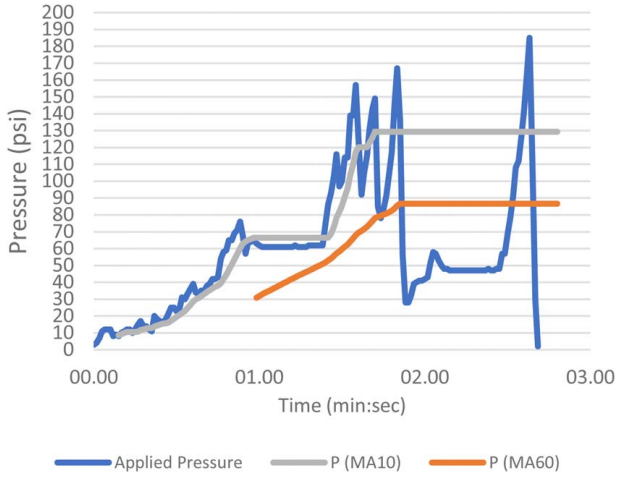

Fig. 5 Example of pressure chart with granular LCM in oil-based drilling fluid

Figure 5 shows the example of a pressure chart where both the highest achieved PHP and SHP are plotted. An oil-based fluid with pill number 5, shown in Table 5, was tested on a 2.0 mm slotted disc. The pressures are calculated according to Eqs. (1)–(3). The raw plot of the applied pressure presents a series of sharp peaks, where the pressure rises for periods shorter than 10 s. The highest recorded pressure reading in the specific test was 185 psi. The PHP was 129 psi, whereas the SHP was significantly less, 87 psi. Considering that the pressure collapsed multiple times and that the peak was only recorded in one instance it seems natural that the peak of 185 psi is not used to represent the sealing capacity of the test. Moving to the PHP, which is calculated as the highest 10 s average, there are four periods where the pressure exceeds the PHP level. However, the longest recorded period above the PHP level was a four-second period. For tests where the PHP and SHP were in the range of less than 1000 psi, the ratio of the SHP and PHP was often in the range of 60–80%. For such tests, it may be that a higher fluid flowrate, facilitated for example by a pressurized gas source instead of a hydraulic pump might have led to a more effective sealing. For tests where the highest pressures obtained were exceeding 2000 psi, the ratio of the SHP to PHP was consistently above 90%. Due to the high losses and high pressures, a gas source was considered to be too risky to operate in a laboratory condition. The four-test series described in the following are therefore presented in terms of the sustainable hold pressure where a high pressure was maintained over time, whereas the PHP is presented for certain tests where it was difficult to achieve a seal with the given fluid flow.

3.2 High Pressure Testing of Preventative Lost Circulation Materials in Oil-Based Drilling Fluid. Two recipes for preventative treatment of lost circulation were mixed into a barite-weighted oil-based drilling fluid with the presence of fine drill solids and measured density of 1.49 s.g. as shown in Table 2. The fluid was described by the supplier as a high-performance nonaqueous drilling fluid, with a low odor hydrocarbon base. Two samples of each fluid were mixed and hot rolled at 90 °C for 16 h. For each fluid, one sample was hot rolled in the conventional way, and one with the addition of a rod to simulate downhole mechanical wear on the fluid particles during the hot rolling. The rod was a 13.5 cm long M16 threaded steel rod placed in a 500 cm^3 cell. A threaded rod was chosen to enlarge the surface area to detect any accretion and to facilitate that both small and large particles may be exposed to the pressure from the rod. With an un-threaded rod, the main wear would be on the largest particles.

After hot rolling, the fluid samples were used in a lost circulation test on a slotted disc with 500 μm slot apertures. The pressure plots

Table 2 Oil-based fluid recipes

LCM additive into recipe for 1 L of fluid	Fluid 1: Granular LCM	Fluid 2: Granular and cellulose LCM
Oil-based drilling fluid (g)	1432	1417
$CaCO_3$ 150 (g)	24.5	24.5
$CaCO_3$ 600 (g)	24.5	24.5
Graphite 100 (g)	24.5	–
Graphite 400 (g)	12.25	–
Ultra-fine cellulose	–	8.6
Granular cellulose	–	28.5

are shown in Fig. 6. For the tests with normal hot rolling, both fluids performed well and enabled high sealing pressures over a 60 s period. For fluid 1, without cellulose-based LCM, the highest sustainable hold pressure was 4182 psi before the fluid loss reached 275 mL, whereas the test for fluid 2 (with cellulose-based LCM) was stopped with an SHP of 5374 psi, due to the pressure approaching the set limit at 5500 psi. At the time, the measured fluid loss was only 13 mL.

Thereafter, the tests were repeated with the fluid samples that have been exposed to mechanical wear by the inclusion of a threaded steel rod in the hot-rolling cell. For fluid 1, the highest recorded SHP was 302 psi when a fluid loss of 275 mL was reached. For fluid 2, also a noticeable change was recorded relative to the first sample. A larger fluid loss was recorded; however, the pressure reached an SHP level of 4689 psi. Following the degradation tests in Sec. 2.2, it may be assumed that only the granular cellulose particles of fluid 2 were intact and equivalent to the slot size after the hot-rolling process with the steel rod. Therefore, in these tests, the concentration of LCM that was similar to or larger than the slot aperture size was around 28.5 kg/m^3 or slightly in excess of 2% by volume.

3.3 High Pressure Testing of Preventative Lost Circulation Materials in Water-Based Drilling Fluid. The preventative LCM mixtures used in Sec. 3.2 were mixed into a water-based drilling fluid as shown in Table 3 and hot rolled with and without a threaded steel rod. The recipes included bentonite to represent fine drill solids.

The pressure tests were conducted on a slotted disc with 0.50 mm apertures, as for the tests with the oil-based drilling fluid. The pressure plots are shown in Fig. 7. Also in these tests, a significant difference was recorded for the samples where the fluid had been exposed to mechanical wear during the hot-rolling process. Without the mechanical wear, the results for fluid 3, with the granular LCM, were very similar to the results obtained for fluid 1 as an SHP pressure in the region of 4200 psi was achieved. For the sample with the mechanical shear, fluid 3 registered an SHP in excess of 1000 psi, or more than three times the SHP for fluid 1, with granular LCM in an oil-based drilling fluid. In contrast, the SHP of 3981 psi obtained for fluid 4 after mechanical wear was a little lower than for fluid 2 after the same mechanical exposure. However, in all tests, the fluid samples with the combined granular and cellulose-based LCM showed significant improvements in sealing strength and fluid loss over the formulations with granular LCM only. Also, it appears that the addition of cellulose-based LCM provided significantly higher sealing strength after exposure to mechanical wear.

3.4 High Pressure Testing of Lost Circulation Materials in Water-Based Drilling Fluid. Three recipes were mixed of LCM pills into a water-based fluid with a density of 1.4 s.g. The recipe of the base fluid and the pills are shown in Table 4.

The LCM pills were tested to achieve the highest sealing pressure before a fluid loss of 275 mL was recorded or until s SHP of

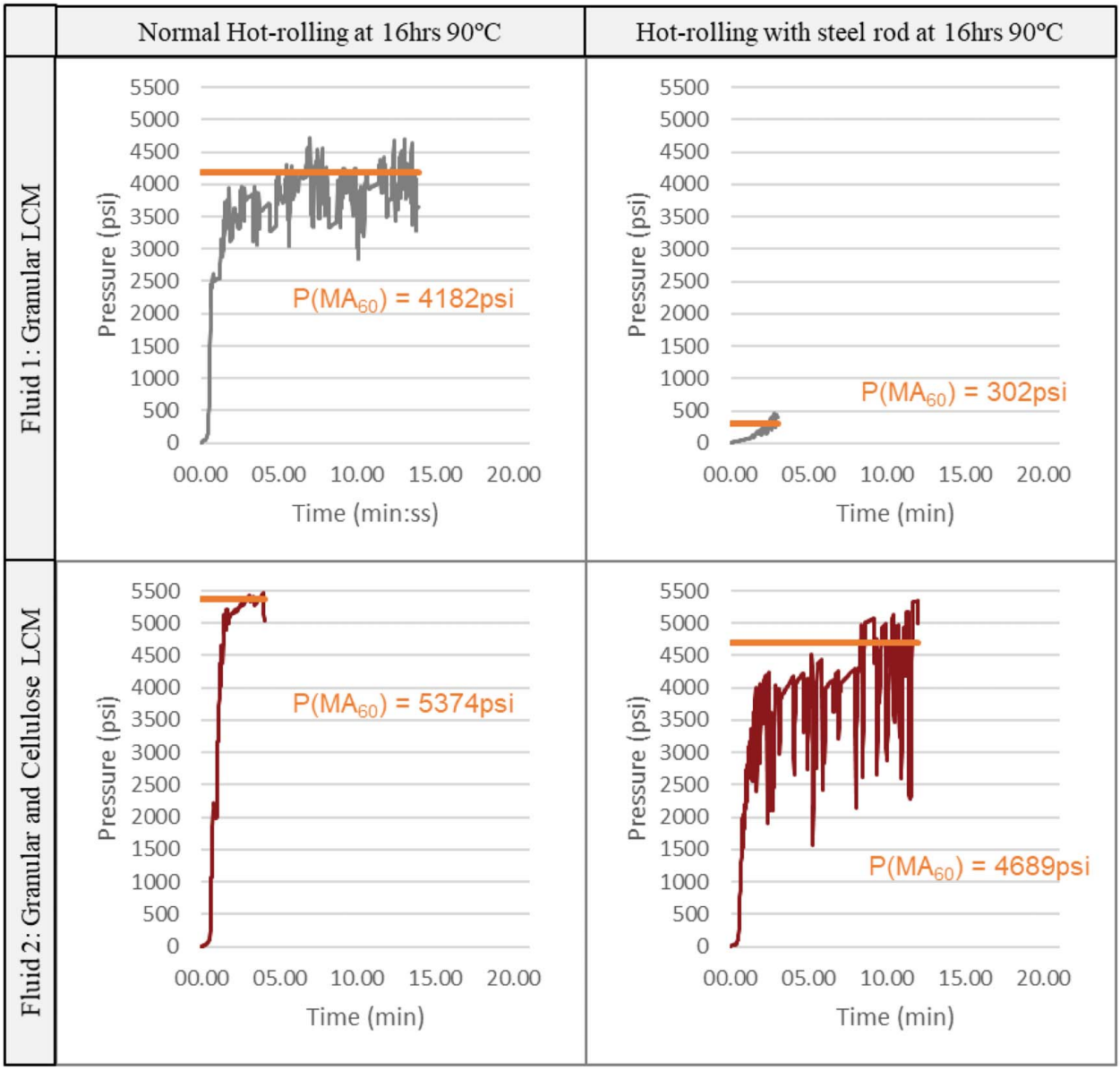

Fig. 6 Pressure charts for preventative LCM in oil-based drilling fluid

Table 3 Water-based fluid recipes

LCM additive into recipe for 1 L of fluid	Fluid 3: Granular LCM	Fluid 4: Granular and cellulose LCM
H_2O (g)	817	817
Na_2CO_3 (g)	0.055	0.055
NaOH (g)	0.69	0.69
Xanthan gum (g)	3.32	3.32
Poly-anionic cellulose (g)	11.05	11.05
MgO (g)	2.77	2.77
KCl (g)	48.3	48.3
Bentonite (g)	13.8	13.8
Barite (g)	464	464
$CaCO_3$ 150 (g)	24.5	24.5
$CaCO_3$ 600 (g)	24.5	24.5
Graphite 100 (g)	24.5	–
Graphite 400 (g)	12.25	–
Ultra-fine cellulose	–	8.6
Granular cellulose	–	28.5

5000 psi was achieved. The sustainable hold pressures are shown in Fig. 8. All three pills achieved a sealing pressure in excess of 5000 psi on the disc with a 750 μm slot width. As the disc slot with increased, the performance of the different pills deviated increasingly more. Pill 1 achieved a PHP of 628 psi on the 1.5 mm disc, whereas pill 2 achieved a PHP of 217 psi on the 2.0 mm disc. In contrast, pill 3 sealed the disc with the 5.0 mm slot up to a PHP of 1347 psi.

3.5 High Pressure Testing of Lost Circulation Materials in Oil-Based Drilling Fluid. The LCM concentrations for pills 1–3 used in Sec. 3.4 were mixed into a barite-weighted oil-based fluid with a density of 1.49 s.g. as per Table 5 to make up three LCM pills. By doing so, pill 4 would correspond to pill 1, pill 5 to pill 2, and pill 6 to pill 3, with the difference being the drilling fluid base.

The first tests were conducted on a disc with a 1.5 mm slot width for comparison of the performance with the results from testing the pill formulations in the water-based drilling fluid.

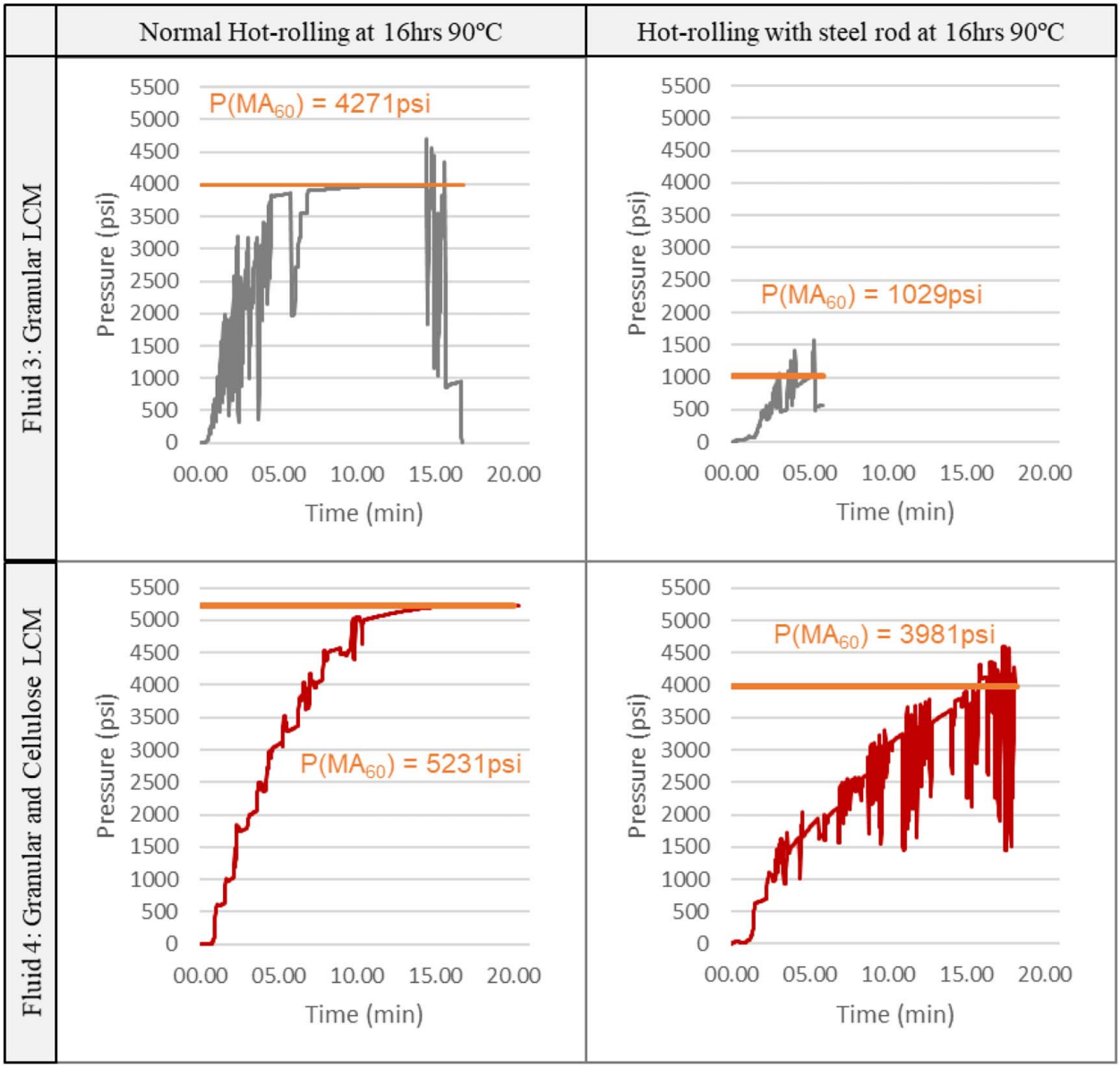

Fig. 7 Pressure charts for preventative LCM in water-based drilling fluid

Table 4 Recipes for LCM pills 1–3

Recipe for 1 L	Pill 1: 350 kg/m^3 granular LCM	Pill 2: 450 kg/m^3 granular LCM	Pill 3: 155 kg/m^3 cellulose
H_2O (g)	718.2	718.2	718.2
Na_2CO_3 (g)	0.05	0.05	0.05
NaOH (g)	0.61	0.61	0.61
Xanthan gum (g)	2.91	2.91	2.91
Poly-anionic cellulose (g)	9.71	9.71	9.71
MgO (g)	2.43	2.43	2.43
KCl (g)	42.5	42.5	42.5
Bentonite (g)	12.14	12.14	12.14
Barite (g)	408	408	408
$CaCO_3$ 150 (g)	100	100	–
$CaCO_3$ 600 (g)	100	100	–
$CaCO_3$ 1200 (g)	–	75	–
Graphite 100 (g)	100	100	–
Graphite 400 (g)	50	75	–
Cellulose LCM blend (g)	–	–	155

The tests were thereafter selected to be on either smaller or larger apertures, due to a limited supply of the oil-based field fluid. As pill 4 only achieved an SHP of 115 psi on the 1.5 mm disc, it was selected to be re-run on the 750 μm slotted disc. On this disc, the sealing pressure increased to 3788 psi. As pill 5 achieved a higher sealing pressure with PHP of 914 psi on the 1.5 mm slotted disc, it was re-tested on the 2.0 mm disc. Here the pill achieved a PHP of 129 psi. In sum, pills 4 and 5 achieved significantly lower sealing pressures when applied into the oil-based drilling fluid. The results for pill 6 were very much in line with the results of the testing in the water-based drilling fluid. The 1.5 mm and 2.0 mm slotted discs were both successfully sealed with pressures exceeding 5000 psi and the 3.5 mm disc was sealed with an SHP 2000 psi. The result on the disc with the 5.0 mm slot gave a PHP than the SHP on the 3.5 mm slot with a small margin. The pressure charts for pills 4–6 are shown in Fig. 9. It should, however, be noted that the fluid loss on the discs with large widths is erratic due to the high loss occurring once a seal is broken and that the slow buildup of hydraulic pressure may provide different results than for field conditions.

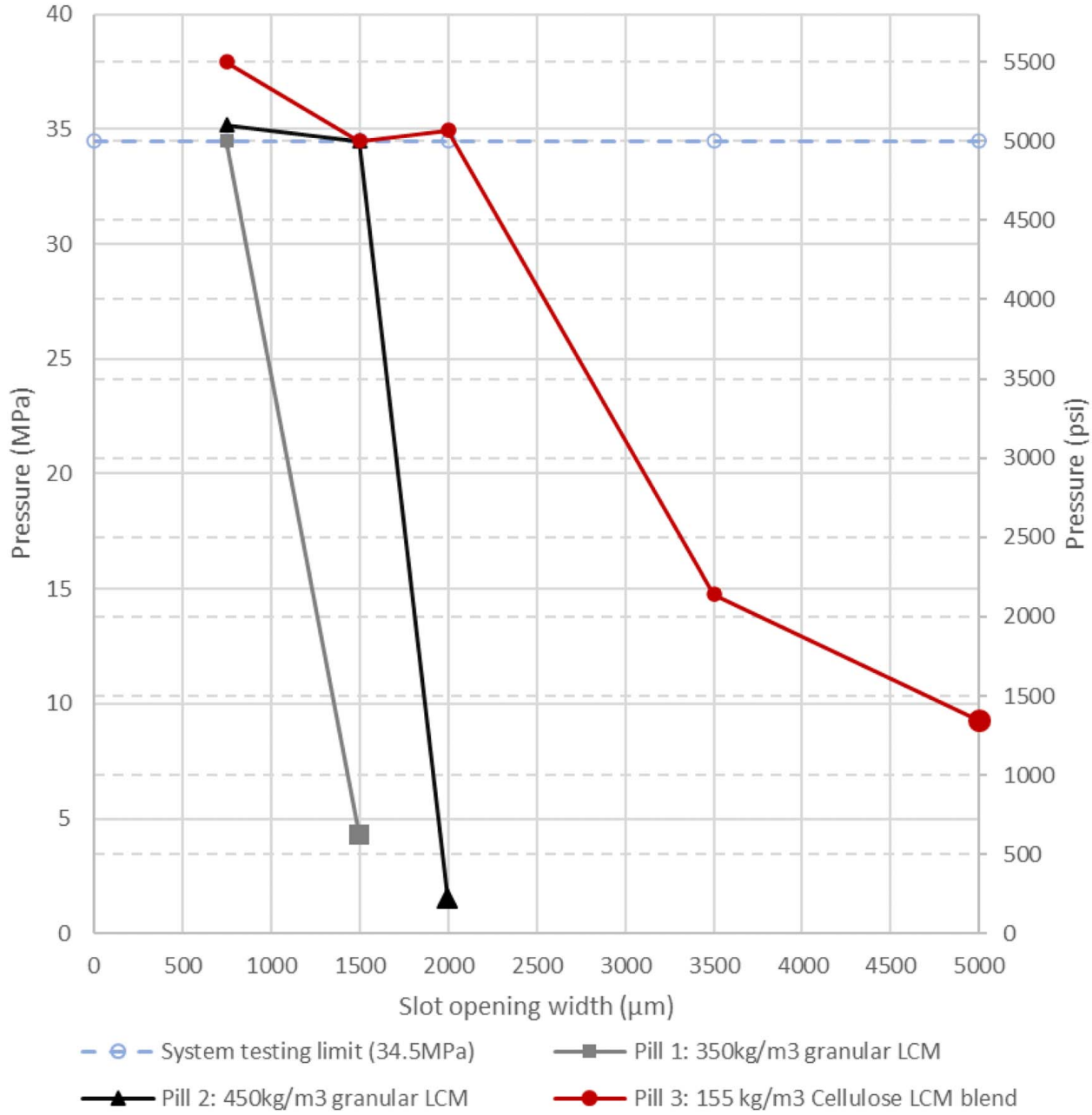

Fig. 8 Pressure charts for LCM pills in water-based drilling fluid

For the tests with cellulose-based LCM pills, the peak hold pressures exceeding 1300 psi were achieved in both oil- and water-based fluids even when the slot size was 1.5 times larger than the D_{90} value of the particles. In contrast, with the granular LCM mixtures, PHP exceeding 1000 psi was only achieved when the largest particles were around the width of the slot.

3.6 Discussion. The results of the testing of preventative LCM treatments are presented in Sec. 3.2 support the findings of Scott et al. [9] for the test conducted with conventional hot rolling, where the particle size (D_{90} or D_{99}) of the $CaCO_3$ 600, graphite 400, and the granular cellulose products was consistent with the sealing of the 500 μm slotted disc. For these tests, LCM particles with sizes equal to or slightly larger than the slot openings were present in adequate concentrations for effective sealing. The exposure to mechanical wear altered these results significantly. This shows the importance of testing fluids and LCM under conditions that replicate the mechanical wear which may be present in a specific field operation. The results differ from those of Vivas and Salehi [11], who tested thermal degradation of LCM for geothermal wells, however, without exposure to mechanical wear and without the presence of drill solids. They found granular materials to function well as LCM for 1000 μm slots and pressure up to 6.2–8.3 MPa or 900–1200 psi.

Two different methods for material degradation were used during the study. Although the PSD changes using the two different methods were not directly compared, the test results showed that both methods led to significant degradation of some materials and little degradation of others. The high-speed mixing process led to a very high degradation (99% >420 μm) of the $CaCO_3$ particles, which was a significant contrast to the resilient graphite that showed some degradation (30% > 420 μm) and the granular cellulose that showed very little degradation (5% >420 μm). The PSD

Table 5 Recipes for LCM pills 4–6

Recipe for 1 L	Pill 4: 350 kg/m^3 granular LCM	Pill 5: 450 kg/m^3 granular LCM	Pill 6: 155 kg/m^3 cellulose LCM blend
Oil-based drilling fluid (g)	1267	1267	1267
$CaCO_3$ 150 (g)	100	100	–
$CaCO_3$ 600 (g)	100	100	–
$CaCO_3$ 1200 (g)	–	75	–
Graphite 100 (g)	100	100	–
Graphite 400 (g)	50	75	–
Cellulose LCM blend (g)	–	–	155

degradation results were also consistent with the measured changes in sealing performance where the $CaCO_3$ particles were combined with either resilient graphite or granular cellulose. The combination of $CaCO_3$ and resilient graphite (fluids 1 and 3) resulted in the SHP falling by 93% in oil-based drilling fluid and 76% in the water-based drilling fluid, whereas the SHP fell only by 13% in oil-based drilling fluid and 24% in water-based drilling fluid with the $CaCO_3$ and cellulose mixture (fluids 2 and 4). For these tests with water-based fluids without degradation, it should be noted that the measured SHP for the tests was limited by the maximum test pressure.

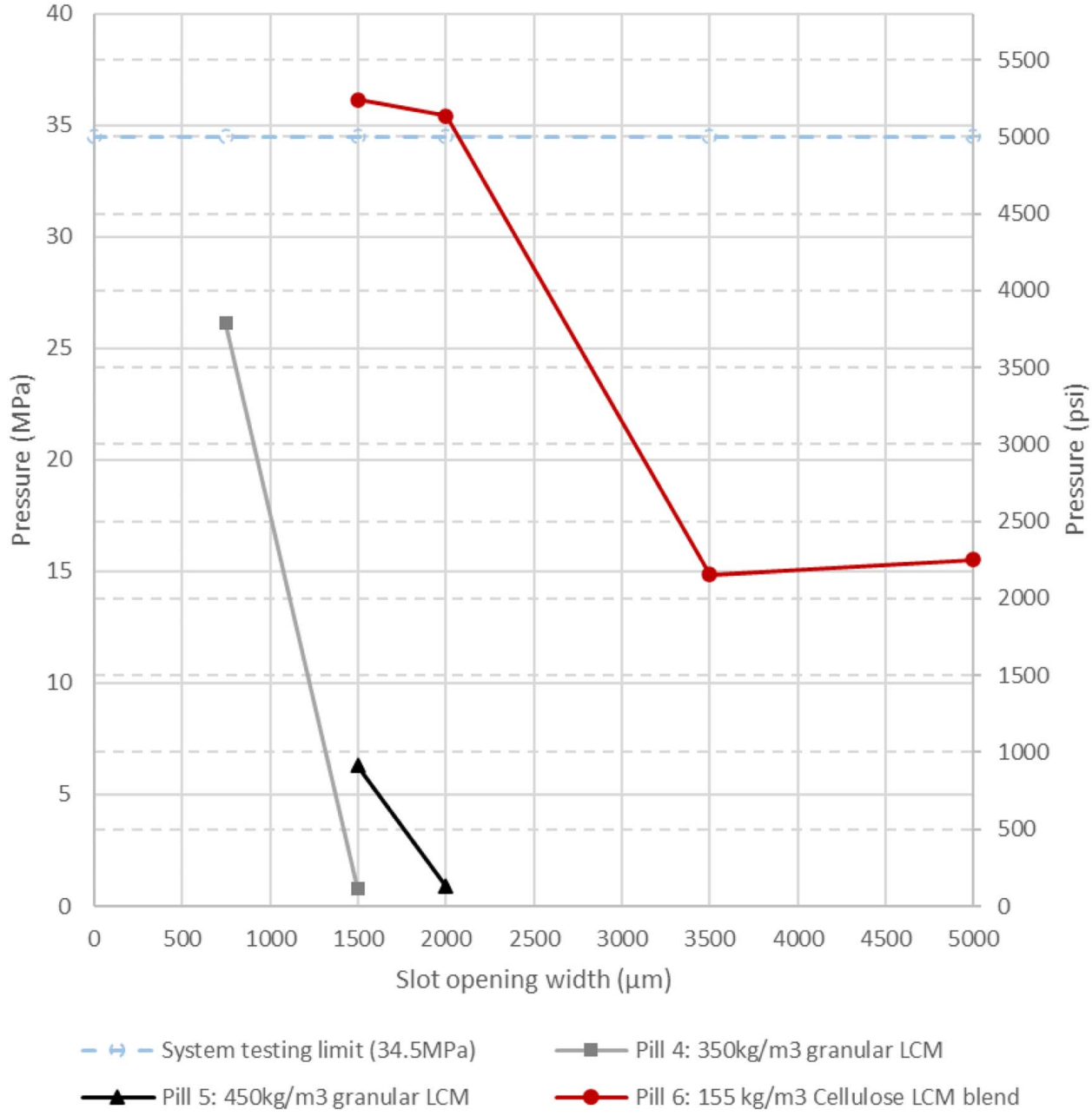

Fig. 9 Pressure charts for LCM pills in oil-based drilling fluid

The results of the degradation tests strongly indicate that ground marble or $CaCO_3$ has clear disadvantages when applied as a fracture-sealing or wellbore-strengthening material. The very high material degradation indicates that the specified product PSD is unsuitable to indicate the material's capacity to seal fractures or large pore-openings in a drilling situation where the material may be exposed to mechanical wear.

The resilient graphite showed considerably better performance than the $CaCO_3$. However, in both tests where mechanical wear had been introduced, the sealing effectiveness fell very significantly so that a high rate of product replenishment would be required to maintain a satisfactory sealing performance.

The granular cellulose particles provided the best resistance toward mechanical degradation and also provided the highest sealing pressures. It should be noted that this was the case despite the granular cellulose particles having a D_{99} value of 600 μm, which is considerably lower than the specified D_{90} values of the $CaCO_3$ of 1125 μm and the resilient graphite of 744 μm.

One likely reason for the difference in sealing strength and mechanical wear resistance of the materials is the mechanical toughness of the particles. In materials science, toughness is described as the ability of a material to absorb energy and plastically deform without fracturing. Equation (4) describes the toughness from a mechanical perspective, where σ is the stress applied, ε is the material strain, and ε_f is the strain upon failure

$$\frac{\text{Energy}}{\text{Volume}} = \int_0^{\varepsilon_f} \sigma d\varepsilon \tag{4}$$

Toughness tests were not conducted on the materials to verify if this could be a method for differentiating the properties of materials. However, by simply grinding a sample of each material between fingers, it is clear that the $CaCO_3$ degrades very quickly, the graphite degrades much less, and the granular cellulose does not degrade noticeably. The findings related to materials degradation may also have some relevance for the tests with the LCM pills, where also the cellulose blend of pill 3 clearly outperformed the sealing capacity of the granular materials used in pills 1 and 2. For the application of LCM in a high-concentration pill, the toughness of the materials may be less relevant from a fluid circulation perspective, as the LCM particles will normally be pumped with a low flowrate to the loss zone. As such, the particles will likely not be degraded in the same manner as LCM particles that are part of the circulating system and sheared whilst being pumped through the bit. During the process of sealing a fracture, the particles will be squeezed together, and less tough particles may degrade during the sealing process.

The degradation tests identified the $CaCO_3$ as a substantially less wear-resistant material than the resilient graphite and the granular cellulose. A hypothesis is, as the seal is formed, the $CaCO_3$ particles break up to fill the voids between the more resilient graphite or granular cellulose particles. If so, this may impact the resilience of the seal toward disturbances in the wellbore relative to seals where the materials elastically adapt to create a low-permeability zone.

Significant differences were observed when applying granular LCM in oil-based fluids relative to water-based fluids. Corresponding differences were not observed when applying cellulose-based LCM materials. A reason for this difference may be related to particle–particle interaction.

In a dispersed water-based fluid, the particles will move independently upon the circulation. When a seal is created in the filter cake against a permeable formation or against a fracture, the particles will be forced together as the filter cake or seal dehydrates. With cellulose-based materials, polar interaction will occur between the cellulose particles themselves, but also between the cellulose particles and other polymers such as poly-anionic cellulose, xanthan gum, and starch. As such, there will be frictional or adhesive forces between the particles, partly like a paper manufacturing process. The filter cake will therefore be very strong and elastic.

When applying inert granular particles in a water-based drilling fluid, it is likely that there will still be present frictional- or adhesive forces between the polymer particles in a seal and that these forces enhance the seal integrity over that which might be achieved by granular particles alone, and that these forces increase as the seal is de-hydrated. The polymers will in such a situation develop an elastic filter cake. Hence, the filter cake can be structured as a separate entity and not be considered to be constructed as a formation of individual particles.

In summary, the higher the concentration of polymers and cellulose-based fibers in the filter cake, the more cohesive it will be. If cellulose-based fibers are replaced in part or in full by inert LCM, the cohesive strength of the filter cake will be reduced correspondingly.

Oil-based drilling fluids are generally considered superior to water-based drilling fluids with regards to lubricity and fluid loss in low- to medium permeability formations. Majid et al. [12] found that in water-in-oil emulsions, water forms small droplets with a size typically smaller than 5 μm in a well-sheared suspension. From a fluid loss perspective, the water may be seen as a particle suspended in the base fluid. Furthermore, Wang and Du [13] found that the D_{50} value of a certain barite powder was in the region of 15–20 μm and that the largest particles may be up to circa 75 μm. Combining the PSD of the water droplets and barite as a weighting agent, a typical oil-based drilling fluid will have a high concentration of particles. Following the Abrams Rule [14], the D_{50} value of the barite suggests that a barite-weighted fluid may effectively seal formations with pore sizes up to circa 60 μm. As a supplement to the barite particles, the high concentration of water droplets with a size <5 μm provides a very effective fine-sealing mechanism.

Unless mechanically or chemically disturbed, water droplets have a high sphericity in a water-in-oil emulsion. For formations where the barite has sufficient size to bridge the pore throats, the smaller water droplets will act as a fine sealant. No polymeric additives are used to create a long strain range elastic gel within the filter cakes.

For LCM used as part of the circulating system, other considerations should also be made with regards to impacting the overall functionality of the drilling fluid in the well. The size, shape, and adhesive forces may impact the equivalent circulating density or the formation of a filter cake on the wellbore wall. Particles that may form a cohesive network may be better suited for pill applications as any increase in fluid viscosity will be less important for such applications. In a dynamic condition, the tensile strength of the filter cake may impact its ability to withstand the erosion caused by the flow of fluid and hence provide a lower continuous fluid loss rate. In such an application, cohesive forces between LCM particles may improve the tensile strength of the filter cake and hence the wellbore stability.

The cellulose-based products used in the test are of different nature and shape. However, when comparing with the $CaCo_3$ and resilient graphite particles, it is clear that the cellulose particles have very low relative sphericity or high aspect ratio. The low sphericity of the cellulose-based particles and the polar interaction between cellulose particles under applied differential pressure may be a differentiating factor relative to the granular LCM particles.

In essence, fluid 1, consisting of a barite-weighted water-in-oil emulsion with $CaCO_3$ and resilient graphite may appear as a high concentration of medium- to high sphericity particles dispersed in a base fluid. Whenever the formation of pore throats or fractures are smaller than a critical size of the particles in the fluid, e.g., where the largest particles in the fluid are equivalent to the fracture aperture or the pore-throat size, the fluid acts very effectively to seal. However, once the pore-throat size or fracture aperture exceeds this critical particle size, the appearance of the fluid may be that of a naturally lubricating roller-bearing system. In contrast to a water-in-oil emulsion, water-based drilling fluid will have dispersed polymers that have very low sphericity and that may

Table 6 Hypothesis for mechanical interaction between particles in various fluid compositions during sealing of pore throats or fractures

	Water-in-oil emulsion	Water-based fluid with polymers for fluid loss and viscosity
Granular inert LCM particles with medium- to high sphericity	Total fluid appears as a dispersed spherical particle system with very high particle concentration and low particle-to-particle adhesive and frictional forces upon defluidization	Total fluid appears as a dispersed particle system with medium concentration of low and high sphericity particles and some particle-to-particle adhesive and frictional forces upon defluidization
Cellulose-based particles with low sphericity	Total fluid appears as a dispersed particle system with very high concentration of high sphericity particles and some low sphericity particles and with some particle-to-particle adhesive and frictional forces upon defluidization	Total fluid appears as a dispersed particle system with medium concentration of low sphericity particles and high particle-to-particle adhesive and frictional forces upon defluidization

Table 7 Hypothesis for sealing effectiveness of various fluid compositions for sealing of pore throats or fractures

	Water-in-oil emulsion	Water-based fluid with polymers for fluid loss and viscosity
Granular inert LCM particles with medium- to high sphericity	Very effective sealing up to critical pore throat or fracture size by effective particle packing Above critical pore throat or fracture size sealing ability sharply drops as the fluid behaves like a roller-bearing system	Effective sealing up to critical pore throat or fracture size by particle packing and interactive forces Above critical pore throat or fracture size sealing ability gradually drops as adhesive and frictional forces become less effective
Cellulose-based particles with low sphericity	Very effective sealing up to critical pore throat or fracture size by effective particle packing Above critical pore throat or fracture size sealing ability gradually drops as the fluid moves toward behaving like a roller-bearing system	Effective sealing up to critical pore throat or fracture size by particle packing and interactive forces Above critical pore throat or fracture size sealing ability slowly drops as adhesive and frictional forces become less effective

combine through polar molecule interaction. Also, by replacing granular inert particles in part or in full by cellulose-based particles, the polar interaction and thereby also the particle-to-particle adhesive and frictional forces are increased.

It may therefore be that the sealing mechanisms may be described as shown in Table 6 and the sealing effectiveness as shown in Table 7.

4 Conclusion

- The application of a simple moving average to identify the peak hold pressure (10 s moving average) and sustainable hold pressure (60 s moving average) provided a good and non-subjective way of measuring the pressures during LCM tests. The PHP became the most relevant metric for measuring when the LCM seal failed, whereas the SHP reflected a more reliable sealing pressure.
- The sealing effectiveness for cellulose-based LCM appeared to be reasonably similar in oil-based and water-based drilling fluids. In contrast, granular LCM was found to create stronger seals in water-based drilling fluids than in oil-based drilling fluids.
- The highest sealing pressures and lowest fluid losses were obtained when applying cellulose-based LCM. Also, the cellulose-based materials showed the ability to seal slotted discs up to 5.0 mm. In contrast, the granular LCM appeared to function very well up to certain limits. Once these limits were reached, the sealing capacity dropped sharply.
- The method for applying mechanical shear in the hot-rolling process strongly differentiated the sealing performance of the materials relative to the samples without mechanical wear. The fluid loss results of the various material classes were impacted in a way that was consistent with the PSD degradation measured using high-speed mixing tests.
- For preventative treatment of lost circulation where the fracture size is known, wear-resistant particles with a size equal to or slightly larger than the fracture size appear to be an effective treatment with a volumetric concentration of 2%.
- For LCM pill application, cellulose-based additives achieved sealing with pressure exceeding 1300 psi when the slot size was around 1.5 times the D_{90} value of the particles, whereas the granular LCM mixture only achieved high sealing pressures when the largest particles were around the slot size.
- For analyzing the effectiveness of preventative treatment of lost circulation, the drilling fluid with LCM additives should be exposed to relevant thermal and mechanical wear prior to testing.

Acknowledgment

The authors would like to thank Jan Kristian Vasshus, Bjørn Berglind, and Swapan Mandal for technical support and the Research Council of Norway for financially supporting the project through RCN# 320646.

Conflict of Interest

There are no conflicts of interest.

Nomenclature

n = time period n
P_t = pressure at time t

Appendix

The equipment setup was as follows.
Conventional equipment used for HTHP fluid loss testing:

- Hamilton Beach Mixer
- Ohaus Pioneer Precision PX3202
- Ofite Filter Press HTHP 175 mL, Double Capped
- Ofite Viscometer model 900
- Ofite roller-oven #172-00-1-C
- Apera pH90, pH meter

Special experimental setup:

- Ohaus MB120 Moisture Analyzer
- Custom built transparent acrylic cell for enabling of reverse flow of fluid through the ceramic discs
- Festo pressure regulator LRP-1/4-2.5 and LRP-1/4-0.25
- Festo pressure sensor SPAN-P025R and SPAN-P10R
- Festo flowmeter SFAH-10U
- Nitrogen source and manifold for pressure up to 1350 psi, Ofite #171-24
- Vacuum machine, DVP EC.20-1
- Custom build permeability plugging apparatus with hydraulic pump for testing on slotted discs or ceramic discs up to 35 MPa (5076 psi)
- AEP transducers JET pressure gauge with data logger

References

[1] Alsaba, M., Nygaard, R., and Hareland, G., 2014, "Review of Lost Circulation Materials and Treatments With an Updated Classification," 2014 AADE Fluids Technical Conference and Exhibition, Houston, TX, Apr. 15–16, Paper No. AADE-14-FTCE-25.

[2] Alshubbar, G., Nygaard, R., and Jeennakorn, M., 2018, "The Effect of Wellbore Circulation on Building and LCM Bridge at the Fracture Aperture," J. Pet. Sci. Eng., **165**, pp. 550–556.

[3] Alsaba, M., Nygaard, R., Saasen, A., and Nes, O. M., 2014, "Lost Circulation Materials Capability of Sealing Wide Fractures," SPE Deepwater Drilling and Completions Conference, Sept. 10–11, Paper No. SPE-170285-MS.

[4] Khalifeh, M., Klungtvedt, K. R., Vasshus, J. K., and Saasen, A., 2019, "Drilling Fluids—Lost Circulation Treatment," SPE Norway One Day Seminar, May 14, Paper No. SPE-195609-MS.

[5] Alvi, M. A. A., Belayneh, M., Fjelde, K. K., Saasen, A., and Bandyopadhyay, S., 2021, "Effect of Hydrophobic Iron Oxide Nanoparticles on the Properties of Oil-Based Drilling Fluid," ASME J. Energy Resour. Technol., **143**(4), p. 043001.

[6] Contreras, O., Alsaba, M., Hareland, G., Hussein, M., and Nygaard, R., 2016, "Effect on Fracture Pressure by Adding Iron-Based and Calcium-Based Nanoparticles to a Nonaqueous Drilling Fluid for Permeable Formations," ASME J. Energy Resour. Technol., **138**(3), p. 032906.

[7] Klungtvedt, K. R., and Saasen, A., "The Role of Particle Size Distribution for Fluid Loss Materials on Formation of Internal Filter-Cakes and Avoiding Formation Damage," ASME 2022 41th International Conference on Ocean, Offshore and Arctic Engineering, Hamburg, Germany, June 21–30, Paper No. OMAE2022-79501.

[8] Grelland, S. S., 2021, "Analysis of Lost Circulation on the Norwegian Continental Shelf," M.Sc. thesis, University of Stavanger, Stavanger.

[9] Scott, P., Redburn, M., and Nesheim, G., 2020, "A Pragmatic Approach to Lost Circulation Treatments: What Every Drilling Engineer Should Know," 2020 AADE Fluids Technical Conference and Exhibition, Houston, TX, Apr. 14–15, Paper No. AADE-20-FTCE-062.

[10] Hoxha, B. B., Yan, L., Hale, A., and van Oort, E., 2016, "Automated Particle Size Analysis Using Advanced Analysers," 2016 AADE Fluids Technical Conference and Exhibition, Houston, TX, Apr. 12–13, Paper No. AADE-16-FTCE-78.

[11] Vivas, C., and Salehi, S., 2022, "Screening of Lost Circulation Materials for Geothermal Applications: Experimental Study at High Temperature," ASME J. Energy Resour. Technol., **144**(3), p. 033008.

[12] Majid, A. A. A., Saidian, M., Prasad, M., and Koh, C. A., 2015, "Measurement of the Water Droplet Size in Water-in-Oil Emulsions Using Low Field Nuclear Magnetic Resonance for Gas Hydrate Slurry Applications," Can. J. Chem., **93**(9), pp. 1007–1013.

[13] Wang, G., and Du, H., 2017, "Viscous Behavior and Wall Slip of Barite-Weighted Water-Based Drilling Fluids Containing a High Particle Fraction," J. Pet. Sci. Eng., **159**, pp. 773–782.

[14] Abrams, A., 1977, "Mud Design to Minimize Rock Impairment Due to Particle Invasion," J. Pet. Technol., **29**(5), pp. 586–592.

VII. Klungtvedt, K.R., Pedrosa, C., and Saasen, A. «Measuring Filter-cake Cohesive Strength and Flowability", Geoenergy Science and Engineering, Volume 221, February 2023, 111298. https://doi.org/10.1016/j.petrol.2022.111298 (open access)

Journal of Petroleum Science and Engineering 221 (2023) 111298

Contents lists available at ScienceDirect

Journal of Petroleum Science and Engineering

journal homepage: www.elsevier.com/locate/petrol

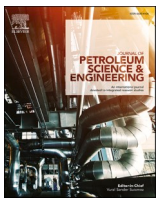

Measuring filter-cake cohesive strength and flowability

Karl Ronny Klungtvedt [a,b], Camilo Pedrosa [c], Arild Saasen [b,*]

[a] EMC AS, NO-4033, Stavanger, Norway
[b] University of Stavanger, NO-4036, Stavanger, Norway
[c] Norwegian University of Science and Technology, NO-7491, Trondheim, Norway

ARTICLE INFO

Keywords:
Measurement of filter cake cohesion
Measurement of filter cake flowability

ABSTRACT

The filter-cake has a critical role in temporarily reducing the permeability of the wellbore to prevent issues such as lost circulation, formation damage, wellbore collapse and differential sticking. The filter-cake's ability to perform these functions may be impaired by its deterioration caused by the circulation of fluid, swabbing or mechanical interaction. Therefore, being able to measure the strength of the filter-cake, and hence its ability to withstand disturbances, is important to ensure optimal drilling fluid design.Two water-based reservoir drilling fluids were used to produce filter-cakes under high differential pressures. The filter-cakes were thereafter analysed using a rheometer with a specially designed cell for accurate powder shear rheology. This enabled measurement of the cohesive strength and flowability of the filter-cakes.It was found that filter-cakes composed of a conventional reservoir drilling fluid with $CaCO_3$ and polymers, showed low cohesive strength and high flowability. The other fluid, which contained cellulose-based fibres in addition to $CaCO_3$ and polymers, showed much higher cohesion and lower flowability.It was concluded that the test methodology could be very useful in relation to optimising drilling fluid design, particularly for wells were lost circulation, wellbore stability and differential sticking may be relevant problems. It was also concluded that the addition of cellulose-based fibres may significantly increase the filter-cake strength in a water-based drilling fluid.

1. Introduction

During testing of drilling fluids, the fluid's ability to seal the formation is tested using API fluid loss tests or HTHP filtration tests. The properties of the filter-cake are typically described in terms of thickness and surface texture, whereas measurements of the filter-cakes' strength and flowability are not normally studied. During an over-balance drilling operation, the filter-cake is the primary barrier that isolate the higher wellbore fluid pressure from the formation pore-pressure, and thereby prevents fluid loss and pressure communication. Ideally, the filter-cake should have very low permeability and high cohesive strength. This would enable low fluid loss, a thin filter-cake and prevent differential sticking.

Differential sticking may appear when the drill-pipe comes in contact with the filter-cake. At the time of first contact, there is no suction pressure on the pipe. If the pipe is allowed to remain in contact with the filter-cake, the fluid pressure on the filter-cake side will start to fall and gradually move towards the formation pore pressure. Therefore, in a long-term static condition, the suction pressure on the pipe will move asymptotically towards being equal to the difference between the fluid pressure in the wellbore and the pore pressure in the formation. By multiplying the suction pressure with the contact area and the coefficient of friction between the drill-pipe and the filter-cake, the frictional force on the pipe is calculated.

The rate at which the suction pressure builds up is governed by the permeability of the filter-cake and the ease of disturbing or eroding the filter-cake in a dynamic setting, or alternatively seen as the cohesive strength and flowability of the filter-cake. Studies were conducted by Sheerwood and Meeten, 1997 with water-based fluids containing bentonite on the ratio of volume of liquid to volume of solids within the filter-cake. They found that lower void ratio was correlated with lower filter-cake permeability. In earlier studies, Sherwood et al. (1991) used a squeeze-film rheometry approach to study filter-cake yield stress, σ_0. They concluded that with a solids volume fraction, φ, between 0.09 and 0.6, the yield stress could be expressed as function of φ for the fluid studied. Also, they showed that the bentonite filter-cakes compacted over time, and that φ reached an equilibrium value for a given applied pressure.

An intact and low-permeability filter-cake will substantially prevent the build-up of suction pressure on the drill-pipe leading to differential

* Corresponding author.
E-mail address: arild.saasen@uis.no (A. Saasen).

https://doi.org/10.1016/j.petrol.2022.111298
Received 6 May 2022; Received in revised form 31 October 2022; Accepted 26 November 2022
Available online 14 December 2022

sticking. In contrast, a high-permeability filter-cake will lead to higher fluid loss and a faster growth of the filter-cake thickness. As the filter-cake thickness grows, the potential area of contact with the drill-pipe increases. Further, if the cohesion of the filter-cake is low it becomes easier for the pipe to become « tucked-in» so that the contact area increases further, and the pressure barrier is damaged. Therefore, to prevent differential sticking, a filter-cake with very low permeability and high cohesive strength is ideal.

Studies of static fluid loss tests shown that after the initial spurt loss, the fluid loss follows a linear function when plotted against the square root of time. Klungtvedt and Saasen, 2023 used such regression models to calculate the permeabilities of filter-cakes for water-based drilling fluids. In a dynamic condition, the filter-cake will reach a state where the rate of erosion equals the rate of filter-cake build-up, such that the fluid loss follows a linear function against time. By measuring the cohesive strength and flowability of the filter-cake, the differences between static and dynamic fluid loss may be better understood.

The study of powder rheology can be done by measuring the dynamic flow and the shear properties of the powders, where the powder itself may be a combination of liquids, solids and gases. Pedrosa et al. (2021) applied the methodology of measuring wet-granular rheology to calculate the internal friction coefficient of cuttings bed, which provides an insight into the particle cohesion properties. The test methodology used in the study by Pedrosa was also selected for the present study. The primary function is to use a powder shear cell to measure the resistance to flow at low shear rates.

The findings that Pedrosa made when studying cuttings beds may also have some relevance to drilling fluid filter-cakes. He concluded that water-based fluids made with KCl and polymers packed cuttings in a dense manner, where the particles moved in clusters. In contrast, the particles were packed in a loose configuration when submerged in an oil-based fluid, and hence single particles could be moved more freely. These data may indicate that an external filter-cake formed by oil-based drilling fluids may erode more readily than that of a water-based drilling fluid.

The main objectives of the study were:

- To determine if a powder shear cell could be used to effectively analyse the cohesive strength and flowability of filter-cakes, and
- To determine if different drilling fluid compositions would lead to significantly different values of cohesiveness and flowability

2. Methods

The flow behaviour of powders is mostly non-Newtonian, where the resistance to flow falls with higher shear rates. Typically filter-cakes have moisture levels in the range of 15–50% by weight, primarily depending on the solids content of the fluids. Therefore, in order to study the rheology of the filter-cakes, it is important that they are kept in original condition, without being dried. The filter-cakes were made in HTHP tests using ceramic discs.

The test is conducted using a 4.5 mL Anton Paar powder shear cell. It is designed for analysis of powders and uses standard test loops with high precision measurements. The methodology uses the Mohs-Coulomb failure envelop theory, which is conventionally used to describe brittle materials or materials where the compressive strength significantly exceeds the tensile strength, by comparing the measured shear stress with the applied normal stress. Labuz et al., 2012 provides a good insight into the mechanisms and governing equations. The Mohr-Coulomb failure is expressed by equation (1).

$$\tau = \sigma \tan(\varphi) + c \tag{1}$$

where τ is the shear strength, σ is the normal stress, φ is the angle of internal friction and c is the cohesion or the inherent shear strength. The coefficient of internal friction μ is calculated using equation (2).

$$\mu = \tan(\varphi) \tag{2}$$

Fig. 1 shows the shear cell and the stem with the blades. The test material is placed into the cell without initial compaction. Excess materials is scraped off to provide an even surface.

After the filter-cake is placed in the test cell, a maximum normal stress is applied, before the sample is sheared at constant rotation until reaching the cake's failure and the shear stress is measured, this procedure is repeated at 30%, 50% and 70% of the maximum initial normal stress. The test cell is designed with a small open area around the top of the test cell, so that it can identify if powders simply overflow when a given normal pressure is applied. For certain free flowing powders, there will hence we a limit to the applied normal pressure. With the three shear-to-failure points is possible to obtain the yield locus of the Mohr-Coulomb failure envelop, and from there calculate the unconfined yield strength and the major principal stress as shown in Fig. 2.

The unconfined yield stress (σ_c) which represents the major principal stress that will cause the cake to in an unconfined state to fail in shear, together with the major principal stress (σ_1) under normal stress, will provide the flowability of the cake in terms of its Flow Function Coefficient (ffc), as described in equation (3). This flowability is divided into five regions, according to the ffc as follows: not flowing (ffc <1), very cohesive (1< ffc <2), cohesive (2< ffc <4), easy flowing (4< ffc <10) and free flowing (ffc>10).

$$ffc = \frac{\sigma_1}{\sigma_c} \tag{3}$$

Equipment used for testing:

- Hamilton Beach Mixer, for mixing of drilling fluids
- Ohaus Pioneer Precision PX3202, for weighing the drilling fluid ingredients
- Custom built Permeability Plugging Apparatus with hydraulic pump for testing slotted discs or ceramic discs up to 35 MPa (5076 psi)
- AEP Transducers JET Pressure Gauge with Data Logger, for measuring and logging applied pressure
- Ofite Viscometer model 900, for measuring fluid rheological parameters
- Ofite roller-oven #172-00-1-C, for aging the drilling fluid samples
- Apera pH90, pH meter, for pH measurements
- Anton Paar MCR-301 Rheometer with Powder Shear Cell

3. Results

3.1. Drilling fluid composition and fluid loss tests

Four fluid compositions, shown in Table 1, were selected to represent typical water-based reservoir drilling fluids. Xanthan Gum was used to provide viscosity, starch for fluid loss control and $CaCO_3$ (ground marble) and cellulose based fibres to provide bridging. To ensure sufficient filter-cake thickness for conducting the tests in the powder shear cell, the concentration of starch was kept a little lower than what might be ideal from a fluid loss perspective. The filter-cakes were made by testing the fluids under high differential pressures on 50 μm ceramic discs. Fluid 1 and 2 were tested with average pressures of 1500 psi for 30 min, whereas Fluid 3 and 4 were tested with average pressures of 2400 psi for 40 min.

3.2. Filter-cake shear rheology measurements

Fluid 1 was tested with a maximum applied normal pressure of 3 kPa, as the sample disintegrated and overflowed above this pressure. The disintegration of the filter-cake is evidence of low cohesion and high flowability. The Mohr-Coulomb failure envelope is presented in Fig. 3. The obtained cohesion was 495 Pa and the internal friction angle 14°.

For Fluid 2, testing was conducted at 3, 6 and 9 kPa applied normal

Fig. 1. Anton Paar Powder Shear Cell and stem.

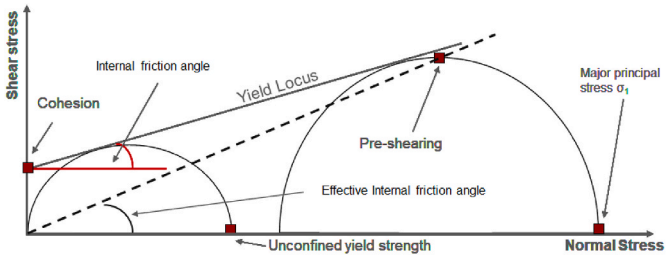

Fig. 2. Mohr-Coulomb failure envelope obtained by rheometry.

Table 1
Drilling fluid recipes 1-4.

Component and mixing sequence	Fluid 1 recipe (kg/m3)	Fluid 2 recipe (kg/m3)	Fluid 3 recipe (kg/m3)	Fluid 4 recipe (kg/m3)
Water	950.6	936	947.6	933
Na2CO3	0.057	0.057	0.057	0.057
NaOH	0.71	0.71	0.71	0.71
Xanthan Gum	4.29	4.29	4.29	4.29
Starch	11.4	11.4	14.25	14.25
MgO	1.43	1.43	1.43	1.43
NaCl	28.57	28.57	28.57	28.57
CaCO3 (<53 μm)	57.14	57.14	57.14	57.14
Cellulose based material with D90 of 75 μm (AURACOAT UF)		14.29		14.29

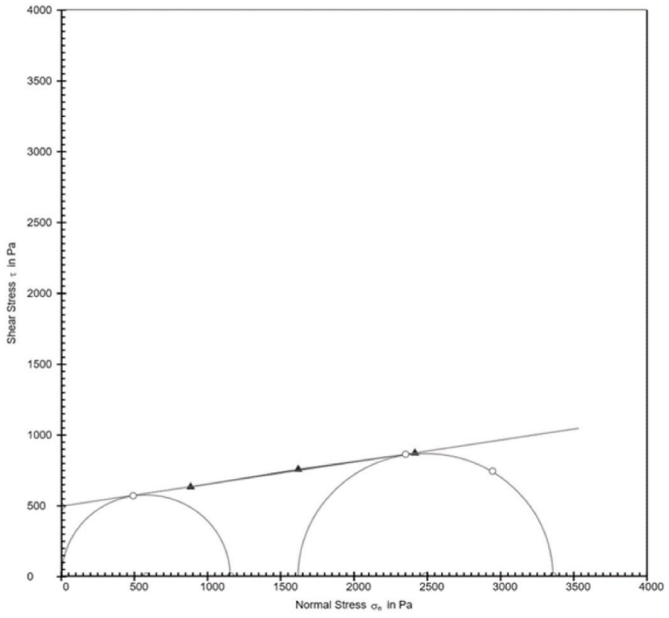

Fig. 3. Mohr-Coulomb failure envelope for Fluid 1 at 3 kPa.

pressures as presented in Fig. 4. The cohesion ranged from 2271 Pa to 3167 Pa, which is around 5 to 6 times that of Fluid 1, and the internal friction angles were from 31° to 44°, indicating lower flowability.

Fluid 4 showed similar characteristics as Fluid 1, and were tested at 1, 2 and 3 kPa normal pressures. Fig. 5 presents these plots, and as for Fluid 1, it can be seen that the Mohr's circles did not overlap for most test conditions. The Cohesion was measured to range from 261 Pa to 361 Pa and the friction angles in the range from 14° to 19°.

Fluid 4 was tested at normal pressures of 1, 2 and 3 kPa, to facilitate a comparison with Fluid 3. The Mohr-Coulomb failure envelopes are presented in Fig. 6. The Cohesion was measured to range from 1032 Pa for the 1 kPa normal pressure test to 1731 Pa for the 3 kPa normal pressure test, and the internal friction angles ranged from 53° to 34°. Relative to Fluid 3, the Cohesion was 4–5 times higher under the same normal pressure conditions, and the friction angle more than double.

The overall unconfined yield strengths were plotted against the major principal stresses for each of the tests. These data are presented in Fig. 7. Using the separation into different flow regimes, it is clear that Fluid 2 and 4 show significantly higher levels of cohesion than Fluid 1 and 3, which appear to be in the range from cohesive to easy flowing. For Fluids 3 and 4, the unconfined yield strength appears to potentially be independent of the major principal stress, within the tested principal stress range. Given that Fluids 2 and 4 are very similar, but tested at different major principal stresses, viewing the two plots together may be relevant. Using this approach it may be interpreted that the unconfined yield strength is constant below a certain major principal stress level, and that when this stress level is exceeded, the unconfined yield strength follows a linear relationship with the major principal stress.

The datapoints for each of the tests are listed in Table 2. Herein, the calculated internal friction angles were lower for higher values of applied normal pressure for all the tests where multiple normal pressures were applied. This also corresponds to higher flowability factors coefficients, for higher applied normal pressures.

4. Discussion

The method of testing filter-cakes using advanced rheometry introduces sources or error and conditions which are unlike those seen in a wellbore. As an example, the filter-cakes were produced under high differential pressures, whereas the rheology studies were conducted without a confining fluid pressure.

The testing using the Anton Paar powder shear cell functioned in a satisfactory manner. The cell required a filter-cake volume of at least 4 mL, and hence the drilling fluid composition and filtration tests need to be conducted in a way that would produce a filter-cake with sufficient thickness. The fluid compositions applied included concentrations of starch ranging from 11.4 to 14.25 kg/m3 to ensure a slightly higher fluid-loss and filter-cake build up. This is somewhat lower than what is conventionally used in wellbore application. Given that the testing was successful, it is natural to conduct future tests with fluid compositions that more closely resemble a field fluid with optimised values of polymers and presence of drilled solids.

The results showed very clear differences between the fluids with and without the cellulose-based fibres. It was clear that the fluid

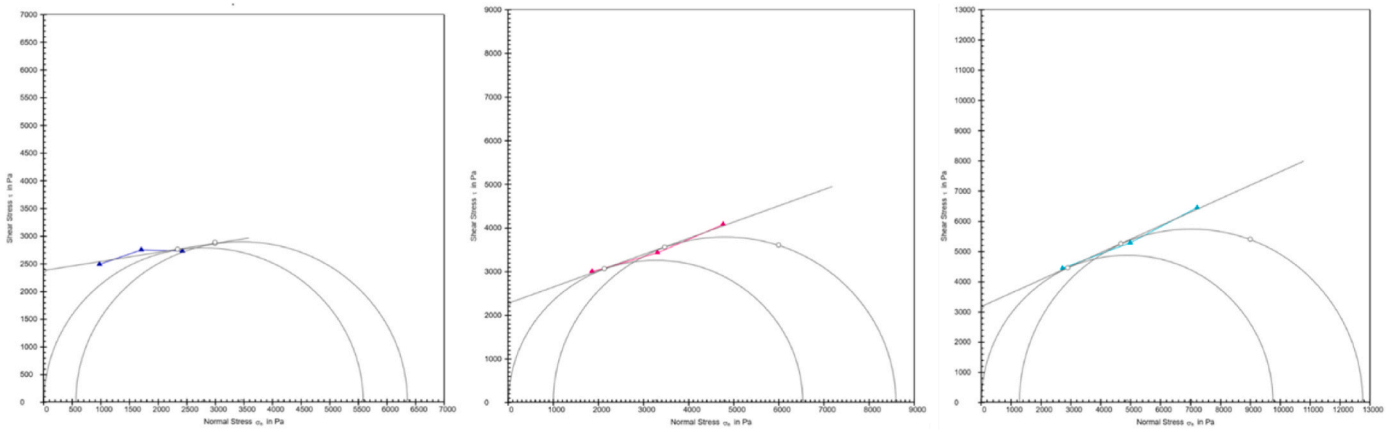

Fig. 4. Mohr-Coulomb failure envelope for Fluid 2 at 3, 6 and 9 kPa.

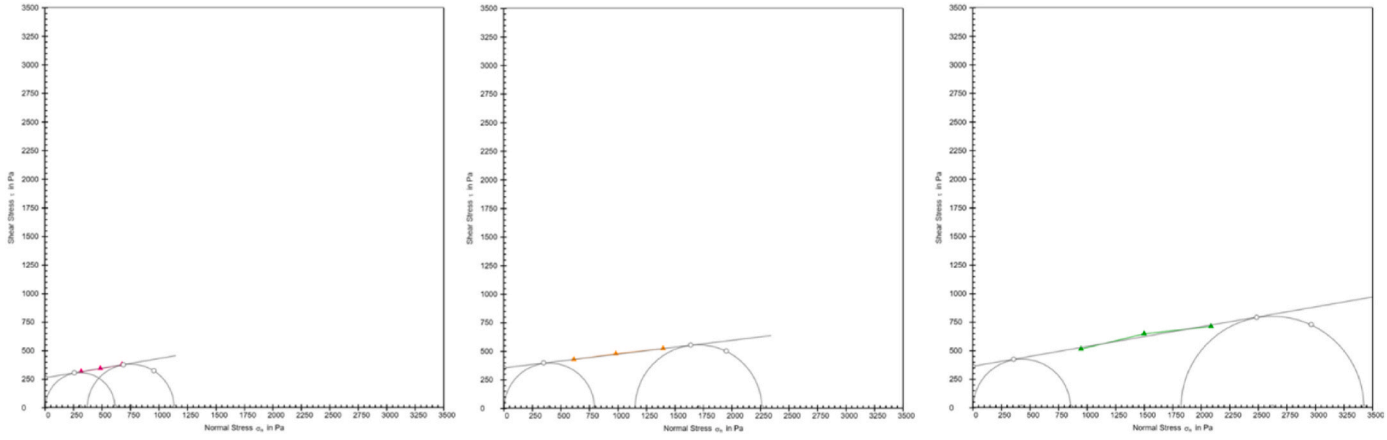

Fig. 5. Mohr-coulomb failure envelope for Fluid 3 at 1, 2 and 3 kPa.

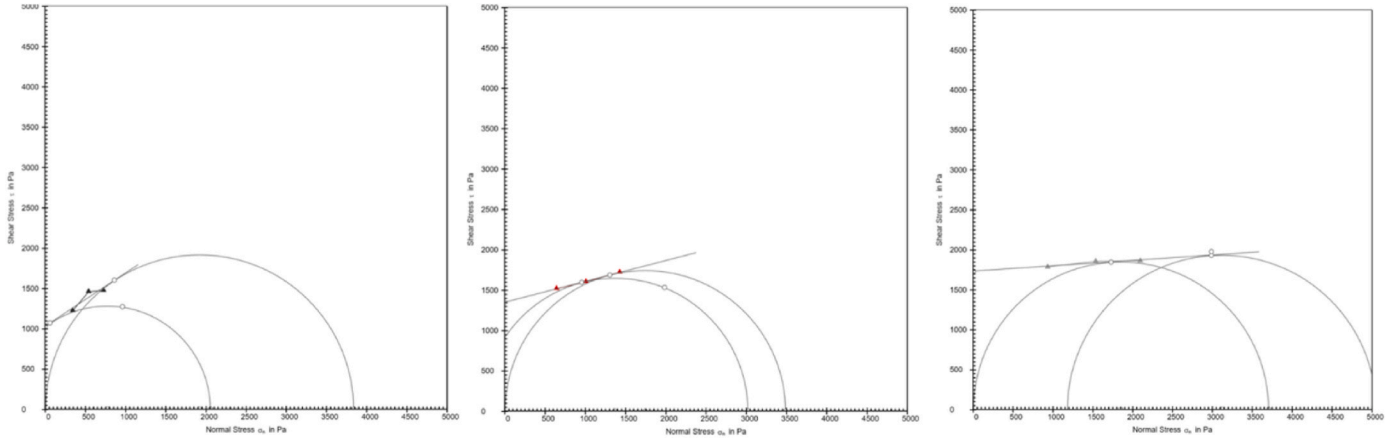

Fig. 6. Mohr-coulomb failure envelope for Fluid 4 at 1, 2 and 3 kPa.

containing $CaCO_3$ as the only solid, created a filter-cake with low cohesive strength and high flowability.

Extending the results to field applications, it may be expected that the fluid without cellulose-based non-invasive fluid additives would be exposed to rapid filter-cake erosion, higher fluid-loss and greater risk of differential sticking, whereas the addition of the tested cellulose-based additives may present a significant reduction of these risk factors.

A cause of the improved filter-cake cohesion for Fluid 2 and 4 may be polar interaction of the cellulose-based fibres and the dispersed polymers in the fluid. Such interaction may take the form of higher adhesive and frictional forces between the particles, and thereby increased shear strength.

Studying the data in further detail, the internal friction angle, or alternatively the coefficient of internal friction, was not constant for either Fluid 2, 3 and 4 as the applied normal stresses varied. For the filter-cakes of each of the three fluids, a higher applied normal pressure led to a lower coefficient of internal friction. For the mentioned filter-cakes, also the highest applied normal pressure led to the largest

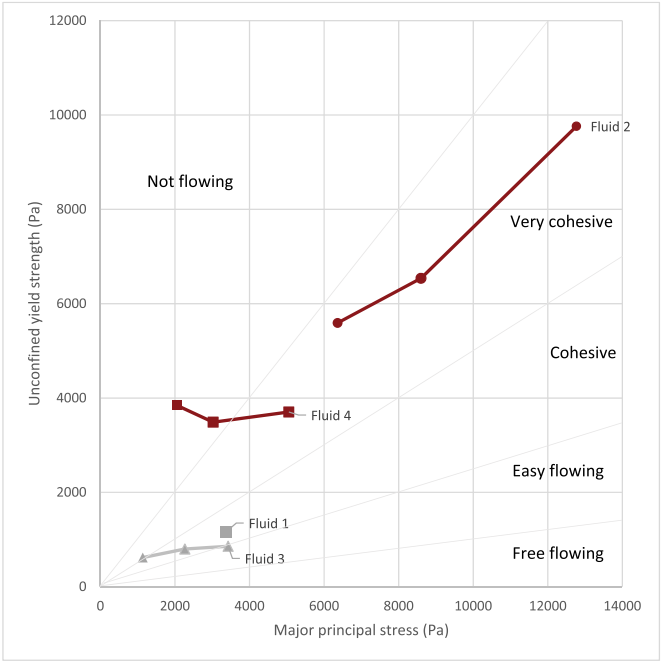

Fig. 7. Flowability of fluid 1–4.

recorded cohesion. The classical Mohr-Coulomb shear strength criterion describes the shear strength as a linear function of the normal stress and the coefficient of internal friction plus the cohesion constant. The observed behaviour indicates that a nonlinear relationship exists when different normal stresses are applied. Shen et al. (2018) presented a nonlinear modified Mohr-Coulomb shear strength criterion for analysing intact rocks. Their model also showed a transition from brittle to ductile behaviour upon reaching a critical level of normal stress, following Barton (1976). At this critical state, the failure envelope becomes horizontal, and the maximum shear strength is half of the normal compressive strength. The tests conducted using the filter-cakes of Fluid 1–4 showed some of the same behaviour as observed by Shen et al. and Barton, however, the testing conducted did not replicate a wide enough range of normal stresses to fully describe the behaviour of the filter-cakes.

5. Conclusions

The conclusions regarding the main objectives of the study are as follows:

- The application of the powder shear cell for measuring the flowability and cohesion of drilling fluid filter-cakes worked well. The test results showed that fluids with relatively similar compositions also yielded similar results.
- A total of four test were conducted successfully and where the primary differences were the addition of an ultra-fine cellulose based non-invasive fluid additive in fluids 2 and 4. The addition of the cellulose-based additive created a significantly higher cohesive strength and lower flowability of the filter-cakes.
- The results from the testing indicate that a Fluid 2 and 4, containing the cellulose-based additive, would provide improved resistance towards erosion of the filter-cake due to fluid circulation and potentially reduced risk of differential sticking.
- Future testing should be attempted across a wider range of pressures to identify if the type of deformation could be identified to change from brittle to ductile at critical normal pressure levels.
- Future testing should be attempted for oil-based filter-cakes to facilitate comparison of the cohesive strength and flowability of filter-cakes made with similar weighting agents and bridging materials, but with different base fluids.

Credit author statement

Karl Ronny Klungtvedt: Conceptualization, Methodology, Validation, Investigation, Writing - Original Draft, Collecting material for experiments, Writing - Review & Editing, Funding acquisition. Camilo Pedrosa; Methodology, Validation, Investigation, Performing experiments, Arild Saasen: Conceptualization, Writing - Original Draft, Writing - Review & Editing, Supervision.

Declaration of competing interest

The authors declare that they have no known competing financial interests or personal relationships that could have appeared to influence the work reported in this paper.

Table 2
Data summary.

	Applied normal pressure (Pa)	Cohesion, c (Pa)	Unconfined yield strength, σ_c (Pa)	Major principal stress, σ_1 (Pa)	Flowability factor coefficient, ffc	Internal fricion angle, φ	Coefficient of internal friction, μ = tan(φ)
Fluid 1	3000	495	1156	3360	2.91	14.14	0.252
Fluid 2	3000	2375	5593	6365	1.14	44	0.966
Fluid 2	6000	2271	6538	8598	1.32	31.07	0.603
Fluid 2	9000	3167	9762	12,770	1.31	30.99	0.601
Fluid 3	1000	261	618	1136	1.84	18.79	0.340
Fluid 3	2000	354	799	2263	2.83	14.39	0.257
Fluid 3	3000	361	858	3425	3.99	13.83	0.246
Fluid 4	1000	1032	3841	2060	0.54	52.92	1.323
Fluid 4	2000	1349	3488	3022	0.87	37.74	0.774
Fluid 4	3000	1731	3704	5054	1.36	33.53	0.663

Data availability

No data was used for the research described in the article.

Acknowledgements

The authors would like to thank Research Council of Norway for financially supporting the project through RCN# 320646 and RCN# 294688.

References

Barton, N., 1976. The shear strength of rock and rock joints. Int. J. Rock Mech. Min. Sci. Geomech. Abstracts 13 (9), 255–279.

Klungtvedt, K.R., Saasen, A., 2023. The role of particle size distribution for fluid loss materials on formation of filter-cakes and avoiding formation damage. Journal of Energy Resources Technology 145 (4), 041702. https://doi.org/10.1115/1.4056187.

Labuz, J.F., Zang, A., Mohr-Coulomb, 2012. Failure criterion. Rock Mech. Rock Eng. 45, 975–979. https://doi.org/10.1007/s00603-012-0281-7.

Pedrosa, C., Saasen, A., Lund, B., Ytrehus, J.D., 2021. Wet drilled cuttings bed rheology. Energies (14), 1644. https://doi.org/10.3390/en14061644.

Sheerwood, J.D., Meeten, G.H., 1997. The filtration properties of compressible mud filtercakes. J. Petrol. Sci. Eng. 18, 73–81.

Sherwood, J.D., Meeten, G.H., Farrow, C.A., Alderman, N.J., 1991. Squeeze-film rheometry of non-uniform mudcakes. J. Non-Newtonian Fluid Mech. 39 (Issue 3), 311–334.

Shen, B., Shi, J., Barton, N., 2018. An approximate nonlinear modified Mohr-Coulomb shear strength criterion with critical state for intact rocks. J. Rock Mech. Geotech. Eng. 10, 645–652, 2018.

VIII. Klungtvedt, K.R., Vasshus, J.K., Nesheim, G., Scott, P.D. "Managing High Differential Pressures in Fractured Carbonate Reservoir by use of Wellbore Strengthening Material", OTC-32173-MS, Offshore Technology Conference 2023, Houston, Texas, USA. https://dx.doi.org/10.4043/32173-MS

Please note: This paper is not included in the repository due to copyright restrictions.

IX. Klungtvedt, K.R., Vasshus, J.K., Saasen, A. “Assessment of induced fracturing and fracture sealing during drilling”, Geoenergy Science and Engineering, Volume 226 (2023) 211816. https://doi.org/10.1016/j.geoen.2023.211816 (open access)

226 (2023) 211816

Contents lists available at ScienceDirect

Geoenergy Science and Engineering

journal homepage: www.sciencedirect.com/journal/geoenergy-science-and-engineering

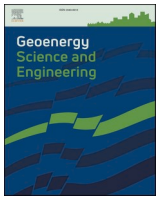

Assessment of induced fracturing and fracture sealing during drilling

Karl Ronny Klungtvedt [a,b], Jan Kristian Vasshus [b], Arild Saasen [a,*]

[a] University of Stavanger, NO-4036, Stavanger, Norway
[b] EMC AS, NO-4033, Stavanger, Norway

ARTICLE INFO

Keywords:
Induced fracture
Fracture sealing
Drilling fluid testing
Wellbore strengthening
Loss prevention
Lost circulation
Dual mode particle size distribution

ABSTRACT

Laboratory testing of lost circulation or loss prevention materials are typically studied either using permeable ceramic discs or sealing of slotted steel discs. Such studies may well reflect the sealing of a permeable formation or the plugging of an existing fracture. When drilling a permeable formation with a high overbalance, the pressure from the wellbore sometimes induces fractures and thereby cause the potential for severe lost circulation incidents. In such situations, it is important that the drilling fluid is composed such that the fracture is sealed rapidly, and that fracture propagation does not occur.

Testing of induced fracturing is very limited due to the complexity of the equipment and access to cores which may adequately represent a formation. The objective of the study was to design an experimental method for assessing the functionality of a drilling fluid to seal induced fractures in a porous formation, and to apply the method for evaluating different fluid compositions. A method was developed using ceramic discs and adapting a conventional permeability plugging apparatus to induce fractures in the disc during a high-pressure fluid-loss test. This permitted a study of the rupturing and re-sealing of the filter-cake when a fracture was induced. The method was applied to water-based (WBM) and oil-based fluids (OBM) containing different loss prevention materials (LPM), and the method facilitated studying the permeability of filter-cakes as well as the fluid loss occurring at the fracturing stage. The method thereby enabled to clearly separate the performance of different fluids for sealing of induced fractures even when the fluids showed similar permeability plugging characteristics.

The loss prevention materials used for the study was selected among mixtures typically applied for drilling campaigns in the North Sea, and cross references to field applications are included. The study showed that lower fluid loss was observed with oil-based fluids than with water-based fluids. However, once the discs fractured, the water-based fluids treated with loss prevention materials sealed the fractures in the discs with lower fluid-loss than similarly treated oil-based fluids.

1. Introduction

When designing a fluid for sealing permeable formations, particles are normally selected based on one of several recognised particle size selection methods. Two such methods are the Ideal Packing Theory (IPT), proposed by Kaeuffer (1973) and Abrams rule (1977). The Ideal Packing Theory aims at selecting a size distribution of particles that allow for forming a low porosity and low permeability filter-cake. It claims that the packing of a filter-cake is optimal when the particle cumulative volume (%) forms a linear relationship with the square root of the particle diameter. The Abrams rule aims at sealing a formation effectively without causing excessive solids-invasion and permeable formation damage. This is achieved by selecting a median particle size $\geq$1/3 the median pore size and with a minimum volumetric concentration of particles of 5%. When it comes to sealing fractured formations, the approach from Alsaba et al. (2017) states that sealing is effective when the D50 particle size $\geq$3/10 of the fracture width and D90 particle size $\geq$6/5 of the fracture width. When studying situations when a fracture is induced in a permeable reservoir formation, it would be natural to consider all three approaches when optimising a drilling fluid design. The difference between the Abrams rule and the Alsaba method are not substantial if the fracture width and the medium pore size are relatively similar. In such conditions, both approaches will yield relatively similar D50 particle size recommendations. It may, however, be difficult to find an approach that satisfies the criteria of Kaeuffer, Abrams and Alsaba if the fracture size deviates considerably from the median pore size.

Fracture initiation and fracture growth are conditions required for

* Corresponding author.
E-mail address: Arild.saasen@uis.no (A. Saasen).

https://doi.org/10.1016/j.geoen.2023.211816
Received 20 February 2023; Received in revised form 9 April 2023; Accepted 18 April 2023
Available online 20 April 2023

lost circulation to occur through an induced fracture. During drilling, leak-of tests (LOT) may be conducted to identify the fracture initiation pressure (FIP) and the fracture propagation pressure (FPP). These pressures are a function of the in-situ stresses, the mechanical properties of the formation, the drilling fluid and the complex interaction of these factors. Feng et al. (2016) presented a review on fracture initiation and fracture propagation and highlighted some important findings. They concluded that the recorded leakoff pressure may be higher than the actual FIP as the drilling fluid may contain particles that seal the initial fracture. Therefore, an observed leakoff pressure may actually be a filter-cake breakdown pressure. Further, they conclude that wellbore strengthening may be achieved through fracture plugging and that this is particularly effective in conditions where the pore pressure is significantly smaller than the minimum horizontal stress, such as for depleted reservoirs. Feng et al. also discuss the importance of capillary-entry pressures and its special importance when the base fluid of the drilling fluid is different to that of the formation fluid. In conditions with high capillary pressures, such as using OBM to drill a water-wet shale, the fluid leakoff may be significantly restricted and hence the fluid pressure is transmitted to the fracture tip. A study by Fekete et al. (2013) also concluded that preventative treatment with lost circulation materials (LCM) was most effective in enhancing the strength of the wellbore in depleted reservoirs.

(Gao et al. 2021a, b) conducted multiple studies on enhancement of wellbore stability in shale formations. They conducted both one dimensional pore pressure response tests and triaxial compressive strength tests with nanomaterials and concluded that 10–30 nm particles could reduce pore pressure transmission and increase uniaxial compressive strength of shales.

Ma et al. (2019) tested various fluid compositions as part of a core fracturing experiment. They used 100 mm diameter and 140–150 mm length cores with a circular hole of 10 mm. The cores were made of Portland cement and quartz sand. Their studies showed that water-based fluids achieved fracture pressures ranging from 19 MPa to 26.6 MPa, whereas the fracture pressures for OBM, with the same LCM additives, ranged from 12.3 MPa to 22.5 MPa. On average, the fracture pressures were 52% higher with WBM and at the same time the API fluid loss values being on average 26% higher with WBM. They concluded that adding barite as a weighting agent increased the fracture pressure, whereas the inclusion of nanomaterials was found to have little effect.

A practical approach to increasing the near-wellbore formation breakdown pressure was presented by Fuh et al. (1993a, b and 2007). The method included use of granular loss prevention materials sized between 250 and 600 μm to seal fractures up to 500 μm. The method was later used by Scott et al. (2012, 2020), Klungtvedt and Saasen (2022) and Klungtvedt et al. (2023b) in laboratory studies and field applications. The laboratory tests were conducted on 500 μm slotted discs to simulate fracture sealing and in certain tests involved exposing the LPM to mechanical wear before application. Klungtvedt et al. (2023a) conducted a study on measuring the cohesion and shear strength of filter-cakes using water-based fluids. They concluded that the inclusion of certain cellulose-based additives in the fluid significantly increased the cohesion and shear strength of the filter-cakes. By designing a study where the filter-cake is formed before the fracture is induced, it may be possible to identify if filter-cakes with high cohesion and shear strength better resist a filter-cake breakdown or aid the re-sealing of a fracture. The present study was designed to study the performance of different fluids and LPMs in the situation when a permeable formation breaks, and a fracture is opened up. Both water-based and oil-based fluids were studied. A combination of $CaCO_3$ and cellulose based LPMs were introduced to reflect relevant fluids for depleted carbonate reservoirs.

The challenge of induced fracturing is relevant for drilling of wells for oil and gas production, geothermal wells and wells for CO_2 injection. The laminar flow of a fluid through a porous medium is described by the Darcy's law, however, when a fracture is induced under high differential pressure, the conditions of flow change abruptly. Also, when new formation is being drilled, any initial formation fluid equilibrium is disturbed during the spurt-loss phase when the drilling fluid filtrate is penetrating the permeable formation and causes changes in the pore-pressure. The hydraulic head losses occurring during the fluid filtration process will impact the formation strength and the induction of fractures. Mohammadizadeh et al. (2021) present an analysis for hydraulic effects of flow through porous media, which may further help to explain such mechanisms.

The paper is structed by first introducing the equipment and method used, followed by laboratory test results and observations and a discussion of the results and the methodology.

Objectives and considerations:

- Evaluate the feasibility of the novel test methodology for assessing induced fracture sealing in permeable formations.
- Establish fluid loss and filter-cake permeability of different fluids and LPM combinations at different pressures.
- Establish fluid loss and re-sealing pressures upon fracturing of the discs
- Identify patterns or differences in performance between the different base fluids and LPMs

Equipment and method:

The method involves using a conventional permeability plugging apparatus designed for application of industry standard ceramic discs. The discs used in the study were supplied by OFITE part number #170–55, with specified mean pore-size of 10 μm, a diameter of 2 ½ inches (≈6.35 mm) and depth of ¼ inch (≈0.635 mm). By making the surface of the end cap slightly uneven, the inflexible ceramic discs fracture at certain applied pressures The difference between the inner diameter of the test cylinder and the outer diameter of the test discs was around 0.6–0.7 mm, thus after fracturing the discs could be forced towards to wall of the test cylinder and the maximum theoretical width of any fracture would be limited to 0.6–0.7 mm. The design pressure of the test assembly was 35 MPa.

Samples of laboratory made WBM and OBM field fluid were treated with different LPMs and hot-rolled for 16 h at either 112° or 120 °C to reflect two different reservoir temperatures. Included in each hot-rolling cell was a 135 mm long threaded M16 stainless steel bar, to simulate mechanical wear that LPM particles would be exposed to during circulation in a field operation as described by Klungtvedt and Saasen (2022). The testing was conducted at an initial temperature of 70 °C and rising towards 75–78 °C during each test. The increase in temperature also raised the pressure in the test cell slightly. During the tests, the mass of the fluid filtrate was logged every 5 s, and the applied pressure was logged every second. The mass of the fluid filtrate was thereafter converted to a volumetric plot, using the average density of the filtrate. Fig. 1 presents a schematic of the test equipment.

The applied cellulose based LPM materials were Supplied by European Mud Company AS and had the following specifications:

- Cellulose fibre A (AURACOAT UF®), D90 value of 75 μm and density of 1.35–1.55 g/cm^3), highly soluble non-invasive fluid additive for increasing filter-cake strength and lowering filter-cake permeability in applications up to 150 °C.
- Cellulose fibre B (AURAFIX UF®), D90 value of 75 μm and density of 1.35–1.55 g/cm^3), non-invasive fluid additive for increasing filter-cake strength and lowering filter-cake permeability in applications up to 200 °C.
- Granular cellulose (AURACOAT C®), D99 value of 600 μm and density of 1.30–1.38 g/cm^3), loss prevention and wellbore strengthening material for sealing of induced or natural fractures

2. Results and observations

Three base fluids were used for the study. Each of these were tested

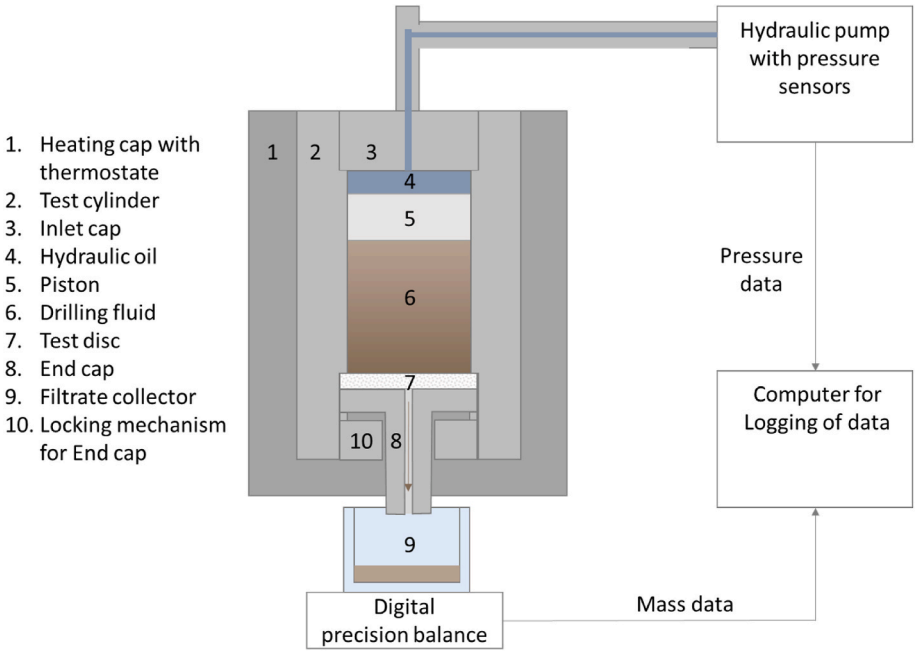

Fig. 1. Schematic of test cylinder and data logging setup.

with different combinations of loss prevention materials. The LPMs were added prior to hot-rolling with the threaded steel rod. For Fluid 1, hot rolling was conducted at 112 °C for 16 h. For Fluids 2 and 3, the temperature was 120 °C. Fluids 1 and 2 were laboratory fluids that had been optimised for reservoir drilling, however without the presence of drilled solids. To simulate the accumulation of fine drilled solids in a carbonate reservoir, $CaCO_3$ particles with a D50 value of 50 μm was added to some of the tests to identify any differences in sealing performance. The tests were also conducted with and without various cellulose based LPMs as presented in Table 1.

Earlier studies have shown that non-degraded $CaCO_3$ with a D50 value of 50 μm can effectively seal 120 μm pore-size ceramic discs when applied in a concentration of 85.5 kg/m^3, e.g. Klungtvedt et al. (2021). This is in line with the Abrams rule (Abrams, 1977), which recommends using particles with a D50 value $\geq$ 1/3 of the formation average pore size. However, after exposing the fluid to mechanical wear during the hot-rolling process it has been shown that the $CaCO_3$ degrades sufficiently to fail a 120 μm ceramic disc test even when applied in 114 kg/m^3 concentration (Klungtvedt and Saasen, 2023). Applying the logic of the Abrams rule, this indicates that the D50 value of the $CaCO_3$ particles degraded to significantly less than 40 μm during the hot-rolling process using the threaded steel rod. This is also consistent with the findings of Scott et al. (2012), where $CaCO_3$ (ground marble) particles larger than 44 μm were shown to degrade during exposure to shearing.

Fluids 1 and 2 were both water-based. The main differences were the finer size of $CaCO_3$ particles in Fluid 2 and the inclusion of polyethylene glycol (PEG) and slightly higher concentration of Xanthan Gum. Jiang et al. (2011) showed that PEG has good effect on shale and gas-hydrate inhibition and can prevent pollution related to presence of calcium and magnesium ions. The specified D50 value of the $CaCO_3$ in Fluid 2 was 5 μm, thus indicating that it would be effective for sealing of formations with pore-size up to 15 μm, following the Abrams rule. The viscosity (at 49 °C) of Fluid 2 was noticeably higher than that of Fluid 1 after hot-rolling, as presented in Fig. 2. The difference in viscosity could be expected to impact the fluid-loss and fracture sealing ability of the fluid.

Table 1
Fluid recipes and additions of LPM materials.

Description	Fluid 1	Fluid 2	Fluid 3
Base Fluid	1.09 sg KCl-polymer fluid, 85.5 kg/m^3 $CaCO_3$, 1–150 μm	1.10 sg KCl-polymer glycol fluid, 57 kg/m^3 $CaCO_3$, 1–15 μm	1.62 sg oil-based field fluid with drilled solids, sieved through API140, 106 μm sieve
A) Cellulose fibre A (D90 = 75 μm)	14.25 kg/m^3	8.55 kg/m^3	
B) Cellulose fibre B (D90 = 75 μm)		8.55 kg/m^3	
C) $CaCO_3$ (D50 = 50 μm, D100 = 150 μm)	28.5 kg/m^3	57 kg/m^3	
G) Granular cellulose (D99 = 600 μm)		28.5 kg/m^3	28.5 kg/m^3

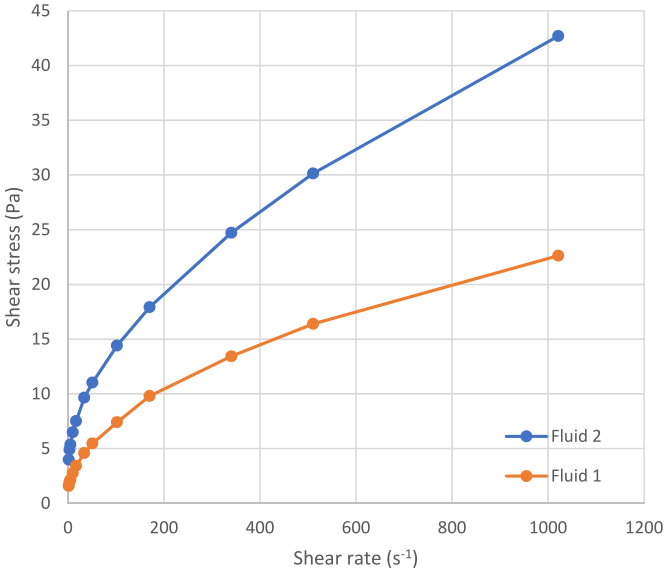

Fig. 2. Flow curves of Fluids 1 and 2 after hot-rolling.

The difference in viscosity of the two fluids reflect that they were designed to be applied in different sections of a well. Fluid 1 was designed for a 6-6 ½ inch diameter reservoir, whereas Fluid 2 was designed for application in a 12 ¼ inch diameter section. The flow curve of Fluid 3 showed high and inconsistent shear stress readings, likely due to high solids content and particle size above 100 μm.

The fractured disc tests were conducted on ceramic discs with a mean pore-size of 10 μm. The discs were selected on the basis of representing a low-to moderate permeability formation such as chalk or limestone, thus creating a contrast to the size of the induced fractures. This enabled a clear separation of when fracturing occurred and a steady state situation before fracturing or after a fracture had been successfully sealed. Fig. 3 shows the pressure and fluid loss plots for Fluid 1 with an additional concentration of $CaCO_3$, referenced as Fluid 1 + C, and with the addition of cellulose fibre A, referenced as Fluid 1 + A. During the early stages of the test with Fluid 1+C, a slight cracking noise could be heard when the pressure reached 7–8 MPa, and a fluid loss of circa 10 ml was observed. Thereafter, the fluid loss remained at a steady state until the pressure reached 16 MPa, after which, a more severe fracturing of the disc occurred. After this point, no stable pressure could be achieved above ca 1 MPa. The induction of a fracture can be detected in the relevant figures as a combination of a sudden drop in pressure accompanied by an increase in the fluid loss rate as visible in Fig. 3 (a) after 6–7 $s^{0.5}$ and at around 18 $s^{0.5}$. During steady state phases without new fractures being induced, the pressure plot reflects the applied differential pressure, whereas the fluid filtrate plot increases with a rate reflecting the gradual build-up of an external filter-cake, such as seen in Fig. 3 (a) between 10 and 15 $s^{0.5}$. Periods with continued changes in pressure and high fluid loss-rates reflect a situation where a disc has been fractured and a seal between the fracture is progressively building and failing. An example of the latter is presented in Fig. 3 (b) in the time period 14–16 $s^{0.5}$. In situations where the fracture is effectively sealed, the initial higher pressure is re-established, and the temporarily higher fluid-loss is reduced, as shown in Fig. 3 (b) after time 20 $s^{0.5}$.

The test with Fluid 1 + A started in a similar manner, with light fracturing occurring around 7–9 MPa and a corresponding fluid loss of around 2 ml. Thereafter, with higher applied pressure the disc fractured multiple times and was repeatedly re-sealed as pressure was increased to 21 MPa.

Fig. 4 shows the disc and the induced fracture when testing with Fluid 1 + C. A clear thin cut can be seen in the filter-cake. This crack led to the high fluid loss. The fracture was measured to be in the range of 74–126 μm on the disc surface using a calibrated Dino-Lite digital microscope. The applied $CaCO_3$ was not able to re-seal this fracture because of the too small a particle size distribution or low filter-cake cohesion.

The disc with filter-cake for the tests with Fluid 1 + A is presented in Fig. 5. After fracturing, the filter-cake re-formed and thus an intact filter-cake can be observed, despite the induced fracture being in the range of 224–365 μm on the surface. Comparing the results with the test with Fluid 1 + C, it is clear that the addition of the ultra-fine cellulose fibres improved the capacity to re-seal the disc and hold a much higher pressure after re-sealing. Given that the fracture width greatly exceeded the size of the Cellulose fibre A particles, the re-sealing was likely not due to particle plugging at the surface, but potentially due to the properties of the filter-cake. It may be that higher cohesion and shear strength in the filter-cake facilitates the re-establishment of a filter-cake after the fracture is induced. Following Klungtvedt et al. (2023a), such a cohesion is expected. However, the strength of the present cohesion is unknown.

The experiments with the other fluids followed the same procedure and the results are presented as two tests side-by side for ease of comparison. To assess the consistency of the testing, two tests were conducted with Fluid 2 without additives and Fluid 2 with extra $CaCO_3$, to reflect the accumulation of fine drilled solids. These two fluid compositions are thus relatively similar to the test with Fluid 1 + C. The recorded pressure and fluid loss data are presented in Fig. 6 and show a behaviour consistent with Fluid 1 + C. Both tests show low fluid loss as the pressure builds towards the first significant fracturing. The test with Fluid 2 without additional LCM was terminated after being fractured at a pressure of 16 MPa, after which it was difficult to obtain a good sealing of the induced fracture. The test with Fluid 2 + C fractured at around 9 MPa and could not be re-sealed to achieve higher pressures thereafter. The addition of coarser size $CaCO_3$ could not be seen to improve the ability of Fluid 2 to re-seal the disc after fracturing. This may be due to inadequate size of the added particles or it may be related to low filter-cake cohesion, or more likely a combination of the two factors, given that Fluid 1 + An effectively re-sealed the fractured disc.

The testes with Fluid 2 were then repeated with the addition of 28.5

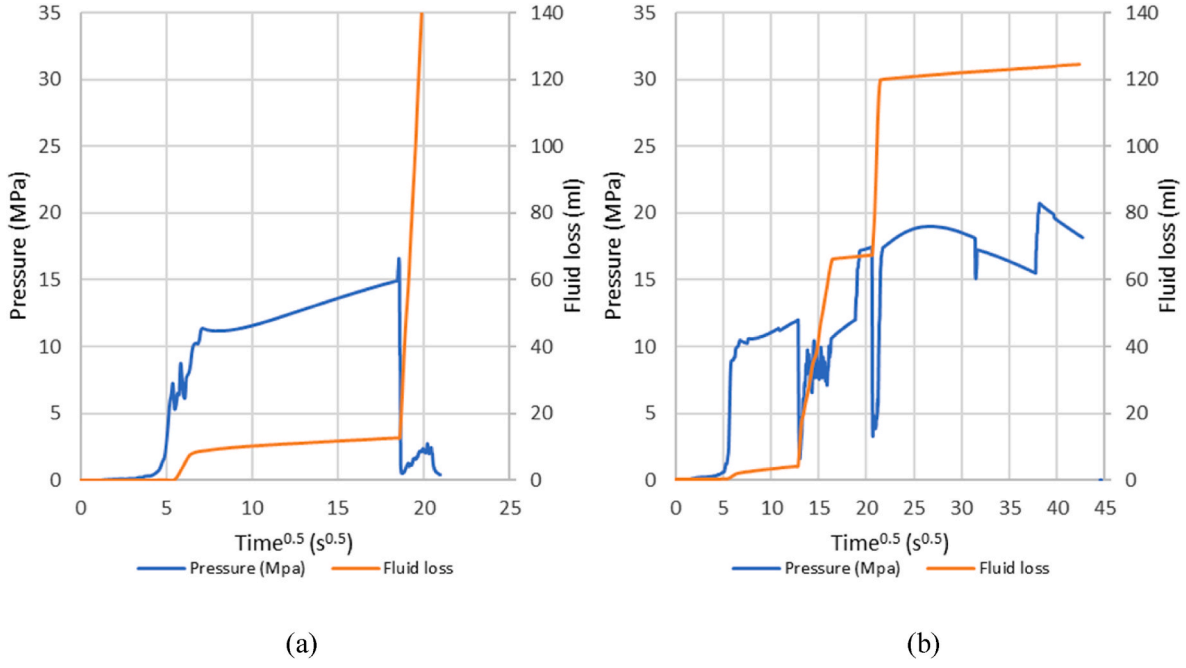

Fig. 3. Pressure and fluid loss for Fluid 1 + C (a), and Fluid 1 + A (b).

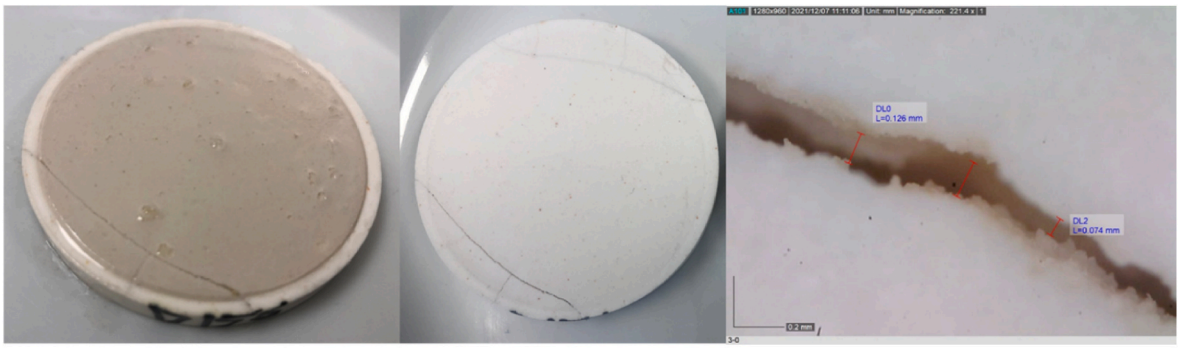

Fig. 4. Disc after test with Fluid 1 + C, with filter-cake (a), after removing filter-cake (b) and measurement of fracture opening (c).

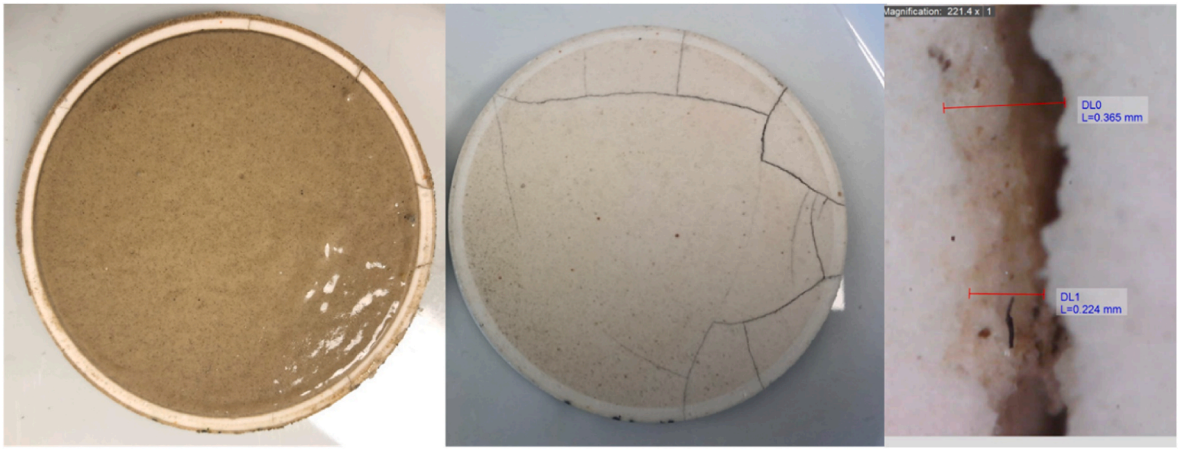

Fig. 5. Disc after test with Fluid 1/14.25 kg/m^3 Cellulose fibre A, with filter-cake (a), after removing filter-cake (b) and measurement of fracture opening (c).

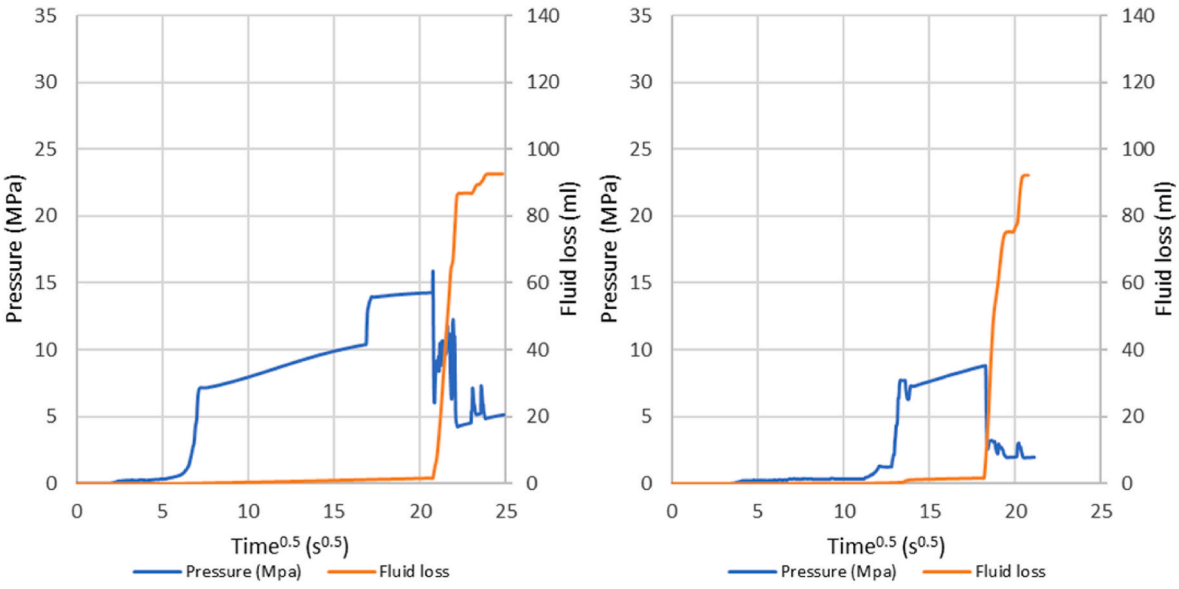

Fig. 6. Pressure and fluid loss for Fluid 2 (a), and Fluid 2 + C (b).

kg/m3 of the Granular cellulose, with and without additional $CaCO_3$. The pressure and fluid loss plots, shown in Fig. 7, reveal a very significant improvement in performance. As the discs fractured, a seal was re-established with steps in the fluid loss of only 0.2–0.5 ml, hence showing an excellent ability to seal fractures as they were occurring. The total fluid loss for each of the tests were around 4 ml and peak pressures of 27–28 MPa were held without the seals failing. From the pressure and fluid loss plots it is not evident that the additional $CaCO_3$ alters the performance of the fluid.

As a next step, the tests with Fluid 2 + G and Fluid 2 + G + C were repeated with the addition of 8.55 kg/m^3 of Cellulose fibre B in two tests and Cellulose fibre A in another test. The pressure and fluid loss data of the tests with Cellulose fibre B are shown in Fig. 8. Overall, the data show similar results as those from the first two tests with the Granular cellulose, with fluid loss ranging from 3.7 to 5 ml under pressures ranging up to 28 MPa. The test with Cellulose fibre A yielded a consistent result as with Cellulose fibre B, since the 2% lower recorded fluid loss is likely within the normal variations of testing.

In summary, the results with water-based fluids provided a consistent set of data, thus indicating that the testing methodology provided data that were repeatable and reliable, despite the natural variations in disc fracturing.

To test the methodology with oil-based fluids, two tests were set up with a 1.62 sg oil-based field fluid, with and without the addition of 28.5 kg/m^3 of the Granular cellulose. The pressure and fluid loss plots of Fluid 3 and Fluid 3 + G are presented in Fig. 9. For Fluid 3 the results are almost identical to the test results with the water-based Fluids 1 and 2 without Granular cellulose. Once the disc fractured at around 9 MPa, a satisfactory re-sealing could not be achieved, despite the high solids content of the drilling fluid. As for the water-based fluids, the addition of 28.5 kg/m^3 of the Granular cellulose enabled a re-sealing of the disc after fracturing and the pressure was elevated as high as 32 MPa. The oil-based fluid loss was, however, considerably higher than that of the tests with water-based once the fractures were induced. The fluid loss was around 30 ml with Fluid 3 + G vs around 4 ml with Fluid 2 + G.

For time periods without any noticeable disc fracturing, the permeability of the filter-cakes for Fluid 2 were estimated using Equation (1). This was established by Klungtvedt and Saasen (2023). K is the permeability (m^2). Note that 1 Darcy = 1 μm^2. The filtrate viscosity is η (Pa*s), ΔP is the applied differential pressure (Pa), A is the flow area (m^2), C_{FL} is the coefficient of fluid loss and k_F the portion of the drilling fluid that is deposited to build the filter-cake.

$$K = \frac{\eta}{2\Delta P A^2} \frac{C_{FL}^2}{1 + \frac{1}{k_F}} \tag{1}$$

The values for C_{FL} were calculated using a linear regression for fluid loss, FL_T, as a function of the square root of time, T, and a spurt loss constant, SL, as per Equation (2) (Klungtvedt and Saasen; 2023).

$$FL_T = C_{FL} * T^{0.5} + SL \tag{2}$$

For simplicity, the viscosity of the fluid filtrate was set to 2 mPa s, which is equivalent to twice the dynamic viscosity of water at 20 °C. The value of k_F was based on a measurement of the moisture content of the filter-cakes, which averaged 50%, and the calculated solids, fibre and polymer contents of the fluids, taken from the fluid recipes. As such, the calculated permeabilities are primarily to be used for comparison within a series of tests for one base fluid, rather than being scientifically precise. A measurement of the fluid filtrate viscosity at the relevant temperature would yield more precise results and may facilitate comparison between fluids.

Fig. 10 shows the estimated filter-cake permeabilities for Fluid 2. For Fluid 2, without any other additives, the permeability was calculated to be 0.017 and 0.019 mD for two different average pressures. Fluid 2 + C contained only a very fine $CaCO_3$ particles, with a D50 value of 5 μm before hot-rolling and degradation, which may explain the low permeability values. With only two data-points, no trend or correlation between permeability and differential pressure can be established with an acceptable level of precision. Once coarser $CaCO_3$ particles were added, the calculated permeability more than doubled to 0.047 mD for Fluid 2 + C. As expected, this indicates that the larger particles, which may be adequate for sealing a coarser formation, increases the permeability of the external filter-cake. For all the three tests with additional $CaCO_3$, the permeabilities increased relative to the tests with only the 5 μm $CaCO_3$. It was noted that all the tests containing cellulose, showed lower permeabilities at higher pressures. The effect is likely caused by the compression of the fibres and hence an improved sealing of the gaps between the particles in the filter-cake. For the test with Granular cellulose, but without Cellulose fibre B, the permeability was significantly

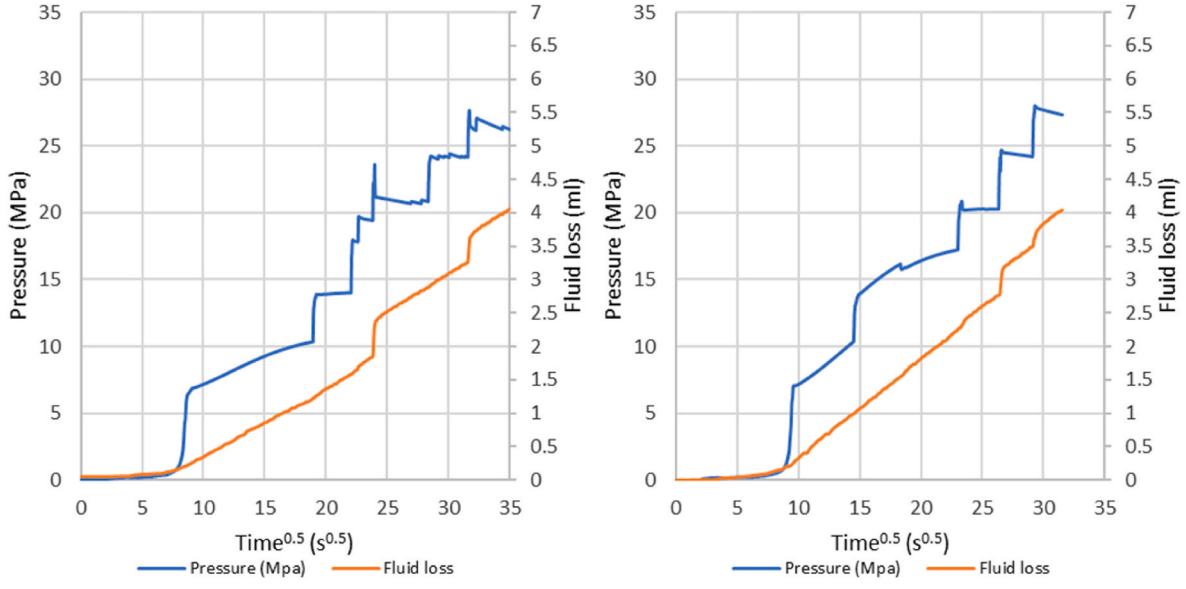

Fig. 7. Pressure and fluid loss for Fluid 2 + G (a), and Fluid 2 + G + C (b).

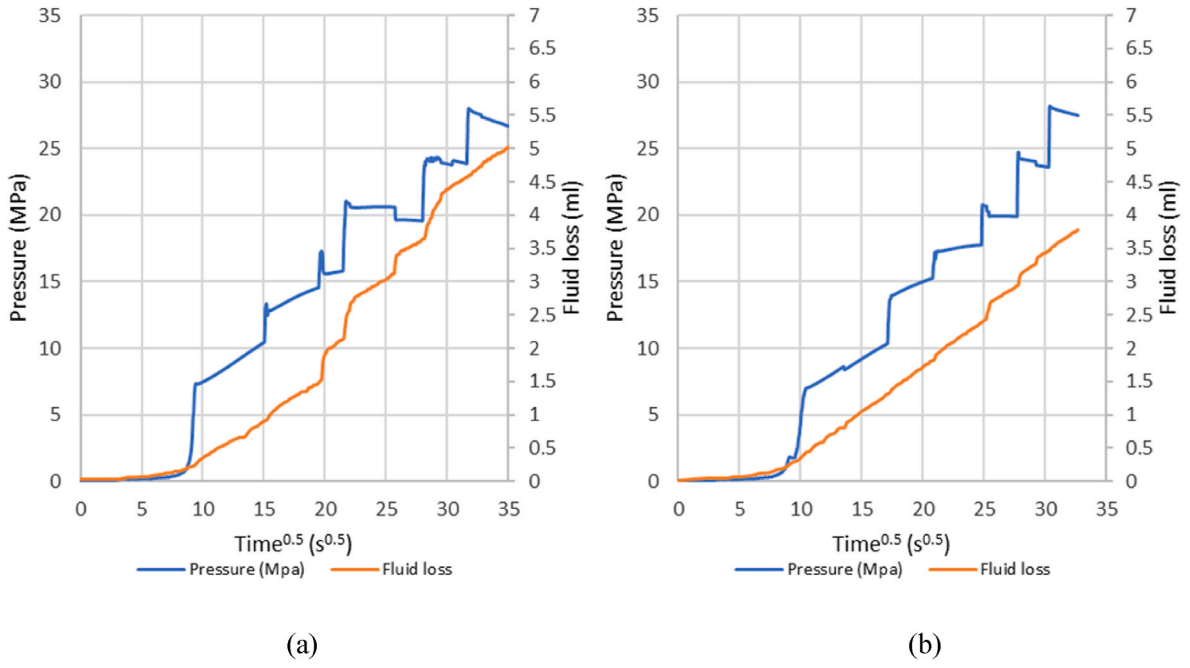

Fig. 8. Pressure and fluid loss for Fluid 2 + G + B, and Fluid 2 + G + B + C (b).

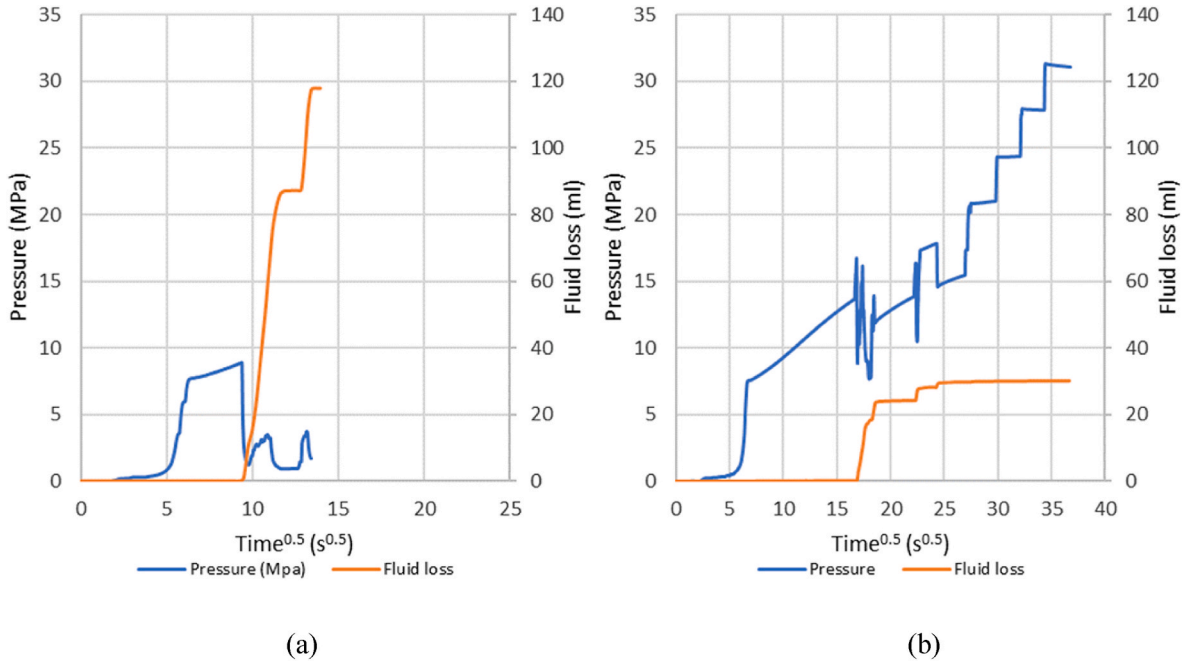

Fig. 9. Pressure and fluid loss for Fluid 3 (a), and Fluid 3 + G (b).

higher when the slightly coarser $CaCO_3$ particles were added to the fluid. This effect was eliminated when Cellulose fibre B or A were present. Considering that the Cellulose fibre B and A particles were of relatively similar size as the $CaCO_3$ particles added to reflect drilled solids, the results indicate that the fibres adapt better than the $CaCO_3$ to reduce filter-cake permeability.

Further, when analysing the test discs and the filter-cakes, the patterns observed in the pressure and fluid loss charts were further established. Firstly, Fig. 11 shows the discs for base Fluid 2 and Fluid 2 + C with $CaCO_3$. Only small fractures in the discs could be observed, and thin hair-like cuts could be seen in the filter-cakes. Considering that both the tests yielded very high fluid loss once the discs had fractured, this indicates that the cohesive strength of the filter-cake or the sealing ability of the particles were ineffective to control the flow at the applied pressure.

For the tests with Granular Cellulose, higher pressures had been applied, and more severe disc fracturing had occurred despite the fluid loss being limited to 4 ml for both tests. As presented in Fig. 12, the Granular Cellulose particles can be seen at the fracture opening. A similar sealing mechanism is presented in Fig. 13, for Fluid 2 + G + C, although the disc fracturing was even more severe. Specifically, it can be seen in Fig. 13 (b) that the Granular cellulose particles gathered to form a seam in the filter-cake above the induced fractures in the disc.

Two tests were conducted with a barite weighted oil-based field

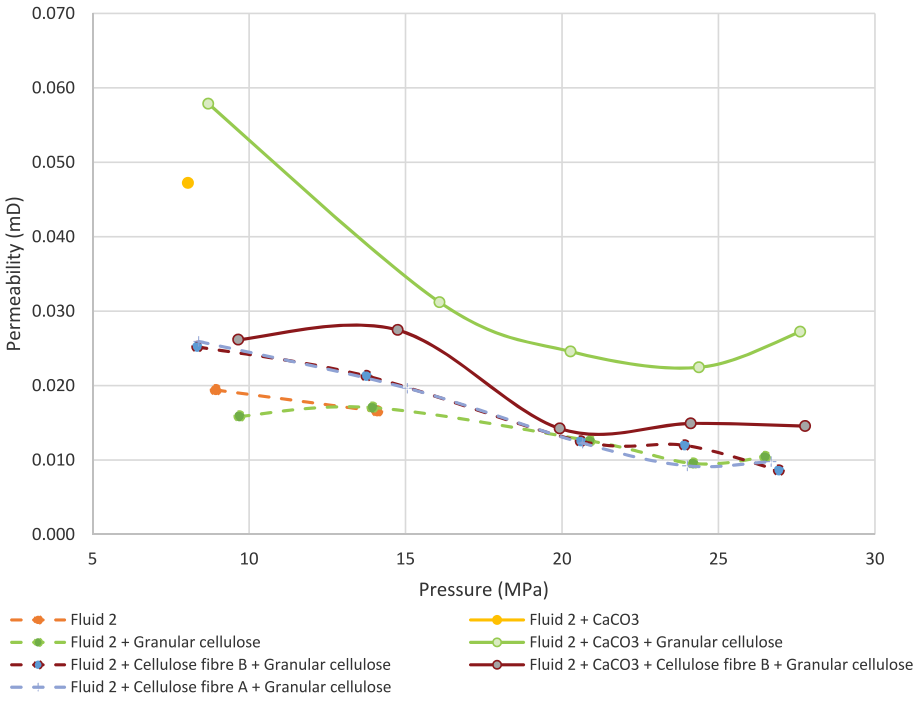

Fig. 10. Calculated permeability of the filter-cakes of Fluid 2 with different additives and at different pressures.

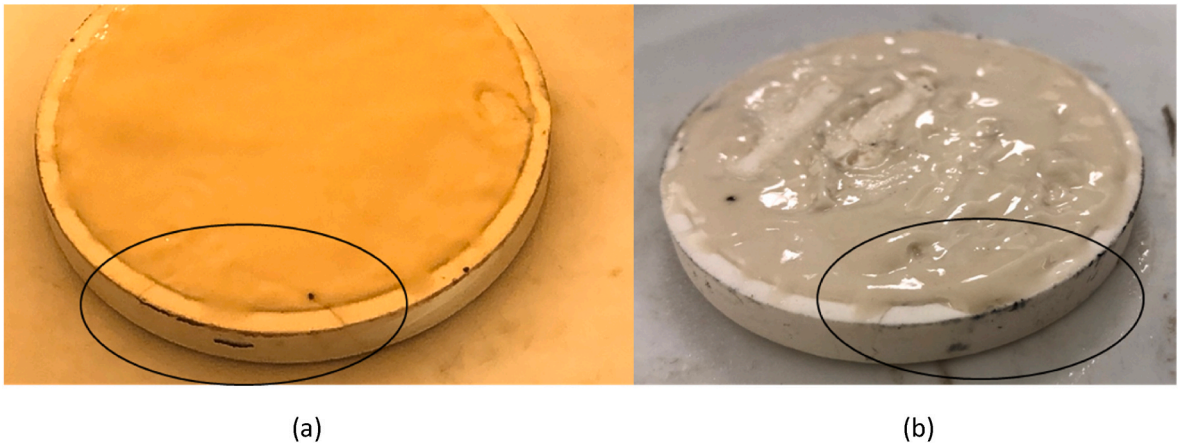

Fig. 11. Discs from tests of Fluid 2 (a) and Fluid 2 + C (b).

fluid, Fluid 3. The test without any Granular cellulose yielded a pressure and fluid loss plot which was consistent with tests with Fluids 1 and 2 without Granular cellulose. Fig. 14 presents images of the disc for the test of Fluid 3. The filter-cake can be seen to have hair-like cuts in multiple places.

Fluid 3 was also tested with the addition of Granular cellulose. Fig. 15 shows the disc with the filter-cake intact in the test cell and also how the disc was fractured. The picture taken with the disc inside the cell clearly shows how the LPM has built ridges over the fractures, which is consistent with the building of LPM seams shown in Fig. 13 (b).

3. Discussion

The methodology was applied to attempt studying the transition from a steady-state fluid loss test to the repeated sealing of induced fractures. The results obtained were remarkably similar for fluids with small variations in composition, such as Fluids 1 and 2. Also, the results were considerably different for different LPM combinations, where addition of $CaCO_3$ had no significant impact on sealing induced fractures, Cellulose fibre A and B improved filter-cake permeability, whereas the Granular Cellulose particles were very effective in sealing the induced fractures. Fig. 16 shows six of the disc's tested, and the similarities in the fracture patterns are evident. The fractures were consistently towards the edge of the discs and often on both sides, thus limiting the fracture width to half of the gap between the disc and the test cylinder, or around 0.3–0.4 mm. This indicates that the test methodology could compare the applied fluids' capability of sealing induced fractures from around 0.1–0.4 mm. With higher applied pressures, more significant disc fracturing was induced, thus potentially enabling distinguishing the performance of more similar LPM materials than those tested.

A weakness of the method is comparing test results conducted with different equipment. This may be solved by establishing a standardized method for inducing the disc fractures, such as e.g. placing thin needles, or cones at fixed locations between the disc and the end cap. An alternative may be to weaken the discs in certain points to control the fracturing patterns, or discs may even be pre-fractured to simulate a situation where natural fractures are present when new formation is

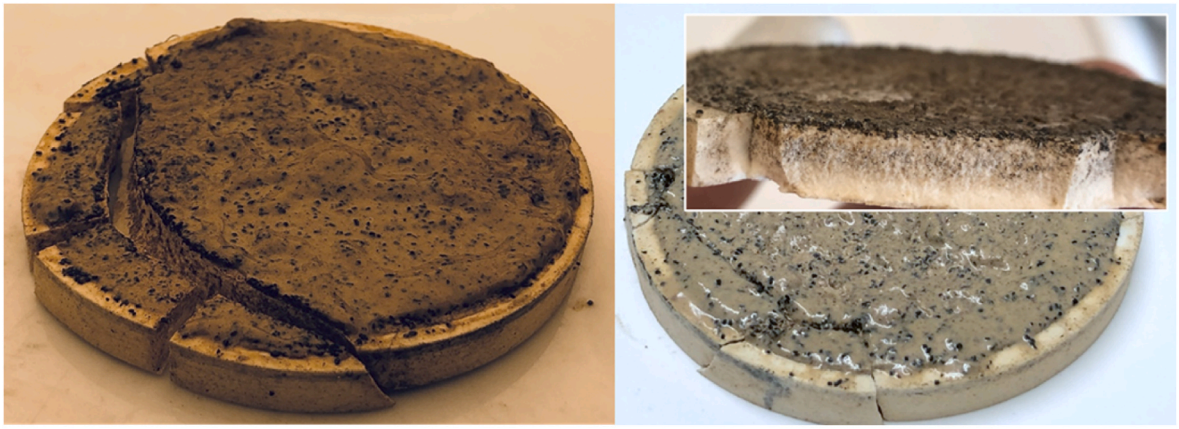

Fig. 12. Discs from tests of Fluid 2 + G (a) and Fluid 2 + G + C (b).

Fig. 13. Disc from tests of Fluid 2 + G + B (a) and reverse side of filter-cake with Granular cellulose seams (b).

Fig. 14. Disc from test with Fluid 3, with filter-cake (a) and with filter-cake removed (b).

being drilled. For the current study, a microscope was used to measure fracture openings. More advanced imaging and scanning analysis may provide additional data to assess fluid and particle invasion into the fractures.

The permeabilities calculated for many of the data-points also include the area of the sealed fractures. As the permeabilities trended downwards with higher pressures where the Granular cellulose had been applied, and more fractures had been induced, it is clear that if the fractures were effectively healed, the permeability of the filter-cake must have been fully restored also over the fracture openings. Certain

Fig. 15. Disc from test with Fluid 3 + G, with filter-cake and LPM ridges (a) and broken disc when taken out of cell (b).

Fig. 16. Fracture patterns in discs.

of the tests yielded relatively similar values for the calculated filter-cake permeabilities, such as the test for Fluid 2 and Fluid 2 with added Granular cellulose, shown in Fig. 10. Therefore, if these fluids were tested using conventional permeability plugging tests on 10 μm discs, the results would also be relatively similar. The pressure and fluid loss plots in Figs. 6 and 7 clearly show how the introduction of the new test methodology provided new insight into how these two fluid compositions function in situations where a fracture is induced.

The similarity between the water-based Fluids 1 and 2 with the oil-based Fluid 3, when $CaCO_3$ was the only applied LPM is apparent. For Fluids 1 and 2 the similarities were also remarkable when the Granular cellulose was applied, as the five tests were successful to above 27 MPa and with very small variations in fluid loss. The contrast was however clear with the oil-based Fluid 3 with Granular cellulose as the fluid loss during fracturing was around 7.5 times that of the water-based fluids. A study by Klungtvedt and Saasen (2022) showed that fluid loss escalates in a more abrupt way for oil-based fluids, when a sealing limit is reached. This may reflect a roller-bearing or lubricity effect caused by the high concentration of brine-particles in the oil-based fluids.

The fluid loss recorded for the tests with water-based fluid and Granular Cellulose was very low at around 4 ml. This is evidence that the fluid composition performed well with regards to sealing of the permeable disc with median pore-size of 10 μm as well as sealing the induced fractures which could be up to 0.3–0.4 mm. When considering the particle size distribution of Fluid 2 with the Granular Cellulose and the Cellulose Fibre B, the results deviate considerably from the recommendations of the Ideal Packing Theory, Abrams rule and the Alsaba method. The closest model is the recommendation that Fuh (1993a) proposed, although the volumetric concentration of Cellulose Fibre B is considerably lower than Fuh's proposal. The polymer and the $CaCO_3$ particles provide a volumetric concentration of particles <10 μm of around 5.6%, the Cellulose fibre B are sized between 5 and 80 μm at a

concentration of 0.63% and the Granular cellulose are sized between 250 and 600 μm at a concentration of 2.1%. In combination this provides a multimodal particle size distribution. The combined functionality is that the fine particles, effectively seal the surface of the formation with a low-permeability filter-cake and the Granular cellulose effectively seal the fracture openings as they are induced. Fig. 17 show the cumulative particle size distribution of Fluid 2 with the Cellulose fibre B and the Granular cellulose compared with the Ideal Packing Theory.

Andreasen (1930) presented a model for designing concrete slurries to optimize the strength of concrete. The model is described by Equation (3), where D is the particle size, D_L is the size of the largest particle and q is the Andreasen packing factor. Through experiments it was shown that smaller values of q led to less voids and higher concrete density.

$$\text{Cumulative Particles Finer Than } (\%) = 100 * \left(\frac{D}{D_L}\right)^q \quad (3)$$

By studying the finer particles in Fluid 2, which are the polymers, $CaCO_3$ and the Cellulose fibre B particles, these may be compared in isolation to the Ideal Packing Theory and the Andreasen packing model. Fig. 18 shows that the particles of Fluid 2 with Cellulose fibre B more closely resemble an Andreasen model with a q of 0.08 than the Ideal Packing Theory, as shown in Fig. 18.

The Granular cellulose materials was sized consistently with the practical approach introduced by Fuh (1993a,b), although at considerably lower concentrations. The fractures that were induced during the experiments were of a size equivalent to the particle size of the Granular cellulose, and thus also reasonably consistent with the Alsaba method for sealing of fractures as well as the Fuh approach.

Considering the very low fluid loss achieved during the induced fracture tests with Fluid 2 + G + B, it may be concluded that multimodal particle size distributions may be useful when a fluid is to be designed for sealing of both a permeable formation and induced fractures simultaneously. Also, the analysis of the finer particles indicate that the Andreasen method may be relevant for optimising fluids to provide a low-permeability filter-cake.

The field application data provided by Klungtvedt et al. (2023b) showed the positive effect of the Granular cellulose material in sealing of fractured limestone/chalk formations under conditions of high differential pressures, confirming the good effect observed in the present study for fluid samples where Granular cellulose had been included.

The hydraulic pump used for the tests provided an accurate measurement of the applied pressure, however, if could not be automatically controlled to provide a constant flowrate or constant applied pressure. For future testing, an automated pump may provide additional insight, particularly if specific differential pressures are to be simulated. Similarly logging of temperature may be relevant as this may facilitate studying any changes in sealing performance as a function of temperature, which may impact particle integrity and fluid viscosity.

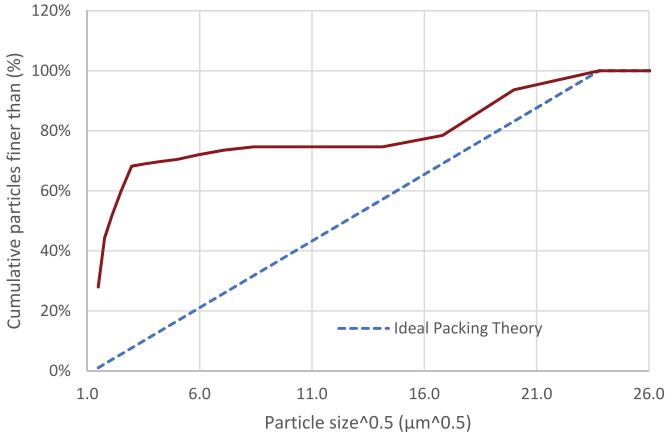

Fig. 17. Particle size distribution of all particles in Fluid 2 + G + B.

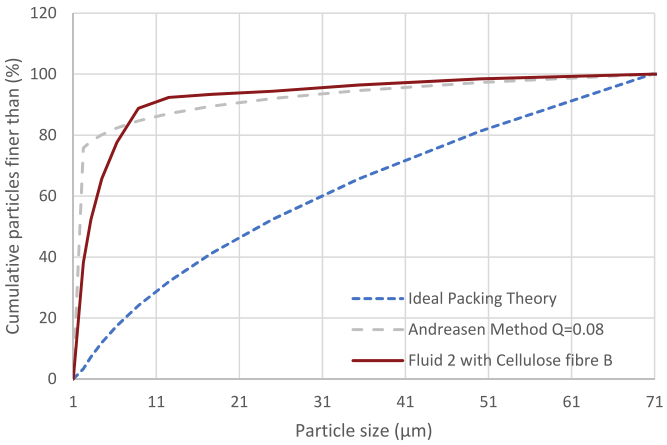

Fig. 18. Particle size distribution of finer particles in Fluid 2 + G + B.

4. Conclusions

The experimental method for testing of fracture induction and fracture sealing using ceramic discs yielded consistent results in terms of fluid loss and fracture patterns, with the fluids tested. The plots of pressure and fluid-loss versus time$^{0.5}$ provided clear insight into periods of stable filtration, disc fracturing and subsequent sealing or failure to seal the induced fracture. The accurate plots of pressure and fluid-loss thus enabled the calculation of filter-cake permeabilities at different pressure intervals. The fluid-loss encountered after disc fracturing and the subsequent success or failure of establishing a new seal across the induced fracture enabled a clear separation of each fluid's capacity to seal induced fractures in the range from 0.1 to 0.4 mm. Further specific conclusions were made:

- The methodology facilitated gradual fracturing of the discs as higher pressures were applied
- The fracture patterns were relatively similar for discs tested up to the same pressures
- The addition of the Granular cellulose LPM enabled effective sealing of the induced fractures with very low fluid loss
- The lowest filter-cake permeabilities were obtained when applying a combination of very fine $CaCO_3$, with D50 of 5 μm, with cellulose based LPM
- The addition of cellulose based LPM eliminated the negative impact that certain sizes of $CaCO_3$ particles had on the filter-cake permeability
- The losses occurring with oil-based fluid was higher than for water-based fluid when fractures were induced
- A multi-modal particle size distribution proved to be effective for simultaneous sealing of a permeable formation and induced fractures
- Further development of the methodology might be attempted to achieve a more standardized methodology which may be transferrable to other permeability plugging apparatuses designed for using ceramic discs

Credit author statement

Karl Ronny Klungtvedt: Conceptualization, Methodology, Validation, Investigation, Performing experiments, Writing – original draft, Collecting material for experiments, Writing – review & editing, Funding acquisition, Jan Kristian Vasshus: Conceptualization, Methodology, Validation, Investigation, Performing experiments, Arild Saasen: Conceptualization, Writing – original draft, Writing – review & editing, Supervision.

Declaration of competing interest

The authors declare that they have no known competing financial interests or personal relationships that could have appeared to influence the work reported in this paper.

Data availability

No data was used for the research described in the article.

Acknowledgement

The authors would like to thank the Research Council of Norway for financially supporting the project through RCN# 320646.

References

Abrams, A., 1977. Mud design to minimize rock impairment due to particle invasion. J. Petrol. Technol. 586–592. May 1977.

Alsaba, M., Al Dushaishi, M.F., Nygaard, R., Nes, O.-M., Saasen, A., 2017. Updated criterion to select particle size distribution of lost circulation materials for an effective fracture sealing. J. Petrol. Sci. Eng. 149, 641–648.

Andreasen, A.H.M., 1930. Ueber die Beziehung zwischen Kornabstufung und Zwischenraum in Produkten aus losen Körnern (mit einigen Experimenten). Kolloid Z. 50, 217–228. https://doi.org/10.1007/BF01422986 (In German).

Fekete, P.O., Dosunmu, A., Anthony, K., Ekeinde, E.B., Anyanwu, C., Odagme, B.S., 2013. Wellbore stability management in depleted and low pressure reservoirs. Paper SPE-167543-MS. In: SPE Nigeria Annual International Conference and Exhibition. https://doi.org/10.2118/167543-MS. Lagos, August 5–7, 2013.

Feng, Y., Jones, J.F., Gray, K.E., 2016. A review on fracture-initiation and -propagation pressures for lost circulation and wellbore strengthening. SPE Drill. Complet. 31, 134–144. https://doi.org/10.2118/181747-PA.

Fuh, G.-F., 1993a. Method for inhibiting the initiation and propagation of formation fractures while drilling and casing a well. U.S. Patent 5, 180, 020 filed Oct. 31, 1991 and issued Jan. 19, 1993.

Fuh, G.-F., 1993b. Method for inhibiting the initiation and propagation of formation fractures while drilling and casing a well. U.S. Patent 5, 207, 282 filed Oct. 5, 1992 and issued May 4, 1993.

Fuh, G.-F., Beardmore, D., Morita, N., 2007. Further Development, Field Testing, and Application of the Wellbore Strengthening Technique for Drilling Operations. SPE/IADC Drilling Conference, Amsterdam, The Netherlands. https://doi.org/10.2118/105809-MS. Paper SPE-105809-MS February 2007.

Gao, C., Miska, S., Yu, M., Dokhani, V., Ozbayoglu, E., Takach, N., 2021a. Geomechanical characterization of shale samples after pore plugging with nanomaterials. J. Petrol. Sci. Eng. 208, 109703 https://doi.org/10.1016/j.petrol.2021.109703.

Gao, C., Miska, S., Yu, M., Dokhani, V., Ozbayoglu, E., Takach, N., 2021b. Experimental and numerical analysis of effective enhancement of wellbore stability in shales with nanopartilces. J. Nat. Gas Sci. Eng. 95, 104197 https://doi.org/10.1016/j.jngse.2021.104197.

Jiang, G., Liu, T., Ning, F., Tu, Y., Zhang, L., Yu, Y., Kuang, L., 2011. Polyethylene glycol drilling fluid for drilling in marine gas hydrates-bearing sediments: an experimental study. Energies 4 (1), 140–150. https://doi.org/10.3390/en4010140.

Kaeuffer, M., 1973. Determination de L'Optimum deRemplissage Granulometrique et Quelques proprieties S'y Rattachant. In: Presented at Congres International de l'A.F. T.P.v. Rouen.

Klungtvedt, K.R., Saasen, A., 2022. Comparison of lost circulation material sealing effectiveness in water-based and oil-based drilling fluids and under conditions of mechanical shear and high differential pressures. J. Energy Resour. Technol. 144 (12), 123011 https://doi.org/10.1115/1.4054653, 2022.

Klungtvedt, K.R., Saasen, A., 2023. The role of particle size distribution for fluid loss materials on formation of filter-cakes and avoiding formation damage. J. Energy Resour. Technol. 145 (4), 041702 https://doi.org/10.1115/1.4056187, 2023.

Klungtvedt, K.R., Saasen, A., Vasshus, J.K., Trodal, V.B., Mandal, S.K., Berglind, B., Khalifeh, M., 2021. The fundamental principles and standard evaluation for fluid loss and possible extensions of test methodology to assess consequences for formation damage. Energies 14 (8), 2021. https://doi.org/10.3390/en14082252 paper 2252.

Klungtvedt, K.R., Pedrosa, C., Saasen, A., 2023a. Measuring filter-cake cohesive strength and flowability. Geoenergy Sci. Eng. 221, 111298 https://doi.org/10.1016/j.petrol.2022.111298.

Klungtvedt, K.R., Vasshus, J.K., Nesheim, G., Scott, P., 2023b. Managing High Differential Pressures in Fractured Carbonate Reservoir by Use of Wellbore Strengthening Material, OTC-32173-MS, Presented at OTC Houston. May 2023.

Ma, B., Pu, X., Zhao, Z., Wang, H., Dong, W., 2019. Laboratory Study on Core Fracturing Simulations for Wellbore Strengthening. Geofluids. https://doi.org/10.1155/2019/7942064, 2019, Article ID 7942064.

Mohammadizadeh, S.M., Mohaddam, M.A., Talebbeydokhti, N., 2021. Analysis of flow in porous media using combined pressurized-free surface network. J. Porous Media 24 (10), 1–15. https://doi.org/10.1615/JPorMedia.2021025407, 2021.

Scott, P., Beardmore, D.H., Wade, Z.D., Evans, E., Franks, K.D., 2012. Size degradation of granular lost circulation materials. In: IADC/SPE 151227, SPE/IADC Drilling Conference and Exhibition Held in San Diego, California, pp. 6–8. March 2012.

Scott, P., Redburn, M., Nesheim, G., 2020. A pragmatic approach to lost circulation treatments: what every drilling engineer should know. In: Paper AADE-20-FTCE-062, AADE Fluids Technical Conference and Exhibition. the Marriott Marquis, Houston, Texas. April 14-15, 2020.